



S-N/99205--002
Shaw/13052-204

Hydrologic Data for the Groundwater Flow and Contaminant Transport Model of Corrective Action Units 101 and 102: Central and Western Pahute Mesa, Nye County, Nevada



Revision No.: 0

February 2004

Prepared for U.S. Department of Energy under Contract No. DE-AC52-03NA99205.

Approved for public release; further dissemination unlimited.

Available for public sale, in paper, from:

U.S. Department of Commerce
National Technical Information Service
5285 Port Royal Road
Springfield, VA 22161
Phone: 800.553.6847
Fax: 703.605.6900
Email: orders@ntis.gov
Online ordering: <http://www.ntis.gov/ordering.htm>

Available electronically at <http://www.osti.gov/bridge>

Available for a processing fee to U.S. Department of Energy and its contractors,
in paper, from:

U.S. Department of Energy
Office of Scientific and Technical Information
P.O. Box 62
Oak Ridge, TN 37831-0062
Phone: 865.576.8401
Fax: 865.576.5728
Email: reports@adonis.osti.gov

Reference herein to any specific commercial product, process, or service by trade name, trademark, manufacturer, or otherwise, does not necessarily constitute or imply its endorsement, recommendation, or favoring by the United States Government or any agency thereof or its contractors or subcontractors.



S-N/99205--002
Shaw/13052-204

HYDROLOGIC DATA FOR THE GROUNDWATER FLOW AND CONTAMINANT TRANSPORT MODEL OF CORRECTIVE ACTION UNITS 101 AND 102: CENTRAL AND WESTERN PAHUTE MESA, NYE COUNTY, NEVADA

Revision No.: 0

February 2004

Prepared by: K. Rehfeldt, W. Drici, B. Lester, D. Sloop, J. Watrus,
T. Beard, M. Sully, W. Fryer, and C. Benedict

Stoller-Navarro Joint Venture
7710 W. Cheyenne, Building 3
Las Vegas, NV 89129

Prepared for U.S. Department of Energy under Contract No. DE-AC52-03NA99205.

Approved for public release; further dissemination unlimited.

HYDROLOGIC DATA
FOR THE GROUNDWATER FLOW AND CONTAMINANT TRANSPORT MODEL
OF CORRECTIVE ACTION UNITS 101 AND 102:
CENTRAL AND WESTERN PAHUTE MESA, NYE COUNTY, NEVADA

Approved by: _____ Date: _____
John McCord, UGTA Project Manager
Stoller-Navarro Joint Venture

Table of Contents

- List of Figures ix
- List of Plates xv
- List of Tables xvi
- Acknowledgement xix
- List of Acronyms and Abbreviations xx

- 1.0 Introduction 1-1
 - 1.1 Background 1-1
 - 1.1.1 Project Background 1-1
 - 1.1.2 Pahute Mesa Background 1-4
 - 1.2 Task Purpose and Scope 1-5
 - 1.2.1 Purpose 1-5
 - 1.2.2 Scope of Work 1-5
 - 1.3 Quality Assurance 1-6
 - 1.4 CAU Model Documentation 1-8
 - 1.5 Document Organization 1-9

- 2.0 Regional Setting and Local Hydrostratigraphic Framework 2-1
 - 2.1 Regional Setting 2-1
 - 2.1.1 Regional Hydrogeologic Framework 2-1
 - 2.1.1.1 Hydrogeologic Units 2-3
 - 2.1.1.2 Hydrostratigraphic Units 2-4
 - 2.1.2 Groundwater Occurrence and Movement 2-7
 - 2.1.2.1 Groundwater Occurrence 2-7
 - 2.1.2.2 Groundwater Movement 2-8
 - 2.2 Local Hydrogeologic Framework 2-9
 - 2.2.1 HSU Model Development 2-9
 - 2.2.2 HSU Alternative Model Screening 2-11
 - 2.2.3 Base HSU Model 2-11
 - 2.2.3.1 Structural Features 2-11
 - 2.2.3.2 Hydrogeologic Units 2-13
 - 2.2.3.3 Hydrostratigraphic Units 2-15
 - 2.2.4 Silent Canyon Caldera Complex HSU Model 2-15
 - 2.2.4.1 Structure 2-18
 - 2.2.4.2 Hydrostratigraphy 2-18

- 3.0 CAU Modeling Approach 3-1
 - 3.1 Overview of CAU Modeling Approach 3-1
 - 3.1.1 Selected Code 3-2
 - 3.1.2 Data Requirements 3-3

Table of Contents (Continued)

3.2	Groundwater Flow Modeling Approach and Data Requirements	3-3
3.2.1	Modeling Approach	3-4
3.2.2	Data Requirements	3-7
4.0	Data Analysis.	4-1
4.1	Data Compilation/Generation	4-1
4.1.1	Data Types	4-1
4.1.1.1	General Description	4-1
4.1.1.2	Description of Hydrologic Data Types	4-2
4.1.2	Data Sources.	4-4
4.2	Data Transfer Methodology.	4-4
4.2.1	Rock Genesis and Evolution Factors Influencing Flow and Transport Parameters	4-5
4.2.2	General Transfer Methodology	4-6
4.2.3	YMP Data Transfer	4-6
4.3	Data Documentation Qualification	4-7
4.4	Data Qualification	4-8
4.5	Analysis Methods Used	4-8
4.6	Data Analysis Limitations	4-9
5.0	Hydraulic Parameters.	5-1
5.1	Objectives.	5-1
5.2	Approach	5-1
5.3	Data Types and Prioritization	5-3
5.3.1	Data Types	5-3
5.3.2	Data Prioritization.	5-4
5.4	Data Compilation and Evaluation	5-4
5.4.1	Existing Data	5-4
5.4.2	Historical Well Testing Data Reanalysis	5-4
5.4.3	Data Evaluation	5-5
5.5	Analysis of Hydraulic Conductivity Data	5-6
5.5.1	Spatial Distribution of Data Points.	5-6
5.5.2	Data Transferability	5-8
5.5.3	Laboratory-Scale Data	5-8
5.5.4	Slug Test Data	5-11
5.5.5	Constant-Rate Scale Data.	5-20
5.5.6	Hydraulic Conductivity Versus Depth	5-28
5.5.7	Scaling and Spatial Variability.	5-28

Table of Contents (Continued)

5.5.8	Vertical Anisotropy	5-29
5.5.9	Alteration of Hydraulic Conductivity in Test Cavities.....	5-30
5.5.10	Hydraulic Conductivity Parameters for Each HSU	5-30
5.6	Analysis of Aquifer Storage Properties	5-30
5.7	Limitations	5-36
5.8	Summary	5-37
6.0	Precipitation Recharge.....	6-1
6.1	Objectives.....	6-1
6.2	Approach	6-1
6.3	Data Types and Prioritization	6-2
6.4	Existing Recharge Model Descriptions	6-2
6.4.1	UGTA Recharge Model	6-2
6.4.1.1	Maxey-Eakin	6-2
6.4.1.2	Modified Maxey-Eakin Method	6-3
6.4.1.2.1	Methodology	6-3
6.4.1.2.2	Construction of the Digital Precipitation Map and Grid File	6-4
6.4.1.2.3	Final Precipitation Distribution	6-8
6.4.1.2.4	Recharge.....	6-10
6.4.1.3	Updated UGTA Recharge Model	6-13
6.4.2	U.S. Geological Survey Recharge Model (Hevesi et al., 2003).....	6-15
6.4.3	Desert Research Institute Recharge Model (Russell and Minor, 2002)	6-20
6.4.4	Nevada Water Resource Study	6-33
6.5	Base Recharge Model	6-38
6.6	Alternative Recharge Models.....	6-38
6.7	Limitations.....	6-42
6.8	Summary	6-42
7.0	Surface Groundwater Discharge	7-1
7.1	Objectives.....	7-1
7.2	Approach	7-1
7.3	Data Types and Prioritization	7-3
7.4	Available Data Description	7-4
7.4.1	Natural Surface Discharge	7-4
7.4.2	Well Discharge.....	7-6
7.5	Natural Surface Discharge	7-7
7.5.1	Description of Oasis Valley Discharge Area	7-7
7.5.2	Methodology.....	7-10

Table of Contents (Continued)

7.5.3	Evapotranspiration Units	7-11
7.5.4	Evapotranspiration Rates and Volumes	7-13
7.5.5	Water Level and Spring Discharge Measurements	7-18
7.5.6	Sensitivity and Uncertainty Analyses of Annual ET	7-19
7.5.6.1	Method	7-19
7.5.6.2	Results	7-20
7.6	Well Discharge	7-22
7.6.1	Well and Pumping Record Description	7-22
7.6.1.1	NTS Water Supply Wells	7-22
7.6.1.2	Oasis Valley Wells	7-25
7.6.1.3	Mine Wells	7-26
7.6.2	Historical Pumping Volumes	7-26
7.7	Limitations	7-26
7.8	Summary	7-28
8.0	Hydraulic Heads	8-1
8.1	Objectives	8-1
8.2	Approach	8-1
8.3	Data Types and Prioritization	8-2
8.4	Data Compilation and Evaluation	8-3
8.4.1	Depth-to-Water and Spring Data	8-3
8.4.2	General Site Information	8-3
8.4.2.1	Land Surface Elevation	8-4
8.4.2.2	EOI Definition	8-4
8.4.2.3	HSU Assignment	8-5
8.5	Evaluation of Water-Level Data	8-5
8.5.1	Effects of Temperature and Borehole Deviation	8-6
8.5.2	Assessment of Temporal Trends	8-7
8.6	Predevelopment Steady-State Hydraulic Heads	8-8
8.7	Steady-State Flow System Behavior	8-9
8.7.1	Horizontal Flow Analysis	8-9
8.7.2	Vertical Flow Analysis	8-9
8.8	Transient Flow System Behavior	8-11
8.9	Limitations	8-12
8.10	Summary	8-12
9.0	Lateral Boundary Fluxes	9-1
9.1	Objectives	9-1
9.2	Approach	9-2

Table of Contents (Continued)

9.3	Analysis Results	9-4
9.3.1	Lateral Fluxes Derived from Regional Model Flow Simulations	9-4
9.3.2	Result Comparison	9-5
9.4	Limitations	9-6
9.5	Summary	9-7
10.0	Groundwater Chemistry	10-1
10.1	Objectives	10-1
10.2	Approach	10-2
10.3	Data Description	10-2
10.4	Data Evaluation	10-7
10.4.1	Data Documentation Evaluation	10-7
10.4.2	Data Quality Evaluation	10-8
10.5	Analysis Process and Results	10-8
10.5.1	Major Ion Chemistry	10-9
10.5.2	Stable and Environmental Isotopes	10-12
10.5.2.1	Hydrogen and Oxygen Isotopes	10-13
10.5.2.2	Carbon Isotopes	10-14
10.5.3	Conservative Tracers	10-17
10.5.3.1	Conservative Tracer Data	10-17
10.5.3.2	Conservative Tracer Data Evaluation	10-17
10.5.4	Geochemical Modeling	10-24
10.5.4.1	NETPATH Modeling Approach	10-25
10.5.4.2	Geochemical Modeling Results Using NETPATH	10-28
10.6	Other Considerations	10-29
10.7	Limitations	10-29
10.8	Summary	10-33
11.0	References	11-1

Appendix A - Hydrostratigraphic Model Supporting Information

A.1.0	Description of the Pahute Mesa-Oasis Valley Model Layers	A-1
A.2.0	Alternative Hydrostratigraphic Models	A-9
A.3.0	HSU Model Screening	A-16
A.3.1	Screening Approach	A-16
A.3.1.1	Dimensionality	A-16
A.3.1.2	Faults	A-17
A.3.1.3	Numerical Model	A-17

Table of Contents (Continued)

A.3.1.4	Boundary Conditions	A-18
A.3.1.5	Calibration	A-19
A.3.1.6	Comparison of Simulations	A-20
A.3.1.7	Final Approach	A-21
A.3.2	Application	A-21
A.3.2.1	Selection of Alternative HSU Models	A-21
A.3.2.2	Screening Process	A-24
A.3.2.3	Permeability Distribution - Depth Decay Case	A-25
A.3.2.4	Boundary Conditions	A-25
A.3.2.5	Impact of Faults and Permeability Distributions	A-25
A.3.2.6	Particle Pathlines	A-26
A.3.2.7	Boundary Flux Results	A-27
A.3.2.8	Particle Path Statistics	A-27
A.3.2.9	Head Residuals	A-28
A.3.2.10	General Conclusions	A-28
A.3.2.11	Figures	A-28
A.4.0	References	A-57

Appendix B - Use of Yucca Mountain Site Characterization Project Data for Developing Pahute Mesa Corrective Action Unit Model Parameter Distributions

B.1.0	Introduction	B-1
B.2.0	Deposition and Alteration of Volcanic Rocks	B-3
B.2.1	Deposition	B-3
B.2.2	Alteration	B-4
B.3.0	Factors Influencing Flow and Transport Parameters of Fractured Rock	B-5
B.4.0	Transferability Rationale	B-8
B.4.1	Geologic Setting	B-8
B.4.2	Lithology	B-9
B.4.3	Alteration	B-10
B.4.4	Influence of Stress	B-10
B.4.5	Groundwater Chemistry	B-11
B.4.6	Summary	B-14
B.5.0	Uncertainties in Data Transfer	B-14
B.6.0	References	B-15

Table of Contents (Continued)

Appendix C - Analyses of Past Aquifer Tests Conducted on the NTS

C.1.0	Introduction	C-1
C.2.0	Aquifer Test Data Reanalysis	C-1
C.2.1	Reanalysis Objectives	C-1
C.2.2	Approaches to Reanalysis	C-2
C.2.2.1	ER Contractor Reanalysis Approach	C-2
C.2.2.2	USGS Reanalysis Approach	C-5
C.2.2.3	Aquifer Thickness	C-6
C.2.3	Results	C-7
C.3.0	Slug Test Data Reanalysis	C-9
C.3.1	Reanalysis Objectives	C-9
C.3.2	Approach	C-9
C.3.2.1	Interval-Specific Equilibrium Head	C-10
C.3.2.2	Initial Injection Head	C-10
C.3.3	Analysis	C-11
C.3.3.1	Types of Head Decline Responses	C-13
C.3.3.2	Application of the Different Models	C-13
C.3.3.3	Results	C-17
C.4.0	References	C-19

Appendix D - Description of Well Discharge Data

D.1.0	Introduction	D-1
D.2.0	Summary Data	D-1
D.3.0	Full Dataset	D-6
D.3.1	Dataset Content Summary	D-7
D.3.2	Table Structure	D-7
D.4.0	Access to Data	D-9
D.5.0	References	D-10

Appendix E - Description of Hydraulic Head Dataset

E.1.0	Introduction	E-1
E.1.1	Hydraulic Head Summary Data	E-1
E.1.2	Water Elevations Dataset and Hydrograph Analysis	E-1
E.2.0	Dataset and Analysis Summary	E-1

Table of Contents (Continued)

E.3.0	Table Structure	E-1
E.4.0	Access to Data	E-18
E.4.1	Water Elevations Table	E-18
E.4.2	Hydrograph Analysis	E-18

Appendix F - Flux Calculations Using Regional Flow Model

F.1.0	Introduction	F-1
F.2.0	Models Evaluated in the Calibration Process	F-3
F.2.1	Geologic Model Alternatives	F-3
F.2.2	Recharge Distribution Models	F-4
F.2.3	Models Calibrated	F-7
F.3.0	Calibration Process	F-11
F.3.1	Calibration Criteria	F-12
F.4.0	Calibration Results	F-14
F.5.0	References	F-25

Appendix G - Supplemental Information

G.1.0	Introduction	G-1
G.2.0	Data Summary	G-1
G.3.0	Access to Data	G-1
G.4.0	References	G-2

List of Figures

Number	Title	Page
1-1	Location of the Pahute Mesa Corrective Action Units	1-2
1-2	Investigation and Pahute Mesa-Oasis Valley Areas for the Pahute Mesa Corrective Action Units (DOE/NV, 1999)	1-7
2-1	Features of the Nevada Test Site Regional Groundwater Flow System.	2-2
2-2	Three-Dimensional View of the Base Hydrostratigraphic Model of the Pahute Mesa-Oasis Valley Area (BN, 2002)	2-12
2-3	Comparison of Silent Canyon Caldera Margins: Base Model and SCCC Alternative (BN, 2002)	2-19
2-4	Typical West - East Cross-Section through the Silent Canyon Caldera for the SCCC Model (BN, 2002) Cross-Section Location Shown in Figure 2-3	2-21
3-1	Data Types and Utilization in the Groundwater Flow Model.	3-8
5-1	Map of the Locations of Hydraulic Conductivity Data	5-7
5-2	Laboratory-Scale Hydraulic Conductivity as a Function of Depth and HSU.	5-9
5-3	Alluvium Laboratory Hydraulic Conductivity Probability Distribution	5-11
5-4	Lower Carbonate Aquifer Laboratory Hydraulic Conductivity Probability Distribution	5-12
5-5	Lower Clastic Confining Unit Laboratory Hydraulic Conductivity Probability Distribution	5-12
5-6	Volcanic Aquifer Laboratory Hydraulic Conductivity Probability Distribution	5-13
5-7	Volcanic Confining Units Laboratory Hydraulic Conductivity Probability Distribution	5-13
5-8	Volcanics Undifferentiated Laboratory Hydraulic Conductivity Probability Distribution	5-14
5-9	Slug Test Scale Hydraulic Conductivity as a Function of Depth and Regional HSU	5-15
5-10	Slug Test Scale Hydraulic Conductivity as a Function of Depth and PM-OV HSU	5-16
5-11	Slug Test Scale Hydraulic Conductivity as a Function of Tested Interval Thickness	5-17
5-12	Alluvium Slug Test Hydraulic Conductivity Probability Distribution.	5-18
5-13	Lower Carbonate Aquifer Slug Test Hydraulic Conductivity Probability Distribution.	5-18
5-14	PBRCM Slug Test Hydraulic Conductivity Probability Distribution	5-19
5-15	PBRCM Slug Test Hydraulic Conductivity as a Function of Depth and Location	5-20
5-16	BRA Slug Test Hydraulic Conductivity as a Function of Depth and Location	5-21
5-17	BFCU Slug Test Hydraulic Conductivity as a Function of Depth and Location	5-21
5-18	TMCM Slug Test Hydraulic Conductivity as a Function of Depth and Location	5-22
5-19	CHZCM Slug Test Hydraulic Conductivity as a Function of Depth and Location	5-22
5-20	CFCM Slug Test Hydraulic Conductivity as a Function of Depth and Location.	5-23

List of Figures (Continued)

Number	Title	Page
5-21	IA Slug Test Hydraulic Conductivity as a Function of Depth and Location	5-23
5-22	Constant-Rate Scale Hydraulic Conductivity as a Function of Depth and HSU	5-24
5-23	Plot of Constant-Rate Scale Hydraulic Conductivity Data (Figure 5-22) with a Linear Trend Line	5-25
5-24	Constant-Rate Scale Hydraulic Conductivity as a Function of Tested Interval Thickness.	5-25
5-25	VCU Constant-Rate Hydraulic Conductivity as a Function of Depth and Location	5-27
5-26	Specific Storage Probability Distributions	5-35
6-1	Precipitation Map for the Nevada Test Site Region	6-5
6-2	Potential Recharge Redistribution Areas in the Nevada Test Site Region	6-12
6-3	NTS Regional Model Recharge Distribution	6-14
6-4	Revised Maxey-Eakin Based Recharge in the NTS Region.	6-16
6-5	USGS Recharge Distribution Model 1, Overland Flow Component Included.	6-26
6-6	USGS Recharge Distribution Model 2, No Overland Flow Component	6-27
6-7	Correlation of Recharge Volumes - UGTA-Revised Recharge Versus DRI Recharge	6-34
6-8	DRI Recharge Distribution with Alluvial Mask (Russell and Minor, 2002)	6-36
6-9	DRI Recharge Distribution with Alluvial and Elevation Mask (Russell and Minor, 2002)	6-37
6-10	Recharge Volumes for Hydrographic Areas for all Recharge Models.	6-41
7-1	Locations of Surficial Hydrologic Features in the Pahute Mesa-Oasis Valley Area and Vicinity.	7-2
7-2	General Spring Locations and Major Structural Features Controlling Spring Discharge in Oasis Valley, NV (Reiner et al., 2002)	7-9
7-3	Locations of ET Units as Defined by Lacznik et al. (2001) for Oasis Valley, Nevada	7-14
7-4	Locations of Pumping Wells in the Pahute Mesa-Oasis Valley Area and Vicinity	7-23
7-5	Total Withdrawals from Pumping Wells Located within the Pahute Mesa-Oasis Valley Area No Data Available between 1968 and 1982.	7-27
8-1	Map Showing Composite Potentiometric Surface with Elevated Heads in the Northeast and HSUs at the Water Table.	8-10
10-1	Groundwater Quality Sample Locations in the Pahute Mesa-Oasis Valley Region.	10-3
10-2	Groundwater Quality Sample Locations Considered During PM-OV Flow System Evaluation	10-6

List of Figures (Continued)

Number	Title	Page
10-3	Piper Diagram of Major-Ion Variations in the Pahute Mesa-Oasis Valley Groundwater Flow System	10-11
10-4	Stable Isotopic Plot of $\delta^{18}\text{O}$ vs. δD Values for Springs, Wells, Tunnels, and Precipitation in the Pahute Mesa-Oasis Valley Region	10-14
10-5	Geographic Distribution of Dissolved Inorganic Carbon Data for Wells and Springs in the Study Area	10-15
10-6	Geographic Distribution of δD Values for Wells and Springs in the Study Area	10-18
10-7	Geographic Distribution of Dissolved Cl^- Concentrations for Wells and Springs in the Study Area	10-19
10-8	Piper Diagram of Major-ion Variations for Pahute Mesa and Upgradient Locations	10-30
10-9	Piper Diagram of Major-ion Variations for Crater Flat, Yucca Mountain, and Amargosa Desert Locations	10-31
10-10	Piper Diagram of Major-ion Variations for the ER-EC Wells, Oasis Valley, and Death Valley Locations	10-32
A.3-1	Base-Case Log-Permeability Values (m^2) at 1,000 m amsl for Case Without Depth-Decay of Permeability	A-29
A.3-2	Base-Case Log-Permeability Values (m^2) at 0 m amsl for Case Without Depth-Decay of Conductivity.	A-29
A.3-3	USGS Log-Permeability Values (m^2) at 1,000 m amsl for Case Without Depth-Decay of Conductivity.	A-30
A.3-4	USGS Log-Permeability Values (m^2) at 0 m amsl for Case Without Depth-Decay of Conductivity.	A-30
A.3-5	RIDGE Log-Permeability Values (m^2) at 1,000 m amsl for Case Without Depth-Decay of Conductivity.	A-31
A.3-6	RIDGE Log-Permeability Values (m^2) at 0 m amsl for Case Without Depth-Decay of Conductivity.	A-31
A.3-7	TCL Log-Permeability Values (m^2) at 1,000 m amsl for Case Without Depth-Decay of Conductivity.	A-32
A.3-8	TCL Log-Permeability Values (m^2) at 0 m amsl for Case Without Depth-Decay of Conductivity.	A-32
A.3-9	PZUP Log-Permeability Values (m^2) at 1,000 m amsl for Case Without Depth-Decay of Conductivity.	A-33
A.3-10	PZUP Log-Permeability Values (m^2) at 0 m amsl for Case Without Depth-Decay of Conductivity.	A-33

List of Figures (Continued)

Number	Title	Page
A.3-11	SEPZ Log-Permeability Values (m^2) at 1,000 m amsl for Case Without Depth-Decay of Conductivity.	A-34
A.3-12	SEPZ Log-Permeability Values (m^2) at 0 m amsl for Case Without Depth-Decay of Conductivity.	A-34
A.3-13	DRT Log-Permeability Values (m^2) at 1,000 m amsl for Case Without Depth-Decay of Conductivity Faults	A-35
A.3-14	DRT Log-Permeability Values (m^2) at 0 m amsl for Case Without Depth-Decay of Conductivity.	A-35
A.3-15	FEHM 3-Dimensional Finite Element Mesh (from LANL).	A-36
A.3-16	Areal View of Mesh Refinement in the Vicinity of the Faults (from LANL)	A-36
A.3-17	Close-up View of Mesh Refinement Around Faults (from LANL)	A-37
A.3-18	Oblique View of Finite Element Mesh Along Faults (from LANL)	A-37
A.3-19	Vertical Section of Finite Element Mesh Along Fault (from LANL)	A-38
A.3-20	Base-Case Log-Permeability Values (m^2) at 1,000 m amsl for the Neutral Fault Case.	A-38
A.3-21	Base-Case Log-Permeability Values (m^2) at 0 m amsl for the Neutral Fault Case	A-39
A.3-22	Base-Case Log-Permeability Values (m^2) at 1,000 m amsl for Case with High-K Faults	A-39
A.3-23	Base-Case Log-Permeability Values (m^2) at 1,000 m amsl for Case with High-K Faults.	A-40
A.3-24	Water-Table Contours in m amsl and SPTR Results for Base Case With a Constant Head Boundary Condition and Neutral Faults.	A-41
A.3-25	Water-Table Contours in m amsl and SPTR Results for Base Case With a Constant Head Boundary Condition and Low-K Faults	A-42
A.3-26	Water-Table Contours in m amsl and SPTR Results for Base Case With a Constant Head Boundary Condition and High-K Faults	A-43
A.3-27	Water-Table Contours in m amsl and SPTR Results for Base Case With a Constant Head Boundary Condition, Neutral Faults and Without Depth-Decaying Conductivity	A-44
A.3-28	Flux Balances for Neutral-Fault Simulations	A-45
A.3-29	Flux Balances for Low-K Fault Simulations	A-45
A.3-30	Flux Balances for High-K Fault Simulations	A-46
A.3-31	Flux Balances for Simulations Without Depth Decay of Hydraulic Conductivity.	A-46
A.3-32	Cumulative Probabilities of Particle Travel Distances at 1,000 Years for the Neutral Fault Cases With Constant-Head Boundaries	A-47

List of Figures (Continued)

Number	Title	Page
A.3-33	Cumulative Probabilities of Particle Travel Distances at 1,000 Years for the Low-K Cases With Constant-Head Boundaries	A-48
A.3-34	Cumulative Probabilities of Particle Travel Distances at 1,000 Years for the High-K Cases With Constant-Head Boundaries	A-49
A.3-35	Cumulative Probabilities of Particle Travel Times for the Cases With No Depth Decay of Permeability and With Constant-Head Boundaries.....	A-50
A.3-36	Cumulative Probabilities of Particle Travel Distances at 1,000 Years for the Cases With Neutral Faults and Flux Boundaries	A-51
A.3-37	Cumulative Probabilities of Particle Travel Distances at 100 Years for the Cases With Neutral Faults and Flux Boundaries	A-52
A.3-38	Head Residuals for Constant-Flux Boundary Condition Simulations With Neutral Faults.....	A-53
A.3-39	Head Residuals for Constant-Flux Boundary Condition Simulations With Faults As Barriers	A-54
A.3-40	Head Residuals for Constant-Flux Boundary Condition Simulations With Faults As Conduits.....	A-55
A.3-41	Head Residuals for Constant-Flux Boundary Condition Simulations With No Depth Decay of Permeability.....	A-56
B.1-1	Location of Pahute Mesa, Yucca Mountain Site, and Relevant Caldera Complexes of the Southwestern Nevada Volcanic Field.....	B-2
B.3-1	Factors Influencing Flow and Transport Parameters in Fractured Rock	B-6
B.4-1	Maximum Excess Horizontal Stress from Yucca Mountain Boreholes (Stock and Healy, 1988) and Rainier Mesa (Carr, 1974).....	B-12
B.4-2	Trilinear Diagram Showing Relative Major Ion Percentages for Groundwater from Pahute Mesa and Yucca Mountain (IT, 2001).....	B-13
C.3-1	Well UE-18r - Injection Test 15-8 Early-Time Storage Effect.....	C-15
C.3-2	Well UE-19e - Injection Test 6-4 Late-Time Packer-Seal Failure.....	C-16
C.3-3	Well UE-20p - Injection Test 1-1 Early-Time Packer-Seal Leakage.....	C-16
C.3-4	Well UE-20p - Injection Test 1-1 Later-Time Formation Response	C-17
C.3-5	Well UE-20h - Injection Test 3-1b Questionable Test	C-18
C.3-6	Distribution of Results as Log K (ft/d).....	C-18
F.1-1	Outline of the Regional Groundwater Flow Model Grid with NTS Perimeter and Area Boundaries Along with Traces of the Major PM-OV Faults and Caldera Perimeters	F-2

List of Figures (Continued)

Number	Title	Page
F.2-1	Recharge Distribution in mm/y for UGTA Recharge Model Used in Final Calibrated Regional Flow Model	F-5
F.2-2	Original Recharge Distribution in mm/y for UGTA Recharge Model Used in Regional Flow Model	F-6
F.2-3	Recharge Distribution in mm/y for USGS Recharge Model Without Redistribution of Recharge	F-8
F.2-4	Recharge Distribution in mm/y for DRI Recharge Model with Recharge Allowed Below an Elevation of 1,237 m	F-9
F.2-5	Recharge Distribution in mm/y for DRI Recharge Model Without Recharge Allowed Below an Elevation of 1,237 m	F-10
F.4-1	Water-Table Contours in m amsl for Regional Groundwater Flow Model with BN PM-OV Geologic Model, Discontinuous LCA and Final Regional Model Recharge (Model G1aR1a)	F-16
F.4-2	Water-Table Contours in m amsl for Regional Groundwater Flow Model with BN PM-OV Geologic Model, Continuous LCA and Final Regional Model Recharge (Model G1bR1a)	F-17
F.4-3	Water-Table Contours in m amsl for Regional Groundwater Flow Model with BN PM-OV Geologic Model, Discontinuous LCA and Original Regional Model Recharge (Model G1aR1b)	F-18
F.4-4	Water-Table Contours in m amsl for Regional Groundwater Flow Model with BN PM-OV Geologic Model, Discontinuous LCA and USGS Recharge Model with no Redistribution (Model G1aR2)	F-19
F.4-5	Water-Table Contours in m amsl for Regional Groundwater Flow Model with USGS PM-OV Geologic Model, Discontinuous LCA and Final Regional Model Recharge (Model G2aR1a)	F-20
F.4-6	Water-Table Contours in m amsl for Regional Groundwater Flow Model with USGS PM-OV Geologic Model, Continuous LCA and Final Regional Model Recharge (Model G2bR1a)	F-21
F.4-7	Water-Table Contours in m amsl for Regional Groundwater Flow Model with BN PM-OV Geologic Model, Discontinuous LCA and DRI Recharge Model (Model G1aR3a)	F-22
F.4-8	Water-Table Contours in m amsl for Regional Groundwater Flow Model with BN PM-OV Geologic Model, Discontinuous LCA and DRI Recharge Model Without Recharge Below 1,237 m (Model G1aR3b)	F-23

List of Plates

<i>Number</i>	<i>Title</i>
1	Hydrostratigraphic Units for the Pahute Mesa - Oasis Valley Area
2	Southwest to Northeast Hydrostratigraphic Cross Section J-J' through the Pahute Mesa - Oasis Valley Area
3	West to East Hydrostratigraphic Cross Section C-C' through the Pahute Mesa - Oasis Valley Area

List of Tables

Number	Title	Page
2-1	Hydrogeologic Units of the NTS Regional Model in the PM-OV Model Area.....	2-3
2-2	Hydrostratigraphic Units of the Pahute Mesa-Oasis Valley Area Included in the NTS Regional Hydrostratigraphic Framework Model	2-6
2-3	Ranges of Hydraulic Conductivity for the Major Aquifers of the Nevada Test Site Region.	2-7
2-4	Estimated Steady-State Groundwater Budget for the Nevada Test Site Regional Groundwater Flow System	2-9
2-5	Additional and Modified Hydrogeologic Units of the PM-OV Model	2-14
2-6	Correlation of Hydrostratigraphic Units of the Pahute Mesa-Oasis Valley Model and Earlier Models	2-16
2-7	Correlation of Hydrostratigraphic Units Between the Silent Canyon Caldera Complex Model and the Base HSU Model	2-20
5-1	Statistics of Laboratory-Scale Hydraulic Conductivity Data	5-10
5-2	Statistics of Slug Test Scale Hydraulic Conductivity Data	5-19
5-3	Statistics of Constant-Rate Scale Hydraulic Conductivity Data as Compared to Statistics of Slug-test and Laboratory Scale Data.	5-26
5-4	Hydraulic Conductivity Distributions of Hydrostratigraphic Units of the Pahute Mesa-Oasis Valley Hydrostratigraphic Framework Model	5-31
6-1	Precipitation Station Data	6-6
6-2	Comparison of Precipitation Volumes to Published Values by Hydrographic Area	6-9
6-3	INFILv3 Input Parameters (Directly from Hevesi et al., 2003)	6-21
6-4	Multiplication Factors for Hydrographic Areas Outside of DRI Study Area.....	6-35
6-5	Recharge Volumes for Hydrographic Areas for all Recharge Models.....	6-39
7-1	Description of Springs Occurring in Oasis Valley	7-8
7-2	Evapotranspiration (ET) Units Determined from Spectral Analysis of Satellite Imagery Data, Oasis Valley Discharge Area, Nevada, June 13, 1992	7-12
7-3	Evapotranspiration Rates Used to Compute Annual Evapotranspiration from Oasis Valley Discharge Area, Nevada	7-15
7-4	Ranges of Evapotranspiration Rates for ET Units Classified In Major Discharge Areas of Death Valley Regional Flow System, Nevada and California	7-16
7-5	Estimated Mean Annual Evapotranspiration and Groundwater Evapotranspiration by Evapotranspiration Unit from Oasis Valley Discharge Area, Nevada	7-17
7-6	Simulated Mean Annual Evapotranspiration from Oasis Valley (Data are simulated means of 1,000 realizations).....	7-20
7-7	Parameters Having the Greatest Effect on Simulated Annual ET Measured by Rank Correlation	7-21

List of Tables (Continued)

Number	Title	Page
7-8	Summary Statistics of Simulated Annual ET from 1,000 Monte Carlo Realizations for the Oasis Valley Discharge Area	7-22
8-1	Temperature Effects on Water Elevation	8-6
9-1	Regional-Scale Model Descriptions	9-3
9-2	Regional Model Groundwater Inflows at CAU-Scale Model Boundaries (m ³ /d)	9-4
9-3	Regional Model Groundwater Outflows at CAU-Scale Model Boundaries (m ³ /d)	9-5
9-4	Total Water Balance for the PM-OV Model Area	9-5
9-5	Summary of Net Boundary Flux Ranges (m ³ /d)	9-7
10-1	Geographic Distribution of Groundwater Sample Locations and Measured Analytical Parameter Groups in the Pahute Mesa Region	10-4
10-2	Statistical Summary of Representative Conservative Tracer Data	10-21
10-3	Description of Plausible Groundwater Flow Paths in the Pahute Mesa-Oasis Valley Flow System (Rose et al., 2002)	10-23
10-4	Summary of Geochemical Flow Path Model Results for the Pahute Mesa-Oasis Valley Flow System from Rose et al., 2002	10-27
A.1-1	Hydrostratigraphic Units of the Pahute Mesa-Oasis Valley Hydrostratigraphic Framework Model	A-2
A.1-2	Hydrogeologic Units of the UGTA Regional Model in the PM-OV Model Area	A-8
A.1-3	Additional and Modified Hydrogeologic Units of the PM-OV Model	A-8
A.2-1	Abridged List of Alternative Scenarios for the Pahute Mesa-Oasis Valley 3-D Hydrostratigraphic Model	A-10
A.3-1	HSU Classification	A-22
A.3-2	Nodal Elevations	A-24
C.2-1	Storage Parameter Constraints	C-4
C.2-2	Summary of Aquifer Test Data Reanalysis Results	C-8
D.2-1	Pumping Well Information	D-1
D.2-2	Historical Groundwater Discharge Volumes and Rates	D-2
E.1-1	Site Information for Selected Wells, Boreholes, and Springs Located in the Pahute Mesa-Oasis Valley Area and Vicinity	E-2
E.1-2	Summary of Hydraulic Heads at Selected Sites within the Pahute Mesa-Oasis Valley Area and Vicinity	E-9
F.2-1	Recharge Models Flux Rates in m ³ /d	F-11
F.2-2	Simulation Names and Associated Hydrostratigraphic and Recharge Models	F-11
F.3-1	Calibration Criteria for Weighted Hydraulic-Head Residuals by Zone (IT, 1996)	F-13

List of Tables (Continued)

Number	Title	Page
F.3-2	Calculation of Criteria for Model-Area Discharge (brackets denote inflow)	F-13
F.4-1	Root Mean Square of Weighted Residuals Values for Individual Residual Zones and Combined Zones in Meters	F-15
F.4-2	Simulation Discharge Rates in m ³ /d at Discharge Calibration Zones	F-15
F.4-3	Regional Model Groundwater Inflows at CAU-Scale Model Boundaries in m ³ /d	F-24
F.4-4	Regional Model Groundwater Outflows at CAU-Scale Model Boundaries in m ³ /d	F-24

Acknowledgement

We thank the many individuals who assisted us in creating this report. In particular, we acknowledge Sig Drellack of Bechtel Nevada for his technical assistance throughout the process; and Merrie Martin, Lisa May, David Rojas, and Sharon Hicks for their assistance in creating the maps and drawings. We greatly appreciate the efforts of Matt Klainer and Carrye Putz for their editing support, and those of Yvonne Lewis and Shirley Murray who were instrumental in preparing this document for publication. We also thank the following individuals for their contributions: Debby Eckardt, Afief Fadil, Pat Fritz, Barbara Ground, Carol Lovelace, Steve Mergenmeier, Toni Miller, Donna Raha, Janice Rose, June Simms, and Jeanne Wightman.

List of Acronyms and Abbreviations

AA	Alluvial Aquifer
ac-ft/yr	Acre-feet per year
amsl	Above mean sea level
ASTM	American Society for Testing and Materials
BA	Benham Aquifer
BAQ	Basal Aquifer
BCU	Basal Confining Unit
BFCU	Bullfrog confining unit
bgs	Below ground surface
BN	Bechtel Nevada
BRA	Belted Range Aquifer
BRD	Biological Resources Division
BRT	Belted thrust range
BWSD	Beatty Water and Sanitation District
C	Carbon
Ca	Calcium
CA	Carbonate Aquifer
CADD	Corrective Action Decision Document
CAI	Corrective Action Investigation
CAIP	Corrective Action Investigation Plan
CAP	Corrective Action Plan
CAS	Corrective Action Site
CAU	Corrective Action Unit
CCU	Clastic Confining Unit
cdf	Cumulative density function
CDR	Common Data Repository
CD-ROM	Compact disk-read only memory
CFCM	Crater Flat Composite Unit
CFCU	Crater Flat Confining Unit
cf	Cumulative frequency distribution
CHZCM	Calico Hills Zeolitized Composite Unit
Cl	Chlorine

List of Acronyms and Abbreviations (Continued)

cm	Centimeters
cm/yr	Centimeters per year
CO ₂	Carbon dioxide
CO ₃	Carbonate
CR	Closure Report
CV	Coefficient of variability
D	Deuterium
DDE_F	Data documentation evaluation flags
DEM	Digital Elevation Model
DGV	Dense to moderately dense grassland
DIC	Dissolved inorganic carbon
DOC	Dissolved organic carbon
DoD	U.S. Department of Defense
DOE	U.S. Department Energy
DQO	Data Quality Objective
DQE_F	Data quality evaluation flags
DRI	Desert Research Institute
DRT	Deeply Rooted Belted Range Thrust Fault
DVA	Detached Volcanic Aquifer
DVCM	Detached Volcanic Composite Unit
EOI	Effective open interval
EPA	U.S. Environmental Protection Agency
ERP	Environmental Restoration Program
ET	Evapotranspiration
FCA	Fortymile Canyon Aquifer
FCCM	Fortymile Canyon Composite Unit
FEHM	Finite-element heat mass transfer code
FFACO	<i>Federal Facility Agreement and Consent Order</i>
ft/d	Foot (feet) per day
ft	Foot (feet)
gal/min	Gallon per minute
GAP	Gap Analysis Program
GCU	Granite Confining Unit

List of Acronyms and Abbreviations (Continued)

GMWL	Global Meteoric Water Line
gpm	Gallon per minute
H	Hydrogen
HA	Hydrographic Area
^3H	Tritium
HCO_3	Bicarbonate
HGU	Hydrogeologic unit
HSU	Hydrostratigraphic Unit
IA	Inlet Aquifer
ICU	Intrusive Confining Unit
ID	Identification number
IICU	Intra-Caldera Intrusive Confining Unit
in.	Inch
in./yr	Inches per year
K	Hydraulic Conductivity
km	Kilometer
km^2	Square kilometer
K^+	Potassium ion
K-S	Kolmogrov-Smirnov
LaGriT	Los Alamos Grid Toolbox
LANL	Los Alamos National Laboratory
LCA	Lower Carbonate Aquifer
LCCU	Lower Carbonate Confining Unit
LFA	Lava flow aquifer
LLNL	Lawrence Livermore National Laboratory
LMWL	Local meteoric water line
m	Meter
m/d	Meter per day
ME	Maxey-Eakin
m^3	Cubic meter
m^3/d	Cubic meters per day
m^3/yr	Cubic meters per year
Mg	Magnesium

List of Acronyms and Abbreviations (Continued)

mg/L	Milligram per liter
Mg/m ³	Megagram per cubic meter
mil	Parts per thousand
min	Minutes
mmoles	Millimoles
Na	Sodium
NDEP	Nevada Division of Environmental Protection
NNSA/NSO	U.S. Department of Energy, National Nuclear Security Administration Nevada Site Office
NTS	Nevada Test Site
NWIS	National Water Information System
O	Oxygen
PBRCM	Pre-Belted Range Composite Unit
pCi/L	Picocurie per liter
PCM	Paintbrush Composite Unit
PEST	Parameter Estimation
PM-CAUs	Central and Western Pahute Mesa Corrective Action Units
PM-OV	Pahute Mesa-Oasis Valley
pmc	Percent modern carbon
Pre-T	Pre-Tertiary
PRISM	Parameter-Elevation Regressions on Independent Slopes Model
PZUP	Raised Pre-Tertiary Surface
QA	Quality assurance
QAPP	Quality assurance project plan
QC	Quality Control
RIDGE	Basement Ridge
R _w	Well radius
S	Storage coefficient
SCCC	Silent Canyon Caldera Complex
SE	Standard error
SEPZ	Contiguous imbricate thrust sheet
Sf	Fracture skin factor
SGV	Moderately dense grassland
S _h	Principle stress

List of Acronyms and Abbreviations (Continued)

Shaw	Shaw Environmental, Inc.
SO ₄	Sulfate
SPTR	Streamline Particle Tracking
S _s	Fracture storativity
S _s '	Matrix storativity
STATSGO	State-computed geostatistical database for soil properties
SVOC	Semivolatile organic compounds
Sw	Well skin factor
SWNVF	Southwestern Nevada Volcanic Field
T	Transmissivity
TC	Tuff cone
TCA	Tivia Canyon Aquifer
TCL	Thirsty Canyon Lineament
TCU	Tuff Confining Unit
TDS	Total dissolved solids
TIN	Triangulated Irregular Network
TM	Thermatic Mapper
TMAQ	Timber Mountain Aquifer
TMCC	Timber Mountain Caldera Complex
TMCM	Timber Mountain Composite Unit
TSA	Topopah Springs Aquifer
TWG	Technical Working Group
UCA	Upper Carbonate Aquifer
UCCU	Upper Clastic Confining Unit
UGTA	Underground Test Area
USGS	U.S. Geological Survey
VA	Volcanic Aquifer
VCU	Volcanic Confining Unit
VOC	Volatile organic compounds
VOIA	Value of Information Analysis
VSMOW	Vienna Standard Mean Ocean Water
VTA	Vitric Tuff Aquifer
VU	Volcanics undifferentiated

List of Acronyms and Abbreviations (Continued)

WESTVEG	Western region vegetation map
WPM-OV	Western Pahute Mesa-Oasis Valley
WTA	Welded Tuff Aquifer
YMP	Yucca Mountain Project
°C	Degree Celsius
°F	Degree Fahrenheit
3-D	Three dimensional
δ	Delta
δ ¹⁴ C	Delta carbon-14
δ ¹⁸ O	Delta oxygen-18

1.0 Introduction

This report documents the analysis of the available hydrologic data conducted in support of the development of a Corrective Action Unit (CAU) groundwater flow model for Central and Western Pahute Mesa: CAUs 101 and 102. Central and Western Pahute Mesa constitute two areas of the Nevada Test Site (NTS) used for underground nuclear testing (Figure 1-1). These nuclear tests resulted in groundwater contamination in the vicinity of the underground test areas. As a result, the U.S. Department of Energy (DOE), National Nuclear Security Administration Nevada Site Office (NNSA/NSO) is currently conducting a corrective action investigation of the Pahute Mesa underground test areas. The CAU groundwater flow model is a component of the CAU model, a major part of the Underground Test Area (UGTA) strategy (FFACO, 1996). A brief summary of the project background is provided, followed by a presentation of the purpose and scope of the work described in this document. Brief descriptions of the CAU model's documentation and this document's contents are provided at the end of this section.

1.1 Background

A brief overview of the project and site background are presented in this section.

1.1.1 Project Background

Between 1951 and 1992, the DOE and the U.S. Department of Defense (DoD) conducted underground nuclear testing at the NTS. To ensure protection of the public and the environment, the NNSA/NSO established a long-term program to monitor groundwater for the presence of radionuclides, and the UGTA Project to investigate and remediate the underground test areas. The UGTA Project is a component of NNSA/NSO's Environmental Restoration Program (ERP).

The UGTA Project activities are conducted under the direction of the NNSA/NSO UGTA Project Manager. A Technical Working Group (TWG) was formed to serve as a technical advisory group and assist the NNSA/NSO UGTA Project Manager with technical management issues. The TWG consists of representatives from the participating organizations which include: Bechtel Nevada (BN), Desert Research Institute (DRI), Shaw Environmental, Inc. (Shaw), Lawrence Livermore National Laboratory (LLNL), Los Alamos National Laboratory (LANL), and the U.S. Geological Survey (USGS). Tasks assigned to the TWG committee include providing technical recommendations to NNSA/NSO, providing expert technical

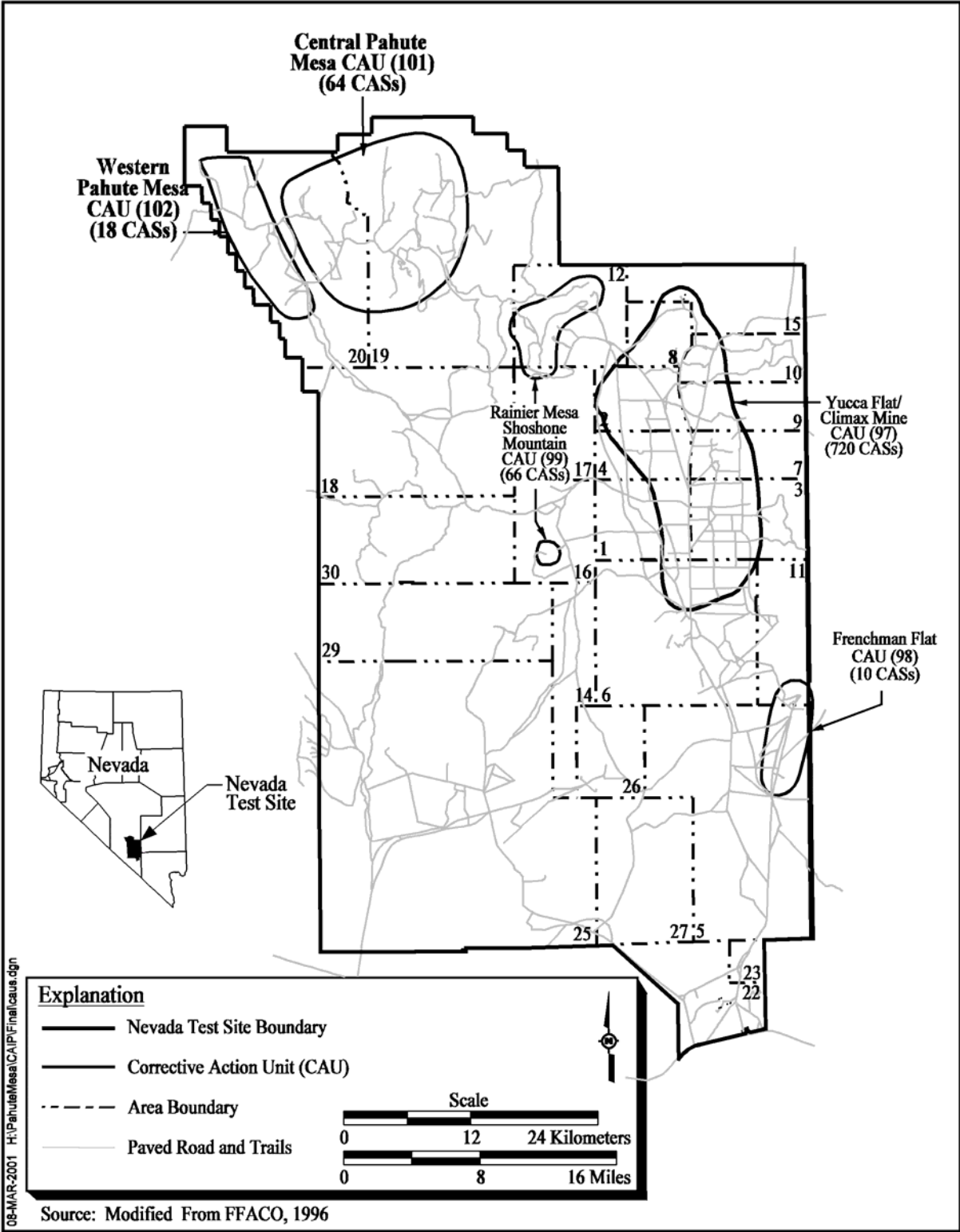


Figure 1-1
Location of the Pahute Mesa Corrective Action Units

support in specific UGTA tasks via subcommittees, and serving as internal peer reviewers of UGTA products.

Since 1996, the Nevada Division of Environmental Protection (NDEP) has regulated NNSA/NSO's corrective actions through the *Federal Facility Agreement and Consent Order* (FFACO) (1996). The individual locations covered by the agreement are known as Corrective Action Sites (CASs), and they are grouped into Corrective Action Units. The UGTA CAUs are Frenchman Flat, Central Pahute Mesa, Western Pahute Mesa, Yucca Flat, and the Rainier Mesa/Shoshone Mountain CAUs (Figure 1-1). Central Pahute Mesa (CAU 101) and Western Pahute Mesa (CAU 102) are addressed together due to their adjacent locations and common groundwater regime as well as similarities in testing practices, geology, and hydrology.

Appendix VI of the FFACO, "*The Corrective Action Strategy*," describes the processes that will be used to complete corrective actions, including those in the UGTA Project. The UGTA corrective action strategy, described in Section 3.0 of Appendix VI of the FFACO (1996), was revised in 2000. The UGTA strategy was modified following completion of the DOE review of the Frenchman Flat CAU model. The UGTA strategy was modified following completion of the DOE review of the Frenchman Flat CAU model (IT, 1999). Any subsequent references to the FFACO or its appendices in this document will be made to the FFACO as a whole (i.e., FFACO, 1996).

The UGTA corrective action strategy consists of two major phases: a regional evaluation of all the UGTA CAUs and a corrective action process for each of the CAUs. The CAU-specific corrective action process includes six major components: Corrective Action Investigation Plan (CAIP), Corrective Action Investigation (CAI), Corrective Action Decision Document (CADD), Corrective Action Plan (CAP), Closure Report (CR), and long-term monitoring.

- The regional evaluation resulted in a regional groundwater flow and contaminant transport model encompassing the NTS and the groundwater flow systems extending to downgradient discharge areas. The NTS regional model is designed to support the entire UGTA program and is developed prior to any CAU-specific activities.
- The CAI planning is documented in the CAIP, an FFACO-required document which provides or references all specific information for planning investigation activities associated with corrective action units or sites.
- The corrective action investigation includes the collection of new data, the evaluation of new and existing data, and the development and use of CAU-specific groundwater flow and transport model(s).
- The CADD is a required report that documents the corrective action investigation. It describes the results of the CAI, the corrective action alternatives considered, the results of their comparative evaluation, the selected corrective action, and the rationale for its selection.

- The CAP is prepared to describe how the selected remedial alternative is to be implemented. The CAP will contain the engineering design and all necessary specifications necessary to implement the selected remedial alternative.
- The UGTA strategy has provisions for CAU closure only if the long-term-monitoring alternative is selected. Closure activities include the preparation of a Closure Report, a review of the CR by NDEP, and long-term closure monitoring by DOE.
- The long-term, post-closure monitoring is designed to ensure the compliance boundary is not violated.

Details on the UGTA corrective action strategy, including the decision process, may be found in Section 3.0 of Appendix VI of the FFACO (1996).

1.1.2 Pahute Mesa Background

Brief overviews of the operational history and work conducted to date are presented in this section.

Pahute Mesa was used as an underground nuclear testing area of the NTS for 27 years. Nuclear testing on Pahute Mesa began with Operation Whetstone in 1965 and ended with Operation Julin in 1992 (DOE/NV, 2000b). Nuclear tests conducted at Pahute Mesa that are of interest to the UGTA Project are those detonated in deep vertical shafts, drilled into volcanic rock near or below the water table. A total of 82 such underground nuclear tests were conducted in Pahute Mesa. Sixty-four of these tests were detonated on Central Pahute Mesa (CAU 101), and 18 tests were detonated in Western Pahute Mesa (CAU 102) (DOE/NV, 1999). Media contaminated by the underground nuclear tests on Pahute Mesa are geologic formations within the unsaturated and saturated zones. Transport in groundwater is the primary mechanism of migration for the subsurface contamination away from the Pahute Mesa underground nuclear tests.

The following is a summary of the activities completed prior to the time of preparation of this document:

- The NTS regional model (IT, 1996 a through f; 1997 a and b; DOE/NV, 1997) was completed prior to the initiation of CAU-specific activities. It was used during the planning and execution of the Pahute Mesa CAI.
- The CAI planning step included the preparation of CAU-specific Data Quality Objectives (DQOs) and the preparation of the CAIP. A Value of Information Analysis (VOIA) (IT, 1998d) using the NTS regional model (DOE/NV, 1997) was conducted to help identify data-collection activities in support of the DQO process. This step is documented in the CAIP (DOE/NV, 1999).

- New data have been collected and added to the data sets. Eight wells have been installed and tested (IT, 2002a through h and j). A tracer test was conducted (IT, 1998a). Major steps of the data analysis process completed at this point include the assessment of geologic data which resulted in the construction of a CAU-specific Hydrostratigraphic Unit (HSU) model (BN, 2002). A summary of the Pahute Mesa HSU model is presented in [Section 2.0](#) of this document.

1.2 Task Purpose and Scope

The purpose and scope of the analysis of hydrologic data for the Pahute Mesa CAUs are presented.

1.2.1 Purpose

The purpose of the tasks documented in this report was to analyze relevant information available for the hydrologic components of the groundwater flow system of Pahute Mesa and vicinity. The information will be used to develop the Pahute Mesa CAU model(s).

Specific task objectives were as follows:

- Compile available hydrologic data and supporting information that may be relevant to the Pahute Mesa corrective action investigation.
- Assess the level of quality of the data and associated documentation.
- Analyze the data to derive expected values or spatial distributions, and estimates of the associated uncertainty and variability.

1.2.2 Scope of Work

The scope of this task includes the assessment of data and information relevant to groundwater flow in the Pahute Mesa subsurface. Hydrologic data described in the NTS regional model documentation (IT, 1996a, b, and c) and the Pahute Mesa CAIP (DOE/NV, 1999) are supplemented with existing data that were not previously used and newly-acquired data.

Data types of interest include hydraulic properties, precipitation recharge, natural surface discharge, well discharge, hydraulic heads, and groundwater chemistry. Descriptions of these data types are provided in [Section 4.0](#).

Data analysis includes: (1) literature searches, (2) data/information compilation, (3) data documentation, (4) data documentation qualification, (5) data quality evaluation, (6), and data assessment and interpretation activities. Data analysis

includes the use of scientific software to assist in estimating and visualizing each of the hydrologic data types.

The area of investigation, as described in the CAIP (Figure 1-2), was selected to encompass the Pahute Mesa CAUs and areas located downgradient that may be impacted by these CAUs. This area includes the Pahute Mesa-Oasis Valley (PM-OV) area and a portion of the Amargosa Desert located downgradient of the Pahute Mesa CAUs. The area of interest to the modeling activities is limited to the PM-OV area (Figure 1-2) as the maximum extent of contamination is expected to remain within this area. This area of over 2,700 square kilometers (km²) encompasses the northwestern portion of the NTS and adjacent lands to the west managed by the U.S. Air Force and the Bureau of Land Management. The PM-OV area includes Timber Mountain, Black Mountain, most of Oasis Valley, and the northern parts of Yucca Mountain and Fortymile Canyon. The groundwater flow model area is a sub-area of the PM-OV area that is practically the same as the PM-OV area (Figure 1-2).

Even though the area of interest is limited to the PM-OV area, information considered to be relevant to this task may be obtained from other nearby sites. Nearby sites include other underground test areas, the Yucca Mountain Site, and other sites located within the NTS region. The justification for the transfer of data from other sites was documented.

1.3 Quality Assurance

Quality assurance measures consistent with the UGTA Project quality assurance (QA) plan (DOE/NV, 2000a) have been taken to control quality during the performance of all UGTA data analysis tasks. These measures include data documentation qualification, data quality assessment, checking procedures, software quality assurance, use of standard methodologies, technical and peer reviews, and corroboration through models.

Data Documentation Evaluation

Each data record will be assigned a data documentation evaluation flag (DDE_F) designed to indicate the level of documentation available for that data record. The five levels of data documentation evaluation flags are described in Section 4.0.

Data Quality Assessment

The criteria used to assess the quality of the different types of required data are dependent on the type and the intended use of the data. The general procedure includes assigning one or more flags to each record compiled in the dataset, indicating the data quality or suitability of the individual data record for the intended usage. Data-type specific quality evaluation procedures are described in detail in the corresponding section of this document.

Checking Procedures

Various checking procedures were designed for quality control purposes. Checking procedures applicable to the UGTA data analysis include those

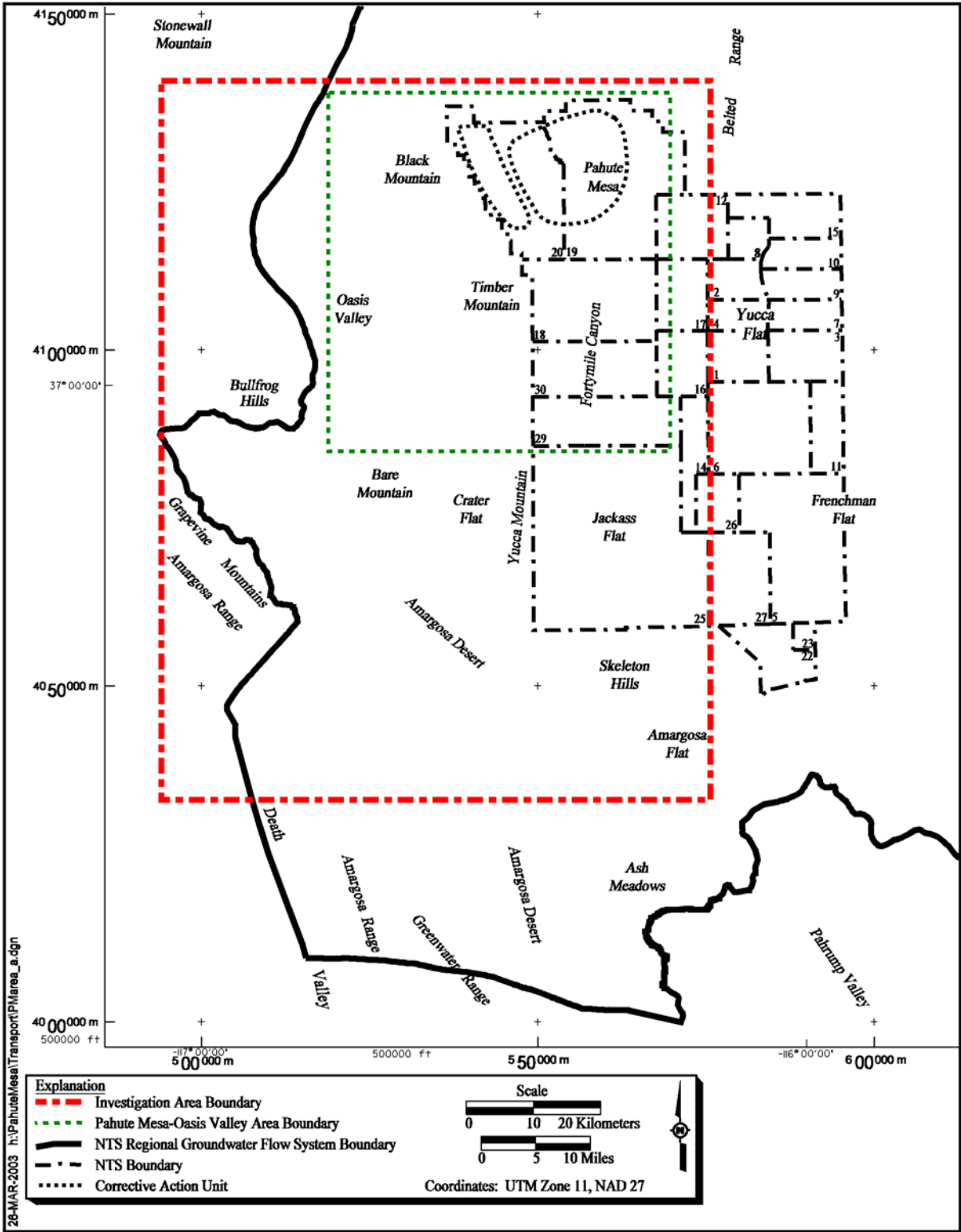


Figure 1-2
Investigation and Pahute Mesa-Oasis Valley Areas for the
Pahute Mesa Corrective Action Units (DOE/NV, 1999)

developed for transcription of data, generation of figures, tables and logs, and performance of calculations. Data compiled by project personnel are subjected to the checking procedures before inclusion in the appropriate dataset. However, the bulk of the available data is comprised of data gathered and compiled by agencies external to the UGTA project. Internal procedures do not govern other UGTA participants; therefore, their data were not subjected to the checking procedures described here.

Standard Methodologies

Only standard and widely accepted methodologies should be used in the development of the interpretive products. The various methodologies used are too numerous to list here; however, they are described and referenced in the sections of this document which discuss their use in the data analysis process.

Technical and Peer Reviews

The review process constitutes an important measure of product quality, and is used throughout the performance of the data analysis activities. The review process may include internal and external technical reviews. The internal reviews are performed by individuals who are independent of the UGTA project. These reviews may include representatives of BN, USGS, DRI, LANL, LLNL, GeoTrans, and Shaw. External reviews may be conducted as directed by NNSA/NSO.

Corroboration of Data Through Models

This step is completed during the development of the groundwater flow and transport model. For example, during the groundwater flow model calibration process, geologic and hydrologic data interpretations are tested and modified as required. This may be accomplished by modifying the extent or thickness of a given HSU or modifying its hydraulic conductivity in areas where no data are available.

1.4 CAU Model Documentation

The Pahute Mesa CAU model is documented in a series of reports describing the data analysis and modeling tasks. The CAU model documentation is as follows:

- *Hydrostratigraphic Model for the Groundwater Flow and Contaminant Transport Model of Corrective Action Units 101 and 102: Central and Western Pahute Mesa, Nye County, Nevada* - This volume describes the evaluation of geologic data and the resulting hydrostratigraphic model (BN, 2002).
- *Hydrologic Data for the Groundwater Flow and Contaminant Transport Model of Corrective Action Units 101 and 102: Central and Western Pahute Mesa, Nye County, Nevada* - This volume describes the assessment of hydrologic data in support of the CAU groundwater flow model.

- *Contaminant Transport Parameters for the Groundwater Flow and Contaminant Transport Model of Corrective Action Units 101 and 102: Central and Western Pahute Mesa, Nye County, Nevada* - This volume describes the assessment of contaminant transport parameter data in support of the CAU radionuclide transport model (Rehfeldt et al., 2003).
- The analysis of data available on the radioactive contaminant sources and extent in support of the CAU radionuclide transport model will be document in a separate report. The report will focus on the unclassified hydrologic source term and radionuclide data only. The classified hydrologic source term will be handled in a separate classified report.
- *Groundwater Flow Model of Corrective Action Units 101 and 102: Central and Western Pahute Mesa, Nye County, Nevada* - This volume describes the results of the groundwater flow modeling activities.
- *Radionuclide Transport Model of Corrective Action Units 101 and 102: Central and Western Pahute Mesa, Nye County, Nevada* - This volume describes the results of the contaminant transport modeling activities.
- *Groundwater Flow and Contaminant Transport Model of Corrective Action Units 101 and 102: Central and Western Pahute Mesa, Nye County, Nevada* - This document includes a summary of the information presented in the six documents listed above.

1.5 Document Organization

This document consists of 11 sections and 7 appendices. Summaries of the section contents follow:

- [Section 1.0](#) provides a description of the project background, the purpose and scope of this data analysis task, QA and quality control (QC) considerations, and a description of the documentation of the CAU model.
- [Section 2.0](#) describes the regional setting and local hydrostratigraphic framework of the PM-OV area. These descriptions are presented to support the analysis of the hydrologic data presented in this document.
- [Section 3.0](#) provides a brief overview of the modeling strategy proposed for the Pahute Mesa CAUs and a more detailed description of the approach used to simulate groundwater flow.
- [Section 4.0](#) presents the approach used to assess the available hydrologic data.
- [Section 5.0](#) describes the compilation and analysis of aquifer property data.

- [Section 6.0](#) describes the compilation and analysis of the available precipitation recharge data.
- [Section 7.0](#) describes the compilation and analysis of the available surface discharge data.
- [Section 8.0](#) describes the compilation and analysis of water level data to derive hydraulic heads.
- [Section 9.0](#) describes the estimation (calculation) of the subsurface boundary fluxes using the NTS regional model.
- [Section 10.0](#) describes the compilation and analysis of groundwater chemistry data.
- [Section 11.0](#) provides a list of references used in the document.
- [Appendix A](#) contains information in support of the hydrostratigraphic model described in [Section 2.0](#).
- [Appendix B](#) contains a justification of the use of Yucca Mountain site characterization data for developing parameter distributions for the Pahute Mesa modeling effort.
- [Appendices C through F](#) contain descriptions of the dataset and supporting information for each of the hydrologic data types considered.
- [Appendix G](#) provides supplemental information including a gallery of visualizations of the PM-OV HSU model.

2.0 Regional Setting and Local Hydrostratigraphic Framework

Selected components of the Pahute Mesa flow system conceptual model are summarized in this section to support the hydrologic data assessment presented in this report. Components described include the regional setting and local hydrostratigraphic framework.

2.1 Regional Setting

The PM-OV flow system is part of the NTS regional flow system ([Figure 2-1](#)), which is part of the Death Valley flow system. A conceptual model of the regional groundwater flow system of the NTS was developed during the regional evaluation (DOE/NV, 1997). Summary descriptions of the NTS regional hydrogeologic framework and groundwater occurrence and movement, as conceptualized in the NTS regional flow model (DOE/NV, 1997), are presented in this section. Information has been updated in some instances.

2.1.1 Regional Hydrogeologic Framework

The hydrogeologic framework used in the NTS regional model is based on the conceptual hydrologic system established for the NTS area by Winograd and Thordarson (1975) and Blankennagel and Weir (1973). This early work was summarized and updated by Laczniaik et al. (1996), and has further been developed by the UGTA Phase I hydrostratigraphic regional modeling team (IT, 1996d).

The rocks of the NTS have been classified using a two-level classification scheme, in which hydrogeologic units (HGUs) are grouped to form HSUs (IT, 1996d). The HGUs are used to categorize rocks according to their ability to transmit groundwater, which is mainly a function of the rocks' primary lithologic properties, degree of fracturing, and secondary mineral alteration. The complex hydrologic properties of the volcanic rocks of the NTS and vicinity are best addressed in terms of HGUs (Blankennagel and Weir, 1973; Winograd and Thordarson, 1975). The concept of HSUs that are made up of groups of similar HGUs is also very useful in volcanic terrains because stratigraphic units can differ greatly in hydrologic character both laterally and vertically. The HSUs serve as "layers" in the NTS regional and CAU-scale hydrostratigraphic framework models.

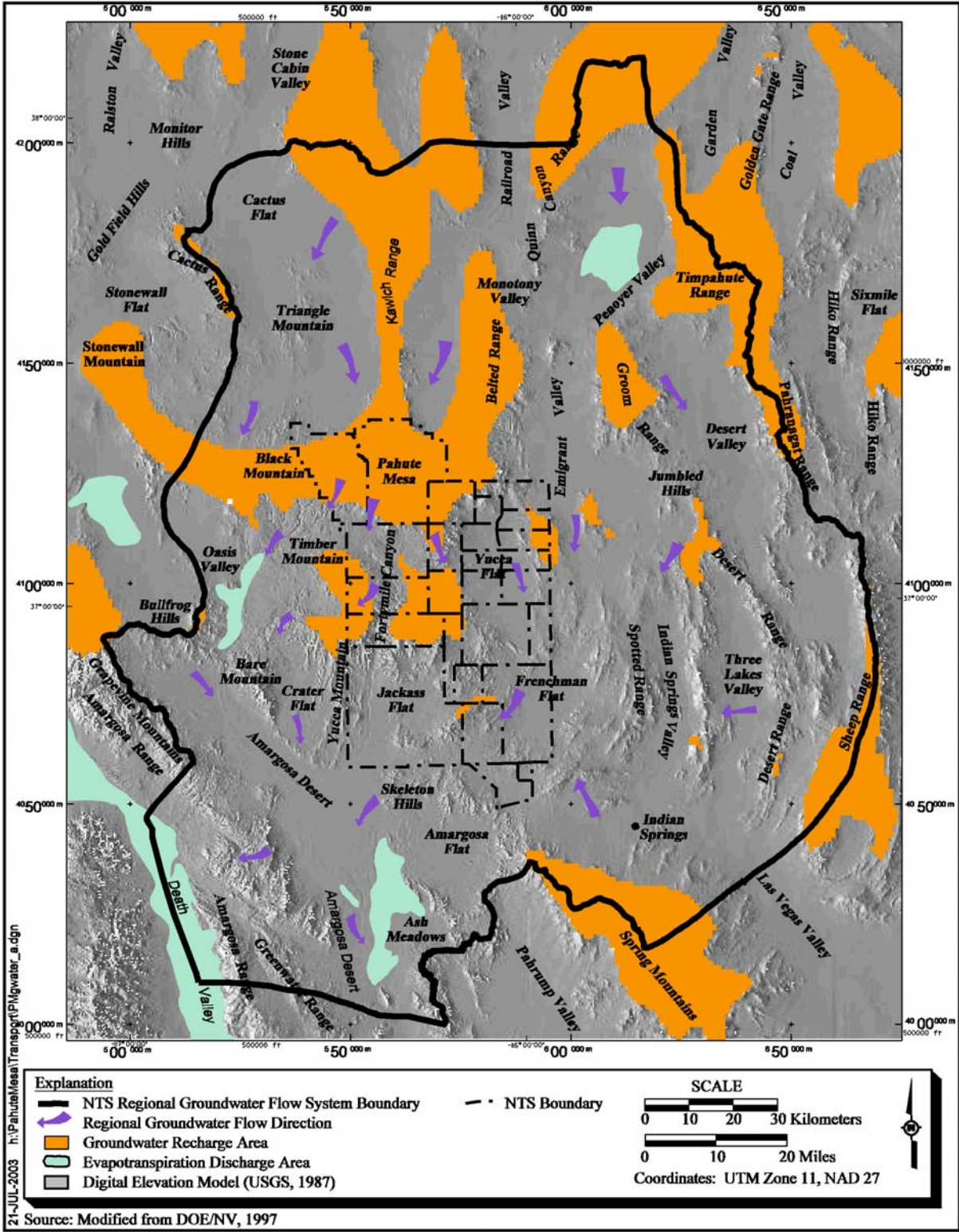


Figure 2-1
Features of the Nevada Test Site Regional Groundwater Flow System

The following paragraphs summarize the hydrogeologic framework of the NTS, first addressing HGUs, then describing HSUs.

2.1.1.1 Hydrogeologic Units

All rocks of the NTS and vicinity can be classified as one of eight hydrogeologic units, which include the alluvial aquifer, four volcanic HGUs, an intrusive HGU, and two HGUs that represent the pre-Tertiary sedimentary and metasedimentary rocks (Table 2-1).

Alluvium

The deposits of alluvium (alluvial aquifer) fill the main basins of the NTS, and generally consist of a loosely consolidated mixture of boulders, gravel, sand, silt, and clay derived from volcanic and Paleozoic sedimentary rocks (Slate et al., 1999).

Table 2-1
Hydrogeologic Units of the NTS Regional Model in the PM-OV Model Area

Hydrogeologic Unit	Typical Lithologies	Hydrologic Significance
Alluvial aquifer (AA) (AA is also an HSU in hydrogeologic models.)	Unconsolidated to partially consolidated gravelly sand, aeolian sand, and colluvium; thin, basalt flows of limited extent	Has characteristics of a highly conductive aquifer, but less so where lenses of clay-rich paleocolluvium or playa deposits are present
Welded-tuff aquifer (WTA)	Welded ash-flow tuff; vitric to devitrified	Degree of welding greatly affects interstitial porosity (less porosity as degree of welding increases) and permeability (greater fracture permeability as degree of welding increases)
Vitric-tuff aquifer (VTA)	Bedded tuff; ash-fall and reworked tuff; vitric	Constitutes a volumetrically minor HGU; generally does not extend far below the static water level due to tendency of tuffs to become zeolitic (which drastically reduces permeability) under saturated conditions; significant interstitial porosity (20 to 40 percent); generally insignificant fracture permeability
Lava-flow aquifer (LFA)	Rhyolite lava flows; includes flow breccias (commonly at base) and pumiceous zones (commonly at top)	Generally a caldera-filling unit; hydrologically complex, wide range of transmissivities, fracture density and interstitial porosity differ with lithologic variations
Tuff confining unit (TCU)	Zeolitic bedded tuff with interbedded, but less significant, zeolitic, nonwelded to partially welded ash-flow tuff	May be saturated but measured transmissivities are very low; may cause accumulation of perched and/or semi-perched water in overlying units
Intrusive confining unit (ICU)	Granodiorite, quartz monzonite	Relatively impermeable; forms local bulbous stocks, north of Rainier Mesa, Yucca Flat, and scattered elsewhere in the NTS regional model area; may contain perched water
Clastic confining unit (CCU)	Argillite, siltstone, quartzite	Clay-rich rocks are relatively impermeable; more siliceous rocks are fractured, but with fracture porosity generally sealed due to secondary mineralization
Carbonate aquifer (CA)	Dolomite, limestone	Transmissivity values vary greatly and are directly dependent on fracture frequency

Source: Adapted from IT (1996d) and BN (2002)

Volcanic HGUs

The volcanic rocks within the study area can be categorized into four HGUs based on primary lithologic properties, degree of fracturing, and secondary mineral alteration. In general, the altered volcanic rocks (typically zeolitic, or hydrothermally altered near caldera margins) act as confining units, and the unaltered rocks form aquifers. The aquifer units can be further divided into welded-tuff and vitric-tuff aquifers (depending on degree of welding) and lava-flow aquifers. Denser rocks, such as welded ash-flow tuffs and lava flows, tend to fracture more readily; therefore, they have relatively high permeability (Blankennagel and Weir, 1973; Winograd and Thordarson, 1975; Laczniaik et al., 1996; IT, 1996d; Prothro and Drellack, 1997).

Pre-Tertiary HGUs

The pre-Tertiary rocks beneath the study area are also categorized as aquifer or confining unit HGUs based on lithology. The silicic clastic rocks (quartzites, siltstones, shales) typically are aquitards or confining units, while the carbonates (limestone and dolomite) tend to be aquifers (Winograd and Thordarson, 1975; Laczniaik et al., 1996).

Intrusives

The intrusive confining unit (ICU) category includes the Mesozoic granite stocks north of Rainier Mesa and Yucca Flat and several intrusives scattered throughout the model area (mostly to the north of the NTS). These rocks are considered to behave as a confining unit. The ICU is the eighth HGU in the NTS regional model area.

2.1.1.2 Hydrostratigraphic Units

Hydrostratigraphic units are groupings of contiguous stratigraphic units that have a particular hydrogeologic character, such as aquifer (unit through which water moves readily) or confining unit (unit that generally is impermeable to water movement). An HSU may contain several HGUs but is defined so that a single general type of HGU dominates (for example, mostly welded-tuff and vitric-tuff aquifers or mostly tuff confining units). Twenty HSUs were defined in the NTS regional HSU model (IT, 1996d).

Structure played a major role in hydrostratigraphy differentiation within the Pahute Mesa-Timber Mountain caldera complex which is part of the Southwestern Nevada Volcanic Field (SWNVF). As defined for the NTS regional HSU model, the Pahute Mesa-Timber Mountain caldera complex includes the nested calderas comprising the Silent Canyon Caldera Complex on Pahute Mesa and the Timber Mountain Caldera. A structural block model covering an area larger than the Pahute Mesa/Timber Mountain caldera areas was used to differentiate volcanic hydrostratigraphic units within the SWNVF. The volcanic stratigraphy differentiation was made based on the HSUs stratigraphic position within the volcanic rocks, their lithologic properties related to depositional environment, post-depositional alteration, and degree of welding. Outside the caldera complex, structural relationships depicted on the hand-drawn cross sections were used to

map volcanic HSUs. The block model was used as guidance in this area. Volcanic units within the caldera complex were mapped as horizontal layers because they have very low dips. The rationale for the block model is presented in Appendix E-3 of the regional geologic model documentation package (IT, 1996d).

In the Pahute Mesa-Timber Mountain caldera complex area, the rocks were divided into six Tertiary volcanic HSUs, one intrusive HSU, and five pre-Tertiary HSUs. The volcanic rocks west of the NTS caldera complex were not subdivided and are represented by a single HSU, volcanics undifferentiated (VU). The HSUs defined for the NTS regional HSU model that are within the PM-OV model area are listed in [Table 2-2](#). These units are listed in approximate order from surface to basement, although some are laterally rather than vertically contiguous, and not all units are present in all parts of the model area. Because the model is very large, geologically and hydrologically complex, with little subsurface data, various simplification steps had to be employed. The entire model area was divided into four geographical areas based on geology and availability of subsurface data (IT, 1996d; Warren et al., 2000b). A hydrostratigraphic nomenclature scheme was developed separately for each of the four areas. A consequence of this procedure are artificial changes at the boundaries of the four geographic mapping areas. Such changes reflect the different HSU nomenclatures and level of detail for the separate geologic domains. For example, the six volcanic HSUs differentiated within the NTS caldera complex become VU to the west and north.

Additionally, the dominant lithology of some units may change or pinch out laterally (e.g., Lava Flow Aquifer [LFA] close to the source vents, Welded-Tuff Aquifer [WTA] further away, and finally nonwelded Tuff Confining Unit [TCU] or Vitric Tuff-Aquifer [VTA] at distal edges). Another simplification addresses the caldera roots. For the NTS regional HSU model, the plutonic or hypabyssal igneous rocks that likely occur at depth below the calderas are modeled as the Lower Clastic Confining Unit (LCCU).

Based on data used in the NTS regional model (IT, 1996b and DOE/NV, 1997), hydraulic conductivity ranges for the main aquifers are as summarized in [Table 2-3](#). The mean hydraulic conductivity of the Alluvial Aquifer is smaller than that of carbonate aquifers, but higher than that of the volcanic aquifers. The ranges extend over orders of magnitude. For example, within the Lower Carbonate Aquifer (LCA), the range of hydraulic conductivity is estimated to be between 0.0008 and 1,570 meters per day (m/d) (0.003 and 5,150 feet per day [ft/d]), representing interstitial and fracture porosity. This large range suggests that at the local scale, large variability in hydraulic conductivity can be expected. At the larger scales, the degree of fracturing controls the heterogeneity. It was also found that a linear trend exists in the logarithm of hydraulic conductivity with increased depth. The data, however, displayed a significant level of scatter. Hydraulic property data for rocks relevant to the PM-OV area have been reassessed and are presented in [Section 5.0](#) of this document.

**Table 2-2
Hydrostratigraphic Units of the Pahute Mesa-Oasis Valley Area Included in the NTS Regional Hydrostratigraphic Framework Model**

Model Layer Number ^a	Hydrostratigraphic Unit (Symbol)	Dominant Hydrogeologic Unit(s) ^b	Stratigraphic Unit Map Symbols ^c	General Description
20	Alluvial Aquifer (AA) (this term is also used to designate a hydrogeologic unit)	AA	Qay, QTc, Qs, Qam, QTa, QTu, Qb, Tgy, Tgc, Tgm, Tgyx, Tt	Consists mainly of alluvium that fills extensional basins such as Gold Flat, Crater Flat, Kawich Valley, and Sarcobatus Flat. Also includes generally older Tertiary gravels, tuffaceous sediments, and nonwelded tuffs (where thin) that partially fill other basins such as Oasis Valley and the moat of the Timber Mountain caldera complex.
19	Timber Mountain Aquifer (TMA)	Mostly WTA, minor VTA; TCU within the Tm caldera complex	Tt, Tf, Tm	"The uppermost welded tuffs" in the PM-OV model area. Consists mainly of extra-caldera welded ash-flow tuffs (aquifer-like lithologies). However, the altered intra-caldera equivalent rocks within the Timber Mountain caldera are modeled as confining units.
18	Tuff Cone (TC)	LFA, TCU	Tp, Th (formerly Ta), Tc	Complex three-dimensional distribution of rhyolite lava and zeolitic nonwelded tuff of the Paintbrush Group, Calico Hills Formation or Crater Flat Group. Present in the northern portion of the PM-OV model area beneath most of eastern and central Area 20.
17	Bullfrog Confining Unit (TCB)	TCU	Tcb	Major confining unit differentiated within the NTS caldera complex area. Unit consists of thick intra-caldera, zeolitic, mostly nonwelded tuff of the Bullfrog Formation.
16	Belted Range Aquifer (TBA)	LFA and WTA, with lesser TCU	Tub, Tcbs, Tr	Consists of welded ash-flow tuff and lava of the Belted Range Group (Tb) above the Grouse Canyon Tuff (Tbg), but may also include the lava flow lithofacies of the commendite of Split Ridge (Tbgs) and the commendite of Quartet Dome (Tbq) where present. Differentiated within the NTS caldera complex area.
15	Basal Confining Unit (BCU)	TCU	Tn, Tub, To, Tr, Tq	Mostly zeolitized nonwelded tuffs differentiated in the NTS caldera complex area.
14	Basal Aquifer (BAQ)	WTA	To, Tlt, Tqm	Mostly aquifer-like older volcanic rocks. Differentiated within the NTS caldera complex area.
11	Volcanics Undifferentiated (VU)	WTA, TCU, lesser LFA	Potentially includes all Tertiary volcanic units	All Quaternary and Tertiary volcanic units outside the NTS proper and the proximal NTS caldera complex.
8	Upper Clastic Confining Unit (UCCU)	CCU	MDc, MDe	Late Devonian through Mississippian siliciclastic rocks. Present in the eastern third of the PM-OV model area.
7	Lower Carbonate Aquifer (LCA)	CA	Dg through Cc	Cambrian through Devonian mostly limestone and dolomite. Widespread throughout the PM-OV area.
6	Lower Clastic Confining Unit (LCCU)	CCU	Cc, Cz, Czw, Zs, Zj	Late Proterozoic through Early Cambrian siliciclastic rocks. Widespread throughout the PM-OV area.
5	Lower Carbonate Aquifer - Thrust Plate (LCA1)	CA	Dg through Cc	Cambrian through Devonian, mostly limestone and dolomite, rocks that occur in the hanging wall of the Belted Range thrust fault.
4	Lower Clastic Confining Unit - Thrust Plate (LCCU1)	CCU	Cc, Cz, Czw, Zs	Late Proterozoic to Early Cambrian siliciclastic rocks that occur within the hanging wall of the Belted Range thrust fault.
1	Intrusives (I)	ICU	Ti, Kg	Consists of granitic rocks that comprise the Gold Meadows stock along the northeastern margin of the PM-OV area and intrusives greater than 2 kilometers in size elsewhere in the NTS regional HSU model.

^aUGTA regional model (IT, 1996d)

^bSee Table 2-2 for definitions of HGUs

^cRefer to Slate et al. (1999) and Ferguson et al. (1994) for definitions of stratigraphic unit map symbols

Source: Adapted from IT, 1996d

Table 2-3
Ranges of Hydraulic Conductivity for the Major Aquifers
of the Nevada Test Site Region

Aquifer	Hydraulic Conductivity	
	Mean (m/d)	Range (m/d)
Alluvial Aquifer	8.44	0.00006-83
Volcanic Aquifers	1.18	0.0003-12
Carbonate Aquifers	31.71	0.0008-1,570

Source: DOE/NV, 1997 and IT, 1996b

2.1.2 Groundwater Occurrence and Movement

Figure 2-1 is a map depicting the characteristics of the NTS regional groundwater flow system including the flow system boundary, areas of recharge, and evapotranspiration (ET) areas. The descriptions provided in this section are based on the data gathered during the regional evaluation (IT, 1996a and c; DOE/NV, 1997). Updates have been incorporated where available.

2.1.2.1 Groundwater Occurrence

Groundwater occurrence within the NTS regional flow system is discussed based on the water level dataset compiled during the regional evaluation (IT, 1996c and DOE/NV, 1997).

Within the NTS region, groundwater occurs in alluvial, volcanic, and carbonate materials. Saturated alluvial materials are present in central and southern Yucca Flat, Frenchman Flat, and Jackass Flats on the NTS and in the basins located throughout the flow system. Saturated Tertiary volcanics are present in the western section of the region. The distribution and thickness of alluvial and volcanic aquifers are highly variable throughout the region and are not interpreted to be continuous. In most instances, an alluvial aquifer is confined to a basin by surrounding mountain ranges. In some basins, alluvial aquifers are discontinuous due to structural controls elevating the bottom of the alluvium above the water table. In general, alluvial and volcanic aquifers are considered depositional elements overlying the regional flow system and only influence regional flow in localized areas. The underlying LCA is the principal aquifer of the NTS regional flow system. The LCA forms a nearly continuous aquifer across the region except where interrupted by calderas, truncated by structural controls, or penetrated by intrusive rocks.

Based on the water level dataset compiled during the regional evaluation (IT, 1996c and DOE/NV, 1997), depths to groundwater beneath the NTS and surrounding region vary greatly. Groundwater depths in the southern NTS range

from about 23 meters (m) (75 feet [ft]) beneath upper Fortymile Wash to over 213.36 m (700 ft) beneath Frenchman Flat compared to more than 610 m (2,000 ft) beneath Pahute Mesa in the northern NTS (IT, 1996c and DOE/NV, 1997). Perched groundwater is found locally throughout the NTS and occurs within the tuff-confining units and, to some extent, overlying units. In the highlands, springs emerge from perched groundwater lenses. Spring discharge rates are low and this water is used only by wildlife.

2.1.2.2 Groundwater Movement

Within the NTS regional flow system, groundwater movement is controlled by structural and geologic conditions, and the distribution of recharge and discharge locations.

The general direction of groundwater flow in the NTS regional flow system is from north to south and east to southwest (Figure 2-1). The direction of groundwater flow is locally influenced in areas where structural and geologic conditions have controlled the distribution and thickness of the Lower Carbonate Aquifer. In some areas of the NTS regional flow system, groundwater encounters structural and geologic conditions, such as structural highs of the Lower Clastic Confining Unit, that promote an upward flow component. The upward flow component brings water to discharge at the surface in the form of a wet playa or springs. Groundwater flow between basins occurs in the form of subsurface inflow and outflow.

Horizontal hydraulic gradients are very low to the east and west of the NTS. In other areas, the prevailing flow direction and hydraulic gradients may locally be influenced by the structural position of geologic units with significantly lower transmissivity than that of the LCA. If the low transmissive units are structurally oriented so that they are perpendicular to flow, flow might be significantly altered, causing large hydraulic gradients. If their structural orientation is parallel to the prevailing flow direction, their effect may be insignificant. Structural uplifts of the Lower Clastic Confining Unit and the distribution of the Upper Clastic Confining Unit have caused several of the observed steep gradients within the flow system. Low-permeability sediments along the Funeral Mountains such as the Tertiary Death Valley Section sediments also cause a steep hydraulic gradient between Amargosa Desert and Death Valley.

Groundwater recharge results from precipitation at higher elevations and infiltration along stream courses and in playas. Recharge rates and distribution may be estimated. The estimates are, however, uncertain. The recharge model used in the NTS regional flow model was based on a modification of the Maxey-Eakin method (Maxey and Eakin, 1949). Several new models have recently been proposed and are described in Section 6.0 of this document.

Groundwater discharges to the surface in the form of springs and seeps and ET in several areas. Major areas of natural groundwater discharge include: Oasis Valley, Ash Meadows, Alkali Flat, Death Valley, and Penoyer Valley. Estimates of ET have recently been updated by the USGS for the first four areas listed above

(Laczniak et al., 2001). Within the NTS region, artificial discharge occurs as groundwater pumpage from drinking water supply wells (public and domestic), agricultural wells, and industrial wells. Public, domestic, and industrial water supply wells for the NTS produce water from the carbonate, volcanic, and valley-fill aquifers. South of the NTS, private and public water supply wells are completed in the valley-fill aquifer. Discharge from the Pahute Mesa-Oasis Valley area is discussed in [Section 7.0](#) of this document.

An estimate of the NTS regional, steady-state, groundwater budget is provided in [Table 2-4](#). Updated regional recharge and discharge volumes are provided in [Appendix F](#).

Table 2-4
Estimated Steady-State Groundwater Budget
for the Nevada Test Site Regional Groundwater Flow System

Recharge	
Recharge from precipitation	177,484 - 289,410 m ³ /d
Subsurface inflow	5,405 - 70,100 m ³ /d
Total Natural Recharge	182,889 - 359,510 m³/d
Discharge	
Surface discharge (ET)	135,340 - 300,700 m ³ /d
Subsurface outflow	850 - 5,100 m ³ /d
Total Natural Discharge	136,190 - 305,800 m³/d

m³/d = Cubic meters per day

Source: DOE/NV, 1997

2.2 Local Hydrogeologic Framework

A three-dimensional (3-D) hydrostratigraphic framework model and alternatives have been built for the PM-OV area. The processes of HSU model development and screening are summarized along with the models retained for use in the CAU groundwater flow and transport model. The details may be found in the HSU model report (BN, 2002).

2.2.1 HSU Model Development

The approach followed to develop the base HSU model and alternatives is described in this section. The HSU model area coincides with the PM-OV area described in [Section 1.0](#) ([Figure 1-2](#)).

The PM-OV area HSU model(s) were constructed using EarthVision[®] (Version 5.1, by Dynamic Graphics), a 3-D geologic model building and visualization software package. Input data included drill-hole data, digital elevation model data, and outcrop and fault data from surface geologic map. Where deemed necessary, the data were supplemented with interpretations in the form of “pseudo drill holes,” cross sections, and structure-contour maps. A “pseudo drill hole” is a fictitious data point used to facilitate the automated

contouring of data. The data for the pseudo drill hole are obtained from surficial geology maps and/or geologist's interpretations.

A preliminary base HSU model was constructed based on the conceptual model of the NTS hydrologic system described by Winograd and Thordarson (1975). Further developments made by Lacznia et al. (1996), IT (1996a, b, and c), and Drellack and Prothro (1997) were also used in the UGTA base HSU model.

To capture the uncertainty associated with the HSU framework, a number of alternatives interpretations were considered in addition to the base HSU model (Table A.2-1). These alternatives were then evaluated and organized into four groups as follows:

- Group A - Recommended changes to the preliminary base model: Alternatives of this group were used to improve the base HSU model.
- Group B - Viable alternative scenarios: These were further developed as alternative HSU models.
- Group C - Proposed Alternatives to address during the Hydrologic Modeling Phase: It was decided that these alternatives would be better addressed during the hydrologic modeling phase.
- Group D - Suggested alternatives that were deemed to be of low priority or not necessary to model

The main criterion for selecting alternatives for full development was the potential impact of the alternative interpretation on groundwater flow and the transport of contaminants in groundwater.

Following this evaluation of the alternatives, the base HSU model was updated using the Group A alternatives and the alternatives placed under Group B were further developed into EarthVision® models. These alternatives are listed below in descending order of inferred potential impact (BN, 2002).

- Alternative #1 - Silent Canyon Caldera Complex (SCCC): Develop structurally uncoupled alternative model for the Silent Canyon caldera complex
- Alternative #2 - Area between the Timber Mountain Caldera and the Silent Canyon Caldera Complex: Explore variations in the interpretation of the basement "ridge" (gravity high) between Timber Mountain and Silent Canyon caldera complexes
- Alternative #3 - Thirsty Canyon Lineament: Explore variations of the Thirsty Canyon lineament
- Alternative #4 - Depth to the Pre-Tertiary Surface: Vary depth to basement/pre-Tertiary surface

- Alternative #5 - Contiguous Sheet of LCA3 Rocks: Change extent and thickness of LCA3 and LCCU1 in the southeastern portion of model
- Alternative #6 - Deeply Rooted Belted Range Thrust Fault: Develop a scenario with a deeply rooted Belted Range Thrust (BRT) fault

A summary description of the alternative HSU models is provided in [Section A.2.0](#). For details, see report titled: *Hydrostratigraphic Model for the Groundwater Flow and Contaminant Transport Model of Corrective Action Units 101 and 102: Central and Western Pahute Mesa, Nye County, Nevada* (BN, 2002).

2.2.2 HSU Alternative Model Screening

The development of groundwater water flow and contaminant transport models for all alternative HSU models would require considerable resources. Therefore, a screening process was developed to evaluate the impact of each alternative on contaminant transport, using simplified transport models (See [Section A.3.0](#) of [Appendix A](#)).

These simplified models were developed using Finite-Element Heat Mass Transfer (FEHM) Computer Code (Zyvoloski et al., 1997a and b). The "particle-tracking" capability of FEHM was used to approximate the transport of radionuclides in groundwater using the base HSU model and the six alternatives.

Except for the SCCC alternative (Alternative 1), the results of the "particle-tracking" analyses for the other five alternatives were statistically similar to those of the base HSU model. The results of the SCCC alternative produced results that were clearly different from those produced by the base HSU model ([Section A.3.0](#) of [Appendix A](#)). Therefore, only the base HSU model and the SCCC alternative will be used to develop alternative CAU models. The other five HSU model alternatives have been eliminated for further consideration. Details of the HSU model screening process and results are presented in [Section A.3.0](#) of [Appendix A](#). Summary descriptions of the base HSU and the SCCC alternative models follow.

2.2.3 Base HSU Model

The structural features, hydrogeologic units, and hydrostratigraphic units of the base HSU model developed for the PM-OV area are described in this section. A 3-D view of this model is shown in [Figure 2-2](#).

2.2.3.1 Structural Features

Geologic structural features are an important part of the hydrologic framework of the groundwater flow system of the PM-OV area. They define the geometric

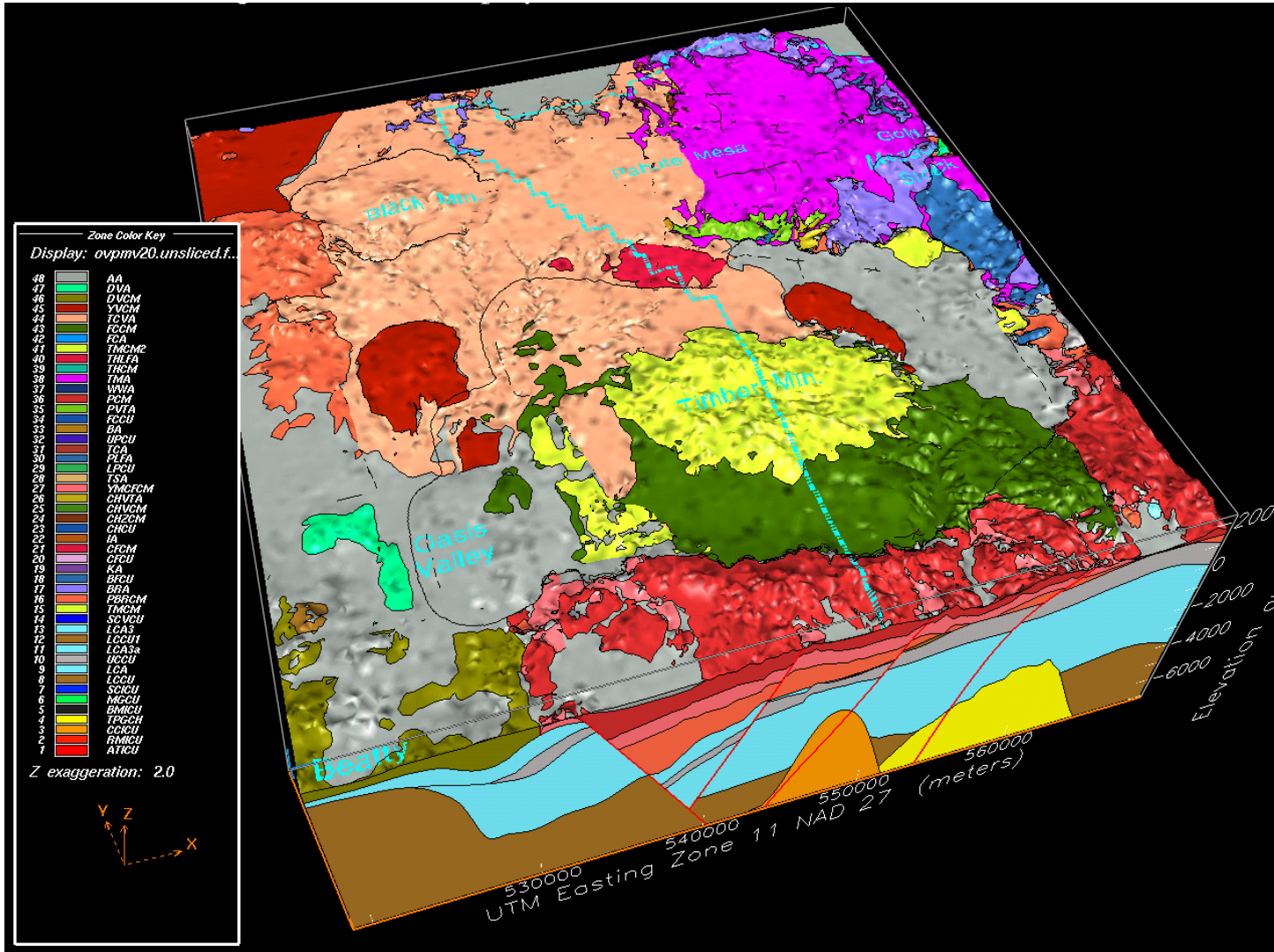


Figure 2-2
Three-Dimensional View of the Base Hydrostratigraphic Model
of the Pahute Mesa-Oasis Valley Area (BN, 2002)

configuration of the flow domain, including the distribution, thickness, and orientation of rock units. The depositional patterns of the geologic units occurring in the area were strongly influenced by syn-volcanic structures, including caldera faults and some normal faults. Faulting, for example, may result in juxtaposition of units with different hydrologic properties. Structures themselves may influence flow patterns by acting as conduits for flow or barriers to flow (BN, 2002).

The structure of the base HSU model is based on the conceptual model developed by Ferguson et al. (1994) and Warren (1994a and b). Ferguson et al. (1994) developed a detailed structural model of the SCCC using seismic refraction, gravity, and drill hole data. Warren (1994a and b) extended the work of Ferguson et al. (1994) to the area surrounding the SCCC. The work of Warren (1994a and b) was later published by Warren et al. (2000a and b).

The base HSU model includes a total of 47 structural elements which are either faults or calderas. Only faults that were considered to be significant were included in the model. These include the larger ones and the ones that seem to form significant structural boundaries. Six calderas have been identified in the PM-OV model area, two of which are buried. These calderas reflect a variety of geometries and collapse processes. Caldera-collapse processes include the “piston,” down-sag, trap-door, and piecemeal collapse. Some calderas seem to have collapsed along pre-existing linear faults, resulting in polygonal boundaries (Kane et al., 1981; Ferguson et al., 1994). Of particular interest is the SCCC, an important and uncertain geologic feature of the PM-OV area. As stated previously, an alternative scenario was developed to evaluate the effect of caldera shape (see following subsection).

In the base HSU model, the SCCC includes two calderas: the Grouse Canyon and Area 20 calderas. As described by BN (2002), *“the caldera-forming faults coincide with north-south striking basin-and-range faults mapped at the surface and with inferred, buried, west-northwest-trending structural zones, which effectively segment the SCCC into numerous fault-bounded sub-basins having the general configuration of half grabens. Thus, the base HSU model incorporates many faults with episodic movements that were synchronous with and associated with caldera formation. Consequently, many of the faults in the base HSU model have significant influence on the distribution of volcanic units.”* The base HSU model for the SCCC area also includes 20 faults and structural zones in addition to the caldera-forming faults. Thirteen of these 20 structural features are basin-and-range type faults mapped at the surface.

2.2.3.2 Hydrogeologic Units

The hydrogeologic framework for PM-OV model established by Blankennagel and Weir (1973) provided the foundation for most subsequent hydrogeologic studies in the area. As described in [Section 2.1](#), the rocks of the NTS have been classified for hydrologic modeling using a two-level classification scheme in which HGUs are grouped to form HSUs (IT, 1996d). New units and additional detail have been added to the basic framework definition, but the systems

developed by these early workers remain the best way to understand the groundwater of the NTS region.

The HGU scheme used for CAU-scale modeling, including the PM-OV framework model, included nine HGUs; the initial eight used in the NTS regional HSU model mentioned in [Section 2.1](#), and an additional ICU. The nomenclature for the intrusive was also modified to Granite Confining Unit (GCU) ([Table 2-5](#)).

Table 2-5
Additional and Modified Hydrogeologic Units of the PM-OV Model

Hydrogeologic Unit	Typical Lithologies	Hydrologic Significance
Intra-caldera intrusive confining unit (IICU)	Highly altered, highly injected/intruded country rock and granitic material	Assumed to be impermeable. Conceptually underlies each of the SWNVF calderas and Calico Hills. Developed for this study to designate basement beneath calderas as different from basement outside calderas.
Granite confining unit (GCU)	Granodiorite, quartz monzonite	Relatively impermeable; forms local bulbous stocks, north of Rainier Mesa and Yucca Flat; may contain perched water.

Source: Adapted from BN, 2002

The intra-caldera intrusive confining unit (IICU) was initially defined for the PM-OV hydrostratigraphic framework model (BN, 2002). Conceptually, an IICU underlies each of the SWNVF calderas, and one other IICU is depicted as the Calico Hills intrusive. Although modeled as single intrusive masses, the exact nature of the rocks beneath the calderas is unknown, as no drill holes penetrate these rocks. We assume these bodies may range from highly altered, highly injected/intruded country rock to granite. The IICUs are considered to behave as confining units due to low primary porosity and low permeability where measured (such as in the granite of Climax stock [Walker, 1962]). Most fractures are probably filled with secondary minerals and/or are poorly connected. The Climax stock in extreme northern Yucca Flat (Houser et al., 1961; Walker, 1962; Maldonado, 1977) and the Gold Meadows stock in the extreme eastern part of the PM-OV model area (Snyder, 1977) may serve as analogs to the IICUs.

Intra-Caldera Intrusive Confining Unit (IICU)

This unit includes highly altered, highly injected/intruded country rock and granitic material. It is assumed to be impermeable. Conceptually, it underlies each of the SWNVF calderas and Calico Hills. It was developed for this study to designate basement beneath calderas as different from basement outside calderas.

Granite Confining Unit (GCU)

This unit includes granodiorite and quartz monzonite, and is relatively impermeable. It forms local bulbous stocks north of Rainier Mesa and Yucca Flat. It may contain perched water.

2.2.3.3 Hydrostratigraphic Units

Brief descriptions of all the HSUs used to construct the PM-OV model are provided in [Table A.1-1 \(Appendix A\)](#). They are listed in approximate order from surface to basement, although some are laterally rather than vertically contiguous, and not all units are present in all parts of the model area.

[Table 2-6](#) shows the correlation of PM-OV HSUs with HSUs from earlier hydrostratigraphic models for this region. [Plate 1](#) is a map showing a plan view of the surficial hydrostratigraphy for the PM-OV model area. A northeast-southwest hydrostratigraphic cross section, along the general flow direction, is provided in [Plate 2](#). A west-east hydrostratigraphic cross section through Pahute Mesa (perpendicular to the general groundwater flow direction) is presented in [Plate 3](#). Both of these cross sections are from the PM-OV 3-D framework documentation package (BN, 2002), where additional cross sections and detailed information regarding this CAU-scale model can be found.

As can be seen from the information presented in this section, the PM-OV hydrostratigraphic framework model (BN, 2002) includes considerable structural detail and stratigraphic enhancement over the NTS regional HSU model (IT, 1996d). The total number of HSUs increased from 20 to 46; most of the increase affected the Tertiary volcanic section. The six Tertiary volcanic HSUs in the Pahute Mesa and Timber Mountain caldera complex and the single volcanics undifferentiated outside the caldera complex (of the NTS regional HSU model) were subdivided into 40 HSUs for the PM-OV model. Except for geometry details, the five pre-Tertiary HSUs remain as initially defined.

The concept of a “composite unit” was first used while developing the PM-OV model. Composite units comprise a mixture of hydraulically variable units. A good example is the Calico Hills Zeolitized Composite Unit (CHZCM). The CHZCM consists of lava-flow aquifers embedded within a zeolitic bedded tuff. The relative distribution of each HGU component of a composite unit is uncertain either due to natural variation or due to lack of definitive subsurface data.

2.2.4 Silent Canyon Caldera Complex HSU Model

The alternative SCCC model is based on the same HGUs as the base HSU model. Despite the considerable differences in basic concepts such as style of caldera formation and number and activity of faults, as well as in scale and level of detail, both models honor the available drill hole and outcrop data. Differences between the two models relate to the structural model used and the categorizing of HGUs into HSUs. Descriptions of these features are summarized from the HSU model report (BN, 2002).

Table 2-6
Correlation of Hydrostratigraphic Units of the Pahute Mesa-Oasis Valley Model and Earlier Models^a
 (Page 1 of 2)

Layer No. ^b	Hydrostratigraphic Unit	Symbol This Report ^b	Correlation with PM-300 Model ^c	Correlation with UGTA Phase I ^d	Correlation with YMP ^e (Lithostratigraphic Units)
46	Alluvial aquifer	AA	TMA	AA	QAL, TPAL, TLIM
45	Younger volcanic composite unit	YVCM	NP ^f	VU	B
44	Thirsty Canyon volcanics aquifer	TCVA	TMA	TMA, VU	NP
43	Detached volcanic aquifer	DVA	NP	VU	
42	Detached volcanics composite unit	DVCM			
41	Fortymile Canyon composite unit	FCCM	TMA	TMA, VA	NP
40	Fortymile Canyon aquifer	FCA	NP	VU	
39	Timber Mountain composite unit	TMCM	TMCU	TMA	
38	Tannenbaum Hill lava-flow aquifer	THLFA	TMA		
37	Tannenbaum Hill composite unit	THCM			
36	Timber Mountain aquifer	TMA		TMA, VA	
35	Subcaldera volcanic confining unit	SCVCU	PreT	BCU	NR
34	Fluorspar Canyon confining unit	FCCU	TMA	TMA, VA	NP
33	Windy Wash aquifer	WWA	WWA	TMA	
32	Paintbrush composite unit	PCM	NP	TMA, VA, TC	UVA
31	Paintbrush vitric-tuff aquifer	PVTA	PVTA	TMA, TC, VA	
30	Benham aquifer	BA	BA	TC	NP
29	Upper Paintbrush confining unit	UPCU	UPCU		NR
28	Tiva Canyon aquifer	TCA	TCA	TMA, TC, VA	UVA
27	Paintbrush lava-flow aquifer	PLFA	PLFA	TC	NP
26	Lower Paintbrush confining unit	LPCU	LPCU	TC	NR
25	Topopah Spring aquifer	TSA	TSA	TC, VA	UVA
24	Yucca Mt. Crater Flat composite unit	YMCFCM	NP	VA, VU	UVCU, MVA
23	Calico Hills vitric-Tuff aquifer	CHVTA	CHVTA	TC	MVA
22	Calico Hills vitric composite unit	CHVCM	CHVCM		
21	Calico Hills zeolitic composite unit	CHZCM	CHZCM		
20	Calico Hills confining unit	CHCU	CHCU	TC	NR

Table 2-6
Correlation of Hydrostratigraphic Units of the Pahute Mesa-Oasis Valley Model and Earlier Models^a
 (Page 2 of 2)

Layer No. ^b	Hydrostratigraphic Unit	Symbol This Report ^b	Correlation with PM-300 Model ^c	Correlation with UGTA Phase I ^d	Correlation with YMP ^e (Lithostratigraphic Units)
19	Inlet aquifer	IA	IA	TC, VA	NP
18	Crater Flat composite unit	CFCM	CFCM	TC, VU	MVA
17	Crater Flat confining unit	CFCU	CFCU		NR
16	Kersarge aquifer	KA	KA	TC	NP
15	Bullfrog confining unit	BFCU	BFCU	TCB	
14	Belted Range aquifer	BRA	BRA	TBA	NR
13	Pre-Belted Range composite unit	PBRCM	PBRCM	BAQ, BCU	MVCU, LVA, LVCU, LCU
12	Black Mountain intrusive confining unit	BMICU	NP	VU	NP
11	Ammonia Tanks intrusive confining unit	ATICU	TMCM	TMA	
10	Rainier Mesa intrusive confining unit	RMICU			
9	Claim Canyon intrusive confining unit	CCICU	NP	VA	NR
8	Calico Hills intrusive confining unit	CHICU		I	NP
7	Silent Canyon intrusive confining unit	SCICU	PreT	LCCU	
6	Mesozoic granite confining unit	MGCU		I	
5	Lower carbonate aquifer–thrust plate	LCA3	NP	LCA3	NR
4	Lower clastic confining unit–thrust plate	LCCU1	PreT	LCCU1	
3	Upper clastic confining unit	UCCU	NP	UCCU	ECU
2	Lower carbonate aquifer	LCA	PreT	LCA	LCA
1	Lower clastic confining unit	LCCU		LCCU	QCU

^aIf correlative to more than one HSU, all HSUs are listed

^bSee BN (2002) and [Table A.1-1](#) of this report for explanation of PM-OV model HSU nomenclature

^cSee Drellack and Prothro (1997) for explanation of PM-300 HSU nomenclature

^dSee IT (1996d) for explanation of the UGTA Phase I HSU nomenclature

^eSee CRWMS M&O (1997 and 2000b) for explanation of the YMP lithostratigraphic unit nomenclature

^fNot present

^gNot recognized as a separate HSU

2.2.4.1 Structure

The alternative structural model of the SCCC is more simplified than the base HSU model. This structural model is based on previous models of calderas of the Pahute Mesa region developed by Noble et al. (1968) and Orkild et al. (1969), and analogies with other calderas of the world.

The SCCC HSU model includes an elliptical ring-fracture fault system elongated to the north-northeast (Figure 2-3). Major structural differences with the base HSU model include the locations of caldera-forming faults and the number depth of the faults considered.

The locations of the SCCC margins are different on the eastern and western sides of the complex (Figure 2-3). In the alternative HSU model, these two margins are located 1 to 3 kilometers (km) further west and east than in the base HSU model.

The number of faults is different. The SCCC HSU model includes the single caldera ring-fracture system, and only 11 of the basin-and-range faults mapped at the surface. Another difference is that the faults in the SCCC HSU model end at shallower depths than in the base HSU model.

2.2.4.2 Hydrostratigraphy

Hydrostratigraphic differences between the two models of the SCCC area are the number of HSUs, their definition, and their distribution (BN, 2002).

Whereas in the base HSU model, the SCCC area includes 25 HSUs, it includes only 12 in the SCCC alternative model (Table 2-7). Six post-Paintbrush HSUs are lumped together in the alternative model. This simplification may not be important because these units are mostly unsaturated, but other simplifications such as the lumping of the four Calico Hills HSUs may be important (BN, 2002).

Significant differences also exist in the configuration of the HSU surfaces. The surfaces of the HSUs are less rugged in the SCCC model than in the base HSU model. Within the SCCC area, the upper surfaces of HSUs in the alternative HSU model are generally bowl-shaped, and dip more gently than those in the base HSU model (Figure 2-4). Upper surfaces of HSUs in the alternative HSU model are also higher along the down-thrown sides of faults, and lower along the up-thrown sides (BN, 2002).

The differences in the locations of caldera margins and in structure result in differences in HSU thicknesses. Generally, the thicknesses of HSUs located within the SCCC vary to a greater degree in the base HSU model. In comparison, in the SCCC model, the HSUs are generally lens-shaped. These lenses are thick in the middle and thin out towards the margins of the SCCC (BN, 2002).

In the alternative HSU model, the HSUs were defined using the drill hole stratigraphy data, without considering lithologic differences present. This led to some differences in the definition of the HSUs. For example, the distribution and

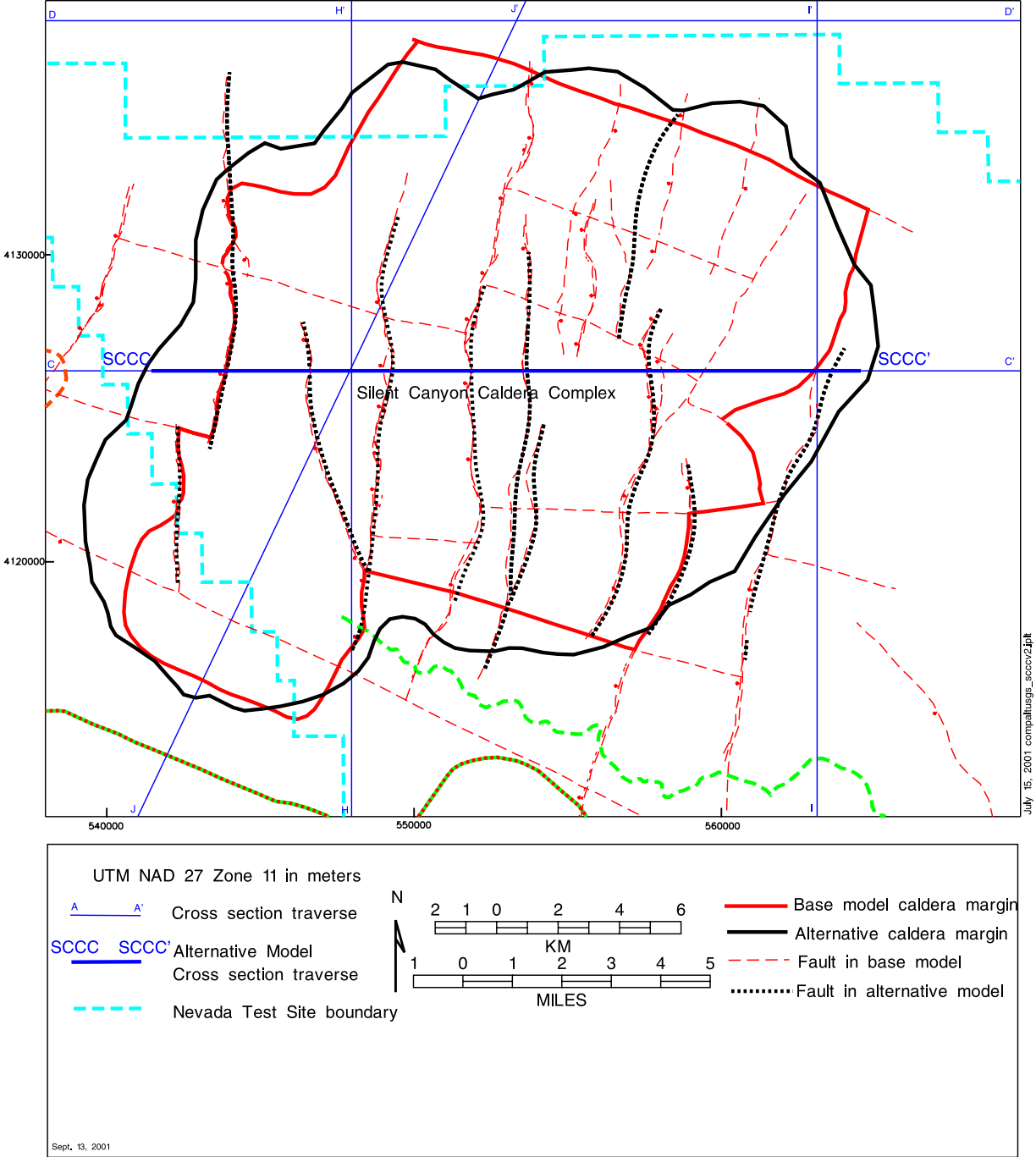


Figure 2-3
Comparison of Silent Canyon Caldera Margins:
Base Model and SCCC Alternative (BN, 2002)

Table 2-7
Correlation of Hydrostratigraphic Units Between
the Silent Canyon Caldera Complex Model and the Base HSU Model

UGTA Base Model HSUs	Alternative SCCC Model HSUs
Thirsty Canyon volcanic aquifer	Silent Canyon Timber Mountain composite unit
Tannenbaum Hill lava-flow aquifer	
Tannenbaum Hill composite unit	
Timber Mountain aquifer	
Fluorspar Canyon confining unit	
Windy Wash aquifer	
Paintbrush vitric-tuff aquifer	
Benham aquifer	Silent Canyon Benham aquifer
Upper Paintbrush confining unit	
Tiva Canyon aquifer	Silent Canyon Tiva Canyon aquifer
Paintbrush lava-flow aquifer	Silent Canyon Lower Paintbrush confining unit
Lower Paintbrush confining unit	
Topopah Spring aquifer	Silent Canyon Topopah Spring aquifer
Calico Hills vitric-tuff aquifer	Silent Canyon Calico Hills composite unit
Calico Hills vitric composite unit	
Calico Hills zeolitic composite unit	
Calico Hills confining unit	
Inlet aquifer	Silent Canyon Inlet aquifer
Crater Flat composite unit	Silent Canyon Crater Flat composite unit
Crater Flat confining unit	
Kearsarge aquifer	
Bullfrog confining unit	Silent Canyon Bullfrog confining unit
Belted Range aquifer	Silent Canyon Belted Range aquifer
Pre-Belted Range composite unit	Silent Canyon Pre-Belted Range composite unit
Silent Canyon intrusive confining unit	Silent Canyon intrusive confining unit

Source: BN, 2002

Note: The HSU names used in the alternative model were modified by adding the prefix "Silent Canyon" for differentiation purposes.

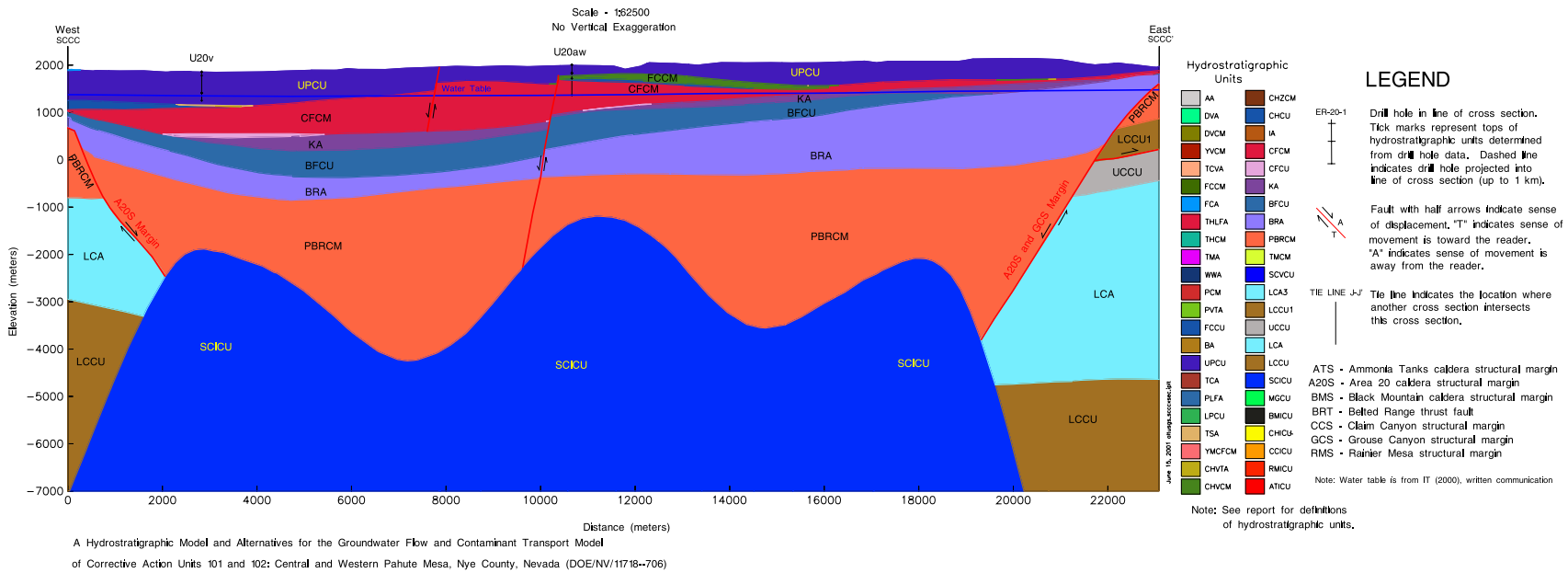


Figure 2-4
Typical West - East Cross-Section through the Silent Canyon Caldera for the SCCC Model (BN, 2002)
Cross-Section Location Shown in Figure 2-3

composition of the Topopah Springs Aquifer (TSA) HSU are different in the two models. In the base HSU model, the TSA includes only the welded ash-flow tuff of the Topopah Spring Tuff, whereas the TSA in the alternative HSU model also includes Topopah Spring vitric and zeolitic, nonwelded, and some bedded tuff.

The hydrogeologic importance of the Calico Hills Formation in the SCCC area is recognized in both the base and SCCC models. It is, however, handled differently in the two models. In the base HSU model, the Calico Hills Formation is subdivided into four HSUs based on differences in lithologic composition and alteration effects, whereas it is treated as a single composite unit in the SCCC alternative model ([Table 2-7](#)). A more detailed discussion of the SCCC alternative model may be found in the HSU model report (BN, 2002).

3.0 CAU Modeling Approach

This section presents an overview of the CAU modeling approach and descriptions of the groundwater flow modeling approach and data requirements.

3.1 Overview of CAU Modeling Approach

Underground nuclear testing at the NTS included a total of 908 detonations in shafts and tunnels with approximately one-third of these tests conducted near or below the water table (DOE/NV, 1997). Groundwater flow from these sources occurs through diverse and structurally complex rocks (Laczniak et al., 1996). Given the complexity of the system, sources, and processes controlling transport, computer models will be required to meet the objectives of the FFACO strategy. The modeling approach used to develop an integrated 3-D model for flow and transport begins with characterization of the system, development of conceptual models based on assumptions of system processes, and representation of these processes mathematically. Mathematical models are then implemented on a computer to represent the system.

The CAU flow and transport models will consist of an integrated set of models. Some of these models focus on a small-scale (relative to the CAU) process such as radionuclide release from source regions and others simplifying CAU-scale processes such as reactive transport in fractures to an abstraction for system sensitivity analysis. Combined, the models (referred to as component models) constitute the CAU predictive model.

The integrating numerical model will be a 3-D finite-element flow and transport simulator that captures the complex geologic structure including units of variable thickness, faults, and offsets, as well as complex transport processes associated with reactive solutes and fractured rock. The CAU groundwater flow model component requires two other component models: the NTS regional groundwater flow model and the recharge model. The CAU contaminant transport model component requires the hydrologic source term model.

To ensure fidelity of the CAU model to the physical system, a ten-step protocol will be utilized. These ten steps are: (1) establishment of model purpose, (2) development of conceptual model, (3) selection of a computer code and verification of the code, (4) model design, (5) model calibration, (6) sensitivity and uncertainty analyses, (7) model verification, (8) predictive simulations, (9) presentation of model results, and (10) postaudit.

3.1.1 Selected Code

The FEHM code (Zyvoloski et al., 1997b), developed by LANL, was chosen for the Pahute Mesa CAU-scale flow and transport model (DOE/NV, 1999). FEHM simulates 3-D, time-dependent, multiphase, nonisothermal flow and multicomponent, reactive groundwater transport through porous and fractured media. FEHM's finite element formulation provides an accurate representation of complex 3-D geologic media and structures and their effects on subsurface flow and transport. Specific capabilities include:

- 3-D
- Flow of air, water, and heat
- Multiple chemically reactive and sorbing tracers
- Colloid transport
- Finite element/finite volume formulation
- Coupled stress module
- Saturated and unsaturated media
- Preconditioned conjugate gradient solution of coupled nonlinear equations
- Porous media equivalent model
- Double porosity and double porosity/double-permeability capabilities
- Complex geometries with unstructured grids
- Two different reactive, dual-porosity, particle-tracking modules
- Coupled to parameter estimation (PEST) software
- Linked with Los Alamos Grid Toolbox (LaGriT) grid generation software
- Supported on SUN, SGI, ALPHA, and Intel (windows)

Documentation includes a description of the mathematical models and numerical methods used by FEHM (Zyvoloski et al., 1997a), the user's manual (Zyvoloski et al., 1997b), documentation of the functional and performance requirements for FEHM, description of the FEHM software, and verification and validation reports (Dash et al., 1997; Dash, 2000 and 2001). Further, the software is maintained in configuration management at LANL. With each new release, the software is subjected to a rigorous verification test to ensure accuracy and functionality of all capabilities.

Assumptions for the flow and energy transport models in FEHM include fluid flow governed by Darcy's law, thermal equilibrium between fluid and rock, immovable rock phase, and negligible viscous heating. Specific assumptions are discussed further by Zyvoloski, et al. (1997a).

Inputs to the flow model include the finite-element grid, initial conditions, lateral boundary conditions, recharge, and material properties for HSUs and faults. For application to isothermal groundwater flow, the calibrated FEHM model produces values of hydraulic head or pressure for each node in the grid.

PEST, a software package developed by Watermark Computing (2000), provides a nonlinear parameter estimation routine that can be used to automatically calibrate a flow model. PEST can be used with any existing modeling computer code for model calibration without making any changes to that code. However, FEHM

was recently modified to efficiently provide data needed by PEST in each iteration with no additional post-processing. LaGriT (George, 1997) is an auxiliary code to the FEHM code (Zyvoloski et al., 1997b), developed by LANL to generate finite-element meshes for FEHM models.

All three codes, FEHM (Zyvoloski et al., 1997b), PEST (Watermark Computing, 2000), and LaGriT (George, 1997) have been used in the Yucca Mountain Project modeling activities. Their usage in the development of the YMP saturated zone flow model is documented in a report titled: *Calibration of the Site-Scale Saturated Zone Flow Model* (CRWMS M&O, 2000a). All YMP models are developed under their quality assurance program (DOE, 2000).

3.1.2 Data Requirements

Data requirements for the CAU model fall into three the categories listed below.

Groundwater Flow

Data types required for the groundwater flow model include permeability (or hydraulic conductivity), storage parameters, precipitation recharge, lateral boundary fluxes, hydraulic heads, and groundwater chemistry. These data types are the subject of this document and are discussed in detail in the following sections.

Contamination Sources and Extent

Potential contaminants are currently located in the 82 test locations and downgradient areas in Western and Central Pahute Mesa. Considering the 1,000-year time frame of interest, the potential contaminants may extend from a few hundred meters away from an underground test to as far as Oasis Valley and the northern area of Yucca Mountain. The information on the unclassified hydrologic source term and radionuclide data for central and western Pahute Mesa are documented in a separate report.

Transport Parameters

Major data types of interest include effective porosity, dispersivity, matrix porosity, matrix diffusion, sorption coefficients, and colloid-facilitated transport parameters. Note that for the purpose of modeling, effective porosity and matrix porosity are considered to be transport parameters rather than hydrologic parameters as they are required input variables in the contaminant transport model. Details for these parameters are the subject of *Contaminant Transport Parameters for Central and Western Pahute Mesa: Corrective Action Units 101 and 102* (Rehfeldt et al., 2003).

3.2 Groundwater Flow Modeling Approach and Data Requirements

This section describes the approach used for groundwater flow modeling and the associated data requirements.

3.2.1 Modeling Approach

Steps for developing the CAU flow model include:

- Identify Simulation Objectives
- Define CAU Geologic Model Boundaries
- Define CAU Flow Model Boundaries
- Generate CAU Model Grid
- Calibrate CAU Flow Model
- Perform Hydraulic Property Sensitivity Analysis.

Simulation Objectives

Simulation objectives are defined in Appendix VI of the FFACO (1996). Briefly, the objective is to develop a tool for predicting contaminant migration from source locations through the hydrogeologic units of Pahute Mesa to forecast locations of specified contaminant concentrations for assessment of the contaminant boundary and to provide a basis for risk assessment, design, and siting of monitoring wells.

Geologic Model Boundaries

The next step in the strategy, defining the geologic model domain, has already been completed. Boundaries were chosen based on a number of considerations. The boundaries were chosen such that: (a) they coincide with perceived geologic and hydrologic domains, (b) the contaminant source areas and discharge areas were included with some buffer regions, and (c) practical constraints on model size were considered. The Pahute Mesa CAU flow and transport models will be developed within the boundaries of the geologic model.

CAU Model Boundaries and Boundary Conditions

The next stage of the process is identification of the CAU model boundaries and boundary conditions. When selecting boundaries for a flow and transport model, natural physical boundaries of the aquifer system such as recharge and discharge zones, impermeable rock, or aquifer connections with surface water bodies are preferred because they provide easily described hydraulic boundary information. The characteristics of the Pahute Mesa CAU are such that natural physical boundaries are too distant to be used for the lateral boundaries of the flow and transport model. The boundaries of the CAU flow and transport model were selected to incorporate all relevant sources, important hydrogeologic features, and wells providing hydrologic and geologic information. These boundaries will be approximately the same as the geologic model boundaries. Lateral boundary conditions will be based on fluxes obtained from the NTS regional groundwater flow model. The recharge model will provide fluxes for the model surface. The bottom of the model will be at an elevation of -3,500 m above mean sea level (amsl) throughout the PM-OV model domain.

Grid Generation

Simulations of flow and transport, including particle tracking, in 3-D domains representing the complex hydrostratigraphy described in the hydrogeologic models will be conducted on finite-element grids. The grids are discrete interconnected tetrahedra which, when connected together, capture the structure of

the hydrostratigraphy. The flexibility of finite-elements allows for the resolution of the grid to vary spatially so as to capture source areas and complex structures such as faults with higher resolution than other areas where coarser discretization is sufficient.

The method developed for the flow of information from hydrogeologic interpretation through grid generation has the following steps. The process begins with incorporation of a given hydrogeologic digital model using EarthVision[®] (Dynamic Graphics, 2002). EarthVision[®] which is a suite of software applications used for geospatial analyses. Elevations describing the surface of each HSU and traces of each fault are extracted from the EarthVision[®] model (Dynamic Graphics, 2002) and become inputs to the grid generation software, LaGriT. This code is composed of a suite of grid generation tools and provides an integrated system for all grid generation steps. Unique properties can be assigned to each HSU and fault in the grid. Grid generation will require decisions on the location of high resolution areas. Possible candidates for high resolution include fault zones and thin hydrostratigraphic units. Calibration efficiency can be increased by keeping the flow model grids coarse, then adding higher resolution to source regions and plume pathways for the transport simulations. A process for transferring hydrogeologic framework model information from an EarthVision[®] model (Dynamic Graphics, 2002) to inputs required by LaGriT has been developed and tested.

Flow Model Calibration

Calibration consists of determining model parameter values such that simulated heads and fluxes are consistent with observed or target values. The parameters for a CAU flow model will include the permeabilities of the HSUs and faults in the model. Specified observations for a CAU model will include hydraulic heads measured in wells within the model domain, fluxes through lateral model boundaries calculated using the NTS regional flow model, and fluxes through the top of the model estimated as recharge. These data provide "targets" for the calibration process. Data required for calibration includes information from hydrologic data analysis including well locations, locations of open intervals, HSUs represented by open intervals, transient head measurements in wells, lateral boundary fluxes from the NTS regional flow model, and fluxes into the water table from the recharge model.

PEST runs the model initially and calculates the sum of weighted squared differences between model-generated heads and observed heads and between simulated flux values and regional model fluxes at the model boundary. This sum is referred to as the objective function. PEST then repeatedly runs the flow model to guide the adjustment of parameters until the objective function is minimized. In principle, PEST can be set up to adjust permeabilities until simulated heads reasonably match measured heads within the CAU model domain and simulated fluxes on the CAU model boundary approximately match those calculated by the NTS regional flow model. Due to random and systematic errors, there will always be some discrepancy between modeled and measured values. PEST attempts to minimize this discrepancy and provides estimates of uncertainty in the results. Since the flow model must be run many times during calibration, this part of the process requires heavy usage of computing resources. A model calibration will be

specific to the hydrogeologic model and recharge specified and the lateral boundary fluxes and hydraulic heads used as calibration targets. Alternative geologic models, alternative recharge models, or changes in calibration targets will require new calibrations.

The PEST optimization process will produce expected values, estimated 95 percent confidence limits, and a measure of sensitivity for HSU and fault hydraulic properties used as parameters. However, it is recognized that the PEST uncertainty results based on the typical linear assumptions will not be appropriate for full uncertainty analysis. Rather, expert judgement will also be important.

For complex models with sparse data, calibration is expected to be non-unique. That is, more than one set of parameter values provided to the flow model could result in the observed hydraulic heads and fluxes. Analysis of geochemical data will be integrated into the calibration process to provide independent lines of evidence to support parameters leading to the prediction of groundwater flow paths and travel times.

Thermal effects may need to be considered during calibration. Sources of heat on Pahute Mesa include flow of heat from deeper layers toward the surface evidenced by the geothermal gradient (Blankennagel and Weir, 1973) and residual thermal pulses from underground nuclear tests. Since warm water is more buoyant than cooler water, hot water injected into the aquifer from nuclear test cavities will tend to rise towards higher layers. This small-scale phenomenon impacts the local exit points for radionuclides to enter the flow system and can be handled easily in the source model. Natural temperature gradients may lead to large-scale thermal upwelling in some areas. The significance of these upwelling processes must be evaluated during calibration and strategies developed to address them. The saturated hydraulic conductivity (K) is dependent on both rock and water properties. Therefore, the presence of warmer water in deeper systems may cause an increase in K, but this can be accounted for by increased K in proportion to the change in temperature, then performing isothermal simulations. Even for steady-state flow fields, FEHM accounts for thermal variation effects based either on elevation in the model or HSU in the model. However, if thermal upwelling is determined to be a significant alternative conceptual model, then transient nonisothermal simulations may be required to assess the impacts of such processes.

Calibration of the CAU flow model will be conducted in two steps. First, a sensitivity/uncertainty analysis will be performed to bound ranges of flux into the model. The range of boundary fluxes will come from the uncertainty in the NTS regional groundwater flow model. Spatial variability within an individual HSU will not be incorporated into the CAU flow model. The hydraulic characteristics of each HSU will be treated in a deterministic, spatially homogeneous fashion. The steady-state CAU model will be calibrated to observed water levels and to the bounds of the fluxes. After the steady-state calibration process is completed, a verification of the calibration using transient simulations will be assessed. The assessment will consist of identifying transient water levels caused by well pumpage, and determining the areal extent of the transient behavior. Temporal recharge or boundary flux variations are not known; hence, hydraulic transient

behavior due to recharge or boundary flux will not be suitable for verification purposes. If the causes of the transient behavior cannot be attributed to well pumpage, or if the areal extent is too small, a transient simulation will not be performed. If transient simulations are performed, aquifer storage properties are adjusted until the simulated drawdowns caused by pumping wells approximately match observed drawdowns. The effectiveness of the model verification will, therefore, depend on the accuracy and completeness of the well discharge dataset, and the availability of water level data exhibiting the effects of pumping.

The groundwater flow model for the PM-OV area will be calibrated using the most current American Society for Testing and Materials (ASTM) standard guidance for calibrating groundwater models. The *Standard Guide for Calibrating a Ground-Water Flow Model Application* (D-5981) (ASTM, 1996) is a guide for calibrating porous medium (continuum) groundwater flow models. The method can be adjusted to use on other types of groundwater models such as multiphase models, noncontinuum (karst or fracture flow) models, or mass transport models. The ASTM standard procedures that will be used to implement the guidance cover the use of site-specific information (D-5490) (ASTM, 1993b), applying modeling to site-specific problems (D-5447) (ASTM, 1993a), defining boundary (D-5609) (ASTM, 1994a) and initial (D-5610) (ASTM, 1994b) conditions, performing sensitivity analyses (D-5611) (ASTM, 1994c), and documenting groundwater flow model applications (D-5718) (ASTM, 1995).

Sensitivity Analysis

Sensitivity analysis is a systematic process of varying the magnitude of model inputs such as hydraulic conductivity, recharge, and boundary conditions and determining the effect on model outputs such as hydraulic head and flux. Sensitivity analyses are conducted before and after calibration of the flow model. Sensitivity analyses conducted before model calibration help identify parameters that can be estimated. Sensitivity analyses conducted after model calibration help identify parameters which affect the model results. The sensitivity analysis process can be automated using the PEST utility SENSAN.

3.2.2 Data Requirements

Specific data types needed to simulate groundwater flow shown in [Figure 3-1](#) are geologic data, hydraulic head data, groundwater recharge estimates, discharge estimates, hydraulic conductivity, and groundwater chemistry data. Geologic data were described in [Section 2.0](#). Hydraulic head data serve as a target to which the flow model is calibrated. Recharge refers to either lateral flow across the CAU-model boundary into the model or recharge that enters from the land surface. Discharge is the lateral flow across the CAU-model boundary out of the model or natural discharge to the surface (e.g., ET, springs, seeps) or wells. The hydraulic conductivity is a measure of the water-transmitting ability of the aquifer system. Hydraulic conductivity may be heterogeneous and vary from location to location within an aquifer unit and vary across geologic units. An understanding of the natural geochemical system may provide constraints on the flow model for the Pahute Mesa CAU. The various data types are described in [Section 4.0](#).

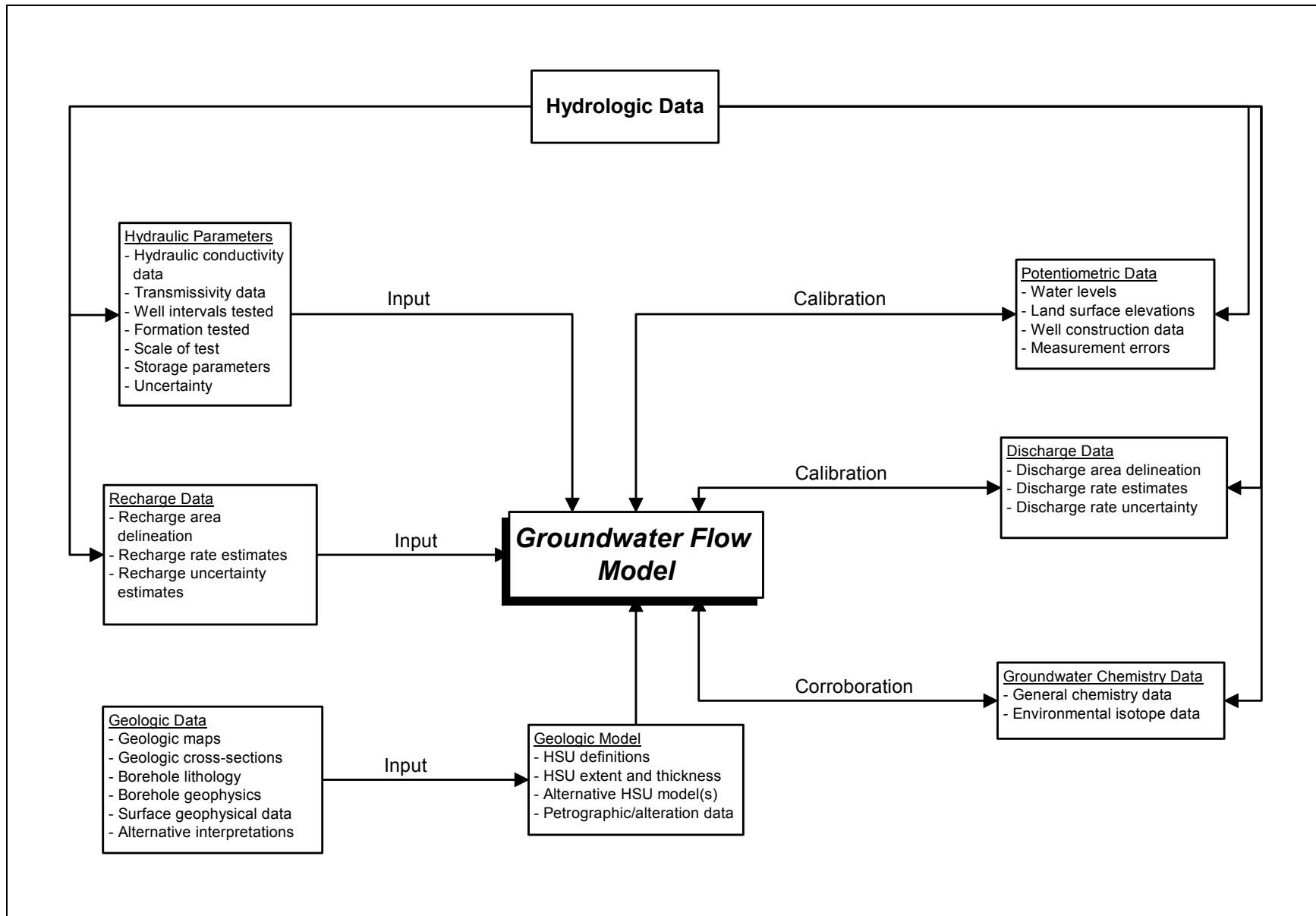


Figure 3-1
Data Types and Utilization in the Groundwater Flow Model

4.0 Data Analysis

Data analysis is the process of compiling, assessing, and interpreting available data in preparation for transport modeling. Data come in a wide variety of types, from a wide variety of sources, and represent a wide variety of scales. The process of analyzing the data can be summarized in the following six steps which are explained below: (1) compilation of existing data in the study area, (2) transfer of applicable data from outside the PM-OV area, (3) assignment of data quality indicators, (4) calculation of the expected values and range of uncertainty, (5) assessment of data scale and likely impacts to the CAU model, as applicable, and (6) discussion of data limitations and the possible impacts to the model.

4.1 Data Compilation/Generation

The compilation of existing data is a multiple step process of identifying existing data, acquiring the data, and compiling the data into structured databases. As will be discussed later, certain data types required for modeling necessitate processing through modeling. Data types of interest and data sources are discussed in the following sections.

4.1.1 Data Types

A general description of the various types of information needed is provided in the following sections. The descriptions are followed by definitions of the hydrologic data types of interest to the CAU models.

4.1.1.1 General Description

Major data types of interest to this report are hydrologic parameters and supporting information.

As stated previously, hydrologic parameters of interest include hydraulic properties, precipitation recharge, discharge to the surface, lateral boundary fluxes, hydraulic heads, and groundwater chemistry. Descriptions of these parameters are provided in [Section 4.1.1.2](#).

The following types of supporting information will be recorded, when applicable and available:

- Site or core information
- Chemical constituent
- Method of data collection or type of test
- Scale of measurement
- Date of data collection
- Stratigraphic unit
- Lithology
- Alteration
- Hydrostratigraphic unit
- Method of data analysis
- Observed parameter value
- Parameter spatial distribution
- Uncertainties
- Any references relating to the data records
- Any noted deficiencies

References to the specific sources of information are provided along with the data. A general description of the data sources is provided in [Section 4.1.2](#).

4.1.1.2 Description of Hydrologic Data Types

Information needed in support of the groundwater flow model include hydraulic properties, precipitation recharge, discharge to the surface, lateral boundary fluxes, hydraulic heads, and groundwater chemistry.

Hydraulic Properties

Hydraulic properties of interest include permeability and storage parameters. Important hydraulic properties include hydraulic conductivity and specific storage coefficient.

The hydraulic conductivity of the geologic units plays a primordial role in the control of groundwater movement. Two data types relating to hydraulic conductivity are required by the model: horizontal hydraulic conductivity and vertical hydraulic conductivity, which is specified in the model as a horizontal to vertical anisotropy ratio. Values of measured hydraulic conductivity will be used in two ways. First, the range of measured values provides an uncertainty range within which the values may be varied during model calibration. Second, the values will be used during the uncertainty analyses to generate realizations that are as realistic as possible.

Specific storage is another property of the geologic units that controls the pattern of groundwater flow, during transient conditions. Transient, or non steady-state, flow conditions are caused when natural or artificial stress is placed on an aquifer.

Precipitation Recharge

Under natural conditions, recharge occurs from precipitation via the unsaturated zone. Recharge is an important component of the hydrologic system. The areal distribution of the recharge affects flow directions. The velocity of groundwater is a function of the amount of recharge entering the flow system. Recharge rates are usually estimated because direct measurements are difficult. Recharge rates may be adjusted during the groundwater flow model calibration. Areal recharge may also be artificially induced by man through irrigation. This type of recharge is very negligible within the area of interest and is, therefore, not accounted for.

Surface Discharge

Under natural conditions, discharge from the groundwater system to the surface occurs by spring flow and by evapotranspiration. Discharge may also be artificially induced by man through well pumping. Natural discharge ranges are used as targets during the flow model calibration process. Well pumping rates may be used to simulate transient conditions.

Lateral Boundary Fluxes

Under natural conditions, subsurface flow occurs across the lateral boundaries of the groundwater flow system. The subsurface inflow and outflow rates are referred to as lateral boundary fluxes. Ranges of lateral boundary fluxes are derived from the NTS regional flow model using several hydrostratigraphic and recharge models to cover the range of uncertainty. Lateral boundary fluxes are used to define model boundary conditions.

Hydraulic Heads

Hydraulic heads are used to define the pressure condition in the aquifer system. They are mostly derived from measured water levels. Land surface elevations at the locations of known regional springs may also be used to approximate hydraulic heads. Existing spring data and water level data measured in wells and boreholes located within the PM-OV area and vicinity were analyzed to derive a hydraulic head dataset. Hydraulic heads for locations inside of the model area are used as targets during the calibration process of the groundwater flow model. Hydraulic heads for locations outside of the model area, but within close proximity, may be used to define model boundary conditions.

Groundwater Chemistry

General groundwater chemistry data and stable/environmental isotope data provide important indications of groundwater recharge, discharge, movement, and storage. Groundwater chemistry data are not incorporated as input in the flow model; rather, interpretations of groundwater chemistry data are used to support calibration of the model. These interpretations can provide an independent check on groundwater flow paths and travel times.

4.1.2 Data Sources

A great many sources for the data have been identified. In many cases, existing databases developed as part of the NTS regional groundwater flow and transport Modeling (DOE/NV, 1997) were used as starting points. These data were supplemented with new data collected as part of ongoing UGTA field investigations and existing data not previously identified.

Data for the Pahute Mesa Area come from numerous organizations including BN, LLNL, LANL, DRI, USGS, Shaw, and the University of Nevada, Las Vegas-Harry Reid Center for Environmental Studies.

Historic data are available in many publications. Typically, much of the data has been compiled during the preparation of the CAIP, but these data need to be supplemented with new data and newly-identified existing data.

Site-Specific Data

Site-specific data refers to data collected within, or near, the boundaries of the CAU study area which is defined as the PM-OV area (Figure 1-2). These are directly applicable to the HSUs within the study area.

Yucca Mountain Data

Yucca Mountain is the proposed geologic storage location for commercial high level waste in the United States. A great deal of high-quality data has been collected and analyzed during investigations of the Yucca Mountain Site. The YMP is located adjacent to the southern edge of the study area. The geology in the YMP region is similar to Pahute Mesa, but not exactly the same. A process was developed to assess the transferability of YMP data for use in the Pahute Mesa CAU model.

Other Data

In some cases, the data from much more distant sites may be used to estimate parameter values. Data from distant sites will only be used in cases where the data from the study area or the YMP site are non-existent or are very limited. As with the YMP data, the transferability of all data will be assessed prior to use in the Pahute Mesa Model.

4.2 Data Transfer Methodology

It has been proposed that using data from other sites to reduce flow and transport parameter uncertainty is an appropriate approach when developing models in a sparse data environment (Freeze et al., 1990), such as that of the PM-OV area. This type of approach incorporates flow and transport parameter data from investigations of similar environments for parameters to be used in modeling of the study area. Note that hydraulic properties are the only hydrologic data types that may be eligible for data transfer. Utilization of data from other sites can be both a cost-effective and necessary step for a modeling effort in a sparse data

environment. Nearby sites considered as sources of additional data for the Pahute Mesa CAUs are other UGTA CAUs and Yucca Mountain which constitutes the most important source. Rock genesis and evolution factors that influence flow and transport parameters, the general transfer methodology, and the case of YMP data transfer are described in this section.

4.2.1 Rock Genesis and Evolution Factors Influencing Flow and Transport Parameters

Numerous factors may influence the flow and transport of groundwater in the subsurface environment in a variety of ways. This section focuses on rock genesis and evolution factors which influence rock characteristics and, therefore, flow and transport parameters. These factors include the overall geologic history of the area, lithology, alteration, stress history, and groundwater chemical composition.

Geologic History

The geologic history of an area has a significant impact on the flow and transport of groundwater. For example, the depositional environment of a rock can influence things such as the primary porosity of sedimentary rocks or the texture of volcanic rocks. In addition, subsequent structural episodes may increase faulting in a given area that could lead to increase in groundwater flow.

Lithology

The specific rock type of a study area has an important impact on the flow and transport of groundwater. Alluvial materials ranging in texture from fine sand to coarse gravels that are well sorted would obviously have different hydraulic properties than an indurated, non-fractured carbonate rock.

Alteration

The alteration of a given rock can play a large factor in the flow and transport of groundwater in the subsurface environment. For example, the formation of zeolitic material in volcanic tuffs can greatly decrease the permeability of a given formation by directly effecting the fracture geometry.

Stress History

The stress history of a given area has a large impact on the flow and transport of groundwater in the subsurface environment. Stress can influence a variety of things such as fracture orientation, aperture distribution, and fracture connectivity. For example, regions of extensional stress tend to form fractures that are open to flow and would tend to increase groundwater movement.

Groundwater Chemical Composition

Groundwater chemistry can play an important role in the flow and transport of groundwater. It can have a large impact on everything from mineral dissolution and precipitation reactions to fracture geometry. For example, mineral

precipitation or dissolution reactions within fractures can cause a reduction in permeability from filling fractures with minerals, or it can cause an enhancement of permeability due to dissolution of flow channels.

4.2.2 General Transfer Methodology

The use of flow and transport data from other study areas to develop parameter distributions for flow and transport modeling of UGTA CAUs can be justified by examining specific similarities that may exist between various investigation areas. It must be shown that there is a sufficient similarity that exists between the two areas, taking into account the various factors mentioned in the previous subsection. A general approach for the transfer of data from one area to another may be accomplished using the following strategy:

- For each parameter of interest, sites need to be identified that may contain data of the same type. Under ideal conditions, sites could be found in the same general area that have roughly the same geologic setting. More likely, however, sites will be identified that are located much farther away but have similar types of rocks. Under less desirable conditions, data may have to be transferred from locations that have no similarities at all to the original study area other than data was collected there for the specific parameter of interest.
- Once the source of the flow and transport parameter data are identified, the factors affecting the specific parameter need to be clarified. If it can be shown that only one factor influences a given parameter, it may make the transfer of data easier to justify. For example, if it can be shown that a parameter is only influenced by lithology, then a comparison of the lithologies of the two HSUs involved in the data transfer would suffice to make a decision.
- Finally, if sufficient data are present in the original study area, a statistical comparison can be made of the data from the other area to see if the two datasets are comparable. If it can be shown that the two datasets have comparable distributions, it would provide further justification for the incorporation of the data into the existing dataset.

4.2.3 YMP Data Transfer

The Yucca Mountain Site Characterization Project has implemented one of the largest hydrologic and geologic characterization studies of volcanic rocks ever conducted. The proximity and similar hydrogeologic environment of the Yucca Mountain Site to Pahute Mesa make it particularly attractive as a source of potential data for the UGTA modeling effort. A detailed rationale for the transfer of data from the YMP is provided in [Appendix B](#); however, a brief summary is presented here:

- Both areas are located in the SWNVE.
- Volcanic rocks in both areas are the result of similar depositional processes.
- Both areas contain similar lithologic units and even lithologic units from the same source area.
- Both areas have experienced similar types of alteration including devitrification and zeolitization of volcanic material.
- Both areas have undergone similar types of regional tectonic stresses resulting in a similarity in the two areas regional fracture orientations.
- Both have similar groundwater chemistry.

As a result of the two areas similarities, the use of flow and transport parameter data from the Yucca Mountain area can be justified in helping to develop parameter distributions for the PM-OV modeling effort. Note that the data are actually transferred on an HSU by HSU basis. In others words, data for a given parameter are transferred only between HSUs that have relevant similar characteristics.

4.3 Data Documentation Qualification

Data documentation provides information on the traceability (or pedigree) of the data. Typically, data collected in the recent past has much better documentation than data collected and reported many years ago. The qualification of the documentation of the data makes it easier to investigate and evaluate the quality of the data being compiled in the model.

Each data record of a given dataset was assigned a DDE_F to indicate the level of documentation available for that data record. This process of data qualification ensures that the pedigree of the data is retained for data users. However, it is important to note the data qualification does not indicate the usefulness of data for Pahute Mesa transport modeling. Historic data, while often poorly documented by today's standards, are often of high quality and extremely useful in the CAU investigations.

The five levels of data documentation evaluation flags are as follows:

Level 1

Data are collected in accordance with NNSA/NSO ERP quality assurance project plans (QAPPs), approved State of Nevada procedures, and/or participant-specific procedures. This ranking indicates that all supporting documentation for the data is on file and available for review by data users.

Level 2

Data are collected in accordance with approved plans and procedures as required for Level 1 with the exception that one or more documentation requirements may be deficient in some way. Examples of data documentation deficiencies may include lost or destroyed field-data collection forms or data acquired using interim or draft procedures.

Level 3

Data are collected using accepted scientific methodology (e.g., ASTM, U.S. Environmental Protection Agency [EPA] methods, USGS procedures) and accompanied by supporting and corroborative documentation such as testing apparatus diagrams, field or laboratory notes, and procedures.

Level 4

Data are collected by a participating NNSA/NSO ERP organization or another organization not associated with the NNSA/NSO ERP prior to the issuance and implementation of project-approved standard policies, procedures, or practices governing data acquisition and qualification. The methods of data collection are documented and traceable; however, the validity of data use or compliance with reference procedures is indeterminate. Supporting documentation may or may not exist.

Level 5

Data are obtained under unknown, undesirable, or uncertain conditions. When data documentation is unknown, any available supporting or helpful descriptions of the intended use and conditions of data capture should be described.

4.4 Data Qualification

The data qualification process varies depending on the type of parameter. The criteria used to evaluate the different types of required data are dependent on the type and the intended use of the data. Thus, various criteria are used to assess data quality. The general procedure includes assigning one or more data quality evaluation flags (DQE_F) to each record or group of records compiled in the dataset, indicating the data quality or suitability of the individual data record for the intended usage. The data quality evaluation flags and their definitions depend on the data type. Data-type specific quality evaluation procedures are described in the corresponding section of this document.

4.5 Analysis Methods Used

Methods of analysis used vary depending on the type of hydrologic data considered. See approach subsections of the analysis sections for the specific methods used.

4.6 Data Analysis Limitations

Data limitations need to be identified. These limitations may be related to the level of data documentation, the data collection method, the data analysis method, or other factors that may limit confidence in the values. Within the discussion of each dataset, data limitations will be noted.

5.0 Hydraulic Parameters

Hydraulic parameters play a vital role in simulating groundwater movement. Specifically, hydraulic conductivity and related parameters such as transmissivity and anisotropy are the most often used parameters in groundwater modeling. The storage coefficient is another hydraulic parameter of interest because it is needed for transient simulations of groundwater flow. The assessment of hydraulic parameter data presented in this section fulfills several project needs. First, the dataset used for this task serves as a repository of hydraulic parameter data for the Central and Western Pahute Mesa CAU. Second, this assessment provides a range of hydraulic conductivities and specific storage coefficients for the major HSUs in the Central and Western Pahute Mesa CAU. The objectives and approach are presented and finally, the assessment provides an evaluation of the relationship of hydraulic properties with depth and scale of measurement.

5.1 Objectives

The specific objectives of this hydraulic parameter assessment include the following:

- Compile and evaluate available hydraulic conductivity and specific storage coefficient data suitable for use in the Central and Western Pahute Mesa CAU.
- Define the ranges of hydraulic conductivity and storage coefficient for the major HSUs.
- Assess the relationship of hydraulic conductivity with depth.
- Assess the relationship of hydraulic conductivity with scale of measurement.

5.2 Approach

This section summarizes the strategies and methods used during the assessment of the hydraulic parameter dataset for the Central and Western Pahute Mesa CAU. The following approach was used to define ranges of hydraulic conductivity and storage coefficients for the major HSUs in the Central and Western Pahute Mesa CAU.

- Hydraulic parameter data were compiled from published and unpublished sources. Additional information associated with each entry included the location, tested interval top and bottom, type of test, method of analysis, hydrostratigraphic unit or units corresponding to the tested interval, and the source of the information.
- In fractured rock materials present within the Pahute Mesa CAU model, three types of hydraulic conductivities can be defined. The three types are fracture hydraulic conductivity, matrix hydraulic conductivity, and bulk hydraulic conductivity. Fracture hydraulic conductivity, as the name clearly define, is the conductivity of the fractures themselves. In nearly all cases, the matrix between the fractures is also permeable and can be defined by its matrix hydraulic conductivity. Finally, a measurement over a region made up of both fractures and matrix is termed the bulk hydraulic conductivity.
- The hydraulic conductivity (and transmissivity) data were separated into three data sets on the basis of the scale of the measurement. The three data sets comprised laboratory, slug-test, and constant-rate test scale data. Laboratory-scale data are generally obtained from measurements of hydraulic conductivity of intact core samples that have been taken to a laboratory for analysis. The cores are generally selected to be nonfractured portions of the aquifer, thus, laboratory measurements most often measure matrix hydraulic conductivity. The scale of these measurements is generally limited to the size of the core. The slug-test scale data are collected by means of short duration aquifer tests in boreholes. These types of tests often use small volumes of water. Although the length of the tested interval may be large (up to several hundred meters), the lateral investigation into the formation is probably quite small. Lastly, the constant-rate test data represent data collected during or after pumping and injection tests. These tests are often conducted over the same, or larger, depth intervals as the slug tests, but because of the longer duration, the volume of formation tested is expected to be larger. The slug and constant-rate scale tests typically measure the bulk hydraulic conductivity.
- Within each scale-dependent data set, the data were further subdivided by hydrostratigraphic unit. In many cases, more than one interpretation of each test is available. Prior to further analysis, multiple interpretations of a single test interval were arithmetically averaged. For each set of multiple interpretations, a mean and standard deviation was determined. This provides an estimate of measurement and interpretation error.
- After multiple interpretations were removed, the resulting data sets were transformed to log base 10, then statistically analyzed to determine mean, standard deviation, and correspondence to a log normal probability distribution. The resulting data are displayed graphically and in tables.
- The storage coefficient data were screened to identify values from multi-well aquifer tests.

5.3 Data Types and Prioritization

The main hydraulic parameters of interest are transmissivity which is a primary calibration parameter in the groundwater flow model and storage coefficient which is a key parameter in transient simulations. Transmissivity is the product of the hydraulic conductivity and the saturated aquifer thickness. Transmissivity is the only hydraulic parameter needed to simulate groundwater flow under steady-state conditions. The thickness of each hydrostratigraphic unit is determined from the geologic model of the Central and Western Pahute Mesa area. To modify the transmissivity during calibration, the hydraulic conductivity must be varied because the thickness of the hydrostratigraphic unit is fixed by the geologic model. As a result, the calibration parameter for the flow model becomes the hydraulic conductivity. The storage coefficient which is used in transient simulations is also of interest. Specific data types needed and their prioritization are discussed in the following sections.

5.3.1 Data Types

Data categories needed for the hydraulic parameter data analysis include site information, well construction data, hydrostratigraphic information, and hydrologic test information. These data are stored in the Pahute Mesa CAU database and include the following data types:

Site Information

- Reporting name
- Site location
- Land surface elevation

Test Interval Information

- Top and bottom elevations of the tested interval
- Stratigraphic unit for the test interval
- Hydrostratigraphic unit designation

Hydraulic Test Information

- Pumping rate
- Pumping duration
- Test start date
- Data availability flag

Test Interpretation Information

- Method of analysis
- Organization performing the analysis
- Hydraulic conductivity
- Transmissivity
- Storage coefficient

- Data documentation evaluation flag (DDE_F)
- Data quality evaluation flag (DQE_F)

Most of these categories are self-explanatory except for the data quality identifiers to be described later in this document.

5.3.2 Data Prioritization

The values of hydraulic conductivity and storage coefficient are the variables that are prioritized for uncertainty evaluation. These two hydraulic properties were selected because they constitute essential building blocks of the groundwater flow model. Both hydraulic properties are derived from hydraulic response measurements collected during single or multiple-well hydraulic tests. Hydraulic conductivity may, however, also be derived from core testing in the laboratory.

5.4 Data Compilation and Evaluation

The transmissivity and hydraulic conductivity data were compiled from interpretations of aquifer tests, packer tests, specific capacity, flow logs, or laboratory analyses. The storage coefficient was also recorded when available. It is generally accepted that relevant storage coefficients are those obtained from multiple-well aquifer tests only. Fortunately, several such tests have been conducted in and around the NTS. These provide a range of storage coefficients applicable to the study area. Additionally, historical well testing data considered to be relevant to the Pahute Mesa CAU were reanalyzed.

5.4.1 Existing Data

Hydraulic property data were obtained from published and unpublished sources. Published data were obtained from reports of the USGS, Sandia National Laboratories, LANL, and LLNL. The publications often included raw or reduced drawdown and recovery data and corresponding interpretations. Specific references are noted in the text, where appropriate. Having the drawdown or recovery data available was important for assessing the adequacy of the interpretation and for assigning data confidence identifiers. Unpublished data and interpretations were obtained from the USGS, DRI, and data collected by the ER Contractor as part of the ERP. Unpublished hydraulic testing documentation generally contains only preliminary interpretations.

5.4.2 Historical Well Testing Data Reanalysis

One step in the interpretation of the hydraulic conductivity data is the reanalysis of historical well testing data (see [Appendix C](#)). Such data were collected prior to the UGTA Project and include aquifer and slug tests conducted in wells located on the NTS.

As presented in Winograd and Thordarson (1975), many of the aquifer tests conducted on the NTS showed a characteristic three-slope drawdown response with an early rapid drawdown, an intermediate period of slowly increasing drawdown, followed at the end by a steepening of the curve. These responses can be explained by a combination of well bore storage effects and boundary influences. Moench (1984) presented a solution of aquifer response from fractured aquifers with dual-porosity and well-bore storage effects that contains the same three-slope response as has been observed. These aquifer tests were, therefore, reevaluated using the Moench solution. It is important to note that correspondence to a solution does not necessarily indicate the solution correctly represents reality. Rather, the reinterpretation provides another means to assess measurement and interpretation uncertainty.

A large number of slug tests using packers were conducted in the 1960s on the volcanic rocks of Pahute Mesa. Multiple tests were run over a series of short intervals along deep open boreholes to evaluate the variation of hydraulic conductivity in the rocks. The tests were originally interpreted using a proprietary method (Blankennagel, 1967) that yielded information on relative hydraulic conductivity between different test intervals. These tests were reanalyzed using slug test models to calculate the actual values of hydraulic conductivity. A total of 261 tests were reanalyzed. The details of the analysis are presented in [Appendix C](#). In the appendix, the interpreted values are presented for several different theoretical models. In most cases, the average of the multiple methods was used in the analyses of all slug test data. In addition, only interpretations of injection tests given by good or fair fits to the data were retained for these analysis.

5.4.3 Data Evaluation

The hydraulic parameter dataset was evaluated for quality of documentation and quality of data for the intended use.

Data Documentation Evaluation

Documentation of the primary prioritized variable (i.e., hydraulic conductivity) was evaluated, and flags were assigned in accordance with data documentation requirements described in [Section 4.0](#). No Level 1 data were noted in the database; therefore, the following defined levels of documentation were assigned to the hydraulic conductivity data:

- Level 2: Data collected in accordance with approved plans and procedures, except that documentation may be deficient, such as data acquired using interim or draft procedures.
- Level 3: Data are collected using accepted scientific methodology (e.g., ASTM Methods, EPA methods, USGS procedures) and accompanied by supporting or corroborative documentation such as testing apparatus diagrams, field or laboratory notes, and procedures.

- Level 4: Data collected by a participating NNSA/NSO ERP organization or another organization not associated with the NNSA/NSO ERP prior to the issuance and implementation of project-approved standard policies, procedures, or practices governing data acquisition and qualification. The methods of data collection are documented and traceable; however, the validity of the data or compliance with referenced procedures is indeterminate. Supporting documentation may or may not exist.
- Level 5: Data are obtained under unknown, undesirable, or uncertain conditions.

Data Quality Evaluation

In addition to the DDE_F which is used to rank the level of documentation, a DQE_F was assigned to qualitatively rank the reported or calculated values of transmissivity or hydraulic conductivity in terms of their usefulness for the intended use. For purposes of modeling groundwater flow in the mostly fractured PM-OV domain, the scale of the data is the most important factor in assessing data quality. Data quality flags were, therefore, assigned based on the scale of the tests as follows:

- The flow data derived from constant-rate tests are considered to be the most reliable and were assigned a "High" quality flag.
- The flow data derived from slug tests are representative of smaller volumes of the tested aquifers and were assigned a "Medium" quality flag.
- The laboratory-scale data may provide data that may be applicable to porous formations, but are not appropriate for any HSU that is dominated by fractures. They were, therefore, assigned a "Low" quality flag.

5.5 Analysis of Hydraulic Conductivity Data

Analysis included evaluations of the spatial distribution of data points, data transferability, laboratory-scale data, slug test data, constant-rate scale data, scaling and spatial variability, vertical anisotropy, and the alteration of hydraulic conductivity in test cavities. Hydraulic conductivity parameters for each HSU are presented at the end of this section. All hydraulic conductivities are in m/d.

5.5.1 Spatial Distribution of Data Points

Figure 5-1 is a map showing the locations of the wells and boreholes from which hydraulic conductivity data were obtained. The locations are coded by the scale of the measurement. In some cases, more than one scale of measurement is available at a single location. The data are not uniformly distributed, rather the data are clustered in several locations such as on Pahute Mesa, near Oasis Valley, and near

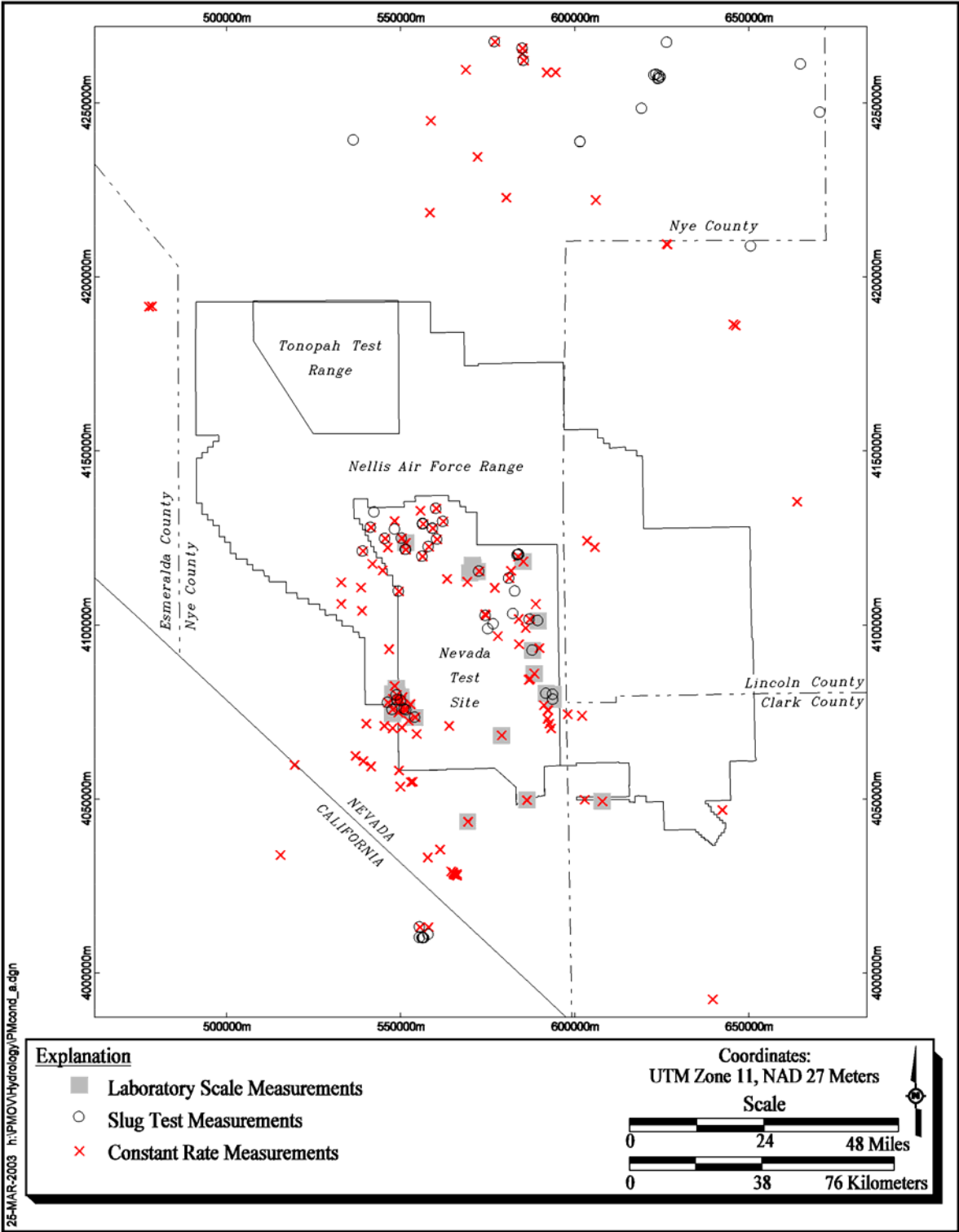


Figure 5-1
Map of the Locations of Hydraulic Conductivity Data

Yucca Mountain. The remaining data are scattered about the CAU and NTS region.

5.5.2 Data Transferability

Not all of the data utilized in the assessment of aquifer properties were collected from within the Pahute Mesa model area. A large portion of the data outside the Pahute Mesa model area were obtained from the YMP, located just south of the study area boundary. Justification of the use of YMP data has been provided in [Section 4.2.3](#) and [Appendix B](#).

Several regional-scale hydrostratigraphic units were sparsely represented by data within the Pahute Mesa model area. These were the alluvial aquifer, the carbonate aquifers (regional [LCA] and on thrust sheets [LCA3]), and clastic confining units including the Eleana Formation and Chainman Shale. The datasets for these regional scale units are substantially similar to the datasets utilized as part of the regional groundwater flow model (DOE/NV, 1997 and IT, 1996b).

The regional model provides constraints on the boundary conditions of the Pahute Mesa CAU model. The parameter distributions established in this work are similar to those of the regional model. This consistency is necessary to provide continuity between the two models. Additionally, with the exception of the alluvial aquifer, the regional units have little influence over the flow and particle tracking from underground tests on Pahute Mesa. This is documented in the screening analysis presented in [Appendix A, Section A.3.0](#). Several alternatives involving different configurations of the regional carbonate and clastic units were shown to produce only small changes in the expected transport of radionuclides from Pahute Mesa. The analysis of the hydraulic properties of the regional carbonate and clastic units will be sufficient to ensure consistency among the models and has been shown to have little influence on the predicted radionuclide migration.

The alluvial aquifer information was also obtained from a variety of areas located outside of the Pahute Mesa region. Nearly all the data were obtained from alluvial basins in southern Nevada. Most of those basins have descriptions similar to the one provided by Bechtel Nevada (2002) for the Pahute Mesa model area:

"Lithologically, the unit [alluvial aquifer] is generally composed of poorly sorted, moderately to poorly bedded, unconsolidated to moderately indurated, angular to rounded, sand and gravel in a locally tuffaceous matrix."

5.5.3 Laboratory-Scale Data

Laboratory-scale data are available for 44 locations, nearly all of which are outside the Pahute Mesa model boundary. As a result, the data are subdivided on the basis of the regional model HSUs. [Figure 5-2](#) is a plot of the laboratory-scale hydraulic conductivity value as a function of depth for six HSUs, the alluvial aquifer (AA), LCA, LCCU, volcanic confining unit (VCU), volcanic aquifer (VA) and VU.

Several key features are visible in [Figure 5-2](#). As a group, the AA data are clustered between log K values of -2 and 1, at depths less than 300 m (900 ft). With a few exceptions, the LCA data are deeper and span a range from -7 to -2. The LCCU data are also deep, but with distinctly smaller log 10 K values than the LCA. The VA and VCU data span very similar ranges of values.

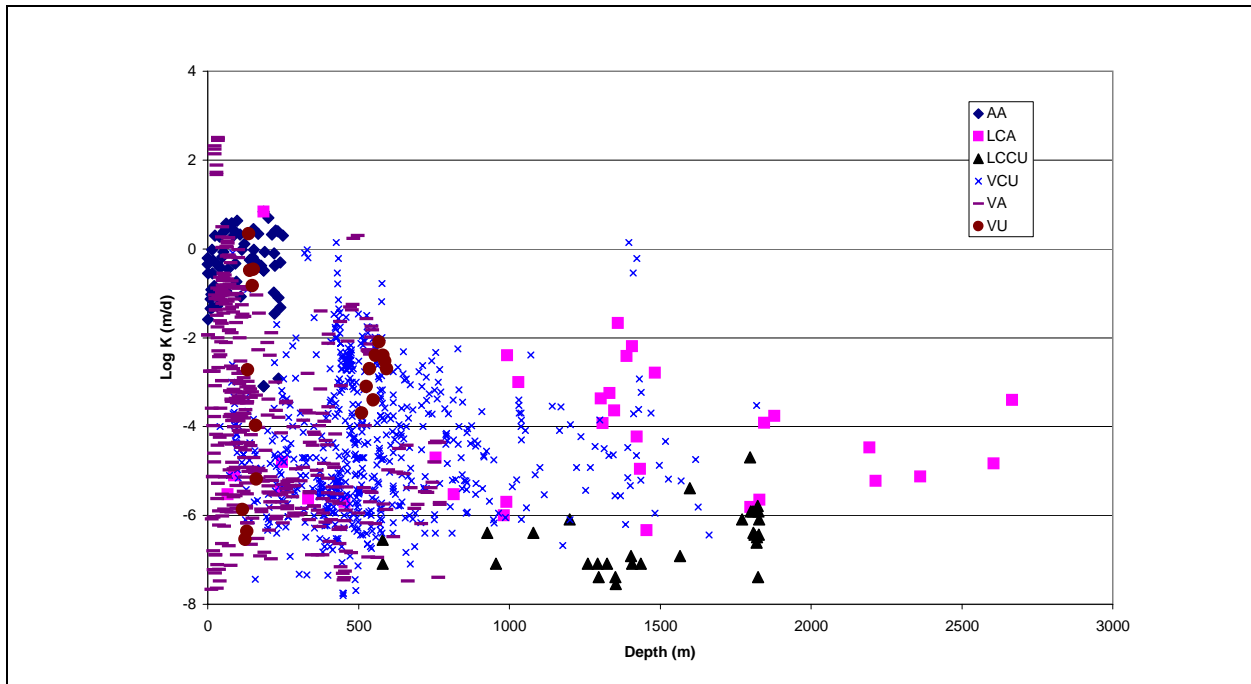


Figure 5-2
Laboratory-Scale Hydraulic Conductivity as a Function of Depth and HSU

When viewed on a per HSU basis, there does not appear to be any depth dependency of the laboratory measured K values. This is not surprising because the measurements are made at low-confining stress. In addition, the cores used for laboratory-scale measurements represent the less fractured portions of the formations (Winograd and Thordarson, 1975; Lahoud et al, 1984). Most rock compression at depth comes from closing of fractures, but the cores represent the predominantly unfractured portion of the formations. The porous units, the AA and perhaps the VU, might be viewed differently. The range of values for the AA in [Figure 5-2](#) is considered a reasonable indicator of the range of values to be expected. The data for the VCU are probably only useful for defining a broad range of possible values. This is primarily because the laboratory-scale K value is going to be most influenced by the lithology of the sample. The VCU is not a homogeneous unit and in fact contains small proportions of aquifer lithologies. The observed wide range of values is an indicator of the variability within the broad designation of VCU.

[Table 5-1](#) is a summary of the log 10 K values of the six HSUs with respect to mean, standard deviation, and whether the data fit a log normal distribution. To test for log normality, a Kolmogorov-Smirnov (K-S) test (Benjamin and

Cornell, 1970) was applied at the 5 percent level of significance to the cumulative frequency distribution (cdf). Both the VA and VCU are rejected as log normal at the 5 percent level. These two HSUs encompass a broad range of overlapping lithologies. It is quite likely that the core scale hydraulic conductivity distributions in the VA and VCU are multimodal on the basis of lithology. Therefore, the broad regional HSUs of VA and VCU defined on the predominance of lithology (VA has more aquifer lithology and VCU more confining lithology) yield overlapping ranges of core scale hydraulic conductivity.

Table 5-1
Statistics of Laboratory-Scale Hydraulic Conductivity^a Data

Hydrostratigraphic Unit	Number of Data Points	Log 10 Mean of Hydraulic Conductivity	Log 10 Standard Deviation of Hydraulic Conductivity	Accept Log Normality at the 5% Level
AA	66	-0.4	0.8	Yes
LCA	33	-4.2	1.6	Yes
LCCU	30	-6.6	0.7	Yes
VA	400	-3.8	2.2	No
VCU	639	-4.4	1.5	No
VU	19	-3.0	2.0	Yes

^a Hydraulic conductivity is in m/d.

An estimate of the range of uncertainty in the log normal parameters can be determined from the K-S test statistic. The K-S statistic, D , is a measure of the maximum difference, in probability space, between the data cdf and the assumed theoretical cumulative density function (cdf). For example, consider the AA data plotted in Figure 5-3. The cdf data are shown by the diamonds and the log normal cdf is given by the dashed line. In this case, the largest difference is 0.11 while the K-S statistic at the 0.05 level of significance for 66 data points is approximately 0.167. Because the observed difference is less than the test statistic, the assumption of log normality is not rejected. As the level of significance is increased, the magnitude of the test statistic decreases. In this case, the test statistic at the 20 percent level of significance is 0.132 and the null hypothesis is again not rejected. If one continues in this manner, a level of significance will be reached where the test statistic equals the observed difference; this represents the smallest value of D for which the null hypothesis is not rejected. Thus, if the observed difference, 0.11 in the case of AA, is used to construct upper and lower bounding curves, the curves represent the smallest region of uncertainty for which the log normal cdf is not rejected. In Figure 5-3, the K-S bounds represent the smallest region that does not reject the null hypothesis based on $D = 0.11$. One point of clarification with respect to Figure 5-3 needs to be made. A difference exists between how the K-S test is applied (at frequency i/n) and how a typical normal probability plot is constructed (with frequency $i/(n+1)$). Therefore, the data cdf and the K-S bounds will not match precisely, especially for small datasets.

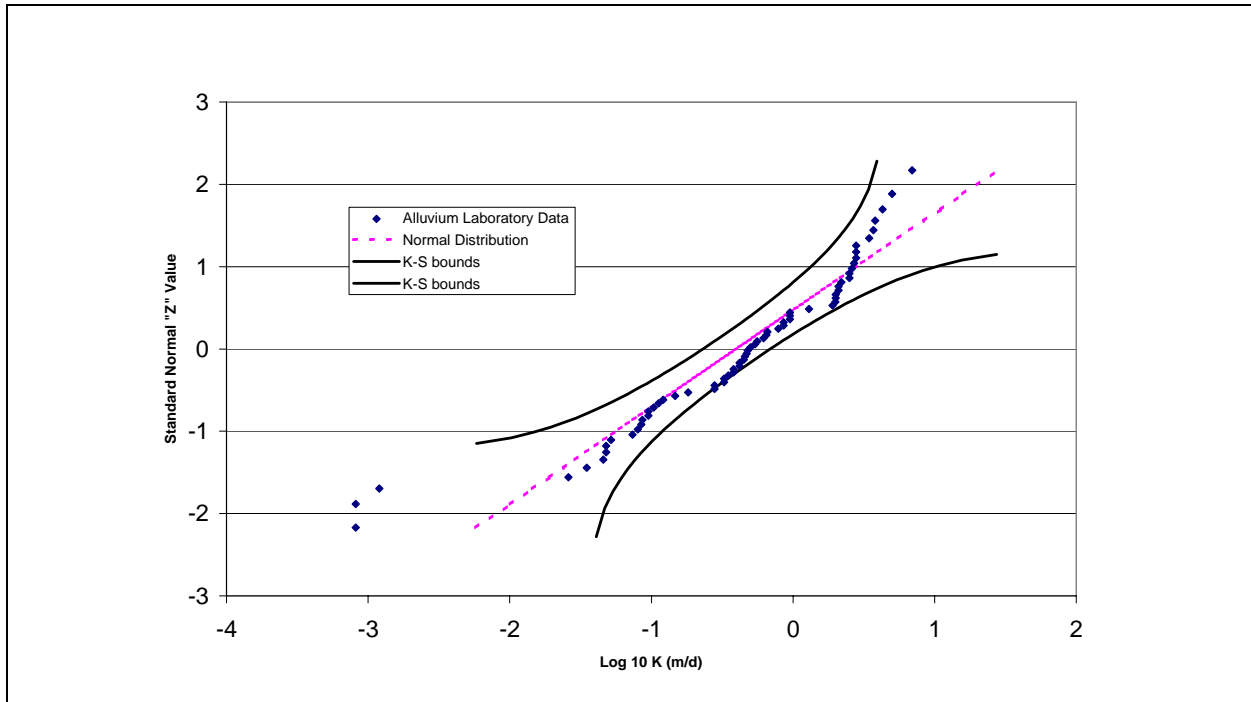


Figure 5-3
Alluvium Laboratory Hydraulic Conductivity Probability Distribution

Within the K-S bounds on [Figure 5-3](#), it is possible to observe the range of parameters describing the log normal cdf. If one holds the standard deviation fixed (i.e., holding the slope constant in the figure), the mean could shift from -0.2 to -0.6 and remain within the bounds. Similarly, if the mean is held fixed, but the slope of the cdf is varied within the bounds, the standard deviation varies between 0.5 and 1.3 . The two ranges cannot be adjusted simultaneously to their limits, or the model would no longer remain within the K-S bounds.

[Figures 5-4](#) through [5-8](#) are plots of the cumulative frequency, theoretical cdf, and the K-S bounds for the LCA, LCCU, VA, VCU, and VU HSUs, respectively. Recall that in each case, the K-S bounds represent the smallest region within which the hypothesis of log normality is not rejected. This applies to the VA and VCU data if one recognizes that the level of significance is less than 1 percent in the VCU case and much less than 1 percent for the VA. If we choose to describe the VA data by a log normal distribution, as in [Figure 5-6](#), the range in the mean will be larger than one order of magnitude. This exercise serves to point out the parameters describing a cumulative density function are themselves uncertain. Thus, the range of parameter values is not constrained by the single log normal distribution fit to the observed data.

5.5.4 Slug Test Data

A large number of hydraulic conductivity values were obtained by methods that have been lumped into the general category of slug tests. The types of tests in this

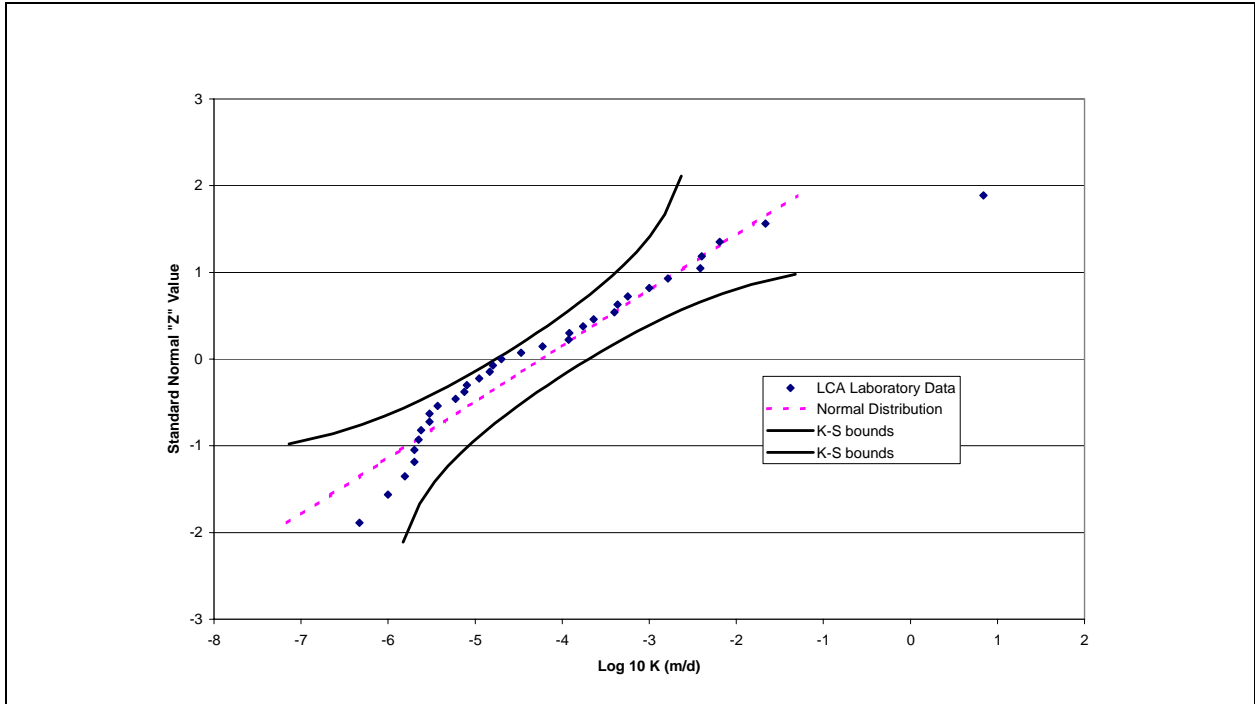


Figure 5-4
Lower Carbonate Aquifer Laboratory Hydraulic Conductivity Probability Distribution

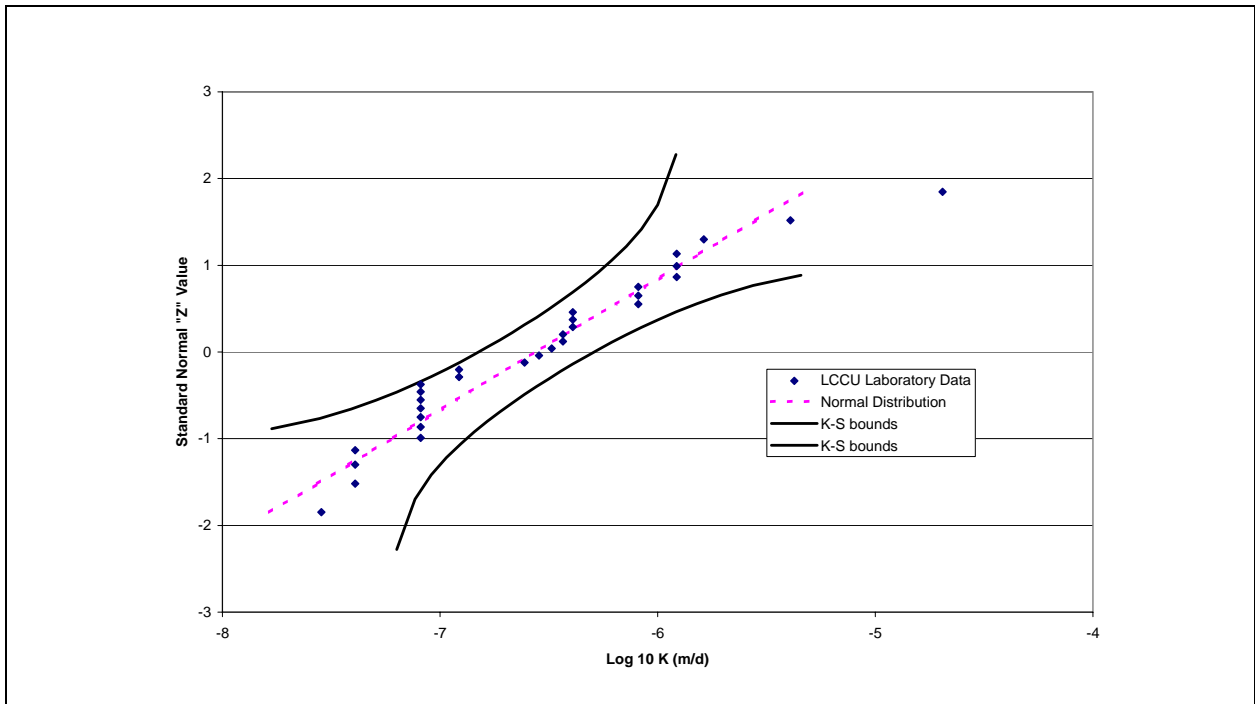


Figure 5-5
Lower Clastic Confining Unit Laboratory Hydraulic Conductivity Probability Distribution

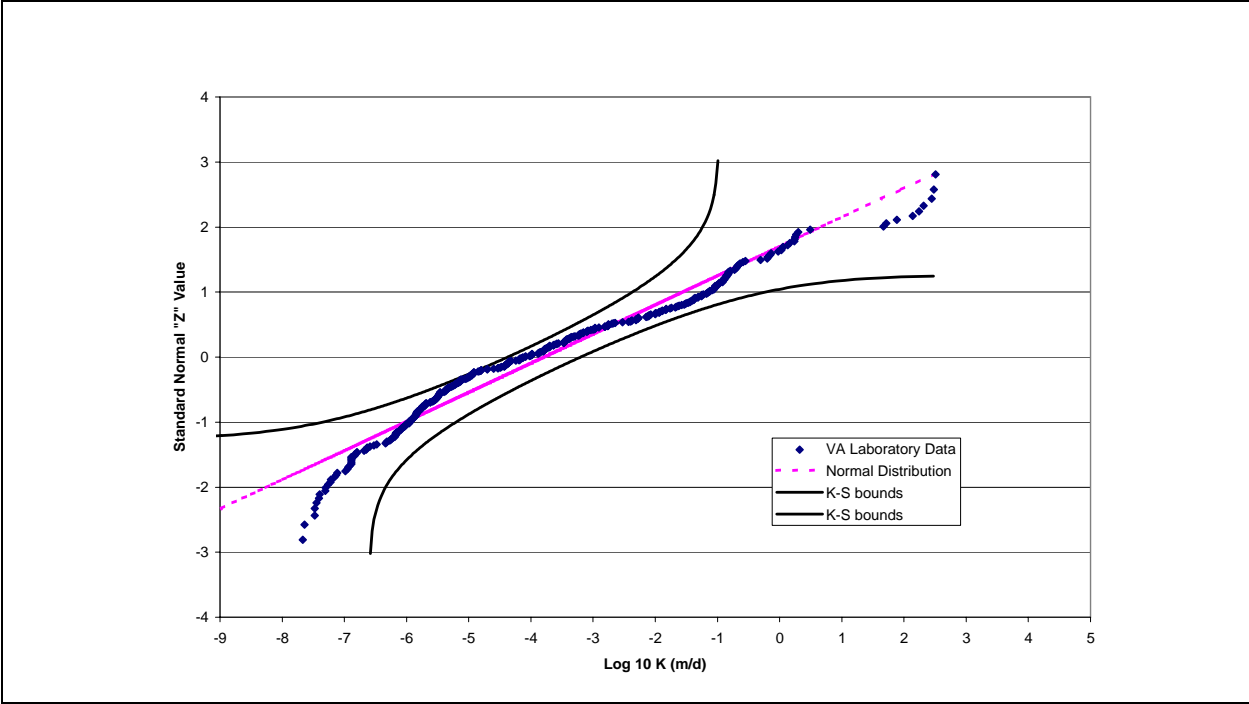


Figure 5-6
Volcanic Aquifer Laboratory Hydraulic Conductivity Probability Distribution

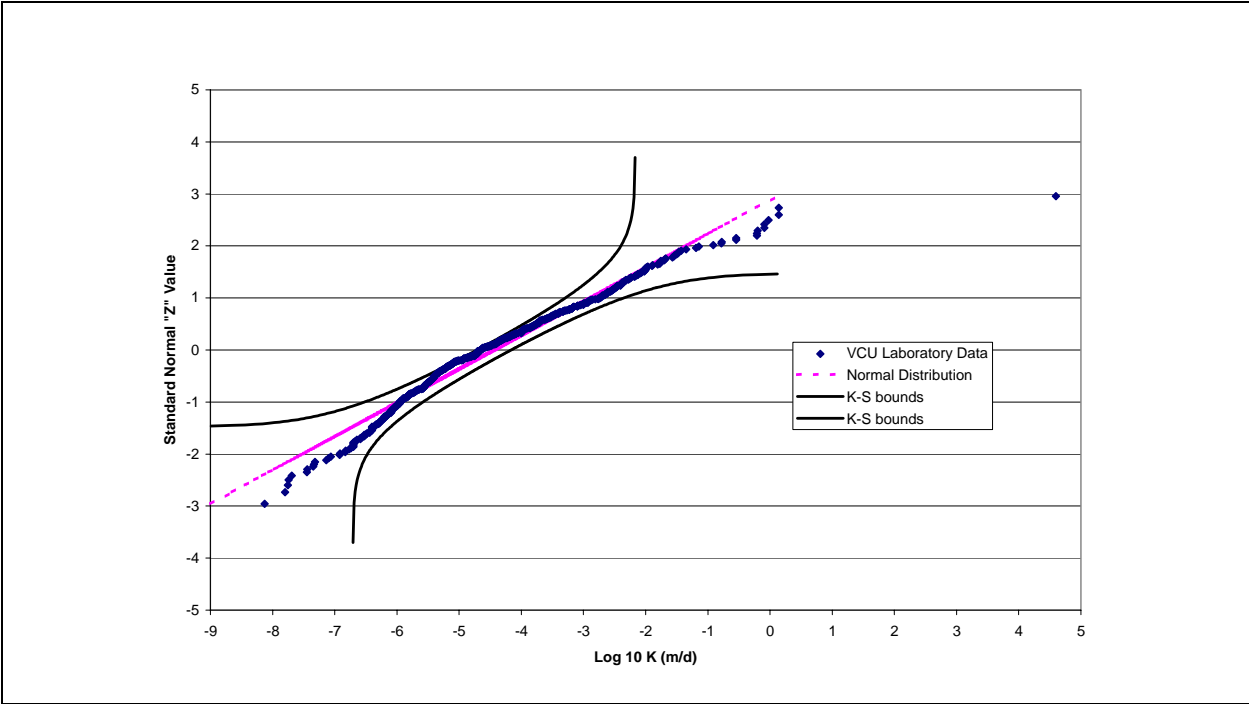


Figure 5-7
Volcanic Confining Units Laboratory Hydraulic Conductivity Probability Distribution

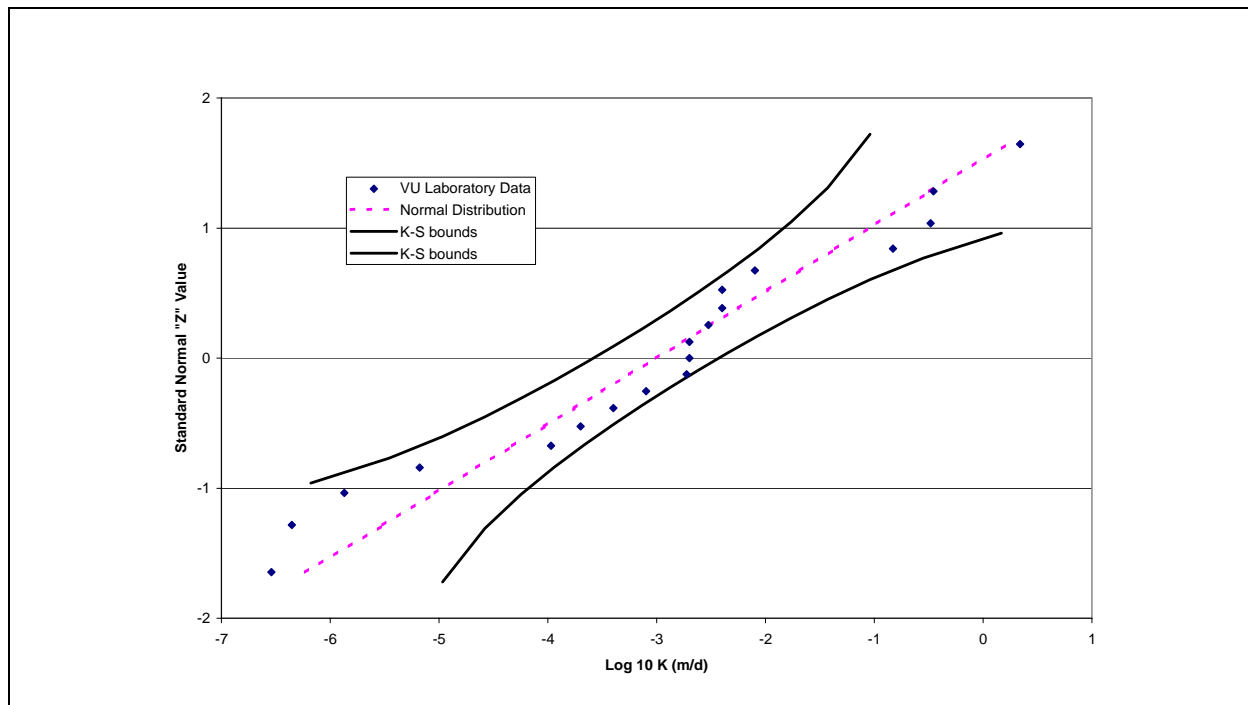


Figure 5-8
Volcanics Undifferentiated Laboratory Hydraulic Conductivity Probability Distribution

category include bailing recovery, drill-stem test, falling-head slug test, packer-injection test, pressure-injection test, slug-injection test, slug-withdrawal test, and swabbing- recovery test. Each of these tests is of relatively short duration with smaller volumes of water than would be typical for a constant-rate test. Therefore, hydraulic conductivity values derived from slug tests represent a smaller volume of the tested formation than either-single well or multiwell constant-rate aquifer tests.

One feature of the slug-scale data that is not part of the laboratory-scale data is multiple interpretations of the same test. For example, a packer-injection test may be interpreted using a variety of theoretical models. Each model may produce a different value of hydraulic conductivity. When multiple interpretations were available, the hydraulic conductivity values were arithmetically averaged prior to conversion to log 10 space. The standard deviation of the multiple measurements was calculated, then converted to log 10 for comparison to the log 10 standard deviation of the entire distribution. Of the 84 tests with multiple measurements, the log 10 standard deviation ranged from 0 to 2.1, with 80 percent of the values less than 0.5. The median standard deviation is 0.25. Four or less multiple interpretations were provided for 76 of the 84 tests. For these small sample sizes, the 95 percent confidence interval about the mean based on a student's t-test ranges from +/- 1.4 times the standard deviation to 3.0 times the standard deviation for the number of multiple interpretations ranging from 4 to 2, respectively. For the median standard deviation of 0.25, the 95 percent confidence interval of the mean value spans a ranges of values from 0.7 to 1.5. Any one value may be in

error by as much as three quarters of an order of magnitude. For the purposes of this discussion, this is being viewed as a measure of the interpretation error.

Figure 5-9 is a plot of the data categorized by major regional-scale HSU. To simplify the presentation in this figure only, all volcanic units on and off Pahute Mesa are included under the heading VU. Figure 5-10 is a plot of the data from volcanic units on the Pahute Mesa model area categorized by the Pahute Mesa-Oasis Valley HSUs.

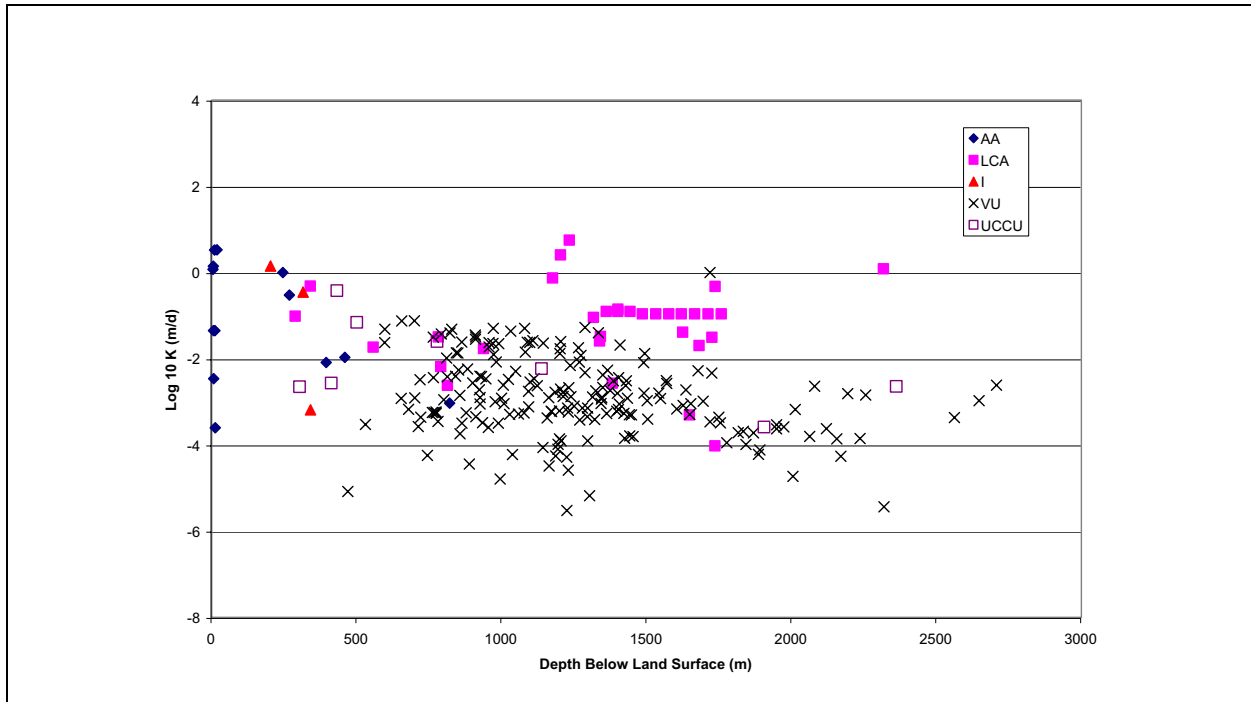


Figure 5-9
Slug Test Scale Hydraulic Conductivity as a Function of Depth and Regional HSU

Several features are evident in the two figures. Beginning with Figure 5-9, there may be a depth-dependent effect of the hydraulic conductivity of the alluvium, but the number of data points is small and the trend is not definitive. The data for the LCA must be viewed with considerable scepticism because a number of the tests probably did not measure formation properties, but rather measured the limitation of the testing device. Therefore, some of the reported values are lower bounds. The line of values at a log 10 K of -1 is an example of questionable data.

The hydraulic conductivity data labeled LCCU have an apparent trend of decreasing values with depth and the values are typically lower than for the LCA. Finally, the hydraulic conductivity of the volcanics, as a group, appear to decrease with depth, but there is a great deal of scatter in the values.

The Pahute Mesa volcanic units are presented in Figure 5-10. To a depth of about 1,500 m (4,500 ft), there is little differentiation between the various HSUs, and there does not appear to be much of a trend with depth. Only the data from the

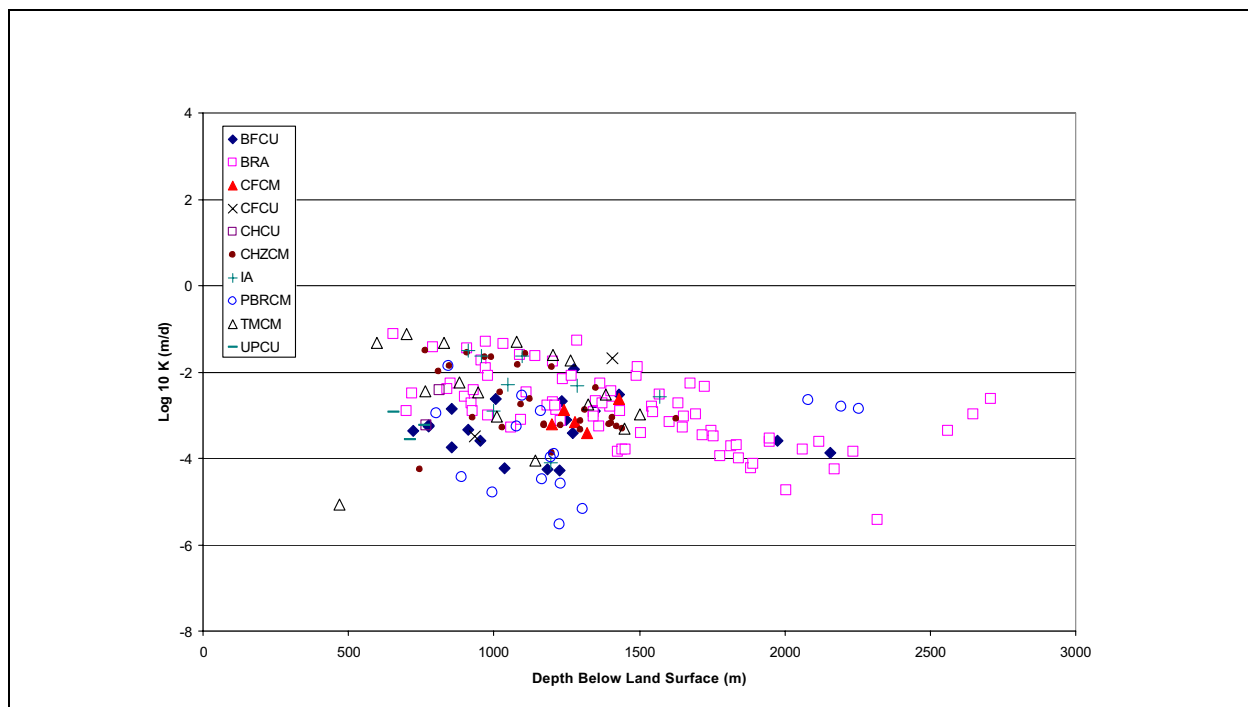


Figure 5-10
Slug Test Scale Hydraulic Conductivity as a Function of Depth and PM-OV HSU

Belted Range Aquifer (BRA) appear to demonstrate an apparent trend with depth. The changes in hydraulic conductivity with depth are not the result of large open intervals being used to calculate hydraulic conductivity from transmissivity. Figure 5-11 is a plot of the slug-scale data as a function of the length of the tested interval. The vast majority of data were collected over a depth interval less than 33 m (100 ft) with only a few data points representing much larger open intervals. The large, open-interval points are not necessarily the deepest, lowest hydraulic conductivity values. Therefore, there may be a few hydraulic conductivity values that are artificially small because a large open interval was used to calculate hydraulic conductivity from transmissivity. However, the small number of such cases will not eliminate the trend of decreasing K with depth.

Figures 5-12 and 5-13 summarize the statistical analysis of the data for the HSUs AA and LCA. The assumption of a log normal distribution is not rejected in either case. Table 5-2 summarizes the statistical analyses of the slug-test scale data. A comparison of the mean and standard deviation of the cdf for AA at the laboratory- and slug-test scale indicates that the two are similar, and in fact a single distribution could be developed for each dataset within the bounds defined by the K-S test. The cdf parameters for the LCA are very different, as would be expected. The slug test data for the LCA includes flow through fractures, whereas the laboratory data almost certainly ignores fractured intervals. For both the AA and LCA data presented in Figure 5-9, there is no apparent depth dependence in the slug-test scale data.

For the volcanic units, the mean Log 10 K values range from -1.9 to -2.9 with standard deviations that are all about 1.0, except for the Pre-Belted Range Composite Unit (PBRCM) which is 1.5. There is no consistent pattern of hydraulic conductivity with HSU type. In the following text, we propose a possible reason for the apparent lack of correspondence between hydraulic conductivity and HSU type. As noted by Laczniaik et al. (1996) and Blankennagel and Weir (1973), the degree of fracturing controls the water yielding characteristics of the volcanic units. Each of the HSUs are generally made up of multiple lithologies, with the dominant lithology providing the basis for categorization. Therefore, a composite or confining unit may contain a small percentage of aquifer lithologies. The slug type tests will respond to the most permeable lithology tested, and because of the relative short duration of these tests may not differentiate between layers of limited areal extent and those of large extent. Figures 5-14 and 5-15 are plots of the cdf and hydraulic conductivity with depth, respectively, for the PBRCM. The log normal distribution has uncertain parameters with the range in the mean from 4.1 to -3.4. From the presentation of the PBRCM data as a function of depth is shown in Figure 5-15, the change in hydraulic conductivity with depth is seen to be a complicated process that is not easily described by a single relationship.

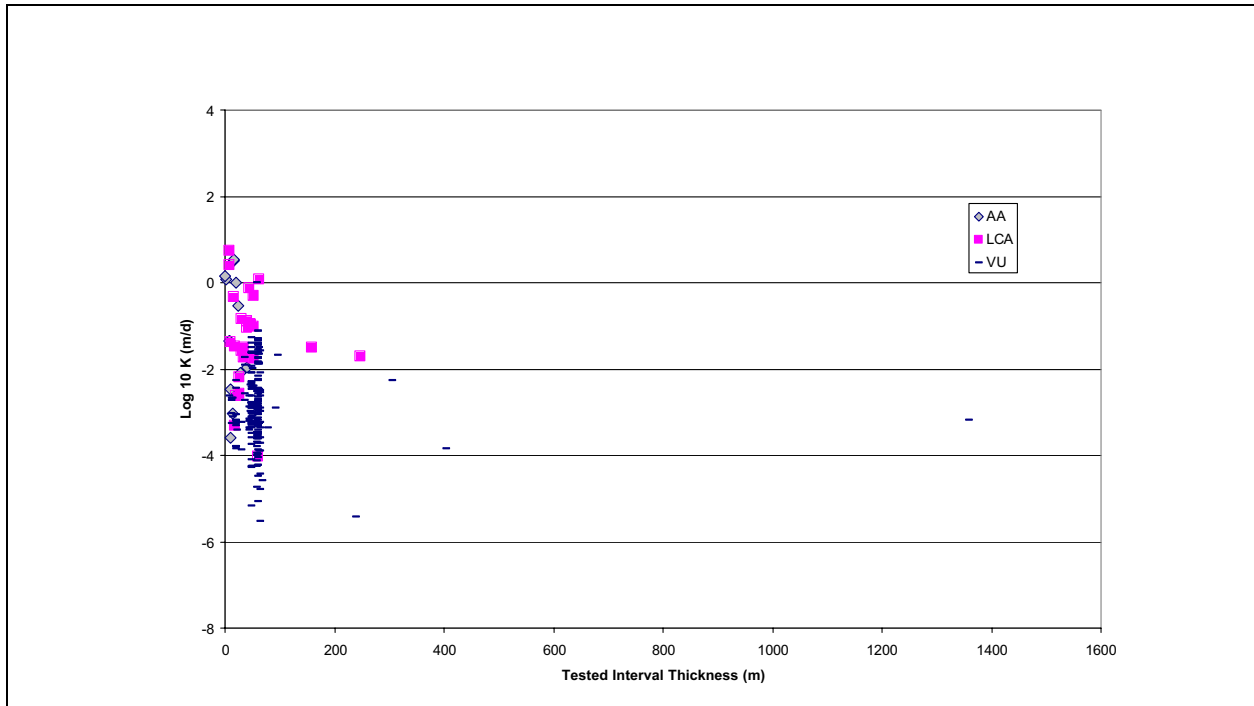


Figure 5-11
Slug Test Scale Hydraulic Conductivity as a Function of Tested Interval Thickness

Depth-dependency plots for data from HSUs BRA, Bullfrog Confining Unit (BFCU), Timber Mountain Composite Unit (TMCM), CHZCM, Crater Flat Confining Unit (CFCU), and Inlet Aquifer (IA) are presented in Figures 5-16 through 5-21, respectively. As can be seen, there is no clear depth dependence in hydraulic conductivity for any of the HSUs. In some cases, what appear to be

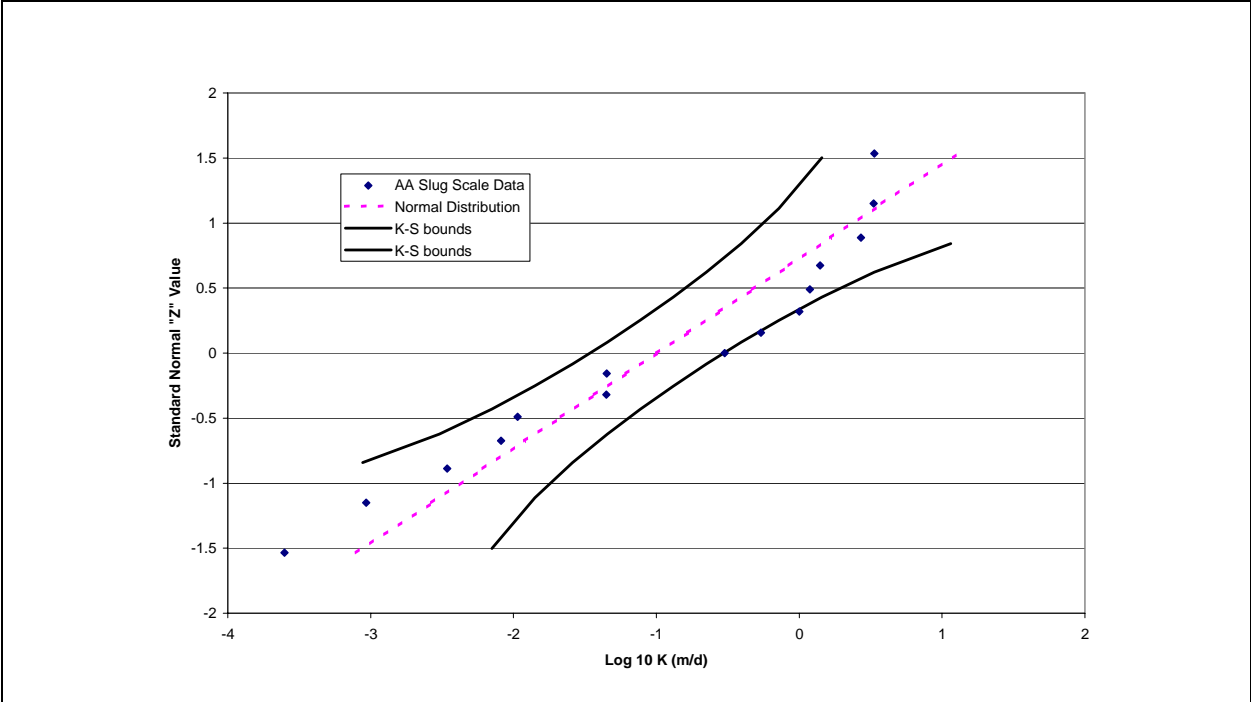


Figure 5-12
Alluvium Slug Test Hydraulic Conductivity Probability Distribution

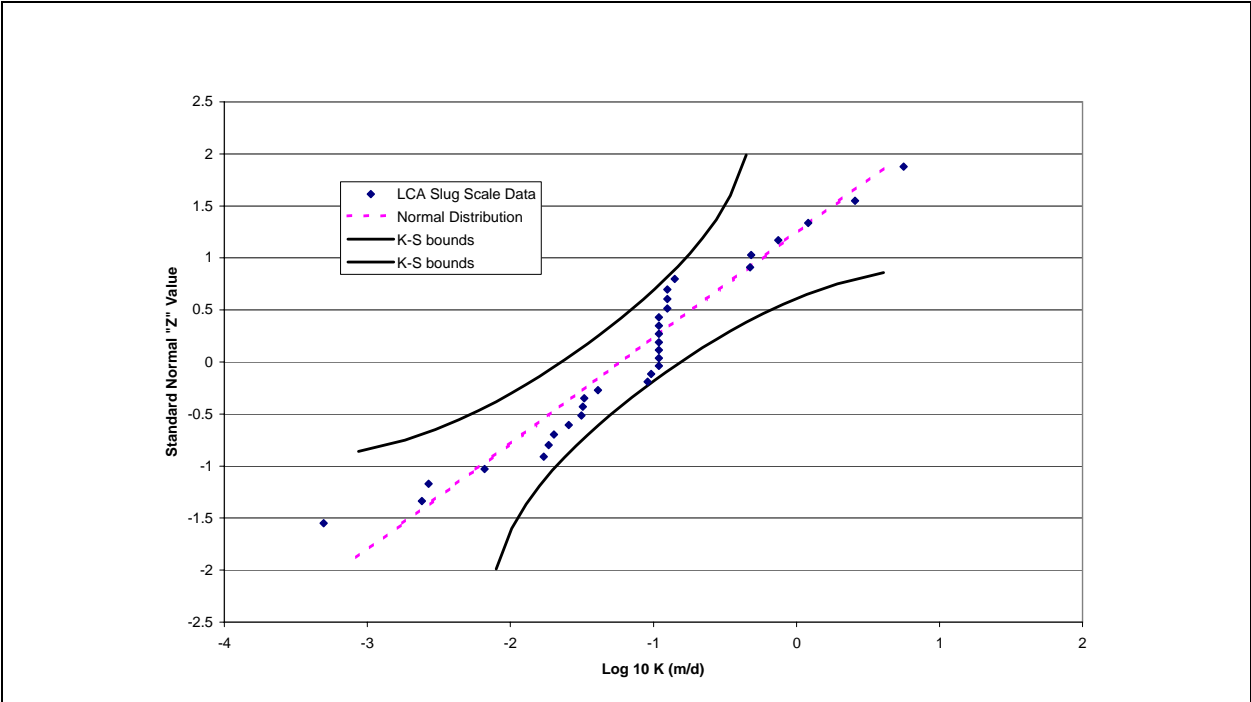


Figure 5-13
Lower Carbonate Aquifer Slug Test Hydraulic Conductivity Probability Distribution

Table 5-2
Statistics of Slug Test Scale Hydraulic Conductivity^a Data

Hydrostratigraphic Unit ^b	Number of Data Points	Log 10 Mean Hydraulic Conductivity	Log 10 Standard Deviation of Hydraulic Conductivity	Accept Log Normality at the 5% Level
AA	15	-1.0	1.4	Yes
LCA	32	-1.2	1.0	Yes
BFCU	19	-3.3	0.6	Yes
BRA	76	-2.9	0.9	Yes
CFCM	5	-3.1	0.3	Yes
CFCU	2	-2.6	1.3	N/A
CHCU	2	-2.8	0.6	N/A
CHZCM	29	-2.7	0.8	Yes
IA	8	-2.4	0.9	Yes
PBRCM	16	-3.7	1.1	Yes
TMCM	16	-2.5	1.1	Yes
UPCU	3	-3.2	0.3	N/A

^a Hydraulic conductivity is in m/d.

^b See Table 2-6 for HSU descriptions.

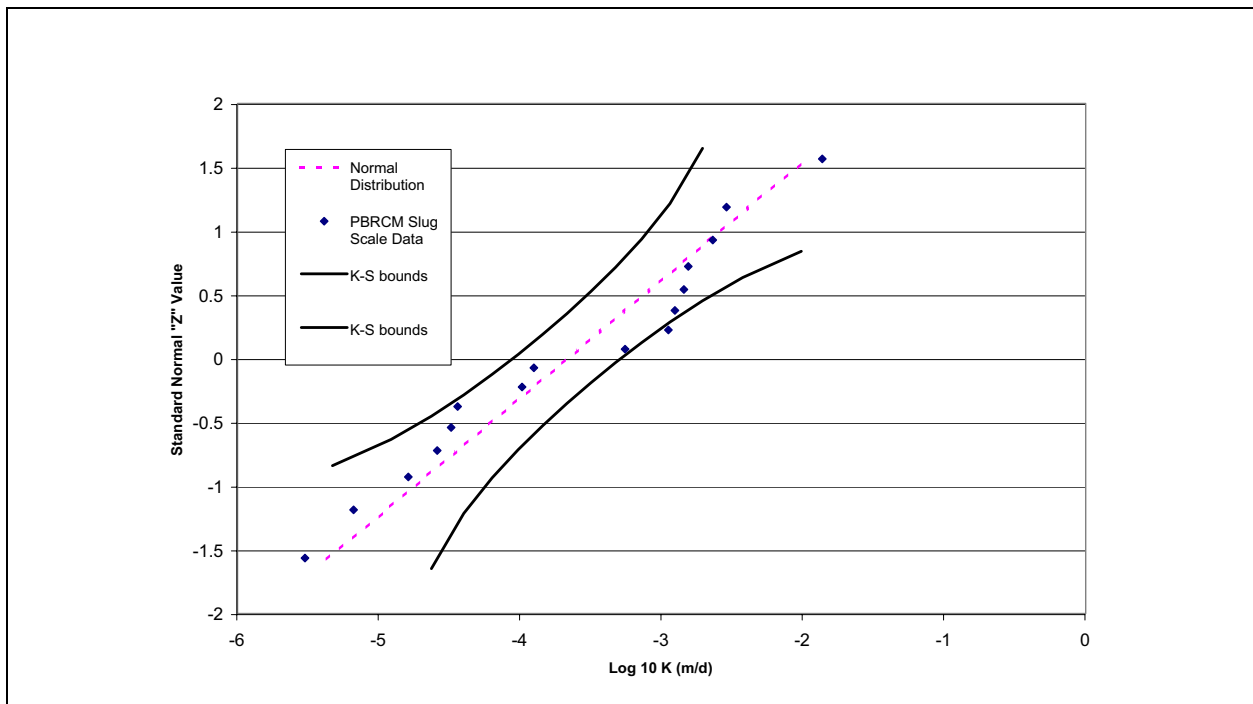


Figure 5-14
PBRCM Slug Test Hydraulic Conductivity Probability Distribution

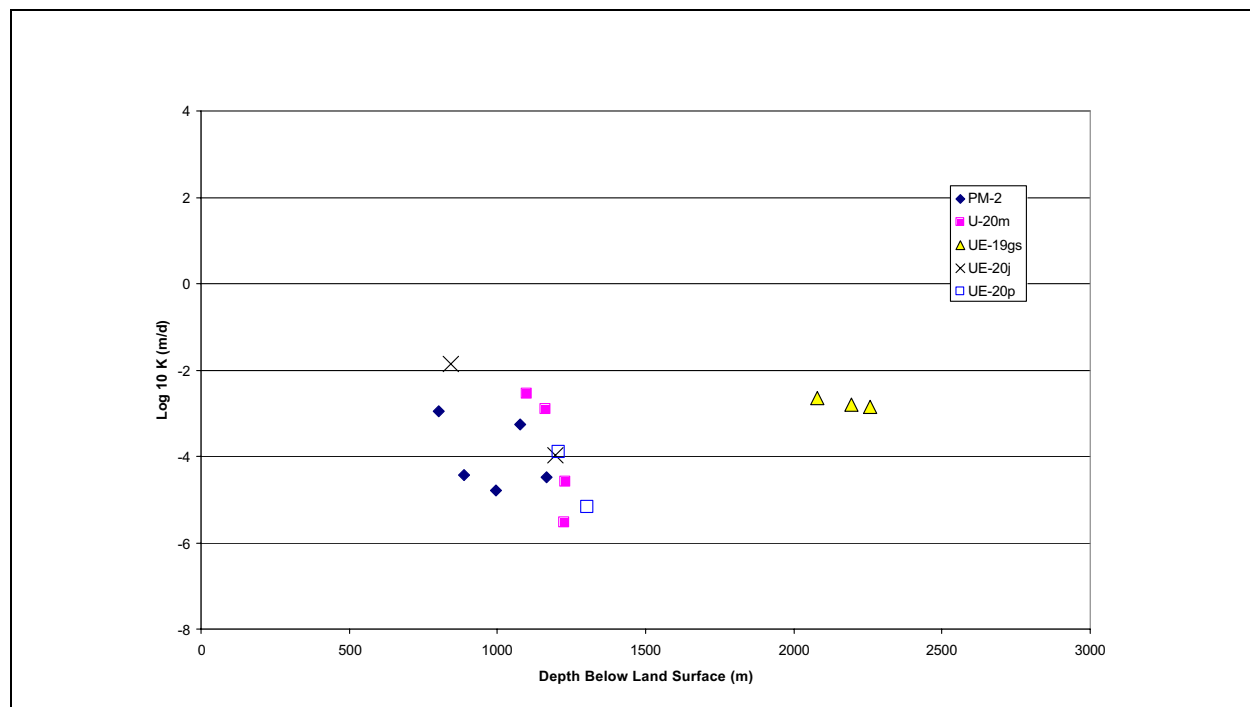


Figure 5-15
PBRCM Slug Test Hydraulic Conductivity as a Function of Depth and Location

changes in K with depth may actually be spatial variability. Consider the BRA (Figure 5-16) where the data from Well UE-19i differ from the other wells. When combined, the entire dataset appears to have a decrease of K with depth, but without Well UE-19i the depth decay is not as obvious.

5.5.5 Constant-Rate Scale Data

The data classified as constant-rate scale represent tests in which water was injected or withdrawn at a constant rate for several hours to several days. As a result, these tests are expected to have sampled a larger volume of the tested formation than either laboratory or slug-scale tests. This group of data contains results from both single and multi-well aquifer tests.

One hundred-six (106) constant-rate tests were interpreted multiple times using different models or different assumptions. Of the 106 tests, 67 percent had 4 or fewer multiples and the median log 10 standard deviation was 0.14. Although this analysis is not a true estimate of interpretation uncertainty, it does suggest that the values can be considered to be accurate to within about one-third of an order of magnitude.

Figure 5-22 is a plot of the constant-rate scale data as a function of depth. Some of the data fall outside the Pahute Mesa model area and these are classified by regional-scale HSUs. The data from wells within the model area are designated by the Pahute Mesa HSU. Several features of the plot are worth noting. As a whole,

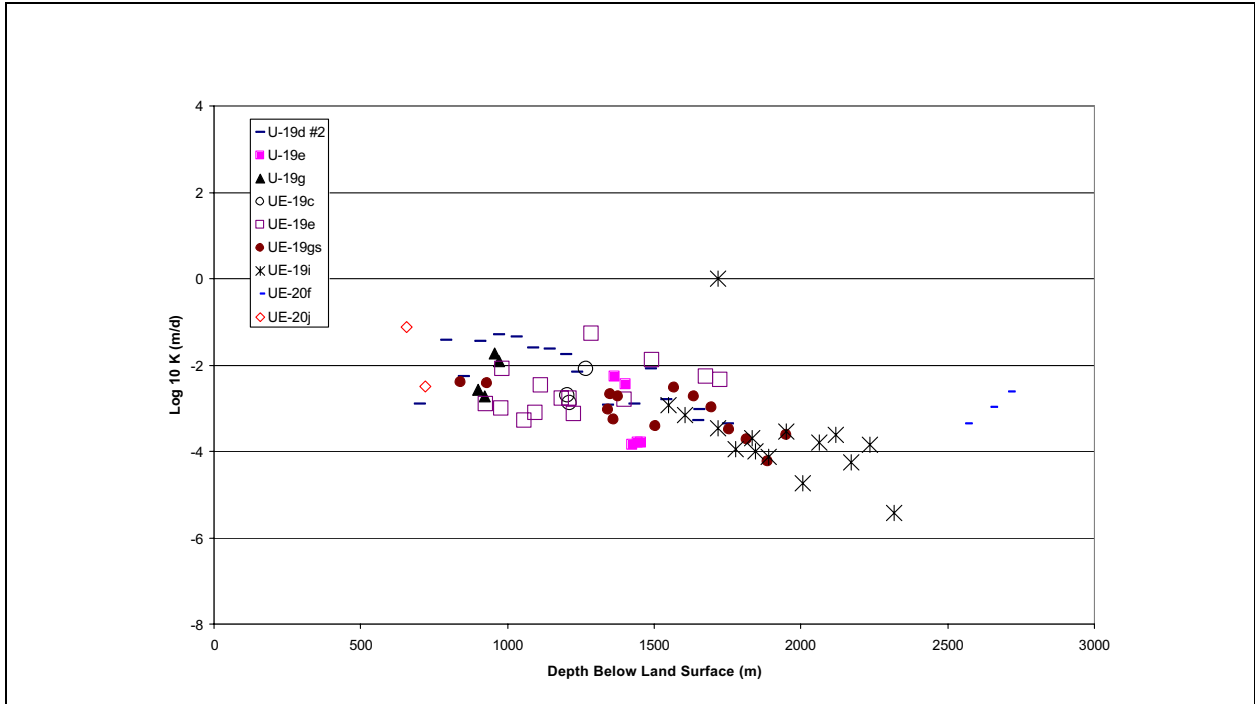


Figure 5-16
BRA Slug Test Hydraulic Conductivity as a Function of Depth and Location

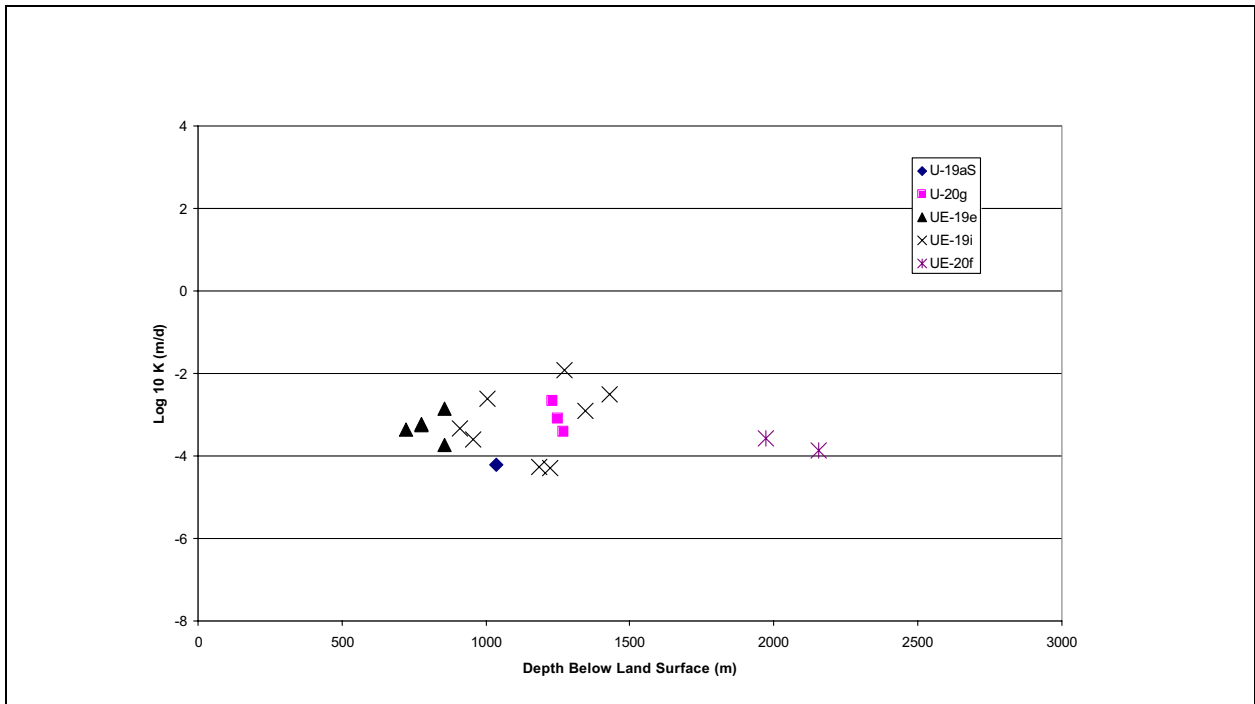


Figure 5-17
BFCU Slug Test Hydraulic Conductivity as a Function of Depth and Location

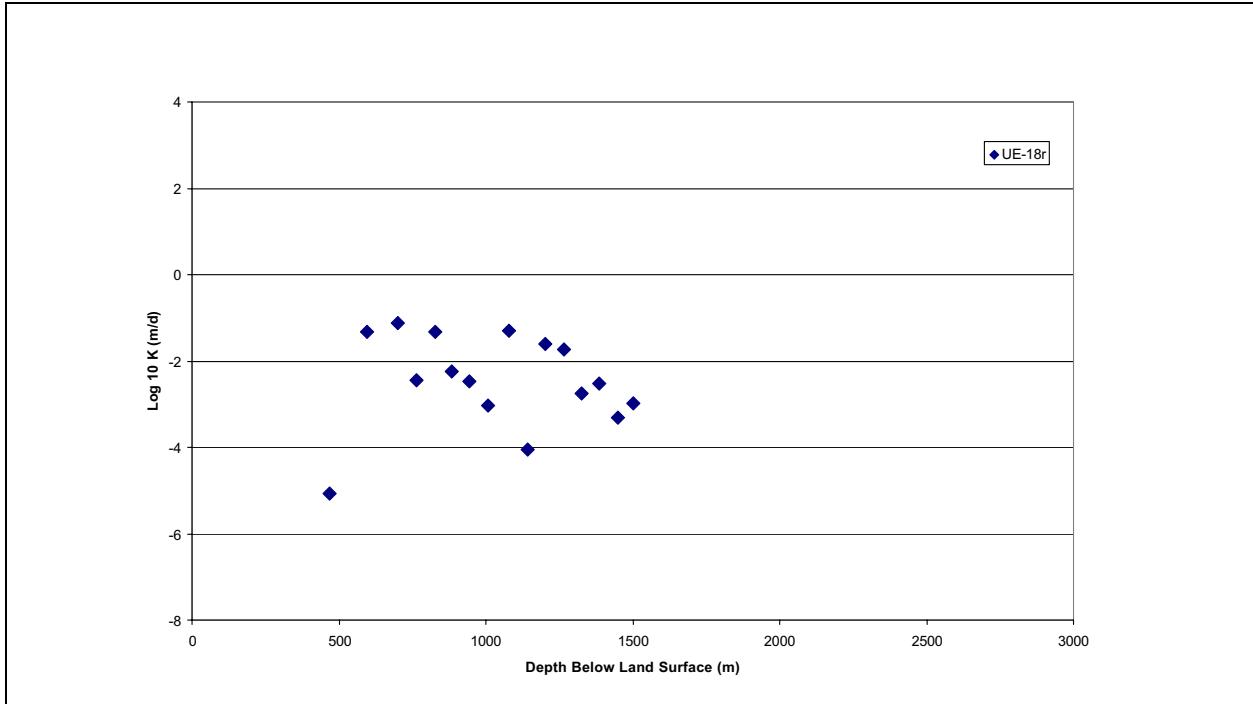


Figure 5-18
TCMC Slug Test Hydraulic Conductivity as a Function of Depth and Location

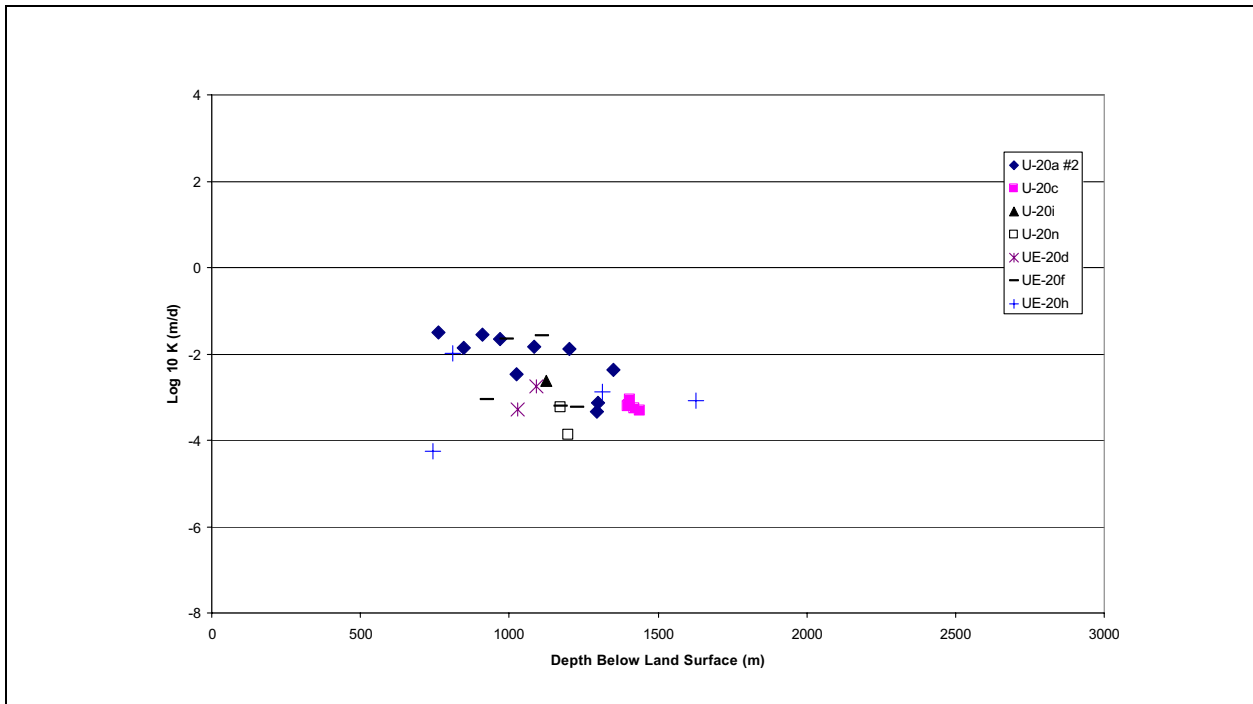


Figure 5-19
CHZCM Slug Test Hydraulic Conductivity as a Function of Depth and Location

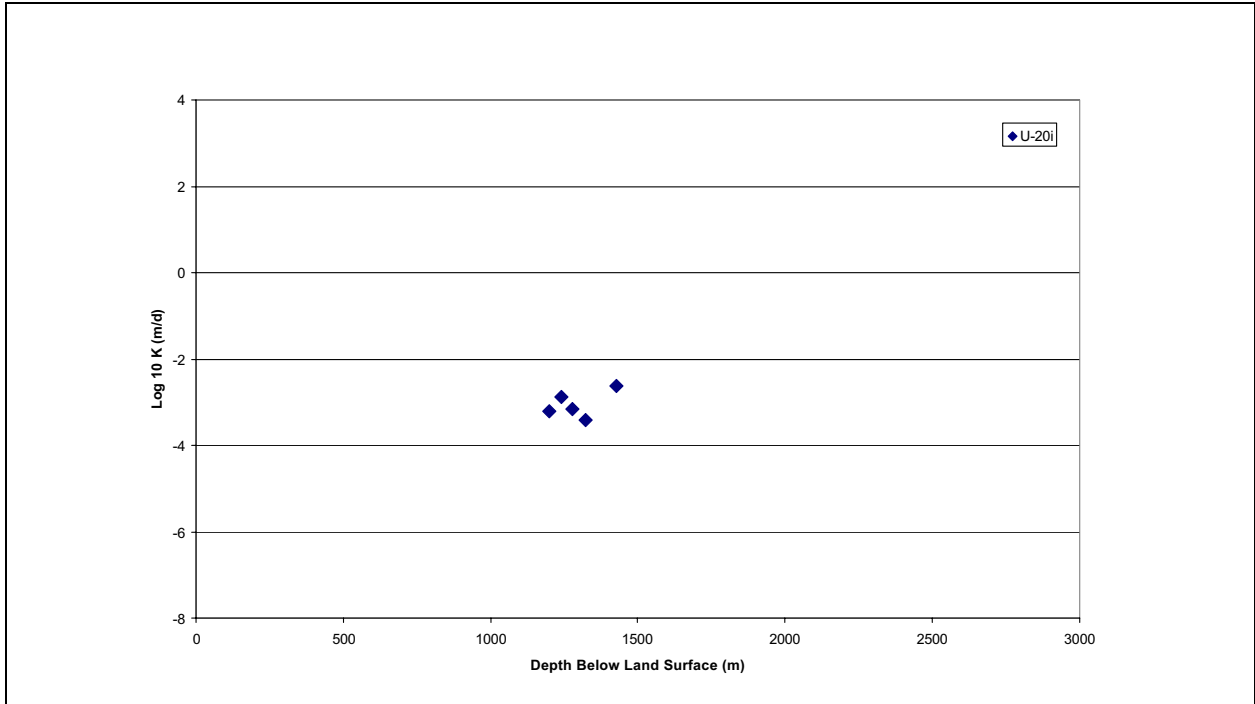


Figure 5-20
CFCM Slug Test Hydraulic Conductivity as a Function of Depth and Location

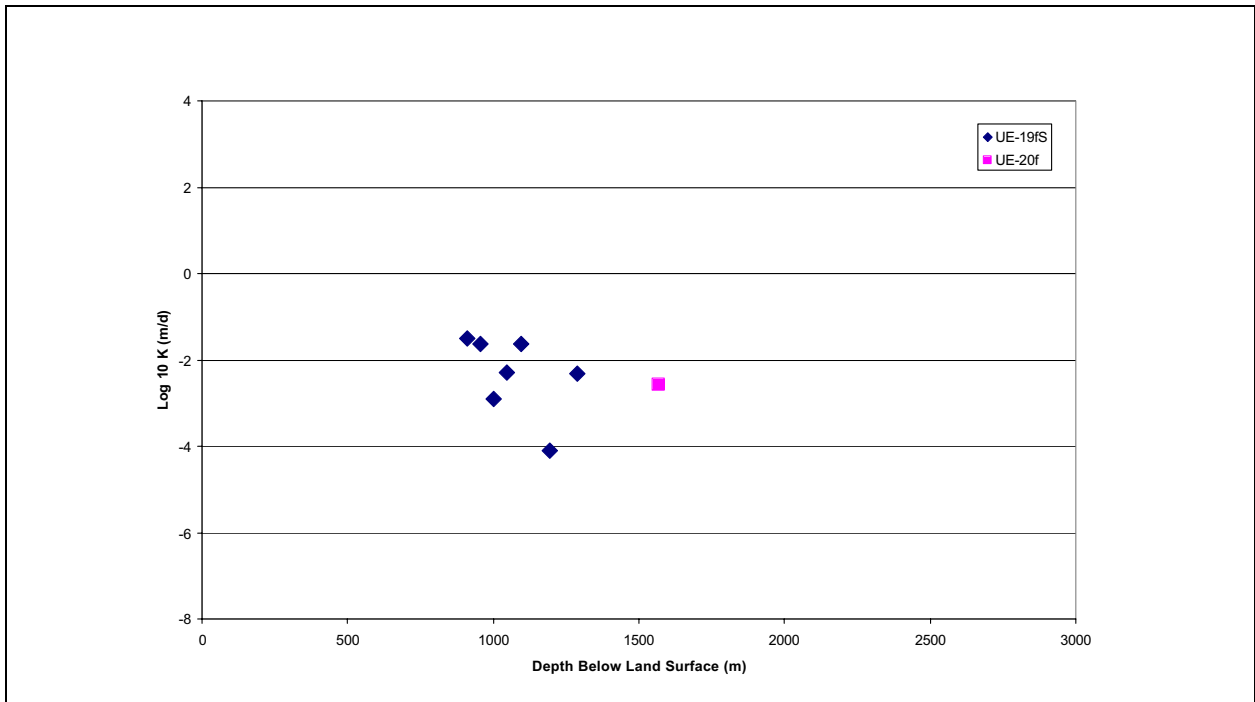


Figure 5-21
IA Slug Test Hydraulic Conductivity as a Function of Depth and Location

the data show a strong trend of decreasing hydraulic conductivity with depth. For some of the individual HSUs such as the LCA and BRA, there is a trend of decreasing hydraulic conductivity with depth. For the VA and VCU, there also appears to be a trend, but the data are much more scattered and a trend is more difficult to discern. Finally, for the AA and the BA, there does not appear to be a trend but the number of data points and the range of depths is limited.

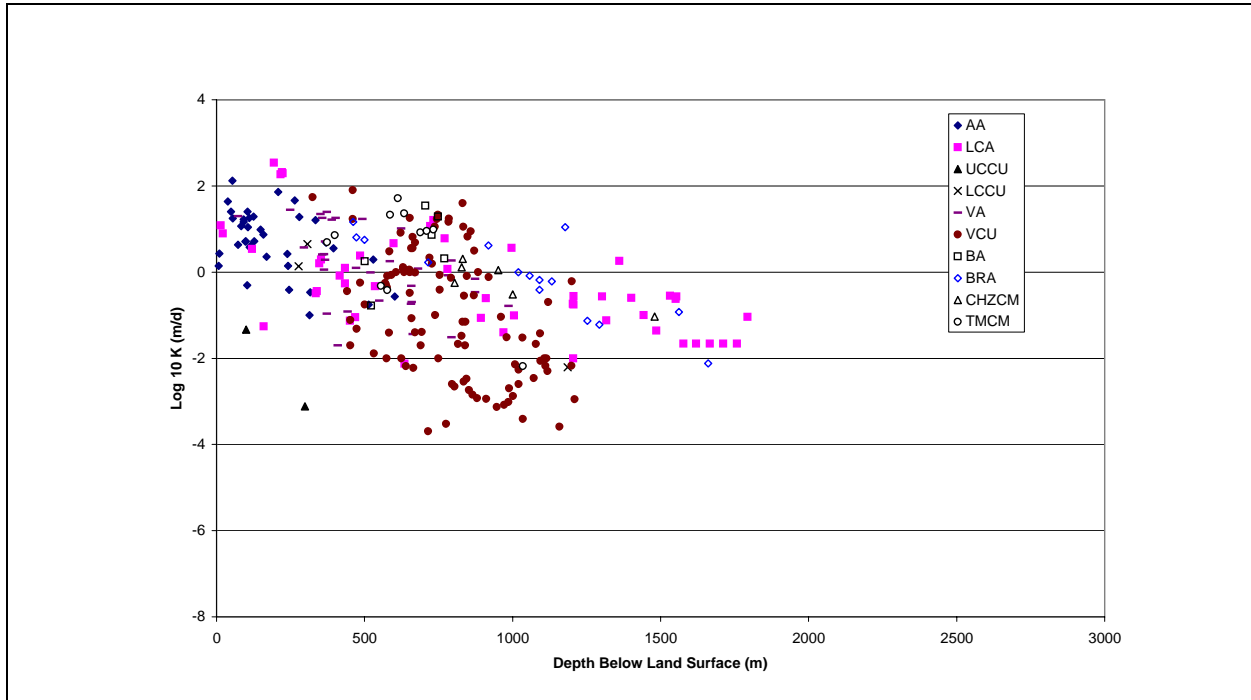


Figure 5-22
Constant-Rate Scale Hydraulic Conductivity as a Function of Depth and HSU

Figure 5-23 is a plot of the data from Figure 5-22 with a linear trend line fitted to the data. This mean trend has a relatively narrow uncertainty range because of the large number of values. Figure 5-24 is a plot of the data as a function of the length of the tested interval. Although a few points represent large open intervals, the vast majority of the data come from test intervals less than 125 m (375 ft). Therefore, it does not appear that length of the tested interval biases the apparent trend with depth, except for the BRA where the deepest, lowest, hydraulic conductivity values have the longest tested intervals.

Table 5-3 summarizes the statistical analysis of the data at the constant-rate scale and also includes corresponding log 10 mean and standard deviation values from the slug test and laboratory scale analysis to aid in comparison. The constant-rate scale parameters were calculated without any correction for depth dependence because, as noted in Section 5.5.6, depth correction may not be an appropriate model at the CAU scale. Therefore, in some cases, the standard deviation will be too large if applied to a depth-corrected mean value. Nonetheless, the presentation of the results in Table 5-3 provides some interesting comparisons to the smaller scale results in Tables 5-1 and 5-2. First, without exception, the mean values in

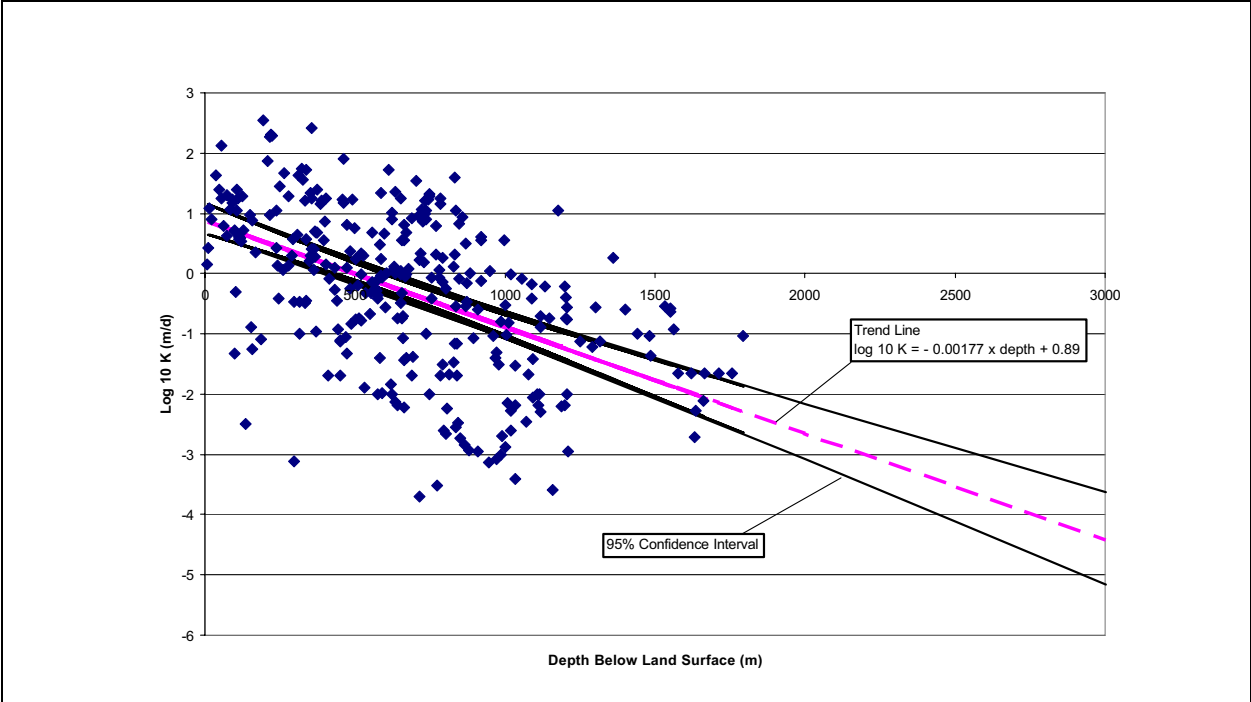


Figure 5-23
Plot of Constant-Rate Scale Hydraulic Conductivity Data (Figure 5-22) with a Linear Trend Line

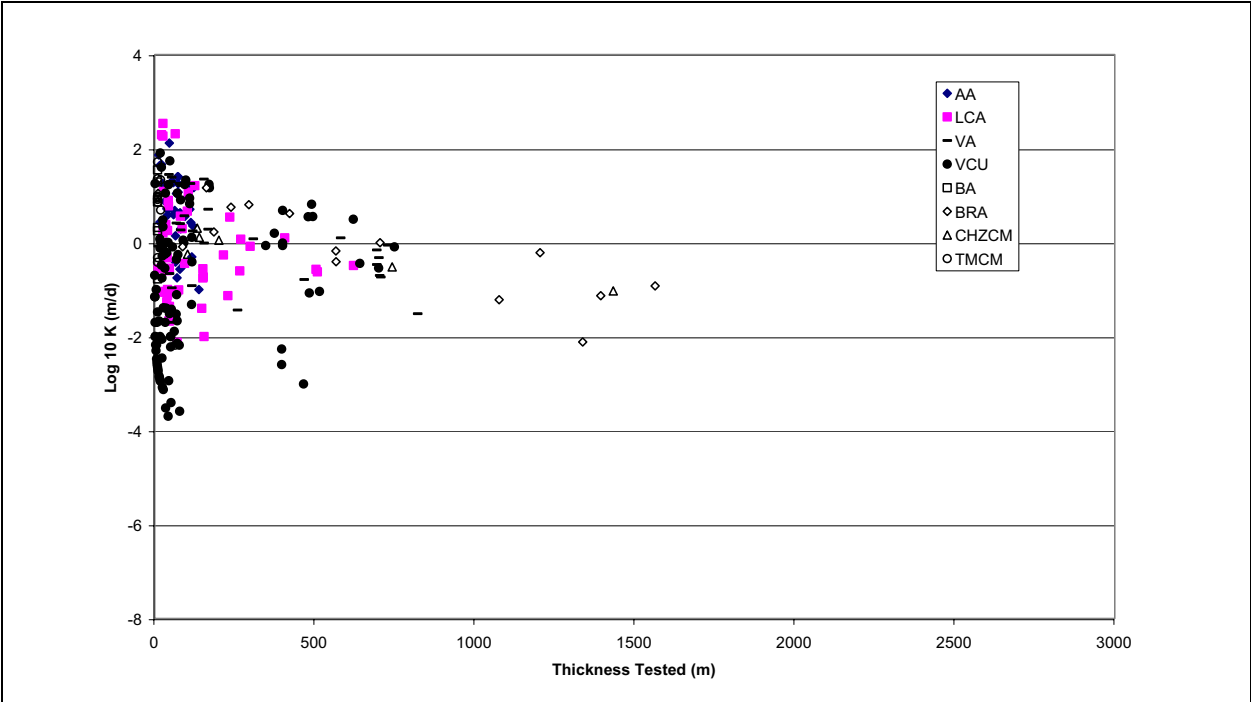


Figure 5-24
Constant-Rate Scale Hydraulic Conductivity as a Function of Tested Interval Thickness

**Table 5-3
Statistics of Constant-Rate Scale Hydraulic Conductivity^a Data as Compared to Statistics of Slug-test and Laboratory Scale Data**

Hydrostratigraphic Unit ^b	Number of Data Points	Log 10 Mean of Hydraulic Conductivity	Log 10 Standard Deviation of Hydraulic Conductivity	Accept Log Normality at the 5% Level	Slug-Test Scale Log 10 Mean of Hydraulic Conductivity	Slug-Test Scale Log 10 Standard Deviation of Hydraulic Conductivity	Laboratory-Scale Log 10 Mean of Hydraulic Conductivity	Laboratory-Scale Log 10 Standard Deviation of Hydraulic Conductivity
AA	38	0.7	0.7	Yes	-1.0	1.4	-0.4	0.8
LCA	49	-0.3	1.2	Yes	-1.2	1.0	-4.2	1.6
I	1	-2.5	NA	NA				
UCCU	2	-2.2	1.3	NA				
LCCU	3	-0.5	1.5	NA			-6.6	0.7
VCU	101	-1.0	1.4	Yes			-4.4	1.5
VA	35	0.1	0.9	Yes			-3.8	2.2
VU	7	-1.3	1.2	Yes			-3.0	2.0
BA	6	0.6	0.8	NA				
BRA	15	-0.1	0.9	Yes	-2.9	1.0		
BFCU	1	-0.3	NA	NA	-2.3	1.0		
IA	3	-1.0	1.6	NA	-2.0	0.9		
CHZCM	6	-0.2	0.5	NA	-1.9	0.9		
FCCM	11	-0.1	1.1	Yes				
PBRCM	2	-0.7	0	NA	-2.8	1.5		
TCVA	4	1.8	0.4	NA				
TMCM	13	0.4	1.1	Yes	-2.1	1.0		
UPCU	3	-0.9	0.9	NA				

^a Hydraulic conductivity is in m/d.

^b See [Table 2-6](#) for HSU descriptions.

NA = Not applicable

Table 5-3 for the constant rate tests are larger than in the other tables. The constant rate means range from 0.9 to 2.8 orders of magnitude larger than the corresponding slug-test scale means for the same HSUs. However, one must be careful not to generalize too much. These data are not always from the same locations; therefore, scale and spatial variability may be linked and are not easily separated. However, this does suggest that CAU-scale parameters should be biased toward larger values, especially if small-scale measurement data are used to guide the setting of parameter ranges. Second, for the first time, there appears to be some mild correlation between the type of HSU and the mean hydraulic conductivity for the volcanic units. The aquifer units tend to have a somewhat larger mean hydraulic conductivity than the confining units. The composite units (i.e., CHZCM, Fortymile Canyon Composite Unit [FCCM], PBRCM, and TCM) are mixed, with some more like aquifers and others more like confining units. However, the reader is cautioned to note that, in several cases, the number of data points is small and it is difficult to draw conclusions.

Figure 5-25 is a plot of selected data from the VCU HSU plotted as a function of depth and identified by well location. As was noted earlier with the slug-scale data, there is generally not a consistent trend of hydraulic conductivity values as a function of depth in any particular well. This is discussed further in the next section.

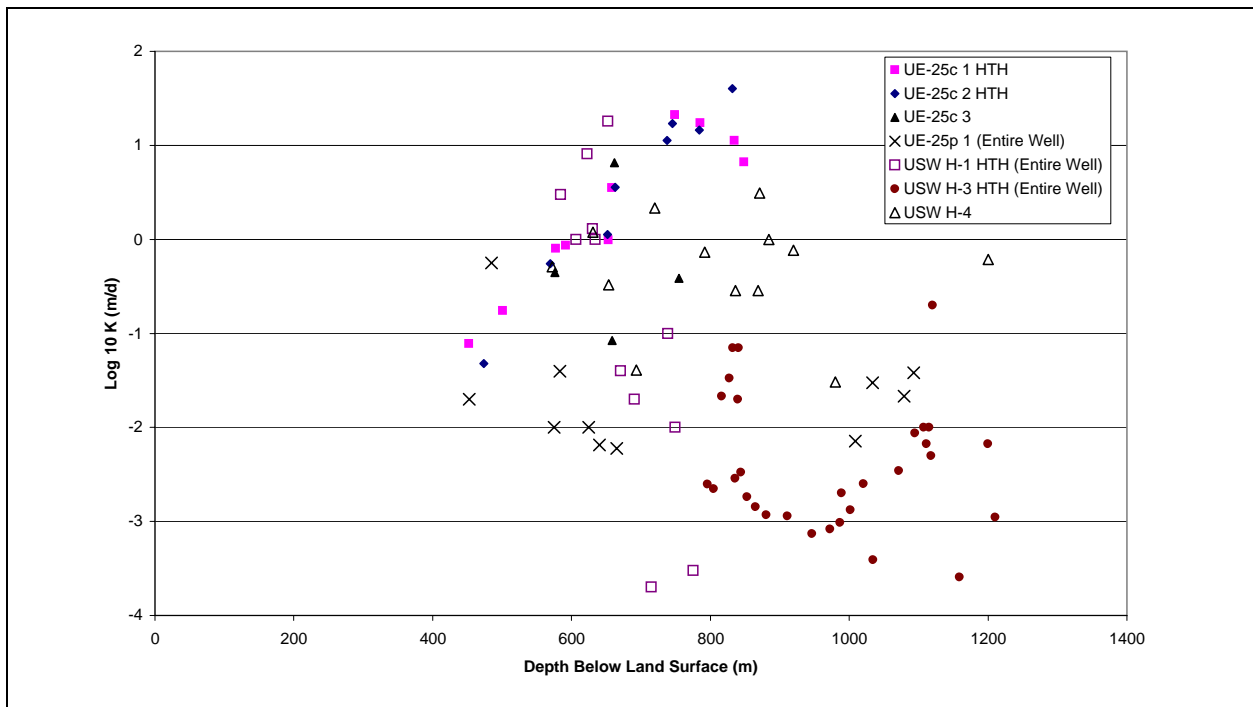


Figure 5-25
VCU Constant-Rate Hydraulic Conductivity as a Function of Depth and Location

5.5.6 Hydraulic Conductivity Versus Depth

The hydraulic conductivity would be expected to decrease with depth in many situations because the pore spaces, or fractures, through which water flows are expected to close under the increasing overburden pressure at greater depths. Viewed in bulk, the plots of hydraulic conductivity with depth presented in [Figures 5-9, 5-10, and 5-22](#) would all support the concept of hydraulic conductivity decreasing with depth. There is considerable scatter in the data, and at any particular depth, the range in values can easily span two orders of magnitude on either side of the trend line. Recalling that the Pahute Mesa flow model will extend to a depth of 3,500 m (9,500 ft) below mean sea level (or as much as 5,500 m [16,500 ft] below land surface). The slope of the hydraulic conductivity trend in [Figures 5-10 and 5-22](#) could lead to decreases of 10 orders of magnitude at the bottom of the model.

When hydraulic conductivity values are plotted at individual well locations such as in [Figures 5-16, 5-18, or 5-25](#), the trend with depth is seen to be very complicated. In fact, at most locations, there is no clear trend with depth.

The following approach to depth dependence of hydraulic conductivity is being proposed for use in the calibration of the Pahute Mesa CAU flow model. For the depth intervals up to 1,500 m (4,500 ft), no depth dependence will be assumed. It is in this depth range that well-specific data indicate no clear trend with depth. At greater depths, where data are particularly sparse, a depth dependence will be used. The apparent trends with depth for the volcanics and LCA in the present study are similar to those developed for the regional model (DOE/NV, 1997); therefore, the relationships developed for the regional model will be applied to the Pahute Mesa CAU modeling, but only for depths greater than 1,500 m (4,500 ft). This proposed approach will be implemented at the start of calibration, but will be assessed throughout the calibration process. Sensitivity of the results to these assumptions about hydraulic conductivity with depth will be thoroughly investigated and documented in the modeling report.

5.5.7 Scaling and Spatial Variability

The hydraulic conductivity of natural geologic formations is known to be spatially variable. The data presented in this report certainly support that claim. Not only is the hydraulic conductivity variable with depth, it varies laterally as demonstrated by distinctly different ranges of values of hydraulic conductivity at different well locations in the same HSU.

Vanmarcke (1983) has shown that as the scale of averaging increases, the variance of a random process decreases and the correlation length increases. Rubin and Gomez-Hernandez (1990) present theoretical and numerical examples of the impact of scaling as a function of block size. As the block size increases relative to the correlation scale, the mean value of the block approaches the geometric mean, and the variance of the mean value is significantly reduced. In their examples, the variance was reduced by a factor of 10 when the block size was 6.5 times the correlation length. The difficulty with application of approaches

such as Rubin and Gomez-Hernandez (1990) is that covariance information, especially correlation length, is needed. In reality, this covariance information is never available. However, several key observations from the theoretical studies can be made. First, the geometric mean is a reasonable estimate of the average hydraulic conductivity of a block. Second, the uncertainty in the hydraulic conductivity as characterized by the log 10 standard deviation is larger than the uncertainty in the block-scale value assuming that the available data represent the full range of variability in the formation. These scaling relationships are all based on the assumption of a constant mean and uniform statistical properties within an HSU. If these assumptions are incorrect, the conclusions of the theoretical studies may not apply.

The effect of measurement scale has been investigated in this study. We have shown that as the scale of measurement increases, the measured value of log 10 hydraulic conductivity increases and log 10 standard deviation decreases. Similar observations have been made in other studies reported in the literature. In contrast, Zlotnik et al. (2000) have reviewed many of these other studies and conclude that there is little evidence for a scale effect in hydraulic conductivity. They conclude, as did we, that the large increases in mean hydraulic conductivity from laboratory- to field-scale measurements are most likely due to sampling bias, not true scale dependence. They also point out the difficulty of quantifying the scale of measurement of field techniques such as slug and constant-rate tests. We have generalized the scale of measurement by slug and constant rate, but do not quantify the difference. In addition, Zlotnik et al. (2000) provide six general principles to apply to screening and comparing data. One of the principles is coverage. They caution that comparison of data collected by two different techniques over two different subdomains is not possible. In other words, if the slug-test data were not collected in the same borehole and same depth interval as the constant-rate data, the comparison of results is not meaningful. In the vast majority of cases, we do not have overlapping domains. For the purposes of the Pahute Mesa CAU flow model, we intend to first rely on constant-rate scale data and then slug-test data. Laboratory-scale data are not applicable to formations characterized by fracture flow, but may be useful in defining hydraulic conductivity in porous formations.

5.5.8 Vertical Anisotropy

In the general case, hydraulic conductivity is not a scalar value, but a second rank tensor, where hydraulic conductivity at a point in space is a function of direction. The measurement of horizontal anisotropy requires multiple observation wells during aquifer testing. Anisotropy in the vertical direction can be determined from oriented core, or observation wells set at depths that differ from the pumped well. Data to define anisotropy are limited. The available data are presented in electronic form (see CD included with this report). Laboratory data are generally not appropriate for large scale model parameters such as those needed for the Pahute Mesa CAU model. Vertical anisotropy data from aquifer testing are presented in the database. Careful testing at the C-well complex at Yucca Mountain yielded a range of anisotropy values (defined as vertical/horizontal hydraulic conductivity) from 0.025 to as large as 2.0. Because the dataset is

limited, it is not possible to provide anisotropy values for each HSU. Rather, the approach to anisotropy will be to begin with anisotropy equal to 1.0 (meaning no directional component to the hydraulic conductivity). This assumption will be tested during sensitivity analyses based, in part, on the ranges determined from the C-wells.

5.5.9 Alteration of Hydraulic Conductivity in Test Cavities

The detonation of underground nuclear tests creates underground cavities and collapse chimneys (Pawloski, et al., 2001). The melt glass that forms at the bottom of the cavity is generally accepted to be of very low permeability as is the crushed zone beneath the cavity. However, the chimney region, because of its rubblized nature, may be more permeable than the surrounding host rock. In their study of flow and transport from an underground test cavity, Pawloski et al. (2001) used chimney hydraulic conductivity values that were at least 70 times larger than in the native rock. As Pawloski et al. (2001) note, these values were estimated using the scant data available from underground nuclear tests, insights gained from calibration of flow and transport models, and understanding of the phenomenology of underground nuclear tests. These assumptions will be tested during the sensitivity analyses.

5.5.10 Hydraulic Conductivity Parameters for Each HSU

[Table 5-4](#) summarizes the hydraulic conductivity parameters for each HSU. The table contains the HSU number and identifier, the log 10 mean and standard deviation, and a description of where the chosen mean and standard deviation were obtained. The given distributions will be applied to the model at the start of calibration.

5.6 Analysis of Aquifer Storage Properties

The storage coefficient (S) is defined as the volume of water that an aquifer releases from or takes into storage per unit surface area of the aquifer per unit change in head (Freeze and Cherry, 1979). It is a dimensionless variable that is generally smaller than 0.005 in confined aquifers and is called the specific yield in unconfined aquifers. In unconfined aquifers, it is a measure of the drainable porosity and is typically less than 0.30. The storage coefficient is calculated from the specific storage (S_s), or amount of water that an aquifer releases from or takes into storage per unit volume, and saturated thickness as $S = S_s \times b$. Specific storage is used to assess storage property variability because it removes the effects of unequal test intervals from the data.

Storage coefficient data have been compiled from aquifer tests with at least two wells, one pumping and the other(s) as observation wells, and converted into specific storage coefficients. [Figure 5-26](#) is a plot of the specific storage on a logarithmic scale with the data categorized by HSU. The data were collected from

Table 5-4
Hydraulic Conductivity^a Distributions of Hydrostratigraphic Units of the
Pahute Mesa-Oasis Valley Hydrostratigraphic Framework Model
 (Page 1 of 5)

HSU Model Layer Number ^b	Hydrostratigraphic Unit (Symbol)	Dominant Hydrogeologic Unit(s) ^c	Log 10 Hydraulic Conductivity Mean	Log 10 Hydraulic Conductivity Standard Deviation	Source of the Parameters	Transport Parameter Category
46	Alluvial Aquifer (AA) (this term is also used to designate a hydrogeologic unit)	AA	0.7	0.7	Values obtained from the constant-rate scale data in Table 5-3 .	Alluvium
45	Younger Volcanic Composite Unit (YVCM)	LFA, WTA, VTA	1.8	0.4	No data were available for this unit. Used values from the TCVA in Table 5-3 because of lithologic similarity. This minor unsaturated unit is not expected to influence the flow model.	WTA 75% VTA 25%
44	Thirsty Canyon Volcanic Aquifer (TCVA)	WTA, LFA, lesser VTA	1.8	0.4	Values obtained from the constant-rate scale data in Table 5-3 .	WTA 75% LFA 25%
43	Detached Volcanics Composite Unit (DVCM)	WTA, LFA, TCU	-1.0	1.4	No data were available for this unit. Used value from the VCU in Table 5-3 because it provides a distribution that spans nearly the full range of observed values. It is expected that composite units have a larger range of values because of the varied lithologies.	WTA 85% TCU 15%
42	Detached Volcanics Aquifer (DVA)	WTA, LFA	0.1	0.9	No data were available for this unit. Used value from the VA in Table 5-3 because it provides a distribution that spans nearly the full range of observed values for an aquifer lithology.	WTA
41	Fortymile Canyon Composite Unit (FCCM)	LFA, TCU, lesser WTA	-0.1	1.1	Values obtained from the constant-rate scale data in Table 5-3 .	LFA 60% TCU 30% WTA 10%
40	Fortymile Canyon Aquifer (FCA)	WTA, LFA	0.1	0.9	No data were available for this unit. Used value from the VA in Table 5-3 because it provides a distribution that spans nearly the full range of observed values for an aquifer lithology.	WTA 80% LFA 20%
39	Timber Mountain Composite Unit (TMCM)	TCU (altered tuffs, lavas) and unaltered WTA and lesser LFA	0.4	1.1	Values obtained from the constant-rate scale data in Table 5-3 .	TCU 75% WTA 25%
38	Tannenbaum Hill Lava-Flow Aquifer (THLFA)	LFA	0.1	0.9	No data were available for this unit. Used value from the VA in Table 5-3 because it provides a distribution that spans nearly the full range of observed values for an aquifer lithology.	LFA
37	Tannenbaum Hill Composite Unit (THCM)	Mostly TCU, lesser WTA	-1.0	1.4	No data were available for this unit. Used value from the VCU in Table 5-3 because it provides a distribution that spans nearly the full range of observed values. It is expected that composite units have a larger range of values because of the varied lithologies.	TCU 75% WTA 25%

Table 5-4
Hydraulic Conductivity^a Distributions of Hydrostratigraphic Units of the
Pahute Mesa-Oasis Valley Hydrostratigraphic Framework Model
 (Page 2 of 5)

HSU Model Layer Number ^b	Hydrostratigraphic Unit (Symbol)	Dominant Hydrogeologic Unit(s) ^c	Log 10 Hydraulic Conductivity Mean	Log 10 Hydraulic Conductivity Standard Deviation	Source of the Parameters	Transport Parameter Category
36	Timber Mountain Aquifer (TMA)	Mostly WTA, minor VTA	0.1	0.9	No data were available for this unit. Used value from the VA in Table 5-3 because it provides a distribution that spans nearly the full range of observed values for an aquifer lithology.	WTA 80% VTA 20%
35	Subcaldera Volcanic Confining Unit (SCVCU)	TCU	-4.4	1.5	No data were available for this unit. Used value from the VCU in Table 5-3 because it is expected that this unit will be of low permeability.	TCU
34	Fluorspar Canyon Confining Unit (FCCU)	TCU	-1.0	1.4	No data were available for this unit. Used value from the VCU in Table 5-3 because it provides a distribution that spans nearly the full range of observed values.	TCU
33	Windy Wash Aquifer (WWA)	LFA	0.1	0.9	No data were available for this unit. Used value from the VA in Table 5-3 because it provides a distribution that spans nearly the full range of observed values for an aquifer lithology.	LFA
32	Paintbrush Composite Unit (PCM)	WTA, LFA, TCU	-1.0	1.4	No data were available for this unit. Used value from the VCU in Table 5-3 because it provides a distribution that spans nearly the full range of observed values. It is expected that composite units have a larger range of values because of the varied lithologies.	WTA 75% TCU 25%
31	Paintbrush Vitric-Tuff Aquifer (PVTA)	VTA	0.1	0.9	No data were available for this unit. Used value from the VA in Table 5-3 because it provides a distribution that spans nearly the full range of observed values for an aquifer lithology.	VTA
30	Benham Aquifer (BA)	LFA	0.6	0.8	Values obtained from the constant-rate scale data in Table 5-3 .	LFA
29	Upper Paintbrush Confining Unit (UPCU)	TCU	-0.9	0.9	Values obtained from the constant-rate scale data in Table 5-3 .	TCU
28	Tiva Canyon Aquifer (TCA)	WTA	0.1	0.9	No data were available for this unit. Used value from the VA in Table 5-3 because it provides a distribution that spans nearly the full range of observed values for an aquifer lithology.	WTA 70% VTA 30%
27	Paintbrush Lava-Flow Aquifer (PLFA)	LFA	0.1	0.9	No data were available for this unit. Used value from the VA in Table 5-3 because it provides a distribution that spans nearly the full range of observed values for an aquifer lithology.	LFA
26	Lower Paintbrush Confining Unit (LPCU)	TCU	-0.9	0.9	No data were available for this unit. Used values from the UPCU in Table 5-3 because of lithologic similarity.	TCU

Table 5-4
Hydraulic Conductivity^a Distributions of Hydrostratigraphic Units of the
Pahute Mesa-Oasis Valley Hydrostratigraphic Framework Model
 (Page 3 of 5)

HSU Model Layer Number ^b	Hydrostratigraphic Unit (Symbol)	Dominant Hydrogeologic Unit(s) ^c	Log 10 Hydraulic Conductivity Mean	Log 10 Hydraulic Conductivity Standard Deviation	Source of the Parameters	Transport Parameter Category
25	Topopah Spring Aquifer (TSA)	WTA	0.1	0.9	No data were available for this unit. Used value from the VA in Table 5-3 because it provides a distribution that spans nearly the full range of observed values for an aquifer lithology.	WTA
24	Yucca Mountain Crater Flat Composite Unit (YMCFCM)	LFA, WTA, TCU	-1.0	1.4	No data were available for this unit. Used value from the VCU in Table 5-3 because it provides a distribution that spans nearly the full range of observed values. It is expected that composite units have a larger range of values because of the varied lithologies.	WTA 75% TCU 25%
23	Calico Hills Vitric-Tuff Aquifer (CHVTA)	VTA	0.1	0.9	No data were available for this unit. Used value from the VA in Table 5-3 because it provides a distribution that spans nearly the full range of observed values for an aquifer lithology.	VTA
22	Calico Hills Vitric Composite Unit (CHVCM)	VTA, LFA	-1.0	1.4	No data were available for this unit. Used value from the VCU in Table 5-3 because it provides a distribution that spans nearly the full range of observed values. It is expected that composite units have a larger range of values because of the varied lithologies.	VTA 75% LFA 25%
21	Calico Hills Zeolitic Composite Unit (CHZCM)	LFA, TCU	-0.2	0.5	Values obtained from the constant-rate scale data in Table 5-3 .	TCU 75% LFA 25%
20	Calico Hills Confining Unit (CHCU)	Mostly TCU, minor LFA	-0.9	0.9	No data were available for this unit. Used values from the UPCU in Table 5-3 because of lithologic similarity.	TCU 90% LFA 10%
19	Inlet Aquifer (IA)	LFA	-1.0	1.6	Values obtained from the constant-rate scale data in Table 5-3 .	LFA
18	Crater Flat Composite Unit (CFCM)	Mostly LFA, intercalated with TCU	-1.4	0.9	Values obtained from the slug-scale data in Table 5-3 . The magnitude of the mean was increased one order of magnitude to account for observed differences between the slug and constant-rate scale.	LFA 75% TCU 25%
17	Crater Flat Confining Unit (CFCU)	TCU	-0.9	0.9	No data were available for this unit. Used values from the UPCU in Table 5-3 because of lithologic similarity.	TCU
16	Kearsarge Aquifer (KA)	LFA	0.1	0.9	No data were available for this unit. Used value from the VA in Table 5-3 because it provides a distribution that spans nearly the full range of observed values for an aquifer lithology.	LFA

Table 5-4
Hydraulic Conductivity^a Distributions of Hydrostratigraphic Units of the
Pahute Mesa-Oasis Valley Hydrostratigraphic Framework Model
 (Page 4 of 5)

HSU Model Layer Number ^b	Hydrostratigraphic Unit (Symbol)	Dominant Hydrogeologic Unit(s) ^c	Log 10 Hydraulic Conductivity Mean	Log 10 Hydraulic Conductivity Standard Deviation	Source of the Parameters	Transport Parameter Category
15	Bullfrog Confining Unit (BFCU)	TCU	-1.3	1.0	Values obtained from the slug-scale data in Table 5-3 . The magnitude of the mean was increased one order of magnitude to account for observed differences between the slug and constant-rate scale.	TCU
14	Belted Range Aquifer (BRA)	LFA and WTA, with lesser TCU	-0.1	0.9	Values obtained from the constant-rate scale data in Table 5-3 .	WTA 50% LFA 50%
13	Pre-belted Range Composite Unit (PBRCM)	TCU, WTA, LFA	-0.7	1.5	Mean Value obtained from the constant-rate scale data in Table 5-3 . The standard deviation was taken from the slug-scale data in Table 5-2 .	TCU 75% WTA 25%
12	Black Mountain Intrusive Confining Unit (BMICU)	IICU	-2.5		Mean Value obtained from the Intrusive (I) in the constant-rate scale data in Table 5-3 . No standard deviation was calculated.	"TCU"
11	Ammonia Tanks Intrusive Confining Unit (ATICU)	IICU	-2.5			
10	Rainier Mesa Intrusive Confining Unit (RMICU)	IICU	-2.5			
9	Claim Canyon Intrusive Confining Unit (CCICU)	IICU	-2.5			
8	Calico Hills Intrusive Confining Unit (CHICU)	IICU	-2.5			
7	Silent Canyon Intrusive Confining Unit (SCICU)	IICU	-2.5			
6	Mesozoic Granite Confining Unit (MGCU)	GCU	-2.5		Mean Value obtained from the Intrusive (I) in the constant-rate scale data in Table 5-3 . No standard deviation was calculated.	
5	Lower Carbonate Aquifer - Thrust Plate (LCA3)	CA	-0.3	1.2	Values obtained from the constant-rate scale data in Table 5-3 for the LCA.	
4	Lower Clastic Confining Unit - Thrust Plate (LCCU1)	CCU	-0.5	1.5	Values obtained from the constant-rate scale data in Table 5-3 . This unit may be broken up and have a larger permeability than when at depth.	

Table 5-4
Hydraulic Conductivity^a Distributions of Hydrostratigraphic Units of the
Pahute Mesa-Oasis Valley Hydrostratigraphic Framework Model
 (Page 5 of 5)

HSU Model Layer Number ^b	Hydrostratigraphic Unit (Symbol)	Dominant Hydrogeologic Unit(s) ^c	Log 10 Hydraulic Conductivity Mean	Log 10 Hydraulic Conductivity Standard Deviation	Source of the Parameters	Transport Parameter Category
3	Upper Clastic Confining Unit (UCCU)	CCU	-2.2	1.3	Values obtained from the constant-rate scale data in Table 5-3 .	
2	Lower Carbonate Aquifer (LCA)	CA	-0.3	1.2	Values obtained from the constant-rate scale data in Table 5-3 for the LCA.	
1	Lower Clastic Confining Unit (LCCU)	CCU	-6.6	0.7	Values taken from the laboratory-scale data in Table 5-1 because this unit is expected to be very impermeable.	

^a Hydraulic conductivity is in m/d

^b PM-OV 3-D Hydrostratigraphic Framework model (BN, 2002)

^c See [Table 2-1](#) and [Table 2-2](#) for definitions of HGUs

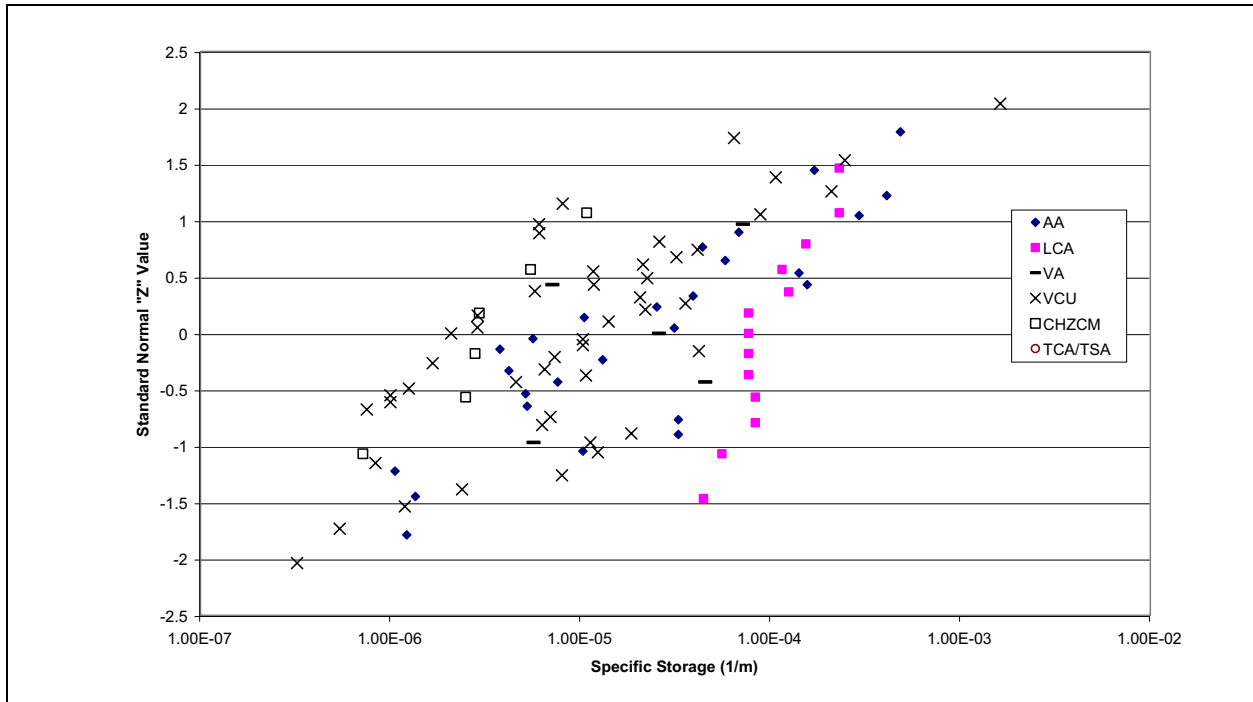


Figure 5-26
Specific Storage Probability Distributions

a variety of locations. The alluvium data are from locations primarily off the NTS. The LCA data are all from the USGS Amargosa tracer test site. The VA data are from several locations in northern Frenchman Flat (i.e., water wells WW-4 and WW-4a). The VCU data are from Yucca Mountain locations. The CHZCM and Tiva Canyon Aquifer (TCA)/TSA are from single locations ER-20-6 and UE-20d, respectively. The data span a 4-order of magnitude range of values. The specific storage value of about 1×10^{-3} is a suspect value because the associated storativity is about 1, which would imply a porosity of nearly 1, meaning the absence of aquifer material (a clearly impossible case).

The distributions for the AA, VA, VCU, and CHZCM are quite similar and could be taken as belonging to the same underlying distribution. The LCA and TCA/TSA appear to be quite different; however, each of those data sets represents only one location. Therefore, it is not clear how representative the data are of the broader distribution over the entire study area. The LCA data are from a location where the LCA is shallow. Consequently, these data likely do not represent the conditions in the LCA in areas where it is deeply buried within the model area. The TCA/TSA data were obtained from the testing of a large open interval crossing several aquifer and confining unit HSUs. The results were assigned to the aquifer units because it is assumed they produced the most water. Nonetheless, the TCA/TSA data are suspect. Finally, Sanchez-Vila et al. (1999) show that in the presence of heterogeneity, which always occurs in reality, storativity estimates will often vary strongly as a function of the relative transmissivity of the flow path between the pumping and observation well. Thus, storativity estimates depend on the degree of transmissivity heterogeneity. Sanchez-Vila et al. (1999) also suggest that a good estimate of true storativity is rarely obtained in practice from pumping tests. It is possible that much of the apparent scatter in specific storage values is unrelated to the actual variability of storage properties.

For the Pahute Mesa CAU model, if transient simulations are required, a log normal distribution through all the data excluding the TCA/TSA and LCA data will be used to bound the range of possible values, and a mean value of 1×10^{-5} 1/m will be used for all units.

5.7 Limitations

The data presented in this section come from a variety of sources and represent data measured at many different scales. Measurements have not been made in all HSUs. As a result, the distributions of hydraulic conductivity for some HSUs have been estimated based on similarity to other units for which data were available. Data from laboratory-scale measurements in fracture flow dominated formations cannot be used for the CAU-scale modeling because of the sampling bias during core recovery and testing. The core data do provide lower bound estimates of the hydraulic conductivity of the bedded and non-fractured confining units. Data from slug-test scale measurements are potentially useful, but appear to be of smaller mean value than corresponding constant-rate scale data. As a result, if slug-scale data are used, they have been increased to make the ranges of values similar to constant-rate scale data. The effect of spatial averaging that will occur

when values are assigned to model grids cells has been noted, but cannot be quantified. Nonetheless, it is apparent that the range of values observed in the data should not be assumed to represent the range of uncertainty at the model scale. During the modeling, scaling relationships will be developed, where possible. If satisfactory scaling relationships cannot be obtained, then the full range of uncertainty will be used, although it is recognized that doing so will overestimate the uncertainty.

Data are available for a number of HSUs within the Pahute Mesa study area; however, not all HSUs are represented by measurements. When data were not available, parameter ranges were assigned on the basis of similarity to other HSUs, or assigned larger ranges of uncertainty.

5.8 Summary

The hydraulic conductivity and specific storage coefficient data have been compiled and analyzed. Hydraulic conductivity measurements appear to be scale-dependent with the constant-rate scale data having a larger mean and somewhat smaller variance than the slug-test scale data. As previously stated, for purposes of modeling groundwater flow in the PM-OV flow domain, data derived from constant-rate tests are considered to be the most reliable, followed by data derived from slug tests. The laboratory-scale data may be applicable to porous formations such as the AA, but certainly are biased for any HSU that is dominated by fracture flow.

There is significant overlap in the ranges of hydraulic conductivity for volcanic units designated as aquifers, composite units, and confining units. A reason for this is the overlap of lithologies within these broad classifications. Composite units and some confining units contain some portions of aquifer lithologies and aquifers contain some portion of confining unit lithology. This leads to overlap in the distributions.

6.0 *Precipitation Recharge*

The groundwater flow system of the Pahute Mesa-Oasis Valley area is replenished by areal recharge from precipitation and underflow. In the arid environment of the NTS region, quantification of precipitation recharge is an important aspect of the groundwater flow system, and is difficult to achieve. This section reviews three different methods used to estimate recharge for the NTS region: an empirical mass-balance method and its derivatives, a deterministic method, and a chloride mass-balance method. The recharge models generated using these methods will be used to support the development of the CAU-scale groundwater flow model for the PM-OV area. The estimates are presented by hydrographic areas, referred to as hydrographic "basins" in some of the source references used.

6.1 *Objectives*

The objective of this data analysis activity is to estimate precipitation recharge rates and their spatial distribution over the NTS region, including the associated uncertainties. The resulting recharge distributions are used in the NTS regional groundwater flow model to generate a range of lateral boundary fluxes for the PM-OV groundwater flow model (see [Section 9.0](#)). These regional recharge distributions will also be used to extract recharge distributions for the PM-OV area during the development of the CAU-scale groundwater flow model.

6.2 *Approach*

The approach was to review all pertinent reports on precipitation and recharge for the NTS region, and to determine if methodologies that currently exist are applicable for defining a range of recharge volumes and areal distributions for use in numerical modeling. The resultant recharge models were then examined, evaluated, and compared for hydrographic area recharge volumes and areal distributions to identify trends and relationships between the methodologies. Limitations to the models were also evaluated. This approach yields a range of recharge volumes and areal distributions for the differing methodologies that can be used to limit the reasonable amount of recharge that could be occurring in the NTS area.

6.3 Data Types and Prioritization

Groundwater recharge data were compiled for the PM-OV area of investigation and surrounding region. The specific data types, their sources, and their prioritization for further evaluation are discussed in this section. Types of data needed for the creation of the predevelopment, steady-state flow model are as follows:

- Primary recharge information
- Precipitation rate distribution
- Land surface elevation distribution
- Method of recharge estimate

Major information sources are the DRI, the USGS, and various reports cited in this section. Information was obtained in the form of published and unpublished documents and datasets. Land surface elevation data were obtained from the USGS or USGS topographic maps.

6.4 Existing Recharge Model Descriptions

The following sections describe the recharge models considered in support of the Pahute Mesa-Oasis Valley groundwater flow model.

6.4.1 UGTA Recharge Model

The UGTA recharge model was first developed during the regional model evaluation (DOE/NV, 1997; IT, 1996a). This recharge model was derived using a modified Maxey-Eakin method (1949). Descriptions of the Maxey-Eakin method and the modified Maxey-Eakin method presented in this section were extracted from the recharge-discharge documentation package (IT, 1996a). A description of the updated UGTA recharge model is also provided.

6.4.1.1 Maxey-Eakin

Maxey and Eakin (1949) first described a method of estimating recharge to groundwater from precipitation in a report on groundwater in White River Valley, Nevada. The method was subsequently modified by Eakin et al. (1951). Maxey and Eakin (ME) (1949) used the Nevada precipitation map developed by Hardman in 1936. In their method, they estimated recharge by assuming that a zone-specific percentage of precipitation infiltrates to groundwater. The initial percentages considered recharge, based on precipitation, for the ME coefficients are as follows: 0 percent, less than 20.3 centimeters (cm); 3 percent, 20.3 to 30.5 cm; 7 percent, 30.5 to 38 cm; 15 percent, 38 to 50.8 cm; and 25 percent, greater than 50.8 cm.

These coefficients were determined by trial and error by balancing of recharge with estimates of groundwater discharge for 13 valleys in east-central Nevada (Maxey and Eakin, 1949). When the Maxey-Eakin method is used, recharge for a given hydrographic area is calculated using Equation 6-1:

$$R = \sum r_i P_i \quad (6-1)$$

where:

- R = Total Maxey-Eakin recharge for a given hydrographic area
 r_i = The Maxey-Eakin recharge coefficient for each delineated precipitation zone
 P_i = The volume of precipitation for each delineated precipitation zone

The Maxey-Eakin method was subsequently modified as it was used in several studies in Nevada to estimate recharge for various hydrographic areas (Eakin et al., 1951; Walker and Eakin, 1963; Malmberg, 1967; and Czarnecki, 1985). Eakin et al. (1951) described a modified Maxey-Eakin method, the area-altitude in a study on the hydrology of eastern Nevada. In this method, the Maxey-Eakin coefficients are associated with areas defined as ranges of altitudes, rather than directly related to precipitation. Recharge is assumed to occur where the mean annual precipitation is above 20.3 cm or the land surface elevation is above 1,700 m. Recharge then increases with elevation according to the Maxey-Eakin coefficients. Note that for all the studies in which the Maxey-Eakin method has been used, the Maxey-Eakin coefficients have remained the same for all precipitation zones, except for the lowest one. For this zone, Maxey and Eakin (1949) used 3 percent, Eakin et al. (1951) used 2 percent, Walker and Eakin (1963) used 1 percent.

6.4.1.2 Modified Maxey-Eakin Method

The recharge distribution used in the regional groundwater flow model (DOE/NV, 1997) was constructed using a modification of the Maxey-Eakin method (1949).

6.4.1.2.1 Methodology

The method included the following activities:

- Construct an updated precipitation map using new and existing data
- Calculate recharge using Maxey-Eakin coefficients
- Calculate total recharge volumes for individual hydrographic areas
- Redistribute a percentage of the total recharge within selected subareas to low-lying areas

The “Precipitation Map of Nevada” (Hardman, 1965) was used as a basis for construction of the precipitation map used to estimate the recharge distribution by the modified Maxey-Eakin method. The “Precipitation Map of Nevada” was adapted by Hardman in 1965 from an earlier version constructed by Hardman in 1936. The map coverage includes the entire state of Nevada, but does not include the Death Valley portion of the NTS regional groundwater flow system. To complete this portion of the precipitation map, the Death Valley section developed by James (1993) was used. Additional data used in the construction of the precipitation map included the precipitation station data (Jacobson, 1996; French, 1996), the Digital Elevation Model (DEM) from the USGS (1987), and a “Nevada Test Site Image Map” prepared by BN (1996). These data were used to validate the existing precipitation maps and any changes made to them in constructing the updated precipitation map.

6.4.1.2.2 Construction of the Digital Precipitation Map and Grid File

To estimate groundwater recharge, it was first necessary to generate a digital precipitation map (DOE/NV, 1997) of the NTS groundwater flow system. As stated previously, a combination of two existing precipitation maps served as the basis for constructing the digital precipitation map (Figure 6-1) by scanning and digitizing the precipitation contours from the existing maps, updating the digital map using current precipitation station data, and validating the map using satellite imagery and land surface elevations. Precipitation contours from the existing precipitation maps of Hardman (1965) and James (1993) were digitized into a three-dimensional design file. The contours were traced onto velum paper and scanned as digital images. The digital images were then geographically registered, and the contours digitized into the three-dimensional design file and set to the appropriate depth as “xyz” data. The z coordinate in the three-dimensional design file was attributed to the average annual precipitation depth in centimeters per year (cm/yr).

The precipitation station data were posted in the design file as “xyz” data with the z-coordinate as the average annual precipitation in inches per year. The coordinates of the station data were converted from geographic coordinates (longitude/latitude) to the projected coordinates (easting/northing, UTM Zone 11, NAD 27). Only those stations with greater than eight years of record were posted in the design file after determining the criteria of a usable station in discussions with regional experts and providers of the data (Jacobson, 1996; French, 1996). The selected precipitation stations are presented in Table 6-1.

Precipitation contours in selected areas were modified to incorporate the new data from the selected precipitation stations (Table 6-1). However, in most instances the precipitation station data validated the existing precipitation contours and only minimal modifications were necessary. The most notable modification was that of the 20.3-cm/yr contour between east Timber Mountain and west Yucca Flat (Figure 6-1). The modification of the 20.3 cm/yr contour in this area was substantiated by stations 29, 34, 36, 46, and 49 (Table 6-1). The extent of the area defined by the 20.3-cm/yr contour line was increased to accommodate these stations. Additional modifications on the NTS included the 12.7-cm/yr contour

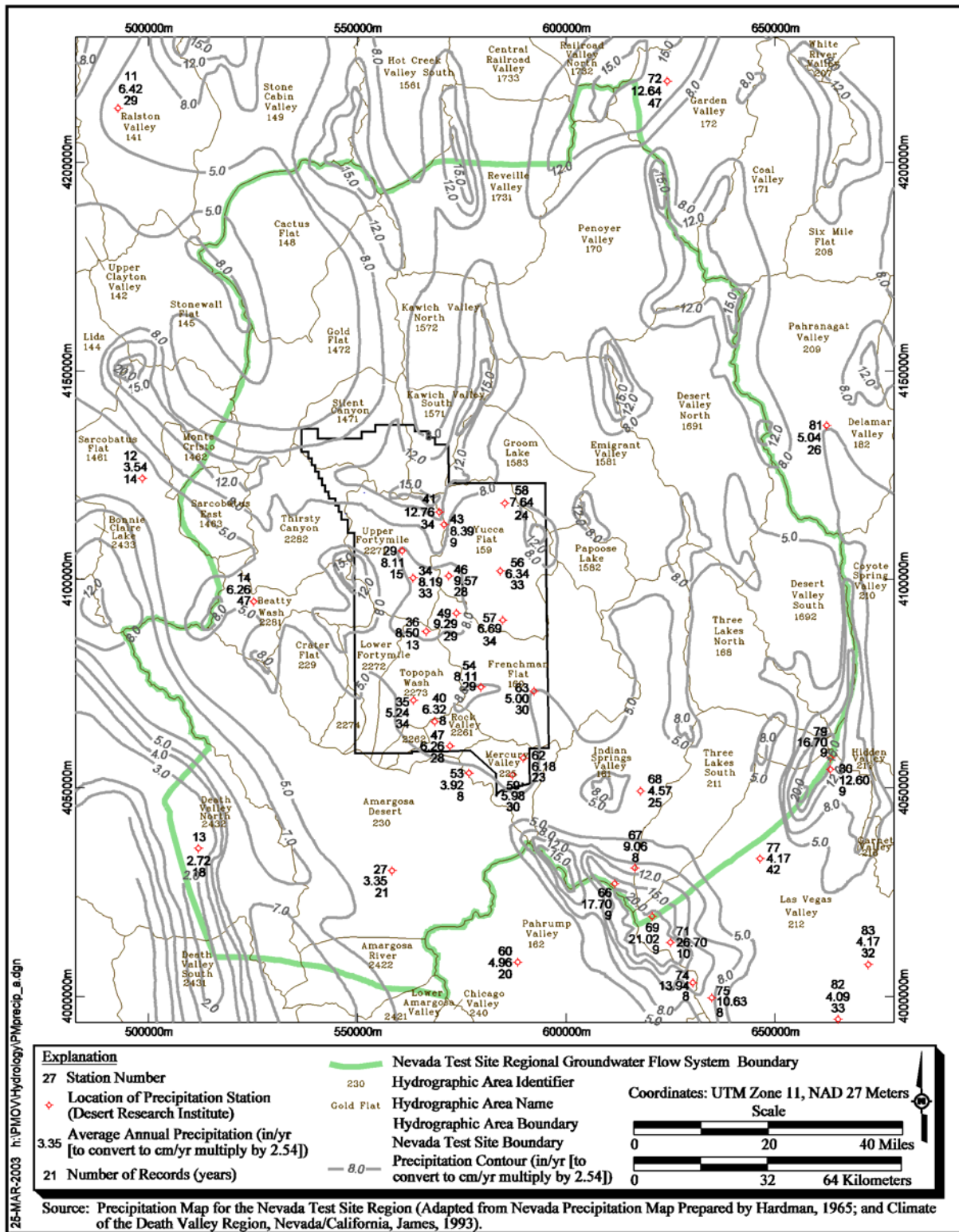


Figure 6-1
Precipitation Map for the Nevada Test Site Region

**Table 6-1
Precipitation Station Data**

Station Number	Station Name	UTM Zone 11, NAD 27		Land Surface Elevation (m)	Average Annual Precipitation	
		Easting (meters [m])	Northing (m)		Depth cm/yr (inches/yr)	Years Record
11	Tonopah Airport	492,689	4,213,009	1,655	16.3 (6.42)	29
12	Sarcobatus	498,522	4,124,251	1,225	9.0 (3.54)	14
13	Death Valley	511,946	4,035,517	-52	6.9 (2.72)	18
14	Beatty	525,210	4,094,706	1,082	15.9 (6.26)	47
27	Lathrop Wells	558,275	4,030,159	664	8.5 (3.35)	21
29	Little Feller 2	560,698	4,106,882	1,573	20.6 (8.11)	15
34	40 MN	563,341	4,100,364	1,469	20.8 (8.19)	33
35	4JA	563,445	4,071,032	1,043	13.3 (5.24)	34
36	Shoshone Basin	566,464	4,087,547	1,725	21.6 (8.50)	13
40	Skull Mountain Pass	568,500	4,065,887	1,186	16.1 (6.32)	8
41	Area 12 Mesa	569,624	4,116,171	2,283	32.4 (12.76)	34
43	Stockade Pass	570,759	4,113,178	2,053	21.3 (8.39)	9
46	Tippiah Spring 2	571,887	4,100,851	1,518	24.3 (9.57)	28
47	RV-1	572,151	4,060,050	1,036	15.9 (6.26)	28
49	Mid Valley	573,701	4,091,914	1,420	23.6 (9.29)	29
53	RV-Wash	576,721	4,053,568	866	10.0 (3.92)	8
54	Cane Springs	579,583	4,074,185	1,219	20.6 (8.11)	29
56	BJY	584,209	4,102,022	1,241	16.1 (6.34)	33
57	Yucca	584,791	4,090,231	1,195	17.0 (6.69)	34
58	PHS Farm	585,301	4,118,280	1,391	19.4 (7.64)	24
59	Desert Rock	587,122	4,053,108	1,005	15.2 (5.98)	30
60	Pahrump	588,385	4,008,227	823	12.6 (4.96)	20
62	Mercury	589,740	4,057,169	1,149	15.7 (6.18)	23
63	Well 5B	592,263	4,073,193	939	12.7 (5.00)	30
66	Trough Spring	610,107	4,026,349	2,512	45.0 (17.70)	9
67	Cold Creek	613,563	4,030,708	1,862	23.0 (9.06)	8
68	Indian Springs	617,793	4,049,256	951	11.6 (4.57)	25
69	Lee Canyon	619,087	4,018,516	2,594	53.4 (21.02)	9
71	Kyle Canyon	623,466	4,012,260	2,365	67.8 (26.70)	10
72	Adaven	624,188	4,219,501	1,905	32.1 (12.64)	47
74	Roberts Ranch	627,418	4,003,163	1,862	35.4 (13.94)	8
75	Red Rock Summit	631,972	3,999,532	1,984	27.0 (10.63)	8
79	Hayford Peak	660,932	4,058,248	2,999	42.4 (16.70)	9
80	Hidden Forest	660,934	4,055,504	2,304	32.0 (12.60)	9
81	Alamo	662,347	4,136,921	1,049	12.8 (5.04)	26
82	Las Vegas Airport	665,072	3,994,546	661	10.4 (4.09)	33
83	Sunrise Manor	672,321	4,007,633	555	10.6 (4.17)	32

Source: Jacobson, 1996; French, 1996

line below Timber Mountain extending from Yucca Mountain to east of Mercury. This contour line was moved south to accommodate stations 35, 40, 47, 53, 56, 57, 59, 62, and 63. Other modifications include refining the contours on Spring Mountain in order to accommodate stations 66, 67, 69, 71, 74, and 75. Modifications in this area consisted of expanding the precipitation area in the southeast portion of the mountains. The last notable modification was that of the 20.3- to 30.5-cm/yr contours at the southern portion of the Grant Range just north of the Worthington Mountains. Modifications in this area included reshaping the contours to accommodate Station 72. The satellite imagery and DEM data were consulted prior to modifying the contours. Contour lines were only modified where there was sufficient data to substantiate any changes.

The precipitation map was validated using the DEM and satellite imagery. The DEM grid was contoured according to the land-area model of Eakin et al. (1951) to show the 1,524- to 2,439-m contour lines. The precipitation map was validated by superposing the precipitation data (contours and station data) on the digital elevation model. The DEM is accurate to 92 meters. The plot was used to ensure the contours were positioned correctly relative to elevation. In general, the contour shape coincides with the shape of the topographic features of the mountain ranges. Due to the poor copy and large scale of the Hardman map, the validation process proved to be a very important step in constructing the digital precipitation map as error was introduced in the tracing and scanning the maps developed by Hardman (1965) and James (1993).

The digital precipitation map was constructed so a precipitation grid file could be generated for calculation of the recharge distribution using the modified Maxey-Eakin method. The precipitation grid was generated after the final modifications to the digital precipitation map were made and the map was validated. To construct the precipitation grid, the precipitation data (contours and station data) in the design file were extracted as “xyz” data to create a Triangulated Irregular Network (TIN) model. A TIN model is a means of representing spatial data using triangles. For example, given three data points in “xyz” space, a triangle is constructed by connecting the data points. The triangle is a plane in “xyz” space; therefore, all “xyz” data on the plane are defined. The TIN model uses triangles to interpolate “xyz” data from known “xyz” data points (contours and precipitation station data). After the TIN model was constructed, a grid file was generated with a 1x1 kilometer node spacing.

The final precipitation distribution was generated by assigning each precipitation data point to its corresponding hydrographic area. This was accomplished by extracting the precipitation data points within a hydrographic area and assigning the hydrographic area number to each one resulting in the following format:
X:easting, Y:northing, Z1:precipitation rate (inches per year [in./yr]),
Z2:hydrographic area number. The final precipitation distribution was completed by assigning zero (0.00000) precipitation to those data points outside the NTS groundwater flow system. The total precipitation was then calculated for each hydrographic area within the NTS groundwater flow system.

6.4.1.2.3 Final Precipitation Distribution

The final precipitation distribution is presented as [Figure6-1](#), with precipitation depth contours and the precipitation station data, the NTS groundwater flow system boundary, and the digital elevation model. As indicated by [Figure6-1](#), the precipitation depth increases with land surface elevation and follows the general topography. The Spring Mountains in the south receive the most precipitation, followed by the Sheep Range to the east. Other mountain ranges in the NTS groundwater flow system receive approximately 30.5 to 38.1 cm/yr. Death Valley receives the least precipitation with approximately 5.08 cm/yr. [Table6-2](#) lists precipitation totals calculated for the hydrographic areas. The total precipitation calculated from the precipitation distribution (column 3) only includes the precipitation within the NTS groundwater flow system boundary. Any precipitation outside the groundwater flow system boundary is not included in the total for the hydrographic area. Total precipitation from Scott et al. (1971) is included in the table for comparison (columns 4 and 5). The highlighted totals in column 4 were prorated based on the area within the flow system boundary using the following equation: (published precipitation total) x ([area within flow system boundary] ÷ [total area of hydrographic area]). 1

In general, the comparison between the calculated precipitation and published precipitation is reasonably good; the difference between the two totals is 118,343 cubic meters per day (m³/d).

For each, the maximum precipitation is found in the Tikaboo and Emigrant Valley hydrographic areas. The precipitation totals for those hydrographic areas including testing areas (Gold Flat, Yucca Flat, and Frenchman Flat) are similar to the published data. The hydrographic areas with the largest discrepancy between totals are the Las Vegas Valley and Amargosa Desert. These hydrographic areas lend very little, if any, recharge to the NTS groundwater flow system and should not effect the modeling results.

Possible causes of discrepancies observed between the calculated precipitation and the published totals are as follows:

- Error introduced during the tracing and scanning of the Hardman (1965) and James (1993) maps
- The use of different methods to construct the precipitation map
- The use of different techniques to calculate the totals (i.e., summing individual grid nodes versus averaging contours within the hydrographic area)
- Rounding errors

Table 6-2
Comparison of Precipitation Volumes to Published Values by Hydrographic Area

Hydrographic Area		Total Precipitation Calculated from Distribution (cubic meters per day [m ³ /d])	Published Precipitation Data (Scott et al., 1971)	
Hydrographic Area No.	Hydrographic Area Name		Total Precipitation within Flow System (m ³ /d)	Total Precipitation in Hydrographic Area (m ³ /d)
145	Stonewall Flat	2,546	4,878	371,737
146	Sarcobatus Flat	202,290	311,556	642,091
147	Gold Flat	889,195	844,856	844,856
148	Cactus Flat	491,956	439,325	439,325
149	Stone Cabin Valley	1,471	2,402	1,182,799
156	Hot Creek Valley	1,846	2,544	1,317,976
157	Kawich Valley	622,296	506,914	506,914
158	Emigrant Valley	1,164,236	959,757	959,757
159	Yucca Flat	461,941	337,942	337,942
160	Frenchman Flat	511,223	506,914	506,914
161	Indian Springs Valley	728,691	912,445	912,445
162	Pahrump Valley	1,531	5,397	1,419,358
168	Three-Lakes Valley North	276,120	371,737	371,737
169	Tikaboo Valley	1,260,641	1,284,181	1,284,181
170	Penoyer Valley	1,127,129	912,445	912,445
171	Coal Valley	835	1,249	574,502
172	Garden Valley	68,283	115,092	777,268
173	Railroad Valley South	681,245	844,856	844,856
209	Pahranaagat Valley	1,446	3,564	912,445
210	Coyote Spring Valley	13,005	18,106	743,473
211	Three-Lakes Valley South	359,289	439,325	439,325
212	Las Vegas Valley	248,265	613,223	2,230,420
225	Mercury Valley	104,576	128,418	128,418
226	Rock Valley	85,759	87,865	87,865
227	Fortymile Canyon	715,443	669,126	669,126
228	Oasis Valley	660,013	506,914	506,914
229	Crater Flat	153,895	206,145	206,145
230	Amargosa Desert	1,131,415	811,062	811,062
242	Amargosa River	117,067	117,067 ^a	
243	Death Valley	398,318	398,318 ^a	
Total Precipitation:		12,481,966	12,363,623	

Source: IT, 1996 a

^aCalculated hydrographic area total included in published precipitation total. Published data for this hydrographic area not available at time of printing.

6.4.1.2.4 Recharge

In Nevada, the ME method has been used to calculate the total volume of recharge to a given hydrographic area. Although the method indirectly correlates recharge magnitude to precipitation zones, the method does not take into account the specific locations where recharge actually occurs. In this investigation, we will assume that the majority of the recharge occurs at higher elevations as assumed in the Maxey-Eakin method. However, smaller portions of the recharge have been shown to occur at lower elevations, in washes, and in canyons. In a study of groundwater recharge in Fortymile Canyon, Savard (1994) reported that recharge does occur along the canyon after streamflow events, as evidenced by rising water levels. Consequently, for the purpose of this regional investigation, recharge was determined in two major steps: generation of a preliminary recharge distribution and reallocation of a fraction of this recharge to canyons and washes.

Preliminary Recharge Distribution

A preliminary recharge distribution was generated using the updated precipitation map and the ME coefficients. The area covering the NTS regional groundwater flow system was subdivided according to the boundaries of hydrographic areas (HA) as defined by Harrill et al. (1988). Thirty major hydrographic areas were identified within this area. Recharge was calculated for each of the HA using the 1x1 kilometer (km) precipitation grid and two sets of ME coefficients.

The recharge rates were first calculated for each 1x1 km grid cell by multiplying the corresponding precipitation value by the Maxey-Eakin coefficients. For the lower zone, recharge was calculated using an ME coefficient of two percent. Total recharge values for the groundwater flow system were also calculated using the one percent and three percent ME coefficient for the lowest recharge zone to evaluate the range of potential recharge. The total recharge calculated from the recharge distribution only includes the recharge within the NTS groundwater flow system boundary. As for precipitation, any recharge that occurs outside of the groundwater flow system boundary is not included in the total for the hydrographic area.

Important recharge areas are located in the Belted, Groom, and Timpahute ranges in the north, in the Pahrnagat and Sheep ranges to the east, and in the Spring Mountains on the southeastern boundary. The estimated total recharge for the NTS regional groundwater flow system is 233,447 m³/d. The discrepancies observed between the calculated values and the literature values for some of the hydrographic areas may be due to two reasons. The first reason is that literature values were derived for recharge from the 1 x 1 km precipitation grid, which can introduce additional errors. The recharge range derived using the one and three percent ME coefficient for the lower recharge zone is from 177,484 to 289,410 m³/d.

Recharge Allocation

A method by which a hydrographic area where recharge to groundwater may occur by infiltration through canyons and washes was developed. The method consists of identifying different types of recharge reallocation zones

corresponding to the canyons and washes, and reallocating portions of the total HA recharge to the identified zones. A given hydrographic area may be subdivided into three types of recharge zones: A, B, and C.

- Type A Zone: Upgradient recharge areas that receive greater than 20.3 cm of annual precipitation per year. This is where the majority of infiltration occurs.
- Type B Zone: Canyon-wash recharge areas that receive less than 20.3 cm of precipitation per year, but include alluvial fans and streams through which recharge may occur.
- Type C Zone: Areas of no recharge that receive less than 20.3 cm of precipitation per year, but contain no alluvial fans or stream reaches to facilitate infiltration.

Recharge volumes were calculated for each subarea as outlined above. Nine hydrographic areas where type B zones occur were identified on the NTS and vicinity. The subject HAs are Topopah Wash, Beatty Wash, Thirsty Canyon, Lower Fortymile Canyon, Upper Fortymile Canyon, Frenchman Flat, Yucca Flat, Silent Canyon, Kawich Valley South, and Groom Lake (Figure 6-2).

Each HA was further subdivided into Types A, B, and C. Type B areas are further subdivided into three types of recharge areas: B1, B2, and B3. Type B1 represents upland canyon and valley washes and stream reaches, Type B2 represents mountain front washes and stream reaches, and Type B3 represents valley bottom washes and stream reaches.

For each HA where Type B areas are known to exist, a portion of the HA recharge volume is redistributed from Type A areas to Type B areas. It is important to emphasize that the total rate of recharge calculated for each area was not modified; only the areal distribution is modified. The calculated total Maxey-Eakin recharge rate (V - total recharge rate τ in the hydrographic area) is redistributed from Type A areas (V_A) where recharge rates are greater than zero to A

Type B areas (V_B) such that:

$$V_T = V_A + V_B \quad (6-2)$$

where:

- V_T = Total recharge rate
- V_A = Recharge rate in Type A areas
- V_B = Recharge rate in Type B areas

The redistribution factor, α , is a fraction of the total recharge (between 0 and 1) so that $V_A = \alpha V_T$ and $V_B = (1-\alpha)V_T$. For example, if $V = 100$ and $\alpha = .30$, then $V_A = 30$ and $V_B = 70$.

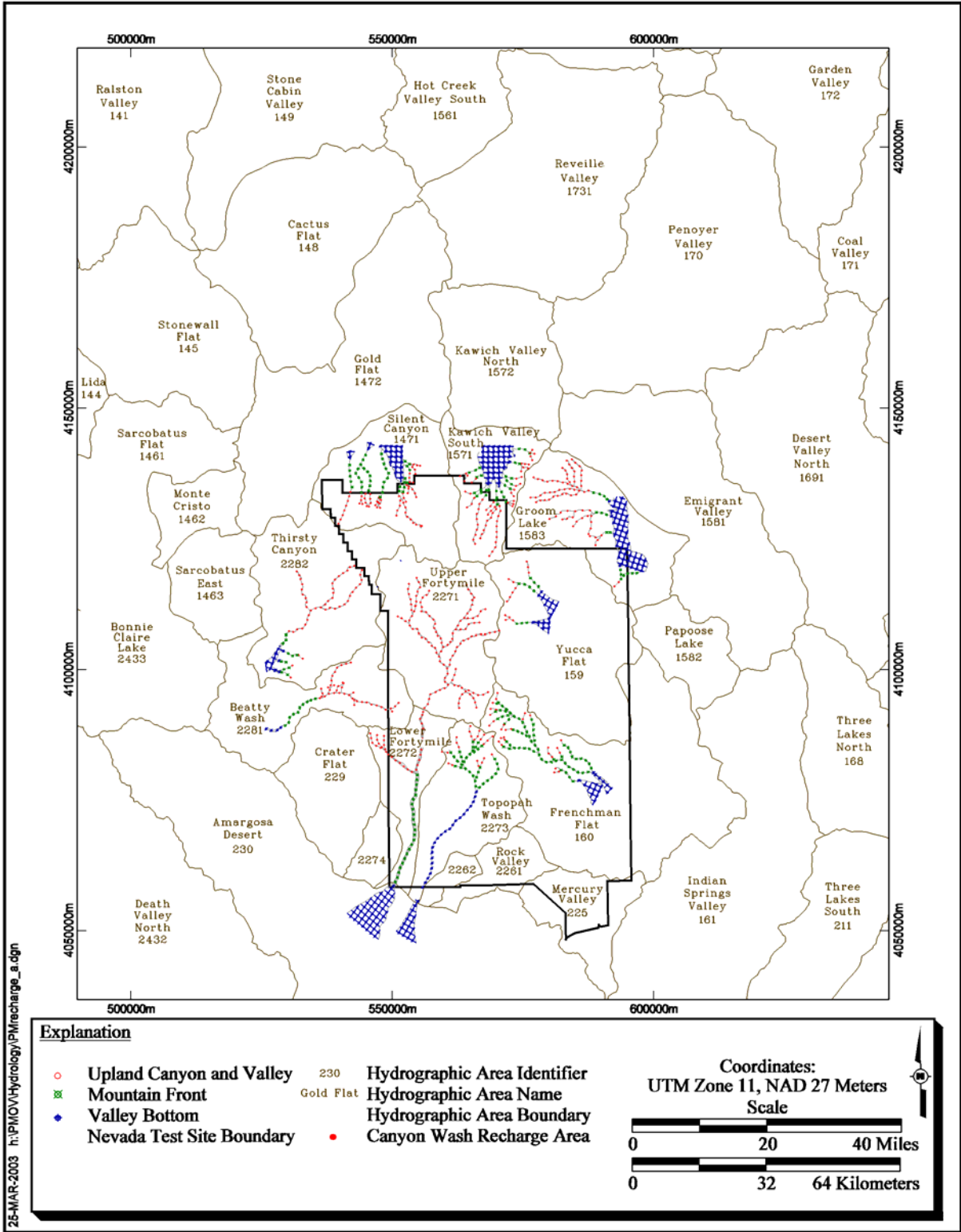


Figure 6-2
Potential Recharge Redistribution Areas in the Nevada Test Site Region

For each HA, the recharge rates in Type B areas are further distributed to each recharge subarea (B1, B2, and B3) based on fractions β , γ , and δ of recharge volume in B (V), such that the B following relationships hold true:

$$\beta + \gamma + \delta = 1 \quad (6-3)$$

where:

β = Fraction of V assigned to Type B1 subareas
 γ = Fraction of V assigned to Type B2 subareas
 δ = Fraction of V assigned to Type B3 subareas

The areas of types B1, B2, and B3 are canyons or washes. Within a given HA, each of them is subdivided into several reaches that are compatible with a selected grid. Recharge rates for each reach are then obtained by dividing the recharge rate assigned to a given subarea type (B1, B2, or B3) by the number of reaches available within a given HA.

A utility FORTRAN code was developed to implement the modified Maxey-Eakin method. The code requires the Maxey-Eakin recharge distribution by HA; the spatial distribution of different types of recharge areas described above; and values for β , γ , δ , and ϵ based on estimates of recharge rates at B-type and subtype areas. The code calculates a new recharge distribution in the form of a grid that is made compatible with the flow model grid, an important feature that allowed adjusting of the recharge grid during the calibration process. The code listing and QA requirements are provided in the *Groundwater Flow Model Documentation Package* (IT, 1997a). The recharge reallocation coefficients (β , γ , δ , and ϵ) are unknown because the amounts of recharge that occur in Type B areas located in the different hydrographic areas are also largely unknown. Arbitrary initial values were assigned to these coefficients to generate the initial recharge distribution. These values were then adjusted during the groundwater flow model calibration process.

The recharge distribution used in the UGTA Regional Groundwater Flow Model was remapped for this document and is shown in [Figure 6-3](#). The process and the results of the recharge data analysis conducted in support of the NTS regional model are detailed in the *Groundwater Recharge and Discharge Data Documentation Package* (IT, 1996a). The final recharge distribution is provided in the *Groundwater Flow Model Documentation Package* (IT, 1997a).

6.4.1.3 Updated UGTA Recharge Model

An additional recharge distribution was generated by updating the original UGTA recharge model. The update included the redigitization and recontouring of the precipitation map, and the redigitization of the hydrographic areas using larger-scale maps. Following the update, a comparison to other recharge models was conducted. The updated UGTA recharge distribution is also referred to as the revised Maxey-Eakin distribution in this document.

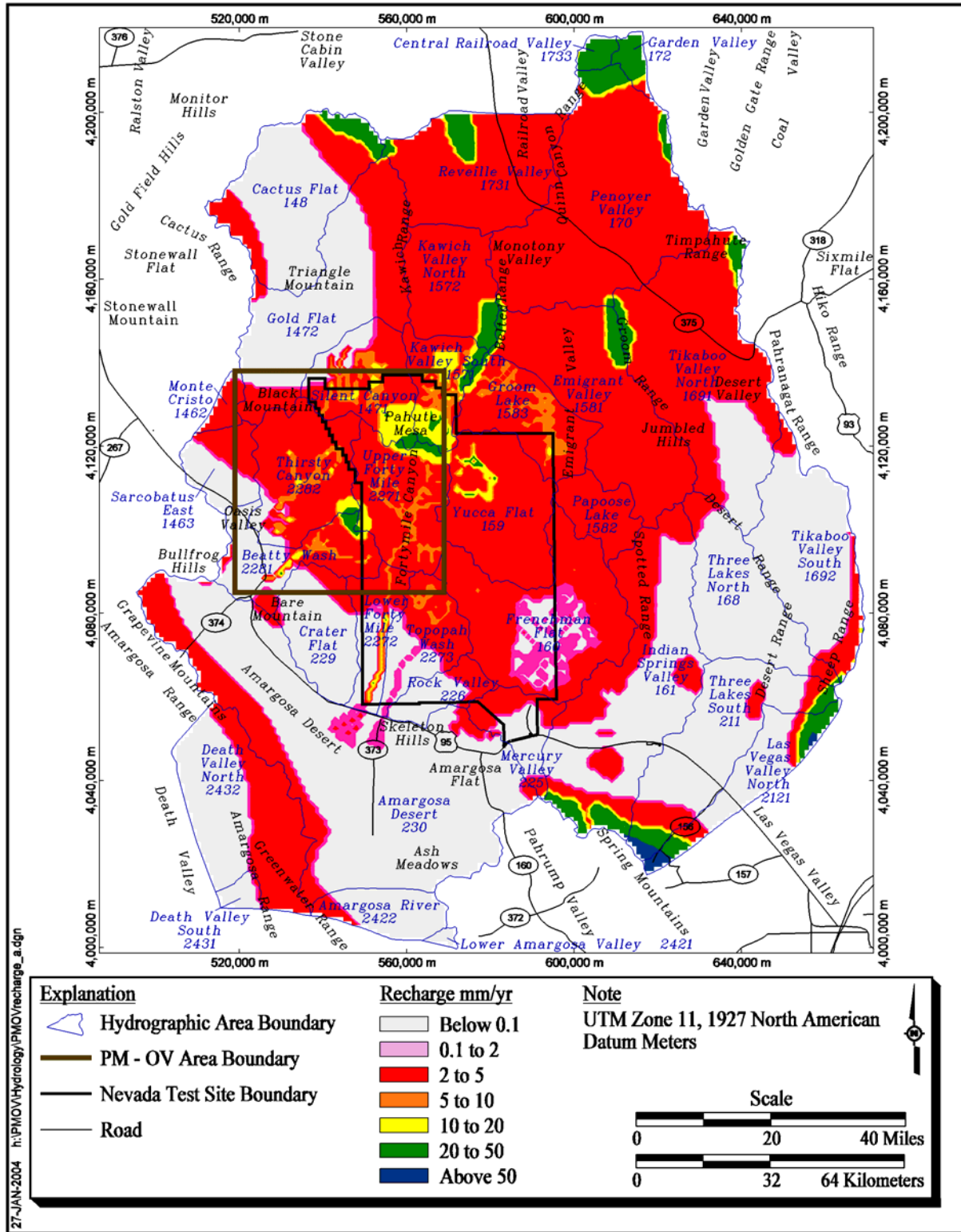


Figure 6-3
NTS Regional Model Recharge Distribution

The main precipitation map was redigitized as some minor locational errors were found in the initial precipitation distribution. A different contouring program (EarthVision®[Dynamic Graphics, 2002]) was used to grid the data. The USGS precipitation distribution in the southeast portion of the NTS area itself was not included in this version. All other aspects of the recharge calculations remained the same, including the redistribution. The results of this version of the UGTA recharge distribution are shown in [Figure 6-4](#).

The digitization of the original hydrographic area boundaries was found to be inaccurate. As a result, a grid cell would be included in the volumetric totals for a neighboring hydrographic area. Also, as a result of the digitization inaccuracies, several hydrographic areas were inadvertently included in the NTS region because one or two grid cells fell into the wrong peripheral hydrographic area. These inaccuracies have been corrected by redigitization of the hydrographic area boundaries at a greater resolution.

Comparisons to other recharge models can be found in the summary section table ([Table 6-5](#)). The recharge volumes for both UGTA-based recharge distributions differ from the original values found in the UGTA regional report because of the changes to the definitions of the hydrographic areas.

6.4.2 U.S. Geological Survey Recharge Model (Hevesi et al., 2003)

The following description of the USGS net infiltration/recharge model is taken verbatim from the abstract of a report entitled: *Simulation of Net Infiltration and Potential Recharge Using a Distributed Parameter Watershed Model For The Death Valley Region, Nevada And California*, by Joseph A. Hevesi, Alan L. Flint, and Lorraine E. Flint (Hevesi et al., 2003).

"The U.S. Geological Survey, in cooperation with the Department of Energy and the National Park Service, is developing a regional saturated-zone groundwater flow model for the Death Valley region to help evaluate potential radionuclide transport and to assess potential impacts of groundwater resources development. To define upper boundary conditions for the flow model, the quantity and spatial distribution of recharge are needed, and the effects of variable climatic conditions on recharge need to be evaluated. Although recharge has been estimated for most of the topographic basins in the Death Valley region, the uncertainty of these estimates remains high, and the spatial variability of recharge within basins has not been quantified. On more localized scales within basins, spatial variability in recharge is likely to be high because of differences in bedrock permeability, soil thickness, and contributions to recharge along active stream channels. A better understanding of the local-scale spatial variability in recharge, along with the effect of climate change on the magnitude and distribution of recharge, is needed to reduce uncertainty in modeling groundwater flow.

This study presents the development and application of a distributed parameter watershed model to estimate the temporal and spatial distribution of net infiltration for the Death Valley region. Net-infiltration estimates quantify the downward percolation of water across the lower boundary of the root-zone and

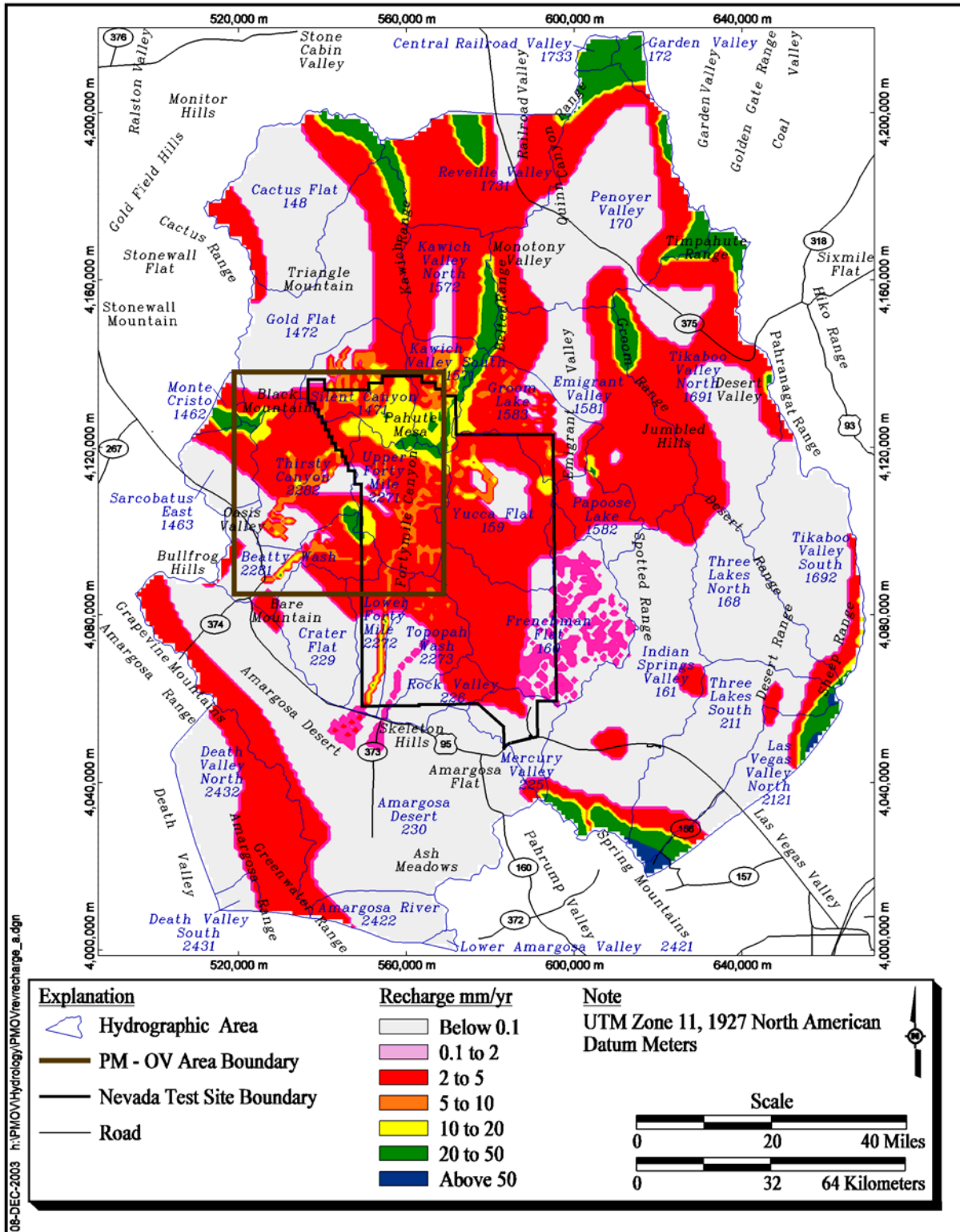


Figure 6-4
Revised Maxey-Eakin Based Recharge in the NTS Region

are used as an indication of potential recharge under current climate conditions. The distributed-parameter watershed model is an application of the water balance method, and provides a deterministic representation of the processes controlling net infiltration and potential recharge. The model uses daily climate input (precipitation and air temperature) and a spatially detailed representation of watershed characteristics to simulate daily net infiltration at all locations in the watershed, including active stream channels. The temporal distribution of daily, monthly, and annual net infiltration can be used to evaluate the potential impact of future climatic conditions on potential recharge.

Model development required application of GIS methods to define a set of spatially distributed input parameters over a modeling grid defined by a digital-elevation model and consisting of more than 1 million nodes. The digital elevation model was used to define many of the required model parameters, including a set of topographic parameters characterizing shading effects and parameters used for surface water flow routing of total daily discharge. Surface water flow routing was performed across all model grid cells using an 8-directional, convergent flow routing algorithm where downstream cells were defined by grid cell elevations. The flow routing parameters consisted of upstream and downstream cell location identifiers, and the total number of upstream cells for each grid cell location. A six-layered root zone system consisting of 5 soil layers and 1 bedrock layer was used to model evapotranspiration, drainage and redistribution of moisture in the root zone, and net infiltration across the bottom of the root-zone.

Model calibration consisted of qualitative and quantitative comparisons of simulated stream flow to historical stream flow records in the Death Valley region, in conjunction with comparisons of basin-wide average net infiltration to previous estimates of basin-wide recharge. In the calibration process, various model parameters were adjusted to establish the best set of model parameters based on a simultaneous fit to all available stream flow records. Parameters adjusted during calibration included bedrock saturated hydraulic conductivity, root density, storm duration, and parameters defining stream-channel characteristics (soil saturated hydraulic conductivity and wetted area). Results from the calibration process indicated that for many locations the spatial coverage of daily climate records in the Death Valley region is not sufficient for representing local-scale, high intensity summer storms that cause a significant portion of the recorded stream flows, especially for smaller-area, higher-elevation watersheds. In addition, the calibration results indicated a high sensitivity in simulated stream flow because of uncertainty in the parameters defining stream channel characteristics. Comparison of simulated net infiltration to basin-wide estimates of recharge indicated model sensitivity to estimates of bedrock hydraulic conductivity and root density.

A selected model was applied to develop 50-year (1950 through 1999) simulations of daily net infiltration for the Death Valley region. Simulation results for the area of the groundwater flow model include an average net infiltration rate of 2.8 mm/year, or a total potential recharge volume of 342,000 cubic meters per day. The net infiltration result represents a potential recharge rate that is about 1.6 percent of a the modeled 1950 to 1999 average annual precipitation rate of

171.3 mm/year over the area of the groundwater flow model. Simulation results also include an average runoff generation rate of 2.2 mm/year and an average run-on infiltration rate of 2.0 mm/year. Average surface water inflow into playa lakebeds is simulated to be 0.20 mm/year, corresponding to an average daily inflow volume of 24,800 cubic meters (less than 10 percent of the runoff generated) that is assumed to evaporate from the playas. The maximum run-on infiltration rate is 1,514 mm/year, and results in the maximum net infiltration rate of 1,262 mm/year for an active channel location.

To evaluate model sensitivity, 3 alternative models were used to develop 50 year simulations of net infiltration. Results indicated that simulated daily stream flow is sensitive to uncertainty in estimates of storm duration and stream channel characteristics, and to a lesser degree uncertainty in estimates of bedrock hydraulic conductivity. Model comparison indicated that infiltration from surface water run-on accounts for only about 14 percent of the total net infiltration volume for the Death Valley regional flow system. However, for some basins within the regional flow system, surface water flow may contribute as much as 40 percent to the total net infiltration volume. Net infiltration showed a high sensitivity to uncertainty in bedrock hydraulic conductivity and root density. Both stream flow and net infiltration are strongly sensitive to uncertainty in spatially distributed precipitation and estimated soil thickness. A more robust estimate of net infiltration may be represented by averaging results for two or more models, as opposed to selecting a single realization.

The 50-year simulation results were evaluated using a comparison of net infiltration estimates with previous basin-wide recharge estimates for 42 hydrographic areas and subareas in the Death Valley region. The net infiltration results are generally consistent with the recharge estimates, although net infiltration shows less variability on a basin-wide scale. Basin-wide net infiltration volumes are lower than recharge volumes for most areas with high recharge estimates, such as Pahrump Valley and Las Vegas Valley, and higher than recharge for most areas with low recharge estimates, including Stonewall Flat, the Lower Amargosa Valley, and Fortymile Canyon. Areas where net infiltration and recharge estimates are in good agreement include Gold Flat, Kawich Valley, Lida Valley, Amargosa Desert, and Tikaboo Valley.

A best-fit model was selected on the combined basis of a comparison to streamflow records and a comparison the previous estimates of basin-wide recharge. The selected model provides a total net infiltration volume of 413,000 cubic meters per day for all hydrographic areas having estimates of recharge, and this is in good agreement with the total estimated basin-wide recharge volume of 431,000 cubic meters per day for the same area. The selected model provides a net infiltration estimate of 342,000 cubic meters per day for the area of the Death Valley regional flow system groundwater model, compared to an estimated recharge volume of 266,800 cubic meters per day obtained by calibrating the groundwater model to the observed potentiometric surface and estimated discharge.

Results from the selected model were compared with results obtained for 3 alternate net infiltration models to evaluate the importance of surface water flow on potential recharge in the Death Valley regional flow system, and to help

evaluate model uncertainty. By averaging results from two or more different realizations of net infiltration, a better agreement is obtained to the total recharge estimated by the groundwater flow model water. Due to uncertainty in many of the input parameters used in modeling net infiltration, averaging results from multiple realizations is likely to provide a more robust estimate of current climate potential recharge (Hevesi et al., 2003)."

It is important to note that the values just cited for volumes of recharge are for a larger area than was applied in this study. Corresponding volumes on a hydrographic area by hydrographic area basis and total equivalent area volumes will be presented later in this section. This study incorporated many parameters not fully discussed in the abstract but that are important to understanding how this methodology was applied. The following discussion elaborates on these parameters and their effects on the resultant recharge distribution and magnitude.

For this study, the base precipitation was developed using the Parameter-Elevation Regressions on Independent Slopes Model (PRISM) code, and is generally consistent with other elevation-correlation models used to estimate precipitation in the Death Valley region. The authors point out that an "extraordinarily high degree of uncertainty remains in estimated precipitation" because of sparse data, and that the uncertainty is highest for remote high elevation locations because of limited records and measurement error associated with snow. For lower elevations, the estimates are more consistent.

Vegetation was also analyzed to develop spatial distribution of types as well as density. Vegetation was mapped from satellite imagery and other records as part of the USGS/Biological Resources Division (BRD) National Gap Analysis Program (GAP). The Western region vegetation map (WESTVEG) was used for this study. This information is critical to estimate the evapotranspiration component for this model.

This model incorporated soils in a quasi-3D methodology by not only inputting the soil types but also their thickness in a layered properties dataset using from one to six layers. A state-compiled geospatial database for soil properties (STATSGO) was used as the base for mapping soil units. From this the maximum and minimum thickness for the layers including their averaged thickness and percent coverage was developed. This produced an input map of calculated averaged soil textures and particle size-based soil properties for the model. The lowest layer in the soil profile was designated as bedrock.

The bedrock was also mapped where soil units were thin or absent so that infiltration rates into the bedrock could be incorporated into the model.

Overland flow originates as excess water within each cell that exceeds the infiltration and evapotranspiration rate for that cell. This excess runoff is routed to downstream cells where it is added to the net water input to the soils in the downstream run-on cells. Stream channel characteristics are a sensitive input parameter for this model as stated in the abstract.

These major components form the conceptual model of precipitation with infiltration of rain, snowmelt, or surface water into the soil or bedrock, with subsequent bare-soil evaporation and transpiration from the root zone. All water percolating past the root zone is considered net infiltration. All excess water can become overland flow to downstream cells.

The model inputs for the INFILv3 (Table 6-3) model consist of:

Climatic: daily climate inputs, model coefficients for monthly climate models, and monthly atmospheric parameters.

Digital Maps: DEM, spatial distribution of rock types, soil types, and vegetation types.

Attribute Tables: bedrock and deep alluvium, soil, and vegetation properties.

Model Control Options: simulation period, initial conditions, seasonal duration, stream channel characteristics, snowmelt and sublimation parameters, and input and output format options.

Table 6-3 from the USGS report details all of the input parameters including the source data, pre-processing (if any), parameter name, description, use, and the units and estimated accuracy of the data. Two of the four USGS models documented in their report are included here. Model 1 (Figure 6-5) includes the runoff/run-on component in recharge, and Model 2 (Figure 6-6) which does not. The table for hydrographic area volumetric totals is discussed in the summary section.

6.4.3 Desert Research Institute Recharge Model (Russell and Minor, 2002)

The following description of the DRI net infiltration/recharge determination is taken verbatim from the abstract of a report titled: *Reconnaissance Estimates of Recharge Based on an Elevation-dependent Chloride Mass-balance Approach* by Charles E. Russell and Tim Minor (Russell and Minor, 2002).

"Significant uncertainty is associated with efforts to quantify recharge in arid regions such as southern Nevada. However, accurate estimates of groundwater recharge are necessary to understanding the long-term sustainability of groundwater resources and predictions of groundwater flow rates and directions. Currently, the most widely accepted method for estimating recharge in southern Nevada is the Maxey and Eakin method. This method has been applied to most basins within Nevada and has been independently verified as a reconnaissance level estimate of recharge through several studies. Recharge estimates derived from the Maxey and Eakin and other recharge methodologies ultimately based upon measures or estimates of groundwater discharge (outflow methods) should be augmented by a tracer-based aquifer response method. The objective of this study was to improve an existing aquifer-response method that was based on the chloride mass-balance approach. Improvements were designed to incorporate

Table 6-3
INFILv3 Input Parameters (Directly from Hevesi et al., 2003)
 (Page 1 of 5)

Source Data	Preprocessing	Input File	Parameter Name	Parameter Description	Parameter Use	Units	Parameter Accuracy
DEM	GIS Calculated	Watershed File	EIEV(rows,cols)	Land surface elevation	Potential evapotranspiration, spatial interpolation models	m	High
		Watershed File	SLP(rows,cols)	Land surface slope	Potential evapotranspiration, Streamflow routing	u	High
		Watershed File	ASP(rows,cols)	Land surface aspect	Potential evapotranspiration	u	High
		Watershed File	EAST(rows,cols)	DEM grid cell east-west coordinate	Grid cell location, spatial interpolation models	m	High
		Watershed File	NORTH(r,c)	DEM grid cell east-west coordinate	Grid cell location, spatial interpolation models	m	High
		Watershed File	LAT(r,c)	DEM grid cell latitude	Potential evapotranspiration	dd	High
		Watershed File	LON(r,c)	DEM grid cell latitude	Potential evapotranspiration	dd	High
	SKYVIEW Calculated	Watershed File	RIDGE(r,c,36)	36 blocking ridge angles	Potential evapotranspiration	d	Medium
		Watershed File	SKYVIEW(r,c)	Reduction in total skyview	Potential evapotranspiration	u	Medium
	GRDSORT01 Calculated	Watershed File	LOCID(r,c)	Location identifier for upstream cell	Streamflow routing	i	Medium
	ROUTER03 Calculated	Watershed File	IROUT(r,c)	Location identifier for downstream cell	Streamflow routing	i	Medium
Watershed File		UPCELLs(r,c)	Number of upstream cells	Streamflow routing	i	Medium	
STATSGO	GIS	Watershed File	SOILTYPE(r,c)	Map code for STATSGO soil units	Spatial distribution of soil properties	i	Medium
	STATSGO34	Watershed File	SOILTHCK(r,c)	Estimated soil thickness for root-zone	Root-zone layer thickness	m	Low
		Soil-attribute Table	SPOR(soiltype)	Soil porosity	Root-zone storage capacity	U	Medium
		Soil-attribute Table	SWP(soiltype)	Soil wilting point	Root-zone storage capacity, evapotranspiration model	U	Medium
		Soil-attribute Table	SKS(soiltype)	Soil saturated hydraulic conductivity	Root-zone infiltration and drainage function	mm/day	Medium
		Soil-attribute Table	SOILB(soiltype)	Soil drainage function coefficient	Root-zone infiltration and drainage function	U	Medium
Faunt and others (1997)*	GIS	Watershed File	ROCKTYPE(r,c)	Map code for Hydrogeologic units	Spatial distribution of bedrock and deep properties	I	Medium

Table 6-3
INFILv3 Input Parameters (Directly from Hevesi et al., 2003)
 (Page 2 of 5)

Source Data	Preprocessing	Input File	Parameter Name	Parameter Description	Parameter Use	Units	Parameter Accuracy
User Defined		Bedrock Attribute Table	RPOR(rocktype)	Effective root-zone porosity for bedrock layer	Defines storage capacity of root-zone in bedrock layer	U	Low
		Bedrock Attribute Table	RK _{Lo} (rocktype)	Effective unsaturated hydraulic conductivity for hydrogeologic unit	Defines lower bedrock hydraulic conductivity	mm/day	Low
		Bedrock Attribute Table	RK _{Hi} (rocktype)	Effective saturated hydraulic conductivity for hydrogeologic unit	Defines upper bedrock and deep alluvium hydraulic conductivity	mm/day	Low
GAP	GIS	Watershed File	VEGTYPE(r,c)	Map code for GAP Vegetation units	Spatial distribution of vegetation properties, root zone layer properties	I	Medium
User defined	GIS	Watershed File	VEGCOV(r,c)	Vegetation cover	Evapotranspiration model	%	Medium
User defined	None	Vegetation Attribute Table	RZDEN(vegtype,l)	Root density for layer l	Evapotranspiration model	%	Low
User defined	None	Vegetation Attribute Table	RZDPTH(vegtype,l)	Root-zone layer thickness	Evapotranspiration model, root-zone drainage model	M	Low
Maidment (1993)*	None	Control File	SNODAY1	Day number 1 for snowmelt model	Define timing of early spring snowmelt model	Day#	Medium
		Control File	SNOPAR1	Snowmelt parameter 1	Degree-day snowmelt rate	Mm/day	Medium
		Control File	SNODAY2	Day number 2 for snowmelt model	Define timing of late spring snowmelt model	Day#	Medium
		Control File	SNOPAR2	Snowmelt parameter 2	Degree-day snowmelt rate	Mm/day	Medium
User Defined	None	Control File	MELTIME	Duration of daily snowmelt	Controls intensity of snowmelt	Hours	Medium
		Control File	SUBPAR1	Sublimation rate parameter #1	Sublimation	U	Low
		Control File	SUBPAR2	Sublimation rate parameter #2	Sublimation	U	Low
User Defined	None	Control File	YRSTART	Simulation start year	Identifies simulation start date	U	NA
		Control File	MOSTART	Simulation start month	Identifies simulation start date	U	NA
		Control File	DYSTART	Simulation start day	Identifies simulation start date	U	NA
		Control File	YREND	Simulation end year	Identifies simulation end date	U	NA
		Control File	MOEND	Simulation end month	Identifies simulation end date	U	NA

Table 6-3
INFILv3 Input Parameters (Directly from Hevesi et al., 2003)
 (Page 3 of 5)

Source Data	Preprocessing	Input File	Parameter Name	Parameter Description	Parameter Use	Units	Parameter Accuracy
User Defined	None	Control File	DYEND	Simulation end day	Identifies simulation end date	U	NA
		Control File	DYSUMBEG	Start day number for summer storms	Defines beginning day number for summer storm events	Day#	Medium
		Control File	DYSUMEND	End day number for summer storms	Defines ending day number for summer storm events	Day#	Medium
		Control File	HSTEP	POTEVAP time step	Define hourly time-step for potential evapotranspiration model	hours	NA
		Control File	STORMSUM	Duration of summer precipitation and streamflow	Defines precipitation and streamflow intensity for summer storms	hours	Low
		Control File	STORMWIN	Duration of winter precipitation and streamflow	Defines precipitation and streamflow intensity for winter storms	hours	Low
Flint and Childs (1987)*	None	Control File	BSEA	Prestley-Taylor model coefficient #1 for bare soil evaporation	ET model coefficient for modified Prestley-Taylor equation, for bare-soil evaporation	U	Medium
		Control File	BSEB	Prestley-Taylor model coefficient #2 for bare soil evaporation	ET model coefficient for modified Prestley-Taylor equation, for bare-soil evaporation	U	Medium
		Control File	ETA	Prestley-Taylor model coefficient #1 for transpiration	ET model coefficient for modified Prestley-Taylor equation, for transpiration	U	Medium
User Defined	None	Control File	ETB	Prestley-Taylor model coefficient #2 for transpiration	ET model coefficient for modified Prestley-Taylor equation, for transpiration	U	Medium
User Defined	None	Control File	CHAN1	Surface-water minimum wetted area factor	Defines wetted area for stream-channel grid cell	U	Low
		Control File	CHAN2	Surface-water wetted area model coefficient	Defines wetted area for stream-channel grid cell	U	Low
		Control File	CHAN3	Surface-water headwater wetted area factor	Defines wetted area for stream-channel grid cell	U	Low
		Control File	CHAN4	Surface-water maximum wetted area factor	Defines wetted area for stream-channel grid cell	U	Low
		Control File	KSCHN1	Model coefficient for stream channel characteristics	Minimum number of upstream cells for using KSCHN2	U	Low
		Control File	KSCHN2	Model coefficient for stream channel characteristics	Scaler for adjusting soil saturated hydraulic conductivity in channels	U	Low

Table 6-3
INFILv3 Input Parameters (Directly from Hevesi et al., 2003)
 (Page 4 of 5)

Source Data	Preprocessing	Input File	Parameter Name	Parameter Description	Parameter Use	Units	Parameter Accuracy
User Defined	None	Control File	KSCHN3	Soil saturated hydraulic conductivity	Maximum soil saturated hydraulic conductivity in channels	U	Low
		Control File	INITOPT	Initial condition option	Defines method for setting initial conditions	i	NA
		Control File	VWCFAC	Scaler for setting initial water content for root-zone	Defines initial water content for soil layers in root zone	U	Low
NOAA/ NCDC	DAYINP14	Precip. File	PPT(day,st)	Daily precipitation	Daily precipitation input	mm	High
		Maximum Air temp. File	TMAX(day,st)	Maximum daily air temperature	Snowfall, snowmelt, sublimation, potential evapotranspiration	Deg. Celsius	High
		Minimum Air temp. File	TMIN(day,st)	Minimum daily air temperature	Snowfall, snowmelt, sublimation, potential evapotranspiration	Deg. Celsius	High
User defined	EXCEL	Monthly Climate Model	PPTMOD(month)	Model type for monthly Precipitation-elevation regression model	Defines model type for daily precipitation spatial interpolation model	i	Medium
		Monthly Climate Model	PPTA(month)	Regression model coefficient for precipitation-elevation regression model	Coefficient for daily precipitation spatial interpolation model	U	Medium
		Monthly Climate Model	PPTB(month)	Regression model coefficient for precipitation-elevation regression model	Coefficient for daily precipitation spatial interpolation model	U	Medium
		Monthly Climate Model	PPTC(month)	Regression model coefficient for precipitation-elevation regression model	Coefficient for daily precipitation spatial interpolation model	U	Medium
		Monthly Climate Model	TMAXMOD(month)	Model type for monthly Maximum air temperature-elevation regression model	Defines model type for maximum daily air temperature spatial interpolation model	I	High
		Monthly Climate Model	TMAXA(month)	Regression model coefficient for maximum air temperature-elevation model	Coefficient for maximum daily air temperature spatial interpolation model	U	High
		Monthly Climate Model	TMAXB(month)	Regression model coefficient for maximum air temperature-elevation model	Coefficient for maximum daily air temperature spatial interpolation model	U	High

Table 6-3
INFILv3 Input Parameters (Directly from Hevesi et al., 2003)
 (Page 5 of 5)

Source Data	Preprocessing	Input File	Parameter Name	Parameter Description	Parameter Use	Units	Parameter Accuracy
User Defined	EXCEL	Monthly Climate Model	TMAXC(month)	Regression model coefficient for maximum air temperature-elevation model	Coefficient for maximum daily air temperature spatial interpolation model	U	High
		Monthly Climate Model	TMINMOD(month)	Model type for monthly Minimum air temperature-elevation regression model	Defines model type for minimum daily air temperature spatial interpolation model	I	High
		Monthly Climate Model	TMINA(month)	Regression model coefficient for minimum air temperature-elevation model	Coefficient for minimum daily air temperature spatial interpolation model	U	High
		Monthly Climate Model	TMINB(month)	Regression model coefficient for minimum air temperature-elevation model	Coefficient for minimum daily air temperature spatial interpolation model	U	High
		Monthly Climate Model	TMINC(month)	Regression model coefficient for minimum air temperature-elevation model	Coefficient for minimum daily air temperature spatial interpolation model	U	High
NWS	None	Monthly Atmospheric Parameter	OZONE(month)	Ozone layer thickness	Potential evapotranspiration model, incoming solar radiation	cm	Medium
		Monthly Atmospheric Parameter	WP(month)	Precipitable water in atmosphere	Potential evapotranspiration model, incoming solar radiation	cm	Medium
		Monthly Atmospheric Parameter	BETA(month)	Mean atmospheric turbidity	Potential evapotranspiration model, incoming solar radiation, net radiation	U	Medium
		Monthly Atmospheric Parameter	CSR(month)	Circumsolar radiation	Potential evapotranspiration model, incoming solar radiation, net radiation	U	Medium
		Monthly Atmospheric Parameter	PG(month)	Surface reflectivity	Potential evapotranspiration model, incoming solar radiation, net radiation	U	Medium

*Source: Hevesi et al., 2003

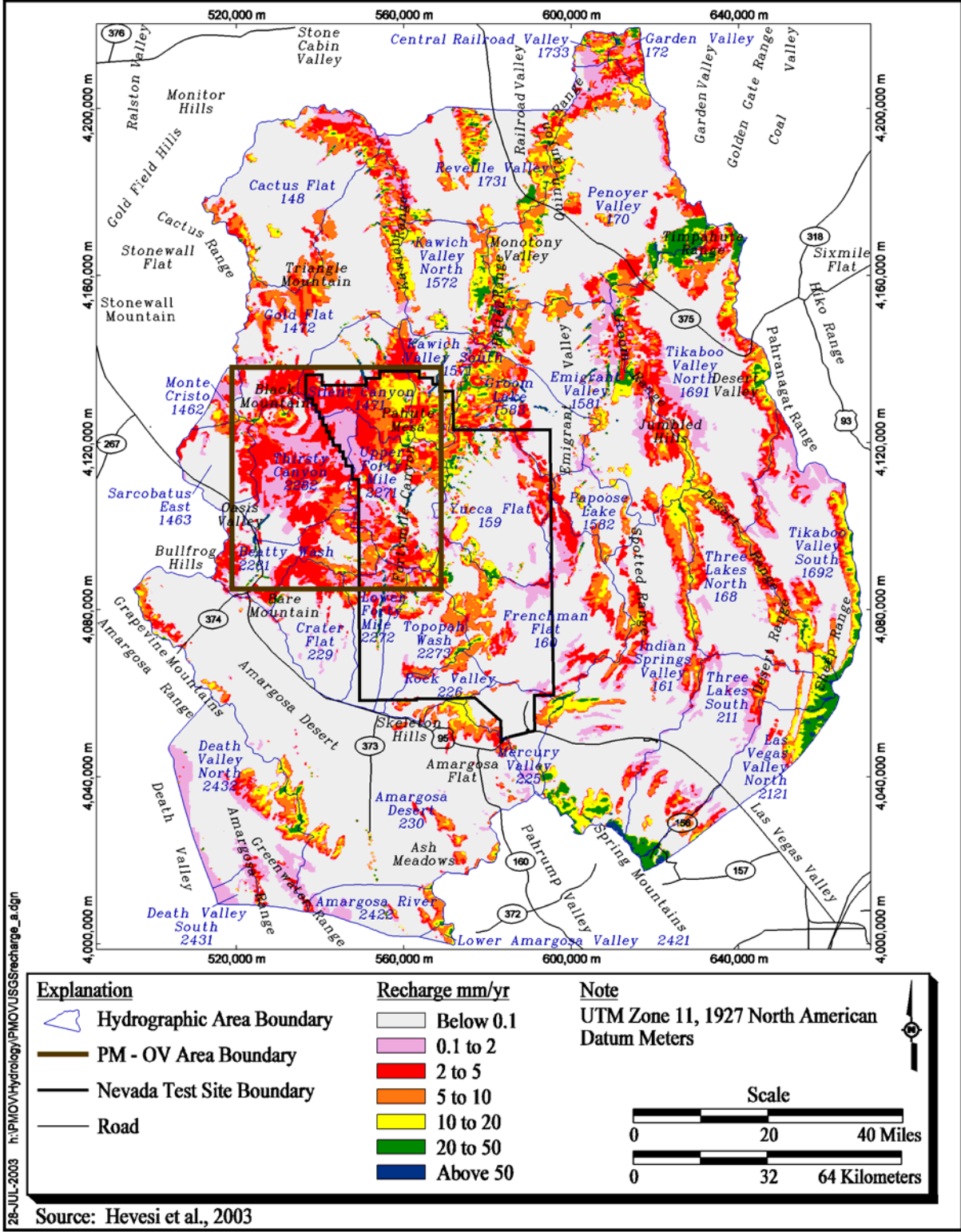


Figure 6-5
USGS Recharge Distribution Model 1, Overland Flow Component Included

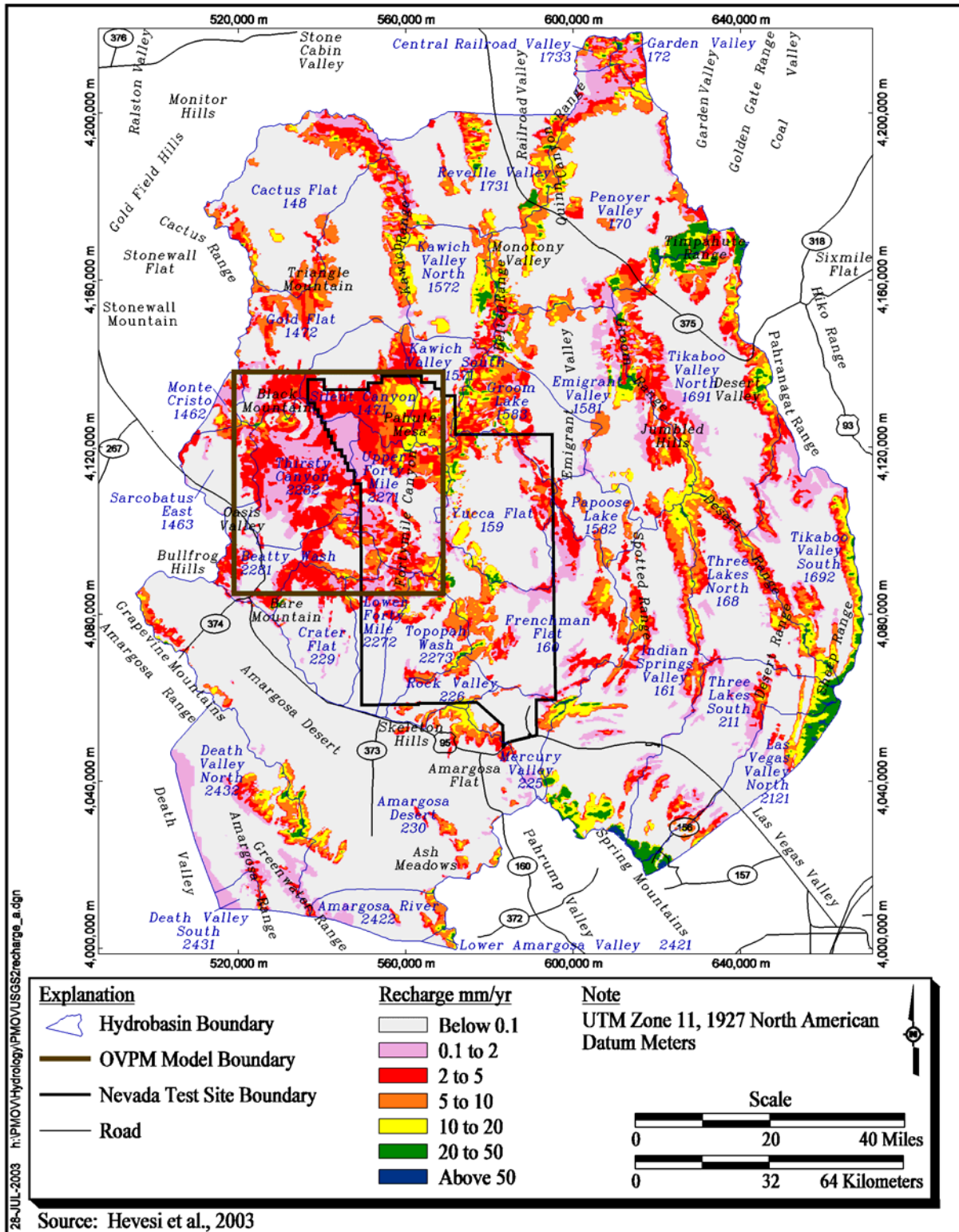


Figure 6-6
USGS Recharge Distribution Model 2, No Overland Flow Component

spatial variability within recharge areas (rather than recharge as a lumped parameter), develop a more defensible lower limit of recharge, and differentiate local recharge from recharge emanating as interbasin flux.

Seventeen springs, located in the Sheep Range, Spring Mountains, and on the Nevada Test Site were sampled during the course of this study and their discharge was measured. The chloride and bromide concentrations of the springs were determined. Discharge and chloride concentrations from these springs were compared to estimates provided by previously published reports. A literature search yielded previously published estimates of chloride flux to the land surface. $^{36}\text{Cl}/\text{Cl}$ ratios and discharge rates of the three largest springs in the Amargosa Springs discharge area were compiled from various sources. This information was utilized to determine an effective chloride concentration for recharging precipitation and its associated uncertainty via Monte Carlo simulations. Previously developed isohyetal maps were utilized to determine the mean and standard deviation of precipitation within the area. A digital elevation model was obtained to provide elevation information. A geologic model was obtained to provide the spatial distribution of alluvial formations. Both were used to define the lower limit of recharge. In addition, 40 boreholes located in alluvial sediments were drilled and sampled in an attempt to support the argument that the areal distribution of alluvial sediments can be used to define a zone of negligible recharge. The data were compiled in a geographic information system and used in a Monte Carlo analysis to determine recharge occurring within the study area. Results of the analysis yielded estimates of the mean and standard deviation of recharge occurring within the study area ($28.168 \times 10^6 \text{ m}^3 \text{ yr}^{-1}$ and $7.008 \times 10^6 \text{ m}^3 \text{ yr}^{-1}$, and $26.838 \times 10^6 \text{ m}^3 \text{ yr}^{-1}$ and $6.928 \times 10^6 \text{ m}^3 \text{ yr}^{-1}$) for two sets of simulations using alternate definitions of the lower limit of recharge. A sensitivity analysis determined the recharge estimates were most sensitive to uncertainty associated with the chloride concentration of the spring discharge. The second most sensitive parameter was the uncertainty associated with the mean precipitation within the recharge areas. Comparison of the analysis to previously published estimates of recharge revealed mixed results with the recharge estimates derived during the course of this project generally greater relative to previously published estimates (Russell and Minor, 2002)."

It is important to note that the values just cited for volumes of recharge are for a smaller area than was applied in this study. Corresponding volumes on a basin-by-basin basis and total equivalent area volumes will be presented later in this section.

The following excerpt from the report describes the methodology employed for this study: *"The methodology used to determine recharge rates within each of the spring watersheds is essentially the same as that employed by Dettinger (1989). The discharge rate of the spring is quantified, the chloride concentration of that spring is measured, and the precipitation and atmospheric flux of chloride falling on the watershed above the spring are estimated. A mass balance approach that relates spring discharge and chloride concentration to precipitation rates and atmospheric chloride flux yields information on recharge rates and an estimate of the size of the watershed required to generate the observed spring discharge. The size of the watershed, and the elevation of the spring orifice and of the ridgeline*

above the spring are used to constrain an estimate of the elevation of the spring watershed. The resultant recharge rates and watershed elevations from multiple springs are used as input into the nonlinear regression analysis.

Uncertainty exists on the actual values of the parameters utilized in the elevation dependent chloride mass-balance approach. For example, multiple measures of the chloride concentration from individual springs demonstrate variability, isohyetal maps of the area disagree on the quantity of precipitation, the quantity of chloride flux is uncertain both temporally and spatially, and uncertainty exists as to the elevation of the watershed for any given spring. Monte Carlo methods were utilized to incorporate the uncertainty associated with each of the variables into an estimate of uncertainty associated with the rate of recharge.

Several types of data were collected to achieve the objective of this project. Seventeen springs, located in the Sheep Range, Spring Mountains, and on the NTS, were sampled during the course of this study and their discharge was measured. The chloride and bromide concentrations of the springs were determined. Discharge measurements and chloride concentrations from these springs were compared to estimates provided by previously published reports. A literature search provided various estimates of chloride flux to the land surface. $^{36}\text{Cl}/\text{Cl}$ ratios and discharge rates of the three largest springs in the Amargosa Springs discharge area were compiled from various sources. This information was utilized to determine an effective chloride concentration of recharging precipitation and its associated uncertainty via Monte Carlo simulations. Previously generated isohyetal maps were compared in terms of parametric variability. A digital elevation model was obtained to provide elevation information and to define the lower limit of recharge based on elevation. A geologic model was obtained to provide the spatial distribution of alluvial formations to define an alternate zone of negligible recharge. In addition, 40 boreholes located in alluvial sediments were drilled and sampled in an attempt to support the argument that the areal distribution of alluvial sediments can be used to define a zone of negligible recharge. The required data types and their respective uses are more thoroughly described in the following sections (Russell and Minor, 2002)."

The precipitation models used by DRI include the PRISM model, the revised Hardman precipitation map (1965), and the Rush (1970) precipitation-elevation relationships. For the PRISM input, precipitation data from 1961 to 1990 was utilized and the resolution set to 16-square kilometers (km^2). The resolution was then refined to 4 km^2 using kriging with a Gaussian model. For comparison the Hardman map was used to recreate the precipitation amounts and distribution and, using the Maxey-Eakin method, recharge rates were estimated. The Rush (1970) method was also recreated for comparison purposes using the elevation-precipitation relationships for that isohyetal map.

The topographic elevations were derived from USGS provided DEM data at 30 and 100 m.

Geologic input was primarily obtained from Wahl et al. (1997), with additional definition of the Sheep and Spring ranges from Burchfiel et al. (1974), and Guth

(1986). This data was digitized and added to the GIS database to delineate alluvial formation distributions in the study area.

The approach is also taken verbatim from the report by Russell and Minor: *"The chloride ion is a conservative ion when dissolved in water. It does not enter oxidation or reduction reactions, forms no important solute complexes with other ions unless the chloride concentration is extremely high, does not form salts of low solubility, is unlikely to be sorbed on mineral surfaces, and plays few vital biogeochemical roles (Hem, 1985). The sources of chloride in the subsurface are generally restricted to evaporites, incompletely leached marine sediments, or porous rocks that have been in contact with the ocean (Hem, 1985). A significant source of chloride in areas where the aforementioned conditions are absent is precipitation and dry deposition. Chloride is present in rain and snow owing primarily to physical processes that entrain marine solutes in air at the surface of the ocean (Hem, 1985). Once entrained, chloride is transported in the atmosphere and reaches land via precipitation (wet-fall) or as an aerosol (dry-fall). Chloride, due to its conservative nature, is transported into the subsurface as precipitation infiltrates into the ground. Evapotranspiration will remove some portion of the infiltrating water, thereby concentrating the chloride. The chloride concentration of the water that infiltrates below the zone of evapotranspiration remains relatively constant and can be an indicator of recharge (Fouty, 1989; Eriksson and Khunakasem, 1969). The chloride mass-balance approach requires an accounting of all sources and sinks associated with the chloride ion. If the sole source of chloride is combined wet-fall and dry-fall atmospheric deposition normalized to precipitation C_p (mg/L) multiplied by the mean annual precipitation P (L/yr), then the quantity of recharge R (L/yr) is defined as (Maurer et al. 1996):*

$$R = (C_p P) / (C_r) - (C_{SW} S_W) / (C_r) \quad (6-4)$$

where:

$C_{SW} S_W$ = the quantity of chloride (mg/L) and water (L/yr) that is removed due to surface water runoff

C_r (mg/L) = the quantity of chloride in water that has recharged.

This equation assumes steady-state deposition, on an annual scale, of chloride and precipitation, no inherent changes in the subsurface storage of either component, atmospheric wet-fall and dry-fall deposition of chloride as the sole source of chloride in the system, and direct infiltration of precipitation as the sole source of recharge. The following is an analysis of these assumptions within the study area (Russell and Minor, 2002)."

The first assumption in this study is that the runoff component is considered negligible. Secondly, steady-state conditions are assumed. Third, no authigenic chloride is found in soils and groundwater, and that all chloride is attributable to atmospheric origin.

Soil chloride samples and spring discharge chloride samples were collected for this study. The results of previous studies of chloride flux to land surface were used to obtain critical data for input to this study.

The vadose zone portion of the study utilized the soil chloride samples taken from 40 shallow borings to develop chloride concentration versus depth profiles for locations in alluvial deposits. The chloride profiles exhibited three signature profiles, bulge, multipeak, and surface maximum. This information was used to determine net infiltration rates for the landforms investigated (e.g., ephemeral streams, alluvial fans).

The investigation of chloride concentrations in spring discharge focused on 17 springs and delineation of their contributory watersheds. Uncertainty relating to the watershed elevation and spatial extent was incorporated into the model by finding end-members for each spring elevation and extent.

The next step of this methodology and approach is the inclusion of the uncertainty of each of the input parameters for parameter estimation. This was accomplished by developing a probability distribution function for each parameter from the mean and standard deviation of the data. Many of the parameters have a high degree of uncertainty and some assumptions were made including that the errors associated with determining the mean and standard deviation using a limited number of samples were not incorporated.

The following text taken directly from the DRI report describes the final determination of recharge:

"The next step was to incorporate the uncertainty in the elevation of 17 spring watersheds and relate that via regression analysis to the rate of recharge that is occurring in those 17 watersheds. The methodology for determining the uncertainty associated with the elevation of each spring watershed was previously discussed. The 17 statistical distributions describing the variability of the area-weighted mean elevation for each spring watershed were randomly sampled 1,000 times, resulting in 17,000 estimates of area-weighted mean watershed elevation. Concurrently, the statistical distributions describing the uncertainty associated with the chloride concentration of each spring were also randomly sampled 1,000 times, resulting in 17,000 estimates of chloride concentration. A single set of 17 simulations of the area-weighted mean elevations, for the 17 springs in the study area, was linked to 17 simulations of chloride concentrations within each spring. The randomly sampled chloride concentrations from all 17 springs were divided by a single estimate of effective chloride concentration in precipitation, determined by randomly sampling the statistical distribution for that parameter. The results consisted of a set of estimated area-weighted mean elevations of spring watersheds and an associated ratio describing the relative enrichment that precipitation has incurred, due to evapotranspiration, within each watershed (C_s/C_p).

The 17 sets of elevations and (C_s/C_p) were utilized to develop a nonlinear regression equation of the following form:

$$(C_r/C_p) = 1.0 + c1 * e^{(c2 * elev)} \quad (6-5)$$

where:

c1 and c2 = the regression coefficients

elev = the area-weighted mean elevation of the watershed of interest.

The regression analysis was conducted using Systat (ver 7.01).

The solved equation was programmed into the GIS system and used, along with data layers incorporating the digital elevation model, a modified version of the PRISM isohyetal map, and the alluvial mask developed from the geologic models to determine the distribution of recharge across the study area. Modifications to the PRISM map consisted of normalizing the values within the PRISM dataset to reflect the randomly sampled, area-weighted mean precipitation falling in the study area that was utilized for that simulation to determine effective chloride concentration in precipitation. Normalization of the PRISM dataset ensured consistency of estimates of precipitation required to determine recharge as a function of elevation versus precipitation required to determine the effective concentration of chloride in precipitation (Figure 7 [in report by Russell and Minor, 2002]) for each simulation.

To calculate recharge, the 100-m-resolution, digital-elevation model was sampled to determine the area-weighted mean elevation of 4-km² grids that coincide with the spatial distribution for the 4-km² resolution of the PRISM isohyetal map (Daley et al., 1994). The area-weighted mean elevation and mean precipitation for the 4-km² sample was used as input to the regression equation. The mean elevation was used to calculate C_r/C_p using Equation 6-5. The corresponding precipitation value for the 4-km² area was divided by C_r/C_p to determine recharge for that area. Results were summed across the study area and ranked. The 50th percentile result was used to map the distribution of recharge across the study area (Russell and Minor, 2002)."

In addition, the results of the 5th, 50th, and 95th percentile were summarized by hydrographic area for comparison to previously published results of recharge. Two versions of the recharge model were calculated one for no recharge (mask) in alluvial areas, and another masked for alluvial areas and for no recharge below an elevation of 1,237 m. These two models differ in the area of alluvium over which recharge is allowed to occur.

A sensitivity analysis indicated that the model was most sensitive to the spring chloride concentration and accounted for 50 percent of the total variance. Mean precipitation was the second most sensitive (26 percent), followed closely by watershed elevation (21 percent). The model was least sensitive to chloride concentration in precipitation (2 percent).

A semi-independent validation was conducted on an independent set of 13 springs in the Spring Mountain range. The results compared very favorably with the initial analysis, and indeed validated the approach.

The recharge models developed by Russell and Minor (2002) are for an area that immediately surrounds the NTS. This area is not entirely coincident with the areas for which recharge estimates were developed by the USGS and the UGTA project. In some instances, recharge estimates reported by Russell and Minor (2002) were for portions of hydrographic basins. DRI, in support of the UGTA project, revisited and expanded their study so that recharge was estimated for the entire area of a hydrographic basin that fell within the original DRI study area.

The recharge models developed by Russell and Minor (2002) did not include all of the hydrographic areas in the UGTA model area. An assessment was, therefore, performed to identify another method that could produce recharge volumes consistent with those developed using the DRI method for hydrographic basins of interest that were not included in the original DRI report and subsequent revision. Recharge volumes were calculated for a number of hydrographic areas using the different methods and compared to those calculated using the DRI method. The highest correlation was found to be with the UGTA revised Maxey-Eakin method at $R^2 = 0.984$ for the alluvial mask 50th percentile distribution and $R^2 = 0.985$ for the alluvial and elevation masked recharge data 50th percentile distribution. Kawich valley recharge was removed from the DRI dataset as it was considered an outlier based on visual inspection of the correlation (Figure 6-7). The correlation formula was then applied to Kawich Valley and to the remaining valleys outside of the DRI dataset, but within the UGTA model area. In general, net recharge in hydrographic areas receiving less than 7 million cubic meters per year had the recharge increased up to 50 percent (see multiplication factors in Table 6-4). Conversely, those valleys with more than 7 million cubic meters per year had their recharge reduced up to 20 percent. The resultant recharge distributions for the entire UGTA regional model area for the alluvial mask 50th percentile is shown in Figure 6-8. The recharge distribution for the alluvial and elevation masks 50th percentile distribution is shown in Figure 6-9. Note that the values for some of the hydrographic areas presented in Table 6-4, Figure 6-8, and Figure 6-9 have been extrapolated from data that are quite distant. The farther the extrapolation distance, the less reliable the recharge estimates become. This is one reason why the value calculated for Kawich is an outlier. Tabled volumetric totals for these recharge distributions are presented in the summary section.

6.4.4 Nevada Water Resource Study

The following description of recharge estimation is based on a report titled: *Water Resources - Reconnaissance Series Report 54* by F.E. Rush (1970).

This study, referred to in most of the literature as the Rush (1970) study, is based primarily on the Maxey-Eakin approach. The difference is the base precipitation model used to derive the percentage recharge estimates. Instead of using the precipitation distribution developed by Hardman (1936, 1965), Rush (1970) used the elevation-based version of the method, as a strong correlation exists between the precipitation and land surface elevation within the study area. The elevation cutoffs were dependent on the hydrographic area under study and were set to 304.8 m elevation zones, with each zone directly correlating to the Maxey-Eakin recharge zone. For example, instead of using precipitation zones of 22.3 to

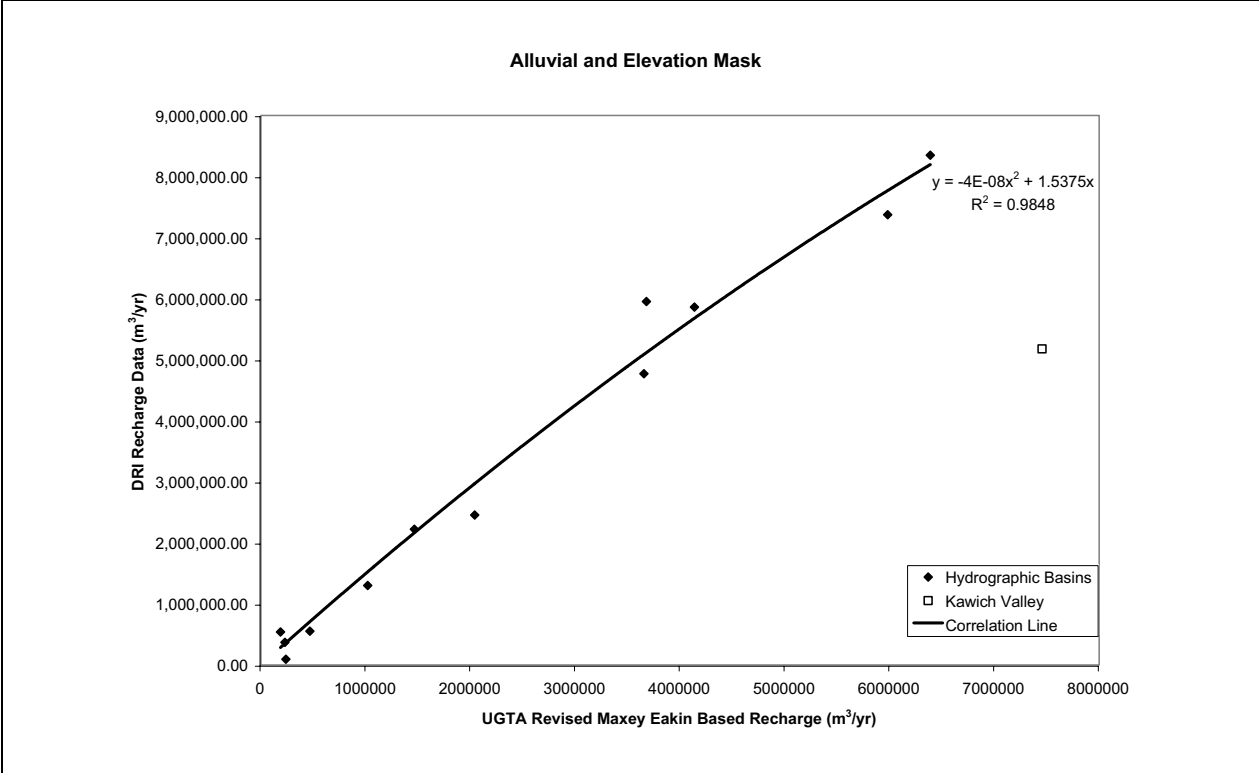
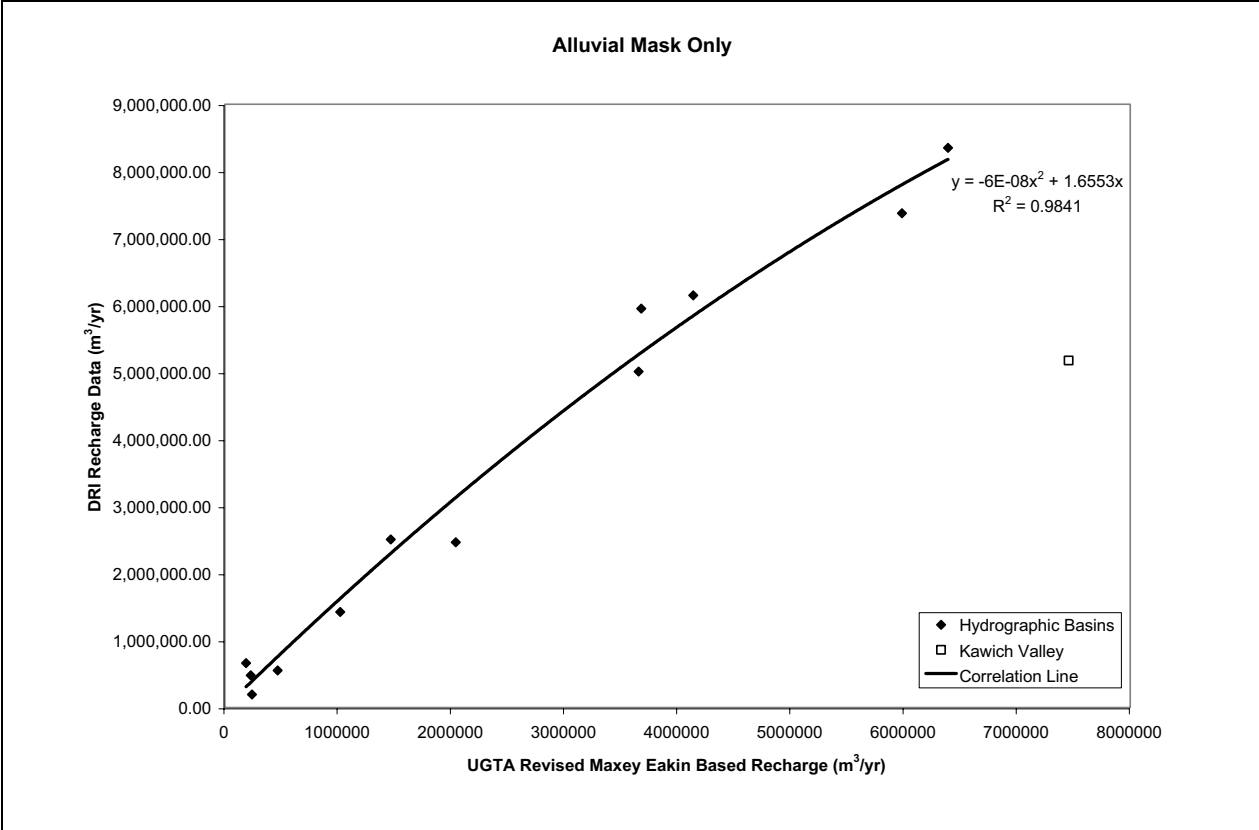


Figure 6-7
Correlation of Recharge Volumes - UGTA-Revised Recharge Versus DRI Recharge

**Table 6-4
Multiplication Factors for Hydrographic Areas Outside of DRI Study Area**

SubArea Number	Area Name	Secondary Name	UGTA	Alluvial Mask			Alluvial and Elevation Mask		
			Revised Maxey-Eakin Based (m ³ /yr)	50th percentile DRI (m ³ /yr)	Est. 50% Recharge (m ³ /yr)	Multiplication Factor	50th percentile DRI (m ³ /yr)	Est. 50% Recharge (m ³ /yr)	Multiplication Factor
1462	Sarcobatus Flat-2	Monte Cristo	794,532.94		1,277,313.42	1.6076		1,196,343.09	1.5057
1463	Sarcobatus Flat-3	Sarcobatus East	568,888.56		922,263.18	1.6212		861,720.79	1.5147
148	Cactus Flat		3,304,088.00		4,814,237.02	1.4571		4,643,355.40	1.4053
1571 & 1572	Kawich Valley		7,455,893.00	5,176,132	9,006,319.26	1.2079	5,176,132	9,239,821.87	1.2393
168	Three Lakes Valley North		319,001.97		521,938.23	1.6362		486,395.04	1.5247
1691	Tikaboo Valley-1	Tikaboo Valley North	6,451,639.00		8,181,979.29	1.2682		8,254,449.13	1.2794
1692	Tikaboo Valley-2	Tikaboo Valley South	760,359.88		1,223,934.88	1.6097		1,145,927.43	1.5071
170	Penoyer Valley		6,487,365.00		8,213,381.01	1.2661		8,290,887.50	1.2780
172	Garden Valley		2,476,189.50		3,730,945.61	1.5067		3,561,880.78	1.4385
1731	Railroad Valley South-1	Reveille Valley	5,464,048.00		7,253,289.42	1.3275		7,206,740.98	1.3189
1733	Railroad Valley South-3	Central Railroad Valley	1,920,032.38		2,957,038.14	1.5401		2,804,588.81	1.4607
211	Three Lakes Valley South		4,219,549.50		5,916,344.41	1.4021		5,775,373.44	1.3687
2121	Las Vegas Valley-1		5,082,539.00		6,863,194.65	1.3503		6,781,115.61	1.3342
2301	Amargosa Desert	NV Portion	648,361.75	1,250,592	1,048,010.83	1.6164	743,101	980,041.27	1.5116
2302	Amargosa Desert	CA Portion	807,343.69		1,297,287.78	1.6069		1,215,218.77	1.5052
2421	Amargosa River-1	Lower Amargosa Valley	0.00		0.00	NA		0.00	NA
2422	Amargosa River-2	Amargosa River	103,700.13		171,009.60	1.6491		159,008.80	1.5334
2431	Death Valley Central-1	Death Valley South	23,983.49		39,665.36	1.6539		36,851.61	1.5365
2432	Death Valley Central-2	Death Valley North	1,559,119.50		2,434,959.29	1.5618		2,299,912.09	1.4751
1471 & 1472	Gold Flat		6,389,219.50	8,350,312	8,126,747.49	1.2719	8,350,312	8,190,539.95	1.2819
1582	Emigrant Valley		466,883.78	552,772	759,753.89	1.6273	552,772	709,114.59	1.5188
1581 & 1583	Emigrant Valley		5,982,482.75	7,375,170	7,755,397.70	1.2964	7,375,170	7,766,463.23	1.2982
159	Yucca Flat		2,040,325.75	2,464,923	3,127,575.46	1.5329	2,455,944	2,970,483.67	1.4559
160	Frenchman Flat		1,465,506.63	2,506,158	2,296,990.54	1.5674	2,224,178	2,167,308.06	1.4789
161	Indian Springs Valley		3,655,453.75	5,012,961	5,249,132.07	1.4360	4,771,832	5,085,766.46	1.3913
225	Mercury Valley		229,304.19	480,636	376,412.40	1.6415	370,736	350,451.98	1.5283
226	Rock Valley		239,180.09	193,175	392,482.38	1.6409	94,937	365,451.10	1.5279
2271	Fortymile Canyon		3,678,718.25	5,951,377	5,277,404.24	1.4346	5,951,377	5,114,710.59	1.3904
2272, 2273	Fortymile Canyon		1,018,842.38	1,425,884	1,624,207.40	1.5942	1,302,536	1,524,948.57	1.4967
2281 & 2282	Oasis Valley		4,137,930.88	6,148,924	5,822,168.67	1.4070	5,860,156	5,677,169.85	1.3720
229	Crater Flat		187,843.92	661,380	308,820.92	1.6440	540,299	287,398.61	1.5300

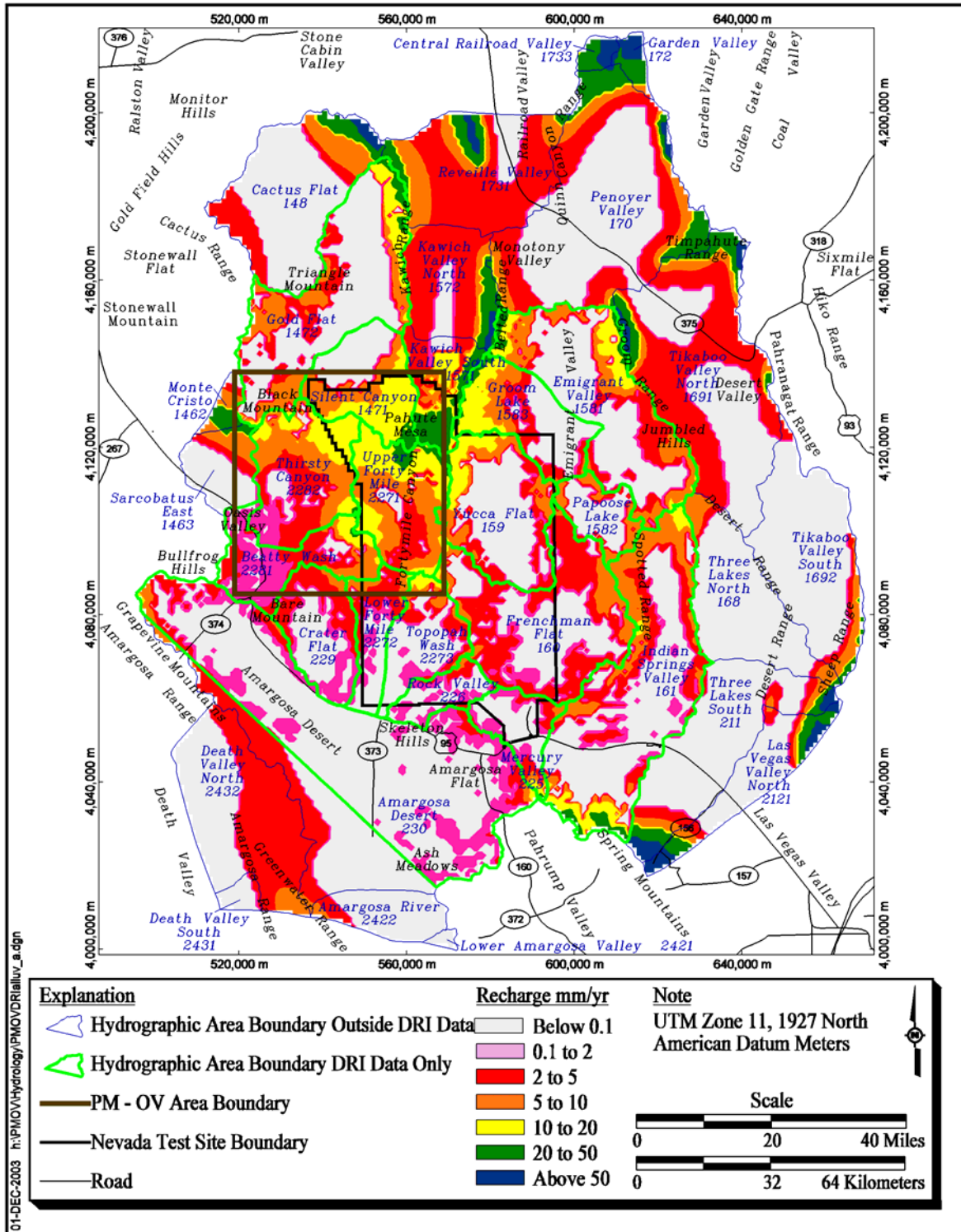


Figure 6-8
DRI Recharge Distribution with Alluvial Mask
(Russell and Minor, 2002)

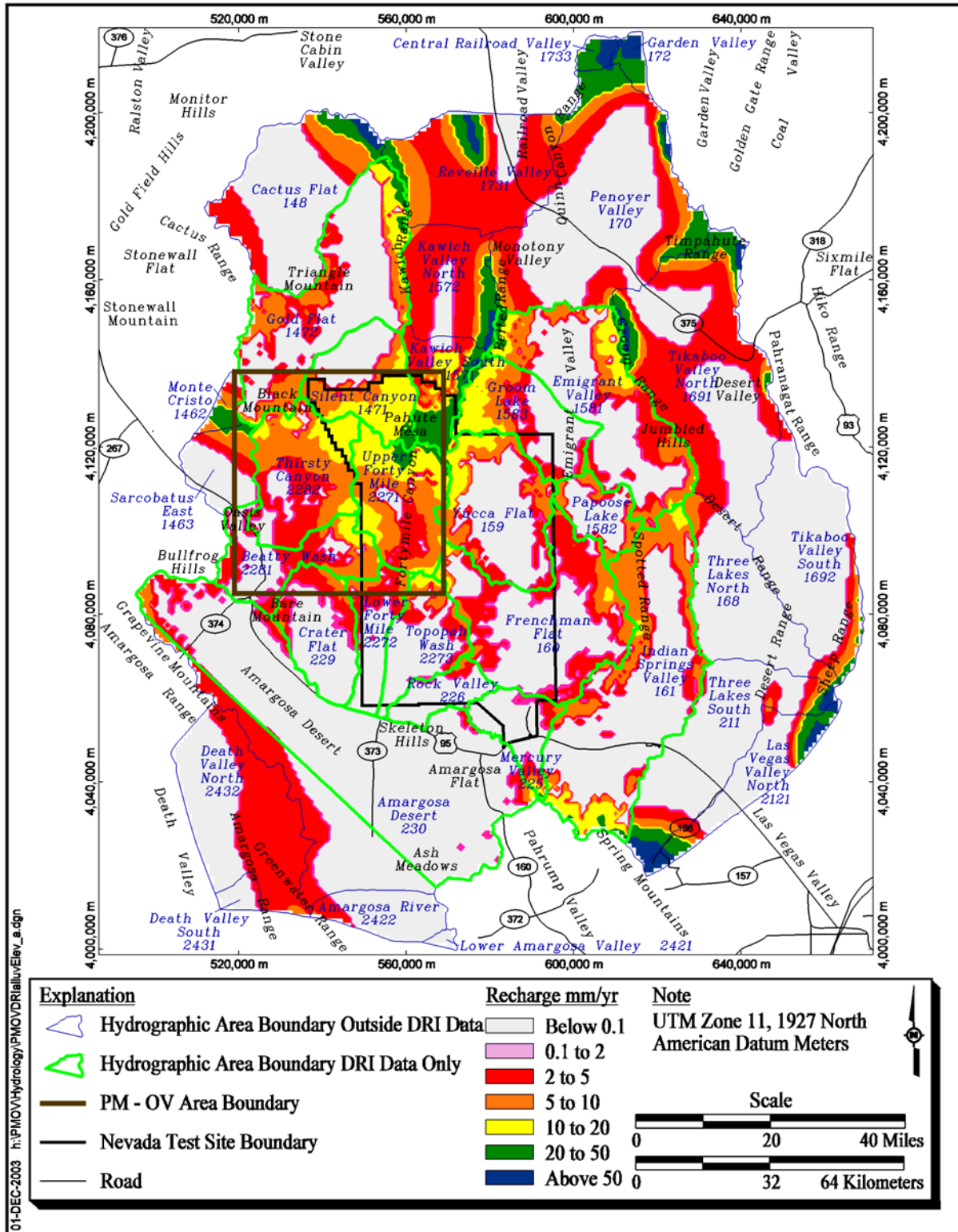


Figure 6-9
DRI Recharge Distribution with Alluvial and Elevation Mask
(Russell and Minor, 2002)

30.5 cm empirically set to a 3 percent recharge rate, the 1,524 to 1,828.8 m elevation zone was set to a 3 percent recharge rate. In theory, the use of this method would yield similar recharge volumes for equivalent Maxey-Eakin (1949) recharge zones. This, however, was not the case for all recharge zones. For example, recharge zones starting at land surface elevations of 1,524 m; 1,828.8 m; and in one case 2,133.6 m produced recharge volumes that differed from those derived using the Maxey-Eakin method (1949) by more than a minor amount. The results of this study are included in the summary table (Table 6-5).

6.5 Base Recharge Model

Where data were available, the recharge volume for each method was listed for each hydrographic area or sub-area in Table 6-5, and graphed in Figure 6-10. Comparisons of the recharge volumes depicts the general trends in the relationships of the methods. The base recharge model chosen for this report is the updated UGTA recharge model based on the modified Maxey-Eakin method. It was chosen because it provides a good starting point for modeling that is, in general, in the middle of the ranges of recharge estimates. In general, the volumes for the base model are bracketed by the other model volumes and fall within the 5 and 95 percent confidence intervals for the DRI methods, where available. For Kawich Valley, the base model value is the highest reported; however, all but Frenchman Flat volumes fall within the DRI 5 and 95 percent confidence intervals. The base model has the lowest reported recharge volume for Three Lakes Valley North, Mercury Valley, Fortymile Canyon 2 & 3, and Amargosa Desert. It is important to note that all DRI recharge values that are not associated with confidence intervals are actually the UGTA model recharge distribution converted using the correlation reported earlier in the DRI recharge model section. The revised UGTA recharge distribution was derived from one precipitation model that was consistently applied and is, therefore, a simpler model than the UGTA calibrated regional model phase I recharge distribution, and was judged to be more readily applicable in light of the newer data.

During the calibration of the Pahute Mesa CAU model, the recharge may be modified to improve calibration. The modifications may range from simple scaling the entire dataset up or down, to changes in a specific hydrographic basin. Every effort will be made to avoid modifying recharge outside the range of values identified by the alternative recharge models.

6.6 Alternative Recharge Models

Groundwater flow modeling of the regional and PM-OV areas will also include calibration to the alternative recharge models described in this section. These volumes will provide a range of recharge estimates that can be used for sensitivity analysis, and evaluation of alternative scenarios during the course of flow model construction and calibration. The range of recharge for any given hydrographic area can vary by more than a factor of 3 or 4 from model to model. In addition, the

Table 6-5
Recharge Volumes for Hydrographic Areas for all Recharge Models
 (Page 1 of 2)

Subarea Number	Area Name	Secondary Name	UGTA	UGTA	USGS	USGS	DRI-Alluvial Mask Only			DRI-Alluvial and Elevation Mask			Rush (1970) (m ³ /yr)
			Regional Model Phase I (m ³ /yr)	Revised Maxey-Eakin Based (m ³ /yr)	Model 1 (m ³ /yr)	Model 2 (m ³ /yr)	5% (m ³ /yr)	50% (m ³ /yr)	95% (m ³ /yr)	5% (m ³ /yr)	50% (m ³ /yr)	95% (m ³ /yr)	
1462	Sarcobatus Flat-2	Monte Cristo	324,700	794,500	162,400	153,300		1,277,000			1,196,000		
1463	Sarcobatus Flat-3	Sarcobatus East	420,300	568,900	297,400	280,800		922,300			861,700		
1471	Gold Flat-1 & 2	Silent Canyon	4,739,000	6,389,000	5,269,000	4,052,000	3,889,000	8,350,000	12,810,000	3,889,000	8,350,000	12,810,000	4,687,000
148	Cactus Flat		3,147,000	3,304,000	1,653,000	1,326,000		4,814,000			4,643,000		740,100
1571	Kawich Valley-1 & 2	Kawich Valley South	6,952,000	7,456,000	4,372,000	2,923,000	2,063,000	5,176,000	8,289,000	2,063,000	5,176,000	8,289,000	4,317,000
1582	Emigrant Valley-2	Papoose Lake	887,800	466,900	412,600	305,300	352,800	552,800	752,700	352,800	552,800	752,700	1,233
1581	Emigrant Valley-1 & 3	Emigrant Valley	7,891,000	5,982,000	6,897,000	4,510,000	3,805,000	7,375,000	10,950,000	3,805,000	7,375,000	10,950,000	3,947,000 ^a
159	Yucca Flat		2,589,000	2,040,000	1,950,000	1,508,000	1,467,000	2,465,000	3,463,000	1,459,000	2,456,000	3,453,000	863,500
160	Frenchman Flat		2,542,000	1,466,000	2,340,000	2,183,000	1,560,000	2,506,000	3,452,000	1,404,000	2,224,000	3,044,000	123,400
161	Indian Springs Valley		4,741,000	3,655,000	4,376,000	4,210,000	2,842,000	5,013,000	7,184,000	2,610,000	4,772,000	6,934,000	1,234,000
168	Three Lakes Valley North		300,600	319,000	1,824,000	1,819,000		521,900			486,400		2,467,000
1691	Tikaboo Valley-1	Tikaboo Valley North	5,997,000	6,452,000	4,595,000	4,241,000		8,182,000			8,254,000		3,207,000
1692	Tikaboo Valley-2	Tikaboo Valley South	606,700	760,400	2,401,000	2,402,000		1,224,000			1,146,000		4,194,000
170	Penoyer Valley		8,382,000	6,487,000	6,289,000	5,175,000		8,213,000			8,291,000		5,304,000
172	Garden Valley		1,859,000	2,476,000	587,500	478,600		3,731,000			3,562,000		
1731	Railroad Valley South-1	Reveille Valley	5,416,000	5,464,000	2,696,000	2,266,000		7,253,000			7,207,000		
1733	Railroad Valley South-3	Central Railroad Valley	1,914,000	1,920,000	373,500	290,000		2,957,000			2,805,000		
211	Three Lakes Valley South		4,221,000	4,220,000	2,143,000	2,117,000		5,916,000			5,775,000		7,401,000

Table 6-5
Recharge Volumes for Hydrographic Areas for all Recharge Models
 (Page 2 of 2)

Subarea Number	Area Name	Secondary Name	UGTA	UGTA	USGS	USGS	DRI-Alluvial Mask Only			DRI-Alluvial and Elevation Mask			Rush (1970) (m ³ /yr)
			Regional Model Phase I (m ³ /yr)	Revised Maxey-Eakin Based (m ³ /yr)	Model 1 (m ³ /yr)	Model 2 (m ³ /yr)	5% (m ³ /yr)	50% (m ³ /yr)	95% (m ³ /yr)	5% (m ³ /yr)	50% (m ³ /yr)	95% (m ³ /yr)	
2121	Las Vegas Valley-1		5,063,000	5,083,000	2,412,000	2,382,000		6,863,000			6,781,000		5,797,000
225	Mercury Valley		424,800	229,300	475,000	446,400	307,600	480,600	653,700	236,500	370,700	504,900	308,400
226	Rock Valley		176,700	239,200	385,200	374,600	103,300	193,200	283,000	58,500	94,940	131,400	37,010
2271	Fortymile Canyon-1	Upper Fortymile	3,477,000	3,679,000	2,545,000	1,709,000	3,241,000	5,951,000	8,662,000	3,241,000	5,951,000	8,662,000	
2272	Fortymile Canyon-2 & 3	Lower Fortymile	1,129,300	1,018,800	1,932,900	1,146,300	916,000	1,426,000	1,936,000	832,700	1,303,000	1,772,000	
2281	Oasis Valley-1 & 2	Beatty Wash	4,022,000	4,138,000	3,041,000	2,380,800	3,866,000	6,149,000	8,432,000	3,642,000	5,860,000	8,078,000	1,234,000
229	Crater Flat		179,800	187,800	347,500	327,500	395,500	661,400	927,300	335,400	540,300	745,200	271,400
230	Amargosa Desert		1,457,000	1,456,000	1,893,000	1,730,000		2,548,000			1,958,000		
2421	Amargosa River-1	Lower Amargosa Valley	0	0	17,920	17,600		0			0		
2422	Amargosa River-2	Amargosa River	105,000	103,700	279,900	257,300		171,000			159,000		
2431	Death Valley Central-1	Death Valley South	15,870	23,980	41,670	37,180		39,670			36,850		
2432	Death Valley Central-2	Death Valley North	1,348,000	1,559,000	1,216,000	1,195,000		2,435,000			2,300,000		

^a The reported recharge volume is only for the Emigrant Valley-3 basin.

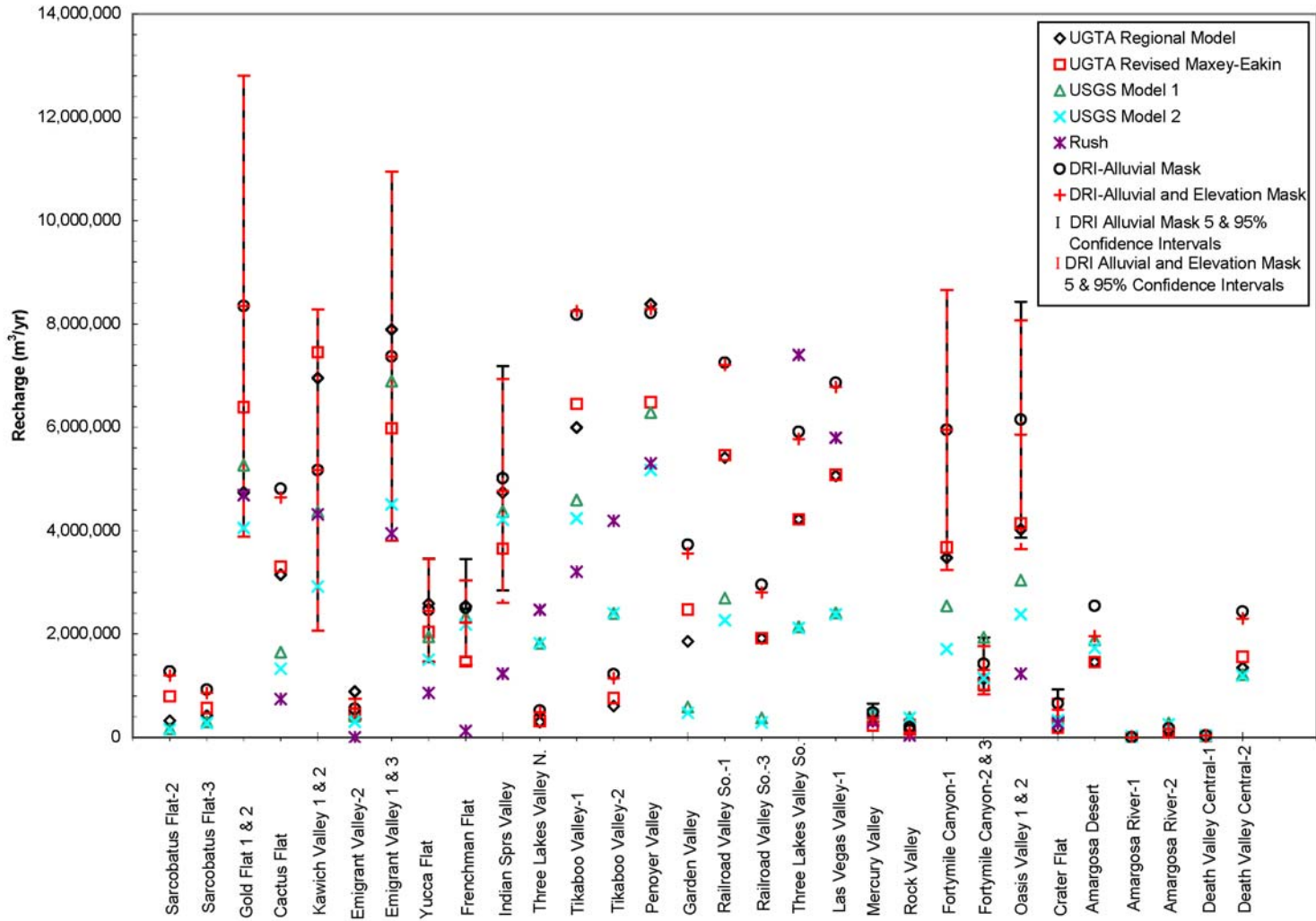


Figure 6-10
Recharge Volumes for Hydrographic Areas for all Recharge Models

recharge areal distributions from model to model vary greatly and this is expected to also have an effect on the resultant flow model predictions. As above, recharge may need to be modified during calibration.

6.7 Limitations

Numerous limitations in the development of the recharge models are documented in each of the reports. The reader is directed to those reports to obtain a complete description of each limitation, including how and at what point in the application of the methodology it affects the resultant recharge estimate. However, there are several limitations that all the authors of the reports found to be in common. These limitations are discussed in this section.

First, all authors agree that the sparsity of precipitation data, especially at higher elevations, and in remote areas greatly increases the uncertainty in the resultant recharge. In addition, the length of record and conversion of snowpack to liquid precipitation have a significant impact on the outcome of the estimates.

Second, the other data types necessary to support each of the methods discussed in this section are limited (e.g., chloride and bromide concentrations in the DRI method [Russell and Minor, 2002]). The regional aspect of the model makes it very difficult and costly to collect sufficient detailed data to develop more than coarse estimates of recharge. The more data types or parameters required for a method would inherently introduce more uncertainty as each parameter would compound the total uncertainty.

Third, the Maxey-Eakin method and to a smaller extent the other methods have depended on a mass balance approach that involves quantification of discharge, which may or may not be accurate. Current studies suggest that the earlier (pre-1980s) estimates of discharge are low, and newer studies support higher discharge values (see discharge section). The increase in discharge, in some cases by a factor of 2 or more, directly relates to an increase by as much to the recharge estimate.

6.8 Summary

This section summarizes three major methods of estimating recharge for the NTS region and proposes application of the recharge models to subsequent groundwater flow modeling activities for the PM-OV area. The Maxey-Eakin approach is an empirically-derived method relating recharge to precipitation zones from a base precipitation map. Several modified versions of this approach are analyzed, including a model from the UGTA regional groundwater flow modeling results, a revised Maxey-Eakin model using a revised base precipitation map, and the Rush (1970) approach which uses elevation contours instead of precipitation contours to determine zonation for recharge estimates.

The USGS deterministic approach models the processes that affect the net rate of infiltration past the root zone. These parameters include precipitation, evapotranspiration, soil type, percent and type of vegetative cover, bedrock type and numerous other input parameters. The USGS approach has two versions. The first includes the overland flow of excess precipitation and redistribution of this water to downstream areas where it can flow onto more permeable soils and infiltrate in those channel locations. In the second version, this redistribution is not included, and the water is removed from the equation.

The DRI chloride mass balance approach estimates recharge by analyzing the chloride ratios of precipitation and groundwater. Higher chloride concentrations in groundwater discharged from springs result from evapotranspiration of precipitation that contains low amounts of conservative atmospheric chloride ion, thus providing a relative gauge of recharge. This information, in conjunction with soil chloride profiles in differing recharge locales (wash versus nonwash), allowed DRI to determine recharge estimates and associated confidence intervals. Two versions of this method are presented, one in which DRI assumed that no recharge was occurring in alluvial deposits (alluvial mask), and the other in which DRI assumed no recharge was occurring in alluvium and up to an elevation of 1,237 m (alluvium and elevation mask).

The UGTA revised Maxey-Eakin method was chosen as the base recharge model for use in groundwater flow modeling because, in general, the method yields recharge volumes that are within the ranges of the other models. The other alternative methods will also be evaluated and used for calibration and sensitivity analysis during the flow modeling process.

Although each method has distinct limitations associated with various steps and assumptions used to determine the resultant recharge, all authors agree that one of the greatest uncertainty can be attributed to the sparsity of precipitation data and length of record over the regional area of investigation.

7.0 *Surface Groundwater Discharge*

Within the PM-OV area and vicinity, most groundwater discharge to the surface occurs naturally in the form of evapotranspiration and springs at the Oasis Valley discharge area. Some groundwater is also withdrawn from the flow system by wells. The area of interest to this activity includes the PM-OV area and all of the Oasis Valley hydrographic area because the discharge area extends outside of the PM-OV area boundary (Figure 7-1). The purpose, approach, and results of the analysis of the data available on groundwater discharge to the surface in the area of interest are presented in this section.

7.1 *Objectives*

The purpose of this data analysis activity is to define locations and rates of groundwater discharge to the surface occurring within the PM-OV area and vicinity.

The specific objectives are as follows:

- Identify locations of natural discharge
- Provide estimates of mean rates of discharge
- Provide a historical record of annual well discharge rates
- Assess and quantify associated uncertainties

7.2 *Approach*

The approach used to complete the data analysis of groundwater discharge to the surface depended on the major data types.

Natural Discharge

Natural discharge to the surface from the PM-OV area and vicinity occurs in the form of springs and ET in the Oasis Valley discharge area. However, because of the processes involved, these two forms of discharge are not independent. In Oasis Valley, most groundwater discharged from springs does not leave the valley by surface flow. Surface water flow out of the valley occurs mostly through the Amargosa River on an intermittent basis. Spring water either re-infiltrates into the flow system or evaporates. Thus, the majority of the groundwater discharged by springs is effectively lost from the groundwater system through ET within the discharge area. In addition, ET estimates include water that moves up from the underlying regional flow system into the shallow flow system.

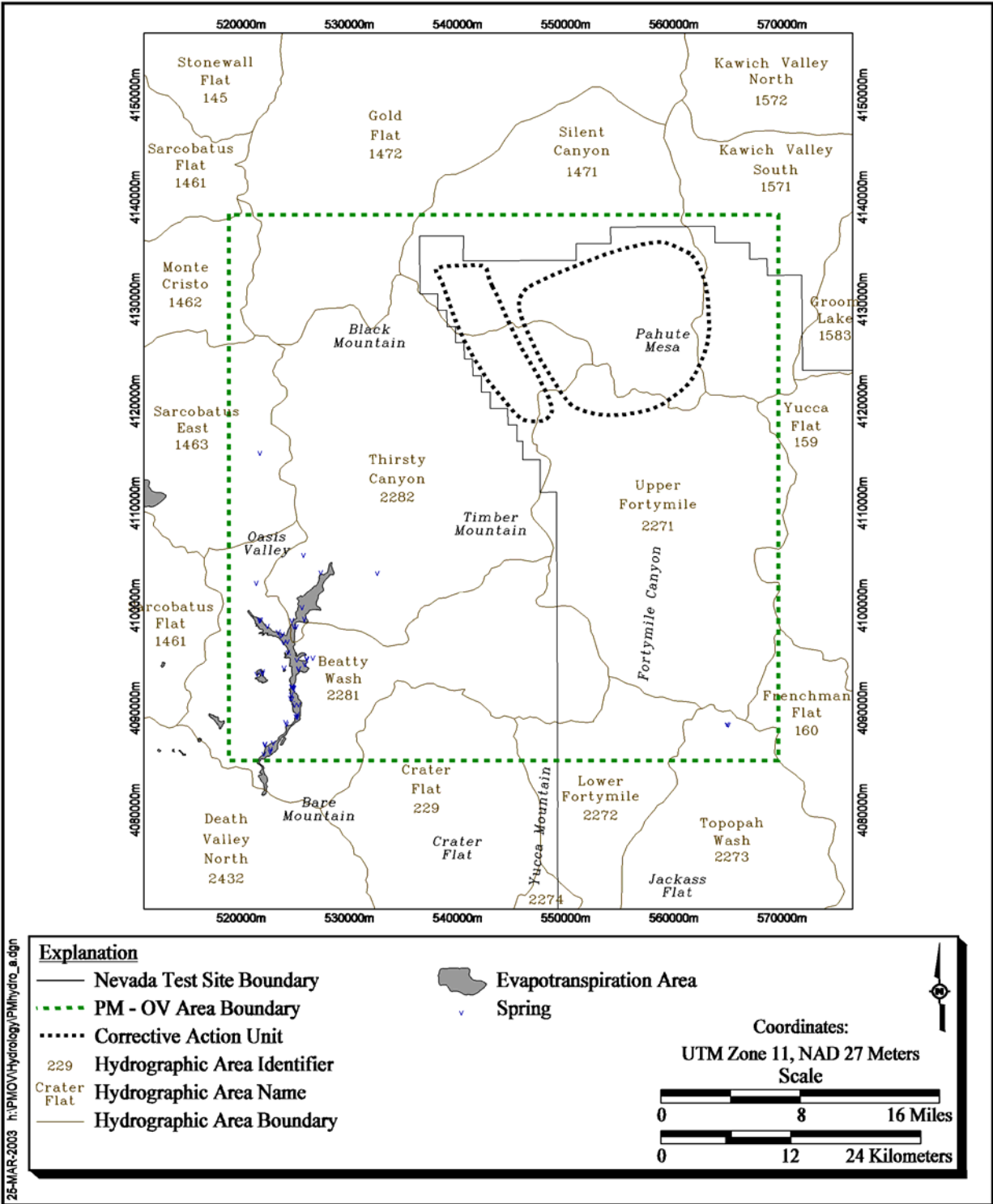


Figure 7-1
Locations of Surficial Hydrologic Features in the
Pahute Mesa-Oasis Valley Area and Vicinity

(Reiner et al., 2002). Total spring discharge could provide a lower bound for ET estimates; however, spring flow rates are difficult to measure at the numerous seeps and at spring locations that are inaccessible. The net natural groundwater discharge to the surface is, therefore, best approximated by an estimate of ET. Thus, the approach used to analyze the natural discharge information is as follows:

- Review and summarize the available ET studies for the PM-OV area and vicinity
- Evaluate their level of documentation
- Evaluate the level of quality
- Describe the ET areas and estimate their extent
- Provide estimates of mean annual ET rates and associated range of uncertainty

Well Discharge

Wells of interest to this activity are only those that pumped or have been pumping for longer than a year. Discharge data collected during short-term pumping such as that conducted during well testing are not included. The approach to analysis of the well discharge data was as follows:

- Compile available historical yearly well pumping data
- Assess pumping record completeness
- Estimate groundwater withdrawal from domestic wells
- Calculate or estimate annual discharge rates

7.3 Data Types and Prioritization

Data types needed for ET and well discharge are as follows:

ET Data

- Location and extent of ET areas within the Oasis Valley discharge area
- Estimates of mean annual ET rates for each area
- Estimates of uncertainty associated with annual ET rates for each area

Well Discharge Data

- Site identification number (ID)
- Reporting Name
- Site coordinates
- Effective open interval
- Date discharge rate measured
- Discharge measurement

Data types were prioritized for uncertainty assessment which includes evaluating the data documentation and estimating ranges of uncertainty.

Two types of flags were assigned to the discharge data: the DDE_F and the DQE_F. The DDE-F is a descriptor of the level of documentation and is described in [Section 4.0](#) of this document. The DQE_F is a descriptor of the level of data quality and depends on the type of data. DDE_Fs and DQE_Fs are described in [Section 7.4](#).

Data types that were prioritized for this activity are as follows:

- ET estimates
- Well discharge rates

7.4 Available Data Description

Available data for natural groundwater discharge and well discharge are summarized in this section. An assessment of the quality of the documentation and the data is also provided.

7.4.1 Natural Surface Discharge

Prior to the 1990s, only two reports provided estimates of ET for the Oasis Valley discharge area: Malmberg and Eakin (1962) and Blankennagel and Weir (1973). Starting in 1993, the U.S. Geological Survey, in cooperation with the U.S. Department of Energy, initiated a series of studies to refine and improve previous estimates of groundwater discharge for the NTS region, including the Oasis Valley discharge area. The first study was focussed on the Ash Meadows discharge area Lacznia et al. (1999). The second study was initiated in 1996 and was focussed on Oasis Valley. Estimates based on early measurements of ET at Oasis Valley during this study were made by Lacznia (1996) and reported in the regional model report (DOE/NV, 1997 and IT, 1996a). The results of the completed Oasis Valley study were later published by Reiner et al. (2002). During the same period of time, Lacznia et al. (2001) estimated annual ET for discharge areas located within the Death Valley flow system, including the Oasis Valley discharge area.

Malmberg and Eakin (1962) estimated the annual ET for Oasis Valley as part of a reconnaissance study. An estimate of the annual ET was calculated as the product of the acreage and the average ET rate. The ET area was delineated using vegetation and soil maps available at the time. The average ET rate was estimated from ET rates reported for other areas of the southwestern United States having similar phreatophytes as Oasis Valley (Lee, 1912; Robinson, 1958; White, 1932; Young and Blaney, 1942). Their estimate of ET was about 7,000 m³/d (2,000 acre-ft per year) (Malmberg and Eakin, 1962). Malmberg and Eakin (1962) also estimated spring discharge rates for selected springs of Oasis Valley.

Blankennagel and Weir (1973) later reported that annual groundwater discharge from Oasis Valley might exceed the Malmberg and Eakin (1962) estimate by a factor of two or more (greater than 14,000 m³/d [4,800 acre-ft per year]). Their estimate was based on unpublished USGS studies conducted at the time by W.A. Beetem and R.A. Young of the USGS.

Early measurements of ET during the Oasis Valley study later reported by Reiner et al. (2002) confirmed the findings reported by Blankennagel and Weir (1973). Using the early measurements of ET, Laczniaik (1996) estimated the range of ET from the Oasis Valley discharge area to be between 5,000 to 8,000 ac-ft/yr (17,000 to 27,000 m³/d). This range was used in the regional model (DOE/NV, 1997).

Reiner et al. (2002) conducted a comprehensive study on groundwater discharge in the Oasis Valley. This study was initiated to address the concern raised by Blankennagel and Weir (1973) and later by the findings of studies by Johnson (1993), Nichols et al. (1997), and Laczniaik et al. (1999) suggesting that ET rates for local phreatophytes may be higher than those used by Malmberg and Eakin (1962) for Oasis Valley. The purpose of this study was to estimate groundwater discharge by quantifying ET, estimating subsurface outflow, and compiling groundwater withdrawal data. In addition to discharge by ET, Reiner et al. (2002) also measured spring discharge and groundwater levels to help evaluate ET and characterize hydrologic conditions. The main objective was to refine and improve the current estimates of ET from the Oasis Valley discharge area.

The study included an extensive field data collection program and detailed analyses. The method used by Reiner et al. (2002) to quantify ET is similar to that used by Laczniaik et al. (1999) for the Ash Meadows discharge area. This method is a refinement of the Malmberg and Eakin (1962) method. Refinements include the incorporation of satellite imagery and remote-sensing techniques to better define the ET units, and the use of long-term micrometeorological data to calculate ET rates for each ET unit. In addition, nearly-continuous measurements of water level collected during the study were used to build confidence in the locations and quantities of ET.

Laczniaik et al. (2001) published the results of studies on groundwater discharge in the Death Valley flow system. The purpose of their study was to estimate mean annual ET from discharge areas located within the Death Valley flow system, including Oasis Valley. The approach used by Laczniaik et al. (2001) was basically the same as the one used by Reiner et al. (2002) and Laczniaik et al. (1999). For the Oasis Valley discharge area, Laczniaik et al. (2001) used most of the data that had been collected by Reiner et al. (2002) at the time. However, their estimates of mean annual ET for the Oasis Valley discharge area are slightly different from those reported by Reiner et al. (2002) due to differences in data interpretation. In addition to mean annual ET, Laczniaik et al. (2001) presented estimates of uncertainty associated with annual ET using Monte Carlo simulations.

DDE_Fs were assigned to ET mean annual rates according to their source report. Estimates from the regional model report (DOE/NV, 1997) were not assigned a

DDE_F level because they were based on preliminary results later reported by Reiner et al. (2002):

- Estimates from Malmberg and Eakin (1962) were assigned a level of 4.
- Estimates from Blankennagel and Weir (1973) were assigned a level of 5 because the documentation of the work of Beetem and R.A. Young was not provided in the Blankennagel and Weir report (1973).
- Estimates from Reiner et al. (2002) and from Laczniaik et al. (2001) were assigned a level of 3 because documentation of the procedures used and the results are either described in the reports or are available from the USGS.

DQE_Fs were assigned to ET mean annual rates according to their source report as follows:

- Estimates from Malmberg and Eakin (1962) were assigned a "low" level of quality because of the approximate methods and non-site specific ET rate data used to derive the estimates.
- Estimates from Blankennagel and Weir (1973) were assigned a "low" level of quality because they did not provide specific values of discharge and because the methods used are unknown.
- Estimates made by Reiner et al. (2002) and Laczniaik et al. (2001) were assigned a "high" level of quality because they are based on comprehensive and well-documented studies relying on field data and sophisticated methods of ET-unit identification.

7.4.2 Well Discharge

The pumping data, their sources, and prioritization for further evaluation are discussed in this section.

Groundwater is withdrawn from the flow system from several wells located within or near the PM-OV area. These wells have been classified into the four following groups:

- NTS water supply wells
- Beatty municipal wells
- Mining pumping wells
- Domestic water wells

Pumping data for the NTS water supply wells are compiled on a monthly and yearly basis by the USGS from records provided by BN. Pumping data for the Beatty municipal wells are recorded by the Beatty Water and Sanitary District (BWSD) and were obtained from the USGS. Discharge data for mining pumping wells were compiled by the USGS from records obtained from the State of

Nevada. No well-specific data are available for domestic wells. Estimates based on water use are, however, available.

DDE_Fs:

- NTS water supply wells: Most records were assigned a level of 3
- Beatty municipal wells: All records were assigned a level of 4
- Mining pumping wells: All records were assigned a level of 4
- Domestic water wells: The estimates were assigned a level of 4

DQE_Fs:

- NTS water supply wells: The available records were assigned a "high" level of quality
- Beatty municipal wells: All records were assigned a "medium" level of quality.
- Mining pumping wells: All records were assigned a "medium" level of quality
- Domestic water wells: The estimates were assigned a "low" level of quality

7.5 Natural Surface Discharge

The studies conducted by Reiner et al. (2002) and Laczniaik et al. (2001) were selected to provide estimates of natural discharge for this activity because of their "high" level of quality. The following description of natural surface discharge from the Oasis Valley discharge area was summarized from the reports prepared by Reiner et al. (2002) and Laczniaik et al. (2001).

7.5.1 Description of Oasis Valley Discharge Area

Natural groundwater discharge to the surface within the PM-OV area and vicinity occurs by springflow or evapotranspiration, mostly within the Oasis Valley discharge area.

Reiner et al. (2002) report that approximately 75 springs and seeps are mapped throughout Oasis Valley. Spring flow rates range from less than 1 gallon per minute (gal/min) to more than 200 gal/min. Water temperatures had previously been reported to be between about 60 degrees Fahrenheit (°F) to more than 100°F (White, 1979; McKinley et al. 1991). Reiner et al. (2002) grouped the springs of Oasis Valley according to their hydrogeologic setting into seven groups as presented in [Table 7-1](#) and [Figure 7-2](#). Except for Group 7 (Bullfrog Hills) which consists of perched springs, all other groups are believed to be regional springs. The source of water is believed to be a portion of the groundwater flowing in the volcanic rocks of Western Pahute Mesa (Reiner et al., 2002). In general, these

Table 7-1
Description of Springs Occurring in Oasis Valley

Group Number	Group Name	Probable Cause	Source
1	Colson Pond Group	Transmissivity change across the Colson Pond Fault	Likely fed by water flowing from the north and northeast
2	Oasis Mountain Hogback Group	Abrupt westward thinning of the welded-tuff aquifer across the Hogback Fault	Likely fed by water flowing from Pahute Mesa
3	Amargosa River Group	Transmissivity change and disruption in aquifer continuity across the Beatty Fault	Likely fed by a mixture of the water flowing into Oasis Valley from the east, west, and north
4	Hot Springs Group	Upward flow along the fault (elevated water temperatures [about 105°F])	Likely fed by flow from the east and north, possibly Timber Mountain and/or Pahute Mesa
5	Lower Amargosa River Group	---	Probably fed primarily by water flowing from the north through Oasis Valley
6	Upper Amargosa River Group	Transmissivity change and disruption in aquifer continuity across the Beatty Fault	Likely fed by inflow from the north and northwest (White, 1979)
7	Bullfrog Hills Group	Permeability changes within the welded-tuff aquifer caused by hydrothermal alteration	Likely fed by local recharge to nearby highlands and therefore perched

Source: Adapted from Reiner et al. (2002)

See [Figure 7-2](#) for locations

source areas are consistent with the end member water types (see [Section 10.5.4](#)) identified by Rose et al. (2002) in the Pahute Mesa-Oasis Valley flow system. It is also likely that as one moves to the south, the springs discharge some mixture of groundwater from recharge areas, as well as contributions from overland flow and infiltration of spring discharge that occurred further to the north.

Once at the surface, groundwater emerging from springs and seeps is captured in local marshes and small pools or is channeled into free-flowing drainages. It then evaporates into the atmosphere or infiltrates valley fill deposits. The valley fill aquifer also receives water from the regional welded-tuff aquifer both by diffuse or preferential, fault-associated upward flow. Water in the valley fill aquifer maintains a variety of plants within the discharge area and vicinity, including grasses, reeds, shrubs, and trees. This vegetation serves as a major vehicle for natural discharge from the area through transpiration.

Little surface water flows out of Oasis Valley except during short periods that follow occasional, intense rainstorms (Reiner et al., 2002). The main drainage is the Amargosa River, which is an intermittent stream. Only reaches located directly downgradient from major springs or spring-fed streams flow on a continuous basis. A small amount of water leaves Oasis Valley through the subsurface across the Amargosa River Narrows (Reiner et al., 2002). Groundwater discharges from Oasis Valley to the Amargosa Desert through alluvium at the Amargosa Narrows in southernmost Oasis Valley

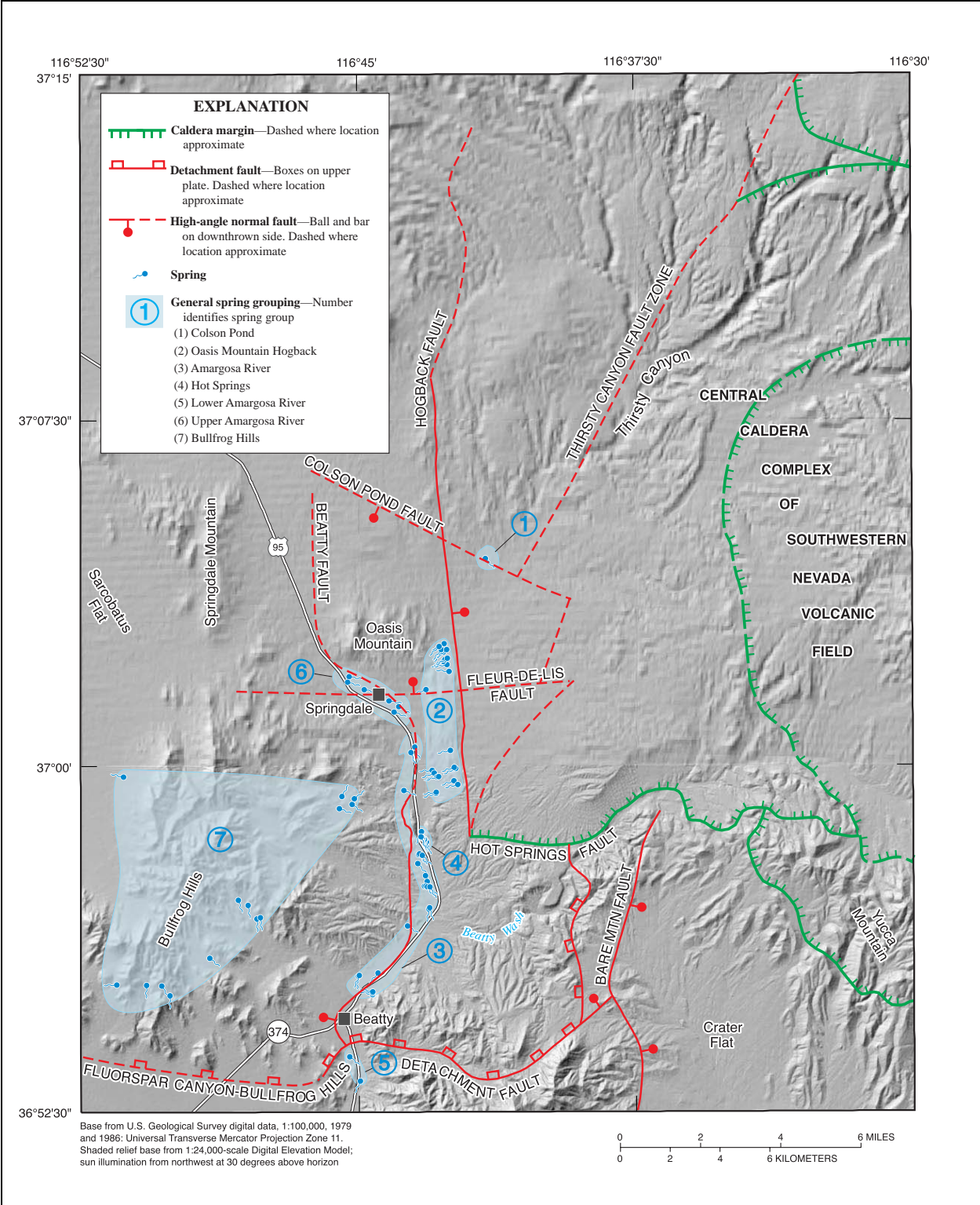


Figure 7-2
General Spring Locations and Major Structural Features Controlling Spring Discharge in Oasis Valley, NV (Reiner et al., 2002)

(Reiner et al., 2002) estimated the amount of outflow using Darcy's Law and average values for the hydraulic gradient (0.0052 m/m), cross-sectional area (8,175 m²), and hydraulic conductivity of the alluvium (0.61 to 3.05 m/d). They calculated an subsurface outflow averaging about 98,678 m³.

7.5.2 Methodology

Reiner et al. (2002) approximated the natural loss of groundwater to the surface from the Oasis Valley discharge area with an estimate of the ET from areas of groundwater discharge. Such an estimate not only includes water losses by spring and seep, but also water flowing upward from the regional welded-tuff aquifer into the alluvial aquifer.

The method used by Reiner et al. (2002) and Laczniaik (2001) to quantify ET from the Oasis Valley discharge area is similar to that used by Laczniaik et al. (1999) for the Ash Meadows discharge area.

As stated by Laczniaik (2001), the method is based on the following assumptions:

- ET rates vary with the health, density, and type of vegetation; and with the wetness of the soil.
- Within a given discharge area, ET rates can be generalized on the basis of similarities in vegetation and soil conditions.

The method consists of the following four basic steps:

- ET units, which are defined as areas of similar plant cover and soil cover, are identified and mapped using Landsat Thematic Mapper (TM) imagery. Spatial changes in vegetation and soil covers are interpreted from remotely-sensed spectral reflectance data and used to delineate ET units on the basis of spectral similarities identified from the TM imagery.
- ET rates are calculated from field measurements of micrometeorological data (localized) using the Bowen-ratio method. An annual ET rate is then estimated for each of the ET units by averaging all ET rates available for sites located within that unit. The ET rates are then adjusted by removing water contributed by local precipitation from the estimates.
- Annual ET from each ET unit is computed as the product of the unit's acreage and ET rate.
- Total ET is calculated by adding estimates of annual ET computed for ET units.

In addition, water-level and spring discharge fluctuations may be used to verify the locations and relative magnitude of ET.

7.5.3 Evapotranspiration Units

In both studies (i.e., Reiner et al., 2002; Laczniaik et al., 2001), the TM data used to classify ET units within the Oasis Valley area was imaged June 13, 1992 (scene identification number LT5040035009216510, Figure 7 in Reiner et al.'s report [2002]). Reiner et al. (2002) and Laczniaik et al. (2001) decided to use the June 1992 TM imagery because of the following reasons:

- June is a period of high vegetation vigor
- 1992 had slightly above-normal precipitation
- The authors wanted to be consistent with the Ash Meadows ET study (Laczniaik et al., 1999)

ET unit definitions were very similar in the two studies (Table 7-2). However, in addition to the nine ET units defined by Reiner et al. (2002), Laczniaik et al. (2001) defined two new ET units (9 and 10) to segregate areas dominated by sparse woodland vegetation, and areas dominated by open playa, respectively.

As shown in Table 7-2, the two studies yielded very similar results in terms of ET unit differentiation for the Oasis Valley discharge area. The areas were, however, not identical for some of the ET areas. The difference was due to difficulty in discriminating between the two grassland ET units, labeled sparse to moderately dense grassland (SGV) and moderately dense to dense grassland (DGV) by Reiner et al. (2002) and sparse grassland and dense to moderately dense grassland by Laczniaik et al. (2001) (Table 7-2). This difficulty led to two different interpretations. Laczniaik et al. (2001) interpreted some of the grassland classified as moderately dense grassland cover by Reiner et al. (2002) to be dense grassland (DGV). This resulted in different ET-unit areas for the two units (Table 7-2).

The values of total ET area were very similar: Reiner et al. (2002) estimated the total ET unit area to be 13,864,542 m², whereas Laczniaik et al. (2001) estimated the total to be 14,054,745 m². The difference in total ET area and other differences in ET unit areas derived from these two studies are minor. The values of total ET area reported by Reiner et al. (2002) and Laczniaik et al. (2001) are also comparable to the 15,378,068 m² of phreatophytes estimated by Malmberg and Eakin (1962). The ET-unit distribution generated by Laczniaik et al. (2001) is presented in Figure 7-3. The distribution generated by Laczniaik et al. (2001) is also available in electronic format as a grid.

The accuracy of the classification method as applied to the Oasis Valley discharge area was assessed by Reiner et al. (2002) using the same method as Laczniaik et al. (1999) for the Ash Meadows discharge area. In this method, a selected number of sites are assigned to ET units on the basis of field observation. The assigned ET unit areas are then compared with those assigned using the classification procedure. The overall accuracy is calculated as the ratio of the number of sites correctly classified to the total number of sites compared.

Table 7-2
Evapotranspiration (ET) Units Determined from Spectral Analysis of Satellite Imagery Data,
Oasis Valley Discharge Area, Nevada, June 13, 1992
 (Page 1 of 2)

Laczniak et al. (2001)			Reiner et al. (2002)		
ET-Unit Number	ET-Unit Area (m ²)	General Description of ET Unit	ET-Unit Identifier	ET-Unit Area (m ²)	General Description of ET Unit
0	0	Area of no significant ET from groundwater source (unclassified); water table typically greater than 50 feet below land surface	UCL	0	Area of no substantial ET from ground-water source (unclassified); water table typically greater than 20 feet below land surface; soil very dry
1	4,047	Area of open water, primarily reservoir or large spring pool	OWB	4,047	Area of open water, primarily spring pool or pond
2	20,234	Area of submerged aquatic vegetation; includes sparse emergent vegetation and shallow part of open water areas; perennially loaded; water at surface	SAV	16,187	Area of submerged and sparse emergent aquatic vegetation; includes primarily shallow part of open water areas; perennially flooded; water at surface
3	161,874	Area dominated by dense wetland vegetation, primarily tall reedy and rushy marsh plants, typically tule, cattail, or giant reed; perennially flooded; water at surface	DWV	161,874	Area dominated by dense wetland vegetation, primarily tall reedy and rushy marsh plants, typically tule, cattail, or giant reed; perennially flooded; water at surface
4	3,767,627	Area dominated by dense meadow and forested vegetation, primarily trees, meadow grasses, or mixed trees, shrubs, and grasses; trees include saltcedar, mesquite, or desert willow; water table typically ranges from a few feet to about 20 feet below land surface; soil moist to dry	DMV	3,366,988	Area dominated by dense meadow and woodland vegetation, primarily trees, meadow and marsh grasses, or mixed trees, shrubs, and grasses; trees include desert ash and cottonwood, with some desert willow and mesquite; water table typically ranges from above land surface to about 20 feet below land surface; soil wet to dry
5	2,610,225	Area dominated by dense to moderately dense grassland vegetation, primarily saltgrass, and/or short rushes with an occasional tree or shrub; intermittently flooded; water table typically less than 5 feet below land surface; soil wet to moist	DGV	1,375,932	Area dominated by moderately dense to dense grassland vegetation, primarily saltgrass, and/or short rushes with an occasional tree or shrub; intermittently flooded; water table typically less than 10 feet below land surface; soil wet to moist
6	3,893,079	Area dominated by sparse grassland vegetation, primarily salt and bunch grasses but also includes areas of very low density shrubs (mesquite); water table typically ranges from a few feet to about 12 feet below land surface; soil dry	SGV	4,916,935	Area dominated by sparse to moderately dense grassland vegetation, primarily salt and bunch grasses with occasional tree or shrub; water table typically ranges from a few feet below land surface to about 10 feet below land surface; soil damp to dry
7	327,796	Area dominated by moist bare soil; vegetation very sparse, primarily grasses; intermittently flooded, water table typically near land surface throughout most of the year but in some areas declines to a maximum depth of about 5 feet below land surface during late summer and early fall; soil typically moist	MBS	412,780	Area dominated by moist bare soil; vegetation very sparse, primarily grasses; intermittently flooded, water table typically near land surface throughout most of the year but in some areas declines to a maximum depth of about 5 feet below land surface during late summer and early fall; soil wet to moist
8	3,265,816	Area dominated by sparse to moderately dense shrubland vegetation, primarily greasewood, rabbitbrush, wolfberry, and seepweed; water table typically ranges from about 5 feet to about 20 feet below land surface; soil dry	SSV	3,609,799	Area dominated by sparse to moderately dense shrubland vegetation, primarily greasewood, rabbitbrush, and wolfberry; water table typically ranges from about 5 feet below land surface to about 20 feet below land surface; soil damp to dry

Table 7-2
Evapotranspiration (ET) Units Determined from Spectral Analysis of Satellite Imagery Data,
Oasis Valley Discharge Area, Nevada, June 13, 1992
 (Page 2 of 2)

Laczniak et al. (2001)			Reiner et al. (2002)		
ET-Unit Number	ET-Unit Area (m ²)	General Description of ET Unit	ET-Unit Identifier	ET-Unit Area (m ²)	General Description of ET Unit
9	NA	Area dominated by sparse woodland vegetation, primarily mesquite; water table typically ranges from about 10 to 40 feet below land surface; soil dry	NA	NA	NA
10	4,047	Area dominated by open playa, primarily bare soil, often encrusted with salts; water table ranges from about 5 to 40 feet below land surface; soil typically dry but can be moist for short periods after intermittent flooding	NA	NA	NA

Source: Laczniak et al. (2001) and Reiner et al. (2002)

NA = Not applicable

The overall accuracy calculated by Reiner et al. (2002) for Oasis Valley was 88 percent. This accuracy is comparable to that reported by Laczniak et al. (1999), 86.6 percent, for the Ash Meadows discharge area. Reiner et al. (2002) also calculated an average accuracy of individual classes to be 91 percent. Both Reiner et al. (2002) and Laczniak et al. (1999) concluded that these accuracy values are above the acceptability criterion established by Anderson et al. (1976).

7.5.4 Evapotranspiration Rates and Volumes

Evapotranspiration rates and volumes as derived by Reiner et al. (2002) and Laczniak et al. (2001) are described in this section.

Reiner et al. (2002) and Laczniak et al. (2001) derived ET rates for the ET units they defined differently. Reiner et al. (2002) derived ET rates from data they collected during their study of Oasis Valley and from data collected at Ash Meadows by Laczniak et al. (1999). ET rates were calculated from field measurements of micrometeorological data (localized) collected from five sites located within the Oasis Valley discharge area between 1996 and 2000, using the energy budget method (Bowen-ratio solution [Bowen, 1926]) (Table 7-3). Data obtained from nine similar ET sites in nearby Ash Meadows (Laczniak et al., 1999) were used to supplement their data (Table 7-3). An annual ET rate was then estimated for each of the ET units by averaging all ET rates available for sites located within that unit (Table 7-3). Laczniak et al. (2001) used ET rates estimated in other studies of areas located in the NTS region. Their primary sources of data were the same as Reiner et al. (2002), ET rates derived from field measurements of micrometeorological data at Oasis Valley (Reiner et al., 2002) and Ash Meadows (Laczniak et al., 1999). However, Laczniak et al. (2001) supplemented these data with rates estimated in other selected studies of ET throughout the region. ET rates for each ET unit are presented as ranges in

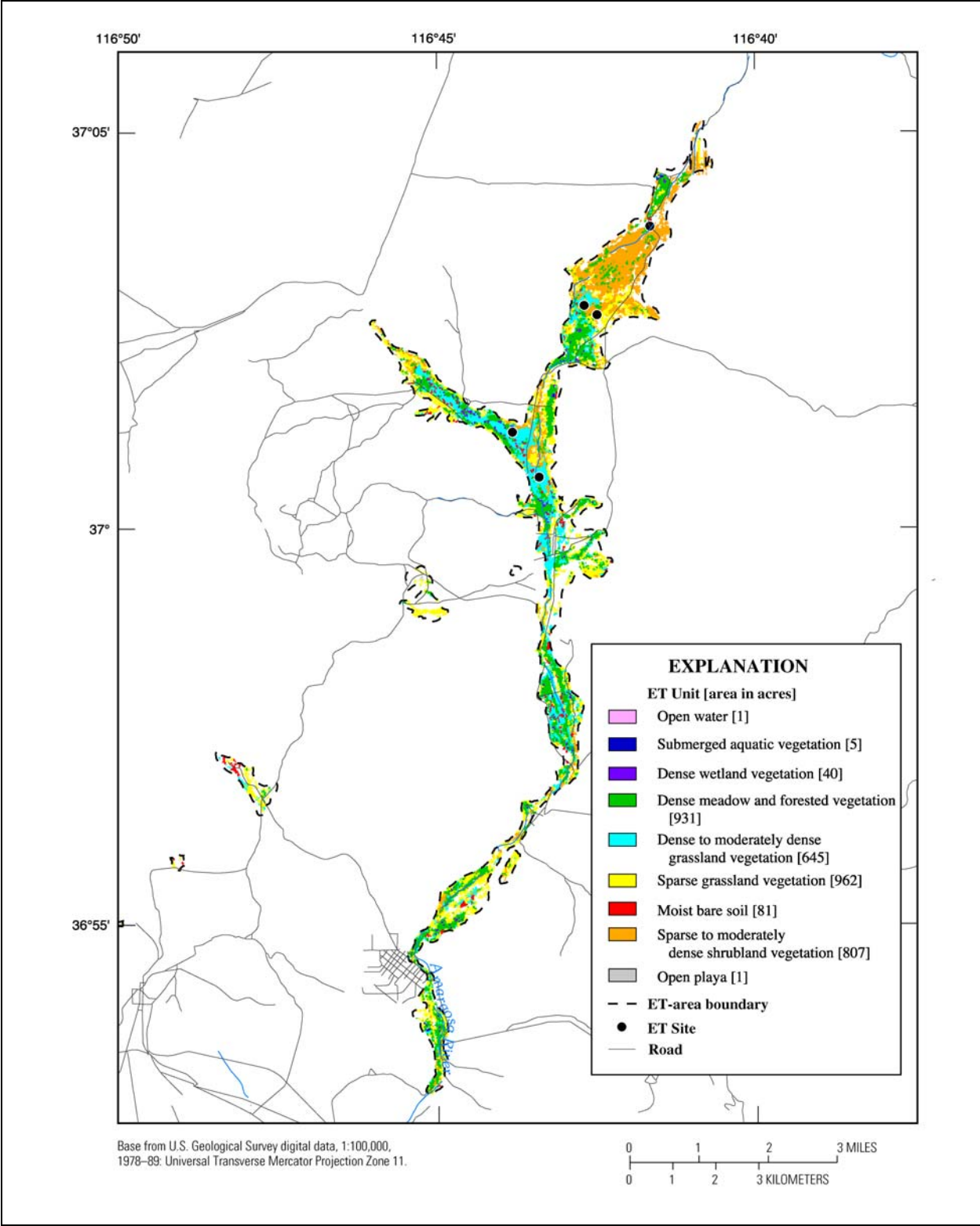


Figure 7-3
Locations of ET Units as Defined by Lacznia et al. (2001) for Oasis Valley, Nevada

Table 7-3
Evapotranspiration Rates Used to Compute Annual Evapotranspiration
from Oasis Valley Discharge Area, Nevada

ET-Unit Identifier ^a	Average ET Rate ^b (m/d)	Site Name	Location	Site Identifier	Measured ET Rate (m/d)	Source
OWB	7.182E-03	Peterson Reservoir	AM	PRESVR	7.182E-03	Laczniak et al. (1999)
SAV	7.182E-03	Peterson Reservoir	AM	PRESVR	7.182E-03	Laczniak et al. (1999)
DWV	3.257E-03	Fairbanks Swamp	AM	FSWAMP	3.265E-03	Laczniak et al. (1999)
DMV	2.756E-03	Carson Meadow	AM	CMEADW	2.873E-03	Laczniak et al. (1999)
		Springdale	OV	SDALE	2.622E-03	Reiner et al. (2002)
DGV	2.672E-03	Fairbanks Meadow	AM	FMEADW	2.564E-03	Laczniak et al. (1999)
		Rogers Spring 2	AM	RGSPR2	2.697E-03	Laczniak et al. (1999)
SGV	1.670E-03	Middle Oasis Valley	OV	MOVAL	2.079E-03	Reiner et al. (2002)
		Bole Spring South	AM	BSSOUT	1.570E-03	Laczniak et al. (1999)
		Rogers Spring 1	AM	RGSPR1	1.603E-03	Laczniak et al. (1999)
		Upper Oasis Valley Middle	OV	UOVMD	1.361E-03	Reiner et al. (2002)
MBS	2.171E-03	Lower Crystal Flat	AM	LCFLAT	2.154E-03	Laczniak et al. (1999)
		Bole Spring North	AM	BSNORT	2.171E-03	Laczniak et al. (1999)
SSV	1.002E-03	Upper Oasis Valley Lower	OV	UOVLO	1.152E-03	Reiner et al. (2002)
		Upper Oasis Valley Upper	OV	UOVUP	5.177E-04	Reiner et al. (2002)

Source: Reiner et al., 2002

^aET unit descriptions are given in [Table 7-2](#).

^bAverage rate is computed as arithmetic mean of measured rates for each ET unit except for SSV. The average rate for SSV is an area-weighted average.

Note: Abbreviations: AM = Ash Meadows; OV = Oasis Valley

[Table 7-4](#). For each ET unit, the range is inclusive of all ET rates calculated for Ash Meadows (Laczniak et al., 1999) and Oasis Valley (Reiner et al., 2002), and the estimated rates obtained from the literature.

Both Laczniak et al. (2001) and Reiner et al. (2002) adjusted the ET rate values by subtracting local precipitation contributions. The local precipitation component was assumed to be equal to the mean, annual, long-term precipitation of $4.175 \cdot 10^{-04}$ m/d. Uncertainty in the precipitation adjustment is due to errors in the

Table 7-4
Ranges of Evapotranspiration Rates for ET Units Classified In Major Discharge Areas
of Death Valley Regional Flow System, Nevada and California

ET-Unit Number	Estimated ET Rate (m/d)		Source (by order of significance)
	Minimum	Maximum	
0	0	0	NA
1	7.015E-03	7.349E-03	Laczniak et al. (1999)
2	6.764E-03	7.099E-03	Laczniak et al. (1999)
3	3.090E-03	3.591E-03	Laczniak et al. (1999)
4	2.505E-03	3.340E-03	Laczniak et al. (1999); Reiner et al. (2002); Johnson (1993); Weeks et al. (1987); Gay and Fritschen (1979); Walker and Eakin (1963)
5	2.088E-03	3.090E-03	Laczniak et al. (1999); Reiner et al. (2002); Walker and Eakin (1963)
6	5.010E-04	1.921E-03	Laczniak et al. (1999); Reiner et al. (2002); Czarnecki (1997); Nichols (2001)
7	1.837E-03	2.505E-03	Laczniak et al. (1999)
8	5.845E-04	2.088E-03	Reiner et al. (2002); Nichols (1993); Nichols (2001); Walker and Eakin (1963)
9	5.845E-04	1.503E-03	Reiner et al. (2002); Walker and Eakin (1963); Young and Blaney (1942)
10	8.351E-05	5.845E-04	DeMeo et al. (1999); Nichols (2001); Czarnecki (1997)

Source: Laczniak et al., 2001

NA = Not applicable

estimate of the average annual precipitation and to the fact that the actual quantity of local precipitation contained in the unadjusted ET rates is unknown.

Surface-water inflow contribution were not accounted for in the estimate of the ET rate due to a lack of data, even though it could be a substantial part of the ET rate in Oasis Valley. The adjusted ET rates are presented in [Table 7-5](#).

Mean annual groundwater ET values calculated by Reiner et al. (2002) and Laczniak et al. (2001) are presented in [Table 7-5](#). Mean annual groundwater ET from each ET unit was calculated by multiplying the unit's area by the adjusted mean groundwater ET rate. Mean annual groundwater ET from the Oasis Valley discharge area was estimated by summing the mean annual groundwater ET from all ET units. The estimates of the mean annual groundwater ET derived by Laczniak et al. (2001) and Reiner et al. (2002) for the Oasis Valley discharge area are very similar.

The estimates of mean annual groundwater ET made by Laczniak et al. (2001) and Reiner et al. (2002) differ from that of Malmberg and Eakin (1962, p. 25) by a factor of 3. The extent of ET area estimated by Malmberg and Eakin (1962) is

Table 7-5
Estimated Mean Annual Evapotranspiration and Groundwater Evapotranspiration
by Evapotranspiration Unit from Oasis Valley Discharge Area, Nevada

Laczniak et al., 2001						Reiner et al., 2002					
ET-Unit Identification	Area (m ²)	ET Rate (m/d)	Annual ET (m ³)	Mean ET Rate (m/d) ^a	Mean Annual ET (m ³)	ET-Unit Identification	Area (m ²)	ET Rate (m/d)	Annual ET (m ³)	Mean ET Rate (m/d) ^a	Mean Annual ET (m ³)
1	4,047	7.182E-03	11,101	6.764E-03	9,868	OWB	4,047	7.182E-03	10,608	6.764E-03	9,991
2	20,234	7.098E-03	51,806	6.681E-03	49,339	SAV	16,187	7.182E-03	41,938	6.764E-03	39,471
3	161,874	3.507E-03	209,692	3.090E-03	185,022	DWV	161,874	3.257E-03	197,357	2.839E-03	172,687
4	3,767,627	2.589E-03	3,577,092	2.171E-03	2,960,352	DMV	3,366,988	2.756E-03	3,330,396	2.338E-03	2,837,004
5	2,610,225	2.589E-03	2,466,960	2.171E-03	2,096,916	DGV	1,375,932	2.672E-03	1,356,828	2.255E-03	1,134,802
6	3,893,079	1.002E-03	1,480,176	5.845E-04	826,432	SGV	4,916,935	1.670E-03	2,960,352	1.253E-03	2,220,264
7	327,796	2.255E-03	271,366	1.837E-03	222,026	MBS	412,780	2.171E-03	333,040	1.754E-03	259,031
8	3,265,816	1.587E-03	1,850,220	1.169E-03	1,356,828	SSV	3,609,799	1.002E-03	1,356,828	5.845E-04	764,758
9	—	—	—	—	—	—	—	—	—	—	—
10	4,047	4.175E-04	1,233	8.351E-06	—	—	—	—	—	—	—
Total	14,054,745	1.921E-03	9,867,840	1.503E-03	7,647,576	—	13,864,542	1.921E-03	9,621,144	1.420E-03	7,400,880

^aSubtract precipitation rate from ET rate (Precipitation rate = 4.175E-04 m/d)

similar to the estimates made by Laczniaik et al. (2001) and Reiner et al. (2002) (within about 10 percent). The ET rate, however, was much smaller at about 1/3 of the average rates estimated by Laczniaik et al. (2001) and Reiner et al. (2002).

7.5.5 Water Level and Spring Discharge Measurements

Reiner et al. (2002) measured groundwater levels and spring discharge rates in the Oasis Valley discharge area during their investigation to gain additional insight into the ET process. They also estimated annual discharge from springs in Oasis Valley for comparison with their ET estimate.

Reiner et al. (2002) measured depth-to-water levels in several shallow wells located throughout the discharge area. The data exhibited a wide range in annual and daily fluctuations between and within the ET units. Reiner et al. (2002) generally observed a declining water table in the summer and fall, and a rising water table in the winter and spring. They also observed a decrease in the magnitude of daily fluctuations during periods of higher ET rates when the water table was near the surface. Reiner et al. (2002) concluded that even though seasonal and daily changes in water levels may indicate the occurrence of ET; their magnitude is not always indicative of ET rates. This is because factors other than ET affect water levels. Reiner et al.'s observations are consistent with Laczniaik et al.'s (1999) in their study of the Ash Meadows discharge area.

Reiner et al. (2002) also measured spring discharge at several springs and channels. Channel measurement sites were located downgradient of groups of springs and seeps where direct measurements could not be made. The annual maximum discharge at channel sites was observed in the winter and early spring when ET was at a minimum. The annual minimum discharge was observed from late spring to early fall when ET was increasing or at a maximum. Reiner et al. (2002) found that flow rates made at spring sites were not seasonally dependent and exhibited smaller fluctuations than those measured at channel sites. Not only did the channel site measurements exhibit larger fluctuations, they were also more variable. Reiner et al. (2002) attributed the larger fluctuations to seasonal changes in ET primarily. They found no relationship between the rates of spring flow and ET.

The estimate of spring discharge made by Reiner et al. (2002) is about 3,700,440 m³/yr. This estimate excludes flow from numerous seeps or springs for which measurements are not available. Their estimated groundwater discharge by ET (7,400,880 m³/yr) is about 2 times greater than the estimated spring discharge. Differences are due to the exclusion of unavailable data for some springs and seeps and to diffuse and fault-associated upward leakage into the alluvial aquifer from the underlying aquifer.

7.5.6 Sensitivity and Uncertainty Analyses of Annual ET

A sensitivity and an uncertainty analyses were conducted by Laczniaik et al. (2001) as part of their ET study of the Death Valley flow system. The objective of the sensitivity analysis was to identify the input parameters that have the greatest effect on the annual ET values. The objective of the uncertainty analysis was to quantify the uncertainty associated with estimates of annual groundwater discharge by ET from the nine discharge areas of the Death Valley flow system, including the Oasis Valley discharge area. The method and results for the Oasis Valley discharge area are summarized from the appendix in the report by Laczniaik et al. (2001).

7.5.6.1 Method

The analyses were conducted using Crystal Ball (*Decision Engineering*, 1996, Crystal Ball Version 4.0), a Microsoft Excel add-in designed to implement the Monte Carlo method. The following input parameters were required for each of the discharge areas considered by (Laczniaik et al., 2001):

- The ET-unit area
- The ET rate for each ET unit
- The annual precipitation rate

The total number of input parameters used to evaluate the uncertainty in estimates of ET was 141 (i.e., 61 ET-unit areas, 61 ET rates, and 9 precipitation rates) (Laczniaik et al., 2001).

Each input parameter was assumed to be normally distributed. Each normal distribution was described by a mean and a coefficient of variability (CV), defined as the standard deviation divided by the mean. The mean of each input parameter is the value of the parameter as estimated by Laczniaik et al. (2001, Table 5 and Table 7).

The ET-unit area CV was assumed to be 10 percent. This value is based on the results of the ET-unit classification accuracy assessment conducted by Laczniaik et al. (1999) and Reiner et al. (2002) for the Ash Meadows and Oasis Valley discharge areas, respectively. As stated previously, this accuracy is about 90 percent.

The CV for each ET rate was calculated from ranges listed in [Table 7-4](#). The CV for each precipitation rate was calculated from measurements given in Table 8 and Table 9 in Laczniaik et al.'s report (2001). CV values for these input parameters were calculated assuming that the ranges represent ± 2 standard deviations of a normal population (95 percent of the measurements are contained in the range).

Each Monte Carlo realization consisted of four steps:

1. Random selection of a value from the normal distribution of each input parameter

2. Subtraction of the selected precipitation rate from the selected ET rate of each ET unit
3. Calculation of the mean annual ET from each ET unit by multiplying the adjusted ET rate by the corresponding area
4. Calculation of total areas and total ET for each discharge area by addition of corresponding values for all ET units

Sample size testing showed that a sample size of 1,000 realizations would be sufficient to produce stable estimates of annual ET probability distributions.

The sensitivity of each parameter was measured by rank correlation (correlation based on ranks rather than on values).

7.5.6.2 Results

Results of the Monte Carlo simulations conducted by Laczniaik et al. (2001) for the Oasis Valley discharge area are presented in this section.

Table 7-6 contains the simulated mean annual ET from the Oasis Valley discharge area by ET-unit. Values shown in Table 7-6 are simulated means of 1,000 Monte Carlo realizations.

Table 7-6
Simulated Mean Annual Evapotranspiration from Oasis Valley
(Data are simulated means of 1,000 realizations)

ET-Unit Identification	Oasis Valley ET-Unit Identification	Area (m ²)	ET Rate (m/d)	Annual ET (m ³)	Adjusted ET rate (m/d) ^a	Mean Annual ET (m ³)
1	OWB	4,047	7.182E-03	10,608	6.764E-03	9,991
2	SAV	20,234	7.098E-03	52,423	6.681E-03	49,339
3	DWV	160,660	3.507E-03	205,621	3.098E-03	181,692
4	DMV	3,757,914	2.589E-03	3,550,819	2.171E-03	2,978,114
5	DGV	2,619,128	2.580E-03	2,466,713	2.163E-03	2,067,559
6	SGV	3,892,270	9.937E-04	1,411,718	5.762E-04	818,537
7	MBS	326,177	2.246E-03	267,418	1.837E-03	218,696
8	SSV	3,271,482	1.603E-03	1,914,484	1.186E-03	1,415,912
9	—	—	—	—	—	—
10	—	4,047	4.175E-04	617	—	—
Total	—	14,054,745	—	9,880,175	—	7,740,087

Source: Laczniaik et al., 2001

^aMean annual precipitation used in Monte Carlo simulations is 2.923E-04 meter.

—, no data or not applicable

The sensitivity of each parameter was measured by rank correlation. The five most sensitive input parameters for the Oasis Valley discharge area are shown in [Table 7-7](#). The sensitivity of the precipitation rate is negative because it is subtracted from the ET rate to calculate the adjusted ET rate.

Table 7-7
Parameters Having the Greatest Effect
on Simulated Annual ET Measured by Rank Correlation

ET Unit	Parameter	Rank Correlation
ET Unit 8	Annual ET Rate	0.56
ET Unit 6	Annual ET Rate	0.43
All	Annual Precipitation	-0.35
ET Unit 4	Area	0.35
ET Unit 5	Annual ET Rate	0.29

Source: Lacznia et al., 2001

Lacznia et al. (2001) found that, generally, the precipitation rate is always one of the more sensitive input parameter. They also found that the two most sensitive parameters are typically the precipitation rate and the ET rate associated with the largest ET unit. This, however, was not the case for Oasis Valley. The ET rate associated with ET unit 8 is the most sensitive parameter, even though ET units 4 and 6 have the largest areas. According to Lacznia et al. (2001), this anomaly can be explained in part by: (1) the low CV of the ET rate for ET unit 4 (0.07) relative to that of ET units 6 and 8 (0.29 and 0.28, respectively; Table 11), and (2) the high ET rate of ET unit 8 relative to ET unit 6.

Oasis Valley, which has nine ET units and only a small area of open playa, has a CV of 0.12. Assuming that CV is a reasonable estimator of the relative uncertainty, Lacznia et al. (2001) found that the discharge estimates for Oasis Valley and those of the Tecopa/California Valley area are most certain (0.12 and 0.11, respectively).

Additional analyses were performed to examine the uncertainty associated with the classification procedure and to evaluate uncertainty related to the assumption of a 10 percent CV for ET-unit areas. The effects of correlation between the classified ET units were found to be minimal. The results of testing the 10 percent CV for ET-unit areas indicate that the predicted uncertainty in the estimate is nearly proportional to the CV of the area.

[Table 7-8](#) shows the summary statistics of simulated annual ET from 1,000 Monte Carlo realizations for the Oasis Valley discharge area.

Table 7-8
Summary Statistics of Simulated Annual ET from 1,000 Monte Carlo Realizations for the Oasis Valley Discharge Area

Statistic	Value	Unit
Mean	7,754,889	m ³
Median	7,758,589	m ³
Minimum	5,142,378	m ³
Maximum	11,005,109	m ³
Standard Deviation	953,480	m ³
5% Confidence Bound	6,185,950	m ³
95% Confidence Bound	9,325,180	m ³
Coefficient of Variability	0.12	unitless

Source: Modified from Laczniaik et al. (2001)

Note: Added 95% confidence range as mean minus 2 standard deviations and mean plus 2 standard deviations

7.6 Well Discharge

The locations of pumping wells located within the PM-OV area and close vicinity are shown in [Figure 7-4](#). The available historical well discharge data for these pumping wells are described in [Appendix D](#). Only wells with long-term pumping of at least one year are included in the dataset.

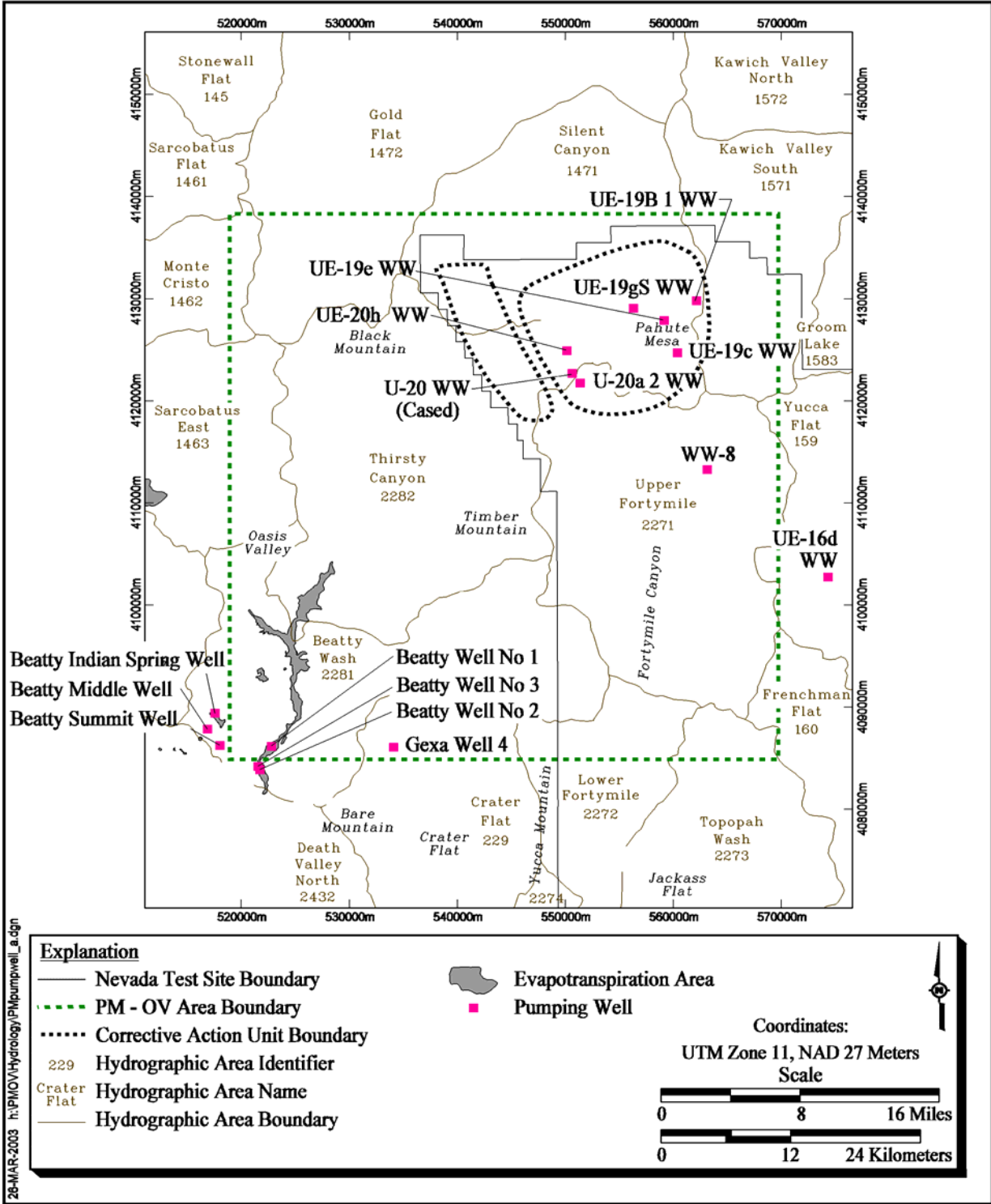
7.6.1 Well and Pumping Record Description

In the PM-OV area, groundwater was pumped from several water supply wells located on and off the NTS. Even though some of the wells are located outside of the PM-OV area, they were included because they are very close to the area of interest and may affect the local groundwater flow system ([Figure 7-4](#)).

The pumping wells were grouped into three categories: NTS Wells, Oasis Valley, and mine wells. Most wells considered are located within the PM-OV boundary. A few wells located outside but near the boundary were also included.

7.6.1.1 NTS Water Supply Wells

NTS water supply wells of interest are located in Areas 19, 20, 18, and 16.



26-MAR-2003 h:\PIMOV\Hydrology\PM\pumpwell_a.dgn

Figure 7-4
Locations of Pumping Wells in the Pahute Mesa-Oasis Valley Area and Vicinity

Area 19

There are four water supply wells in Area 19 on the NTS: UE-19b 1 WW, UE-19c WW, UE-19e WW, and UE-19Gs WW. Groundwater withdrawal data for these and other NTS water supply wells were recompiled by the USGS from totalizing flowmeter readings provided by BN.

UE-19b 1 WW is located in Central Pahute Mesa (Figure 7-4). It was installed as a water-supply well in 1964. The well has a total depth of 1,371.6 m below ground surface (bgs). The open interval is from a depth of 667.5 to 1,371.6 m bgs within the BRA HSU. The pumping record for this well is available for a few months in 1964 and 1965. The data are insufficient to calculate yearly totals. Groundwater may have been withdrawn from this well up to 1982, but no records are available. The well has since been destroyed.

UE-19c WW is located near the center of Area 19 on Pahute Mesa. It was originally drilled in 1964 as an exploratory hole to determine the adequacy of the site for underground nuclear testing. During drilling, the drill pipe became stuck at a depth of approximately 2,587.4 m bgs. As a result, the hole was abandoned. UE-19 c WW was then completed as a water supply well in 1975, and was again recompleted in 1992. The current well depth is 2,587 m bgs. The well is open to the BRA HSU from a depth of 737.9 to 2,401.8 m bgs, and to the PBRCM HSU from a depth of 2,401.8 to 2,587.4 m bgs. Pumping data for this well are available from 1983 through 2000. It is unknown whether this well was pumped prior to 1983 as no pumping records are available.

UE-19e WW is located in Central Pahute Mesa (Figure 7-4). It was installed as a water-supply well in 1964 with a total depth at 1,981.2 m. The well is open to the BFCU HSU from a depth of 754.38 to 894 m bgs, and to the BRA HSU from a depth of 894 to 1,830.47 m bgs. The pumping record for this well is available for years 1965 through 1967. This well has since been destroyed.

UE-19gS WW is located in Central Pahute Mesa (Figure 7-4). It was installed as a water-supply well in 1965 with a total depth at 2,286 m bgs. The well is open to the BRA HSU from a depth of 807.72 to 2,002.5 m bgs, and to the PBRCM HSU from a depth of 2,002.5 to 2,286 m bgs. The well pumping record for this well is available for years 1966 and 1967. The data for 1966 are insufficient to calculate a total pumpage for 1966; no water may have been withdrawn. This well has since been destroyed.

Area 20

There are three water supply wells in Area 20 of the NTS: U-20 WW, U-20a 2 WW, and UE-20h WW.

U-20 WW is located in western Pahute Mesa (Figure 7-4). It was installed as a water-supply well in 1982 with a total depth at 996.1 m (3,268.0 ft). The open interval is from 692.2 to 996.1 m bgs within the CHZCM HSU. The pumping record for this well is available for years 1985 through 1999.

U-20a 2 WW is located in western Pahute Mesa (Figure 7-4). It was installed as a water-supply well in 1963 with a total depth at 1,371.6 m. The well is open to the CHZCM HSU from a depth of 629 to 1,371.6 m bgs. The pumping record for this well is available for years 1964 through 1967. The data for 1966 are, however, insufficient to calculate a yearly total. This well has since been destroyed.

UE-20h WW is located in western Pahute Mesa, north of U-20 WW (Figure 7-4). It was installed as a water-supply well in 1964 with a total depth at 2,196.69 m. The well is open to the CHZCM HSU from a depth of 763.82 to 1,653.8 m bgs, to the BFCU HSU from a depth of 1,653.8 to 2,196.4, and to the CFCM from a depth of 2,196.4 to 2,196.69 m bgs. The pumping record for this well is available for a few months in 1965. It is unknown whether this well was pumped in 1966. This well has since been destroyed.

Area 18

Only one water supply well is located in Area 18: Water Well 8. This well is located on the western edge of Pahute Mesa (Figure 7-4). It was installed in 1962. The total depth is 1,676.10 m (5,499 ft). The well is open to the BRA HSU from a depth of 381 to 542.5 m bgs. The pumping record for this well is available from 1963 to 1967 and from 1983 to 2000.

Area 16

Only one water supply well is located in Area 16, UE-16d WW. This well is located outside of the PM-OV area but very near its eastern boundary (Figure 7-4). The total depth is 1,676.1 m. The well is open to the (upper carbonate aquifer) [UCA]) HSU from a depth of 229 to 252.98 m bgs. The pumping record for this well is available from 1983 to 2000.

7.6.1.2 Oasis Valley Wells

Groundwater withdrawal data were compiled from local public water supply records and estimates of non-municipal use. The largest water user is the BWSD, the main water supplier of municipal water to the city of Beatty, Nevada. Homes and ranches located outside of Beatty but within Oasis Valley obtain their water from springs and non-municipal wells.

Currently, BWSD pumps groundwater from six wells located in Oasis Valley (Figure 7-4) and one well located in the Amargosa Desert. Only one well, Beatty Well No. 1 is located within the PM-OV area. The others are located outside of the southern boundary of this area to the southwest of Beatty. Beatty Well No. 1 is located near Beatty (Figure 7-4). The well is open to the AA HSU from a depth of 28.96 to 48.77 m bgs. The pumping record for this well is available for years 1994 through 2000.

Five other wells used by the BWSD are located outside of the PM-OV area but within Oasis Valley (Figure 7-4). These wells are described here along with their pumpage records because they are located within the Oasis Valley hydrographic

area and are very close to the boundary of the PM-OV area. Beatty Well No. 2, and Beatty Well No. 3 are open to the AA HSU from a depth of 27.43 to 59.44 m bgs, and 21.336 to 39.62 m, respectively. The other wells: Beatty Middle Well, Beatty Summit Well, and Beatty Indian Spring Well are also shallow wells that are all open to the Detached Volcanics Aquifer (DVA) HSU. Their open intervals are: 30.48 to 213.36 m bgs, 147 to 210.3 m bgs, 115 to 213.3 m bgs, respectively. Pumping records for these wells are available for years 1991 through 2000.

During their study of groundwater discharge in Oasis Valley, Reiner et al. (2002) identified approximately 15 springs and 20 non-municipal wells within the valley. Assuming that each of these sources discharges about 1,233.48 m³/yr based on an estimate made by Coache (1999), they calculated a total annual groundwater withdrawal of 43,171.8 m³ from all 35 non-municipal sources.

7.6.1.3 Mine Wells

One mine is located within the PM-OV area: Glamis Daisy Gold Mine currently operated by Glamis Gold Inc. (Figure 7-4). The Daisy Gold Mine was previously owned by Rayrock Mines, Inc. GEXA Well 4 is the main pumping well for the Daisy Gold mine. Another well, PW-2, located near the GEXA Well 4 was pumped for about two years before the pump failed and was never repaired. The pumping record for these wells is available for years 1997 through 2000.

7.6.2 Historical Pumping Volumes

The total yearly water withdrawals for wells located within the boundaries of the PM-OV area are shown in Figure 7-5. Only NTS water supply wells that contributed to the total pumpage from 1963 to 1993 are included in this figure. In 1995 and 1996, the totals include contributions from Beatty Well No. 1. For the remainder of the years, the totals also include the mine wells. The total yearly volumes are based on available data only and are, therefore, an underestimation of the actual volumes pumped. Records for NTS water supply wells are not available from 1972 to 1982. For the area of interest, the gap in the dataset is from 1968 to 1982, as shown on the graph (Figure 7-5). The graph shows a general increase in pumping from 1983 to 1989. The peak annual production of 1,154,700 m³ occurred in 1989. All water was pumped from U-20 WW (cased), UE-19c WW, and WW-8 at that time. A decreasing trend started in 1990 and ended in 1993. A drastic drop in pumping occurred from 1992 to 1993. This drop marks the end of nuclear testing in 1992.

7.7 Limitations

Limitations associated with the ET estimates and well discharge data are discussed in this section.

Limitations associated with the ET estimates are as follows:

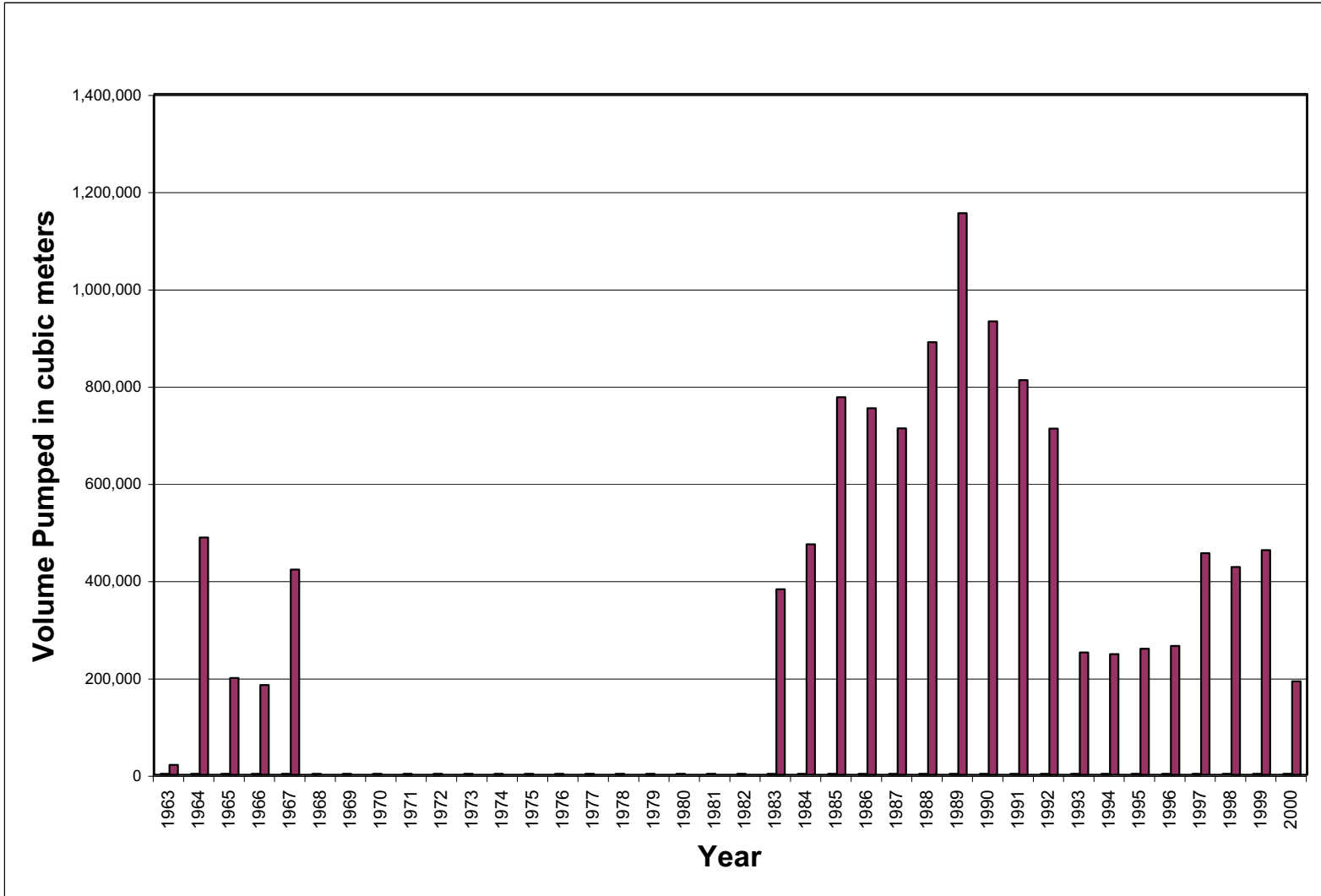


Figure 7-5
Total Withdrawals from Pumping Wells Located within the Pahute Mesa-Oasis Valley Area
No Data Available between 1968 and 1982

- The assumption that ET is negligible in areas other than the Oasis Valley area discharge area is supported by a lack of vegetation, soil dryness, and greater depths to water. It could, however, still result in some error. The volumetric loss would be minimal since the rate of ET from these areas is likely to be less than 0.01 ft/yr as shown by Andraski (1997) in his study of soil-water movement in the Mojave Desert of Nevada. Andraski (1997) estimated water fluxes from water potential and temperature data. From these data, he concluded that isothermal liquid, isothermal vapor, and nonisothermal vapor fluxes need to be included in the conceptual model of unsaturated flow at the study sites. Estimated vapor fluxes ranged between approximately 4×10^{-9} and 5×10^{-4} ft/yr.
- The use of the 1992 TM imagery to delineate ET-unit area, a year of slightly-above-normal rainfall, may have lead to an overestimate of ET. The use of TM imagery from multiple years would likely result in area estimates that would be more representative of the desired long-term ET average.
- The mean annual ET estimates of each ET unit were computed from Oasis Valley and Ash Meadows data acquired over a relatively short period of a few years. These data may not be representative of long-term averages.
- It is assumed that most of the water flowing at the surface is either lost to evapotranspiration or infiltrated into the alluvial aquifer. Thus, overland flow is not factored out of the total ET estimate.
- Other limitations include: (1) the assumption that all springflow is ultimately evaporated or transpired from within the bounds of one of the ET units, (2) the short-term nature of the data used to compute mean values, (3) the limited number of sites used to estimate ET from each ET unit, (4) the uncertainty in the adjustment applied to remove precipitation from ET estimates, and (5) the non-inclusion of local groundwater recharge from areas outside ET unit boundaries (Reiner et al., 2002).

Limitations associated with the well discharge data include missing pumping records for NTS water supply wells from 1972 to 1982 and a lack of data for the domestic water wells of Oasis Valley. The available data may not account for all groundwater discharged since the beginning of development in the area.

7.8 Summary

Groundwater discharge to the surface within the PM-OV area and vicinity occurs by natural means and by withdrawal from wells.

Natural discharge to the surface in the area of interest is best approximated by an estimate of ET. Laczniak et al. (2001) and Reiner et al. (2002) used TM imagery to delineate the ET subareas (ET units), and field data to estimate the ET rates.

The mean annual ET was calculated by both Lacznia et al. (2001) and Reiner et al. (2002) to be about 7,700,000 m³/yr. Reiner et al. (2002) estimated groundwater discharge from Oasis Valley by all means, including subsurface flow and wells, and found that ET represents about 90 percent of the discharge from that area. Discharge by evapotranspiration constitutes the majority of natural discharge to the surface from the PM-OV groundwater flow system. A range of uncertainty for the ET was derived by Lacznia et al. (2001) using Monte Carlo simulations of annual ET. The range of annual ET is between 5,142,378 and 11,005,109 m³/yr or between 14,089 and 30,151 m³/d. In comparison, the discharge flux estimates used for the Oasis Valley discharge area in the regional model ranged between 5,000 to 27,000 m³/d. The mean annual ET of 7,700,000 m³ should be used as a target during the calibration of the flow model. The range of uncertainty associated with this target should be the confidence range derived from the Monte Carlo simulations (6,185,950 m³ to 9,325,180 m³).

Ten pumping wells have been used to withdraw groundwater from the PM-OV area. Eight of them are NTS water supply wells located in Pahute Mesa and vicinity. The two other wells are Beatty Well No 1 and Gexa Well 4, located outside of the NTS. All other wells discussed in this section are located outside but near the boundary of the PM-OV area. Up to 1996, water pumped out of the NTS wells accounted for most of the volume. Starting in 1997, most of the groundwater withdrawals may be attributed to mine wells. The amount of groundwater discharged through wells is small compared to that of natural discharge. Even the maximum volume of 1,154,700 m³ in 1989 represents only 15 percent of the ET estimate.

Given the incomplete pumping record, the spatial concentration of most of the pumpage, and the relatively small volume of water withdrawn from the PM-OV groundwater flow system, a full verification of the model is not possible. Depending on the availability of drawdown data and the significance of their magnitude, a partial model verification may be possible for areas of significant pumping such as the area around U-20 WW. This will be further evaluated following the completion of the water level data analysis (See [Section 8.0](#)).

8.0 Hydraulic Heads

Observed hydraulic heads are derived from depth-to-water measurements and well information. Hydraulic heads may also be approximated by the land surface elevations of regional springs. This section provides descriptions of the objectives of the potentiometric data analysis including the data types and their prioritization, data compilation and evaluation, data analysis, and results.

8.1 Objectives

The purpose of this data analysis activity is to evaluate the existing potentiometric data for use in the CAU-scale groundwater flow model for the PM-OV area.

The specific objectives are as follows:

- To derive a set of hydraulic heads for the PM-OV area and vicinity from the available potentiometric data
- To evaluate the groundwater flow system behavior under both steady-state and transient conditions in support of the groundwater flow model for the PM-OV area

8.2 Approach

The approach used to analyze the available potentiometric data was as follows:

- Collection, compilation, and qualification of existing potentiometric data for the PM-OV area and vicinity, including depth-to-water measurements and spring data
- Analysis of the temporal trends in these data using hydrograph creation and statistical analysis of the water elevations
- Identification of a subset of hydraulic head data that is representative of predevelopment, steady-state conditions for the PM-OV area and vicinity; this dataset will include the location of the measurement point, land surface elevation and associated error, and the HSU(s) represented
- Creation of a potentiometric-surface map using the predevelopment, steady-state hydraulic head dataset for the PM-OV area and vicinity

- Analysis of vertical gradients using the predevelopment steady-state hydraulic head dataset for the PM-OV area and vicinity
- Identification and evaluation of any transient response to groundwater pumping based on the hydrograph analysis

8.3 Data Types and Prioritization

The data types needed and their prioritization for quality evaluation are presented in this section.

Data categories needed for the hydraulic head data assessment include general site information, depth-to-water data, well construction data, and hydrostratigraphic information for the PM-OV area and vicinity. A site is defined as a well, a test hole, a separate completion zone within a well, or a spring. The data types needed are as follows:

General Site Information

- Unique site identifier
- Site location
- Land surface elevation
- Error on land surface measurement

Depth-to-Water Data

- Depth-to-water measurement
- Method of depth-to-water measurement
- Measurement method error
- Date of measurement

Well Construction Data

- Well total depth
- Open interval top
- Open interval bottom

Stratigraphic/Hydrostratigraphic Data

- Well hydrostratigraphy
- Well stratigraphy
- Well lithology
- Source hydrostratigraphic unit

Measurements of the land surface elevation and depth-to-water are the priority data types required for hydraulic head calculations. The additional data types are needed for site description, data qualification, uncertainty evaluation, and hydrostratigraphic unit assignment. The well construction and stratigraphy/hydrostratigraphy data are discussed in later sections.

8.4 Data Compilation and Evaluation

Well and spring data for the PM-OV area and vicinity were obtained from several sources. The USGS National Water Information System (NWIS) on-line database was the primary source of this data (USGS, 2001). Additional data were obtained from NTS reports including the *Potentiometric Data Documentation Package* (IT, 1996c), and depth-to-water measurement forms from the UGTA Project records. More than 3,800 depth-to-water records were compiled and analyzed as part of this study. The period of record spans from 1941 to 2001. In addition, 28 springs were selected to supplement the available water level data.

The level of documentation of the available data was assessed, based on the criteria established in [Section 4.3](#), to provide the user of the data with some basis for traceability of the reported values. The levels were assigned to each record in the water elevation table ([Appendix E](#)) to assess the documentation available for each water-level measurement point. The levels assigned do not reflect the accuracy or reliability of the reported data, only the level of documentation.

Descriptions of the available well data that are relevant to hydraulic heads and spring data are provided in the following text.

8.4.1 Depth-to-Water and Spring Data

Water-level measurements are available for approximately 292 wells or separate well completions in the PM-OV study area. During the analysis of these water levels, 152 wells or completions were selected as appropriate for the PM-OV area and vicinity.

Land surface elevations at regional spring locations are used as estimates of hydraulic heads to supplement the dataset derived from water level measurements. As described in [Section 7.0](#), numerous regional springs occur within the groundwater discharge area of Oasis Valley ([Figure 7-1](#)). Site information is not available for all of those springs because many of them are located in areas that are inaccessible. However, it is not necessary to include all of them for this purpose. A selected number of springs spread over the discharge area should be sufficient to characterize the hydraulic heads in the discharge area. Twenty-eight spring locations were selected from the NWIS database.

8.4.2 General Site Information

General site information for wells, boreholes or completions, and for springs is presented in [Table E.1-1](#).

For wells, boreholes, or completions, the general site information of interest includes location, land surface elevation, and well construction and hydrostratigraphy, which are used to identify the effective open interval (EOI) and the HSU associated with a given water-level measurement. General site

information for the 152 wells or completions is presented in [Table E.1-1](#), including the EOI and the HSU associated with each site.

For springs, site information of interest includes location, land surface elevation (with accuracy) and the HSU contributing water to the spring. Site information for the 28 regional springs selected for inclusion in the hydraulic head dataset is also presented in [Table E.1-1](#).

8.4.2.1 Land Surface Elevation

Land surface elevations at well locations have been determined in a wide variety of ways including reading them off of a topographic map to the use of a global positioning system. Land surface elevations at spring locations were obtained from topographic maps. The level of uncertainty in the measurement has been documented in the site information table presented in [Appendix E](#). The level of documentation for the land surface elevation is not shown in the table. The level of documentation is not shown because all of the land surface elevations in the dataset would receive a Level 5 documentation qualifier. The Level 5 qualifier would be assigned based on a lack of standard procedures and documentation for the measurements.

8.4.2.2 EOI Definition

Well construction data are used to identify the EOI for a given site. The EOI and stratigraphy information are then used to identify the hydrostratigraphic unit or units associated with each site. The process of defining an effective open interval is described in the following text.

Well construction data of primary interest are the depths to the top and bottom of each open interval within a given completion zone or the total depth for open boreholes. The term "open interval" refers to any type of opening through which water may flow from the rock formation into the borehole. Examples of open intervals include open borehole (uncased) or the intervals in which well screens and perforated casing are gravel packed.

An EOI was defined for each site for which well construction data are available. Determination of the top of the EOI was based upon whether the water level was above or below the top of the open interval. The bottom of the EOI was defined as the bottom of the open interval.

If the average water level was below the top of the open interval, then the EOI was defined as follows:

- Depth of EOI top = average depth-to-water measurement
- Depth of EOI bottom = greater of the depths to either the bottom of the screen or gravel pack

If the average water level was above the top of open interval, then the EOI was defined as follows:

- Depth of EOI top = depth to top of open interval
- Depth of EOI bottom = greater of the depths to either the bottom of the screen or gravel pack

For cases where the borehole was open, the EOI was defined as the length of the saturated thickness.

- Depth of EOI top = average depth-to-water measurement
- Depth of EOI bottom = total depth (or depth to top of backfill)

8.4.2.3 HSU Assignment

For wells, assignment of hydrostratigraphic units to a given site was made based on the calculated EOI and the hydrostratigraphic units defined in the base HSU model described in [Section 2.0](#). A list of these HSUs is provided in [Appendix A](#). The base HSU model is fully documented in the HSU model report (BN, 2002). Most of the wells and holes of interest have available open interval and stratigraphic data. Thus, assigning hydrostratigraphic units to sites consisted of identifying the stratigraphic units to which the well was open, using the EOI previously defined, and then identifying the corresponding HSU based on the hydrostratigraphic organization ([Appendix A](#)).

For springs, assignment of hydrostratigraphic units was made based on the water moving upwards through faults in the Tertiary volcanics and alluvium. Therefore, the AA HSU was assigned with a caveat to stipulate that the water may be derived from the Tertiary volcanics below.

8.5 Evaluation of Water-Level Data

For the purposes of constructing a groundwater flow model, a set of hydraulic heads consistent with natural and undisturbed groundwater flow system conditions needed to be identified. In theory, this dataset consists is derived from water levels measured prior to the start of pumping and underground nuclear testing in the PM-OV area and vicinity. The existing data are insufficient to define natural, steady-state conditions. Thus, the entire period of record for each site was used in the data evaluation and reduction process.

Hydraulic heads are calculated as the water level elevation adjusted for borehole deviation and temperature effects. For each depth-to-water measurement, the water-level elevation was calculated as the difference of the land surface elevation and the depth-to-water measurement. Effects of temperature and borehole deviation were evaluated and adjustments were made to derive hydraulic head

values, where possible. Measurements for which the effects of temperature and borehole deviation are negligible, are equal to the corresponding water-level elevation. Finally, a temporal evaluation, which identified water-level data as part of predevelopment steady-state or transient conditions, was performed for each site.

8.5.1 Effects of Temperature and Borehole Deviation

Abnormal temperatures can affect water levels by altering the density of the water. Table 8-1 demonstrates how a change in temperature over different columns of water can influence the elevation of the water. This table was prepared using the Thiesen-Scheel-Diesselhorst (Equation 8-1) in conjunction with Equation 8-2.

**Table 8-1
Temperature Effects on Water Elevation**

Temperature Differential ^a	Water-Column Length ^b		
	100 meters	500 meters	1,000 meters
+5 Degrees Centigrade	+0.14 meters	+0.70 meters	+1.40 meters
+10 Degrees Centigrade	+0.30 meters	+1.51 meters	+3.03 meters
+20 Degrees Centigrade	+0.69 meters	+3.45 meters	+6.90 meters
+30 Degrees Centigrade	+1.15 meters	+5.76 meters	+11.52 meters

^aInitial Temperature 25 Degrees Centigrade

^bDistance from point of lowest inflow to the top of the water column

$$\rho = 1000 \left[1 - \frac{(T + 288.9414)}{508929.2 \times (T + 68.12963)} (T - 3.9863)^2 \right] \quad (8-1)$$

where:

ρ = The density of the water in kilograms per cubic meter

T = The temperature of the water in degrees centigrade

$$\eta' = \eta \left(\frac{\rho}{\rho'} \right) \quad (8-2)$$

where:

η' = The length of the water column above the point of inflow after a given temperature change

- η = The measured water column length above the point of inflow
 ρ = The density of water in the column at the mean water-column temperature and hydrostatic pressure
 ρ' = The density of water in the column at the new temperature and identical hydrostatic pressure

Spatial and temporal changes in temperature may be an important consideration when analyzing horizontal and vertical hydraulic gradients. In order to perform such corrections, data on zones of inflow and vertical temperature profiles for each water-level measurement must be available. Unfortunately, the data required to perform temperature corrections are not available for most wells in the PM-OV region (Fenelon, 2000).

Borehole deviation may result in groundwater depth measurements that are greater than the true depth to water. Fenelon (2000) reports that a survey of readily available documentation of borehole deviation for wells in the Pahute Mesa region show very small deviations that would not significantly alter water levels. There are, however, two boreholes on Pahute Mesa that have significant deviations. Significant borehole deviations occur in boreholes U-19v PS 1D and U-20n PS 1DD-H. These wells were purposely drilled at an angle into or near detonation cavities (Fenelon, 2000). Of the two boreholes, a hydraulic head was only determined for U-20n PS 1DD-H. Borehole deviations for the ER wells were studied in greater detail. For a correction to be applied, the wells had to have a borehole directional log available and the value of the calculated correction factor had to be greater than the error on the water-level measurement. The correction factors were determined to be insignificant for all but a single ER well. The only well requiring a significant correction was ER-20-5-3 (Open Borehole). The correction factor determined for this well was approximately 1.90 meters. This well was subsequently eliminated from further consideration during data analysis for reasons not associated with the correction.

8.5.2 Assessment of Temporal Trends

A temporal data analysis was performed for each site to identify water levels as representative of either steady-state or transient conditions.

The procedure used in the temporal analysis of the water-level data consisted of the following steps:

- Preparation and review of a hydrograph for each site for which multiple records of water-level measurements exist.
- Performance of a detailed review and evaluation of individual water-level records by reviewing the hydrograph for general shape, scatter, and apparent trends.
- Establishment of whether or not suitable steady-state and/or transient trends exist. If a hydrograph is completely vertical or consists of erratic

points, the site may not be suitable for use. If one or more trends are present, they are noted along with pumping trends.

- Flagging of each measurement based on its applicability to a calibration target.
- Elimination of measurements that are considered unrepresentative.
- Generation of statistical information on the steady-state data including mean, standard deviation, and variance on the mean for each of the sites included in the dataset.

Historical water-level values for each of the sites are presented in the water level table in [Appendix E](#). Hydrographs with summary information for the wells (with sufficient data) listed in [Table E.1-1](#) are also presented in [Appendix E](#). The water-level datasets, including the results of the temporal analyses are presented in [Appendix E](#).

8.6 Predevelopment Steady-State Hydraulic Heads

Predevelopment steady-state hydraulic heads and a measure of their uncertainty are discussed in this section. The results are presented in [Table E.1-2](#).

The results of the water level data analysis were used to identify hydraulic head values that are most representative of steady-state, predevelopment conditions at specific boreholes and well locations. Each temporal subset of measurements that represents steady-state conditions was reduced statistically to a mean, standard deviation, and variance of the mean. The hydraulic head data derived from the water level data were supplemented with land surface elevations of the selected regional springs.

The uncertainty associated with each of the hydraulic head values was estimated differently depending on the case. The uncertainty associated with hydraulic heads derived from multiple water level measurements is represented by the total variance. In this case, a given steady-state hydraulic head's variance was calculated as the sum of the variance of the mean hydraulic head and the variance of the land surface elevation derived from the accuracy estimates provided in [Appendix E](#). The uncertainty associated with hydraulic heads derived from land surface elevations at spring locations was equated to the variance of the land surface elevation derived from the accuracy estimates also provided in [Appendix E](#). It was not possible to quantify the measurement variance for many of the wells due to a lack of information. No estimates of uncertainty have been made for these cases. A variance of 100 m² could be used as was done in the NTS regional flow model (DOE/NV, 1997). This variance is based on the assumption that the combined error in the measuring point elevation and depth-to-water measurements is about 10 m. As part of the modeling effort, weights will be derived using the total variances and other available information and assigned to the hydraulic heads.

8.7 Steady-State Flow System Behavior

Analyses of the horizontal and vertical flow patterns using the predevelopment steady-state hydraulic heads will help understand the flow system. The results will be used to guide the calibration of the flow model.

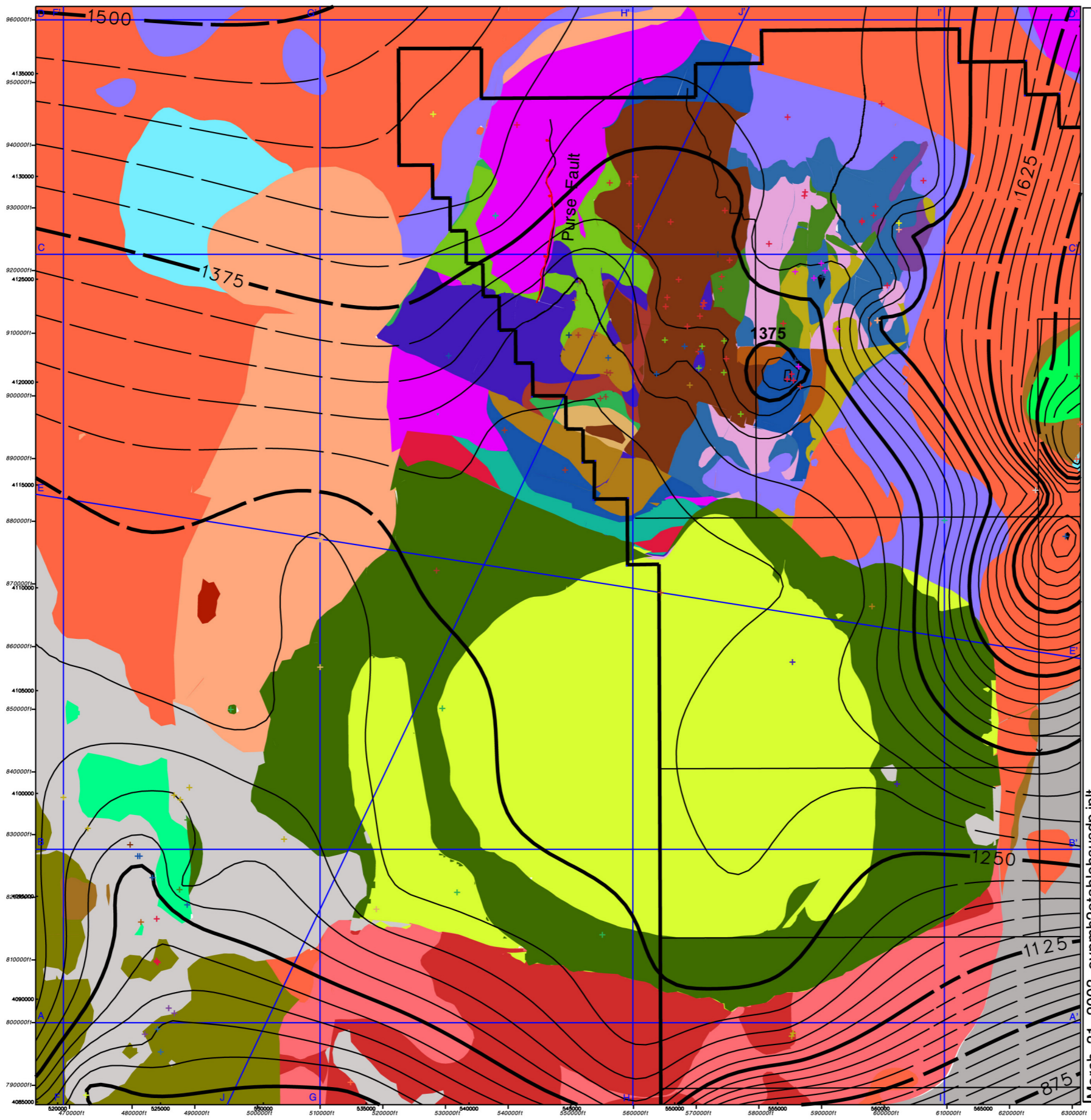
8.7.1 Horizontal Flow Analysis

A potentiometric contour map was prepared using composite water-level data to provide a general understanding of the hydraulic gradient and direction of groundwater flow. The map was prepared using the automatic contouring program of the EarthVision[®] (Dynamic Graphics, Inc. 2002) software package. A table of x, y, z data based on the hydraulic head dataset ([Table E.1-1](#) and [Table E.1-2](#)), the spring location information ([Table 8-1](#)), and additional water-level data outside of the model boundary ([Appendix E](#)) was prepared as the input data file for EarthVision[®]. The data were then split into two datasets, one with elevated and potentially perched water levels and the other without. Wells with multiple completions were represented in both datasets. The highest water level was used for the elevated water-level dataset and the lowest water-level elevation was used in the other dataset. The difference in these two sets is apparent in the northeast portion of the model boundary where the elevated heads are several hundred meters higher.

The data were then gridded at 250, 500, and 1,000-m spacing using both a 4-point and 8-point distance weighting. For areas containing a favorable data density, the 250-m contouring was too jagged and at 1,000-m more than 12 wells were averaged together in a grid node. No differences were observed in the potentiometric surfaces using the 4-point or 8-point distance weighting. The resulting potentiometric surfaces were evaluated and a single potentiometric surface showing the elevated and potentially perched data was prepared using the 500-m grid spacing with a 4-point distance weighting. [Figure 8-1](#) shows the elevated composite potentiometric surface overlaid on top of the HSUs at the water table.

8.7.2 Vertical Flow Analysis

Vertical flow analysis was performed with the aid of the EarthVision[®] software program (Dynamic Graphics, 2002) to produce an isocontour model. The amount of information available on the vertical distribution of hydraulic heads in the region is sparse. The EarthVision[®] model was, therefore, only used to observe regions with sufficient data. A table of x, y, z data based on the water-level data analysis was prepared as the input data file for EarthVision[®] ([Appendix E](#)). The predevelopment steady-state hydraulic heads were assigned to a z-position in the middle of the effective open interval. In wells with multiple screened intervals, the unit vertical gradient was calculated as the difference in hydraulic heads versus the difference in vertical distance between open intervals. The unit vertical gradient was then applied to the midpoint between effective open intervals. A 3-D



LEGEND

- Cross section traverse
- Nevada Test Site boundary
- Major water level contours, elevation (m)
- Minor water level contours, elevation (m)

AA	TCA	PBRCM
DVA	PLFA	TMCM
DVCM	LPCU	SCVCU
YVCM	TSA	LCA3
TCVA	YMCFCM	LCCU1
FCCM	CHVTA	UCCU
FCA	CHVCM	LCA
THLFA	CHZCM	LCCU
THCM	CHCU	SCICU
TMA	IA	MGCU
WWA	CFCM	BMICU
PCM	CFCU	CHICU
PVTA	KA	CCICU
FCCU	BFCU	RMICU
BA	BRA	ATICU
UPCU		

4000 0 4000 8000

METERS

2 0 2 4 6

MILES

Elevation Contour Interval 25 meters
UTM Easting NAD 27 Zone 11 in meters

Nevada State Plane Zone 2702 in feet

Figure 8-1 Map Showing Composite Potentiometric Surface with Elevated Heads in the Northeast and HSUs at the Water Table

March 31, 2003 ovpmh2otablehsusdp.ipit

vertical gradient isocontour model was then generated in EarthVision®. The upper limit of the contours was +0.9 m head per meter vertical distance, while the lower limit was -0.1 m head per meter vertical distance. In this model, a negative number implies an upward gradient, while a positive number is a downward gradient. All data below 0 meters elevation were clipped as a result of insufficient data to contour.

The results of the isocontour model are as follows:

- A strong downward vertical gradient occurs near the water table in the Rainier Mesa region with a slight upward gradient at depth. There is also a strong downward vertical gradient near U-20bb #1.
- A moderate downward vertical gradient occurs in the area of the Coffey Middle ET Well.
- There is a slight upward vertical gradient at intermediate depths throughout the central portions of NTS Area 19 and Area 20.
- The Oasis Valley region contains a mixture of vertical gradients. Near the surface, there is a very weak upward gradient as well as areas of localized downward vertical gradients.

8.8 Transient Flow System Behavior

As described in [Section 7.0](#), ten pumping wells have been historically used to withdraw groundwater from the PM-OV area. Eight of them are NTS water supply wells located in Pahute Mesa. The two other wells are Beatty Well No. 1 and Gexa Well 4, located outside of the NTS. In 1989, the maximum volume of 1,154,700 m³ was pumped. This volume represents only 15 percent of the ET estimate. The three largest producing wells are Water Well 8, UE-19c Water Well, and U-20 Water Well. The effects of pumping at U-20 Water Well can be seen as drawdown at several wells located up to 5.9 km away (Fenelon, 2000). The drawdown is apparent in the hydrographs for U-20be, U-20bf, U-20bg, UE-20bh #1, UE-20n #1, and U-20n PS 1 DD-H ([Appendix E](#)). As observed by Fenelon (2000), the correlation of monthly withdrawal rates and drawdown is hindered because of relatively long periods of no pumping interspersed with periods of pumping. The lack of spatial concentration of pumpage data throughout the model area, as well as the intermittent pumpage at U-20 Water Well, will make it difficult to perform even a partial model verification. In conclusion, transient well-related effects are very localized and likely not representative of conditions over a majority of the model area. A full verification of the flow model is, therefore, not feasible.

8.9 Limitations

Limitations associated with the hydraulic head analysis include a sparse data environment, and data that may or may not have been corrected for borehole deviations and/or temperature by earlier investigators, potential effects from nuclear testing, misinterpretation of non-steady state water levels as steady state, and misidentification of perched water levels. A particular data gap also exists beneath the topographic high of Timber Mountain, beneath which a potentiometric mound may exist. Data limitations associated with the NWIS database have also been documented by Wood (1994). Limitations cited include duplicate site identification numbers, unverified data, and inaccurate land surface elevations.

8.10 Summary

In summary, the primary objective of the water-level data analysis was to derive a set of hydraulic heads which can be used to support the development of a flow model for the PM-OV area. This dataset was prepared through the collection, compilation, and qualification of existing depth-to-water and spring data, and analysis of temporal trends using hydrograph and statistical analyses. The resulting hydraulic head dataset is provided in [Appendix E](#). The mean hydraulic heads are the suggested target heads to be used for flow model calibration. A secondary objective of this data analysis was to generate a composite potentiometric surface map for the PM-OV model domain to depict general flow directions. A vertical gradient analysis showed a strong downward vertical gradient at the water table in the area of Rainier Mesa. This gradient is consistent with recharge occurring on Rainier Mesa. Based on the available historical pumping information, it is apparent that pumpage is not widely-distributed over the PM-OV area. Furthermore, the total pumpage represents a small portion of the natural discharge from the area (less than 15 percent). In addition, the transient flow system response to pumping is localized to the vicinity of wells where significant pumpage occurred, such as U-20 Water Welland. This lack of a widely-spread transient response makes full model verification using pumpage/drawdown data impossible. Partial model verification may be possible but would be of little value.

9.0 Lateral Boundary Fluxes

Inflow and outflow through the lateral boundaries of the Pahute Mesa CAU-scale flow model constitute an important portion of the groundwater budget of the modeled system. The lateral fluxes, combined with recharge, control the rate of water flow through the modeled system. Unfortunately, there is no practical way to directly measure groundwater fluxes at the scale and spatial frequency needed to define boundary conditions for the CAU flow model. In addition, field study-based gradients and hydraulic conductivities are also not well defined for the boundaries, making analytic estimates difficult (e.g., the type of estimates made by Blankennagel and Weir [1973]). Due to the lack of field study-based data, the flux data for estimating CAU flow model lateral boundary flux were derived by calibrating a set of alternate regional-scale flow models. The set of different regional-scale flow models was developed to allow for consideration of the uncertainty in the boundary fluxes associated with differences in the conceptualization of the HSU model and the methodology used to approximate the surficial recharge distributions.

9.1 Objectives

The specific objective of this modeling effort was to generate a set of lateral flux boundary conditions that could be used in conjunction with the CAU flow model. These fluxes were derived by calibrating a set of eight alternate regional-scale flow models using USGS's finite-difference code MODFLOW ([Appendix F](#)). Once a satisfactory calibration was reached for a regional-scale model, the MODFLOW utility package ZONEBUDGET was used to postprocess the associated water budget file. The postprocessing generated a set of fluxes that could be used as a first approximation to assess the flux variability along the boundaries of the CAU flow model. The modeling effort and associated postprocessing produced a set of boundary fluxes for each of the eight alternate regional-scale models. The use of the eight alternate regional flow models allowed for consideration of boundary flux uncertainty associated with the choice of plausible geologic models that still honor the site data and the choice of recharge models based upon different methodologies.

The regional-model-derived boundary fluxes are intended to be the basis for constraints on boundary flow into the CAU-scale models. In other words, fluxes into the CAU model will be expected to remain within the range of values derived from the regional model under the uncertainty of different HSU and recharge scenarios. This may be accomplished in two different approaches. In the first approach, hydraulic heads are specified at the model boundary while boundary fluxes are not specified. The boundary fluxes are allowed to vary within specified

limits during the flow model calibration. In the second approach, three different sets of boundary fluxes are applied to the CAU model boundary. The first set would represent the lower range fluxes, the second set the middle range fluxes, and the third set the upper range fluxes. For each set of fluxes, the CAU model is calibrated, thus, yielding a range of calibrated parameters, each of which would provide acceptable calibration to observed water levels and discharges at Oasis Valley.

9.2 Approach

Water budgets for the approximate CAU flow model domain were generated from a series of alternate regional-scale flow models. These numbers are approximate because regional model MODFLOW cells are not exactly coincident with the CAU model along its boundary, and the CAU model is tilted relative to the regional model. The UGTA calibrated regional flow model (IT, 1997a) served as the base model. The HSU models used to generate the hydraulic conductivities for the alternate regional-scale flow models were based upon the UGTA base regional HSU model and a hybrid of this model. The hybrid was basically the same HSU construction throughout most of the model, but used a slightly different conceptual model for the LCA in the northern portion of the model. The alternate conceptual model assumes that the LCA is more continuous in the northern portion of the geologic model than in the base case. Although this is not the favored conceptual model, it was considered as an alternative because it is true to the data and it may have a large influence on the northern lateral boundary flux boundary condition.

In addition, the EarthVision® (Dynamic Graphics, 2002) generated regional-scale geologic models for the UGTA base conceptualization and the "continuous LCA" alternative were updated for this modeling effort. Both regional-scale geologic models were fitted with high-resolution PM-OV submodels replacing the PM-OV area of the coarser model (see [Appendix A](#)). Two high-resolution PM-OV submodels were considered (see [Appendix A](#); [Appendix F](#); and BN, 2002), one representing a finer-scale interpretation of the UGTA base geologic model and the other a simpler PM-OV conceptual model developed by the USGS (BN, 2002). The choice of the two submodels was based upon a screening analysis that indicated that the UGTA base model and the USGS model would cover the range of possible radionuclide transport results that could be expected from the set of conceptual models considered by the TWG (see [Appendix A](#); [Appendix F](#); and BN, 2002). The high-resolution segment of the PM-OV model based upon the UGTA conceptual model was comprised of 47 HSUs. The second alternative high-resolution segment of the PM-OV model based upon the USGS conceptual model was comprised of 42 HSUs.

In addition to considering the uncertainty in the flux boundary conditions caused by differences in conceptual models, uncertainty associated with various methods of approximating recharge was also considered ([Appendix A](#) and [Section 6.0](#)). The three methods used to approximate the recharge distribution were an empirical mass-balance method and two derivatives of this method, a deterministic method, and a chloride mass-balance method (see [Section 6.0](#)). The first method, a Maxey-Eakin approach ([Section 6.0](#); Maxey and Eakin, 1949; and

Eakin et al., 1951) is an empirically-derived approach relating recharge to precipitation zones from a base precipitation map. The second approach (used by USGS) is a deterministic approach based upon modeling the processes that affect the net rate of infiltration past the root zone (Section 6.0; and Hevesi, et al., 2003). The third method is DRI’s chloride mass-balance approach, which estimates recharge by analyzing and comparing the chloride ratios of precipitation and groundwater (Section 6.0; and Russell and Minor, 2002). In addition, submodels of the first and third methods were also used to generate other possible recharge distributions. The two recharge distributions generated from the Maxey-Eakin approach include an original version used for the regional flow modeling task and the final version used in the calibrated model. The final version included updates in the amount of precipitation needed to generate recharge. The two recharge distributions based on the chloride mass-balance approach include one where recharge is found at elevations below 1,237 m and one where recharge is not found below 1,237 m elevation.

Twenty alternate groundwater flow conceptual models could be generated by combining the two HSU models, the two LCA conditions, and the five recharge models. Because of large computational demands, eight out of the twenty alternate groundwater flow models were selected to calculate a range of lateral boundary fluxes using the regional flow model (Table 9-1). These eight conceptual models were selected to cover the range of uncertainty.

**Table 9-1
Regional-Scale Model Descriptions**

Model Name	Pahute Mesa-Oasis Valley Geologic Model	Northern Region LCA Submodel	Recharge Model
G1aR1a	BN	Discontinuous LCA	UGTA Calibrated Regional
G1bR1a	BN	Continuous LCA	UGTA Calibrated Regional
G1aR1b	BN	Discontinuous LCA	UGTA Original Regional
G1aR2	BN	Discontinuous LCA	USGS - no redistribution
G2aR1a	USGS	Discontinuous LCA	UGTA Calibrated Regional
G2bR1a	USGS	Continuous LCA	UGTA Calibrated Regional
G1aR3a	BN	Discontinuous LCA	DRI
G1aR3b	BN	Discontinuous LCA	DRI - no recharge below 1,237 m

A set of boundary fluxes for the CAU flow model was generated from the set of alternate regional-scale flow models by using the MODFLOW utility package ZONEBUDGET to postprocess the water budget files generated from the flow models. The ZONEBUDGET output included inflow and outflow fluxes for each lateral boundary of the CAU flow model.

9.3 Analysis Results

The lateral fluxes derived from the regional model flow simulations using the eight alternate conceptual models are presented, followed by a comparison of the results.

9.3.1 Lateral Fluxes Derived from Regional Model Flow Simulations

Lateral fluxes derived from the eight alternate regional model flow simulations are presented followed by a comparison of the results.

The results of the alternate flow model simulations at the regional scale include a set of files containing the MODFLOW flow budgets for each of eight simulations ([Appendix F](#)). Included in the flow budgets are volumetric flow rates across each face of every finite-difference block within the regional-scale flow models. Based on the regional-scale flow model (finite difference blocks through which the trace of the northern, southern, eastern, and western boundaries of the CAU-scale model traverse), ZONEBUDGET was used to sum up the inflow and outflow volumes (m^3/d) that would cross the lateral boundaries of the CAU-scale model. The flux boundary conditions generated from the eight alternate regional-scale flow models were reported in terms of inflow and outflow volume along the northern, southern, eastern, and western boundaries of the PM-OV CAU-scale model.

The inflow volumes derived from each of the alternate regional-scale models for the northern, southern, eastern, and western lateral boundaries of the CAU-scale model are presented in [Table 9-2](#). The outflow volumes derived from each of the alternate regional-scale models for the northern, southern, eastern, and western lateral boundaries of the CAU flow model are presented in [Table 9-3](#). The HSU model and recharge distributions used in each of the alternate regional-scale models are presented in [Table 9-1](#).

Table 9-2
Regional Model Groundwater Inflows
at CAU-Scale Model Boundaries (m^3/d)

Model Number	Northern Boundary Influx	Southern Boundary Influx	Eastern Boundary Influx	Western Boundary Influx
G1aR1a	22,763	452	10,453	13,478
G1bR1a	22,494	458	12,407	14,652
G1aR1b	23,880	413	11,828	17,257
G1aR2	13,828	248	5,572	1,723
G2aR1a	26,895	3,280	13,950	8,325
G2bR1a	27,693	3,477	16,943	9,285
G1aR3a	27,948	502	13,678	8,803
G1aR3b	24,216	804	10,531	5,815

Table 9-3
Regional Model Groundwater Outflows at
CAU-Scale Model Boundaries (m³/d)

Model Number	Northern Boundary Outflux	Southern Boundary Outflux	Eastern Boundary Outflux	Western Boundary Outflux
G1aR1a	5,127	40,747	4,598	13,858
G1bR1a	4,985	41,651	4,507	14,676
G1aR1b	5,034	41,996	3,979	17,305
G1aR2	139	26,339	305	2,440
G2aR1a	6,703	53,109	4,120	9,537
G2bRa1	6,669	54,405	5,007	10,225
G1aR3a	2,417	50,979	1,959	7,251
G1aR3b	1,419	50,224	1,568	5,839

Table 9-4 summarizes the water budget for each simulation. The recharge is the total inflow from areal recharge over the model area and the drain cell outflow represents the outflow by evapotranspiration within the Oasis Valley discharge area. The eight cases presented in Table 9-4 adequately cover the range of possible outcomes.

Table 9-4
Total Water Balance for the PM-OV Model Area

Model Number	Perimeter Influx (m ³ /d)	Perimeter Outflux (m ³ /d)	Recharge (m ³ /d)	Drain Cell Outflow (m ³ /d)	Difference in Total Inflow (m ³ /d)
G1aR1a	47,146	64,330	32,336	15,152	0
G1bR1a	50,011	65,819	32,336	16,533	-5
G1aR1b	53,378	68,314	36,462	21,527	-1
G1aR2	21,371	29,223	20,173	12,514	-193
G2aR1a	52,450	73,469	32,336	11,317	0
G2bR1a	57,398	76,306	32,336	13,429	-1
G1aR3a	50,931	62,606	57,387	45,919	-207
G1aR3b	41,366	59,050	41,683	24,000	-1

9.3.2 Result Comparison

The results of the alternate flow model simulations were compared with respect to changing the HSU model, the LCA condition, and the recharge model.

Effect of Changing the HSU Model

Two direct comparisons between the two HSU models are provided by pairs of models G1aR1a/G2aR1a and G1bR1a/G2bR1a where G1 refers to the BN HSU model and G2 is the USGS HSU model. For the two sets, the USGS model yields larger total boundary fluxes, but smaller drain outflow at the Oasis Valley discharge area. The net outflow from the USGS model is larger than the BN case.

Effect of Changing the LCA Condition

The continuity condition of the LCA north of the model area also had an impact on total flux. Paired simulations G1aR1a/G1bR1a and G2aR1a/G2bR1a indicate the continuous LCA case yields slightly larger boundary fluxes than the discontinuous case. The drain discharge varied in the two cases.

Effect of Changing the Recharge Model

Based on total recharge, DRI models have the most recharge and the USGS model has the least. From [Figure 6-10](#), it can be seen that for hydrographic areas present within the PM-OV model area, the highest recharge case is associated with the DRI model with alluvial mask or the UGTA model. The lowest recharge is associated with the USGS Model 2 or the UGTA model.

A second comparison is made between simulations G1aR1a, G1aR2, G1aR3a, and G1aR3b. In these cases, the only difference is the recharge model. The USGS Model 2, simulation G1aR2 yields the lowest boundary fluxes. This simulation also uses the BN HSU model with discontinuous LCA - all of which produce smaller boundary fluxes. It seems reasonable to take case G1aR2 as representing the lower bound of the possible cases.

The high recharge cases G1aR3a and G1aR3b using DRI recharge do not produce the largest boundary fluxes, but do produce the largest drain discharge. In fact, the drain flows are out of range when compared with observed ET discharge at Oasis Valley. The expected Oasis Valley ET discharge from [Section 7.0](#) is about 21,000 m³/day, with a range of values from 14,000 to 30,000 m³/day. Therefore, if the DRI model runs were further calibrated to match observed mean discharge by ET at Oasis Valley, the perimeter outfluxes might be expected to increase by about 20,000 to 81,000 m³/day.

From the eight simulations presented, it is possible to set reasonable bounds on perimeter fluxes for the PM-OV model area.

9.4 Limitations

The major limitation associated with assessing the lateral boundary fluxes to be used for the CAU flow model is associated with the indirect manner with which the data must be derived. First, there is no technically practical way to directly measure groundwater fluxes at the scale and spatial frequency needed. Secondly, field study-based gradients and hydraulic conductivities are also not well defined

for the boundaries. This leaves the indirect method of measuring the internal fluxes generated by a regional-scale flow model.

The limitations associated with deriving the fluxes from a regional-scale flow model are a function of the degree to which the model accurately represents the physical system. The model's representation of the system is in turn a function of: (1) the appropriateness of the conceptual model, (2) the accuracy of the geologic model used to define parameter heterogeneity, (3) the complexity of the system, (4) the degree to which the model can be calibrated, and the (5) the applicability of the recharge model describing the surficial infiltration of water from precipitation.

9.5 Summary

A set of boundary fluxes to be used with the CAU flow model have been developed based on results generated for eight alternate regional-scale flow models using MODFLOW. The eight models represent different flow system conceptual models and recharge models. Hydrostratigraphic models reflecting the different conceptual models were chosen from a larger set of conceptual models based on the marked difference in the flow fields (and associated radionuclide transport) they generate ([Appendix A](#)). The recharge models represent different methods of approximating recharge for the NTS area ([Section 6.0](#)). The alternate flux boundary conditions can be used to help evaluate the uncertainty in the CAU flow model associated with the choice of flow system conceptual model (and associated HSU model) and recharge model.

The range in net boundary flux across each of the CAU model boundaries is summarized in [Table 9-5](#). These fluxes are rounded to the nearest 100 m³/d for presentation. This approach does not specify the location or locations on the boundary where the flux occurs; just bounds on the total amount of flow. More specific ranges will be developed for the CAU model using the interpolation approach and tools developed by LANL (Gable and Cherry, 2001). If a suitable calibration cannot be achieved within the range of values obtained from the regional model results, additional justification will need to be added to the model documentation explaining the difference.

Table 9-5
Summary of Net Boundary Flux Ranges (m³/d)

Model Boundary	Range in Net Inflow	Range in Net Outflow
Northern	14,000 to 28,000	100 to 6,700
Southern	200 to 3,500	26,000 to 54,000
Eastern	5,600 to 17,000	300 to 5,000
Western	1,700 to 17,000	2,400 to 17,000

10.0 Groundwater Chemistry

Groundwater chemistry data are considered during the evaluation of the groundwater flow system because they provide a means for determining the origin, pathway, and timescale of groundwater flow that is independent of estimates based on conventional hydraulic data. Geochemical and hydraulic data reflect distinct but complimentary aspects of a groundwater flow system, and must be considered in unison in order to develop a consistent, comprehensive, and defensible flow system assessment. For example, geochemical data may identify flow paths and source areas that would otherwise not be recognized on the basis of hydraulic information alone; however, these flow paths must be consistent with potentiometric data in order to be valid (and vice versa). Geochemical data, specifically groundwater chemistry and reactive mineral distribution, are also important constraints on solute transport. As described in the Pahute Mesa transport report (Rehfeldt et al., 2003), these data comprise fundamental components in defining distribution coefficients for assessing solute mobility. Groundwater chemistry data aid in the calibration of groundwater flow and transport models and are essential to understanding the fate and transport of contaminants of potential concern in the subsurface environment.

The assessment of groundwater chemistry data for the Central and Western Pahute Mesa CAUs (PM-CAUs) fulfills several project needs. First, the dataset compiled for this task represents the current repository for groundwater geochemical data pertinent to the PM-CAUs. Second, the flow path, water budget, and travel time evaluations presented here are based on geochemical data and methodologies that can provide an independent means to verify flow and contaminant transport modeling efforts for the PM-CAUs.

10.1 Objectives

The specific objectives of this groundwater chemistry assessment include the following:

- Present a comprehensive groundwater chemistry dataset for the PM-CAUs and surrounding area
- Using this dataset, present a characterization of the groundwater chemistry of the wells, springs, and seeps in this area
- Based on the groundwater chemistry characterization, present the evaluation of groundwater sources, flowpaths, and travel times

The assessment provided in this chapter is based primarily upon geochemical data from groundwater collected from wells and springs located within the PM-CAUs. Data from wells and springs located in surrounding areas that are likely to be influential to, or a continuation of, the PM-OV flow system are also included. The groundwater geochemistry data used in this evaluation include general chemical parameters, major ions, minor and trace elements, and stable and environmental isotopes. The results of geochemical data evaluation and modeling are also included. Data are available for groundwater samples taken from various geologic formations including Quaternary and Tertiary alluvial materials, Tertiary volcanic rocks, Paleozoic sedimentary rocks, and Precambrian metamorphic rocks.

10.2 Approach

This section summarizes the strategies and methods applied during the geochemical assessment of the groundwater data for the PM-CAUs. The primary purpose of this assessment is to support conceptual model development and refinement, and to assist with the verification of the flow and transport modeling efforts for the PM-CAUs. The following steps were taken in the course of this assessment.

1. Available geochemical data were extracted from GEOCHEM02.mdb, the UGTA groundwater quality database (IT, 2002i), for wells and springs within a region encompassing the Central and Western Pahute Mesa study area.
2. Using the data from Step 1, variations in water chemistry and isotopic composition were identified for the geographic region (and subregions) of interest. The processes whereby representative groundwater data were defined and selected (based on data quality, distribution, and completeness of the necessary parameter suite) for use in these geochemical evaluations are discussed in [Section 10.3](#).
3. A variety of geochemical evaluations were performed on the representative data in order to identify and assess viable flow paths and groundwater mixing models. These evaluations include the application of conservative tracers and the evaluation of non-conservative tracers to provide additional supporting evidence. The NETPATH computer program (Plummer et al., 1994) was used as part of the evaluation process to calculate the net geochemical mass-balance reactions, groundwater mixing ratios, and apparent groundwater travel times along viable flow paths (Rose et al., 2002). The geochemical evaluation processes are discussed in [Section 10.5.4](#).

10.3 Data Description

The groundwater chemistry dataset for the PM-CAUs includes data generated during 2,233 recorded sampling events at 466 different locations within the area shown in [Figure 10-1](#). This area includes the western portion of the NTS, areas upgradient of the NTS to the north, and downgradient areas as far south as the

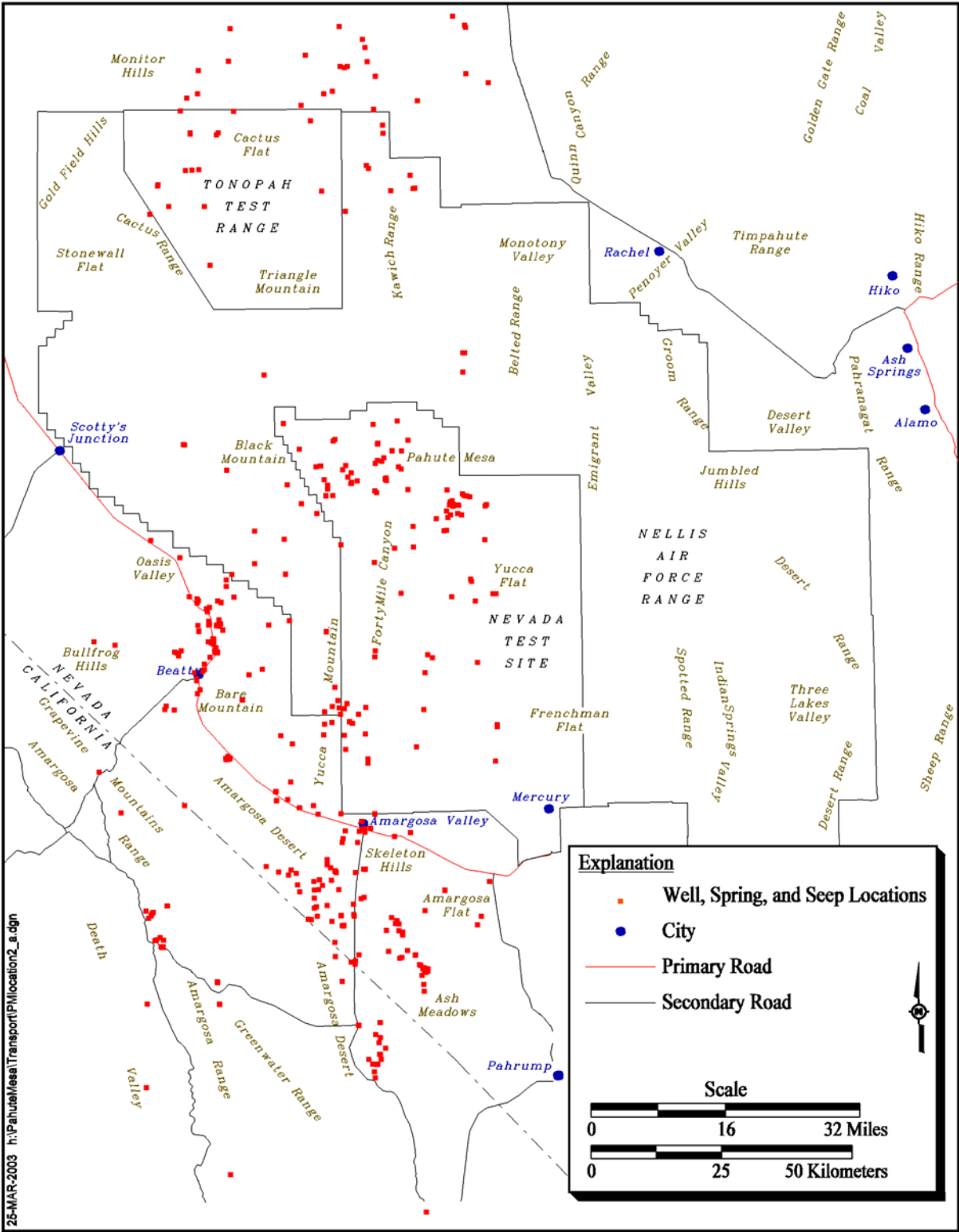


Figure 10-1
Groundwater Quality Sample Locations in the Pahute Mesa-Oasis Valley Region

Table 10-1
Geographic Distribution of Groundwater Sample Locations and
Measured Analytical Parameter Groups in the Pahute Mesa Region

Geographic Areas	Individual Sample Locations ^b	Parameter Group Types ^a					
		Minor and Trace Elements	Environmental Tracers	Radionuclides	Organic Compounds	Other Parameters	Major Ions
Pahute Mesa (Area 19)	23	23	6	10	3	22	23
Pahute Mesa (Area 20)	32	25	17	21	3	24	25
Oasis Valley	66	51	33	26	1	59	54
ER-EC Wells	10	10	8	8	0	8	8
Rainier Mesa (Area 12)	20	20	2	3	0	20	20
Upgradient Locations	54	53	24	8	1	54	54
Crater Flat/Yucca Mountain	29	27	28	25	10	27	27
Amargosa Valley	40	36	29	26	4	35	38
Amargosa Desert	51	50	30	41	2	51	50
Ash Meadows	35	32	17	14	6	35	33
Death Valley	24	23	11	8	1	24	23
Franklin Lake	22	19	16	1	0	22	19
Other	60	60	20	30	5	60	60

^aDetails how many of the individual sample locations have been sampled for a given parameter group for the specified geographic area

^bIndividual locations include wells, separate completions in multiple completion wells, spring discharge orifices, or seeps

Amargosa Desert and as far southwest as Death Valley. [Table 10-1](#) summarizes the distribution of groundwater sample locations and measured analytical parameter groups within this area. Individual sample locations were grouped with other geographically similar locations into 13 geographic areas for the table. The geographic areas summarized in [Table 10-1](#) include three NTS areas (i.e., 12, 19, and 20), locations north of the NTS, the ER-EC wells, locations in Oasis Valley, locations in the Crater Flat/Yucca Mountain area, locations south of the NTS (e.g., Amargosa Valley, Amargosa Desert proper, Ash Meadows, Death Valley, Franklin Lake area), and an "Other" category which consists of locations that did not fit into any of the other areas. The various geochemical data parameter groups sampled for the following:

- Minor and Trace Elements - includes relatively low-concentration metals such as arsenic, lead, or selenium
- Environmental Tracers - includes carbon, hydrogen, and oxygen isotopes

- Radionuclides - includes radionuclides in groundwater such as tritium (^3H)
- Organic Compounds - includes volatile organic compounds (VOC), semivolatile organic compounds (SVOC), and pesticides
- Other Parameters - includes physical, field, and miscellaneous parameters such as pH, total dissolved solids (TDS), or temperature
- Major Ions - includes major cation and anions such as sodium or bicarbonate

Over 1,800 of these sampling events have been conducted on 316 different well, spring, and seep locations within a smaller area around Pahute Mesa (Figure 10-2, between 36.75 and 38.00 degrees north latitude and between 116.20 and 116.85 degrees west longitude). It is important to point out that the number of individual sample locations, the suite of water quality parameters generated, and the associated data quality can vary as a function of sample location and/or time of sampling. The data have been generated over a significant period of time using various sampling and analytical methods to accomplish a variety of objectives. For instance, within the area shown in Figure 10-2 there are locations with only a single sampling event and a minimal number of measured parameters (e.g., Beatty Wash Windmill Well, with data for two field parameters only), while other locations have numerous sampling events and numerous measured parameters (e.g., J-12 Water Well has been sampled during 15 individual sampling events with data generated for 289 different parameters). More than 1,200 sampling events, conducted prior to 1992, generated data from 220 individual locations for over 280 different parameters within the area of interest (oldest recorded sample date within the area of interest is 2/22/1956). Note that only 95 of the total number of individual parameters measured prior to 1992 were analyzed 10 or more times. Since 1992 (and the initiation of the Environmental Restoration Project), more than 600 sample events have generated data from 138 individual well, spring, and seep locations within the same area of interest for over 500 different parameters. Note that only 307 of the total number of individual parameters measured since 1992 were analyzed 10 or more times. There are 54 locations that have been sampled both before and since 1992.

Water quality samples are typically collected as composite samples either from wells with single completions that transect multiple hydrostratigraphic unit boundaries or from wells with multiple completions that are all pumped simultaneously. Local vertical variability in water quality can be evaluated by the cluster wells located at ER-20-5, ER-20-6, ER-30-1, and PM-3. Depth discrete sampling would provide additional information on the vertical variability in groundwater quality at the multiple completion wells (ER-EC-1, ER-EC-2A, ER-EC-4, ER-EC-5, ER-EC-6, ER-EC-7, ER-EC-8, ER-18-2, J-13 Water Well, Test Well 1, Water Well 8, and USW H-1) located within the area of interest.

To the extent possible, in the process of compiling GEOCHEM02.mdb, data have been made internally consistent (i.e., parameter names, units, and data qualifiers have been standardized). All data entry and modifications to the dataset were

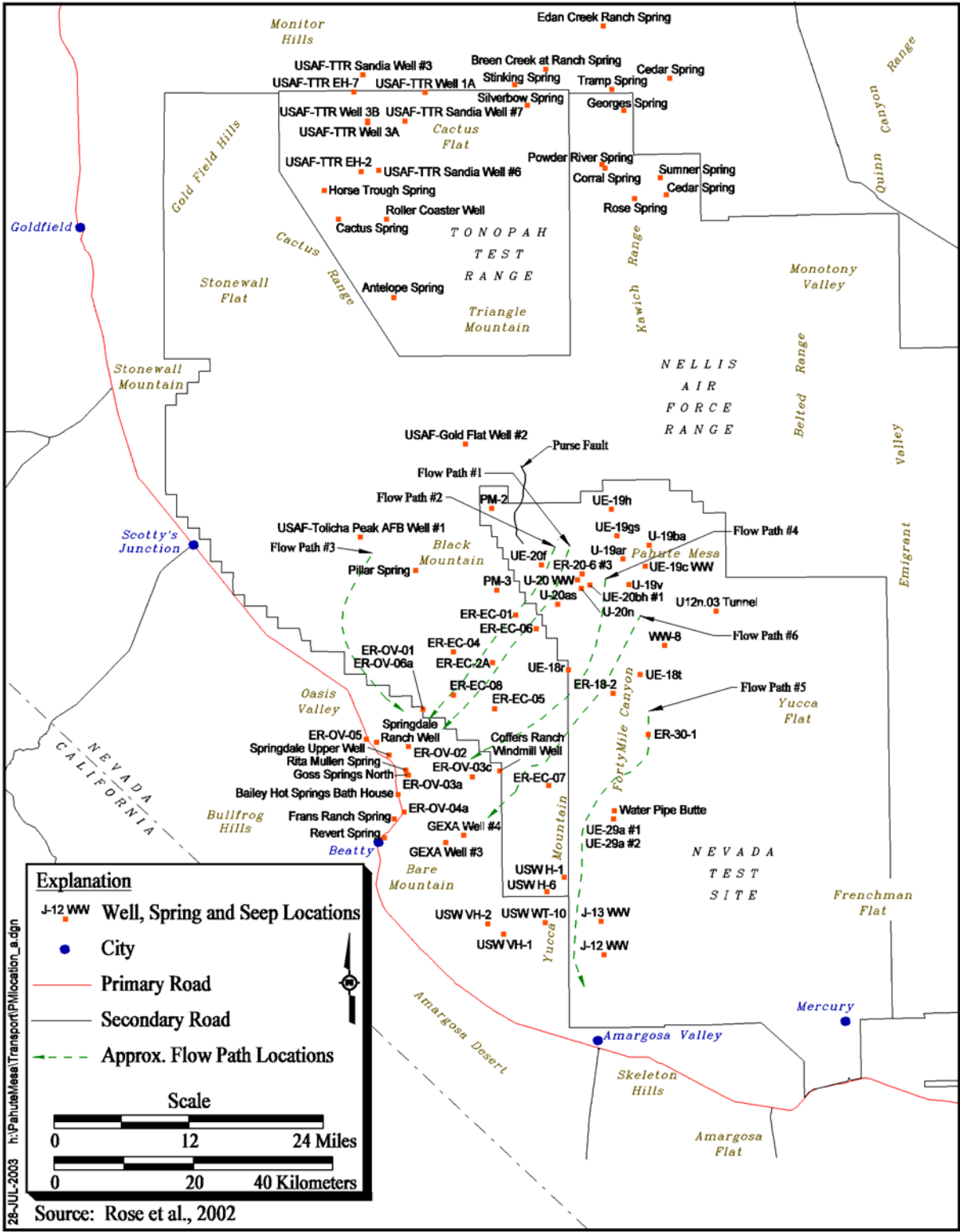


Figure 10-2 Groundwater Quality Sample Locations Considered During PM-OV Flow System Evaluation

documented and verified in accordance with the UGTA QAPP (DOE/NV, 2000a). Most non-radiological parameters are reported in concentration units of milligrams per liter (mg/L), and most radiological parameters are reported in activity units of picocuries per liter (pCi/L). Other parameters are reported in the appropriate conventional units (e.g., water temperature is reported in degrees Celsius (°C), pH is reported in standard units). Analytical data qualifiers are also included in the groundwater chemistry dataset. Qualifier definitions are as follows:

- < - Compound was analyzed for, but not detected above the reported sample quantitation limit. The detection limit (quantitation limit) is reported in the value field.
- B - Reported value is less than the Contract Required Detection Limit, but greater than the instrument detection limit.
- J - Estimated value.

10.4 Data Evaluation

The groundwater chemistry dataset was evaluated with respect to the level of available data documentation and with respect to the quality and/or diagnostic utility value of the reported data measurements.

10.4.1 Data Documentation Evaluation

The available data documentation for the groundwater chemistry dataset has been evaluated and flags were assigned in accordance with data documentation requirements described in [Section 4.3](#). Accordingly, the following levels of data documentation have been defined and assigned to the groundwater chemistry data for the Central and Western Pahute Mesa CAUs.

- Level 3: Data are collected using accepted scientific methodology (e.g., ASTM, EPA methods, USGS procedures) and accompanied by supporting or corroborative documentation such as testing apparatus diagrams, field or laboratory notes, and procedures.
- Level 4: Data are collected by a participating NNSA/NSO ERP organization or another organization not associated with the NNSA/NSO ERP prior to the issuance and implementation of project-approved standard policies, procedures, or practices governing data acquisition and qualification. The methods of data collection are documented and traceable; however, the validity of the data or compliance with referenced procedures is indeterminate. Supporting documentation may or may not exist.

- Level 5: Data are obtained under unknown, undesirable, or uncertain conditions.

10.4.2 Data Quality Evaluation

In addition to the data documentation evaluation flag which is used to rank the level of documentation, a DQE_F was assigned to qualitatively rank the reported chemical values in terms of the relative confidence that might be expected. The following levels of relative confidence have been defined and assigned to the groundwater chemistry data:

- Level C: Consistent - Analytical results are consistent with historical or regional trends for the reported location(s); or, for a given sample there are no anomalous results within the suite of parameters that would indicate sample contamination due to improper sample collection or erroneous laboratory procedures.
- Level NC: Not Consistent - Analytical results are not consistent with historical or regional trends for the reported location(s); or, for a given sample there are data anomalies within the suite of parameters that may indicate sample contamination or laboratory errors.
- Unknown - Data has not been formally evaluated in order to assess the accuracy and/or consistency of the data; or, there does not exist enough information (e.g., regionally, temporally, or within the dataset) to determine whether or not the data is consistent with historical or regional trends for the reported location.

Other data quality criteria exist and are commonly applied in the course of conducting evaluations of groundwater geochemical data. For example, the evaluation of major ion charge balance (Hem, 1985) serves as an indicator that the analytical data quality and/or verification account for the predominant constituents in a given water sample. The presence of bromide concentrations above background levels can be an indication of groundwater samples that have been contaminated by residual drilling fluids and are, therefore, not representative of ambient conditions. These data quality criteria have been applied in the process of evaluating groundwater data from the PM-CAUs and are discussed in the following section.

10.5 Analysis Process and Results

A synopsis of the geochemical evaluation of water quality data from the Central and Western Pahute Mesa is provided in the following section. For a more detailed discussion of this assessment, the reader is referred to Rose et al. (2002) and Thomas et al. (2002). The geochemical processes that accompany the movement of groundwater at the NTS include a variety of interactions (e.g., water-rock, solute-solute, and water-atmospheric) that occur in response to

changes in the hydrogeologic environment. These geochemical processes, and the changes in the hydrogeologic environment that they are indicative of, are identified through the evaluation of a diverse suite of geochemical parameters. The parameters occur as groups (e.g., major ions, stable isotopes) that tend to respond in systematic ways to similar geochemical processes. The following subsections discuss these various groups of geochemical parameters in terms of their respective ability to function as diagnostic hydrogeological indicators. The utility of geochemical data in evaluating groundwater systems is a function of having data (that meet data quality criteria) for the suite of parameters that have diagnostic value for the system or hydrogeologic processes of interest. Within the Pahute Mesa region groundwater quality dataset, samples collected from 77 individual locations generated representative major ion data that satisfy charge balance criteria (± 5 percent). Seventy-two (72) of these locations have provided both representative major ion data (that meet data quality criteria) and environmental tracer data (i.e., Carbon-13 [^{13}C], Carbon-14 [^{14}C], delta deuterium [δD], and delta oxygen-18 [$\delta^{18}\text{O}$]) to support the geochemical evaluation of groundwater flow. The following discussion highlights the geochemical evaluation process conducted by Rose et al. (2002) and Thomas et al. (2002) to provide a corroborative and independent means of verifying the conceptual models for groundwater flow in the Pahute Mesa area.

10.5.1 Major Ion Chemistry

This subsection of the report discusses the major ion chemistry characteristics of Central and Western Pahute Mesa groundwater. The dissolved constituents in groundwater provide a record of the minerals encountered as water moves through geologic materials. Accordingly, major ion water chemistry can be used to characterize the interaction and help trace the movement of groundwater through aquifer materials. The group of parameters comprising the major ions typically consists of calcium (Ca^{2+}), potassium (K^{+}), magnesium (Mg^{2+}), sodium (Na^{+}), chloride (Cl^{-}), sulfate (SO_4^{2-}), bicarbonate (HCO_3^{-}), and carbonate (CO_3^{2-}). Other constituents (such as silica or boron) are occasionally at concentrations high enough to be considered major constituents of groundwater. These constituents, however, more commonly occur as minor or trace constituents at significantly lower concentration levels. The techniques (Hem, 1985) used to evaluate data quality (charge balance) and to characterize and categorize principal groundwater types focus on the major ionic species listed above.

Evaluation of the major ion characteristics of Central and Western Pahute Mesa groundwater can provide insights on the source areas and flow directions for groundwater movement.

Using the dissolved constituents in groundwater to provide a record of the minerals encountered as water moves through an aquifer, Schoff and Moore (1964), Blankennagel and Weir (1973), and Winograd and Thordarson (1975) identified three distinct hydrochemical water types, or facies, in NTS groundwaters. These include a Na-K- HCO_3 groundwater facies commonly found in volcanic rock aquifers, a Ca-Mg- HCO_3 facies commonly occurring in Paleozoic carbonate aquifers, and a Ca-Mg-Na- HCO_3 facies assumed to be a mixture of the

volcanic and carbonate facies. Chapman and Lyles (1993) confirmed the occurrence of the Na-K-HCO₃ volcanic groundwater facies beneath Pahute Mesa, but noted a transition in the chemical composition from east to west. The groundwater in eastern Pahute Mesa (i.e., Area 19) contains a relatively higher proportion of Ca²⁺ while western Pahute Mesa (i.e., Area 20) groundwater contains a relatively higher proportion of Cl⁻ and SO₄²⁻. These changes in water quality occur in spatial proximity to hydrothermally altered volcanic rocks present in the Western PM-OV area.

A Piper diagram is a graphical tool used to represent the relative concentrations of major ions in a groundwater sample or group of samples (Hem, 1985). Ion concentrations are expressed in percent milliequivalents per liter and are used to classify various groundwater chemistry types, or facies, and illustrate the relationships that may exist within or between a group or groups of water samples. A Piper diagram consists of three different component representations of major-ion chemistry. Cation (i.e., Ca²⁺, K⁺, Mg²⁺, Na⁺) data are plotted in the left-hand triangle, while anion (i.e., Cl⁻, SO₄²⁻, HCO₃⁻, and CO₃²⁻) data are plotted in the right-hand triangle. Both cation and anion data are projected on to the central diamond-shaped area so that compositional relationships (such as mixing or evolutionary trends) within or between a group or groups of groundwater sample locations can be visually presented.

Figure 10-3 is a Piper diagram illustrating the variations in major ion concentrations within the PM-OV flow system. The data used in the construction of the Piper diagram are the most recent major ion analyses available in GEOCHEM02.mdb (IT, 2002i) for a particular location that meet charge balance criteria (± 5 percent). As shown, Na⁺ is the dominant cation and HCO₃⁻ is the dominant anion at most of the locations in the flow system. This is shown on the cation triangle where almost all of the samples plot very near the lower right corner indicating Na⁺ dominance. Similarly, most locations plot in the lower left corner of the anion triangle which indicates HCO₃⁻ dominance. However, data distribution within the anion triangle in the figure shows that Cl⁻ and SO₄²⁻ are locally present in appreciable quantities. This is indicated by some of the locations plotting more toward the center of the anion triangle. The evaluation by Rose et al. (2002) identified the highest Cl⁻ and SO₄²⁻ concentrations in wells ER-EC-1, ER-EC-4, and PM-3, located in western Pahute Mesa, west of the Purse Fault (WPM, stars in Figure 10-3). Drill core and cuttings from wells in this area show evidence of hydrothermal alteration (IT, 1998e), which could potentially account for the observed high dissolved Cl⁻ and SO₄²⁻ concentrations. This is consistent with previous observations by Blankennagel and Weir (1973). It was also noted by Rose et al. (2002) that eastern Pahute Mesa groundwater (east of the Purse Fault) is relatively dilute with respect to Cl⁻ and SO₄²⁻ when compared to groundwater west of the Purse Fault. Similarly, dilute groundwater is also present in Crater Flat (EPM & CF, open triangles in Figure 10-3). Further, inspection of the Piper diagram shows that other wells from central and western Pahute Mesa, the remaining ER-EC wells, and groundwater in Oasis Valley (PM, ER-EC, OV, open circles in Figure 10-3) exhibit Cl⁻ and SO₄²⁻ concentrations that are intermediate between groundwater west of the Purse Fault and the relatively dilute eastern Pahute Mesa groundwater samples. Groundwater in the Oasis Valley discharge area also has less Cl⁻ and SO₄²⁻ than western Pahute Mesa groundwater,

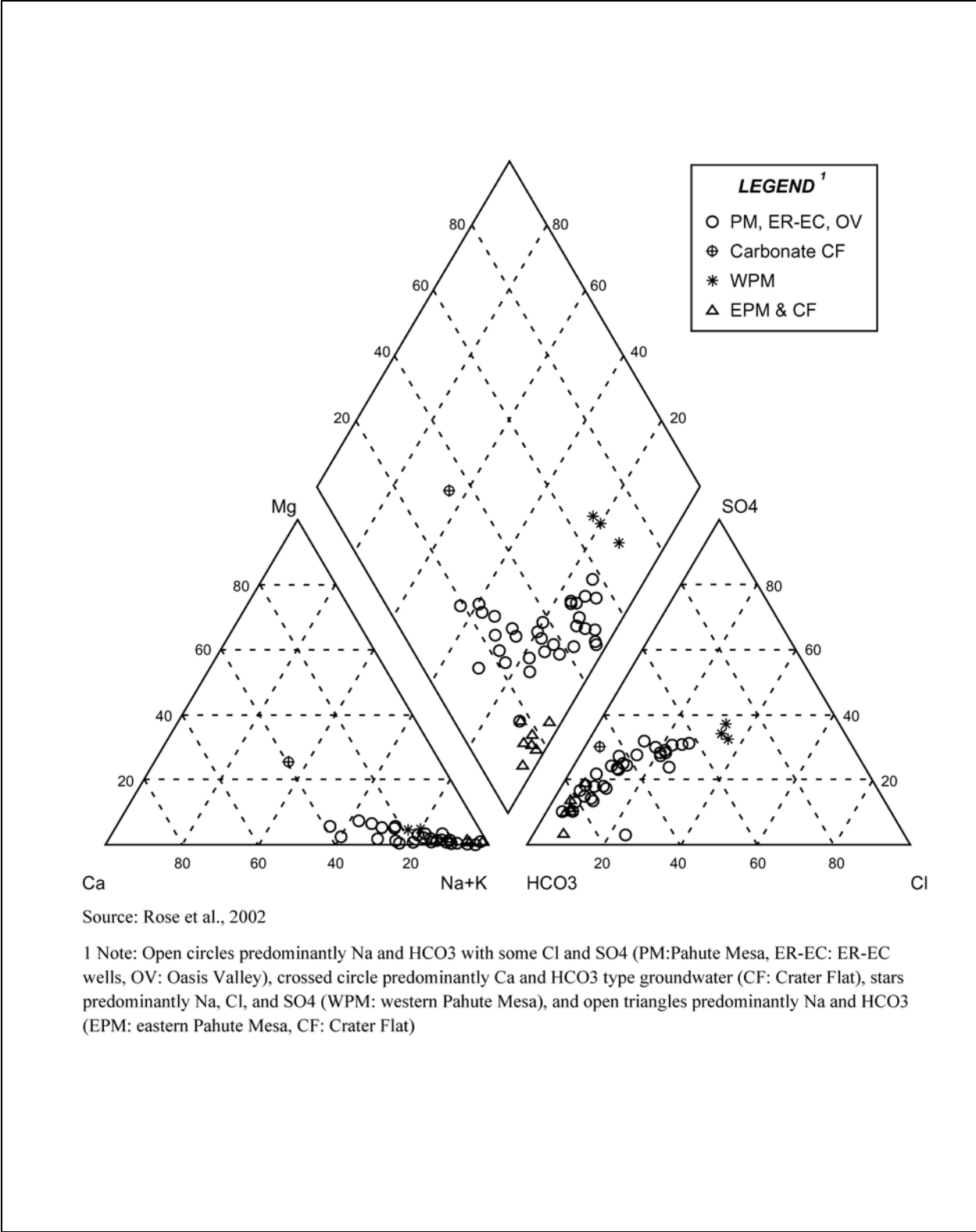


Figure 10-3
Piper Diagram of Major-Ion Variations in the Pahute Mesa-Oasis Valley Groundwater Flow System

indicating a predominance of groundwater originating beneath eastern Pahute Mesa and/or the mixing of western Pahute Mesa groundwater with more dilute local recharge. It can also be seen from the Piper diagram that one well (USW VH-2) in Crater Flat (Carbonate CF, hachured circle) shows a distinct carbonate aquifer signature (based on the Ca + Mg concentration).

10.5.2 Stable and Environmental Isotopes

This subsection discusses distribution of the stable isotopes of hydrogen, oxygen, and carbon, and the radioisotope ^{14}C in the PM-OV Valley flow system. The stable isotopes of hydrogen ($^2\text{H}/^1\text{H}$) and $^{18}\text{O}/^{16}\text{O}$ are perhaps the most conservative of all environmental tracers because they are uniquely intrinsic to the water molecule. In the water cycle, hydrogen and oxygen isotopes are fractionated (partitioned) between the liquid and vapor phases during evaporation and condensation processes. Once the precipitation has infiltrated the water table, the stable isotope values are unaffected by water-rock interaction at temperatures below approximately 100°C , and can be used to trace the groundwater origin and flow path, and to quantitatively determine mixing ratios of different water masses. The carbon isotopes are strongly influenced by recharge processes and water-rock interaction. The stable isotopes of carbon ($^{13}\text{C}/^{12}\text{C}$) provide a means to identify the degree of interaction with the available carbon reservoirs along the flow path while radiocarbon (^{14}C) provides a means by which groundwater travel times or apparent groundwater ages can be estimated.

Stable isotopes are reported as the abundance ratio of the two most common isotopes of a given element relative to a standard. For example, considering hydrogen isotopes in groundwater, it is the ratio of the hydrogen-2, or deuterium (^2H or D), isotope to the more common hydrogen-1 (^1H or H) isotope. Isotopic concentrations are expressed as the difference between the measured ratios of the sample and a reference over the measured ratio of a reference using the delta (δ) notation in units of per mil (parts per thousand). The reference standard for hydrogen and oxygen isotopes is known as the "Vienna Standard Mean Ocean Water" (VSMOW). The stable isotopes of hydrogen, oxygen, and carbon are important indicators of geochemical processes. Each of these elements is relatively light and the relative mass differences between the isotopes for a given element are relatively large. This mass difference can result in significant fractionation during physical processes and associated chemical reactions. Fractionation occurring in the natural environment during hydrogeological processes can provide information on the origin and evolution of groundwater. As a result, the stable isotopes of carbon, hydrogen, and oxygen function as tracers for water, carbon, and nutrient and solute movement and cycling.

Radioactive environmental isotopes are also important geochemical indicators. Groundwater residence times can be inferred from the decay of radioactive tracers present in the water if the input concentration of the tracer is reasonably well known and constant over time. Naturally occurring radionuclides such as ^{14}C or ^3H can be used to estimate the apparent age or travel time of groundwater.

10.5.2.1 Hydrogen and Oxygen Isotopes

Under ambient conditions (and temperatures $< 100^{\circ}\text{C}$) significant isotopic fractionation of hydrogen and oxygen does not occur in the subsurface environment. Therefore, an evaluation of the hydrogen and oxygen isotopic composition of groundwater can provide information on prevailing environmental conditions (i.e., latitude, elevation, and distance from the ocean) at the time of groundwater recharge. The observed variability in groundwater $\delta^{18}\text{O}$ and δD measurements result from fractionation effects that have occurred during evaporation and precipitation or in response to the mixing of groundwaters that have recharged under different conditions.

Figure 10-4 is a plot of the $\delta^{18}\text{O}$ composition versus the δD composition of NTS spring discharge, Rainier Mesa tunnel seepage, shallow groundwater from Fortymile Wash, representative regional precipitation, and groundwater from the PM-OV area. For reference, the global meteoric water line (GMWL) defined by Craig (1961) and the local meteoric water line (LMWL) defined by Ingraham et al. (1990) are included in this figure. The meteoric water lines represent the observed correlations in $\delta^{18}\text{O}$ - δD values of precipitation samples from around the world and from the Nevada Test Area, respectively. The GMWL is defined by the equation $\delta\text{D} = 8\delta^{18}\text{O} + 10$ (Craig, 1961), while the LMWL is defined by the equation $\delta\text{D} = 6.87\delta^{18}\text{O} - 6.5$ (Ingraham et al., 1990).

Figure 10-4 shows that the precipitation data tend to plot along both of the meteoric water lines. Further inspection of the figure reveals, however, that groundwater data tend to plot beneath the meteoric water lines. This is indicative of an isotopic shift or fractionation toward heavier (enriched in the heavier isotope) values in the groundwater data and has been ascribed to fractionation that takes place during the sublimation of snowpack or evaporation during infiltration (White and Chuma, 1987). Because recent regional precipitation plots along both the GMWL and the LMWL, it is suggested that evaporation of modern precipitation can be ruled out as the cause for the isotopic shift observed in the groundwater data. It can also be seen from the figure that the deep, regional groundwater from Pahute Mesa ($\delta\text{D} \sim -113$ per mil), Oasis Valley ($\delta\text{D} \sim -111$ per mil), and the ER-EC wells ($\delta\text{D} \sim -115$ per mil) have much lighter (more negative) stable isotope signatures than shallow groundwater from Fortymile Wash which has a similar isotopic signature to local modern mean annual precipitation. Rose et al. (2002) interpret this to indicate that recent groundwater recharge taking place at the NTS is not the dominant source of the deep groundwater. This implies that the primary source of deep groundwater observed beneath Pahute Mesa was either local recharge occurring during a colder climatic period (with little subsequent movement), or distal recharge (occurring at higher elevation, more northerly latitudes, or greater distance from the oceanic source) that has been relatively rapidly "imported" as a result of regional groundwater flow. Evidence presented by Rose et al. (2002) and Thomas et al. (2002) for deep groundwater in the PM-OV flow system is consistent with conclusions presented by Rose and Davisson (2002) which indicate that the bulk of deep groundwater presently in southern Nevada is likely to have been recharged in central Nevada and moved relatively rapidly to the present location.

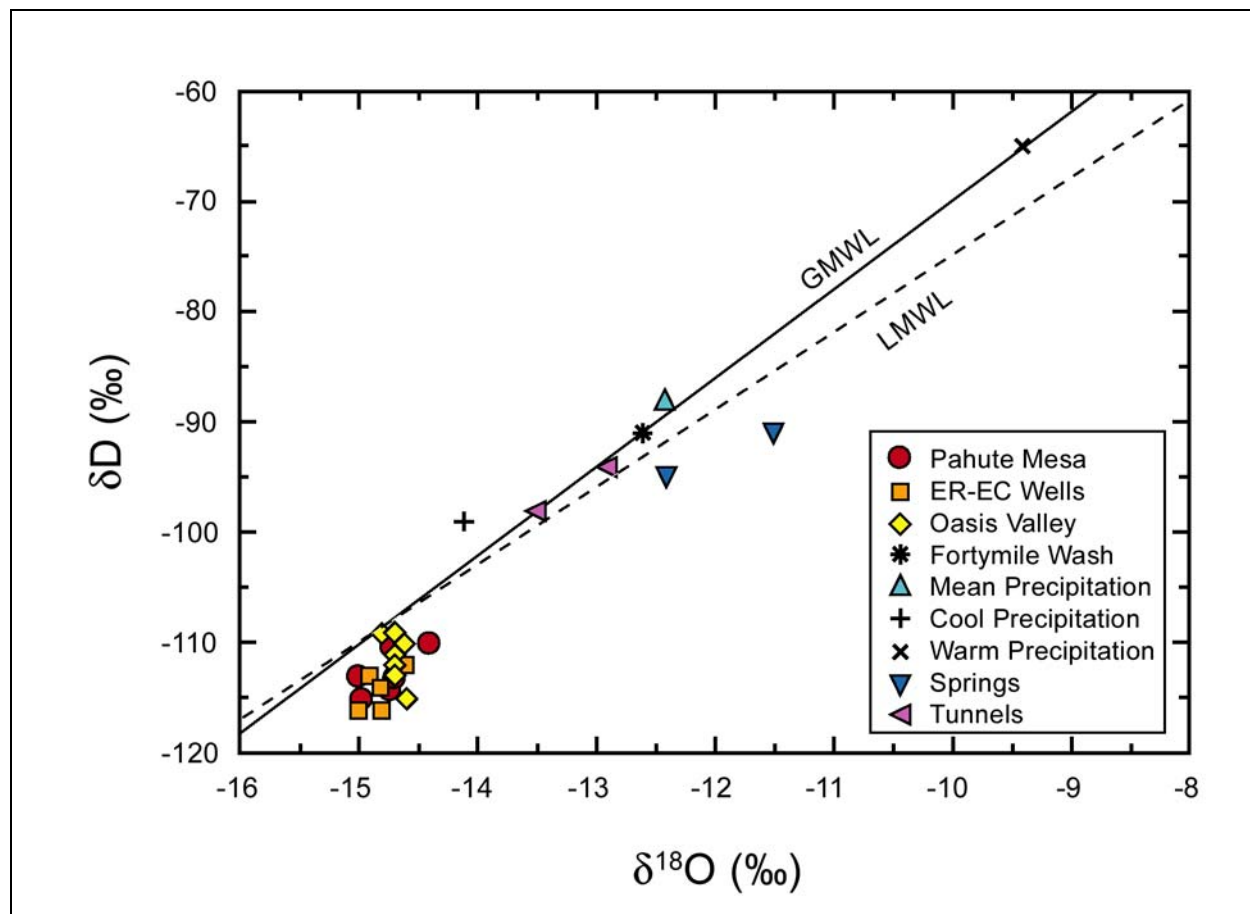


Figure 10-4
Stable Isotopic Plot of $\delta^{18}\text{O}$ vs. δD Values for Springs, Wells, Tunnels, and Precipitation in the Pahute Mesa-Oasis Valley Region

10.5.2.2 Carbon Isotopes

Carbon isotope values were measured in samples of both dissolved inorganic carbon (DIC) and dissolved organic carbon (DOC) fractions in groundwater from the PM-CAUs. DIC, attributed to the biochemical production of carbon dioxide (CO_2) gas in the soil zone and the chemical dissolution of carbonate minerals (Rose and Davisson (2002), was analyzed for both $\delta^{13}\text{C}$ and ^{14}C activity. The differences in the $\delta^{13}\text{C}$ characteristics of contributory carbon reservoirs provide the means to estimate their interaction with relative carbon contribution to groundwater DIC. It has been pointed out (Rose et al., 2002; Thomas et al., 2002) that any chemical dissolution of carbonate minerals during water-rock interaction can significantly modify the ^{14}C content of the DIC. As a result, any interpretation of ^{14}C ages may require significant corrections based on the careful evaluation of mineral dissolution and isotope exchange processes (Mook, 1980).

Variations in groundwater DIC concentrations and carbon isotope values ($\delta^{13}\text{C}$ and ^{14}C) as a function of location are shown in Figure 10-5. It can be seen from

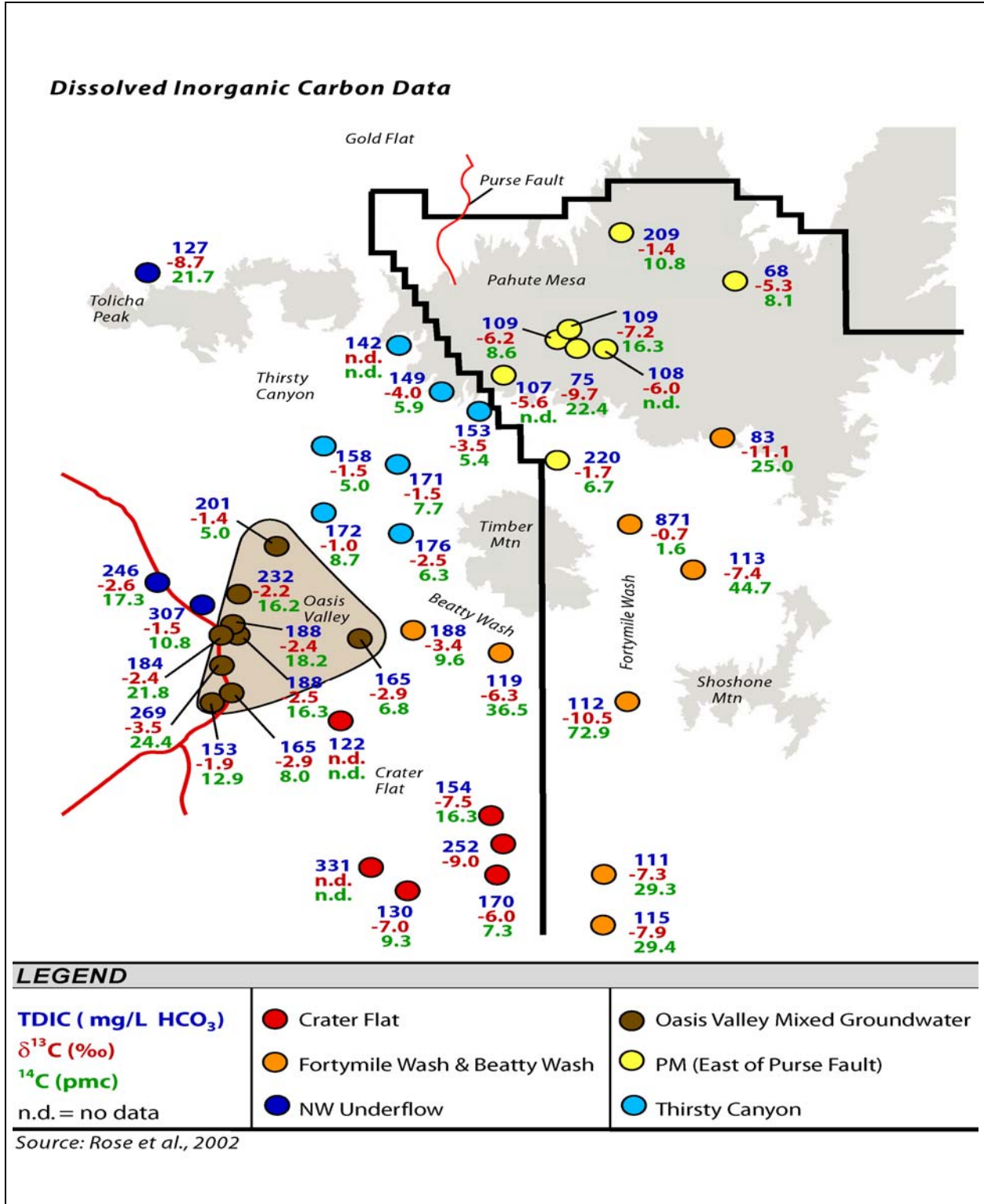


Figure 10-5
Geographic Distribution of Dissolved Inorganic Carbon Data
for Wells and Springs in the Study Area

the figure that groundwater from the Pahute Mesa underground testing area (east of the Purse Fault) has $\delta^{13}\text{C}$ values ranging from -11.1 to -1.4 per mil, with ^{14}C values ranging between 6.7 and 25 percent modern carbon (pmc). Rose et al. (2002) interpret the heterogeneous distribution of carbon isotopes in this area as an indication that local groundwater has been derived from more than one source. It can also be seen from this figure that, in groundwater west of the Purse Fault (in the Thirsty Canyon region), carbon isotope values are less variable. Less variability in or more effective mixing of groundwater sources in the Thirsty Canyon area are indicated by $\delta^{13}\text{C}$ values ranging from -4.0 to -1.0 per mil, and ^{14}C values ranging between 5.0 and 8.7 pmc.

Figure 10-5 shows that the ^{14}C values increase in Oasis Valley (8.0 to 24.4 pmc) relative to groundwater compositions immediately upgradient of the discharge area. Thomas et al. (2002) point out that the $\delta^{13}\text{C}$ values in Oasis Valley groundwater (-3.5 to -1.5 per mil) are, however, similar to groundwater in the ER-EC wells in Thirsty Canyon. Rose et al. (2002) suggest that this observed increase in ^{14}C values closer to Oasis Valley indicates mixing with a local recharge component in or near the discharge area. While isotopic exchange with soil CO_2 gas near the discharge area is likely and would account for the observed increase in ^{14}C values, coupled dissolution of carbonate minerals during water-rock interaction would be required to maintain the relatively heavy $\delta^{13}\text{C}$ values that are observed in Oasis Valley groundwater (Rose et al., 2002). Micrographic observations of calcite in cores and cuttings from boreholes in the Oasis Valley area (Benedict et al., 2000) identify the dissolution of calcite in wells in this area.

The ^{14}C data presented in Figure 10-5 indicate that a significant amount of recharge is taking place in Fortymile Wash and upper Beatty Wash. This is apparent from the higher ^{14}C values (e.g., 44.7, 72.9, and 36.5 pmc) in wells located in or near those features. According to Rose et al. (2002), data indicate that local recharge in these washes originates as precipitation or snow melt runoff from Pahute Mesa and Timber Mountain. Water Well 8, also shown in Figure 10-5, is located northeast of Fortymile Wash and has the highest ^{14}C value (25 percent modern carbon [pmc]) and the lowest $\delta^{13}\text{C}$ value (-11.1 per mil) observed in wells on Pahute Mesa. Stable isotope data for Water Well 8 indicate that it has characteristics commensurate with a significant contribution from local recharge (i.e., more positive, δD and $\delta^{18}\text{O}$ values). Rose et al. (2002) point out that similarly "young" ^{14}C signatures (high percent modern carbon values) persist further downgradient along Fortymile Wash and include samples from ER-30-1 (44.7 pmc), UE-29a #1 and #2 (72.9 pmc), J-12 (29.4 pmc) and J-13 (29.3 pmc). Similar values are observed in upper Beatty Wash at ER-EC-7 (36.5 pmc). The δD and $\delta^{18}\text{O}$ values observed in these wells are also consistent with a significant recent recharge component (Rose et al., 2002). The ^{14}C value (1.6 pmc) observed in Well ER-18-2, located east of Timber Mountain in upper Fortymile Wash, is significantly lower than any of the other wells in Fortymile Wash. The high dissolved carbonate species in this well and the relatively heavy $\delta^{13}\text{C}$ (-0.7 per mil) suggest that the dissolution of aquifer calcite (and introduction of "dead" carbon) may result in this local anomaly. It should be noted that ER-18-2 was completed in an interval where the groundwater production rate was very low (IT, 2002h).

10.5.3 Conservative Tracers

Conservative tracers are geochemical species that move with groundwater, exhibiting little or no change in concentration caused by reactive processes. Conservative tracers can be used to support the identification of groundwater flow paths, mixing ratios, and time scales of environmental processes (Cook and Bohlke, 2000). The Cl^- and often SO_4^{2-} ions, and the stable isotopes of hydrogen and oxygen are considered conservative tracers. These parameters provide the fundamental basis for the flow path identification and mixing model estimates developed by Rose et al. (2002).

10.5.3.1 Conservative Tracer Data

Figure 10-6 and Figure 10-7 illustrate the geographic variations in groundwater δD values and chloride concentrations, respectively, in the PM-OV flow system. As discussed above, these figures illustrate that groundwater in upper Thirsty Canyon, west of the Purse Fault, has relatively light δD values (as light as -116 per mil) and high Cl^- concentrations (up to 97 mg/L) that are distinct from Pahute Mesa groundwater immediately to the east. In the Pahute Mesa area east of the Purse Fault, the δD values ranged from -110 to -115 per mil and the Cl^- values ranged from 5 to 25 mg/L. The Purse Fault is spatially associated with a major discontinuity in regional water levels, in the western part of Area 20 (O'Hagan and Lacznik, 1996; Lacznik et al., 1996). According to Rose et al. (2002), the difference in the conservative tracer compositions of groundwater on either side of the Purse Fault indicates that two distinct water masses are present in that area. Downgradient from this water level discontinuity, changes in δD and Cl^- values indicate (Rose et al., 2002) that mixing of these two water masses occurs in the area downgradient from ER-EC-1 and PM-3 toward the Oasis Valley discharge area.

10.5.3.2 Conservative Tracer Data Evaluation

Representative well sites were selected for the conservative tracer modeling effort. The following section describes the criteria applied by Rose et al. (2002) in the selection process to define representative data for use in the conservative tracer modeling. Conservative tracer data for a number of well locations within the PM-OV flow system are summarized in Table 10-2. As previously described in Section 10.2, these data were extracted from the GEOCHEM02.mdb as part of the flow system dataset that meets quality and parameter suite criteria. The range in reported values is indicated for those sites that have been sampled on more than one occasion. The "n" value after each record indicates the number of independent analyses. The data in Table 10-2 have been subdivided into three categories (i.e., Pahute Mesa - West of Purse Fault, Pahute Mesa - East of Purse Fault, and "Local" Recharge) to represent the end-member mixing components that are present in the flow system. These components are inferred to mix within the flow system and contribute to groundwater discharge in central Oasis Valley.

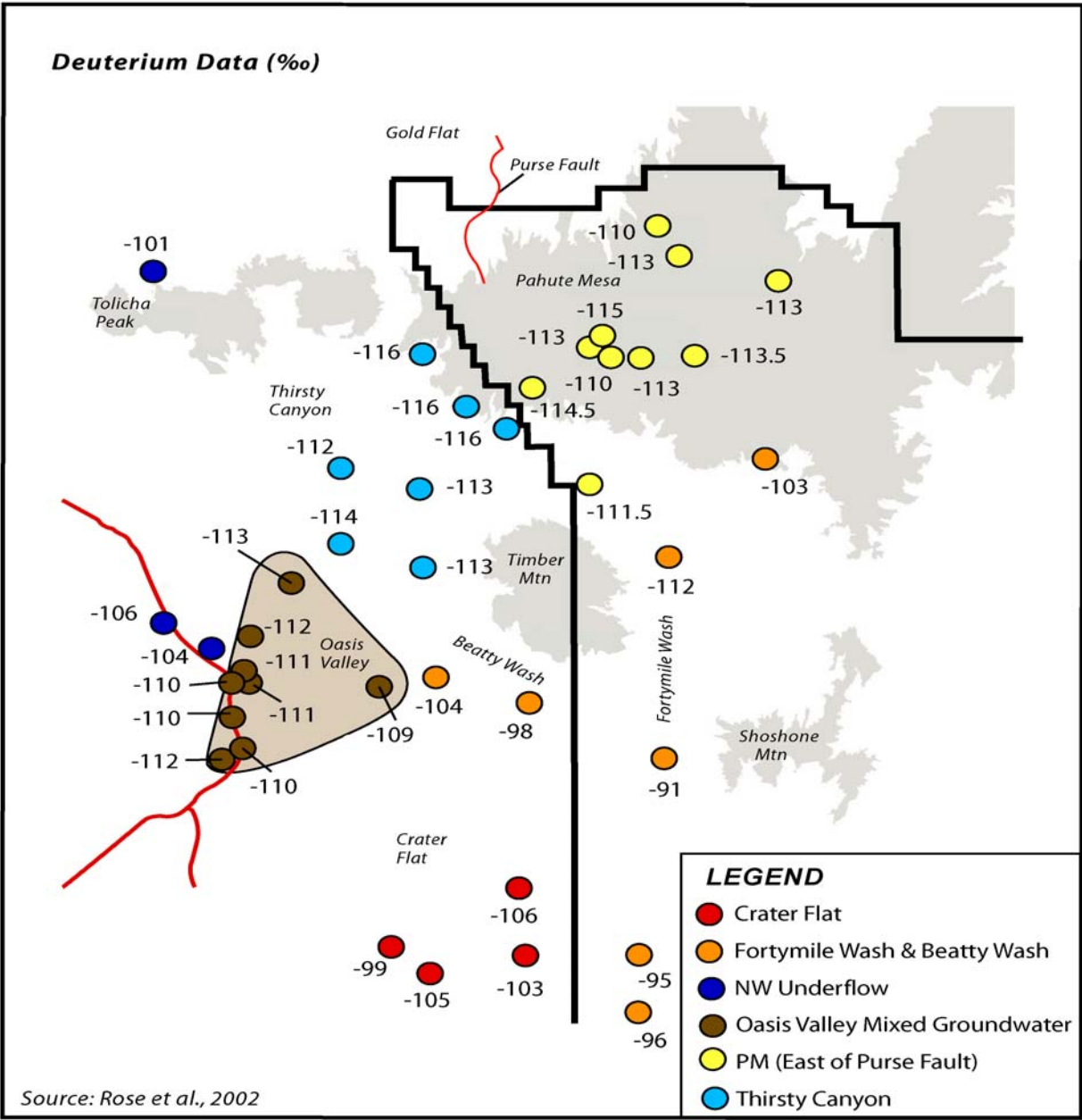


Figure 10-6
Geographic Distribution of δD Values for Wells and Springs in the Study Area

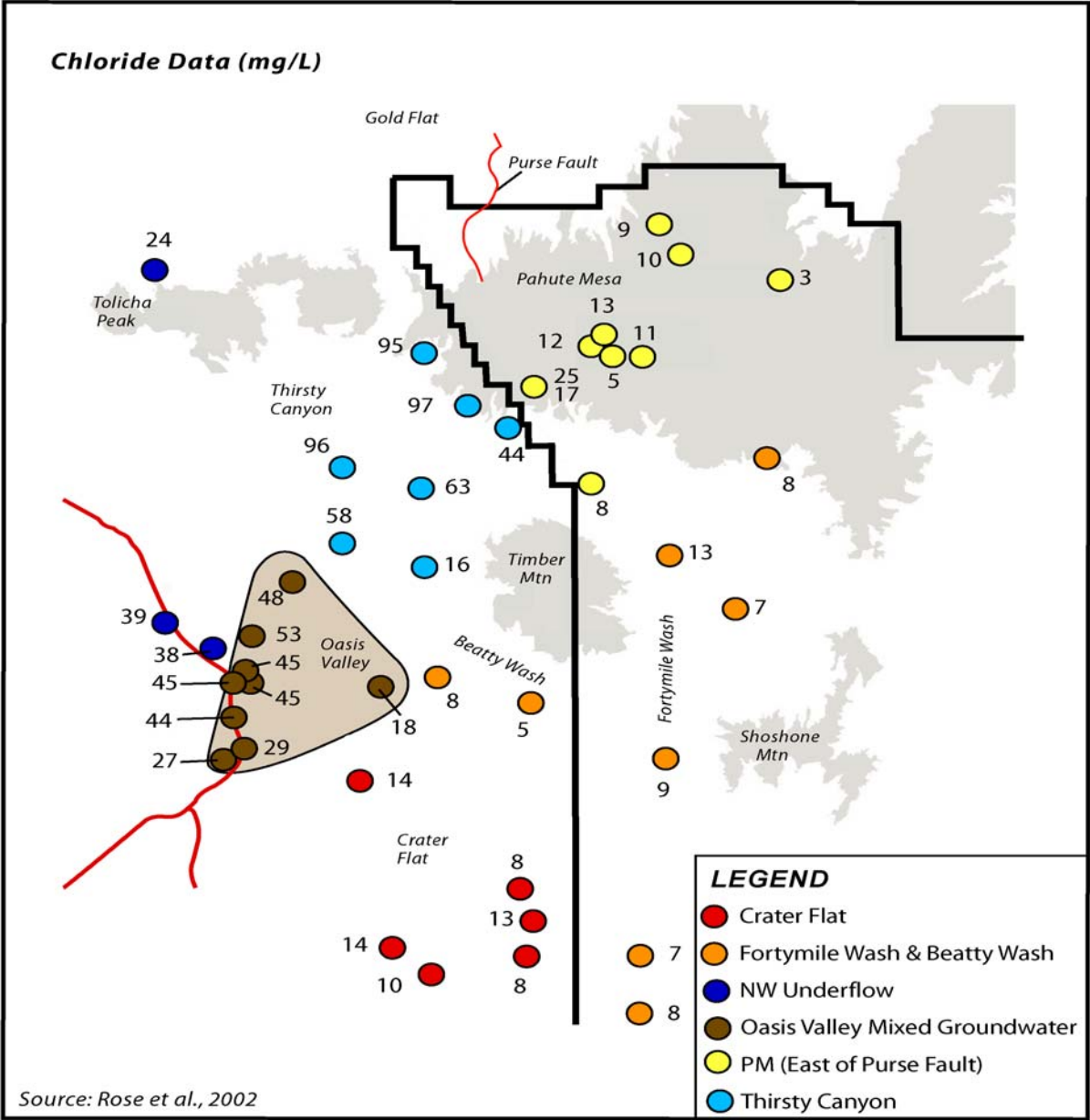


Figure 10-7
Geographic Distribution of Dissolved Cl⁻ Concentrations for Wells and Springs in the Study Area

Conservative tracer data are also presented for the Oasis Valley groundwater discharge area.

Simple statistical methods were used to identify the well locations most representative of a particular end member group. The overall range in δD , $\delta^{18}O$, Cl^- and SO_4^{2-} values are provided along with the mean and median values for each group. Note that the mean and median values were determined using the average values for each well location. This avoids "weighting" the group statistics with data from locations that have been sampled on a number of occasions. Using these results, well locations that are compositionally similar to the statistical mean and median values are readily identified.

Some of the "end-members" used for conservative tracer models were chosen largely on the basis of these statistical criteria. For example, Well ER-OV-3a was used to represent central Oasis Valley discharge in many of the mixing models, and is a good "statistical match" with the mean and median values of the Oasis Valley samples listed in [Table 10-2](#). Following the same rationale, U-20 Water Well was commonly used to represent Pahute Mesa groundwater east of the Purse Fault.

In addition to statistical information, the selection process also included more subjective criteria such as geographic location, or proximity to an underground test. For example, well UE-19h was sometimes used to represent groundwater east of the Purse Fault instead of U-20 Water Well. This decision was based on the fact that UE-19h is the northernmost well on Pahute Mesa, and is a fairly good match to the statistical data. Deep groundwater beneath the Mesa is inferred to originate as regional underflow from the north, and UE-19h may, therefore, be representative of this underflow component prior to mixing with groundwater from other sources. In a similar manner, the UE-29a wells were used to represent "local recharge" both because of their being representative of the group "average" composition, and because they are located in a similar setting (with respect to the collection of local runoff) to that of Thirsty Canyon Wash. Most of the local recharge in the Oasis Valley region is inferred to occur by infiltration of runoff in the washes.

Of the Pahute Mesa wells located west of the Purse Fault, Well PM-3 is perhaps the best match to the statistical data, but most of the models were run using either ER-EC-1 or ER-EC-4. This decision was based on the fact that the ER-EC wells are the most concentrated end-members for representing the high-solute mixing component present in this area, and are situated geographically near the northern boundary of the study area.

Another issue addressed in the data selection process focused on the range in reported values for the individual wells selected to represent the end-member groups. Variation at a given site may reflect systematic procedural influences among the various sampling and/or analytical contractors or differences in water chemistry over time. For instance, a well that is extensively purged on one occasion but only briefly pumped on another occasion may show conspicuous differences between sample sets. However, much of the observed variation at individual sites is likely due to differences in analytical precision and standardization practices of different laboratories. In this case, consistency

Table 10-2
Statistical Summary of Representative Conservative Tracer Data

Site ID	δD	n	$\delta^{18}O$	n	Cl (mg/L)	n	SO ₄ (mg/L)	n
Pahute Mesa - West of Purse Fault								
ER-EC-1	-116	2	-14.8	2	92 - 97	4	120 - 145	4
ER-EC-2A	-113 / -116	2	-14.9	2	59 - 63	3	87 - 99	3
ER-EC-4	-112 / -115	2	-14.6	2	78 - 95.7	5	110 - 130	5
ER-EC-6	-116	2	-15.0	2	44 - 52	4	56 - 79	4
Pahute Mesa #3 (PM-3)	-116	1	-14.8	1	84.2 - 95.2	2	92.3 - 114	2
Range	-112 / -116	9	-14.6 / -15.0	9	44 - 97	18	56 - 145	18
Mean	-115.2	5	-14.82	5	76.1	5	102.7	5
Median	-116	5	-14.8	5	85.5	5	103.2	5
Pahute Mesa - East of Purse Fault								
ER-20-5 #3 (Tybo)	-114	3	-15.0 / -15.1	4	17.0 - 18.9	4	33.3 - 35.3	4
ER-20-6 #3 (Bullion)	-114 / -115	3	-15.0 / -15.1	4	11.9 - 15.3	4	30.5 - 34.0	4
U-19ba #1	---	---	---	---	40.9	1	10.2	1
U-19q PS#1d (Camembert)	-113	1	-14.6	1	10.4	1	29.7	1
U-20 Water Well	-113	1	-14.7	1	11 - 12.1	2	31 - 31.5	2
U-20a #2 Water Well	-114	1	-14.75	1	9.5 - 11.2	3	28 - 38.4	3
U-20al (Egmont)	---	---	---	---	30.5 - 32.8	2	68 - 77.6	2
U-20n PS#1 DDH (Cheshire)	-113	3	-14.6 / -15.0	9	11.1 - 14.1	7	26.5 - 35.3	7
UE-18r	-110 / -112	2	-14.6 / -14.7	2	6.3 - 12	4	18 - 24	3
UE-19c Water Well	---	---	-15.0	1	2.4	2	5.8 - 6.2	2
UE-19gs	-113.5	1	-14.5	1	9.9	1	75 - 100	2
UE-19h	-110 / -112	2	-14.4 / -14.8	2	8.5 - 9.7	2	38.2	1
UE-20bh #1	-109 / -112	3	-14.7 / -14.8	3	3.5 - 4.7	3	8.3 - 14	2
Range	-109 / -115	20	-14.4 / -15.1	29	2.4 - 40.9	36	8.3 - 100	34
Mean	-112.8	10	-14.77	11	14.0	13	33.6	13
Median	-113	10	-14.73	11	10.4	13	31.3	13
"Local" Recharge								
NTS Springs	-88 / -101	5	-11.0 / -12.7	5	4.7 - 11	4	7.7 - 33.2	4
Rainier Mesa Tunnel Seeps	-90 / -101	80	-11.9 / -14.2	80	6 - 12	17	7.9 - 28.8	17
NTS Surface Runoff	-82.3 / -88.1	2	-11.3 / -12.4	2	3.2 - 4.3	2	8.3 - 9.0	2
UE-29a wells	-91	2	-12.6	2	7.7 to 9.0	6	15 - 16.5	6
Range	-82.3 / -101	89	-11.0 / -14.2	89	3.2 - 12	29	7.7 - 33.2	29
Mean	-91.3	4	-12.39	4	7.1	4	14.8	4
Median	-92	4	-12.28	4	7.7	4	16.1	4
Central Oasis Valley Discharge								
Bailey's Hot Spring	-108 / -110	2	-14.6	2	39.5 - 43.5	7	111 - 119	7
ER-OV-2	-112	1	-14.7	1	49.2 - 53.1	2	86 - 90.2	2
ER-OV-3a	-111	1	-14.7	1	41.6 - 44.6	2	76 - 76.1	2
ER-OV-4a	-109	1	-14.8	1	27.6 - 28.8	3	58.7 - 61	3
Goss Spring	-110 / -112	2	-14.7	2	41.9 - 44.8	3	76 - 77	3
Mullen Spring	-111	1	-14.7	1	42.5 - 45.1	2	76 - 76.7	2
Range	-108 / -112	8	-14.6 / -14.8	8	27.6 - 53.1	19	58.7 - 119	19
Mean	-110.3	6	-14.7	6	41.8	6	82.1	6
Median	-110.5	6	-14.7	6	43.1	6	76.6	6

became an important selection criterion, and it was decided that the stable isotope and conservative solute data generated by the DRI for the most recent sample date of record for the representative well locations would be used in the modeling effort. While this introduces some bias to the data selection and modeling processes, the results of mixing models using different well sites will generally vary more than the results based on modeling the range in values for an individual well site. There are, however, some instances where this is not the case.

Conservative mixing models are fairly sensitive to variations in stable isotope values. Using one of the most extreme examples, the δD values reported for well ER-EC-4 range from -112 to -115 per mil. For a mixing model involving ER-EC-4 + UE-19h + UE-29a to yield the final composition of ER-OV-3a, the two different δD values for ER-EC-4 resulted in the following two models:

$$\delta D = -112 \text{ ‰} \quad \text{ER-OV-3a} = (0.406)\text{ER-EC-4} + (0.546)\text{UE-19h} + (0.048)\text{UE-29a}$$

$$\delta D = -115 \text{ ‰} \quad \text{ER-OV-3a} = (0.471)\text{ER-EC-4} + (0.414)\text{UE-19h} + (0.115)\text{UE-29a}$$

Hence, the range in the possible proportions of the end-member mixing components increases with increasing input parameter uncertainties. For this particular set of wells, the issue is further exacerbated by the fact that UE-19h also has a range in reported δD values. Using different combinations, δD values for ER-EC-4 and UE-19h will somewhat increase the range in model uncertainty. Hence, while the models that were reported in Rose et al. (2002) are generally self-consistent with respect to data source, it is incumbent upon the geochemists to ensure that the parameters that are used in the geochemical models represent the best possible results. This is particularly critical for "high sensitivity" parameters such as δD .

Rose et al. (2002) used various combinations of the conservative tracer data to identify six plausible paths for groundwater flow from Pahute Mesa. These flow paths, and the wells/source areas considered as contributory sources, are described in [Table 10-3](#). The location of these flow paths are shown in [Figure 10-2](#). Relatively abundant data from the well characterized flow path directly between Pahute Mesa and Oasis Valley (Flow Path 1) suggest that central Oasis Valley discharge consists of 29 to 47 percent groundwater from west of the Purse Fault, 45 to 57 percent groundwater from east of the Purse Fault, with 0 to 16 percent local recharge. Several other potential flow paths for groundwater movement away from Pahute Mesa are also identified by Rose et al. (2002) using conservative tracers. While these other flow paths are plausible based on existing data, they exhibit greater uncertainties with respect to contributory water sources because of data limitations (scarcity of wells or lack of diagnostic parameters in key areas). It should be kept in mind that the reported range in mixing ratios of the various water sources for a given flow path is narrower than it would be had every possible combination of data and location been used in the calculations. This bias is a reflection of the data selection process.

**Table 10-3
Description of Plausible Groundwater Flow Paths in the Pahute Mesa-Oasis Valley Flow System (Rose et al., 2002)**

Groundwater and/or recharge source end-member groups (with list of individual well and/or spring locations used in flowpath modeling)																							
Flow path designation and description	Pahute Mesa Groundwater from East of the Purse Fault			Pahute Mesa Groundwater from West of the Purse Fault					Gold Flat/TTR				NW Ground Water Inflow	Timber Mountain Area		Local Recharge	Oasis Valley					Amargosa Valley	Crater Flat
	U-20 WW	UE-19h	WW-8	ER-EC-1	ER-EC-2a	ER-EC-4	ER-EC-6	ER-EC-8	Cedar Pass	Sandia #6	Roller Coaster	Rose Spring	Tolicha Peak	ER-EC-7	Coffers Windmill	UE-29a#2	ER-OV-1	ER-OV-3a	ER-OV-4a	ER-OV-5	Springdale	J-12	USW-VH-1
Flow Path 1 ^a	Pahute Mesa groundwater + local recharge → Oasis Valley groundwater																						
	M1	M1	M1	M1	M1	M1	M1	M1								R	T	T	T	T	T		
Flow Path 2 ^b	Pahute Mesa groundwater + Gold Flat/TTR groundwater + local recharge → Oasis Valley groundwater																						
	M1	M1	M1	M1	M1	M1	M1	M1	M2	M2	M2	M2				R	T	T	T	T	T		
Flow Path 3 ^c	Tolicha Peak +/- Pahute Mesa groundwater +/- Gold Flat/TTR groundwater +/- local recharge → Oasis Valley groundwater																						
	M1	M1	M1	M1	M1	M1	M1	M1	M2	M2	M2	M2	M3			R	T	T	T	T	T		
Flow Path 4 ^d	Pahute Mesa groundwater + local recharge (in Timber Mtn area) → Beatty Wash to Oasis Valley discharge area																						
	M1	M1	M1	M1	M1	M1	M1	M1						R	R		T	T	T	T	T		
Flow Path 5 ^e	Pahute Mesa groundwater + local recharge → flow down Fortymile Wash toward the Amargosa Valley																						
	M1	M1	M1	M1	M1	M1	M1	M1								R							T
Flow Path 6 ^f	Pahute Mesa groundwater + local recharge → Crater Flat																						
	M1	M1	M1	M1	M1	M1	M1	M1						R	R	R							T

Groundwater mixing components M1- Pahute Mesa Groundwater, M2- Gold Flat/TTR Groundwater, M3- NW Groundwater Inflow
 Recharge components R- Timber Mountain Area or Local Recharge
 Mixing target T- Mixing target in either Oasis Valley, Amargosa Valley, or Crater Flat

^aThis flow path considers mixing of Pahute Mesa groundwater with local recharge to yield central Oasis Valley discharge. Reasonable models for this flow path can be derived using three end-member compositions: (1) Pahute Mesa groundwater from wells east of the Purse Fault, (2) Thirsty Canyon groundwater from wells west of the Purse Fault, and (3) local recharge.

^bFlow path 2 represents groundwater from north of Pahute Mesa (Cactus Flat area) mixing with Pahute Mesa groundwater and local recharge and then flowing to Oasis Valley.

^cFlow path 3 represents groundwater flow from north of Oasis Valley into Northwest Oasis Valley. Potential mixing sources of inflow to northwest Oasis Valley include groundwater from the Tolicha Peak area, groundwater from the Cactus Flat area north of Oasis Valley, and groundwater from Pahute Mesa. Groundwater in wells ER-OV5 and Springdale Upper have deuterium values that are significantly different than wells and springs in the rest of the Oasis Valley area therefore justifying an attempt to identify potential sources for that water.

^dFlow path 4 represents groundwater flow from Pahute Mesa to southern Oasis Valley through the Timber Mountain-Beatty Wash area. Local recharge along this flow path may include Timber Mountain recharge (represented by ER-EC-7) and/or recharge from surface water flow in Beatty Wash (represented by UE-29a#1). Well ER-OV-4a is used to represent southern Oasis Valley groundwater because it has the lowest carbon-14 value of the three samples in this area and does not appear to have interacted with shallow local groundwater or been subjected to exchange with soil-zone gases (Thomas et al., 2002).

^eFlow path 5 represents groundwater flow from Pahute Mesa down Fortymile Wash toward Amargosa Valley combining with local recharge. Thomas et al. (2002) developed models for groundwater from wells WW-8 and UE-29a#1 mixing to produce the water chemistry observed at well J-13.

^fFlow path 6 represents groundwater from Pahute Mesa mixing with local recharge and flowing south toward Crater Flat.

10.5.4 Geochemical Modeling

Flow paths defined by Rose et al. (2002) based on conservative mixing models were further evaluated using the NETPATH geochemical computer code (Plummer et al., 1994). NETPATH is a computer code for geochemical calculations developed by the U.S. Geological Survey. This code is freely available from their website. The specific code capabilities sought for use by Rose et al. (2002) included geochemical speciation calculations, mass balance calculations, isotopic exchange, and the ability to calculate apparent water ages based on carbon isotope data (^{13}C and ^{14}C). Code options for a peer reviewed, non-proprietary geochemical code capable of conducting isotopic exchange and apparent water age calculations (without modifications), in addition to the other capabilities, are limited to NETPATH. The geochemical calculations performed using NETPATH were conducted in accordance with procedures described in Plummer et al. (1994) and summarized in Rose et al. (2002) and Thomas et al. (2002).

The NETPATH modeling performed by Rose et al. (2002) incorporates data for the ER-EC (and ER-18-2) wells and builds on previous NETPATH modeling done in the PM-OV flow system by Thomas et al. (2002). The NETPATH program is used to define the net geochemical mass-transfer that takes place between initial and final water compositions (i.e., well locations) along a hydrologic flow path as a result of water-rock interaction processes. NETPATH can also compute the mixing proportions of up to five contributory source waters, along with the net geochemical reactions, required to account for the observed composition of the final water. Plausible flow paths that are consistently described using both the conservative tracer and NETPATH modeling approaches are considered to have a high probability of representing realistic groundwater pathways (Rose et al., 2002).

Geochemical modeling is used to evaluate the consistency between the groundwater sources, flow paths, and mixing processes identified using geochemical and hydrogeologic data and the water-rock interaction processes assumed to be taking place. As described in the previous section, conservative geochemical tracers were used first by Rose et al. (2002) to delineate probable water sources, flow paths, and mixing ratios. The plausible flow paths identified were then modeled using the computer code NETPATH (Plummer et al., 1994). NETPATH performs speciation calculations to determine mineral saturation states, net mass transfer of major ions during chemical reactions along a proposed flow path, and carbon isotope fractionations for carbon (both ^{14}C and $\delta^{13}\text{C}$) entering and exiting the groundwater. By modeling the isotopic evolution of DIC that occurs between individual wells along a flow path, it is also possible to calculate the apparent groundwater travel time between those wells. Viable water-rock geochemical models developed in this way, using measured water chemistry and representative aquifer mineral compositions and phase relations, provide independent validation of proposed flow paths and mixing processes.

Geochemical reactions in the NETPATH model are constrained by thermodynamic calculations and by the $\delta^{13}\text{C}$ composition of the phases involved in the reactions. Travel time calculations using NETPATH require that DIC isotope

data are available for water samples along the flow path and the minerals interacting with the groundwater. The evaluation of carbon isotopes of DOC has also been used to provide estimates of apparent groundwater travel times (Rose et al., 2002; Thomas et al., 2002). As discussed in Thomas et al. (2002), travel time estimates based on DOC fate and transport are considered less susceptible to the complex water-rock interaction processes that can strongly influence the fractionation of DIC.

The water-rock interaction process calculations performed within NETPATH are constrained by both user-defined aquifer mineralogical data and speciation calculations (using groundwater quality data) performed by the computer program. Representative mineral phases are determined using micrographic and chemical analyses of aquifer materials. For the PM-OV flow system, micrographic and chemical data for aquifer mineralogy are available in various reports (Benedict et al., 2000; IT, 1998b and c; and Drellack et al., 1997) and databases (IT, 2002i; Warren et al., 2000a). These data support the definition of chemical composition and reactive tendencies of aquifer minerals to be used during the NETPATH modeling process. Minerals that have been identified to be under-saturated (based on speciation calculations) and/or dissolving (based on micrographic observation) are constrained in NETPATH to only dissolve. Similarly, those that are super-saturated and/or precipitating can only precipitate from groundwater or form by incongruent dissolution. The NETPATH models are limited by (1) site-specific data (including the chemical and isotopic compositions) for aquifer minerals and gases, and (2) availability of groundwater chemistry data along specific flow paths. Since NETPATH model solutions are non-unique, and more than one model can, therefore, be calculated to describe the chemical changes along a particular flow path, the evaluation of potential flow paths using conservative tracers (as discussed in the previous section) is an effective verification process.

10.5.4.1 NETPATH Modeling Approach

The NETPATH modeling conducted by Rose et al. (2002) builds on earlier flow path modeling presented by Thomas et al. (2002). Rose et al. (2002) incorporate new mineralogical data (from the ER-EC and ER-OV wells) and new chemical and isotopic data for groundwater samples (from the ER-EC and ER-18-2 wells) from the immediate PM-OV area. As discussed in Thomas et al. (2002) and Rose et al. (2002), multiple well locations for each source area that met charge balance criteria (± 5 percent) were used in individual NETPATH simulations for a given flow path. The chemical and isotopic compositions of mineral and glass phases for the HSUs present in EOIs in individual wells were used to constrain the modeling of the specific flow paths which include those wells. The reactive or exchangeable phases used in the models include calcite, dolomite, volcanic glass, feldspar, clay (illite and smectite), zeolite, silica, pyrite, gypsum, biotite, carbon dioxide (CO₂) gas, chloride ion, and Ca/Mg-Na ion exchange. The chemical compositions of the volcanic glass, feldspar, clay, zeolite, and biotite represent average compositions for these phases measured on samples from each HSU. For flow paths where groundwater moves through more than one HSU, or wells where EOI(s) is hosted by multiple HSUs, a composite chemical composition was

calculated for each mineral phase using the compositions of the individual phases from each HSU present. A detailed description of the construction process and the limitations of geochemical models is found in Thomas et al. (2002). An updated discussion of the modeling process, which includes the ER-EC wells, is provided in Rose et al. (2002).

The results from successful NETPATH geochemical models for flow paths identified using conservative tracers are summarized in [Table 10-4](#). Complete NETPATH modeling results are included in Rose et al. (2002). NETPATH calculates the percentages of the different source waters required to make the target groundwater composition based on best fit to the major-ion chemistry. This approach differs from mixing models defined based on best fit to conservative tracers as indicated by Rose et al. (2002) and discussed in [Section 10.5.3](#) of this report. Rather than calculating the optimal mixture of groundwater and recharge sources required to produce the final mixed composition, NETPATH calculates the mixing ratios on the basis of largely non-conservative parameters that can be influenced by chemical reactions that occur along the flow path. As discussed by Rose et al. (2002) and summarized in [Table 10-4](#), the final mixing ratios of the contributory end-members calculated using NETPATH tend to overlap with and occasionally differ somewhat from those calculated using conservative tracers. These differences have been attributed (Rose et al., 2002) to differences in the respective geochemical modeling approaches and validation criteria. These differences are, however, considered (Rose et al., 2002) to be consistent with observed local variability in groundwater chemistry.

As described by Thomas et al. (2002) and Rose et al. (2002), valid NETPATH mixing models must have predicted final water compositions with calculated δD values within 3 per mil (parts per thousands) of the observed value in the target well. Final calculated Cl and SO₄ values are required to be equal to or less than the observed concentration in the target well. If these criteria are met, then the mineral saturations calculated by NETPATH are checked. Valid NETPATH models are those in which predicted mineral dissolution and precipitation behavior is in accordance with aqueous speciation calculations and micrographic observations of aquifer materials.

Once a valid geochemical model has been defined for a given flow path, a geochemically based estimate of groundwater travel time along that flow path can be calculated. As discussed in Rose et al. (2002) and Thomas et al. (2002) estimated travel times vary depending on the $\delta^{13}C$ composition of calcite in equilibrium with groundwater. Rose et al. (2002) use a range in $\delta^{13}C$ values for aquifer calcite from lightest (most negative) to heaviest (most positive) value measured along the flow path to calculate a range in travel times. This approach accommodates the natural variability in calcite $\delta^{13}C$ values observed within individual boreholes and individual HSUs. In the NETPATH modeling conducted in the PM-OV flow system, allowable CO₂ gas exchange was limited to the addition of up to 0.20 millimoles (mmoles) of CO₂ gas (more in areas of local recharge) to groundwater and the exsolution of CO₂ gas from groundwater in spring areas.

Table 10-4
Summary of Geochemical Flow Path Model Results for the Pahute Mesa-Oasis Valley Flow System from Rose et al., 2002

Flow Path Designation and Description	Groundwater and/or recharge source and contributory fraction (with flowpath target)								Apparent Travel Time (yrs)
	Pahute Mesa Groundwater from East of the Purse Fault	Pahute Mesa Groundwater from West of the Purse Fault	Gold Flat/TTR/Tolicha Peak	Timber Mountain Area	Local Recharge	Oasis Valley	Amargosa Valley	Crater Flat	
Flow Path 1 Pahute Mesa groundwater + local recharge = Oasis Valley groundwater									
Conservative Tracers	0.45 - 0.56	0.39 - 0.42			0.02 - 0.16	Target			
NETPATH	0.39 - 0.57	0.29 - 0.56			0.05 - 0.14	Target			> 1,000 to 3,900
Flow Path 2 Pahute Mesa groundwater + Gold Flat/TTR groundwater + local recharge = Oasis Valley groundwater									
Conservative Tracers	0.09 - 0.12	0.24 - 0.50	0.34 - 0.60		0.33 - 0.42	Target			
NETPATH	0.10 - 0.83	0.10 - 0.40	0.17 - 0.72			Target			> 1,000 to 2,300
Flow Path 3 Tolicha Peak +/- Pahute Mesa groundwater +/- Gold Flat/TTR groundwater +/- local recharge = Oasis Valley groundwater									
Conservative Tracers		0.23 - 0.27	0.73 - 0.77			Target			
NETPATH			1			Target			1,500
Flow Path 4 Pahute Mesa groundwater + local recharge (in Timber Mtn area) = Beatty Wash to Oasis Valley discharge area									
Conservative Tracers	0.47 - 0.53	0.22 - 0.23		0.24 - 0.31		Target			
NETPATH	0.00 - 0.76			0.24 - 1.0		Target			> 1,000 to 1,600
Flow Path 5 Pahute Mesa groundwater + local recharge = flow down Fortymile Wash toward the Amargosa Valley									
Conservative Tracers	0.13 - 0.39			0.05 - 0.29	0.56 - 0.57		Target		
NETPATH	0.08 - 0.37			0.32 - 0.65	0.14 - 0.54		Target		1,000 to 3,800
Flow Path 6 Pahute Mesa groundwater + local recharge = Crater Flat^a									
Conservative Tracers	0.44 - 0.57	0.00 - 0.02		0.20 - 0.54	0.00 - 0.22			Target	
NETPATH								Target	

^aNo Valid NETPATH models were obtained for flow path 6, for discussion see Rose et al., 2002

As shown in [Table 10-4](#), NETPATH modeling results from Rose et al. (2002) often produce "modern" groundwater travel times. However, as discussed in Thomas et al. (2002) and Rose et al. (2002), these results do not necessarily imply rapid groundwater flow. The apparent "modern" travel times are interpreted to be a consequence of the relatively small variations in ^{14}C within the flow system. This is complicated by the dissolution of calcite along the flow path and introduction of "dead" carbon to groundwater. Hence, most of the apparent "aging" of the groundwater along flow paths is interpreted (Rose et al., 2002) to simply reflect calcite dissolution. Given the complexity of carbon behavior in the PM-OV flow system, it is difficult to obtain more precise travel time estimates using DIC. Analytical uncertainties in the ^{14}C measurements (± 1 pmc) compound this problem by introducing a significant level of uncertainty to travel times estimated between locations with allow contrast in ^{14}C abundance. Accordingly, "modern" travel times reported calculated by Rose et al. (2002) have been assigned an effective travel time of less than 1,000 years in [Table 10-4](#).

10.5.4.2 Geochemical Modeling Results Using NETPATH

The results of NETPATH geochemical models for the six conceptual flow paths identified by Rose et al. (2002), and defined in [Table 10-2](#), are summarized (along with the results from the conservative tracer modeling) in [Table 10-4](#). These flow paths are illustrated in [Figure 10-2](#).

The NETPATH program calculates the changes in major ion chemistry that occur along a flow path, and determines groundwater-mixing ratios on the basis of chemical mass balance relationships. The models generated by Rose et al. (2002), incorporating new data from the ER-EC wells, provide generally consistent results using both NETPATH and the conservative tracer models presented earlier in this report ([Section 10.5.3.2](#)). The variation between results generated by these two methodologies is considered (Rose et al., 2002) to reflect differences in the approach of the two modeling techniques. This variation is also consistent with the natural variability in water chemistry within the system. Whereas the wells used as mixing "end-members" in the respective models are specific in composition, the groundwater compositions within each end-member sub-region or source area of the flow system are more variable, and cannot be completely described using specific individual wells.

Five of six potential groundwater flow paths identified by Rose et al. (2002) using conservative tracers ([Figure 10-2](#)) also had valid NETPATH models. Valid NETPATH models were not obtained for flow path 6, which considered southerly groundwater flow from Pahute Mesa to the Crater Flat area. Rose et al. (2002) conclude that insufficient data are available at this time to adequately determine the viability of this flow path. Groundwater travel time estimates generated using $\delta^{13}\text{C}$ mass balance calculations in NETPATH for flow paths 1 through 5 range from less than 1,000 to 4,200 years.

10.6 Other Considerations

The detailed evaluation of geochemical data, in the course of flow path analysis, has extended downgradient to the south and southwest to the southern border of the NTS and the Oasis Valley, respectively. This analysis has focused on a selected data subset, defined and screened based on the data quality and data completeness criteria required for this purpose. In order to place this data subset (as described above in [Section 10.5.1](#)) into context within the larger regional dataset, we can consider the larger body of major ion data. In order to facilitate presentation of major ion data from the hundreds of individual sample locations (including the flow path evaluation data subset previous described in [Section 10.5.1](#)), three Piper diagrams have been prepared for the Pahute Mesa region. [Figure 10-8](#) includes locations within areas 19 and 20 on Pahute Mesa and upgradient locations in the Kawich and Cactus Ranges, and Cactus and Gold Flats. While locally elevated chloride and/or sulfate concentrations are evident, these data define a highly coherent trend of compositional consistency. [Figure 10-9](#) shows a Piper diagram which includes the data from [Figure 10-8](#) augmented by down gradient data from the Yucca Mountain, Crater Flat, and Amargosa Desert areas to the south. [Figure 10-9](#) shows two distinct divergent trends in this down gradient area based on both cation and anion distributions. A continuation of the trend defined in [Figure 10-8](#) is also accompanied by a divergent trend toward higher magnesium (relative to calcium) concentrations and a trend toward increased sulfate concentrations (relative to chloride). These trends support the projection of distinct regional flow paths to the south. [Figure 10-10](#) shows a Piper diagram which includes the data from [Figure 10-8](#) augmented by downgradient data from the ER-EC wells, Oasis Valley locations, and Death Valley locations to the southwest. [Figure 10-10](#) also shows two compositional trends in this area. While these trends are compositionally similar to those defined in [Figure 10-9](#), the tendency toward relative magnesium and sulfate enrichment is not as distinct. This suggests that groundwater flow to the southwest may occur along a less heterogeneous pathway. A quantitative geochemical evaluation of the continuity of the relatively well defined southwesterly flow path from Pahute Mesa to Oasis Valley has not been done. This would require a thorough evaluation of water quality data between Oasis Valley and Death Valley. Steinkampf and Werrell (2001) indicate that (based on composition and stable isotope signatures) probable source areas for spring discharge in parts of the Funeral Mountains and Grapevine Mountains in Death Valley lie east and/or northeast of the Amargosa Range. While this is consistent with and would include groundwater flow from the PM-OV area, an assessment of the water sources, pathways, and time scales for flow toward Death Valley has not been performed.

10.7 Limitations

There is an irregular distribution of wells that have been sampled for the parameter suite necessary to support geochemical flow path analysis and characterization. To date, the geochemical evaluation of groundwater in the Pahute Mesa area has focused primarily on the shortest potential flow path (Pahute Mesa to Oasis Valley) between the underground testing areas and off-site water users (e.g., Rose et al., 2002; Thomas et al., 2002; White and Chuma, 1987). This

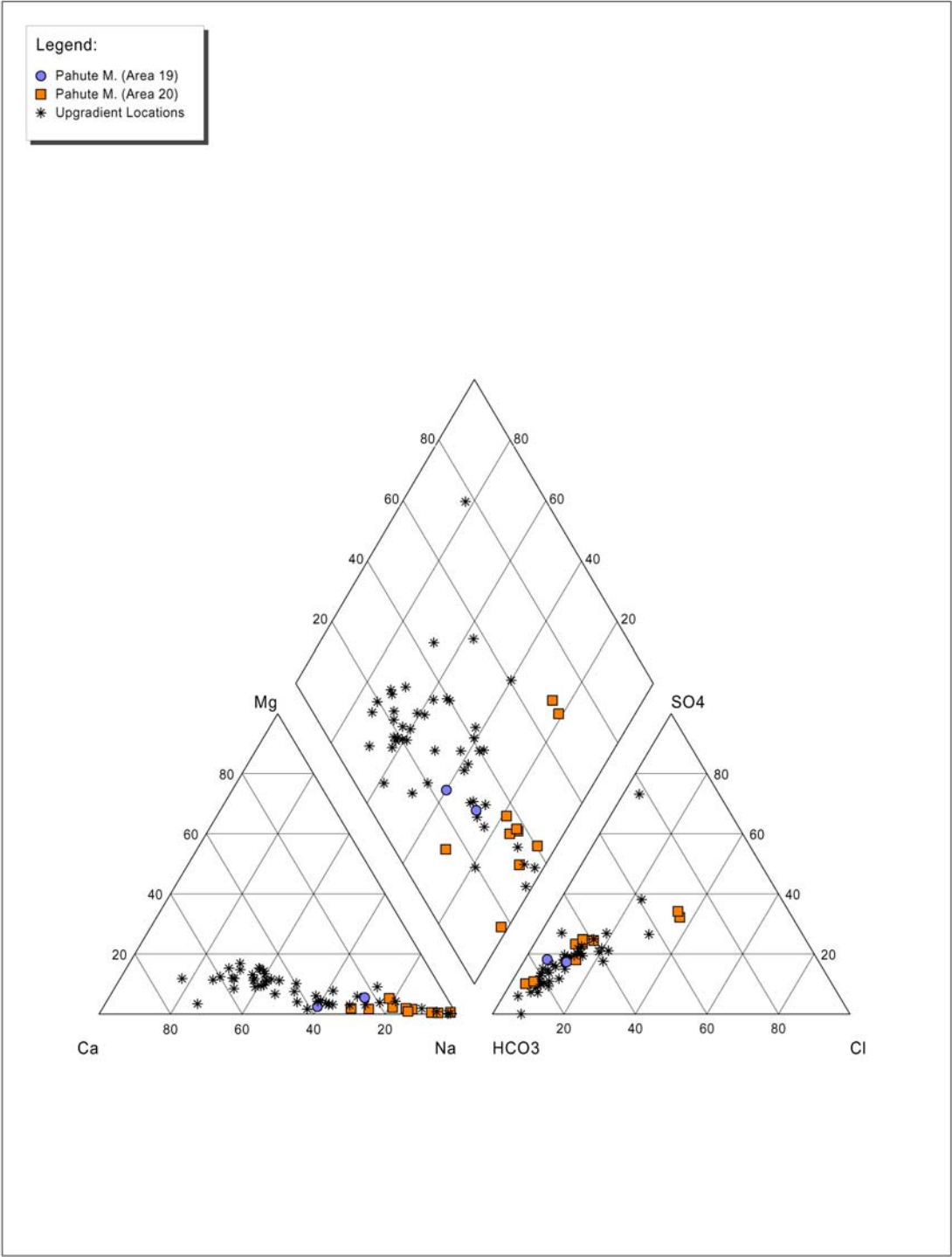


Figure 10-8
Piper Diagram of Major-ion Variations for Pahute Mesa and Upgradient Locations

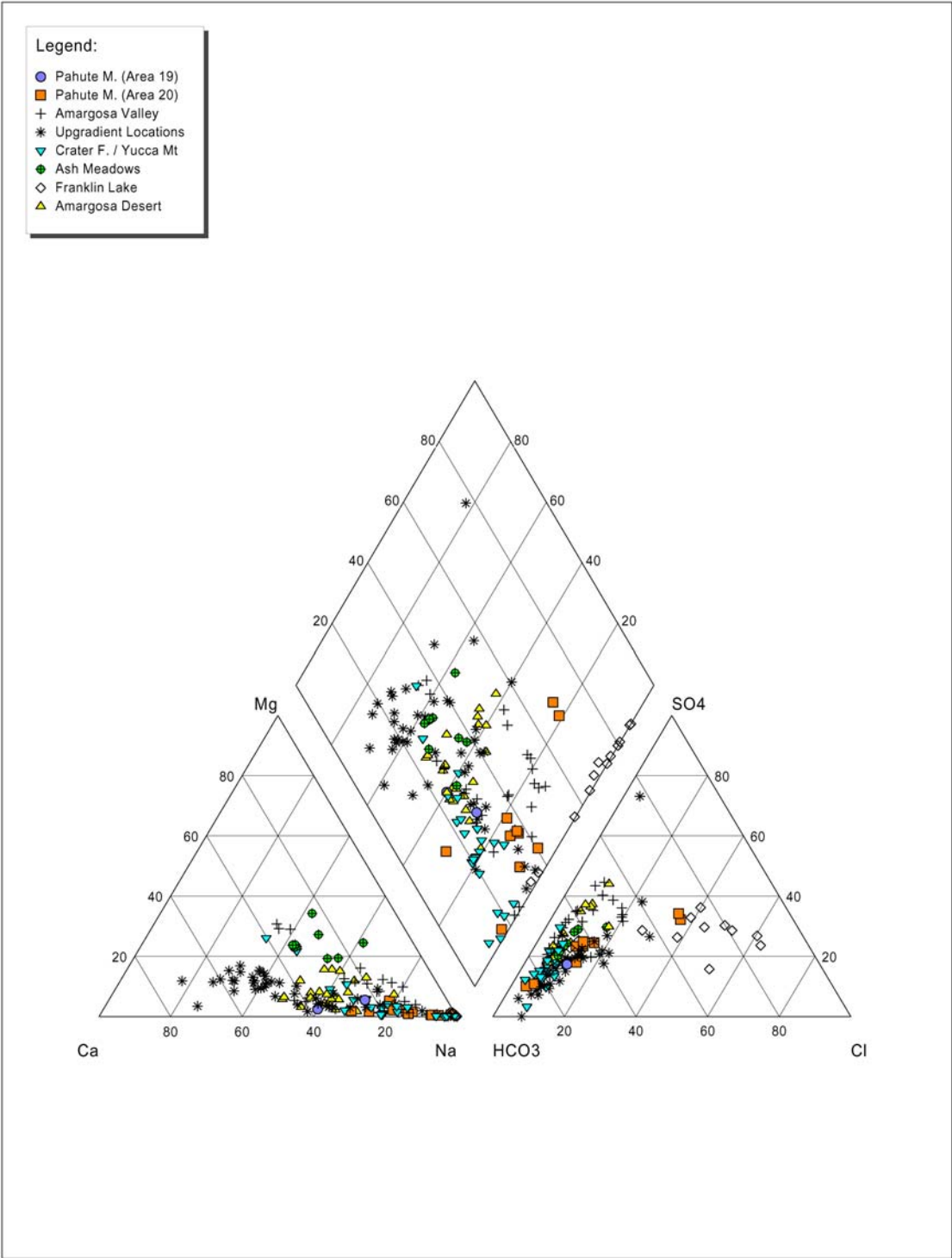


Figure 10-9
Piper Diagram of Major-ion Variations for Crater Flat, Yucca Mountain,
and Amargosa Desert Locations

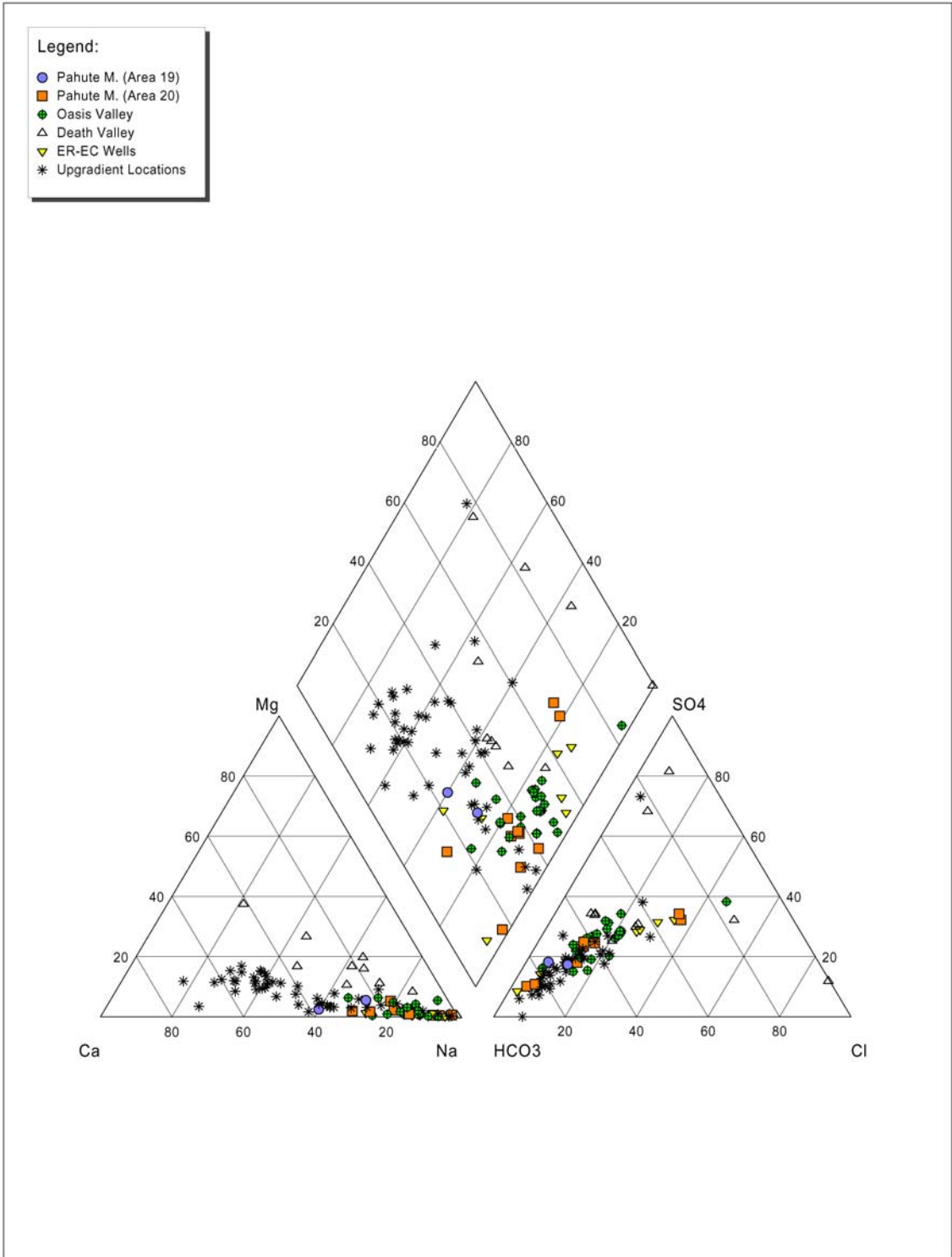


Figure 10-10
Piper Diagram of Major-ion Variations for the ER-EC Wells, Oasis Valley, and Death Valley Locations

evaluation process has been supported by the installation and sampling of additional new wells in this area (ER-OV and ER-EC wells). Several other potential flow paths for groundwater movement away from Pahute Mesa have been identified using geochemical data. The characterization of these other flow paths has been accomplished with a less complete and/or more sparsely distributed dataset. Accordingly, there are greater uncertainties associated with the groundwater source identification, mixing calculations, influence of water-rock interaction processes, and groundwater travel times determined using geochemical data for these other flow paths.

Current well placements have limited capabilities to support geochemical characterization of regional groundwater inflow from the Kawich Valley and/or Gold Flat-Cactus Flat areas. Other water budget components that are not well defined by existing geochemical data include recharge in the Timber Mountain, Beatty Wash, and Thirsty Canyon areas. While assumptions have been made that allow for existing data to proxy for these water budget components, uncertainties in the geochemical characteristics of these water budget components propagate into geochemically based mixing models.

Available water quality data provide limited insights into vertical groundwater variability. Flow logging has demonstrated that, within multiple completion wells or wells with large effective open intervals that cross multiple HSUs, water production is often dominated by a single HSU. Corresponding depth discrete water quality sample data are very sparse. Geochemical evaluations have, therefore, not been able to derive maximum benefit from the flow logging results. Most existing wells have effective open intervals constructed across multiple hydrostratigraphic units. Depth-discrete samples have not been systematically collected from existing multiple completion wells or analyzed for the suite of geochemical parameters necessary to support the evaluation of water sources, flow paths, or time scales of movement.

10.8 Summary

The chemistry of groundwater in the Pahute Mesa area has been shown to reflect interactions between regional groundwater flow and local hydrogeologic conditions. As shown in Rose et al. (2002) and Thomas et al. (2002), these result in local variations that are observed in the distributions of major ion, conservative tracer, and minor and trace element data. These variations are attributed to chemically distinct sources of regional groundwater underflow, local recharge, and processes of water-rock interaction within localized areas of hydrothermal alteration. These observations have been better defined as a result of the installation and sampling of the ER-EC wells (IT, 1998c) and are consistent with previous interpretations (e.g., Schoff and Moore, 1964; Winograd and Friedman, 1972; Blankennagel and Weir, 1973; Winograd and Thordarson, 1975; Winograd and Pearson, 1976; Claassen and White, 1979; White, 1979; White et al., 1980; White and Chuma, 1987; Chapman and Lyles, 1993; and Thomas et al., 1996).

Trends in major ion and stable isotope chemistry indicate that regional groundwater underflow components mix with local recharge and flow to the south

and/or southwest along a number of plausible flow paths. During groundwater flow, water-rock interaction with areas of hydrothermal alteration in volcanic rocks and increasingly common areas of carbonate rock (to the south and southwest toward Ash Meadow and Death Valley respectively), water chemistry shows increasing trends in relative sulfate, calcium, magnesium, and total dissolved solids concentrations. While these trends are generally consistent with the detailed analysis of the PM-OV flow system (Rose et al., 2002; Thomas et al., 2002), the evaluation of specific flow paths for movement of Pahute Mesa groundwater has not been extended to the southwest beyond Oasis Valley or to the south beyond the NTS border.

The detailed evaluation of the Pahute Mesa-Oasis Valley flow system, conducted by Rose et al. (2002), indicates that the earlier conceptual model for the area of interest is generally consistent with new data from the ER-EC wells and other recent samples. There are, however, several specific observations that are emphasized by Rose et al. (2002) on the basis of the new data.

1. Groundwater in upper Thirsty Canyon, west of the Purse Fault, is geochemically distinct from groundwater in central Pahute Mesa. These two distinct water masses occur along either side of the Purse Fault, and are spatially associated with a major discontinuity that has been identified in water levels in this area. Down gradient from this discontinuity, groundwater conservative tracer concentrations are intermediate to the two "end-members." This suggests that mixing of the end members may be taking place in this area.
2. Tritium was not observed in any of the ER-EC wells, indicating that detectable amounts of recent groundwater recharge is not present in samples from these wells.
3. All of the ER-EC wells in the Thirsty Canyon region have relatively low dissolved inorganic ^{14}C values and heavy $\delta^{13}\text{C}$ values indicating extensive water-rock reaction with secondary calcite. Substantial mixing with is observed in the Oasis Valley discharge area, locally within Beatty Wash, and along Fortymile Wash.
4. Helium isotope data support the conclusion that deep-seated faults are contributing a significant amount of mantle helium to the groundwater system in the Oasis Valley - Thirsty Canyon region.
5. Minor and trace element data (including the concentration and isotopic ratios of naturally occurring uranium) reflect more localized geochemical processes. The distribution of these data is locally consistent with possible southerly flow paths through the area.

Six conceptual flow path models were tested by Rose et al. (2002) using conservative tracer and water-rock reaction modeling techniques. Groundwater discharge in central Oasis Valley can be modeled as a three-component mixture consisting of 29 to 47 percent groundwater from western Pahute Mesa in upper Thirsty Canyon (west of the Purse Fault), 45 to 57 percent groundwater from central Pahute Mesa (east of the Purse Fault), and between 0 and 16 percent local recharge, presumably in Thirsty Canyon Wash. Assuming a groundwater discharge rate of 6,100 ac-ft/yr in Oasis Valley (Reiner et al., 2002), these mixing ratios imply that approximately 2,750 to 3,500 ac-ft of the annual discharge in

Oasis Valley originates from the underground testing area beneath Pahute Mesa. Consistent water-rock reaction models were also obtained for this flow path, and groundwater travel times based on modeled dissolved inorganic ^{14}C values range from less than 1,000 to 2,900 years. While this model is strongly supported by the existing data, it does not necessarily represent a unique or exclusive description of the flow system.

Rose et al. (2002) also identified a number of additional potential flow paths along which flux of significant amounts of Pahute Mesa groundwater is likely to occur. These alternatives have variable degrees of uncertainty reflecting the amount, distribution, and quality of data that are available to constrain them. For example, geochemical models were successfully developed for Oasis Valley discharge reflecting mixtures of regional inflow from the north with Pahute Mesa groundwater. However, the composition of groundwater influx from the north is relatively poorly constrained by the existing well locations, and these model results exhibit higher levels of uncertainty than the models for direct groundwater flow from Pahute Mesa to Oasis Valley. Southerly groundwater flow along Fortymile Canyon has been successfully modeled as a mixture of local recharge with a small component of central Pahute Mesa groundwater. Groundwater flow from central Pahute Mesa to the Crater Flat area was also evaluated, and although successful NETPATH models (and ^{14}C travel time estimates) were not obtained, several conservative geochemical parameters suggest this flow path may be plausible. Modeled ^{14}C groundwater travel times for all Pahute Mesa flow paths are less than 4,200 years. It should be noted that the apparent travel times indicated are HCO_3 travel times and that these times will have been subject to the influence of matrix diffusion and should be considered as maximum water travel times. In a number of cases, calculated travel times are below the resolution of the ^{14}C dating system.

11.0 References

ASTM, see American Society for Testing and Materials.

American Society for Testing and Materials. 1993a. *Standard Guide for Application of a Ground-Water Flow Model to a Site-Specific Problem*, ASTM D 5447-93. Philadelphia, PA.

American Society for Testing and Materials. 1993b. *Standard Guide for Comparing Ground-Water Flow Model Simulations to Site-Specific Information*, ASTM D 5490-93. Philadelphia, PA.

American Society for Testing and Materials. 1994a. *Standard Guide for Defining Boundary Conditions in Ground-Water Flow Modeling Designation*, ASTM D 5609-94. Philadelphia, PA.

American Society for Testing and Materials. 1994b. *Standard Guide for Defining Initial Conditions in Ground-Water Flow Modeling*, ASTM D 5610-94. Philadelphia, PA.

American Society for Testing and Materials. 1994c. *Standard Guide for Conducting a Sensitivity Analysis for a Ground-Water Flow Model Application*, ASTM D 5611-94. Philadelphia, PA.

American Society for Testing and Materials. 1995. *Standard Guide for Documenting a Ground-Water Flow Model Application*, ASTM D 5718-95. Philadelphia, PA.

American Society for Testing and Materials. 1996. *Standard Guide for Calibrating a Ground-Water Flow Model Application*, ASTM D 5981-96. Philadelphia, PA.

Anderson, J.R., E.E. Hardy, J.T. Roach, and R.E. Witmer. 1976. *A Land Use and Land Cover Classification System for use with Remote Sensor Data*, Professional Paper 964, p 28. Denver, CO: U.S. Geological Survey.

Andraski, B.J. 1997. "Soil-water Movement Under Natural-site and Waste-site Conditions—a Multiple-year Field Study in the Mojave Desert, Nevada." In *Water Resources Research*, v. 33, no. 8, p. 1901–1916. Washington, DC: American Geophysical Union.

BN, see Bechtel Nevada.

- Bechtel Nevada. 1996. Nevada Test Site Region Image Map, SIGIS-NTS-96038. Las Vegas, NV: Remote Sensing Laboratory.
- Bechtel Nevada. 2002. *Hydrostratigraphic Model and Alternatives for the Groundwater Flow and Contaminant Transport Model of Corrective Action Units 101 and 102: Central and Western Pahute Mesa, Nye County, Nevada*, DOE/NV/11718-646. Prepared for U.S. Department of Energy, National Nuclear Security Administration Nevada Operations Office. Las Vegas, NV.
- Benedict, F.C., Jr., T.P. Rose, and X. Zhou. 2000. *Mineralogical, Chemical, and Isotopic Characterization of Fracture-coating Minerals in Borehole Samples From Western Pahute Mesa and Oasis Valley, Nevada*. Prepared for U.S. Department of Energy, Nevada Operations Office. Livermore, CA: Lawrence Livermore National Laboratory.
- Benjamin, J.R., and Cornell, C.A. 1970. *Probability, Statistics, and Decision for Civil Engineers*. New York, NY: McGraw-Hill Book Co.
- Blankennagel, R.K. 1967. *Hydraulic Testing Techniques of Deep Drill Holes at Pahute Mesa, Nevada Test Site*. Washington, DC: U.S. Geological Survey
- Blankennagel, R.K., and J.E. Weir, Jr. 1973. *Geohydrology of the Eastern Part of Pahute Mesa, Nevada Test Site, Nye County, Nevada*, Professional Paper 712-B. Denver, CO: U.S. Geological Survey.
- Bowen, I.S. 1926. "The Ratio of Heat Losses by Conduction and by Evaporation from any Water Surface." In *Physical Review*, v. 27, p. 779-787. New York, NY: American Physical Society.
- Burchfiel, B.C., R.J. Fleck, D.T. Secor, R.R. Vincelette, and G.A. Davis. 1974. "Geology of the Spring Mountains, Nevada." In *Geological Society of America Bulletin*, 85(7): 1013-1022. Boulder, CO: Geological Society of America, Inc.
- CRWMS M&O, see Civilian Radioactive Waste Management System Management and Operating Contractor.
- Chapman, J.B., and B.F. Lyles. 1993. *Groundwater Chemistry at the Nevada Test Site: Data and Preliminary Interpretations*, Publication No. 45100. Las Vegas, NV: Desert Research Institute.
- Civilian Radioactive Waste Management System Management and Operating Contractor. 1997. *ISM2.0: A 3D Geologic Framework and Integrated Site Model of Yucca Mountain*, B00000000-0717-5700-004, Rev. 00. Las Vegas, NV.
- Civilian Radioactive Waste Management System Management and Operating Contractor. 2000a. Calibration of the Site-Scale Saturated Zone Flow Model, MDL-NBS-HS-000011, REV 00. Las Vegas, NV.

- Civilian Radioactive Waste Management System Management and Operating Contractor. 2000b. *Integrated Site Model Process Report*, TDR-NBS-GS-000002, REV 00, ICN 01. Prepared for the U.S. Department of Energy, Yucca Mountain Site Characterization Office by TRW Environmental Safety Systems, Inc. Las Vegas, NV.
- Classen, H.C., and A.F. White. 1979. "Application of Geochemical Kinetic Data to Ground-water Systems: A Tuffaceous-Rock System in Southern Nevada." In *Chemical Modeling in Aqueous Systems*, American Chemical Society Symposium Series No. 93, p. 771-793.
- Coache, R.A. 1999. *Las Vegas Valley Water Usage Report*. Clark County, NV: Nevada Division of Water Resources.
- Cook, P., and J.K. Bohlke. 2000. "Determining Timescales for Groundwater Flow and Solute Transport." In *Environmental Tracers in Subsurface Hydrology*, pp.1-30. Boston, MA: Kluwer.
- Craig, H. 1961. "Isotopic Variations in Meteoric Waters." In *Science*, 26 May, Vol. 133, p. 1702-1703. Washington, DC: American Association for the Advancement of Science.
- Czarnecki, J.B. 1985. *Simulated Effects of Increased Recharge on the Ground-Water Flow System of Yucca Mountain and Vicinity, Nevada-California*, Water-Resources Investigations Report 84-4344. Denver, CO: U.S. Geological Survey.
- Czarnecki, J.B. 1997. *Geohydrology and Evapotranspiration at Franklin Lake Playa, Inyo County, California, with a Section on Estimating Evapotranspiration using the Energy-Budget Eddy-correlation Technique by Stannard, D.I.*, Water-Supply Paper 2377, p 75. Denver, CO: U.S. Geological Survey.
- DOE, see U.S. Department of Energy.
- DOE/NV, see U.S. Department of Energy, Nevada Operations Office.
- Daley, C., R.P. Nielson, and D.L. Phillips. 1994. "A Statistical-Topographic Model for Mapping Climatological Precipitation over Mountainous Terrain." In *Journal of Applied Meteorology*, 33:140-158. Boston, MA: American Meteorological Society.
- Dash, Z.V. 2000. *Validation Test Report (VTR) for the FEHM Application Version 2.10, Yucca Mountain Project Identification Numbers SAN: LANL-1999-046; STN: 10086-2.10-00*. Los Alamos, NM: Los Alamos National Laboratory.

- Dash, Z.V. 2001. *Validation Test Report (VTR) for the FEHM Application Version 2.12, Yucca Mountain Project Identification Numbers SAN: LANL-2001-133; STN: 10086-2.12-00*. Los Alamos, NM: Los Alamos National Laboratory.
- Dash, Z.V., B.A. Robinson, and G.A. Zyvoloski. 1997. *Software Requirements, Design, and Verification and Validation for the FEHM Application - A Finite-Element Heat- and Mass-Transfer Code*, LA-13305-MS. Los Alamos, NM: Los Alamos National Laboratory.
- Decision Engineering. 1996. *Crystal Ball Software*, Version 4.0 for Windows. Denver, CO.
- DeMeo, G.A., R.J. Laczniaik, and W.E. Nylund. 1999. "Estimating Evapotranspiration Rates in Death Valley, California." In *Proceedings of Conference on Status of Geologic Research and Mapping in Death Valley National Park, Las Vegas, Nevada*, April 9-11, Open-File Report 99-153, p. 68. Denver, CO: U.S. Geological Survey.
- Dettinger, M.D. 1989. "Reconnaissance Estimates of Natural Recharge to Desert Basins in Nevada, U.S.A., by using Chloride-Balance Calculations." In *Journal of Hydrology*, Vol. 106: 55-78. New York, NY: Elsevier Publishing Co.
- Drellack, S.L., and L.B. Prothro. 1997. *Descriptive Narrative for the Hydrogeologic Model of Western and Central Pahute Mesa Corrective Action Units*. Las Vegas, NV: Geology/Hydrology Group, Geotechnical Services, Bechtel Nevada.
- Drellack, S.L., L.B. Prothro, K.E. Roberson, B.A. Schier, and E.H. Price. 1997. *Analysis of Fractures in Volcanic Cores from Pahute Mesa, Nevada Test Site*, DOE/NV/11718-160. Las Vegas, NV: Bechtel Nevada.
- Dynamic Graphics, Inc. 2002. *EarthVision 7: Software for 3-D Modeling and Visualization*. Alameda, CA.
- Eakin, T.E., G.B. Maxey, T.W. Robinson, J.C. Fredericks, and O.J. Loeltz. 1951. "Contributions to the Hydrology of Eastern Nevada." In *Water Resources Bulletin*, No. 12. Carson City, NV: State of Nevada, Office of the State Engineer, U.S. Geological Survey.
- Eriksson E., and V. Khunakasem. 1969. "Chloride Concentrations in Groundwater, Recharge Rate and Rate of Deposition of Chloride in the Israel Coastal Plain." In *Journal of Hydrology*, 7:178-197. New York, NY: Elsevier Publishing Company.
- FFACO, see *Federal Facility Agreement and Consent Order*.

- Federal Facility Agreement and Consent Order*. 1996 (as amended). Agreed to by the State of Nevada, the U.S. Department of Energy, and the U.S. Department of Defense.
- Fenelon, J.M. 2000. *Quality Assurance and Analysis of Water Levels in Wells on Pahute Mesa and Vicinity, Nevada Test Site, Nye County, Nevada*, USGS-WRIR 00-4014. Carson City, Nevada: U.S. Geological Survey.
- Ferguson, J.F., A.H. Cogbill, and R.G. Warren. 1994. "A Geophysical-Geological Transect of the Silent Canyon Caldera Complex, Pahute Mesa, Nevada." In *Groundwater*, Vol. 99 (B3): 4323-4339. Columbus, OH: Groundwater Publishing Co.
- Fouty, S.C. 1989. *Chloride Mass-balance as a Method for Determining Long-Term Groundwater Recharge Rates and Geomorphic-Surface Stability in Arid and Semi-Arid Regions, Whiskey Flat and Beatty, Nevada*, University of Arizona, Master of Science Thesis, p. 12, 3rd chp.
- Freeze, R.A., and J.A. Cherry. 1979. *Groundwater*. Englewood Cliffs, NJ: Prentice Hall.
- Freeze, R.A., J. Massmann, L. Smith, T. Sperling, and B. James. 1990. "Hydrogeological Decision Analysis: I. A Framework." In *Groundwater*, Vol. 28: (5) 738-766. Columbus, OH: Groundwater Publishing Co.
- French, R.H., Desert Research Institute. 1996. Memorandum to E. Jacobson, Desert Research Institute, regarding additional high altitude precipitation data, 21 August. Las Vegas, NV.
- Gable, C., and T. Cherry, Los Alamos National Laboratory. 2001. Technical Note on Interpolation of MODFLOW flux onto a piecewise linear surface. Los Alamos, NM: Los Alamos National Laboratory.
- Gay, L.W., and L.J. Fritschen. 1979. "An Energy Budget Analysis of Water Use by Saltcedar." In *Water Resources Research*, v. 15, no. 6, p. 1589-1592. Washington, DC: American Geophysical Union.
- George, D.C. 1997. *Unstructured 3D Grid Toolbox for Modeling and Simulation*, LA-UR-97-3052. Los Alamos, NM: Los Alamos National Laboratory.
- Guth, P.L. 1986. *Bedrock Geologic Map of the Black Hills, 1:24,000 Quadrangle, Nevada*, Open-File Map 86-438. Las Vegas, NV: U.S. Geological Survey.
- Hardman, G. 1936. *Nevada Precipitation and Acreages of Land by Rainfall Zones*, Bulletin 183. Reno, NV: U.S. Department of Agriculture, University of Nevada Experimental Station.
- Hardman, G. 1965. *Nevada Precipitation and Acreages of Land by Rainfall Zones*. Reno, NV: U.S. Department of Agriculture, University of Nevada Experimental Station.

- Harrill, J.R., J.S. Gates, and J.M. Thomas. 1988. "Major Groundwater Flow Systems in the Great Basin Region of Nevada, Utah, and Adjacent States." In *U.S. Geological Survey Hydrologic Investigations Atlas*, ATLAS-HA-694-C, Scale: 1,000,000. Denver, CO: U.S. Geological Survey.
- Hem, J.D. 1985. *Study and Interpretation of the Chemical Characteristics of Natural Water*, Water-Supply Paper 2254, 3rd. ed., p. 118. Denver, CO: U.S. Geological Survey.
- Hevesi, J.A., A.L. Flint, and L.E. Flint. 2003. *Simulation of Net Infiltration and Potential Recharge Using a Distributed Parameter Watershed Model for the Death Valley Region, Nevada and California*. Water-Resources Investigations Report 03-4090. Sacramento, CA: U.S. Geological Survey.
- Houser, F.N., R.E. Davis, and W.L. Emerick. 1961. *Geologic Reconnaissance of Granite Intrusive Masses at Gold Meadows, Tem Piute, and Trappman's Camp, Lincoln and Nye Counties, Nevada, and Comparison with Climax Stock of the Nevada Test Site*, USGS-TEI-793. Denver, CO: U.S. Geological Survey.
- Ingraham, N.L., R.L. Jacobson, J.W. Hess, and B.F. Lyles. 1990. Stable Isotopic Study of Precipitation and Spring Discharge on the Nevada Test Site, DOE/NV/10845-03, Publication No. 45078. Las Vegas, NV: Desert Research Institute.
- IT, see IT Corporation.
- IT Corporation. 1996a. *Groundwater Recharge and Discharge Data Documentation Package (Phase I Data Analysis Documentation, Volume III)*. Prepared for the U.S. Department of Energy, Nevada Operations Office. Las Vegas, NV.
- IT Corporation. 1996b. *Hydrologic Parameter Data Documentation Package (Phase I Data Analysis Documentation, Volume IV)*. Prepared for the U.S. Department of Energy, Nevada Operations Office. Las Vegas, NV.
- IT Corporation. 1996c. *Potentiometric Data Documentation Package (Phase I Data Analysis Documentation, Volume II)*. Prepared for the U.S. Department of Energy, Nevada Operations Office. Las Vegas, NV.
- IT Corporation. 1996d. *Regional Geologic Model Data Documentation Package (Phase I Data Analysis Documentation, Volume I)*. Prepared for the U.S. Department of Energy, Nevada Operations Office. Las Vegas, NV.
- IT Corporation. 1996e. *Transport Parameter and Source Term Data Documentation Package (Phase I Data Analysis Documentation, Volume V)*. Prepared for the U.S. Department of Energy, Nevada Operations Office. Las Vegas, NV.

- IT Corporation. 1996f. *Tritium Transport Model Documentation Package (Phase I Data Analysis Documentation, Volume VII)*. Prepared for the U.S. Department of Energy, Nevada Operations Office. Las Vegas, NV.
- IT Corporation. 1997a. *Groundwater Flow Model Documentation Package (Phase I Data Analysis Documentation, Volume VI)*. Prepared for the U.S. Department of Energy, Nevada Operations Office. Las Vegas, NV.
- IT Corporation. 1997b. *Risk Assessment Documentation Package (Phase I Data Analysis Documentation, Volume VIII)*. Prepared for the U.S. Department of Energy, Nevada Operations Office. Las Vegas, NV.
- IT Corporation. 1998a. *Report and Analysis of the BULLION Forced-Gradient Experiment*, ITLV/13052-042, DOE/NV-13-52. Las Vegas, NV.
- IT Corporation. 1998b. Summary of micrographic analysis of selected core samples from Well ER-20-6#1, in support of matrix diffusion testing, Rev. 0, September, ITLV/13052-048. Las Vegas, NV.
- IT Corporation. 1998c. Summary of micrographic analysis of fracture coating phases on drill cores from Pahute Mesa, Nevada Test Site, Rev. 1, December, ITLV/13052-050. Las Vegas, NV.
- IT Corporation. 1998d. *Value of Information Analysis for Corrective Action Units Nos. 101 and 102: Central and Western Pahute Mesa, Nevada Test Site, Nevada*, ITLV/13052-041. Prepared for the U.S. Department of Energy, Nevada Operations Office. Las Vegas, NV.
- IT Corporation. 1998e. Western Pahute Mesa – Oasis Valley Hydrogeologic Investigation Wells Drilling and Completion Criteria, Rev. 0, Report prepared for the U.S. Department of Energy, Nevada Operations Office, September, ITLV/13052-049, p. 439. Las Vegas, NV.
- IT Corporation. 1999. *Underground Test Area Project Corrective Action Unit 98: Frenchman Flat, Vol. II, Groundwater Data Documentation Package*, Rev. 0, DOE/NV/13052-044-V2. Prepared for U.S. Department of Energy, Nevada Operations Office. Las Vegas, NV.
- IT Corporation. 2002a. *Analysis of Well ER-EC-1 Testing, Western Pahute Mesa-Oasis Valley FY 2000 Testing Program*, Rev. 0, ITLV/13052--173, DOE/NV/13052--846. Las Vegas, NV.
- IT Corporation. 2002b. *Analysis of Well ER-EC-2a Testing, Western Pahute Mesa-Oasis Valley FY 2000 Testing Program*, Rev. 0, ITLV/13052--174, DOE/NV/13052--851. Las Vegas, NV.
- IT Corporation. 2002c. *Analysis of Well ER-EC-4 Testing, Western Pahute Mesa-Oasis Valley FY 2000 Testing Program*, Rev. 0, ITLV/13052--175, DOE/NV/13052--850. Las Vegas, NV.

- IT Corporation. 2002d. *Analysis of Well ER-EC-5 Testing, Western Pahute Mesa-Oasis Valley FY 2000 Testing Program*, Rev. 0, ITLV/13052--176, DOE/NV/13052--848. Las Vegas, NV.
- IT Corporation. 2002e. *Analysis of Well ER-EC-6 Testing, Western Pahute Mesa-Oasis Valley FY 2000 Testing Program*, Rev. 0, ITLV/13052--177, DOE/NV/13052--849. Las Vegas, NV.
- IT Corporation. 2002f. *Analysis of Well ER-EC-7 Testing, Western Pahute Mesa-Oasis Valley FY 2000 Testing Program*, Rev. 0, ITLV/13052--178, DOE/NV/13052--852. Las Vegas, NV.
- IT Corporation. 2002g. *Analysis of Well ER-EC-8 Testing, Western Pahute Mesa-Oasis Valley FY 2000 Testing Program*, Rev. 0, DOE/NV/13052--847, ITLV/13052--179. Las Vegas, NV.
- IT Corporation. 2002h. *Analysis of Well ER-18-2 Testing, Western Pahute Mesa-Oasis Valley FY 2000 Testing Program*, Rev. 0, ITLV/13052--172, DOE/NV/13052--845. Las Vegas, NV.
- IT Corporation. 2002i. GEOCHEM02.mdb - A comprehensive chemistry database for groundwater at the Nevada Test Site, Rev. 4, September. Las Vegas, NV.
- IT Corporation. 2002j. *Summary of Well Testing and Analysis, Western Pahute Mesa-Oasis Valley FY 2000 Testing Program*, Rev. 0, ITLV/13052--180, DOE/NV/13052--853. Las Vegas, NV.
- Jacobson, B., Desert Research Institute. 1996. Personal Communication from B. Jacobson to O. Drici (IT Corporation) regarding Precipitation Data, 20 September. Reno, NV.
- James, J.W. 1993. *Climate of the Death Valley Region, Nevada/California*. Prepared for the National Park Service. Reno, NV: State of Nevada, Office of the State Climatologist.
- Johnson, M.J. 1993. *Micrometeorological Measurements at Ash Meadows and Corn Creek Springs, Nye and Clark Counties, Nevada, 1986-87*, Open-File Report 92-650, p 41. Denver, CO: U.S. Geological Survey.
- Kane, M.F., M.W. Webring, and B.K. Bhattacharyya. 1981. *A Preliminary Analysis of Gravity and Aeromagnetic Surveys of the Timber Mountain Area, Southern Nevada*, Open-File Report 81-189. Denver, CO: U.S. Geological Survey.
- Laczniak, R.J., U.S. Geological Survey. 1996. Personal communication to O. Drici (IT Corporation) regarding groundwater discharge in Ash Meadows and Oasis Valley, 13 February. Las Vegas, NV.

- Laczniak, R.J., J.L. Smith, P.E. Elliott, G.A. DeMeo, M.A. Chatigny, and G. Roemer. 2001. *Ground-Water Discharge Determined from Estimates of Evapotranspiration, Death Valley Regional Flow System, Nevada and California*, USGS-WRIR 01-4195. Denver, CO: U.S. Geological Survey.
- Laczniak, R.J., G.A. DeMeo, S.R. Reiner, J.L. Smith, and W.E. Nylund. 1999. *Estimates of Ground-Water Discharge as Determined from Measurements of Evapotranspiration, Ash Meadows Area, Nye County, Nevada*, USGS-WRIR 99-4079: Denver, CO: U.S. Geological Survey.
- Laczniak, R.J., J.C. Cole, D.A. Sawyer, and D.A. Trudeau. 1996. *Summary of Hydrogeologic Controls on Ground-Water Flow at the Nevada Test Site, Nye County, Nevada*, USGS-WRIR-96-4109. Denver, CO: U.S. Geological Survey.
- Lahoud, R.G., D.H. Lobmeyer, and M.S. Whitfield, Jr. 1984. *Geohydrology of Volcanic Tuff Penetrated by Test Well UE-25b#1, Yucca Mountain, Nye County, Nevada*, USGS-WRIR 84-4253. Denver, CO: U.S. Geological Survey.
- Lee, C.H. 1912. *An Intensive Study of the Water Resources of a Part of Owens Valley, California*, Water-Supply Paper 294. Denver, CO: U.S. Geological Survey.
- Maldonado, F. 1977. *Summary of the Geology and Physical Properties of the Climax Stock, Nevada Test Site*, USGS-OFR-77-356. Denver, CO: U.S. Geological Survey.
- Malmberg, G.T. 1967. *Hydrology of the Valley-fill and Carbonate-rock Reservoirs Pahrump Valley, Nevada-California*, Water Supply Paper 1832. Denver, CO: U.S. Geological Survey.
- Malmberg, G.T., and Eakin, T.E. 1962. *Ground-Water Appraisal of Sarcobatus Flat and Oasis Valley, Nye and Esmeralda Counties, Nevada: Nevada Department of Conservation and Natural Resources, Ground-Water Resources-Reconnaissance Series Report 10, p 39*. Carson City, NV: U.S. Geological Survey.
- Maurer, D.K., D.L. Berger, and D.E. Prudic. 1996. *Subsurface Flow to Eagle Valley from Vicee, Ash, and Kings Canyons, Carson City, Nevada, Estimated from Darcy's Law and the Chloride-Balance Method*, USGS-WRIR 96-4088, p. 38. Denver, CO: U.S. Geological Survey.
- Maxey, G.B., and T.E. Eakin. 1949. *Groundwater in White River Valley, White Pine, Nye and Lincoln Counties, Nevada*, Water Resources Bulletin No. 8. Carson City, NV: State of Nevada, Office of the State Engineer.

- McKinley, P.W., M.P. Long, and L.V. Benson. 1991. *Chemical Analyses of Water From Selected Wells and Springs in the Yucca Mountain Area, Nevada and Southeastern California*, USGS Open-File Report 90-355. Denver, CO: U.S. Geological Survey.
- Moench, A.F. 1984. "Double-Porosity Models for a Fissured Groundwater Reservoir with Fracture Skin." In *Water Resources Research*, 20 (7), p. 831-846. Washington, D.C.: American Geophysical Union.
- Mook, W.G. 1980. "Carbon-14 in Hydrogeological Studies." In *Handbook of Environmental Isotope Geochemistry*, Volume 1, The Terrestrial Environment, pp 49-74. Amsterdam: A. Elsevier.
- Nichols, W.D. 1993. "Estimating Discharge of Shallow Groundwater by Transpiration from Greasewood in the Northern Great Basin." In *Water Resources Research*, v. 29, no. 8, p. 2771-2778. Washington, DC: American Geophysical Union.
- Nichols, W.D. 2001. *Regional Ground-Water Evapotranspiration and Ground-Water Budgets, Great Basin, Nevada*, Professional Paper 1628. Denver, CO: U.S. Geological Survey.
- Nichols, W.D., R.J. Laczniaik, G.A. Demeo, and T.R. Rapp. 1997. Estimated Ground-Water Discharge by Evapotranspiration, Ash Meadows Area, Nye County, Nevada, 1994 USGS WRIR 97-4025, p 13. Denver, CO: U.S. Geological Survey.
- Noble, D.C., G.D. Bath, R.L. Christiansen, and P.P. Orkild. 1968. *Zonal Relations and Paleomagnetism of the Spearhead and Rocket Wash Members of the Thirsty Canyon Tuff, Southern Nevada*, USGS Professional Paper 600C: C61-65. Denver, CO: U.S. Geological Survey.
- O'Hagan, M.D., and R.J. Laczniaik. 1996. *Ground-Water Levels Beneath Eastern Pahute Mesa and Vicinity, Nevada Test Site, Nye County, Nevada*, USGS-WRIR 96-4042. Denver, CO: U.S. Geological Survey.
- Orkild, P.P., K.A. Sargent, and R.P. Snyder. 1969. *Geologic Map of Pahute Mesa, Nevada Test Site and Vicinity, Nye County, Nevada*, USGS-MI-567. Denver, CO: U.S. Geological Survey.
- Pawloski, G.A., A.F.B. Tompson, and Carle, S., editors. 2001. *Evaluation of the Hydrologic Source Term from Underground Nuclear Tests on Pahute Mesa at the Nevada Test Site*, UCRL-ID-147023. Livermore, CA: Lawrence Livermore National Laboratory.
- Plummer, L.N., E.C. Prestemon, and D.L. Parkurst. 1994. *An Interactive Code (NETPATH) for Modeling Net Geochemical Reactions Along a Flow Path*, Version 2.0, USGS WRIR 94-4169. Denver, CO: U.S. Geological Survey.

- Prothro, L.B., and S.L. Drellack, Jr. 1997. *Nature and Extent of Lava-Flow Aquifers Beneath Pahute Mesa, Nevada Test Site*, DOE/NV-11718-156. Las Vegas, NV: Bechtel Nevada.
- Rehfeldt, K., W. Drici, D. Sloop, J. Watrus, T. Beard, M. Sully, C. Benedict, A. Wolfsbergand, P. Reimus. 2003. *Contaminant Transport Parameters for the Groundwater Flow and Contaminant Transport Model of Corrective Action Units 101 and 102: Central and Western Pahute Mesa, Nye County, Nevada*, Shaw/13052-201, Rev. 0. Las Vegas, NV: Shaw Environmental, Inc.
- Reiner, S.R., R.J. Laczniak, G.A. DeMeo, J. LaRue Smith, P.E. Elliott, W.E. Nylund, and C.J. Fridrich. 2002. *Ground-Water Discharge Determined from Measurements of Evapotranspiration, Other Available Hydrologic Components, and Shallow Water-Level Changes, Oasis Valley, Nye County, Nevada*, USGS-WRI-01-4239. Carson City, NV: U.S. Geological Survey.
- Robinson, T.W. 1958. *Phreatophytes*, Water-Supply Paper 1423. Denver, CO: U.S. Geological Survey.
- Rose, T.P., and M.L. Davisson. 2002. "Isotopic and Geochemical Evidence for Holocene-Age Groundwater in Regional Flow Systems of South-Central Nevada." In *Hydrologic Resources Management Program and Underground Test Area Project FY2000 Progress Report*, Report UCRL-ID-145167, PP. 99-139. Livermore, CA: Lawrence Livermore National Laboratory.
- Rose, T.P., F.C. Benedict, J.M. Thomas, W.S. Sicke, R.L. Hershey, J.B. Paces, I.M. Farnham, and Z.E. Peterman. 2002. *Geochemical Data Analysis and Interpretation of the Pahute Mesa - Oasis Valley Groundwater Flow System, Nye County, Nevada*. Lawrence Livermore National Laboratory report attached to a memorandum to files by W. Drici (Stoller-Navarro Joint Venture), February 23, 2004. Las Vegas, NV.
- Rubin, Y., and J.J. Gomez-Hernandez. 1990. "A Stochastic Approach to the Problem of Upscaling of Conductivity in Disordered Media: Theory and Unconditional Numerical Simulations." In *Water Resources Research*, 26(4), p. 691-701. Washington, DC: American Geophysical Union.
- Rush, F.E. 1970. *Regional Ground-Water Systems in the Nevada Test Site Area, Nye, Lincoln, and Clark Counties, Nevada*, Division of Water Resources, Reconnaissance Series, Report 54, p. 21. Carson City, NV: Nevada Department of Conservation and Natural Resources.
- Russell, C.E., and T. Minor. 2002. *Reconnaissance Estimates of Recharge Based on an Elevation-dependent Chloride Mass-balance Approach*, DOE/NV/11508-37. Prepared for the U.S. Department of Energy, National Nuclear Security Administration Nevada Operations Office. Las Vegas, NV: Desert Research Institute.

Systat, see Systat Software Inc.

Sanchez-Vila, X., P.M. Meier, and J. Carrera. 1999. "Pumping tests in heterogeneous aquifers: An analytical study of what can be obtained from their interpretation using Jacob's method", In *Water Resources Research*, 35(4), pp. 943-952. Washington, DC: American Geophysical Union.

Savard, C.S. 1994. "Groundwater Recharge in Fortymile Wash Near Yucca Mountain, Nevada, 1992-1993." In *Radioactive Waste Management*, Vol. 4: pp. 1,805-1,813. Washington, DC: American Nuclear Society.

Systat Software Inc. 1997. SYSTAT® Version: 7.01, Systat Software Inc. Richmond, CA. Webpage: <http://www.systat.com>, accessed on 7/24/2003.

Schoff, S.L., and J.E. Moore. 1964. *Chemistry and Movement of Ground Water, Nevada Test Site*, Report TEI-838, p. 75. Denver, CO: U.S. Geological Survey.

Scott, R.B., T.J. Smales, R.E. Rush, and A.S. Van Denburgh. 1971. *Water for Nevada, Nevada's Water Resources*, "State of Nevada Department of Conservation and Natural Resource, Water for Nevada Report 3." Carson City, NV: Nevada Division of Water Resources.

Slate, J.L., M.E. Berry, P.D. Rowley, C.J. Fridrich, K.S. Morgan, J.B. Workman, O.D. Young, G.L. Dixon, V.S. Williams, E.H. McKee, D.A. Ponce, T.G. Hildenbrand, W.C. Swadley, S.C. Lundstrom, E.B. Ekren, R.G. Warren, J.C. Cole, R.J. Fleck, M.A. Lanphere, D.A. Sawyer, S.A. Minor, D.J. Grunwald, R.J. Laczniak, C.M. Menges, J.C. Yount, and A.S. Jayko. 1999. *Digital Geologic Map of the Nevada Test Site and Vicinity, Nye, Lincoln, and Clark Counties, Nevada, and Inyo County, California*, USGS-OFR-99-554-A. Denver, CO: U.S. Geological Survey.

Snyder, R.P. 1977. *Geology of the Gold Meadows Stock, Nevada Test Site*, USGS-474-179 (Areas 12-26). Denver, CO: U.S. Geological Survey.

Steinkampf, W.C., and W.L. Werrell. 2001. *Ground-water Flow to Death Valley as Inferred from the Chemistry and Geohydrology of Selected Springs in Death Valley National Park, California and Nevada*, USGS-WRIR 98-4114, p. 37. Denver, CO: U.S. Geological Survey.

Thomas, J.M., A.H. Welch, and M.D. Dettinger. 1996. *Geochemistry and Isotope Hydrology of Representative Aquifers in the Great Basin Region of Nevada, Utah, and Adjacent States*, Professional Paper 1409-C, p. 100. Denver, CO: U.S. Geological Survey.

Thomas, J.M., F.C., Jr. Benedict, T.P. Rose, R.L. Hershey, J.B. Paces, Z.E. Peterman, I.M. Farnham, K.H. Johannesson, A.K. Singh, K.J. Stetzenbach, G.B. Hudson, J.M. Kenneally, G.F. Eaton, and D.K. Smith. 2002. *Geochemical and Isotopic Interpretations of Groundwater Flow in the Oasis Valley Flow System, Southern Nevada*, Water Resources Center, Publication 45190. Las Vegas, NV: Desert Research Institute.

USGS, see U.S. Geological Survey.

U.S. Department of Energy. 2000. Quality Assurance Requirements and Description. DOE/RW-0333P, Rev. 10. Washington, D.C.: U.S. Department of Energy, Office of Civilian Radioactive Waste Management. ACC: MOL.20000427.0422.

U.S. Department of Energy, Nevada Operations Office. 1997. *Regional Groundwater Flow and Tritium Transport Modeling and Risk Assessment of the Underground Test Area, Nevada Test Site, Nevada*, DOE/NV--477. Las Vegas, NV.

U.S. Department of Energy, Nevada Operations Office. 1999. *Corrective Action Investigation Plan for Corrective Action Units 101 and 102, Central and Western Pahute Mesa, Nevada Test Site, Nevada*, DOE/NV--516, Rev. 1. Las Vegas, NV.

U.S. Department of Energy, Nevada Operations Office. 2000a. *Underground Test Area Quality Assurance Project Plan, Nevada Test Site, Nevada*, DOE/NV-341, Rev. 3. Las Vegas, NV.

U.S. Department of Energy, Nevada Operations Office. 2000b. *United States Nuclear Tests, July 1945 through September 1992*, DOE/NV-209, Rev. 15. Las Vegas, NV.

U.S. Geological Survey. 1987. *Digital elevation models: U.S. Geological Survey, National Mapping Program Technical Instructions Data Users Guide 5*, p. 38. Denver, CO: U.S. Geological Survey.

U.S. Geological Survey. 2001. *National Water Information System (NWISWeb)*. As accessed at <http://waterdata.usgs.gov/nwis> on multiple occasions the latest being 15 October.

Vanmarcke, E. 1983. *Random Fields: Analysis and Synthesis*. Cambridge, MA: The MIT Press.

Wahl, R.R., D.A. Sawyer, S.A. Minor, M.D. Carr, J.C. Cole, W.C. Swadley, R.J. Laczniak, R.G. Warren, K.S. Green, and C.M. Engle. 1997. *Digital Geologic Map of the Nevada Test Site Area, Nevada*, Open-File Report 97-140. Denver, CO: U.S. Geological Survey.

Walker, G.E. 1962. *Ground Water in the Climax Stock, Nevada Test Site, Nye County, Nevada*, USGS-TEI-813. Denver, CO: U.S. Geological Survey.

- Walker, G.E., and T.E. Eakin. 1963. *Geology and Ground Water of Amargosa Desert, Nevada-California*, Ground-Water Resources - Reconnaissance Series Report 14. Denver, CO: Nevada Department of Conservation and Natural Resources and U.S. Geological Survey.
- Warren, R.G. 1994a. *Structural Elements and Hydrogeologic Units of the Southwestern Nevada Volcanic Field*. Los Alamos National Laboratory informal technical report prepared for the DOE/NV Underground Test Area Project, January 19. Los Alamos, NM.
- Warren, R.G., Los Alamos National Laboratory. 1994b. Written communication to Ed Price (GeoTrans), Subject: Structural Elements and Hydrogeologic Units of the Southwestern Nevada Volcanic Field. Attachment to Los Alamos National Laboratory letter, May, pp. 19, 4 figures, structural block model map, 2 cross sections. Los Alamos, NM.
- Warren, R.G., D.A. Sawyer, F.M. Byers, Jr., and G.L. Cole. 2000a. *A Petrographic/Geochemical Database and Stratigraphic and Structural Framework for the Southwestern Nevada Volcanic Field*, LA-UR-00-3791. Los Alamos, NM: Los Alamos National Laboratory.
- Warren, R.G., G.L. Cole, and D. Walther. 2000b. *A Structural Block Model for the Three-Dimensional Geology of the Southwestern Nevada Volcanic Field*, LA-UR-00-5866. Los Alamos, NM: Los Alamos National Laboratory Report.
- Watermark Computing, see Watermark Numerical Computing and Waterloo Hydrogeologic.
- Watermark Numerical Computing and Waterloo Hydrogeologic. 2000. *Visual PEST User's Manual (Includes PEST2000 & WinPEST) - Graphical Model-Independent Parameter Estimation*. Ontario, Canada, and Tampa, FL.
- Weeks, E.P., H.L. Weaver, G.S. Campbell, and B.D. Tanner. 1987. *Water Use by Saltcedar and by Replacement Vegetation in The Pecos River Flood Plain Between Acme and Artesia, New Mexico*, Professional Paper 491-G, p. 33. Denver, CO: U.S. Geological Survey.
- White, A.F. 1979. *Geochemistry of Ground Water Associated with Tuffaceous Rocks, Oasis Valley, Nevada*, Professional Paper 712-E. Denver, CO: U.S. Geological Survey.
- White, A.F., and N.J. Chuma. 1987. "Carbon and Isotopic Mass Balance Models of Oasis Valley-Fortymile Canyon Groundwater Basin, Southern Nevada." In *Water Resources Research*, Vol. 23, (4): 571-582. Washington, DC: American Geophysical Union.

- White, A.F., H.C. Claassen, and L.V. Benson. 1980. *The Effect of Dissolution of Volcanic Glass on the Water Chemistry in a Tuffaceous Aquifer, Rainier Mesa, Nevada*, Water-Supply Paper 1535-Q. Denver, CO: U.S. Geological Survey.
- White, W.N. 1932. *A Method of Estimating Ground-Water Supplies Based on Discharge by Plants and Evaporation from Soil*, Water-Supply Paper 659-A, p. 165. Denver, CO: U.S. Geological Survey.
- Winograd, I.J., and F.J. Pearson, Jr. 1976. "Major Carbon-14 Anomaly in a Regional Carbonate Aquifer: Possible Evidence for Megascale Channeling, South Central Great Basin." In *Water Resources Research*, 12, 1125-1143. Washington, DC: American Geophysical Union.
- Winograd, I.J., and I. Friedman. 1972. *Deuterium as a Tracer of Regional Groundwater Flow, Southern Great Basin, Nevada and California*, Bulletin 83, 3691-3708. Boulder, CO: Geological Society of America.
- Winograd, I.J., and W. Thordarson. 1975. *Hydrogeologic and Hydrochemical Framework, South-Central Great Basin, Nevada-California, with Special Reference to the Nevada Test Site*, USGS-PP-712-C. Denver, CO: U.S. Geological Survey.
- Wood, D.B., U.S. Geological Survey. 1994. Personal communication to J. Eberlin (IT Corporation) regarding water level data, 15 February. Las Vegas, NV.
- Young, A.A., and H.F. Blaney. 1942. *Use of Water by Native Vegetation*, Division of Water Resources Bulletin 50, 154 p. Sacramento, CA: California Department of Public Works.
- Zlotnik, V.A., B.R. Zurburchen, T. Ptak, and G. Teutsch. 2000. "Support Volume and Scale Effect in Hydraulic Conductivity: Experimental Aspects." In *Theory, Modeling, and Field Investigation in Hydrogeology: A Special Volume in Honor of Shlomo P. Neuman's 60th Birthday Special Paper*, 348, p. 215-231. Boulder, CO: Geological Society of America.
- Zyvoloski, G.A., B.A. Robinson, Z.V. Dash, and L.L. Trease. 1997a. *Summary of Models and Methods for the FEHM Application - A Finite-Element Heat- and Mass-Transfer Code*, LA-13307-MS. Los Alamos, NM: Los Alamos National Laboratory.
- Zyvoloski, G.A., B.A. Robinson, Z.V. Dash, and I.L. Trease. 1997b. *User's Manual for the FEHM Application - A Finite-Element Heat- and Mass-Transfer Code*, LA-13306-M. Los Alamos, NM: Los Alamos National Laboratory.



Appendix A

Hydrostratigraphic Model Supporting Information

A.1.0 Description of the Pahute Mesa-Oasis Valley Model Layers

Brief descriptions of the HSUs used to construct the PM-OV model are provided in [Table A.1-1](#). They are listed in approximate order from surface to basement, although some are laterally rather than vertically contiguous, and not all units are present in all parts of the model area. Other information supporting [Table A.1-1](#) is provided in [Table A.1-2](#) and [Table A.1-3](#).

Table A.1-1
Hydrostratigraphic Units of the Pahute Mesa-Oasis Valley Hydrostratigraphic Framework Model
 (Page 1 of 6)

Model Layer Number ^a	Hydrostratigraphic Unit (Symbol)	Dominant Hydrogeologic Unit(s) ^b	Stratigraphic Unit Map Symbols ^c	General Description	Transport Parameter Category
46	Alluvial Aquifer (AA) (this term is also used to designate a hydrogeologic unit)	AA	Qay, QTc, Qs, Qam, QTa, QTu, Qb, Tgy, Tgc, Tgm, Tgyx, Tt	Consists mainly of alluvium that fills extensional basins such as Gold Flat, Crater Flat, Kawich Valley, and Sarcobatus Flat. Also includes generally older Tertiary gravels, tuffaceous sediments, and nonwelded tuffs (where thin) that partially fill other basins such as Oasis Valley and the moat of the Timber Mountain caldera complex.	Alluvium
45	Younger Volcanic Composite Unit (YVCM)	LFA, WTA, VTA	Typ, Tgy, Ts, Tyb, Tyr	A minor unsaturated HSU that consists of Pliocene to late Miocene basaltic rocks such as those at Thirsty Mountain and Buckboard Mesa. Also includes welded and nonwelded ash-flow tuff of the Volcanics of Stonewall Mountain. Mainly occurs in the northwestern portion of the model area.	WTA 75% VTA 25%
44	Thirsty Canyon Volcanic Aquifer (TCVA)	WTA, LFA, lesser VTA	Ttg, Tth, Tts, Ttt, Ttp, Ttc	Consists mainly of welded ash-flow tuff and lava of the Thirsty Canyon Group. Unit is very thick within the Black Mountain caldera. Also is present east and south of the caldera, including the northwestern moat area of the Timber Mountain caldera complex and the northern portion of the Oasis Valley basin.	WTA 75% LFA 25%
43	Detached Volcanics Composite Unit (DVCM)	WTA, LFA, TCU	Tf through Tq	Consists of a very complex distribution of lavas and tuffs that form a relatively thin, highly extended interval above the FC-BH detachment fault in the southwestern portion of the model area.	WTA 85% TCU 15%
42	Detached Volcanics Aquifer (DVA)	WTA, LFA	Tgyx, Tf, Tma, Tmr	Consists of welded ash-flow tuff and lava assigned to the Ammonia Tanks Tuff and units of the Volcanics of Fortymile Canyon. Although (like the DVCM) the DVA also overlies the FC-BH detachment fault, it is considered a separate HSU because of the preponderance of welded-tuff and lava-flow aquifers that compose the HSU and much smaller degree of alteration present.	WTA
41	Fortymile Canyon Composite Unit (FCCM)	LFA, TCU, lesser WTA	Tfu, Tfs, Tfd, Tfr, Tfb, Tfl, Tff	Consists of a complex and poorly understood distribution of lava and associated tuff of the Volcanics of Fortymile Canyon. Generally confined within the moat of the Timber Mountain caldera complex, where the unit forms a ring around Timber Mountain. Unit is also present in areas southwest of the Timber Mountain caldera complex.	LFA 60% TCU 30% WTA 10%
40	Fortymile Canyon Aquifer (FCA)	WTA, LFA	Tff, tuff of Cutoff Road	Composed mainly of welded ash-flow tuffs and lesser amounts of rhyolitic lava, and is generally less than 305 m (1,000 ft) thick. It is located between two composite units that are much more hydrologically diverse, although they include some of the same units as the FCA. The FCA is completely saturated.	WTA 80% LFA 20%

Table A.1-1
Hydrostratigraphic Units of the Pahute Mesa-Oasis Valley Hydrostratigraphic Framework Model
 (Page 2 of 6)

Model Layer Number ^a	Hydrostratigraphic Unit (Symbol)	Dominant Hydrogeologic Unit(s) ^b	Stratigraphic Unit Map Symbols ^c	General Description	Transport Parameter Category
39	Timber Mountain Composite Unit (TMCM)	TCU (altered tuffs, lavas) and unaltered WTA and lesser LFA	Tmay, Tmaw, Tma, Tmx, Tmat, Tmt, Tmr	Consists mainly of intra-caldera, strongly welded ash-flow tuff of the Timber Mountain Group, and is confined within the Timber Mountain caldera complex. Although consisting mainly of strongly welded tuff which is assumed to be considerably fractured and thus behave as an aquifer, the TMCM is designated a composite unit because of the potential for hydrothermal alteration within this deep intra-caldera setting. Alteration would have significantly altered the hydraulic properties of the rocks, particularly filling fractures with secondary minerals such as quartz.	TCU 75% WTA 25%
38	Tannenbaum Hill Lava-Flow Aquifer (THLFA)	LFA	Tmat	Composed entirely of rhyolitic lava of the rhyolite of Tannenbaum Hill. Occurs just outside the northwestern structural boundary of the Timber Mountain caldera complex. Tannenbaum Hill lava occurring inside the caldera complex is grouped with the TMCM.	LFA
37	Tannenbaum Hill Composite Unit (THCM)	Mostly TCU, lesser WTA	Tmat	Zeolitic tuff and lesser welded ash-flow tuff of the rhyolite of Tannenbaum Hill that occurs stratigraphically below Tannenbaum Hill lava and above the rhyolite of Fluorspar Canyon. Distribution is similar to the THLFA.	TCU 75% WTA 25%
36	Timber Mountain Aquifer (TMA)	Mostly WTA, minor VTA	Tmay, Tmaw, Tma, Tmx, Tmat, Tmt, Tmr	Consists mainly of extra-caldera welded ash-flow tuffs of Ammonia Tanks Tuff and Rainier Mesa Tuff. These rocks are the extra-caldera equivalent of the rocks comprising the TMCM. Unit occurs mostly north and west of the Timber Mountain caldera complex.	WTA 80% VTA 20%
35	Subcaldera Volcanic Confining Unit (SCVCU)	TCU	Tm, Tp, Tc, and older, undifferentiated tuffs	A highly conjectural unit that is modeled as consisting of highly altered volcanic rocks that occur stratigraphically between the Rainier Mesa Tuff and basement rocks (ATICU and RMICU) within the deeper portions of the Timber Mountain caldera complex.	TCU
34	Fluorspar Canyon Confining Unit (FCCU)	TCU	Tmrf	Consists of zeolitic, nonwelded tuff of the rhyolite of Fluorspar Canyon that generally occurs beneath the THCM, and thus has a similar distribution. Typically, the rhyolite of Fluorspar Canyon is higher structurally, and vitric in other areas.	TCU
33	Windy Wash Aquifer (WWA)	LFA	Tmw	Minor HSU consisting of the lava-flow lithofacies of the rhyolite of Windy Wash. Occurs along the western (down-thrown) side of the West Greeley fault in Area 20.	LFA

Table A.1-1
Hydrostratigraphic Units of the Pahute Mesa-Oasis Valley Hydrostratigraphic Framework Model
 (Page 3 of 6)

Model Layer Number ^a	Hydrostratigraphic Unit (Symbol)	Dominant Hydrogeologic Unit(s) ^b	Stratigraphic Unit Map Symbols ^c	General Description	Transport Parameter Category
32	Paintbrush Composite Unit (PCM)	WTA, LFA, TCU	Tmr, Tmrf, Tmn, Tp	Consists mostly of units of the Paintbrush Group that occur in the southern portion of the model area in the vicinity of the Claim Canyon caldera. Unit is dominated by thick, strongly welded Tiva Canyon Tuff within the Claim Canyon caldera. Outside the caldera this unit is more variable, consisting of welded and nonwelded tuff and rhyolitic lava assigned to various formations of the Paintbrush Group. Stratigraphically equivalent units of the Paintbrush Group that occur in the northern portion of the model area beneath Pahute Mesa have been grouped into seven separate HSUs.	WTA 75% TCU 25%
31	Paintbrush Vitric-tuff Aquifer (PVTA)	VTA	Pre-Tmr tuffs, Tp	Typically includes all vitric, nonwelded, and bedded tuff units below the Rainier Mesa Tuff to the top of a Paintbrush lava (e.g., Tpb or Tpe) but may extend to base of Paintbrush Tuff in eastern Area 19 where Tpe or Tpr lavas are not present. May also include the vitric pumiceous top of the Tpe lava. Unit occurs in the northern portion of the model area beneath Pahute Mesa.	VTA
30	Benham Aquifer (BA)	LFA	Tpb	Lava-flow lithofacies of the rhyolite of Benham. Occurs north of the Timber Mountain caldera complex and beneath the southwestern portion of Pahute Mesa.	LFA
29	Upper Paintbrush Confining Unit (UPCU)	TCU	Pre-Tmr tuffs, Tp	Includes all zeolitic, nonwelded and bedded tuffs below the Rainier Mesa Tuff to base of the rhyolite of Delirium Canyon. Unit occurs in the northern portion of the model area beneath Pahute Mesa.	TCU
28	Tiva Canyon Aquifer (TCA)	WTA	Tpc	The welded ash flow lithofacies of the Tiva Canyon Tuff in southern Area 20. May not be differentiated where thin or where sandwiched between vitric bedded tuffs as in Area 19.	WTA 70% VTA 30%
27	Paintbrush Lava-flow Aquifer (PLFA)	LFA	Tpd, Tpe, Tpr	Lava-flow lithofacies of the rhyolite of Delirium Canyon (Tpd), rhyolite of Echo Peak (Tpe), and rhyolite of Silent Canyon (Tpr). Also includes moderately to densely welded ash-flow tuff of Tpe. Unit occurs in the northern portion of the model area beneath Pahute Mesa.	LFA
26	Lower Paintbrush Confining Unit (LPCU)	TCU	Tpe, Tpp, Tpt	Includes all zeolitic nonwelded and bedded tuffs below the rhyolite of Delirium Canyon to the base of the Topopah Spring Tuff. Unit occurs in the northern portion of the model area beneath Pahute Mesa.	TCU
25	Topopah Spring Aquifer (TSA)	WTA	Tpt	The welded ash-flow lithofacies of the Topopah Spring Tuff in southern Area 20.	WTA

Table A.1-1
Hydrostratigraphic Units of the Pahute Mesa-Oasis Valley Hydrostratigraphic Framework Model
 (Page 4 of 6)

Model Layer Number ^a	Hydrostratigraphic Unit (Symbol)	Dominant Hydrogeologic Unit(s) ^b	Stratigraphic Unit Map Symbols ^c	General Description	Transport Parameter Category
24	Yucca Mountain Crater Flat Composite Unit (YMCFCM)	LFA, WTA, TCU	Tc, Th	Includes all units of the Crater Flat Group and Calico Hills Formation that occur in the southern portion of the model area in the vicinity of Yucca Mountain. Stratigraphically equivalent units that occur in the northern portion of the model area beneath Pahute Mesa have been grouped into nine separate HSUs.	WTA 75% TCU 25%
23	Calico Hills Vitric-tuff Aquifer (CHVTA)	VTA	Th (Tac)	Structurally high, vitric, nonwelded tuffs of the Calico Hills Formation. Present in the northern portion of the model area beneath the eastern portion of Area 19. May become partly zeolitic in the lower portions.	VTA
22	Calico Hills Vitric Composite Unit (CHVCM)	VTA, LFA	Th	Structurally high, lava and vitric nonwelded tuff of the Calico Hills formation. Present in the northern portion of the model area beneath the western portion of Area 19. May become partly zeolitic in the lower portions.	VTA 75% LFA 25%
21	Calico Hills zeolitic composite unit (CHZCM)	LFA, TCU	Th	Complex three-dimensional distribution of rhyolite lava and zeolitic nonwelded tuff of the Calico Hills Formation. Present in the northern portion of the model area beneath most of eastern and central Area 20.	TCU 75% LFA 25%
20	Calico Hills Confining Unit (CHCU)	Mostly TCU, minor LFA	Th	Consists mainly of zeolitic nonwelded tuff of the Calico Hills Formation. May include minor lava flows along the eastern margin. Present in the northern portion of the model area beneath the western portion of Area 20.	TCU 90% LFA 10%
19	Inlet Aquifer (IA)	LFA	Tci	Lava-flow lithofacies of the rhyolite of Inlet. Occurs as two thick isolated deposits beneath Pahute Mesa in the northern portion of the model area.	LFA
18	Crater Flat Composite Unit (CFCM)	Mostly LFA, intercalated with TCU	Th (Tac), Tc	Includes welded tuff and lava flow lithofacies of the tuff of Jorum (Tcjp), the rhyolite of Sled (Tcps), and the andesite of Grimy Gulch (Tcg). Occurs in central Area 20 in the northern portion of the model area.	LFA 75% TCU 25%
17	Crater Flat Confining Unit (CFCU)	TCU	Tc	Includes all zeolitic, nonwelded and bedded units below the Calico Hills Formation (Th) to the top of the Bullfrog Tuff (Tcb). Occurs mainly in Area 19 in the northern portion of the model area.	TCU
16	Kearsarge Aquifer (KA)	LFA	Tcpk	Minor HSU that consists of the lava-flow lithofacies of rhyolite of Kearsarge. Unit is present as a small isolated occurrence in the northeastern portion of the model area.	LFA
15	Bullfrog Confining Unit (BCU)	TCU	Tcb	Major confining unit in the northern portion of the model area. Unit consists of thick intra-caldera, zeolitic, mostly nonwelded tuff of the Bullfrog Formation.	TCU

Table A.1-1
Hydrostratigraphic Units of the Pahute Mesa-Oasis Valley Hydrostratigraphic Framework Model
 (Page 5 of 6)

Model Layer Number ^a	Hydrostratigraphic Unit (Symbol)	Dominant Hydrogeologic Unit(s) ^b	Stratigraphic Unit Map Symbols ^c	General Description	Transport Parameter Category
14	Belted Range Aquifer (BRA)	LFA and WTA, with lesser TCU	Tb	Consists of welded ash-flow tuff and lava of the Belted Range Group (Tb) above the Grouse Canyon Tuff (Tbg), but may also include the lava flow lithofacies of the commendite of Split Ridge (Tbgs) and the commendite of Quartet Dome (Tbq) where present. Occurs in the northern portion of the model area.	WTA 50% LFA 50%
13	Pre-belted Range Composite Unit (PBRCM)	TCU, WTA, LFA	Tr, Tn, Tq, Tu, To, Tk, Te	Laterally extensive and locally very thick HSU that includes all the volcanic rocks older than the Belted Range Group.	TCU 75% WTA 25%
12	Black Mountain Intrusive Confining Unit (BMICU)	IICU	Tti	Although modeled as single intrusive masses beneath each of the Black Mountain, Ammonia Tanks, Rainier Mesa, Claim Canyon, and Silent Canyon calderas, and the Calico Hills area, the actual nature of these units is unknown. They may consist exclusively of igneous intrusive rocks, or older volcanic and pre-Tertiary sedimentary rocks that are intruded to varying degrees by igneous rocks ranging in composition from granite to basalt.	"TCU"
11	Ammonia Tanks Intrusive Confining Unit (ATICU)	IICU	Tmai		
10	Rainier Mesa Intrusive Confining Unit (RMICU)	IICU	Tmri		
9	Claim Canyon Intrusive Confining Unit (CCICU)	IICU	Tpi		
8	Calico Hills Intrusive Confining Unit (CHICU)	IICU	Thi		
7	Silent Canyon Intrusive Confining Unit (SCICU)	IICU	Tc, Tb		
6	Mesozoic Granite Confining Unit (MGCU)	GCU	Kg	Consists of granitic rocks that comprise the Gold Meadows stock along the northeastern margin of the model area.	
5	Lower Carbonate Aquifer - Thrust Plate (LCA3)	CA	Dg through Cc	Cambrian through Devonian, mostly limestone and dolomite, rocks that occur in the hanging wall of the Belted Range thrust fault.	

Table A.1-1
Hydrostratigraphic Units of the Pahute Mesa-Oasis Valley Hydrostratigraphic Framework Model
 (Page 6 of 6)

Model Layer Number ^a	Hydrostratigraphic Unit (Symbol)	Dominant Hydrogeologic Unit(s) ^b	Stratigraphic Unit Map Symbols ^c	General Description	Transport Parameter Category
4	Lower Clastic Confining Unit - Thrust Plate (LCCU1)	CCU	Cc, Cz, Czw, Zs	Late Proterozoic to Early Cambrian siliciclastic rocks that occur within the hanging wall of the Belted Range thrust fault.	
3	Upper Clastic Confining Unit (UCCU)	CCU	MDc, MDe	Late Devonian through Mississippian siliciclastic rocks. Present in the eastern third of the model area.	
2	Lower Carbonate Aquifer (LCA)	CA	Dg through Cc	Cambrian through Devonian mostly limestone and dolomite. Widespread throughout the model area outside the calderas.	
1	Lower Clastic Confining Unit (LCCU)	CCU	Cc, Cz, Czw, Zs, Zj	Late Proterozoic through Early Cambrian siliciclastic rocks. Widespread throughout the model area outside the calderas.	

^aPM-OV 3-D Hydrostratigraphic Framework model (BN, 2002)

^bSee [Table A.1-2](#) and [Table A.1-3](#) for definitions of HGUs

^cRefer to Slate et al. (1999) and Ferguson et al. (1994) for definitions of stratigraphic unit map symbols

Adapted from BN, 2002

Table A.1-2
Hydrogeologic Units of the UGTA Regional Model in the PM-OV Model Area

Hydrogeologic Unit	Typical Lithologies	Hydrologic Significance
Alluvial aquifer (AA) (AA is also an HSU in hydrogeologic models.)	Unconsolidated to partially consolidated gravelly sand, aeolian sand, and colluvium; thin, basalt flows of limited extent	Has characteristics of a highly conductive aquifer, but less so where lenses of clay-rich paleocolluvium or playa deposits are present
Welded-tuff aquifer (WTA)	Welded ash-flow tuff; vitric to devitrified	Degree of welding greatly affects interstitial porosity (less porosity as degree of welding increases) and permeability (greater fracture permeability as degree of welding increases)
Vitric-tuff aquifer (VTA)	Bedded tuff; ash-fall and reworked tuff; vitric	Constitutes a volumetrically minor HGU; generally does not extend far below the static water level due to tendency of tuffs to become zeolitic (which drastically reduces permeability) under saturated conditions; significant interstitial porosity (20 to 40 percent); generally insignificant fracture permeability
Lava-flow aquifer (LFA)	Rhyolite lava flows; includes flow breccias (commonly at base) and pumiceous zones (commonly at top)	Generally a caldera-filling unit; hydrologically complex, wide range of transmissivities, fracture density and interstitial porosity differ with lithologic variations
Tuff confining unit (TCU)	Zeolitic bedded tuff with interbedded, but less significant, zeolitic, nonwelded to partially welded ash-flow tuff	May be saturated but measured transmissivities are very low; may cause accumulation of perched and/or semiperched water in overlying units
Intrusive confining unit (ICU)	Granodiorite, quartz monzonite	Relatively impermeable; forms local bulbous stocks, north of Rainier Mesa, Yucca Flat, and scattered elsewhere in the regional model area; may contain perched water
Clastic confining unit (CCU)	Argillite, siltstone, quartzite	Clay-rich rocks are relatively impermeable; more siliceous rocks are fractured, but with fracture porosity generally sealed due to secondary mineralization
Carbonate aquifer (CA)	Dolomite, limestone	Transmissivity values vary greatly and are directly dependent on fracture frequency

Source: Adapted from IT (1996) and BN (2002)

Table A.1-3
Additional and Modified Hydrogeologic Units of the PM-OV Model

Hydrogeologic Unit	Typical Lithologies	Hydrologic Significance
Intra-caldera intrusive confining unit (IICU)	Highly altered, highly injected/intruded country rock and granitic material	Assumed to be impermeable. Conceptually underlies each of the SWNVF calderas and Calico Hills. Developed for this study to designate basement beneath calderas as different from basement outside calderas.
Granite confining unit (GCU)	Granodiorite, quartz monzonite	Relatively impermeable; forms local bulbous stocks, north of Rainier Mesa and Yucca Flat; may contain perched water.

Source: Adapted from BN (2002)

A.2.0 Alternative Hydrostratigraphic Models

Multiple hydrostratigraphic models have been created to describe the geologic structure of the PM-OV flow system. The flow system contains the Western and Central Pahute Mesa CAUs (the site of 85 underground nuclear tests) along with the HSUs through which the radionuclides from these tests could potentially leave the Pahute Mesa underground test areas. The flow system includes areas within and around the NTS. A summary description is provided here. The report titled *Hydrostratigraphic Model for the Groundwater Flow and Contaminant Transport Model of Corrective Action Units 101 and 102: Central and Western Pahute Mesa, Nye County, Nevada* (BN, 2002) provides more detail.

Each of the alternative hydrostratigraphic models honor the data available, with differences between the models representing differences in interpretations of various features described by the data. Thus, each alternative model can be considered a possible representation of reality. The original list of alternatives was developed by an alternative scenario working group, under the auspices of the TWG. The complete list included 48 "alternative scenarios" (Table A.2-1). The list of 48 "alternative scenarios" was then distilled into four groups based upon the action deemed needed. The four groups were as follows:

Group A: Recommended changes to the base model

Group B: Viable alternative scenarios

Group C: Proposed alternatives that would be better addressed during the hydromodeling phase rather than as alternatives to the geologic framework model

Group D: Suggested alternatives that were deemed to be of low priority or not necessary to model at this time

The final listings for Groups A, B, and C, based on the work of the alternative scenario working group, were as follows (note that because they are considered be of lesser consequence to the potential mobility of the radionuclides from the Central and Western Pahute Mesa test sites, the scenarios that fall into Group D are not presented in this report).

Group A - Recommended Changes to the Base Model

1. Subdivide the Fortymile Canyon Composite unit. The lower part of the FCCM in the Oasis Valley area tends to have more welded ash-flow tuffs, and so was differentiated as the Fortymile Canyon Aquifer (FCA).

Table A.2-1
Abridged List of Alternative Scenarios for the Pahute Mesa-Oasis Valley 3-D Hydrostratigraphic Model
 (Page 1 of 4)

Alternative	Priority Group	Comment
1.0 HYDROSTRATIGRAPHY-RELATED ALTERNATIVES		
1.1 Alternatives to Simplify Hydrostratigraphy		
1.1.1 Combine intra-caldera intrusives into a single HSU	D	Are all the intra-caldera intrusives the same hydrologically? Can we combine the intrusives beneath the Ammonia Tanks and Rainier Mesa calderas?
1.1.2 Simplify HSUs above the water table	D	Can HSUs in the unsaturated zone be lumped, simplified, or ignored?
1.1.3 Decrease the depth of the model	D	Is there any merit in raising the bottom of the model? Work on the regional model demonstrated that even after removing the lowest 2 km (1.2 miles) from the bottom of the model, there was no difference in the outcome compared to the original model. The elevation of the bottom of the framework model is now consistent with the regional model.
1.2 Alternatives to Add Hydrostratigraphic Detail		
1.2.1 Include all alluvium (AA) as mapped on USGS surface geologic maps	D	In parts of the current base model alluvium (typically thin surficial deposits) is lumped with an underlying HSU. Thick deposits of AA; however they are differentiated. Could this affect recharge, e.g., alluvium filling a wash or small structural valley?
1.2.2 Add collapse breccias along (within) caldera margins	D	We do not know how permeable the breccias are, and we do not know exactly where they are located. Are they confining or conductive units? To explore this, collapse breccias would be added as another HSU. One way to do this is to symbolically add a wedge-shaped volume along the inside of the caldera.
1.2.3 Subdivide the Fortymile Canyon composite unit (FCCM)	A	For example, this unit consists of lavas in the southeastern Timber Mountain moat area, but welded ash-flow tuffs become more common in the lower portion of the FCCM in Oasis Valley. These units may also become saturated in the deepest portion of the valley. A separate unit would allow more vertical resolution in the model.
1.2.4 Differentiate units of the Twisted Canyon caldera	D	The Twisted Canyon caldera (after Fridrich et al., 1999a) is relatively small and generally above the static water level. The Timber Mountain units are currently included with the detached volcanics composite units (DVCM) but could be differentiated to permit more detailed modeling.
1.2.5 Subdivide the detached volcanics composite unit	A	Is there enough information (e.g., in Fridrich et al., 1999a, b), and are the differences significant and/or predictable enough to warrant subdividing these units?
1.2.6 Define areas of hydrothermal alteration	D	Should we treat alteration as another HSU? This may be possible where there is evidence of alteration on the surface and in drill holes. Drill holes where hydrothermal alteration is documented include: ER-EC-1, ER-EC-6, PM-2 (deep), UE-20f (below 10,000 ft), UE-19w1 (shallowest; the hole cuts through Area 20 caldera margin, where the footwall is hydrothermally altered but the hanging wall is not), ER-EC-7 and ER-EC-2A, all at various depths. To define hydrothermal alteration without evidence does not make sense. Are occurrences of hydrothermal alteration predictable?
1.2.7 Map caldera moat-filling unit	D	Differentiate moat gravels from other alluvium, though these units typically are not saturated.

Table A.2-1
Abridged List of Alternative Scenarios for the Pahute Mesa-Oasis Valley 3-D Hydrostratigraphic Model
 (Page 2 of 4)

Alternative	Priority Group	Comment
1.2.8 Subdivide the Paintbrush composite unit (PCM) in the southern end of the model	C	Although dominated by the Paintbrush Group, the PCM also includes remnants of the Rainier Mesa and Ammonia Tanks welded ash-flow tuffs and thin alluvium. In the north (the 1997 PM-300 model area), the various Paintbrush tuffs are differentiated where drill hole data are available. We might be able to add more geologic detail, but we have almost no hydrologic data. Is the YMP information adequate to differentiate and map out various HSUs?
1.2.9 Subdivide the Kearsarge lavas identified in Well ER-EC-1	D	The Kearsarge lava is a minor aquifer in the northwest corner of the model area and is currently modeled as the Kearsarge aquifer HSU. However, detailed petrographic analysis has identified the Kearsarge lava in Well ER-EC-1, farther south, which represents a newly recognized separate lobe of the lava. Currently, this lobe is lumped with the Crater Flat composite unit (CFCM), which contains lavas of uncertain thicknesses and extent.
1.3 Alternatives to Develop Different Distributions for Pre-Tertiary HSUs		
1.3.1 LCCU in the southwestern portion of the model area	D	Determine whether this outcrop is really LCCU (hydrologic "basement") or LCCU1, with LCA beneath it.
1.3.2 Outcrop of Paleozoic carbonate rocks west of Black Mountain	D	It is currently modeled as LCA. Should it be LCA3?
1.3.3 Continuity of LCA	D	Model LCA as discontinuous from east to west across the model area. (Alternative 2.4.7 creates this geometry.)
1.3.4 Basement subcrop	D	Change the extent and thickness of LCA3 and LCCU1. Instead of only two small LCA3 subcrops in the southwestern corner, make a more extensive LCA3 plate(s)
1.3.5 Vary the Paleozoic stratigraphy in the southern area	D	Differentiate the LCA3 sandwiched between the two occurrences of UCCU, as in the YMP model.
1.3.6 Vary the occurrence of the UCCU	A	It was suggested to change the base model to have the western UCCU contact move eastward down along a line that goes through the middles of the calderas.
1.3.7 LCCU1	A	Depict as a continuous sheet in the southeastern portion of the model area.
1.4 Other Hydrostratigraphy-Related Alternatives		
1.4.1 Intrusive confining unit beneath the Silent Canyon caldera	D	Is this ICU different from that of the other resurgent calderas? What is the nature of this material? Can we define the hydrologic properties of a highly injected/altered rock mass?
1.4.2 Composite units	D	Change/divide composite units into aquifers and/or confining units.
1.4.3 Pre-Belted Range composite unit (PBRM)	D	Show PBRM everywhere overlying the "basement." Thin the younger units as necessary at basement highs to accommodate some added thickness of PBRM.
1.4.4 Mesozoic granite	D	Make the Gold Meadows stock larger in the subsurface.
2.0 STRUCTURE-RELATED ALTERNATIVES		
2.1 Silent Canyon caldera alternative	B	Develop an alternative based on McKee et al. (1999 and 2001) to explore a "structurally uncoupled" model for the SCCC.
2.2 Simplify the model	D	Omit all but the most profound structures and faults.

Table A.2-1
Abridged List of Alternative Scenarios for the Pahute Mesa-Oasis Valley 3-D Hydrostratigraphic Model
 (Page 3 of 4)

Alternative	Priority Group	Comment
2.3 Add More Structural Detail		
2.3.1 Faults and caldera margins	C	Add width to these structures, modifying them from simple two-dimensional surfaces to a 3-D feature having some width. Can we predict where and why they might be a barrier and/or conduit to groundwater flow?
2.3.2 Add more Tertiary faults or fault zones	D	Perhaps begin by adding the mapped faults (shown on Slate et al. [1999] or USGS quadrangle maps). Most reviewers thought that structurally the model contained the individual appropriate level of detail.
2.3.3 Show several more older calderas	D	Where is the source caldera for the Topopah Spring Tuff? If the gravity lows depicted on the USGS gravity maps are really older calderas, would it make any difference? Are they too deep to significantly affect groundwater flow?
2.3.4 Add the CP thrust fault in the south	D	The CP thrust is a poorly characterized, west-to-northwest-vergent thrust fault, that appears to be mostly outside the boundaries of the model area. Do we really need to add this complexity to the southeastern margin of the model? Could the fault be elsewhere, too? The YMP geologic model includes the Calico Hills thrust, while the UGTA model shows a simpler variation without this thrust. Alternatively, the LCA3 might be more continuous in the southeast corner. In the southeast, there are potentially three versions of pre-Tertiary geometry: (1) As depicted in the current UGTA base model; (2) Alternative with LCA at the pre-Tertiary surface not covered with LCCU; (3) Base model with LCA3 as a continuous sheet, not as isolated islands.
2.3.5 Juxtapose aquifers	C	Deliberately juxtapose aquifer units across faults. See Alternative 2.5.3.
2.4 Develop Different Structural Scenarios		
2.4.1 Vary fault dips	C	The basin-and-range normal faults are modeled using an 80-degree dip. Varying fault dips would present more consequences in the source areas, where fault proximity to working points is important. This might be better addressed in sub-CAU-scale models.
2.4.2 Other fault variations	C	Model faults as either present, a single plane, and/or a zone with multiple planes.
2.4.3 Vary the depth to basement rocks	B	The uncertainty in depth to basement based on geophysical data is roughly 2,000 m (6,560 ft). This may not be geologically permissible in some areas. And where it is possible, what units would be thinned or thickened? Could the depth to the Ammonia Tanks and Rainier Mesa resurgent intrusive granites be raised or lowered?
2.4.4 Modify the shapes of calderas	D	Do small differences in the shapes of calderas matter? Compare round vs. rectangular shapes; round the corners as a compromising geometry. The western and eastern lobes of the Timber Mountain caldera complex could be smaller, or extended. Separate the Rainier Mesa structural margin and the Ammonia Tanks structural margin in the north and south sides. Presently, the UGTA base model shows these structural margins merging together (the Ammonia Tanks margin as a reactivation of the Rainier Mesa margin) at those locations.
2.4.5 Explore variations of the Thirsty Canyon lineament	B	Because of its northeast trend and the short distance from testing areas on Pahute Mesa to Oasis Valley, if this lineament exists, it would be the most direct path for migration. Could it be a single (or zone of) north-northeast trending features or faults rather than a series of en echelon, more north-south-trending faults and caldera margins?
2.4.6 Model a "trap-door" caldera geometry	D	"Trap-door" type collapse of the Ammonia Tanks caldera (hinge at the south side) may be another interpretation to explain the gravity inversion data.

Table A.2-1
Abridged List of Alternative Scenarios for the Pahute Mesa-Oasis Valley 3-D Hydrostratigraphic Model
 (Page 4 of 4)

Alternative	Priority Group	Comment
2.4.7 Vary the geometry/position of the BRT fault	B	The current UGTA base model depicts the BRT as not deeply rooted. An alternative interpretation developed by the USGS depicts the BRT as a very deeply rooted and throughgoing thrust. What latitude do we have in moving this feature (what does it do between outcrops)? The BRT is modeled as a low-dip feature except where it ramps up, especially at the top of the pre-Tertiary surface (e.g., 40 degrees as per Jim Cole).
2.4.8 Model Oasis Valley as an extensional basin	D	The preferred interpretation, based on drill hole MyJo Coffey #1 and mapped units in the Transvaal Hills, shows Oasis Valley as part of the Timber Mountain caldera and not an extensional basin. Some disagree. Magnetic data do show north-south faults.
2.5 Other Structure-Related Alternatives		
2.5.1 Add structural detail in Oasis Valley	D	Study structural features in the Oasis Valley discharge area. There are indications of north-south trending faults. Is Chris Fridrich's structural model best?
2.5.2 "Smooth" versus "rough" HSU surface	D	Computer idiosyncrasies have produced "hills" and "indentations" on HSU surfaces where none were intended. Does it matter? A rough surface might better approximate the effect of faulting.
2.5.3 Explore interconnected groundwater pathways	C	Consider increasing or decreasing fault displacements so aquifers are juxtaposed across faults. Conversely, if aquifers are juxtaposed, adjust relative fault displacement to prevent aquifer-aquifer juxtaposition. This may best be handled with sub-CAU-scale models. See Alternative 2.3.5.
2.5.4 Consider defining basin/low with faults	D	The UGTA base model portrays many of the gravity lows as syncline-type structures and not half-grabens related to basin-and-range extension (e.g., northeast of the Black Mountain caldera). However, most reviewers and modelers seem to feel that the present fault detail is about right.
3.0 OTHER ALTERNATIVES		
3.1 Explore variations of the gravity ridge between the TMCC and the SCCC	B	This feature appears as a gravity high between two calderas. Possible explanations include an intrusive resurgent-type body, a hydrothermally altered area, etc.
3.2 Reposition the topographic margins of calderas	D	In some areas their placement seems strange, such as too far removed from the inferred structural margin or not recognizable at all.
3.3 Account for lower hydraulic heads at wells ER-EC-4 and ER-EC-2A	D	These two wells show a significant downward gradient.
3.4 Maximize detail within 1,000 m (3,280 ft) of the water table	D	Add the water table to the model. Will detail above the SWL affect the model? Will small differences at, or just beneath the water table make big differences in the flow and transport modeling results (e.g., raise or lower an HSU, or, add or remove HSUs)?
3.5 Add spring locations	A	Add the locations of springs, particularly those near the TLC and the western margin of the TMCC.

Source: BN, 2002

2. Subdivide the Detached Volcanic Composite unit (DVCM). Based on information from C. Fridrich (of the USGS), the rocks of Oasis Mountain are more aquifer-like (less altered) than the rest of the detached volcanic domain. This portion was designated as the DVA.
3. Clean up the fragmented Lower Clastic Confining Unit (LCCU1) at the leading edge of the BRT in the southeastern portion of the model. This was the consequence of a computer idiosyncrasy in handling of a thinning-wedge geometry.
4. Move the western Upper Clastic Confining Unit (UCCU) contact eastward.
5. Add the locations of springs, particularly those in the vicinity of the Thirsty Canyon lineament, and the western margin of the Timber Mountain Caldera Complex (TMCC).

Group B - Viable Alternative Scenarios

1. Develop a structurally uncoupled alternative model for the Silent Canyon caldera.
2. Explore variations in the interpretation of the basement "ridge" (gravity high) between Timber Mountain and Silent Canyon caldera complexes.
3. Explore variations in the Thirsty Canyon lineament.
4. Vary depth of basement/pretertiary surface.
5. Change the extent and thickness of the Lower Carbonate Aquifer-thrust plate (LCA3) and the LCCU1 in the southeastern portion of the model.
6. Develop a scenario with a deeply rooted, Belted Range thrust fault.

Group C - Alternatives to Address During Hydrologic Modeling

1. Subdivide the Paintbrush Composite unit (PCM) located only in the southern portion of the model.
2. Model faults as 3-D features having some width.
3. Model faults as either: not present, a single plane, and/or a zone with multiple planes.
4. Vary fault dips.
5. Intentionally juxtapose aquifers across faults.

The alternatives listed in Group A are considered to be of high priority and reflect the need to update the HSU model in order to examine the influence of the alternative interpretations on radionuclide mobility. The PM-OV section of the base HSU model has been refined and modified by applying to it the

recommendations presented in Group A. The regional flow model, updated to include the changes in structure associated with the updated PM-OV, has been calibrated using ModFlow 2000 in conjunction with PEST.

Group C alternatives are important and can be implemented in the flow model without the need to update the HSU model. Group C alternatives will be simulated as part of the FEHM Pahute Mesa flow modeling effort.

The alternatives posted in Group B represent the important alternatives that for full consideration would entail major modifications of both the HSU and numerical models. Associated calibrations would also become major efforts. A full calibration effort on all the alternatives would be hard to complete within the administrative constraints associated with the efforts. A screening method was developed to reduce the number of alternatives requiring further consideration. The screening method and associated results are presented in the following section.

A.3.0 HSU Model Screening

Within the framework of uncertainty analysis, one primary consideration is that simulation results span the range of possible outcomes. In a conservative sense, if the model results span all reasonable possibilities, but the likelihood of outlying results is overstated relative to the more likely possibilities, a factor of safety is built into the less accurate results. To meet this end, an acceptable analysis could be performed by screening the six alternatives, then choosing to look at the most likely model (as defined by the committee) in conjunction with the extreme models (that are physically possible). This represents the safest plausible scenario and the scenario that presents the greatest likelihood of transporting radionuclides to the accessible environment at levels of risk. To decide on a smaller set of alternatives that span the plausible range of possibilities, a screening procedure was implemented. By definition, a screening procedure implies the use of a simpler analogue that can be used to decide upon which of the alternatives should be considered further. The problem is whether a simpler procedure can be used to rank the alternatives that faithfully reflects the processes that physically discern the radionuclide transport potential of the modeled alternatives. Of equal importance is the question of how to examine all six alternatives and make sure that a single methodology is applied to consistently model each alternative.

A.3.1 Screening Approach

The general approach being considered herein is comprised of performing flow simulations for each of the alternative models and assessing the impact of the various generated flow fields on the advective transport of the radionuclides as defined by particle tracking. The methodology upon which the screening approach was based involved several considerations related to the choice of dimensionality of the model, the type of code used, the need for calibration, how faults are modeled, the type of boundary conditions, and how to evaluate the results. The options used in for the screening effort were as follows.

A.3.1.1 Dimensionality

The dimensionality of the model refers to the number of dimensions in the flow simulation. It is the 3-D aspects of the model that will define whether the path of least resistance is under, over, around, or through the 3-D structures defined by the faulting, as well as complex intrusive and extrusive igneous processes. In addition, numerous underground test locations are spread out laterally as well as vertically. Different alternative HSU models may impact only a small subset of the total number of tests, but the impact to those few tests may be important for

radionuclide transport. To properly account for the impact of alternative HSU models on all tests, it was considered critical to examine the 3-D nature of the flow system during the screening process. Therefore, the screening approach used the simulation of 3-D flow.

A.3.1.2 Faults

The role of faults in controlling the migration of radionuclides from underground test areas is not known. Faults may act as barrier to flow, may be conduits that direct flow into a narrow area, or may have no noticeable influence at all. Several of the alternative HSU models have different representations of faults. For example, the Thirsty Canyon Lineament is treated as a continuous feature in one alternative, but as a discontinuous feature in others. As a second example, the number and depth of faults differ among several of the alternative models. Anticipating the important future role faults will play in the Pahute Mesa CAU modeling; therefore, it seems clear that any screening methodology must include the impact of faults on the flow system.

It is expected that CAU modeling of groundwater flow on Pahute Mesa will strive to faithfully represent the location of faults in three dimensions. Faults dip at various angles; therefore, the CAU modeling will also represent dipping faults as necessary. For screening, however, it may not be necessary to faithfully represent the fault geometry in all aspects.

Dipping faults more faithfully represent the reality on Pahute Mesa. However, the computation burden on any model is large when dipping faults are used. In finite-difference or finite-element, a large number of nodes are required to represent faults in three-dimensions. This creates a large numerical burden making the simulations slow and in some cases may prevent the model from running on some computers.

Approximating faults as vertical simplifies the modeling tremendously because grid refinement can be limited to plan view. For the purpose of screening, the vertical fault approximation is preferable. In this case, the HSU model will not be revised to include vertical faults, rather the flow model will assume the faults are vertical. This simplification will create blocks of material from the HSU model that will be located on the wrong side of a vertical fault in the flow model. This inaccuracy is considered acceptable for screening purposes. To best represent the proximity of underground tests to faults, the location of the faults in plan view was chosen to coincide with the intersection of the fault and a plane following the spatially variant trend of the average depth of the underground tests in the vicinity of the faults.

A.3.1.3 Numerical Model

FEHM, LANL's 3-D finite-element model (Zyvoloski et al., 1997a and b), was considered to be the best choice of model for screening purposes. The FEHM

model, which has been chosen for the Pahute Mesa CAU modeling, has been used for simulations at Yucca Mountain and is maintained in configuration management to ensure that the code has been validated against analytical solutions and other numerical simulations. In addition, UGTA personnel have some experience using the model outside and within the NTS project.

The FEHM model is designed so that it can mathematically and geometrically handle vertical or dipping faults. As noted earlier, the most efficient method of implementing faults in FEHM is the use of vertical faults. This would minimize the number of nodes needed, and mesh generation would be efficient. An advantage of the finite-element approach is the ability to refine locally around faults without extending the refinement across the entire model as with the finite-difference approach. A disadvantage of the finite-element approach is the time spent to create the mesh for each alternative model. Presently, a unique mesh is required for each alternative to capture the detail of changes in stratigraphy. One way to avoid this limitation is to limit the vertical discretization to uniform thickness layers as in the finite difference approach. The hydraulic properties would be assigned as in the regional finite difference model where the arithmetic mean of HSU hydraulic properties defines the horizontal hydraulic conductivity of the block, and the harmonic mean of the HSU hydraulic properties defines the vertical hydraulic conductivity of the block. This approach is not acceptable for later CAU modeling, but should be adequate for screening purposes. This simplification was used to add greater efficiency to the screening simulation process at a minimal cost in accuracy.

A.3.1.4 Boundary Conditions

For screening purposes, relatively simple boundary conditions could be consistently applied to each alternative model. The simplest to apply and use from a finite-difference or finite-element model solution-stability aspect would be constant head boundaries based upon contouring of field data or a regional model simulation. An advantage of this method is the implicit quantification of flux differences. The disadvantage of this type of boundary is the strong control of a perimeter assigned head boundary on boundary-value problems based upon Laplace's equation (Bear, 1972). The differences in transport pathways that would be reflected by head distributions for alternative geologic models may become obfuscated by the strong control of the boundary conditions. The constant head boundaries will accentuate differences in groundwater flux through each of the alternative models and can be used to compare to measured fluxes at Oasis Valley.

A second manner of handling the boundary conditions would be to apply an upgradient boundary flux based upon the results of the regional model simulations. Since the eastern and western sections of the boundary were comprised of both inflow and outflow zones, it was decided that the regional influxes and outfluxes for each boundary (western, eastern, and northern) needed to be applied separately. The method used was designed to take advantage of the knowledge derived from prior constant-head boundary FEHM simulations. The regional model-based boundary influxes and outfluxes for the western, eastern,

and northern faces were applied to the finite-element boundary nodes based upon the direction and proportion of total boundary face influx (or outflux) seen in the constant-head boundary FEHM simulations. The discharge areas of the model in Oasis Valley were then assigned constant-head values based upon the field data available. The differences between the alternative models should be more accurately reflected in these simulations. Problems with the conceptualizations upon which the alternative models are based, as indicated by the generation of spurious results, is much more likely to show up using the flux boundary condition than using the constant-head perimeter boundary approach. Both types of boundary condition were simulated used to allow for comparisons to both measured fluxes and measured hydraulic heads.

A.3.1.5 Calibration

The effort involved with setting up the first numerical simulation for each alternative model is dependent on the model type and the degree of sophistication in which the discretization and/or fault definition is handled. Once a base simulation is successfully run, the major amount of effort involved is associated with the calibration of the model. This can be a very tedious process even when an automatic parameter estimation is involved (note that there are a maximum of 940 parameters that can be estimated with the base-case MODFLOW regional model). If calibration is neglected, the efforts involved in modeling can be minimized. In a screening procedure to decide which of the alternative models to choose for continued modeling efforts, the decision criteria is based upon choosing alternatives that allow for spanning the possible range of outcomes. This does not necessarily entail the need for accurate results (Morelon and Guerillot, 1995). If the objective is to span the possible results, careful choice of parameters and setting up of models can yield results that, although possibly incorrect, allow for a relative sorting of the possible results which can then be used to choose the models that best span the range of the results. Morelon and Guerillot (1995), noting that for three-dimensional oil-reservoir production modeling, flow simulations are too expensive to perform for a large number of geostatistical representations. Therefore, they suggested that for many of the generated reservoir images, production behavior of the reservoirs would be similar. With this in mind, they suggested selecting a subset of reservoir images representative of the possible production behaviors. Their selection or screening process was based upon simplifying the flow simulations by computing only one constant pressure field corresponding to a steady-state flow field within the reservoir for each reservoir image. The boundary conditions for each simulation were kept the same. Production results of the simulations may have been wrong, but the results could be sorted relative to each other. The validity of the results could also be discerned.

In an analogous effort, one way of performing a screening model would be to take a calibrated model and its HSU-based parameters and use those parameters for a single simulation with each alternative model. To guarantee the proper flux balance, the models would have upgradient flux boundary conditions in the North and constant head outlet boundaries in discharge zones such as Oasis Valley. The alternative models would all use the same HSU parameter values and boundary conditions. Differences would then be a function of the HSU geometries and fault

structures. To make sure the mobility potential is not missed in the effort, two limiting simulations could also be performed for each alternative. The limiting simulations would consider enhanced and dampened conductivity ratios between potential high-flow and low-flow zones. A set of three simulations would be performed for each alternative geologic model, and particle tracking from the test sites would be performed to examine the transport potential of each model. From the range of travel distances derived from the particle tracking results, a subset of alternative models which span the possible transport distance ranges of the complete alternative-model set will be chosen as part of a more detailed analysis.

A.3.1.6 Comparison of Simulations

The comparison of the simulations of the different alternative HSU models will be performed in three different ways. As a general rule, the hydraulic conductivity for each HSU will be set based on the calibration of the BN HSU model performed in fiscal year 2001. Constant head boundary values will be set based on observed head maps. The boundary flux values will be consistent with published values in the literature and the regional groundwater model.

The first set of simulations, with constant head boundaries on the model, will determine the flux of groundwater from various sections of the model (for example from Areas 19 and 20, across the northern boundary, into Oasis Valley). These groundwater fluxes will be compared with published values of flux into the Pahute Mesa region, discharging at Oasis Valley, and to the regional groundwater model results. Of course, it is recognized that fluxes can be easily increased or decreased by model calibration, but the use of consistent hydraulic conductivity values for each simulation should provide a valid basis for comparison of simulations.

The second set of simulations, with constant flux boundaries to the north, will determine the hydraulic head distribution. The head distributions for each alternative will be compared with observed head measurements in a manner similar to calibration. The differences between observed and simulated head will be quantified for the entire model and for subregions to look for subtle differences.

A third set of comparisons will be performed on both sets of model runs using Streamline Particle Tracking (SPTR) to identify differences in pathways from all the underground tests. It is possible that significant differences in transport may be manifested in a limited region of the model, yet that difference may be important to the location of the contaminant boundary.

Each of these comparisons will be performed and tabulated. This quantitative comparison will be used as the basis for selecting two alternative HSU models for inclusion in the CAU modeling process.

A.3.1.7 Final Approach

Based on an assessment of approaches and models for screening the alternative HSU models of the PM-OV region, the following approach was applied:

- Create 3-D simulations of flow using the finite-element code FEHM.
- Treat all faults as vertical in the flow model (ignore clips portions of HSUs).
- Mesh refinement in the vicinity of faults.
- Use constant thickness flow model layers and effective horizontal and vertical hydraulic conductivity (K_h and K_v).
- Chose representative parameter values based on the calibrated base model.
- Simulate flow under constant head boundaries to assess flux.
- Simulate flow under flux boundary conditions to assess heads.
- Compare alternatives on the basis of comparisons to measured heads and fluxes.
- Choose two alternatives to span the range of outcomes.
- Document the process and the choice of alternatives

A.3.2 Application

The application of the screening procedure is described in this section. All figures may be found in the last section of this report.

A.3.2.1 Selection of Alternative HSU Models

Seven alternative HSU models were constructed within the EarthVision[®] system (Dynamic Graphics, 2002), one base model and six others. For the purposes of these simulations, the base model is considered one of the alternatives. The alternative models are: (1) UGTA base model (base-case), (2) Silent Canyon Caldera Complex Model (USGS), (3) Basement Ridge model (RIDGE), (4) Thirsty Canyon Lineament model (TCL), (5) Raised Pre-Tertiary Surface model (PZUP), (6) Contiguous imbricate thrust sheet model (SEPZ), and (7) Deeply Rooted Belted Range Thrust Fault model (DRT).

The base-case, and the six alternatives are described by BN, 2002. The base model contains 47 separate hydrostratigraphic units ranging from alluvium to

granitic intrusives. This model provides much more detail with respect to the caldera region than the previous regional model (DOE/NV, 1997). For the purposes of the screening calculations, the HSUs were lumped into a smaller number of categories streamlining assigning of modeling properties. [Table A.3-1](#) contains the seven different classes of HSUs and an assessment of the appropriate flow and transport property.

**Table A.3-1
HSU Classification**

HSU Class	Hydraulic Conductivity	Porosity
Volcanic Aquifer	Aquifer permeability	Fracture porosity
Volcanic Composite Unit	~12 times smaller K than VA	Fracture porosity
Volcanic Composite Unit	~100 times smaller K than VA	Porous
Alluvial Aquifer	~ 3 times smaller K than VA	Porous
Carbonate Aquifer	~ 35 times smaller K than VA	Fracture porosity
Clastic Confining Unit	~ 2,000 times smaller K than VA	Fracture porosity
Intrusive	~ 35,000 time smaller K than VA	Fracture porosity

These material properties are in general agreement with the values chosen for the regional model (DOE/NV, 1997). This simplification allows the alternative HSU models to be visually compared with one another on the basis of likely impact to the flow system and also particle travel. In the simulations, the decay of hydraulic conductivity with depth was retained as the conceptual model. If the decay with depth is ignored, the resulting permeability maps display the relative positions of aquifers, composite units, confining units, etc.

[Figure A.3-1](#) is a map of the base-case model log-permeability distribution at the 1,000-meter elevation, assuming the property model in [Table A.3-1](#) and no decay of hydraulic conductivity with depth. Moderate to high-permeability units are shown in the Silent Canyon Caldera region. The high-permeability region extends southwest of the Silent Canyon Caldera. At the 0-meter elevation ([Figure A.3-2](#)), more of the western and eastern boundary of the model area is shown to be of lower permeability. The Silent Canyon Caldera region continues to have high permeability units, but to the south only moderate permeability units are mapped.

The USGS model is shown in [Figures A.3-3](#) and [A.3-4](#), for the 1,000-m and 0-m elevation cases, respectively. This model differs from the base-case in a number of areas: (1) it is based on a traditional cylindrical caldera collapse model, (2) the Silent Canyon Caldera region is uncoupled from the rest of the model region, (3) it was developed from the basement up, (4) it was entirely generated within EarthVision[®] (Dynamic Graphics, 2002), (5) has fewer HSUs than the base model, (6) fault depths are limited with only a few faults penetrating deeper than the water table, and (7) the eastern and western margins are extended relative to the base model. Despite these differences, the USGS model, like the base-case model, honors available stratigraphic data.

The RIDGE model is shown in [Figures A.3-5 and A.3-6](#), for the 1,000-m and 0-m elevation cases, respectively. Data indicate a gravity high between the Silent Canyon and Timber Mountain caldera complexes. This alternative interpretation of the gravity high produces lateral variation and juxtaposition of overlying volcanic units causing aquifer units to truncate against older, with less conductive units forming the gravity-high ridge. The impact of the greater amount of lower permeability units is most evident in the 1,000-m elevation plot.

The TCL model is shown in [Figures A.3-7 and A.3-8](#) for the 1,000-m and 0-m elevation cases, respectively. In this alternative, the Thirsty Canyon Lineament is treated as a continuous feature structurally connecting the Silent Canyon and Timber Mountain Caldera complexes. In this alternative, the southern margin of the Silent Canyon Caldera Complex is extended westward to account for connection of the two complexes. Minor differences between the TCL and base-case models are evident along the western edge of the Silent Canyon Caldera at both the 1,000-m and 0-m elevations.

The PZUP model is shown in [Figures A.3-9 and A.3-10](#) for the 1,000-m and 0-m elevation cases, respectively. In this alternative, the depth of the pre-Tertiary surface is raised to the highest elevation that could be geologically permitted. In addition, the basement complexes are also raised as much as possible within the caldera complexes. In general, larger areas of the model have smaller permeability in the PZUP case than the base case, but the changes occur outside of the caldera margins.

The SEPZ model is shown in [Figures A.3-11 and A.3-12](#) for the 1,000-m and 0-m elevation cases, respectively. In this alternative, the extent and thickness of the LCA3 and LCCU1 in the southeast corner of the model area are adjusted. The differences between the SEPZ and base case models are evident only in the southeast corner of the model. At the 1,000-m elevation, the material along the eastern edge of the model is more permeable than in the base case.

The DRT model is shown in [Figures A.3-13 and A.3-14](#) for the 1,000-m and 0-m elevation cases, respectively. In this final alternative, the Belted Range Thrust Fault is modeled as more deeply rooted than in the base case model. This produces a very thick thrust sheet over most of the model area in which the LCA is discontinuous. The upper pre-Tertiary rock immediately downgradient of Pahute Mesa is low permeability LCCU1, rather than more permeable LCA. The differences between the DRT and base case models are not very evident at either the 1,000-m or 0-m elevations. Rather, the differences occur much deeper in the model.

The FEHM code was chosen for the simulations. The PM-OV model area was discretized into 14 nodal layers with the top layer of nodes at an elevation of 1,400 m and the bottom layer of nodes at -2,000 m. [Table A.3-2](#) contains the nodal elevations chosen for the screening model.

This nodal spacing emphasizes the portions of the flow system most likely to be involved in transport of radionuclides from underground test cavities on Pahute Mesa.

Table A.3-2
Nodal Elevations

Nodal Layer Number	Nodal Elevation (MASL)
14	1,400
13	1,300
12	1,200
11	1,100
10	1,000
9	900
8	750
7	600
6	450
5	300
4	0
3	-500
2	-1,000
1	-2,000

A.3.2.2 Screening Process

The screening models were built using the FEHM code (Zyvoloski et al., 1997a and b). This will maintain consistency with the CAU-scale model which will also be constructed using the FEHM code (Zyvoloski et al., 1997a and b), as described in [Section 3.0](#). As noted above, the model geometry was simplified by using horizontal model layers, as was used in the regional flow model. Faults in the model are represented by vertical zones of altered permeability. The faults are located spatially at the true location corresponding to the depth of nearby underground tests. A planar function was fit to depths of the underground tests, excluding the few very deep tests. The location where this plane intersected the fault surfaces is the map view location of the fault in the screening model. No attempt was made to correct the HSUs that were left on the "wrong" side of the fault when they were made vertical in the flow model. This error was assumed to be minor.

The finite element mesh for the seven alternative HSU models is shown in [Figures A.3-15 through A.3-19](#). [Figure A.3-15](#) is an oblique view of the entire model from the southeast and horizontal layers and the refinement along the faults. [Figure A.3-16](#) shows more detail of the faults zones in the northern part of the Silent Canyon Caldera. [Figure A.3-17](#) is a close up of the intersection of two faults. An oblique view of the faults only is presented in [Figure A.3-18](#). Finally, [Figure A.3-19](#) is a cross-sectional view of the mesh along two of the faults. This mesh, which has a maximum nodal spacing of 1,000 m, and a minimum spacing of 125 m, has 261,912 total nodes.

A.3.2.3 Permeability Distribution - Depth Decay Case

In a majority of the model simulations, the hydraulic conductivity of individual units is assumed to decrease with depth as was the case for the regional flow model. The permeability distribution at an elevation of 1,000 m for the base case model is presented in [Figure A.3-20](#). [Figure A.3-21](#) shows the same information at the 0-m elevation. There is a substantial decrease in permeability at depth in these cases with a higher permeability pathway on the western edge of Timber Mountain clearly visible. When faults are treated as conduits, [Figures A.3-22 and A.3-23](#), the permeability of the faults is increased two orders of magnitude over the surrounding material. This can be seen clearly in [Figure A.3-23](#).

A.3.2.4 Boundary Conditions

Two sets of boundary conditions were simulated for this screening analysis. First, constant head boundaries were placed around the entire screening model. The boundary heads were determined by mapping the heads from the regional model on the screening model boundary. This was performed using utilities provided by LANL that run with the LaGriT mesh generation software. The hydraulic head at each node on the model boundary was specified and the code simulated the hydraulic head distribution within the interior of the model. The amount of water entering or leaving a model boundary, integrated over the entire side, was calculated for each set of simulations. In this manner, the total inflow across the northern boundary could be calculated.

For the flux boundary, the total flux along each side of the model was equated to the total boundary flux as determined from the regional model. In this case, the USGS utility (ZONEBUDGET) was used to determine the amount of water entering each boundary of the screening model. The distribution of flux, node-to-node, along each boundary was determined from the constant head simulations. The flux at each boundary node was determined from the relative proportion of flow at each node in the constant head simulations and scaled such that the total boundary flux matched the flux in the regional model. The fluxes were provided on the western, northern, and eastern boundaries. The southern boundary was left constant head.

A.3.2.5 Impact of Faults and Permeability Distributions

Four different cases were considered for the simulations. Three different fault permeability cases were simulated: (1) faults neutral, (2) faults as barriers, and (3) faults as conduits. A fourth case was simulated where the permeability does not decrease with depth.

The impact of faults is always included in the HSU models in the offset and juxtaposition of HSU against other HSU across fault boundaries. In the neutral case, the permeability of the faults is the same as the surround rock, so the faults do not impact flow except to offset one HSU with respect to another.

With faults as barriers, the permeability of all the faults were decreased one order of magnitude relative to the surrounding rock material. This provided a narrow impediment to flow across faults.

Increasing the permeability of faults two orders of magnitude above the surrounding rock produced a series of conduits in which water would preferentially flow. These three cases were simulated to see if the nature of faults might influence the importance of the different alternative HSU models.

The final case examined the assumption of decreasing K with depth. If the permeability is large at depth, it would surely influence how water and radionuclides move at depth.

A.3.2.6 Particle Pathlines

Particle pathlines used in the screening process were generated using the SPTR option of FEHM. Particles were placed at every underground test location beginning at a depth of 1.5 cavity radii (calculated from maximum announced yield) below the working point and then every 50 m up to the water table. This approximates the results of the Cheshire (LLNL) and Benham (LANL) simulations which showed that due to residual temperature anomalies due to testing, radionuclides can migrate to overlying aquifers and be transported away from underground tests.

The particle pathlines for the four cases of the base-case HSU model are presented in [Figures A.3-24](#) through [A.3-27](#). [Figure A.3-24](#) contains the head contours and the pathlines for the base case with constant head boundaries. It shows general particle travel to the southwest, around the western side of Timber Mountain, and discharge out the south end of the model, east of Oasis Valley. When faults are barriers, ([Figure A.3-25](#)) a very similar flow pattern develops, but travel distances are less because the faults create impediments to flow. In addition, water levels are generally higher because of the overall lower permeability of the flow system.

In [Figure A.3-26](#), the impact of faults as conduits is clearly visible. Where possible, the flow paths preferentially flow in the fault zones. In this case, a few of the flow paths discharge to the springs at Oasis Valley, but the majority of flow paths exit the southern boundary of the model. In this example, a few paths flow east of Timber Mountain. In general, water levels are lower than in the fault neutral case because overall permeabilities are larger than in this case.

The last case, [Figure A.3-27](#), the pathlines for the case of no depth decay of hydraulic conductivity show a dramatically different flow system. The pathlines head almost due south from the testing areas, directly beneath Timber Mountain, and discharge across almost the entire southern boundary of the model area.

A.3.2.7 *Boundary Flux Results*

When constant head boundaries are set in the model, the code adjusts the amount of flow through the system. Therefore, it was expected that with constant head boundaries, the amount of water flowing through the system under the seven alternative models would differ. By examining these differences, it may be possible to differentiate between the models. Figures A.3-28 through A.3-31 show the groundwater fluxes, integrated across each model face, for each of the seven alternative models.

Figure A.3-28 is the case with faults neutral and shows that in general, flow through the screening model is greater than the regional model. This suggests the permeabilities in the screening model are probably too large. Several of the alternatives differ in small ways from the others. For example, the SEPZ has more flow through the eastern boundary. The USGS model has more flux through the northern boundary, and the DRT has more spring flow and discharge through the western boundary. Beyond that, the results for the seven alternatives are really quite similar.

When the faults are barriers (Figure A.3-29), the pattern of results is the same as the fault neutral case, but the overall boundary fluxes are smaller because the bulk permeability of the system is less.

When faults are conduits (Figure A.3-30), total fluxes are larger than in the fault neutral case, but the pattern of fluxes from one alternative model to the next is unchanged.

The last case (Figure A.3-31) with no depth decay of permeability, produces enormous total fluxes with DRT and PZUP producing less flow than the other cases because of the greater amounts of low permeability clastic units in those models.

With few exceptions, it is difficult to distinguish between the different cases on the basis of boundary flux alone. It appears quite easy to calibrate any of these alternatives to total flux simply by decreasing the permeability of the units by an amount equal to the ratio of boundary flux in the screening model to boundary flux in the regional model.

A.3.2.8 *Particle Path Statistics*

The particle path statistics were compiled as a way to view the results from all the paths at the same time. The particle travel distance is defined as the distance from the starting location to the location at 100 or 1,000 years. This is determined as the straight line distance (as the crow flies) and does not account for total pathlength. This matches the definition in the FFACO for the maximum extent of the contaminant boundary. The results to follow are for the constant head case.

Figure A.3-32 shows the particle distance cdf for the case with neutral faults. Of the seven alternatives, the USGS model has the greater number of slow paths

(primarily those from Area 19). The other alternative that differs slightly is the TCL which shows a greater number of paths with distances between 10,000 and 25,000 m, but fewer paths greater than 25,000 m than the other cases.

When faults are barriers, [Figure A.3-33](#), the USGS model again appears to be the most unique, with some variability among the other alternatives. In [Figure A.3-34](#), the case with faults as conduits, the USGS model is clearly different, with the other alternatives barely distinguishable. [Figure A.3-35](#) is the case of no depth decay. In this case, the fluxes were so great that nearly all the particles exit the system in less than 1,000 years, so the plot is presented as time of exit, rather than distance at 1,000 years. Again, there is some variability among the alternatives, but the USGS model is the only truly different alternative.

[Figure A.3-36](#) is a plot of particle distance statistics at 100 years. It shows the same pattern as for 1,000 years in that the most unique case is the USGS model. [Figure A.3-37](#) is also at 100 years, but for the case of faults as conduits.

The general conclusion from the particle statistics is that the USGS model is clearly unique compared with the other six alternatives. Several of the other alternatives appear to be different in selected distance intervals or selected time intervals, but no alternative (with the exception of the USGS model) is clearly unique. More importantly, the proportion of flow paths that reach a specific distance (say 30,000 m) is impacted much more by the nature of the faults (barrier or conduit) than by the differences in the HSU models (again excluding the USGS model).

A.3.2.9 Head Residuals

The last four figures show the hydraulic head residuals, calculated as the simulated head minus the measured head, for the flux boundary condition cases. In [Figures A.3-38 through A.3-41](#), it is clear that the differences between HSU models in terms of head residuals is much smaller than between the different fault permeability cases.

A.3.2.10 General Conclusions

The USGS model is clearly structurally different than the other six alternative models. The other alternatives are not different enough to warrant separate simulations. We recommend only two alternatives be carried forward, the USGS and the base case.

A.3.2.11 Figures

This section contains all the figures previously called out in this appendix.

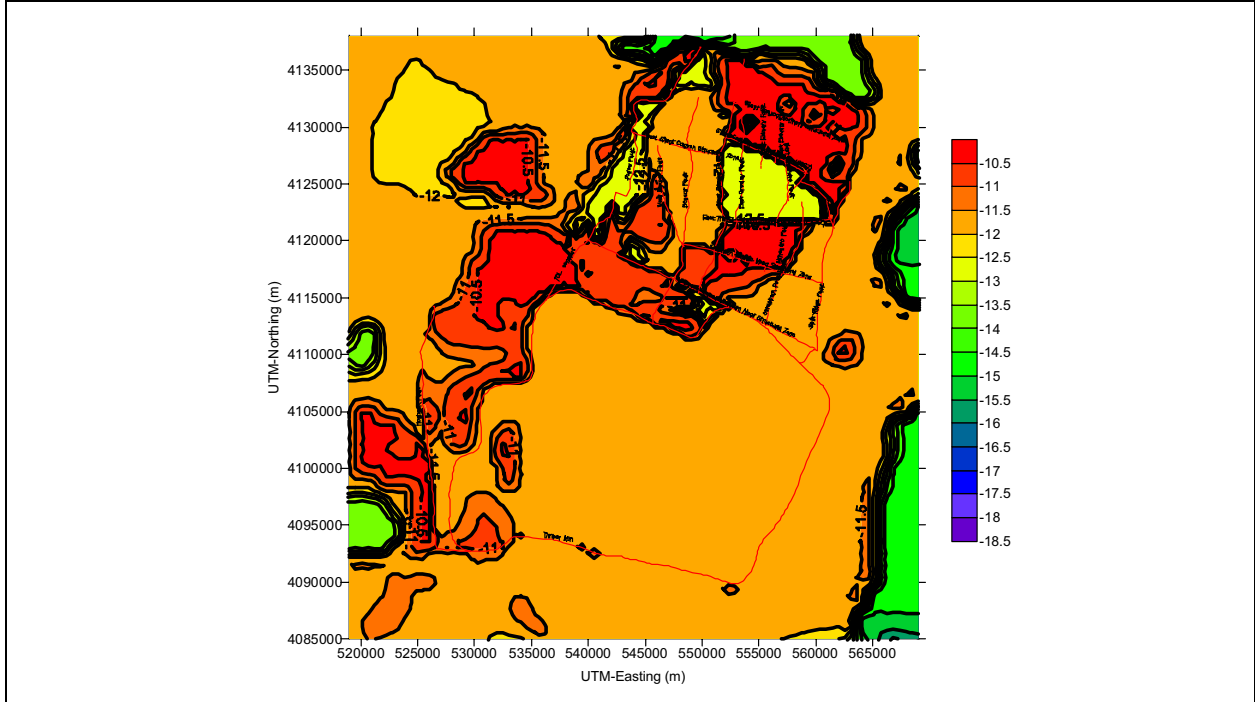


Figure A.3-1
Base-Case Log-Permeability Values (m^2) at 1,000 m amsl for Case Without Depth-Decay of Permeability

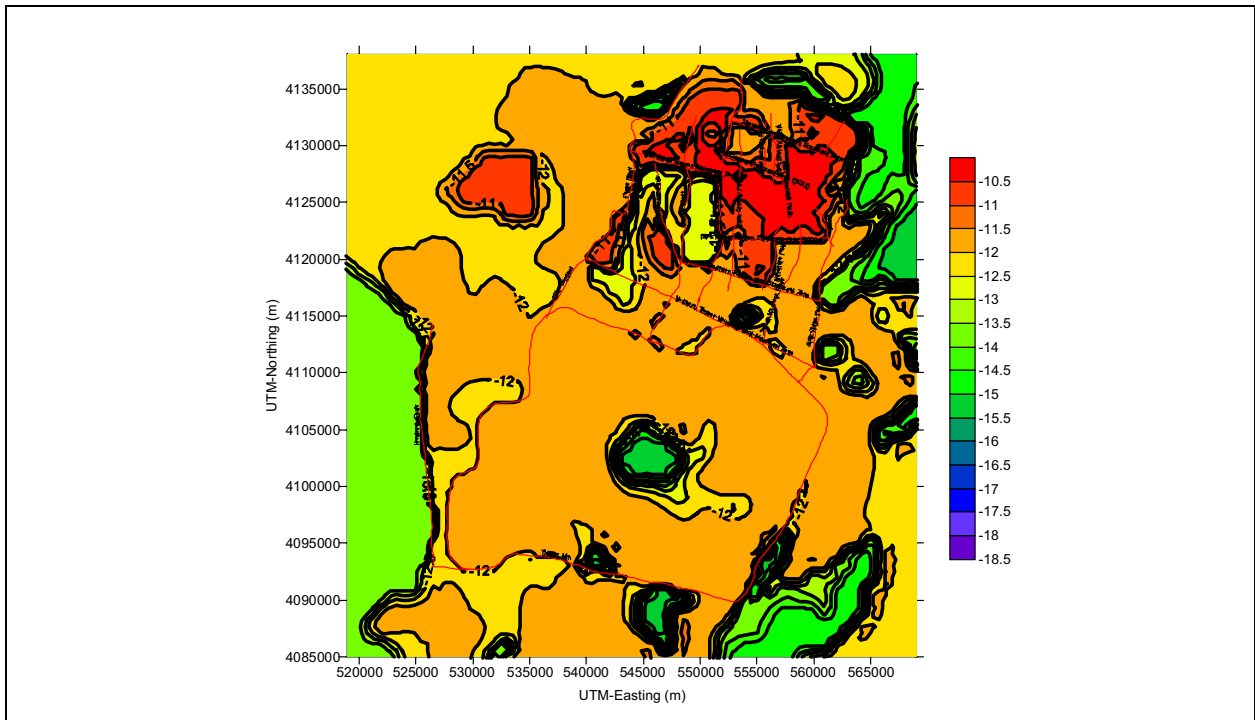


Figure A.3-2
Base-Case Log-Permeability Values (m^2) at 0 m amsl for Case Without Depth-Decay of Conductivity

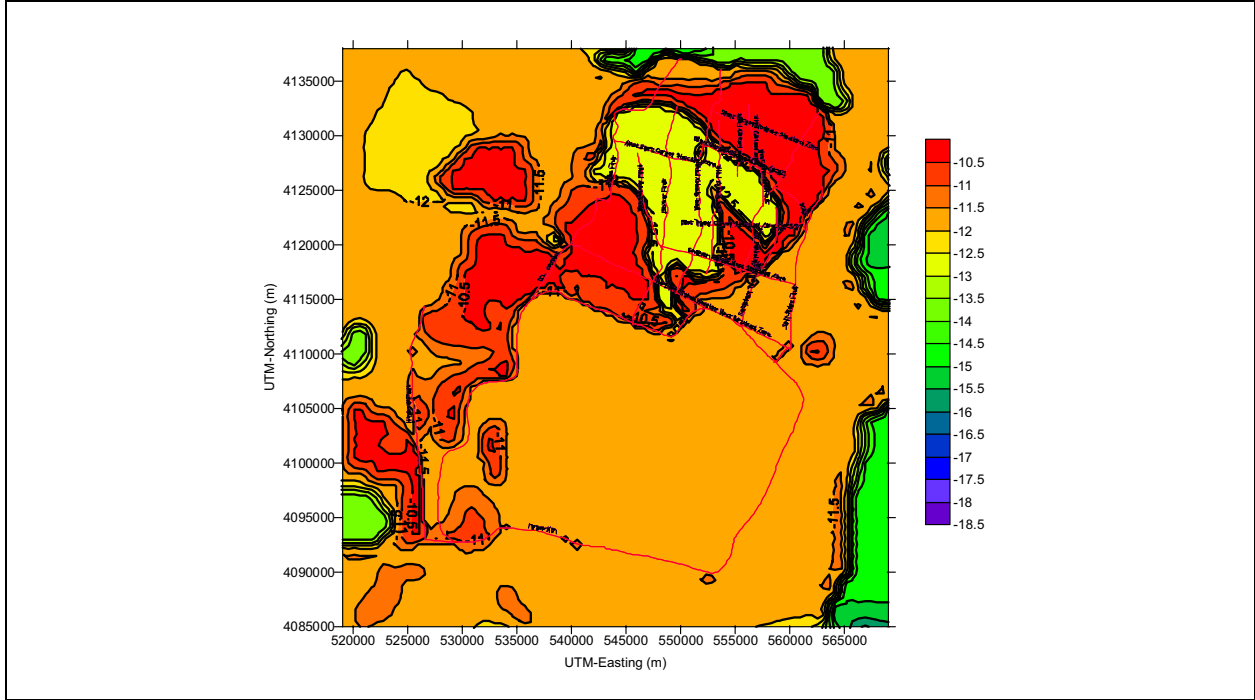


Figure A.3-3
USGS Log-Permeability Values (m^2) at 1,000 m amsl for Case Without Depth-Decay of Conductivity

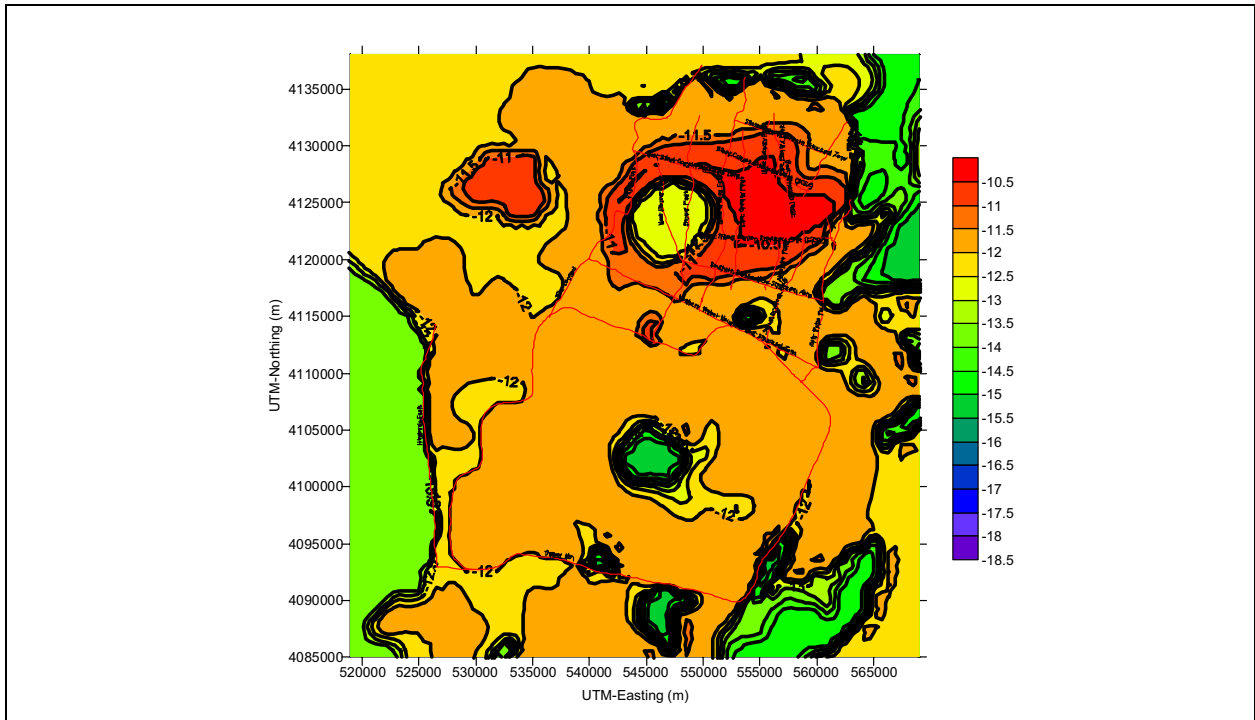


Figure A.3-4
USGS Log-Permeability Values (m^2) at 0 m amsl for Case Without Depth-Decay of Conductivity

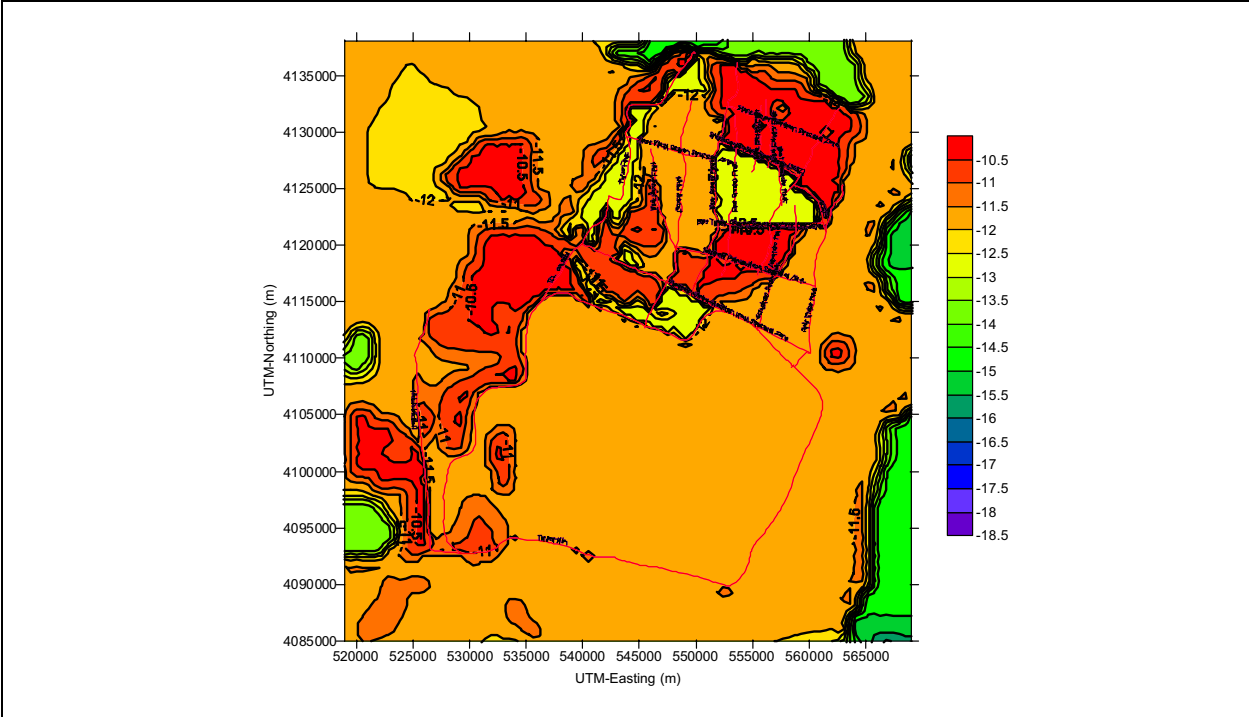


Figure A.3-5
RIDGE Log-Permeability Values (m^2) at 1,000 m amsl for Case Without Depth-Decay of Conductivity

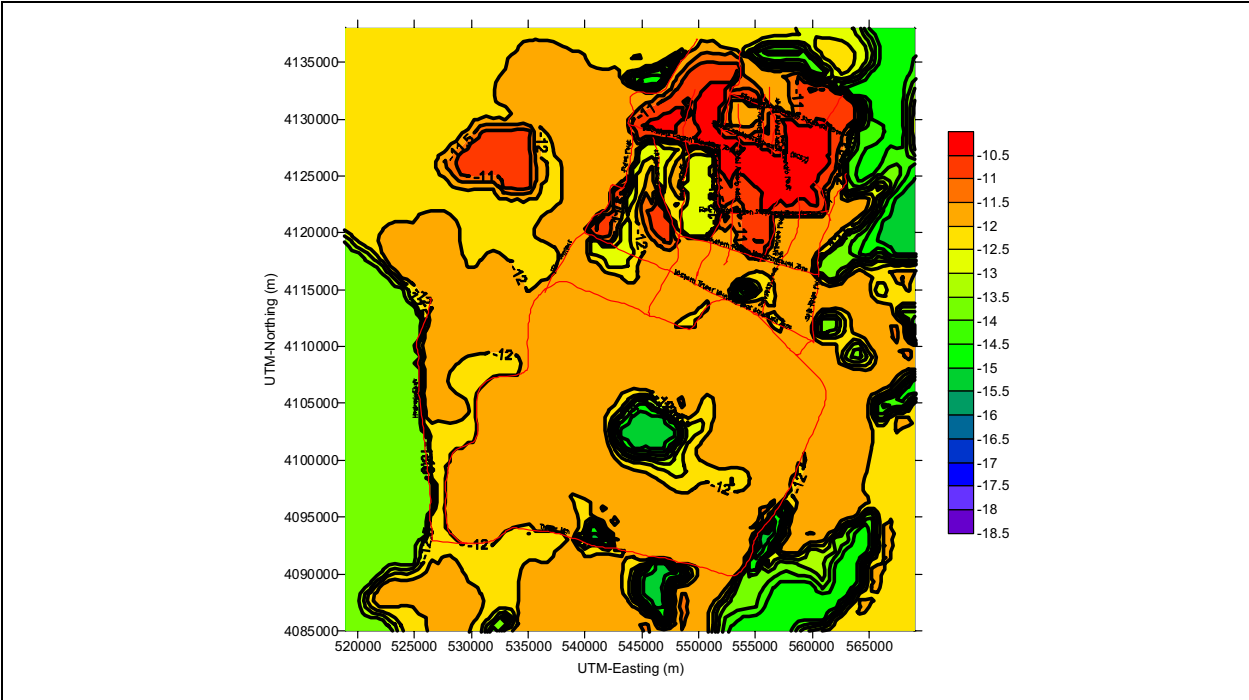


Figure A.3-6
RIDGE Log-Permeability Values (m^2) at 0 m amsl for Case Without Depth-Decay of Conductivity

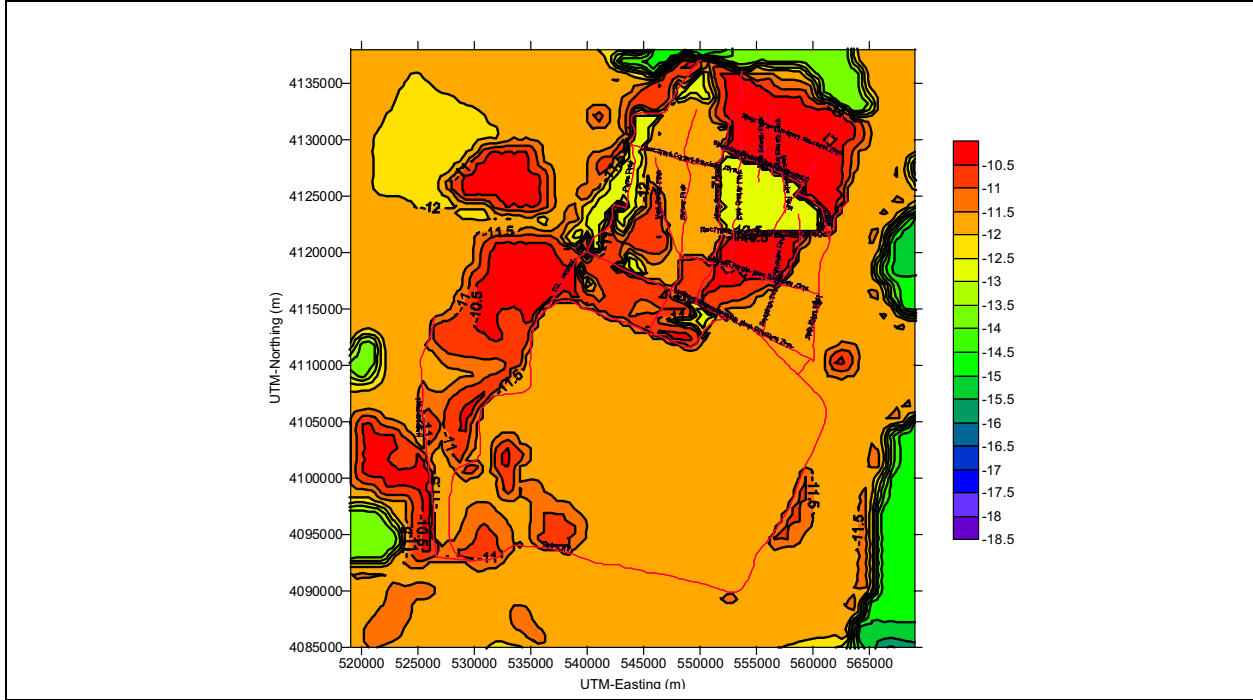


Figure A.3-7
TCL Log-Permeability Values (m²) at 1,000 m amsl for Case Without Depth-Decay of Conductivity

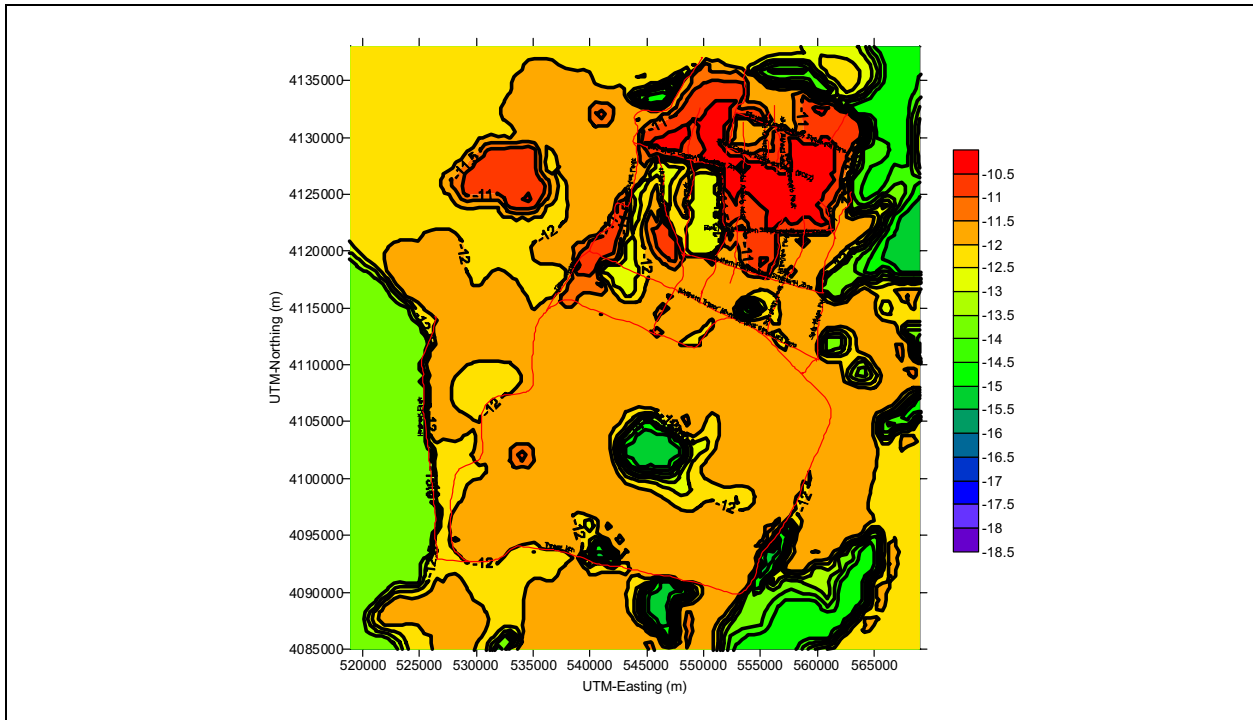


Figure A.3-8
TCL Log-Permeability Values (m²) at 0 m amsl for Case Without Depth-Decay of Conductivity

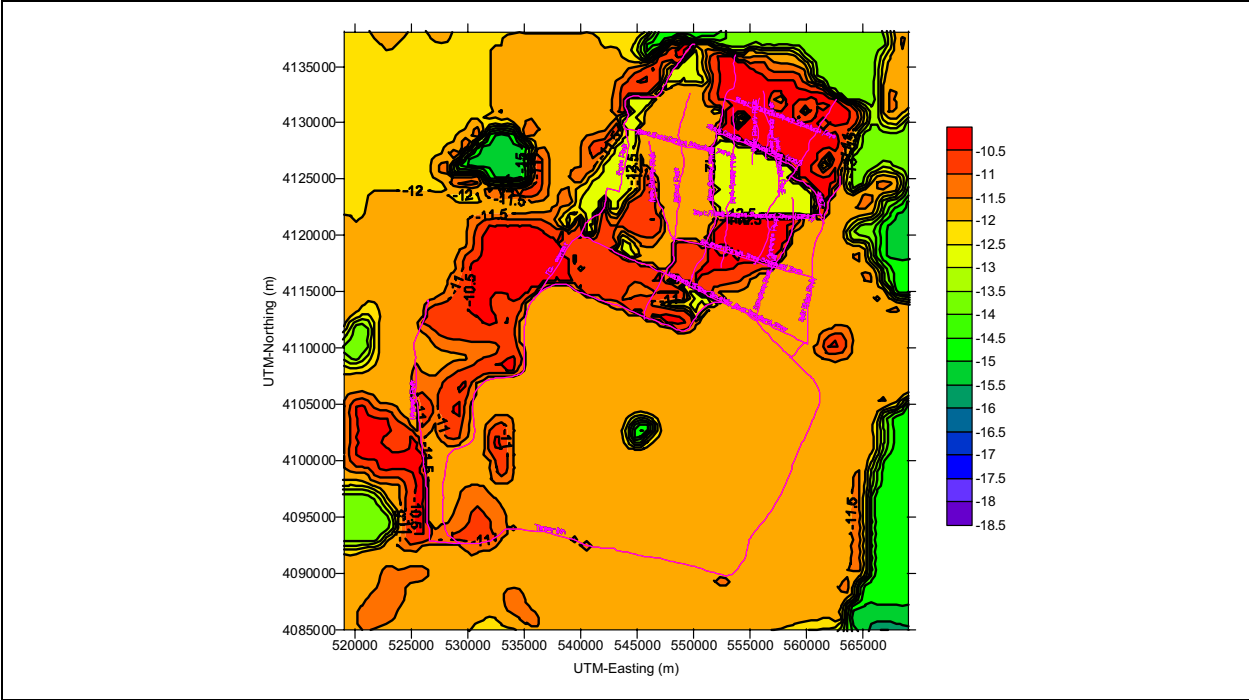


Figure A.3-9
PZUP Log-Permeability Values (m^2) at 1,000 m amsl for Case Without Depth-Decay of Conductivity

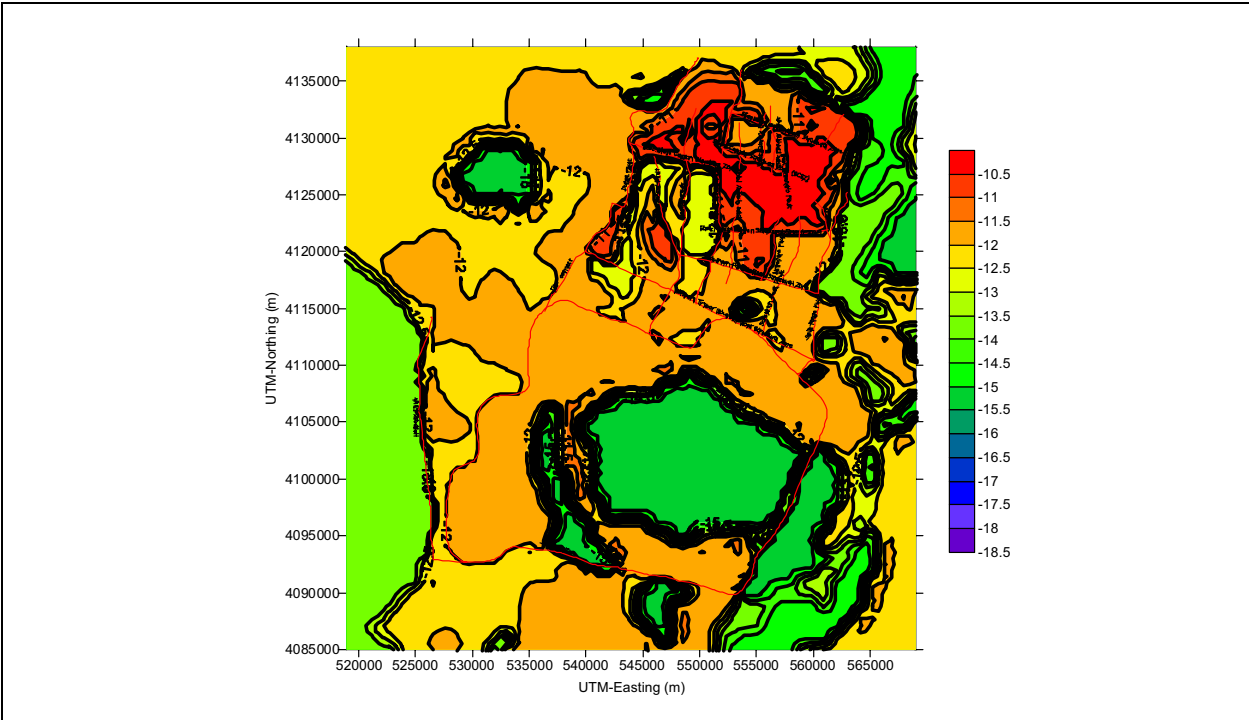


Figure A.3-10
PZUP Log-Permeability Values (m^2) at 0 m amsl for Case Without Depth-Decay of Conductivity

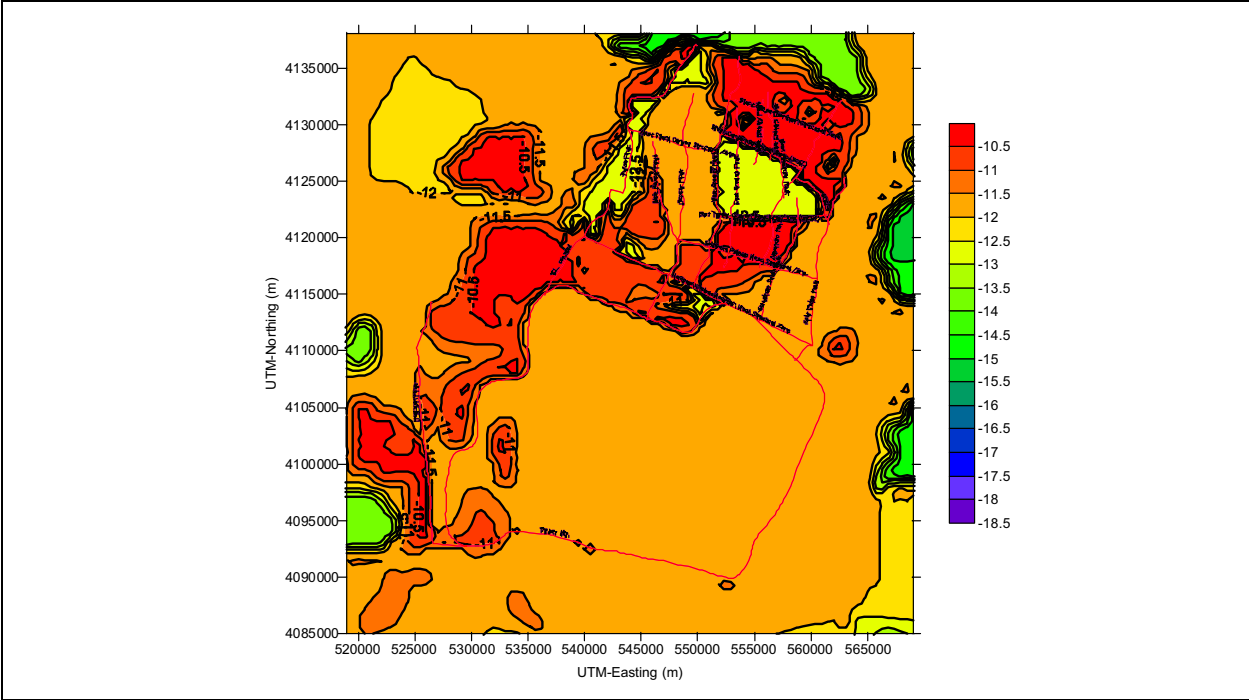


Figure A.3-11
SEPZ Log-Permeability Values (m^2) at 1,000 m amsl for Case Without Depth-Decay of Conductivity

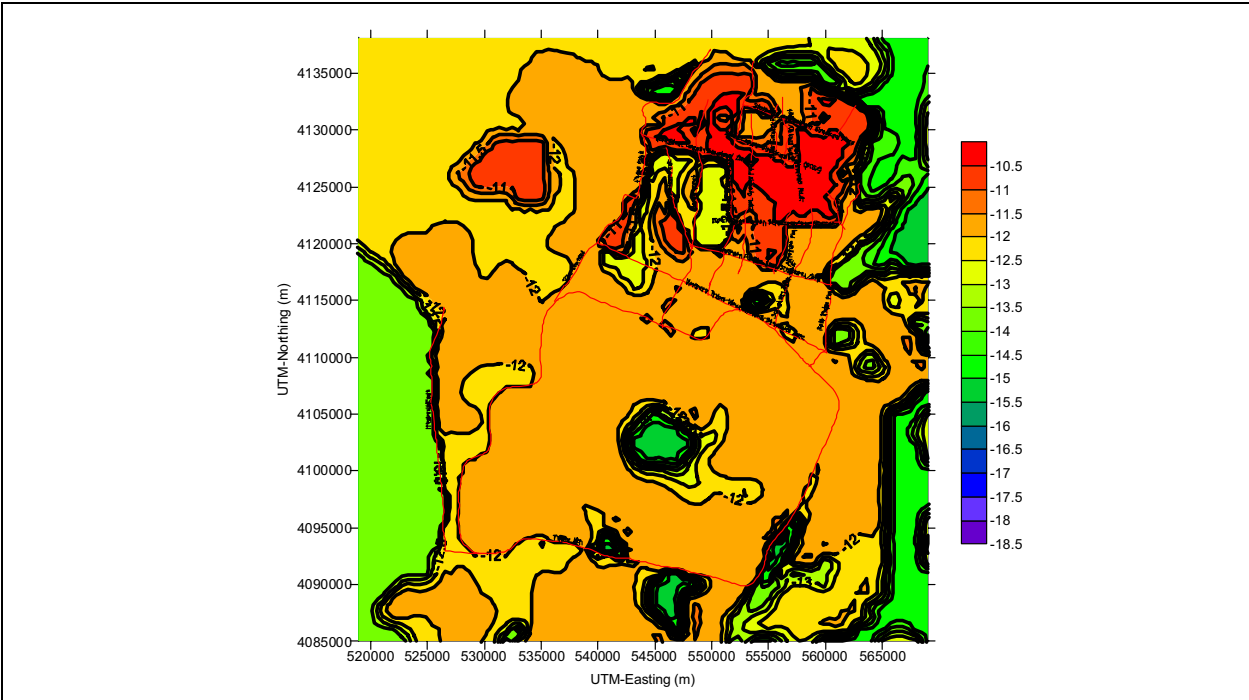


Figure A.3-12
SEPZ Log-Permeability Values (m^2) at 0 m amsl for Case Without Depth-Decay of Conductivity

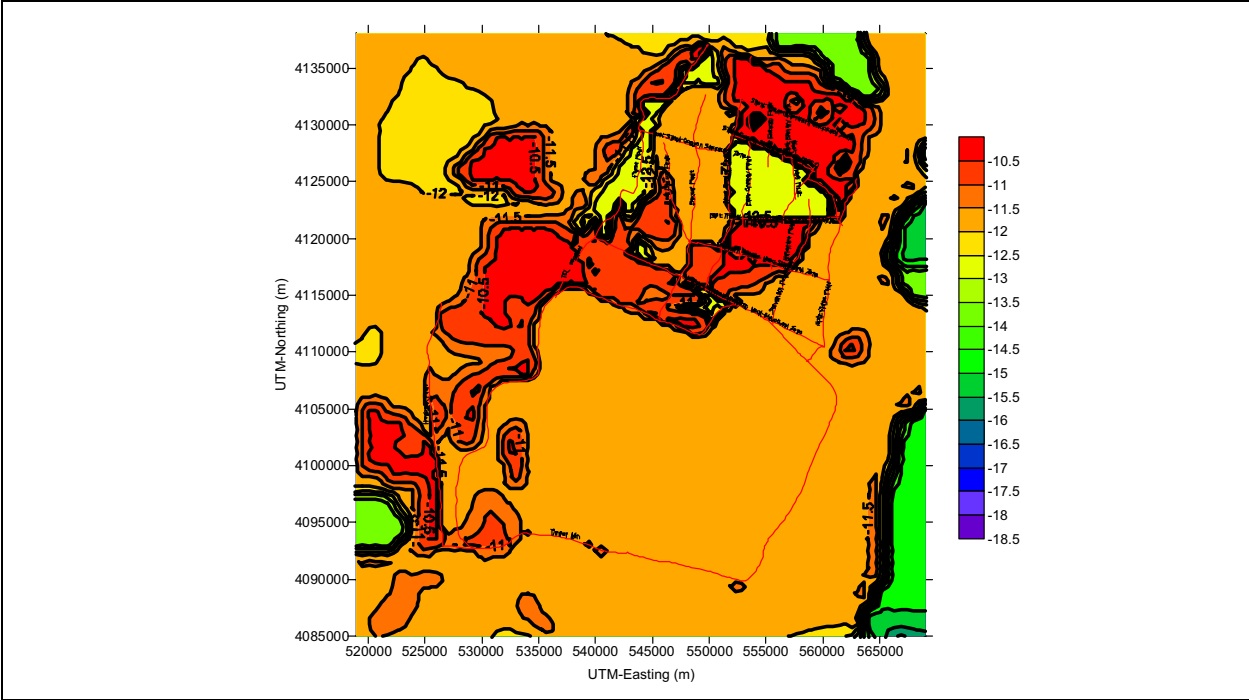


Figure A.3-13
DRT Log-Permeability Values (m^2) at 1,000 m amsl for Case Without Depth-Decay of Conductivity Faults

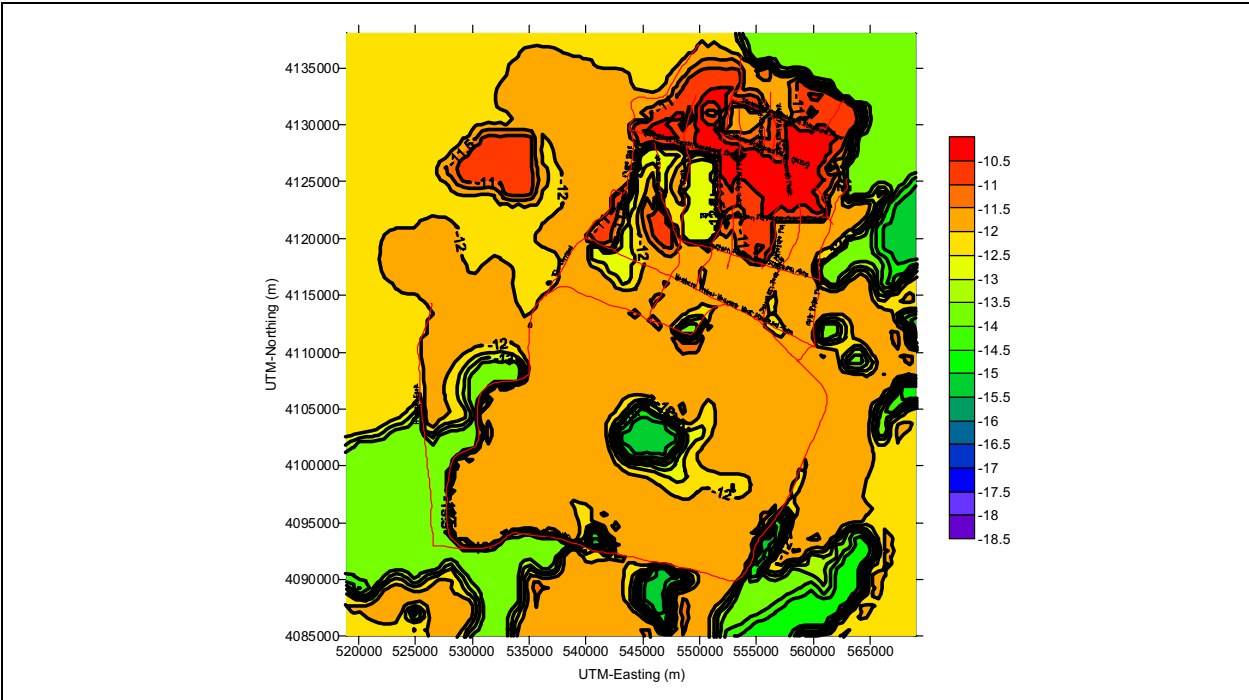


Figure A.3-14
DRT Log-Permeability Values (m^2) at 0 m amsl for Case Without Depth-Decay of Conductivity

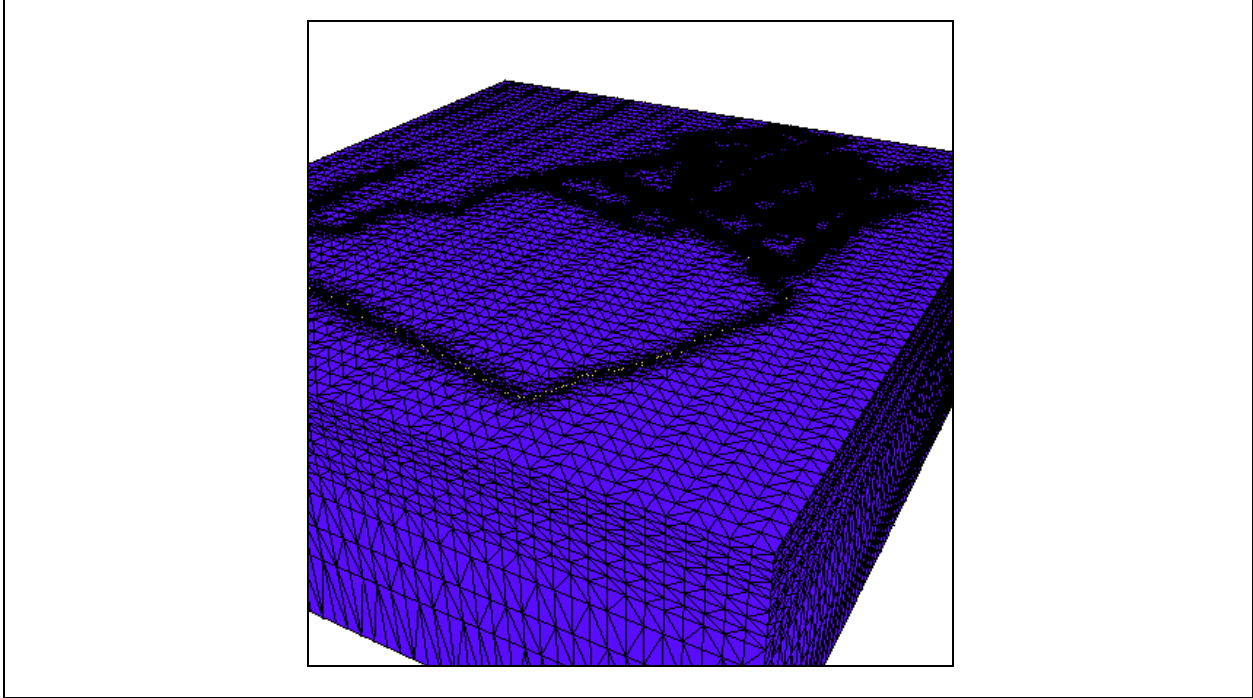


Figure A.3-15
FEHM 3-Dimensional Finite Element Mesh (from LANL)

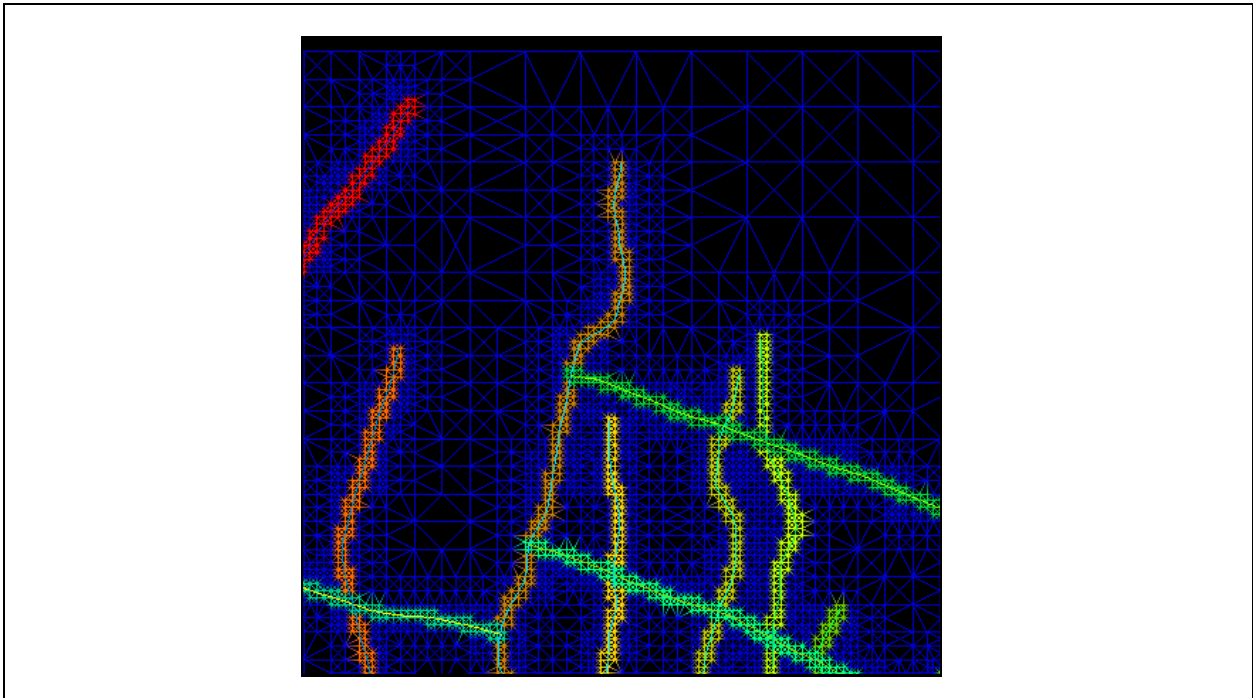


Figure A.3-16
Areal View of Mesh Refinement in the Vicinity of the Faults (from LANL)

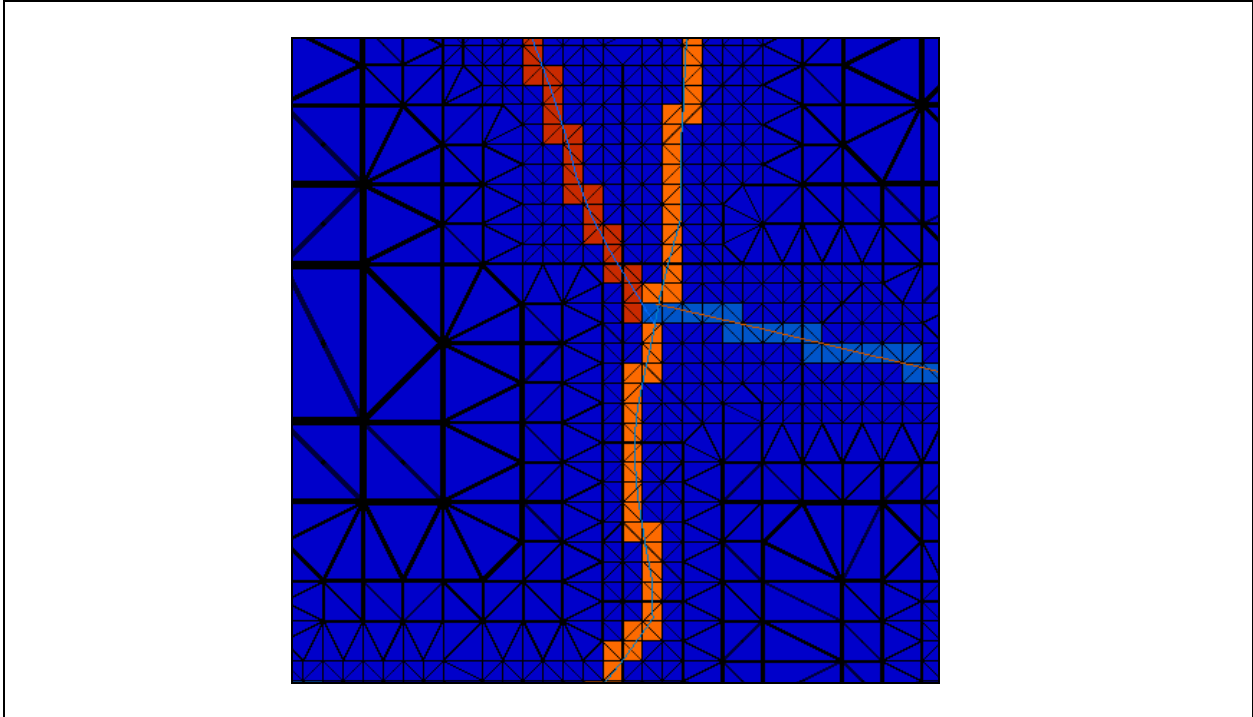


Figure A.3-17
Close-up View of Mesh Refinement Around Faults (from LANL)

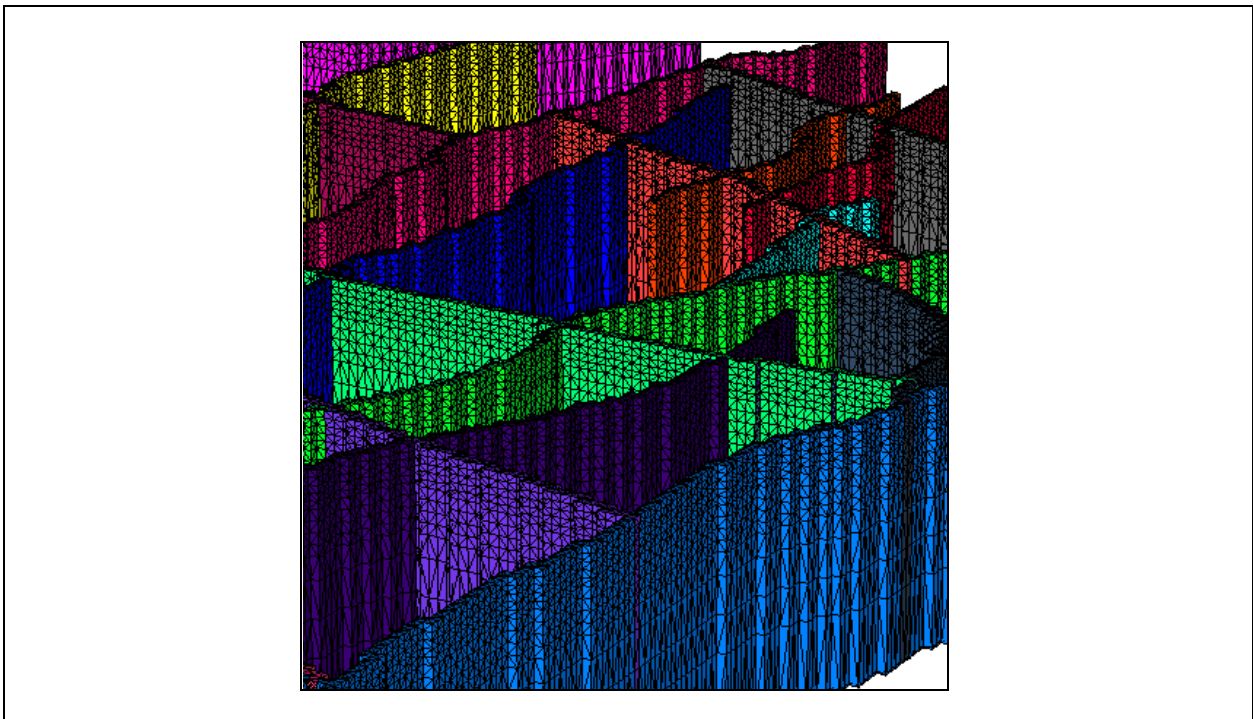


Figure A.3-18
Oblique View of Finite Element Mesh Along Faults (from LANL)

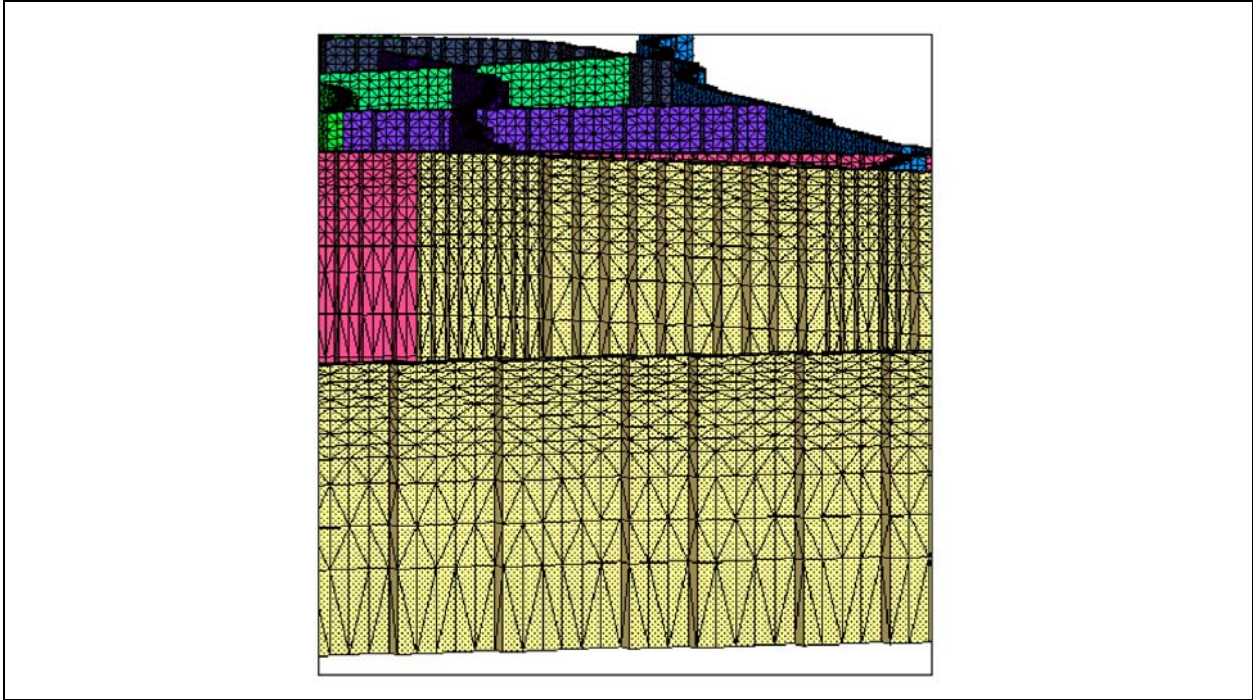


Figure A.3-19
Vertical Section of Finite Element Mesh Along Fault (from LANL)

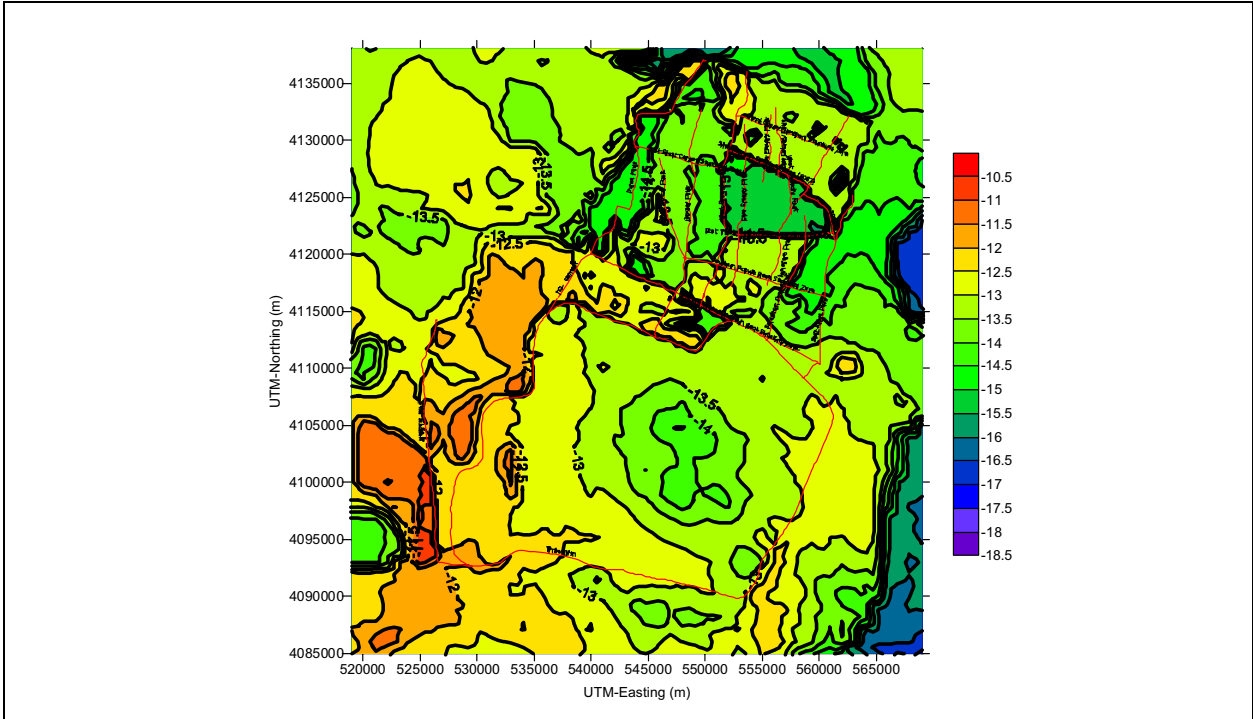


Figure A.3-20
Base-Case Log-Permeability Values (m^2) at 1,000 m amsl for the Neutral Fault Case

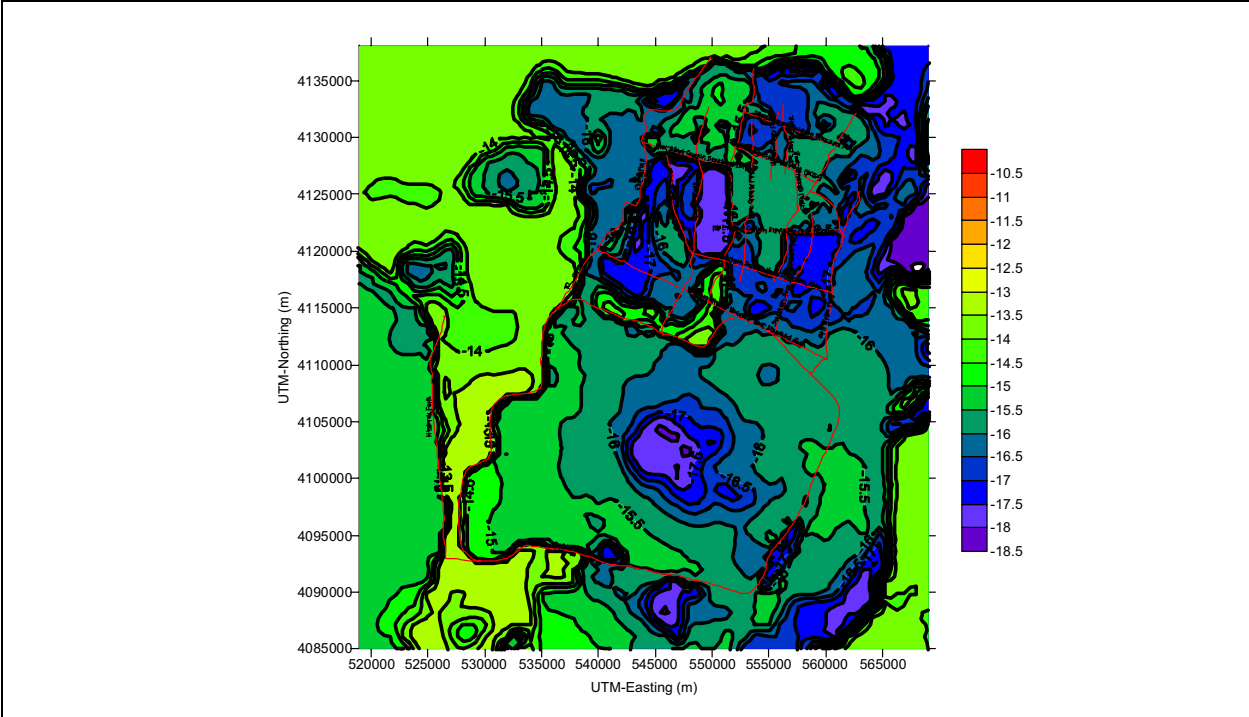


Figure A.3-21
Base-Case Log-Permeability Values (m²) at 0 m amsl for the Neutral Fault Case

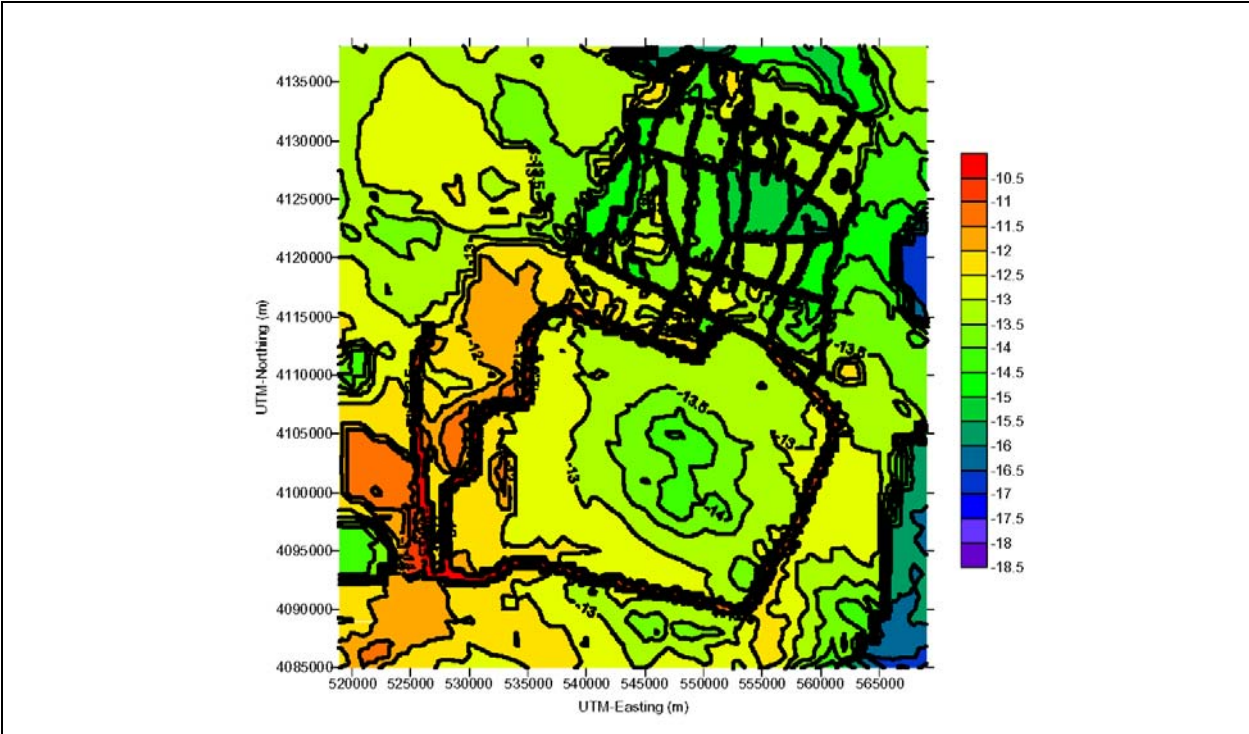


Figure A.3-22
Base-Case Log-Permeability Values (m²) at 1,000 m amsl for Case with High-K Faults

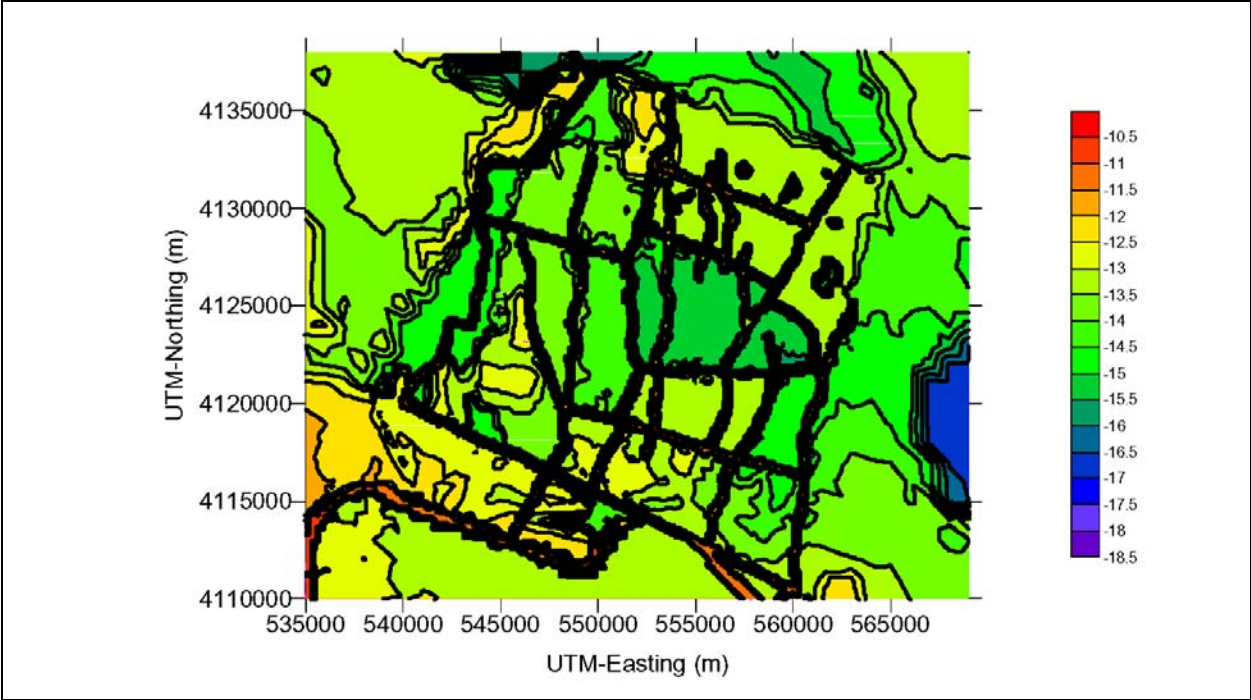


Figure A.3-23
Base-Case Log-Permeability Values (m²) at 1,000 m amsl
for Case with High-K Faults

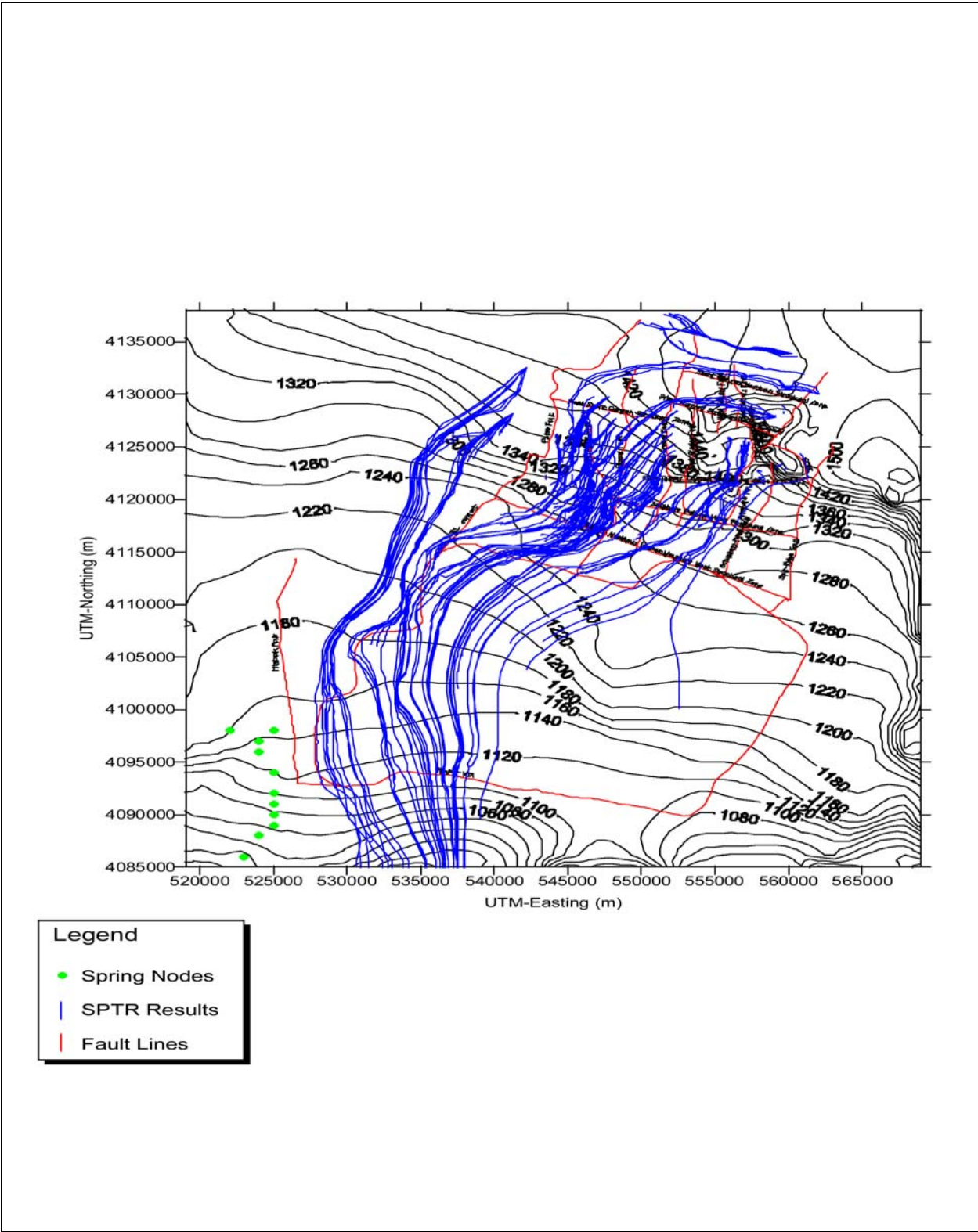


Figure A.3-24
Water-Table Contours in m amsl and SPT Results for Base Case
With a Constant Head Boundary Condition and Neutral Faults

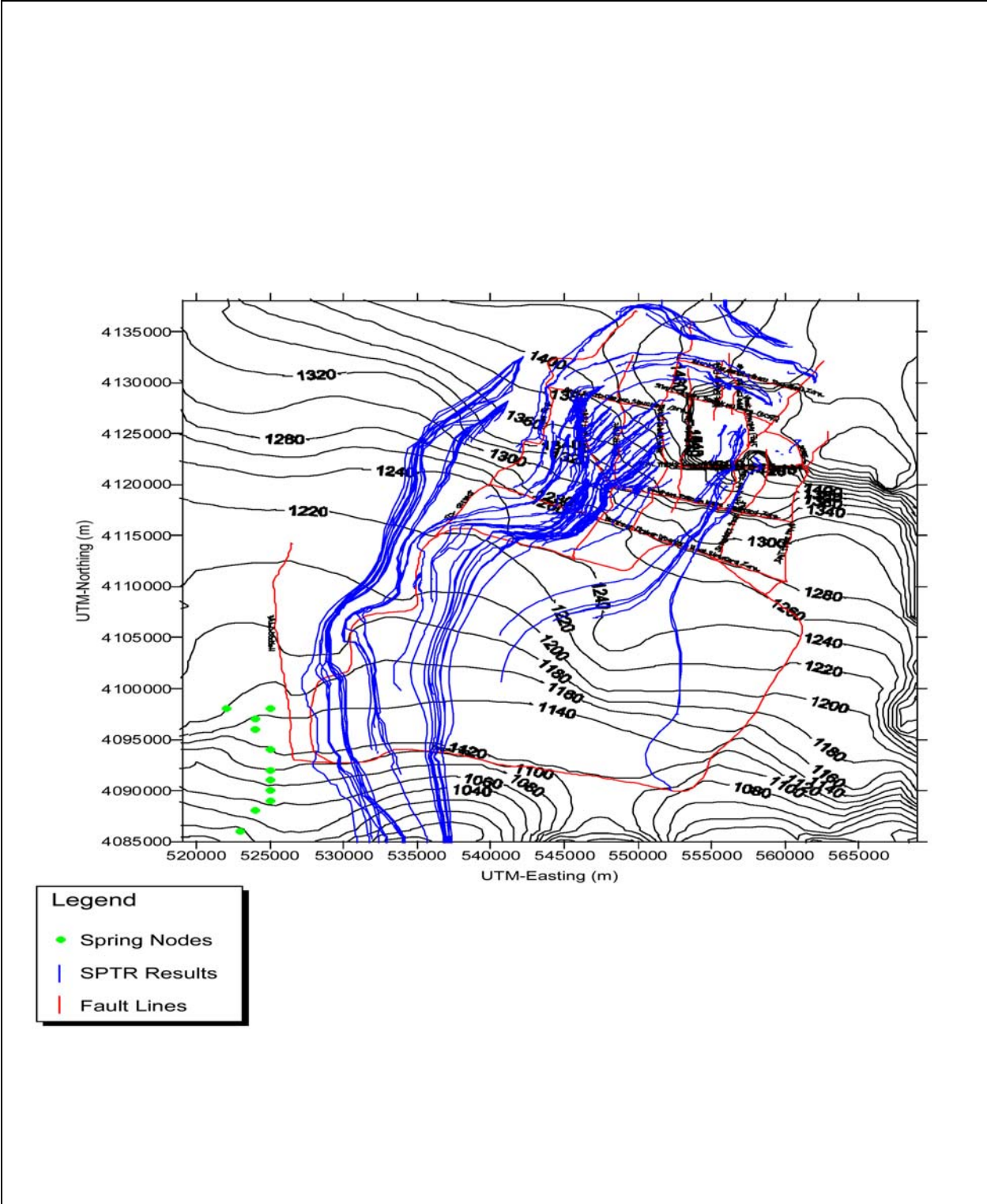


Figure A.3-25
Water-Table Contours in m amsl and SPTR Results for Base Case
With a Constant Head Boundary Condition and Low-K Faults

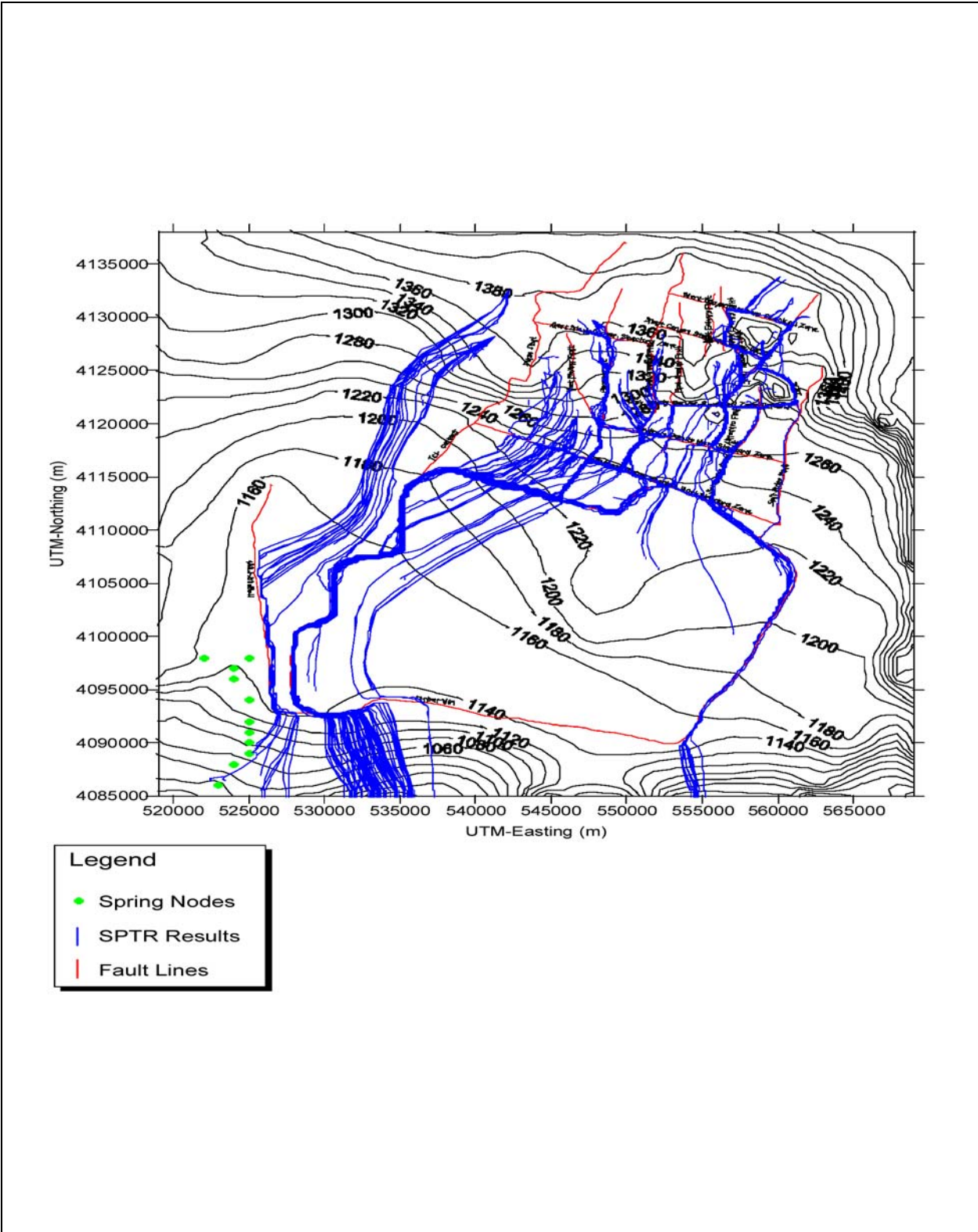


Figure A.3-26
Water-Table Contours in m amsl and SPTR Results for Base Case
With a Constant Head Boundary Condition and High-K Faults

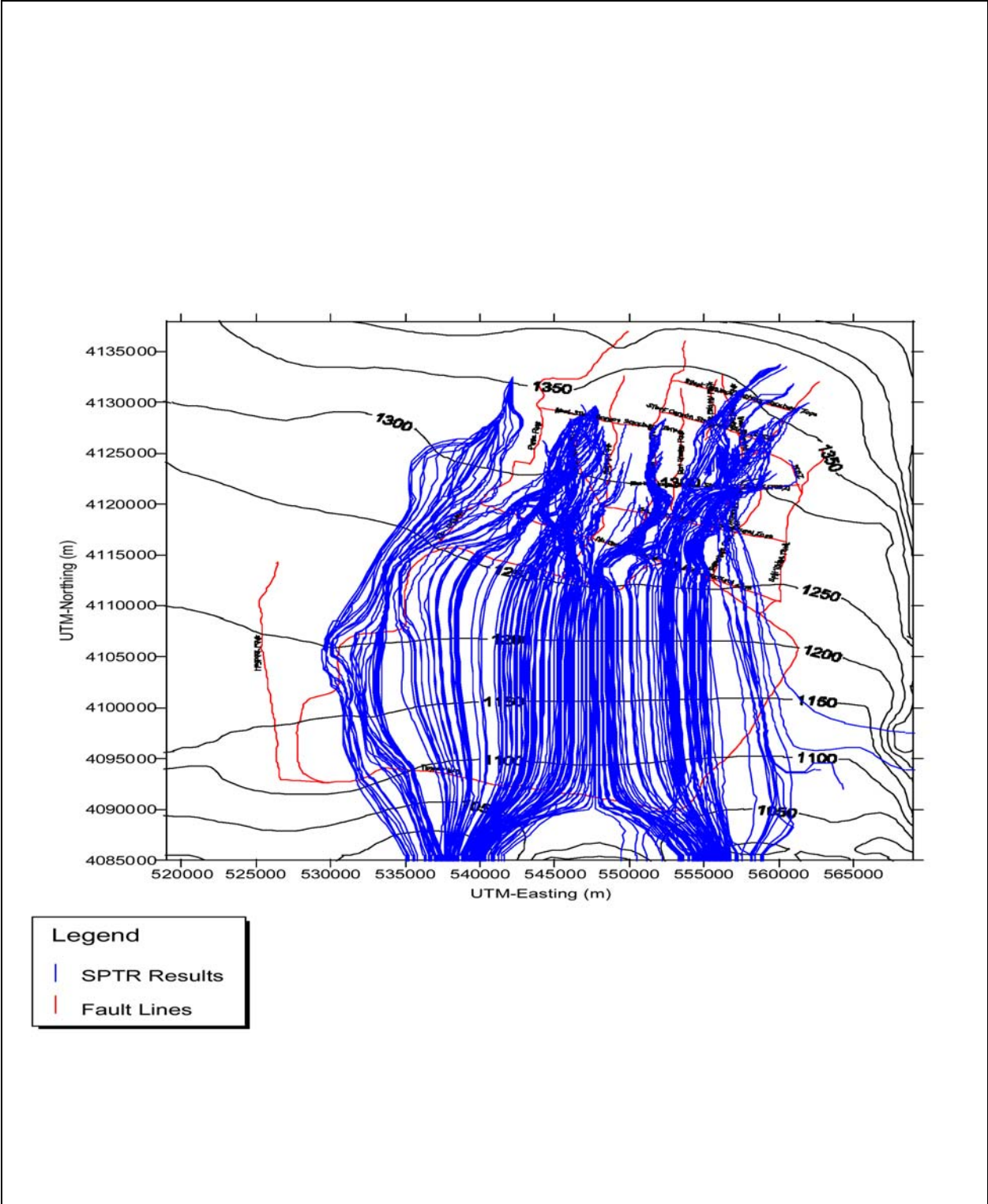


Figure A.3-27
Water-Table Contours in m amsl and SPT Results for Base Case
With a Constant Head Boundary Condition, Neutral Faults and
Without Depth-Decaying Conductivity

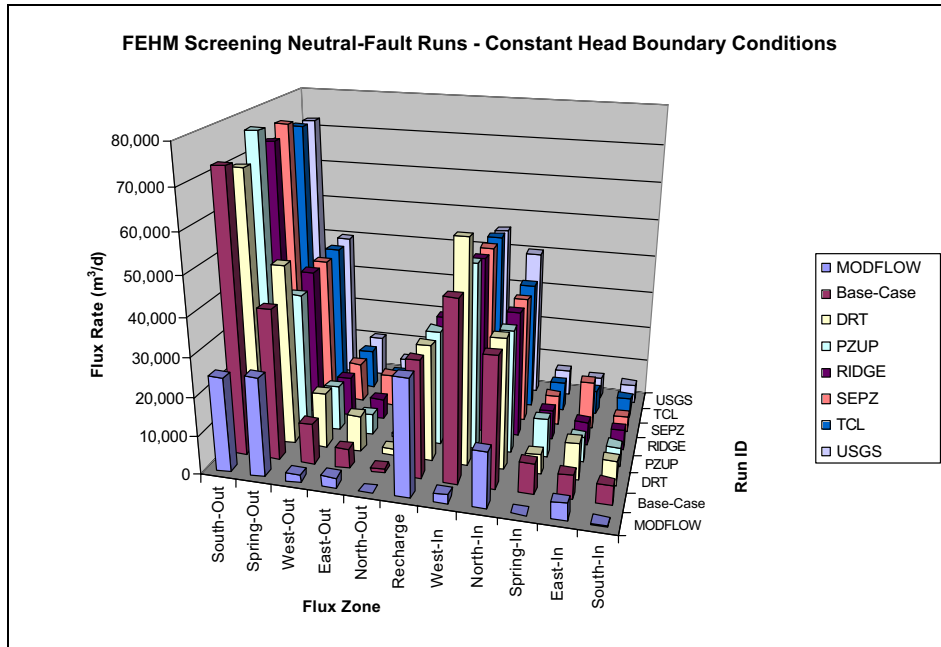


Figure A.3-28
Flux Balances for Neutral-Fault Simulations

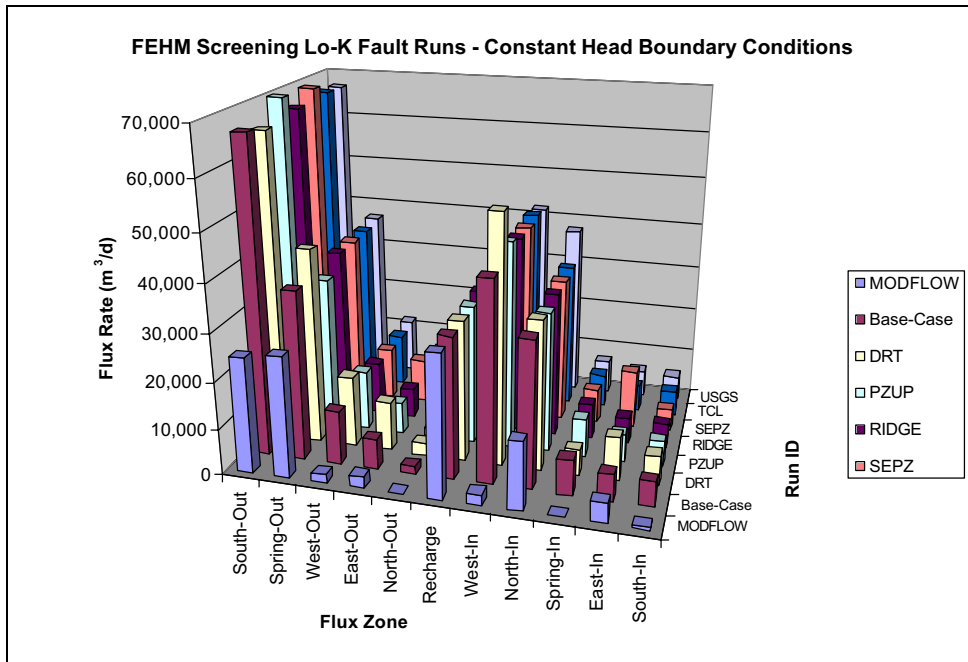


Figure A.3-29
Flux Balances for Low-K Fault Simulations

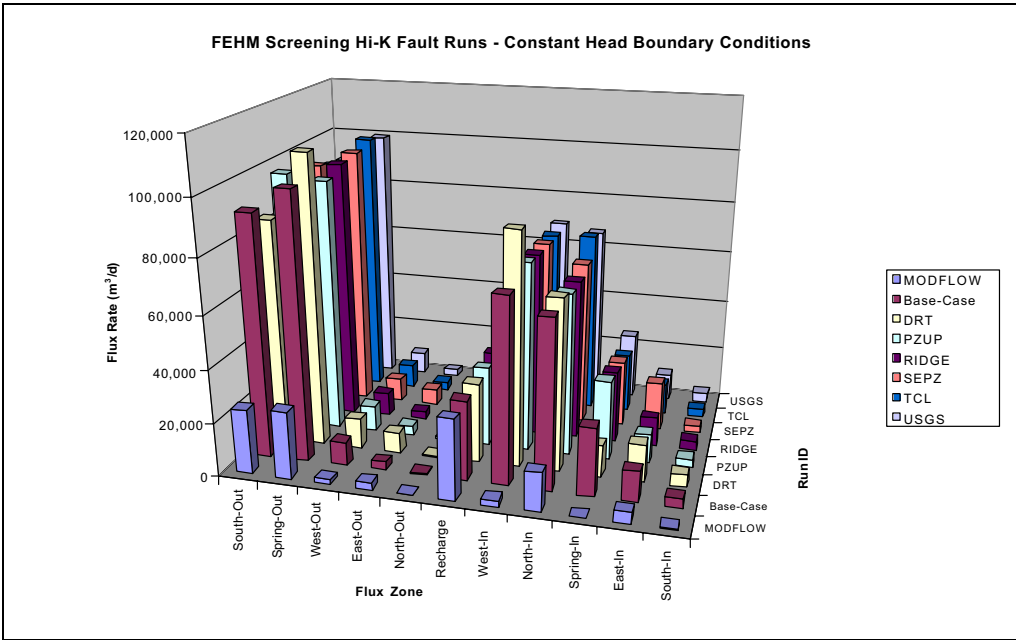


Figure A.3-30
Flux Balances for High-K Fault Simulations

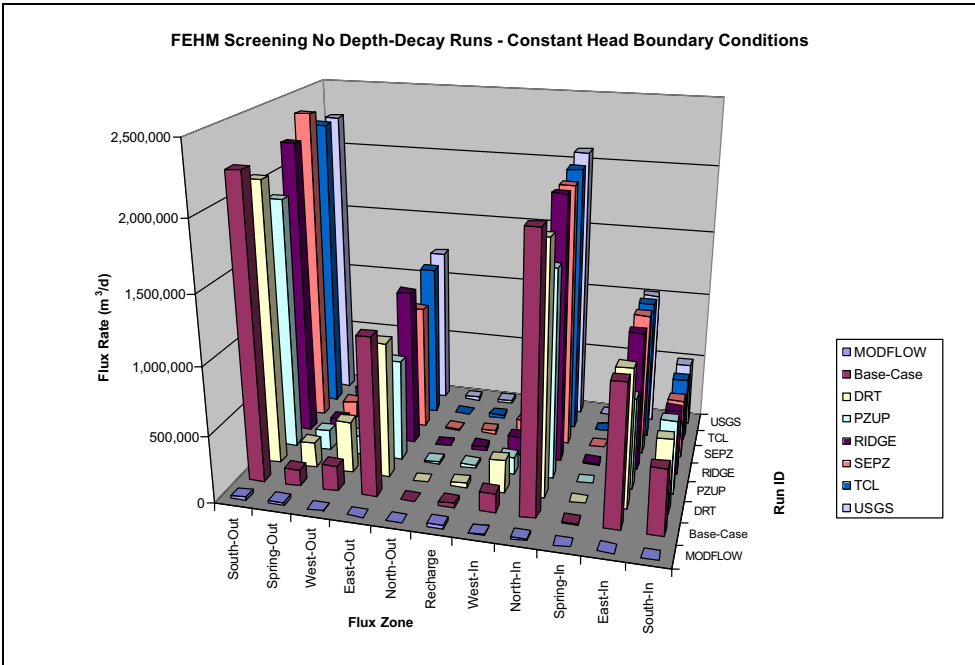


Figure A.3-31
Flux Balances for Simulations Without Depth Decay of Hydraulic Conductivity

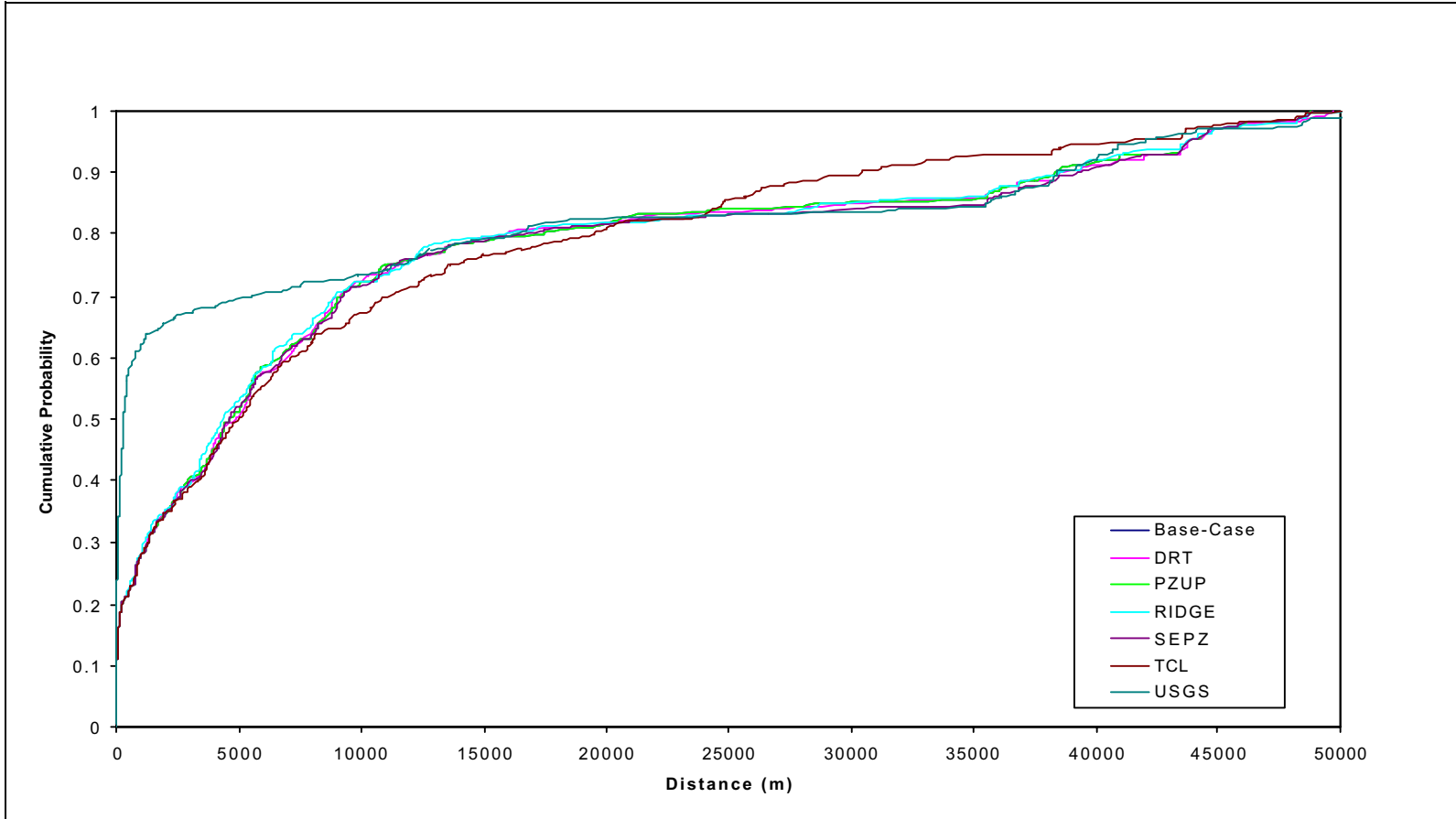


Figure A.3-32
Cumulative Probabilities of Particle Travel Distances at 1,000 Years for the Neutral Fault
Cases With Constant-Head Boundaries

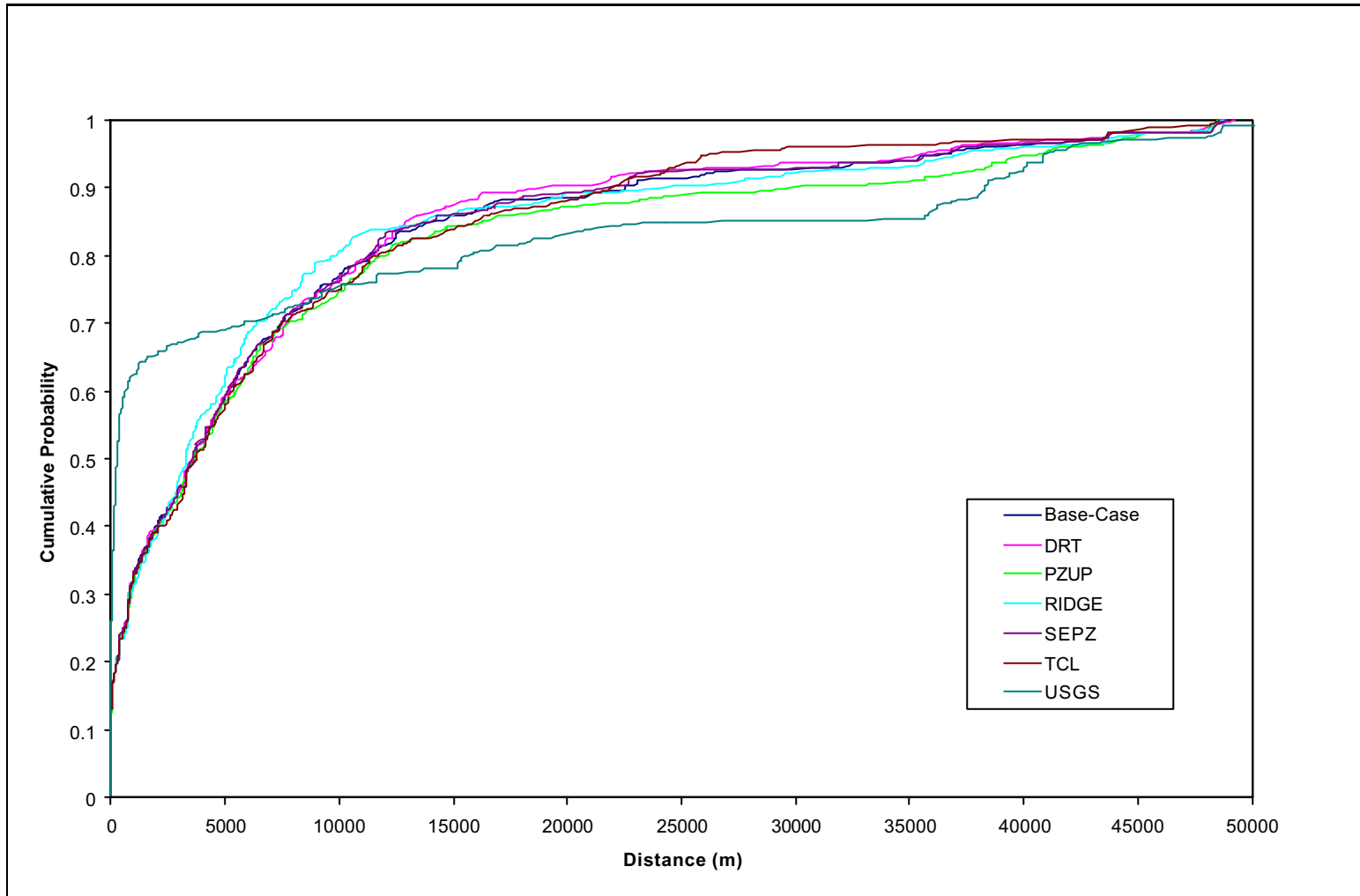


Figure A.3-33
Cumulative Probabilities of Particle Travel Distances at 1,000 Years for the Low-K Cases
With Constant-Head Boundaries

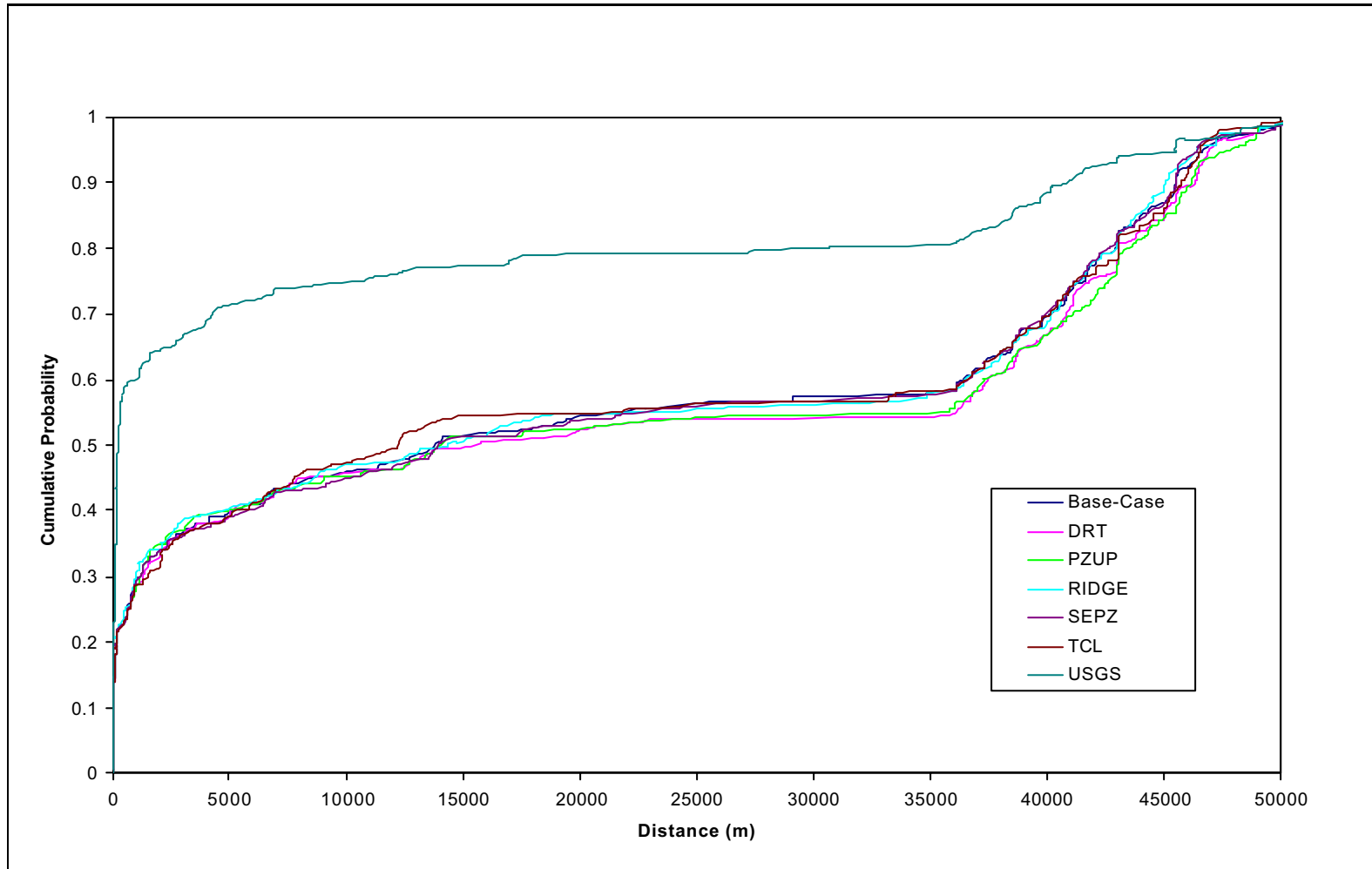


Figure A.3-34
Cumulative Probabilities of Particle Travel Distances at 1,000 Years for the High-K Cases
With Constant-Head Boundaries

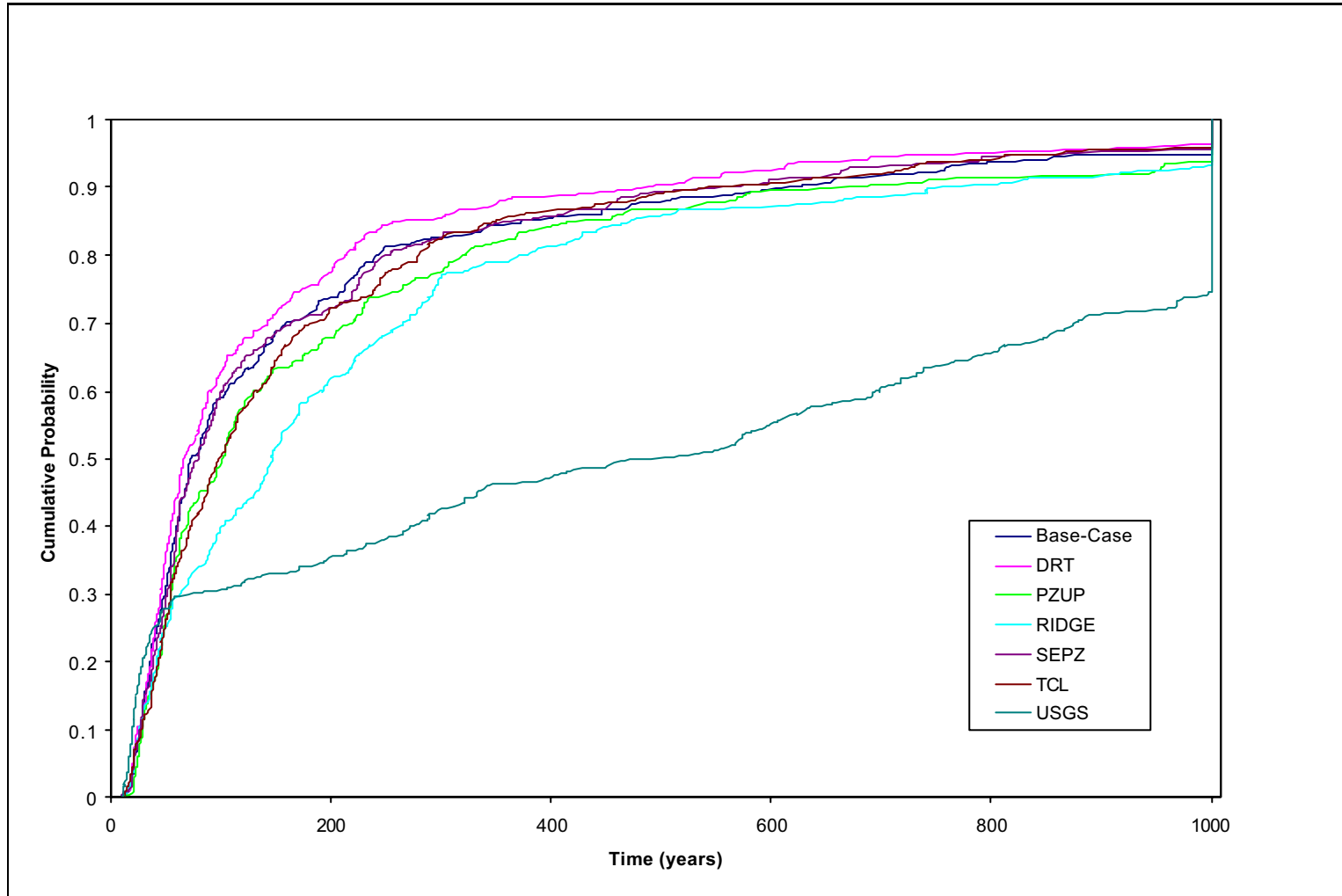


Figure A.3-35
Cumulative Probabilities of Particle Travel Times for the Cases
With No Depth Decay of Permeability and With Constant-Head Boundaries

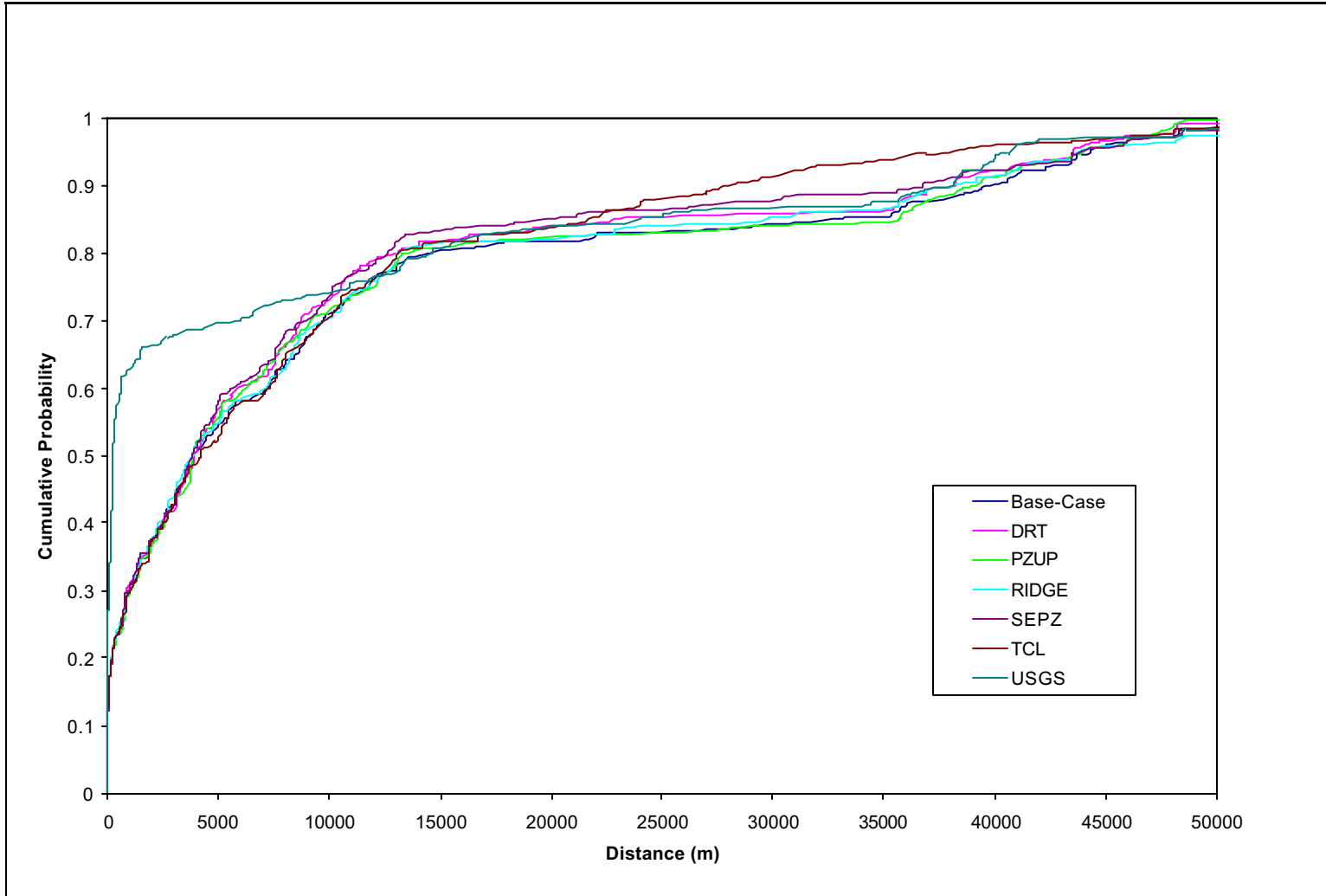


Figure A.3-36
Cumulative Probabilities of Particle Travel Distances at 1,000 Years for the Cases
With Neutral Faults and Flux Boundaries

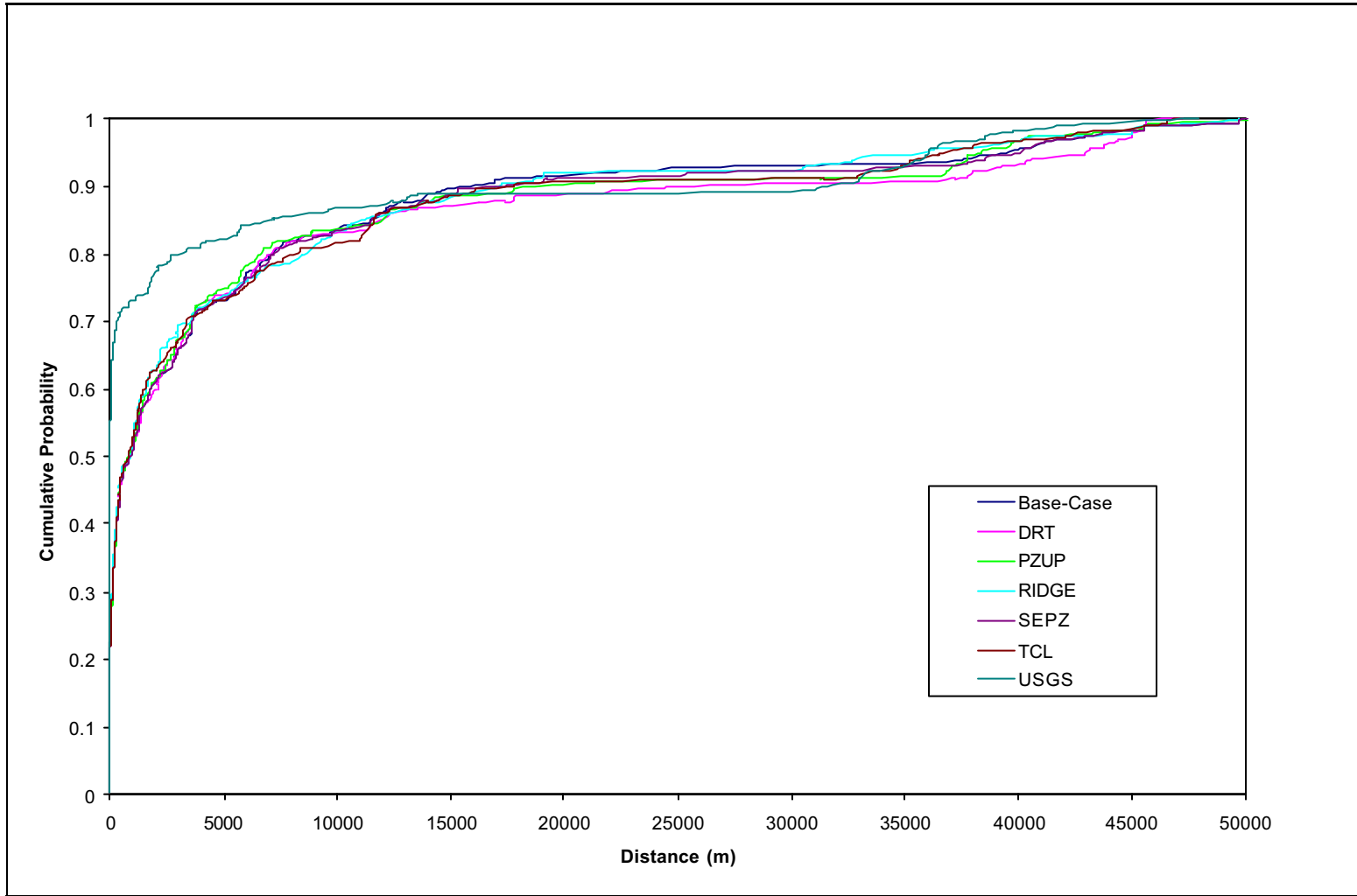


Figure A.3-37
Cumulative Probabilities of Particle Travel Distances at 100 Years for the Cases
With Neutral Faults and Flux Boundaries

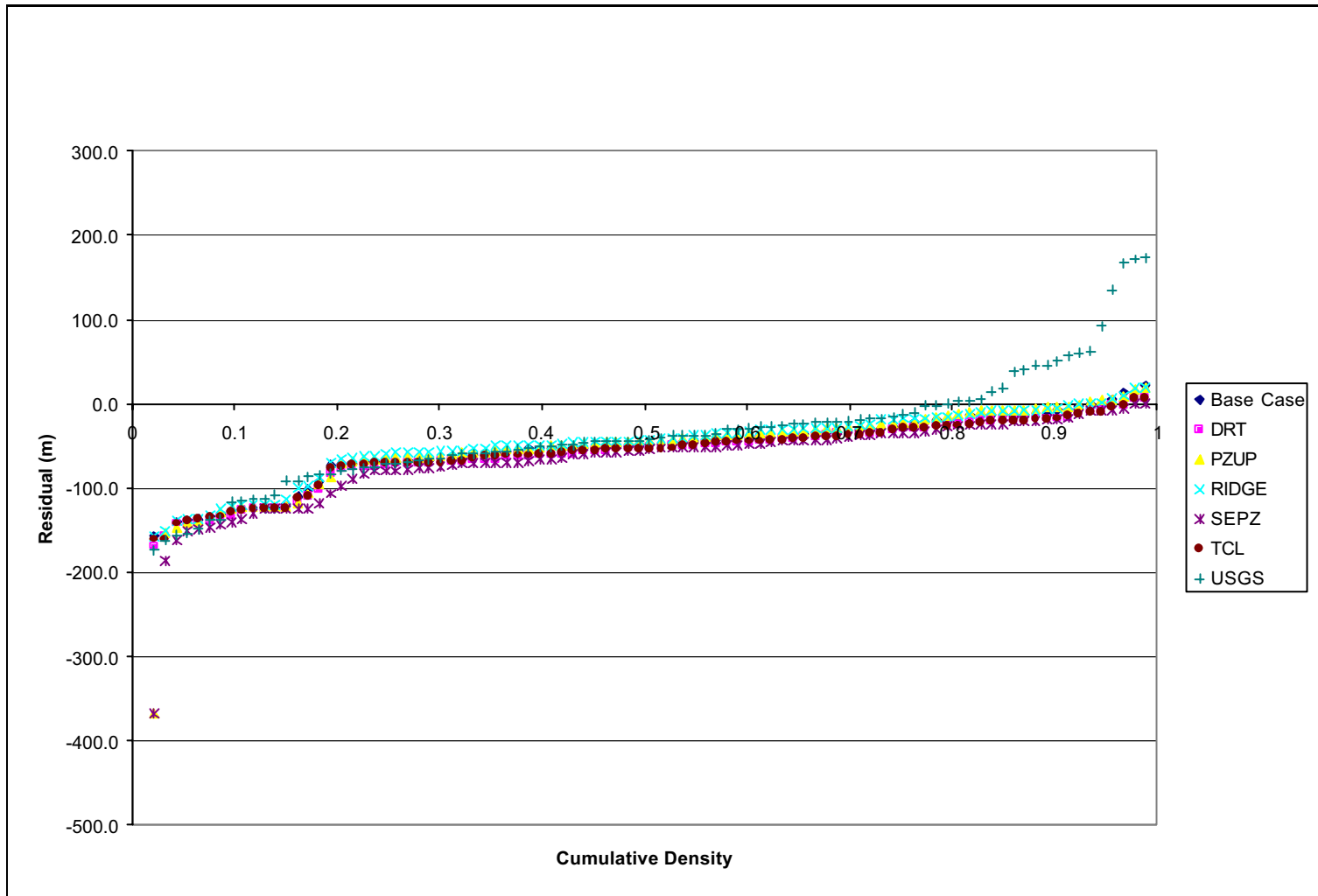


Figure A.3-38
Head Residuals for Constant-Flux Boundary Condition Simulations
With Neutral Faults

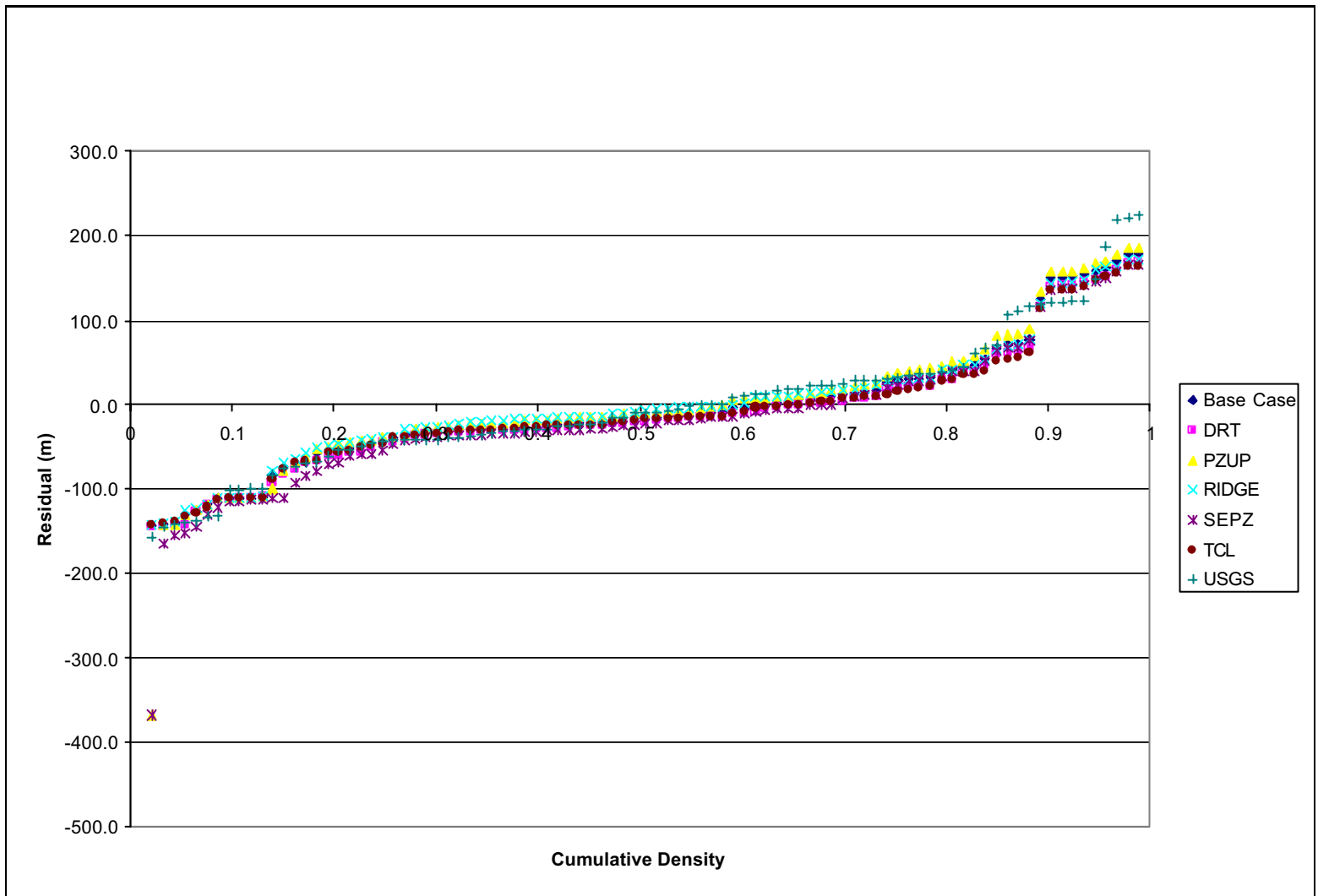


Figure A.3-39
Head Residuals for Constant-Flux Boundary Condition Simulations
With Faults As Barriers

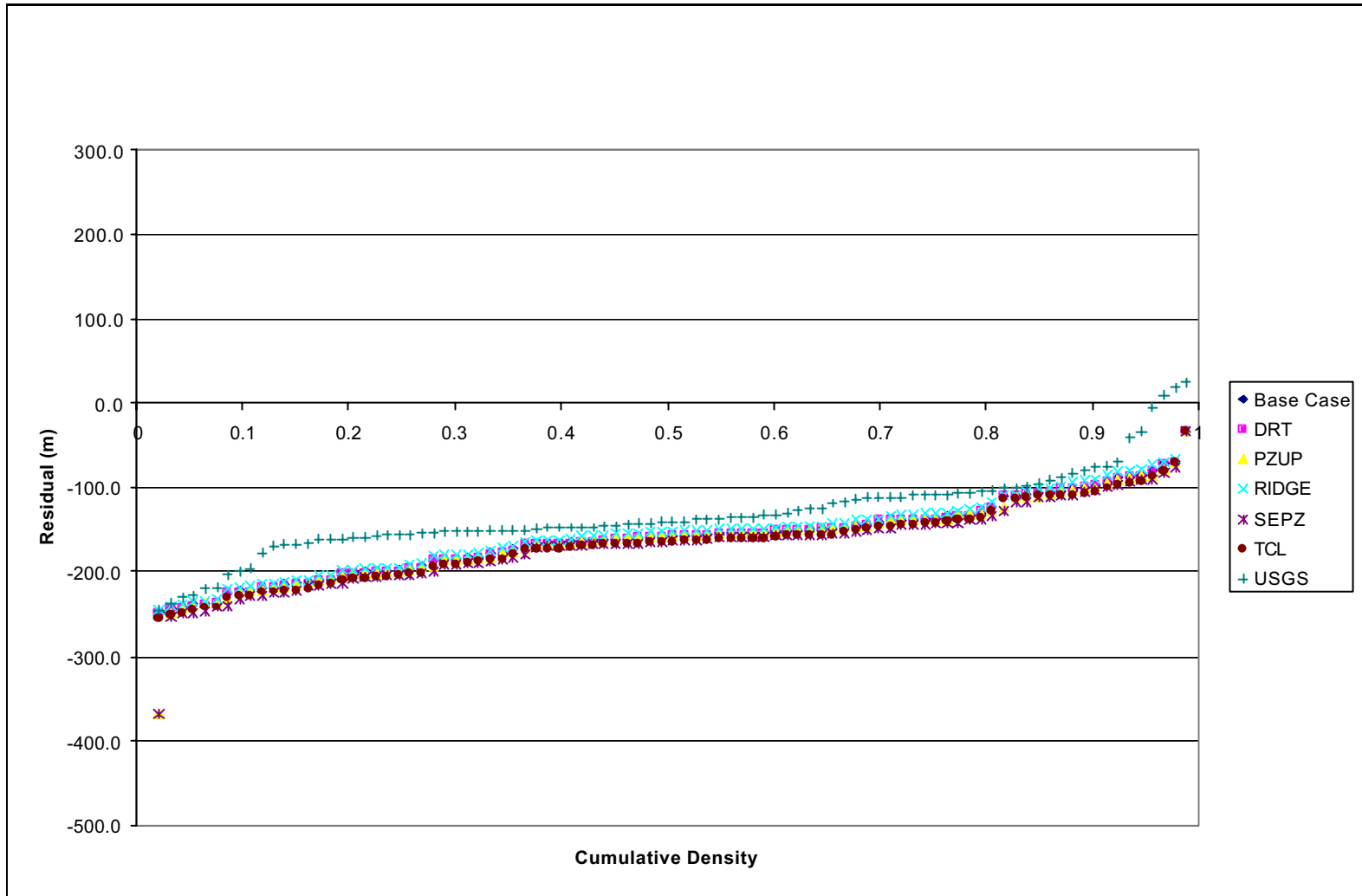


Figure A.3-40
Head Residuals for Constant-Flux Boundary Condition Simulations
With Faults As Conduits

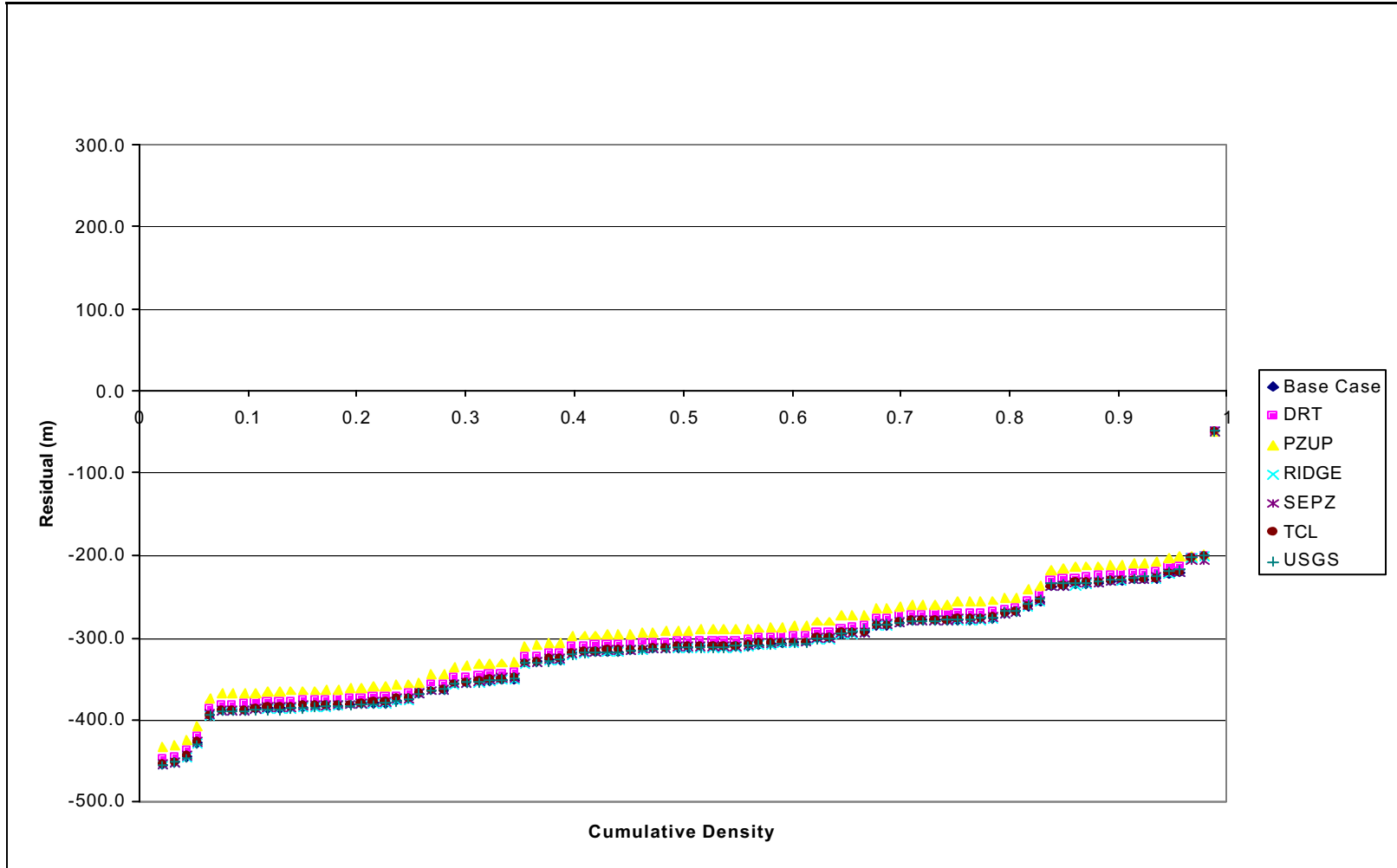


Figure A.3-41
Head Residuals for Constant-Flux Boundary Condition Simulations
With No Depth Decay of Permeability

A.4.0 References

- BN, see Bechtel Nevada.
- Bear, J., 1972. *Dynamics of Fluids in Porous Media*. New York: Dover Publications.
- Bechtel Nevada. 2002. *Hydrostratigraphic Model for the Groundwater Flow and Contaminant Transport Model of Corrective Action Units 101 and 102: Central and Western Pahute Mesa, Nye County, Nevada*, DOE/NV/11718-646. Prepared for U.S. Department of Energy, National Nuclear Security Administration Nevada Operations Office. Las Vegas, NV.
- DOE/NV, see U.S. Department of Energy, Nevada Operations Office.
- Dynamic Graphics, Inc. 2002. *EarthVision 7: Software for 3-D Modeling and Visualization*. Alameda, CA.
- Ferguson, J.F., A.H. Cogbill, and R.G. Warren. 1994. "A Geophysical-Geological Transect of the Silent Canyon Caldera Complex, Pahute Mesa, Nevada." In *Groundwater*, Vol. 99 (B3): 4323-4339. Columbus, OH: Groundwater Publishing Company.
- Fridrich, C.J., S.A. Minor, and E.A. Mankinen. 1999a. *Geologic Evaluation of the Oasis Valley Basin, Nye County, Nevada*, U.S. Geological Survey Open-file Report 99-533-A.
- Fridrich, C.J., S.A. Minor, P.L. Ryder, and J.L. Slate. 1999b. *Geologic Map of the Oasis Valley Basin and Vicinity, Nye County, Nevada*, U.S. Geological Survey Open-File Report 99-533B, scale 1:62,500.
- IT Corporation. 1996. *Regional Geologic Model Data Documentation Package (Phase 1 Data Analysis Documentation, Volume I)*. Prepared for the U.S. Department of Energy, Nevada Operations Office. Las Vegas, NV.
- McKee, E.H., G.A. Phelps, and E.A. Mankinen. 2001. *The Silent Canyon Caldera—A Three-Dimensional Model as part of a Pahute Mesa - Oasis Valley, Nevada, Hydrogeologic Model*, U.S. Geological Survey Open-File Report 01-297. Denver, CO: U.S. Geological Survey.

- McKee, E. H., T.G. Hildenbrand, M.L. Anderson, P.D. Rowley, and D.A. Sawyer. 1999. *The Silent Canyon Caldera Complex—A Three Dimensional Model Based on Drill-Hole Stratigraphy and Gravity Inversion*, U.S. Geological Survey Open-File Report 99-555, 38 p.
- Morelon, I, and D. Guerillot. 1995. *Selection of 3D Geostatistical Reservoir Representations Based on Dynamic Production Criteria*, AAPG Bulletin, Vol. 79, Issue 8. Tulsa, OK: The American Association of Petroleum Geologists.
- Slate, J.L., M.E. Berry, P.D. Rowley, C.J. Fridrich, K.S. Morgan, J.B. Workman, O.D. Young, G.L. Dixon, V.S. Williams, E.H. McKee, D.A. Ponce, T.G. Hildenbrand, WC Swadley, S.C. Lundstrom, E.B. Ekren, R.G. Warren, J.C. Cole, R.J. Fleck, M.A. Lanphere, D.A. Sawyer, S.A. Minor, D.J. Grunwald, R.J. Laczniak, C.M. Menges, J.C. Yount, and A.S. Jayko. 1999. *Digital Geologic Map of the Nevada Test Site and Vicinity, Nye, Lincoln, and Clark Counties, Nevada, and Inyo County, California*, USGS-OFR-99-554-A. Denver, CO: U.S. Geological Survey.
- U.S. Department of Energy, Nevada Operation Office. 1997. *Regional Groundwater Flow and Tritium Transport Modeling and Risk Assessment of the Underground Test Area, Nevada Test Site, Nevada*, DOE/NV--477. Las Vegas, NV.
- Zyvoloski, G.A., B.A. Robinson, Z.V. Dash, and L.L. Trease. 1997a. *Summary of Models and Methods for the FEHM Application - A Finite-Element Heat- and Mass-Transfer Code*, LA-13307-MS. Los Alamos, NM: Los Alamos National Laboratory.
- Zyvoloski, G.A. B.A. Robinson, Z.V. Dash, and I.L. Trease. 1997b. *User's Manual for the FEHM Application - A Finite-Element Heat- and Mass-Transfer Code*, LA-13306-M. Los Alamos, NM: Los Alamos National Laboratory.



Appendix B

Use of Yucca Mountain Site Characterization Project Data for Developing Pahute Mesa Corrective Action Unit Model Parameter Distributions

B.1.0 Introduction

The UGTA project is modeling flow and transport in aquifers of the NTS that have been contaminated from underground testing of nuclear weapons. Modeling is used as a method of forecasting how the hydrogeologic system, including the underground test cavities, will behave over time with the goal of assessing the migration of radionuclides away from these cavities. To this end, flow and transport models are being developed over a range of scales for the UGTA CAUs. For the Central and Western Pahute Mesa CAUs, the predominant hydrologic flow pathways from the test cavities are through locally hydrologically conductive Cenozoic volcanic rocks that were erupted and deposited during multiple eruptive cycles of the Timber Mountain and Silent Canyon caldera complexes (Christensen et al., 1977; Byers et al., 1976; Broxton et al., 1989; Byers et al., 1989; Sawyer et al., 1994). Probability distributions for flow and transport parameters for these rocks are required input for the models.

A major effort of the UGTA project is to compile and assess the suitability of the existing data for these models. Modeling of the UGTA CAUs is not a common groundwater contaminant modeling problem. Most groundwater contamination problems consist of migration of contaminants from relatively well-characterized sources over short flow paths through shallow aquifers. There is often some information about contaminant distribution as a result of monitoring and site characterization. In contrast, the Pahute Mesa CAU model will require prediction of contaminant movement through deep aquifers in a large system (tens of kilometers on a side). Seventy-six widely distributed contaminant sources must be considered for the Pahute Mesa CAU. Information about sources and radionuclide distribution in the aquifer is sparse. Test cavities on Pahute Mesa are as deep as 1,450 m, making extensive characterization of the source and contaminant migration difficult and expensive.

Using experience from other sites to reduce parameter uncertainty is an appropriate approach when developing models in a sparse data environment (Freeze et al., 1990). This approach incorporates flow and transport parameter data from investigations of similar environments when developing prior distributions for parameters to be used in modeling the study area. Utilization of such existing data can be both a cost-effective and necessary step to a modeling effort in a sparse data environment.

Volcanic rocks formed from ash or lava from the Timber Mountain, Silent Canyon, and Claim Canyon Caldera complexes comprised the host environment for the nuclear tests on Pahute Mesa. The Yucca Mountain repository site, located approximately 40 km south of the most southerly test location on Pahute Mesa ([Figure B.1-1](#)), is composed of similar and related volcanic rocks formed by

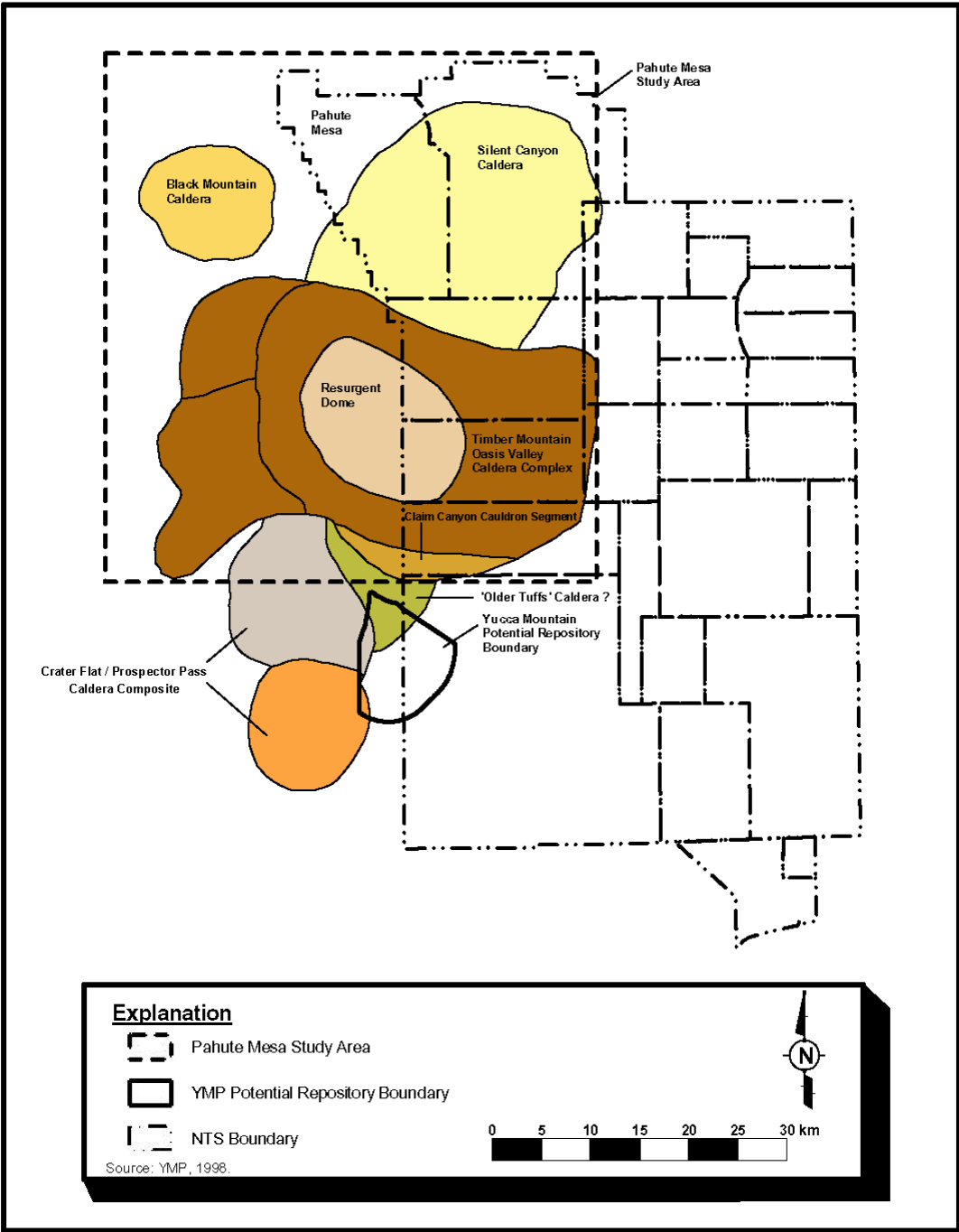


Figure B.1-1
Location of Pahute Mesa, Yucca Mountain Site, and Relevant Caldera Complexes
of the Southwestern Nevada Volcanic Field

eruptions of ash or lava from volcanic vents to the south of Pahute Mesa. The YMP has implemented one of the largest hydrologic and geologic characterization studies of volcanic rocks ever conducted in any setting. The proximity and similar hydrogeologic environment of the Yucca Mountain site to Pahute Mesa make it particularly attractive as a source of potential data for the UGTA modeling effort.

The purpose of this appendix is to provide technical justification for use of YMP characterization data in determining parameter distributions for physical, hydrological, and chemical properties of volcanic rocks for use as input to flow and transport models for Central and Western Pahute Mesa CAUs:

- [Section B.1.0](#) is the introduction.
- [Section B.2.0](#) provides a description of the processes involved in the deposition and alteration of volcanic rocks that influence their characteristics.
- [Section B.3.0](#) discusses the factors influencing flow and transport properties of fractured rock.
- [Section B.4.0](#) provides the technical justification for use of YMP data in Pahute Mesa model parameter distributions.
- [Section B.5.0](#) discusses the uncertainties associated with the use of data from other sites.
- [Section B.6.0](#) provides a list of references used in this appendix.

B.2.0 Deposition and Alteration of Volcanic Rocks

This section provides descriptions of deposition and alteration processes for the volcanic rocks in the Yucca Mountain and Pahute Mesa areas. A discussion of these topics is essential because the flow of groundwater within the volcanic aquifers of the NTS is controlled largely by the physical characteristics of the volcanic rocks that were deposited, in general, as pyroclastic rocks (Winograd and Thordarson, 1975). The physical properties of these rocks vary systematically with the eruptive-emplacement mechanism, temperature of emplacement, and distance from the source vent of the eruptions (Smith, 1960a and b). In addition, superimposed on these properties are the jointing or fracture characteristics of the rocks and the alteration processes of devitrification, zeolitization, and hydrothermal alteration.

B.2.1 Deposition

The geology of the NTS and the surrounding area is the product of a complex history marked by major structural events. For example, the volcanic rocks of the NTS and the surrounding area were emplaced during eruptions of the SWNVF

during the Tertiary Period. Successive eruptions produced at least six large and partially overlapping calderas such as the Timber Mountain and Silent Canyon Caldera complexes, Claim Canyon Caldera, and the Black Mountain Caldera that were filled with ash flows and lava flows, and blanketed surrounding Paleozoic and Precambrian rocks with vast deposits of tuff (DOE/NV, 1999). These vast tuff deposits were emplaced by processes of ballistic fallout and pyroclastic flows (ash-flow tuffs). Individual eruptive units are thickest adjacent to their source calderas and extend radially outward for distances of several tens of kilometers.

An ash fall deposit is formed after material has been explosively ejected from a vent producing an eruption column, which is a buoyant plume of tephra and gas rising high into the atmosphere (Cas and Wright, 1988). As the plume expands, pyroclasts fall back to Earth, under the influence of gravity, at varying distances from the sources, depending on their size and density (Cas and Wright, 1988). As a result, air-fall deposits mix efficiently with the atmosphere and are cooled before deposition resulting in deposits that are well sorted by grain size, if they are not altered to assemblages of clays and zeolites. Fall deposits have low densities and high porosities (20 to 35 percent). Ash-flow tuffs, on the other hand, are the deposits left by surface flows of pyroclastic debris which travel as a high particle concentration gas-solid dispersion (Cas and Wright, 1988). They are gravity controlled and may be deposited at a variety of temperatures (less than 100 degrees celsius [$^{\circ}\text{C}$] to temperatures approaching 800°C), dependent upon such things as the initial magmatic temperature, the specific eruption mechanism, and the transport distance of the ash-flow from the source caldera. In addition, pyroclastic flows that are deposited above the minimum annealing temperatures of volcanic glass will weld (Smith, 1960a). Welding refers to the process of compaction and cohesion of glassy fragments by viscous deformation. The extent of welding is controlled by the depositional temperature and lithostatic load. Generally, the greater the temperature and lithostatic load, the greater the degree of welding with some additional variation from the chemistry of the volcanic glass. Ash-flow tuff, when initially deposited, varies vertically in temperature due to initial variations in the eruption column dynamics (degree of mixing with the atmospheric) and conductive heat loss from the top and bottom of the pyroclastic flow. The vertical variations in temperature and lithostatic load result in distinct zones of welding characterized by bulk density differences. Bulk densities can range from about 1.4 Megagram per cubic meter (Mg/m^3) in the outer cool and non-welded top and bottoms of an ash-flow sheet to about $2.5 \text{ Mg}/\text{m}^3$ in the densely welded interiors of an ash-flow tuff. Porosities are inversely correlated with density and range from greater than 30 to less than 10 percent. The vertical variations in welding of volcanic tuff also occur laterally with distance from the source vents because of heat loss during turbulent flow of the hot density currents that deposit the rocks. Generally, depositional temperatures decrease systematically with distance from vents with correlated lateral decreases in the degree of welding and density, and increases in the porosity of the tuff.

B.2.2 Alteration

Superimposed on the vertical and lateral variations in ash-flow tuff are zones of primary and secondary alteration. Primary alteration refers to devitrification, or the subsolidus recrystallization of original metastable volcanic glass. The main

products of devitrification are cristobalite and alkali feldspar. The primary effect of devitrification is that stable assemblages of minerals are formed that cannot easily be affected by secondary alteration. Generally, the extent of devitrification is controlled by temperature with the hot, welded interiors of ash-flow tuff showing the greatest extent of devitrification. These densely welded, devitrified interiors of sheets of ash-flow tuff tend to maintain open fractures formed as cooling joints during the cooling of a deposit. The narrow spacing of cooling joints leads to a high fracture permeability and these types of rocks, at the NTS, tend to be some of the most productive aquifers.

Secondary alteration of non-welded ash-flow tuff consists primarily of alteration of volcanic glass to assemblages of clays and zeolites. This alteration occurs primarily in the vitric (glassy) exterior top and bottoms of the ash-flow sheets where the initial high porosities of the non-welded rocks transmit water that promotes the secondary alteration. The secondary alteration tends to dramatically reduce the conductivity and effective porosity of volcanic rocks and greatly reduces the ability of the rocks to transmit water. These rocks tend to also have a less brittle nature and a low fracture density due to the absence of cooling joints. Most of the major aquitard units of the NTS region occur in sequences of zeolitized volcanic rocks. These rocks predominate in thick sections of air-fall tuff and the distal (cool emplacement) parts of ash-flow tuff where there is limited welding of the deposits.

B.3.0 Factors Influencing Flow and Transport Parameters of Fractured Rock

The flow of groundwater beneath Pahute Mesa occurs almost exclusively through interconnected natural fractures in volcanic rocks (DOE/NV, 1997). Consequently, the parameters required to appropriately represent flow and transport in the rock mass are influenced significantly by the characteristics of the fracture system. While quantitative predictions of flow and transport parameters cannot be made from characteristics such as rock type or stress, sufficient evidence exists to identify factors that influence flow and transport parameters in fractured rock. A diagram representing these factors and their influence on flow and transport parameters is shown in [Figure B.3-1](#).

Influences on Flow Parameters

Flow in fractured rocks is controlled by fracture geometry and fracture connectivity. Fracture geometry includes characteristics such as orientation, spacing, aperture, and length. Geologic history, lithology, alteration, mineral precipitation or dissolution, and stress history influence fracture geometry.

The emplacement of volcanic rocks during multiple eruptive cycles leads to stratigraphic sequences of ash-flow tuffs and magmas of varying thicknesses. Thermal stress due to cooling of these layers leads to the formation of polygonal joints.

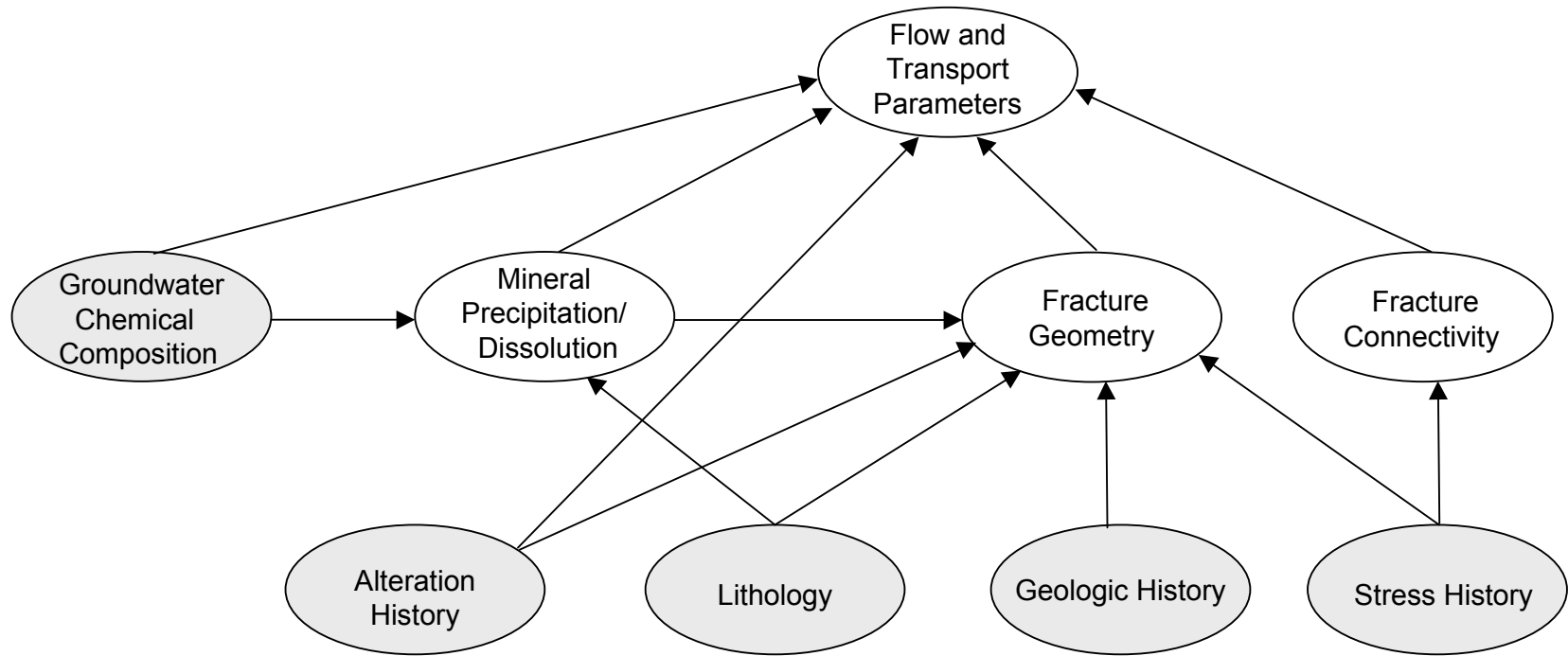


Figure B.3-1
Factors Influencing Flow and Transport Parameters in Fractured Rock

Processes of welding and alteration following emplacement discussed in [Section B.2.0](#) influence matrix porosity and fracture geometry. The geologic and alteration histories contribute to a rock's lithologic classification.

Mineral precipitation or dissolution within fractures also influences fracture geometry and, thus, permeability. The effect on permeability can range from a reduction in permeability from filling fractures with minerals to enhancement of permeability due to fracture fillings forming bridges that prop open fractures (NRC, 1996). Mineral precipitation and dissolution are influenced by lithology and groundwater chemical composition.

Stress can influence fracture orientation and aperture distribution. Regions characterized by extensional stress tend to form extensional fractures oriented perpendicular to the intermediate stress direction. Unless the fractures are filled, fracture permeability in these regions is enhanced due to opening of the fractures (NRC, 1996).

Fracture connectivity is strongly influenced by the state of stress. The degree of connectivity is considered to be inversely related to the magnitude of differential regional stress (NRC, 1996).

Influences on Transport Parameters

Solute transport depends on the distribution of fluid velocities in the rock mass. Velocity distributions are influenced by fracture geometry. Solute dispersion as multiple pathways in the rock mass are encountered; thus, fracture geometry and connectivity influence dispersion.

Diffusion of solutes from fluid in fractures into fracture coatings and the rock matrix is influenced by fracture-coating characteristics, lithology, and alteration of the rock. In addition, fracture geometry influences the amount of rock surface area available for matrix diffusion.

Chemical reactions occurring within the fracture depend on chemical composition of the groundwater, the extent and composition of mineral fillings, and the nature of the rock matrix. Groundwater composition and lithology of the host rocks influence the presence and composition of mineral coatings. Lithology and the alteration history control the sorption characteristics of the rock matrix.

Basis for Correlation Between Sites

Similarities between factors influencing flow and transport parameters shown in [Figure B.3-1](#) provide a basis for incorporation of characterization data for volcanic rocks from other sites into prior distributions of PM-CAU model parameters. The rationale for use of YMP data presented in [Section B.4.0](#) will be based on similarities in geologic history, lithology, alteration, groundwater composition, and stress.

B.4.0 Transferability Rationale

The use of data from the YMP area and proximal CAUs on the NTS in flow and transport modeling of a specific UGTA CAU can be supported by examining specific similarities between the two areas. The previous section identified the factors that influence flow and transport parameters for fractured rock. This section considers these factors specifically for Yucca Mountain and Pahute Mesa to develop the similarities of the two areas.

B.4.1 Geologic Setting

Pahute Mesa

Pahute Mesa is an elongated, east-to-west-oriented volcanic plateau within the SWNVF and consists mainly of Miocene rhyolitic rocks that erupted from local calderas (Lacznik et al., 1996). Its eastern portion occupies the northwestern corner of the NTS, including Areas 19 and 20. The surface of the Pahute Mesa study area consists primarily of ash-flow tuffs of the Thirsty Canyon and Timber Mountain Groups that erupted from calderas located just west and south of the area (Drellack and Prothro, 1997). These Tertiary volcanics, along with volcanic rocks of the underlying Paintbrush Group, bury an older group of calderas that compose the Silent Canyon Caldera complex (Drellack and Prothro, 1997). The Silent Canyon Caldera complex along with the Timber Mountain Caldera complex are the dominant geologic features in the PM-OV region. The Silent Canyon Caldera complex consists of at least two nested calderas, the Area 20 caldera and the older Grouse Canyon caldera. The Grouse Canyon caldera was formed and then filled by Tertiary eruptions of tuff and lava of the Belted Range Group. The Area 20 caldera was formed by eruptions of tuff of the Crater Flat Group, and then filled by eruptions of tuff and lava of the Crater Flat Group and Volcanics of Area 20. The volcanic rocks of the Belted Range Group, the Crater Flat Group, and Volcanics of Area 20 are underlain by a considerable thickness of older volcanic rocks, which were probably erupted locally from unidentified calderas, some possibly beneath Pahute Mesa. In the eastern portion of Pahute Mesa outside the calderas, the Tertiary volcanic rocks probably overlie an unknown thickness of late Precambrian to Cambrian quartzites and siltstones. Paleozoic carbonates may underlie the volcanic rocks in the western portion of Pahute Mesa (Drellack and Prothro, 1997).

Yucca Mountain

Yucca Mountain is a remnant of a Miocene-Pliocene volcanic plateau that was centered around the Timber Mountain/Oasis Valley caldera complex in the SWNVF. Yucca Mountain consists of a series of volcanic outflow sheets that frame the southern margin of the Claim Canyon caldera. North-to-south trending basin and range faults have disrupted the volcanic plateau and formed linear mountain ranges separated by sediment-filled troughs. Yucca Mountain is an east-tilted fault block consisting of a thick sequence of tuffs erupted from the middle to late Miocene Timber Mountain-Oasis Valley caldera complex located to

the north and west (Broxton et al., 1987; Byers et al., 1976; Christiansen et al., 1977).

The exposed stratigraphic sequence at Yucca Mountain is dominated by Tertiary ash-flow tuffs and ash-fall tuffs, with minor lava flows and reworked volcanic material (Broxton et al., 1987). Most tuffs are high-silica rhyolites, but two large-volume, ash-flow cooling units in the upper part of the sequence are compositionally zoned grading upward in composition from rhyolite to quartz latite. Exposed rocks at Yucca Mountain consist primarily of these two zoned tuffs, the Topopah Spring Tuff and Tiva Canyon Tuff of the Paintbrush Group (Broxton et al., 1987). The Paintbrush Group erupted from the Claim Canyon caldera just north of Yucca Mountain. According to Sawyer et al. (1994), the Topopah Spring Tuff has an age of 12.8 million years while the Tiva Canyon Tuff has an age of 12.7 million years. Beneath the Paintbrush Group, the principal stratigraphic units are in descending order: Calico Hills Formation (Volcanics of Area 20), Crater Flat Group, Lithic Ridge Tuff of the Tram Ridge Group, Tunnel Formation, and older tuffs and Tertiary sediments. Wells on Yucca Mountain have penetrated to depths of 1.8 km without leaving volcanic rocks, and the volcanic section east of Yucca Mountain is about 1.2 km thick and overlies the Silurian Lone Mountain Dolomite (Broxton et al., 1987).

B.4.2 Lithology

Intensive studies associated with the YMP and the weapons-testing program have shown that hydrologic properties can generally be correlated with major volcanic rock types (Blankennagel and Weir, 1973; Winograd and Thordarson, 1975; Drellack and Prothro, 1997; Prothro and Drellack, 1997). For example, Blankennagel and Weir (1973) state that ash-fall tuffs and nonwelded (or slightly welded) ash-flow tuffs have similar physical properties and hydraulic characteristics, although their origin and mode of emplacement differs. This suggests that hydrologic data gathered from field or laboratory studies of volcanic rocks at one site can be applied or transferred to another less well-studied site if it contains comparable types of volcanic rocks. This has important implications for the modeling of UGTA CAUs because the Yucca Mountain area contains comparable types of volcanic rocks that have been more extensively studied than the volcanic rocks found at the Pahute Mesa study area. For example, the widely distributed ash-flow sheets of the Timber Mountain and Paintbrush Groups that were erupted from the Timber Mountain and Claim Canyon calderas, respectively. These rocks are generally similar in chemical composition and exhibit mostly similar patterns in their vertical and lateral variations in welding. Both groups of rocks are present in the subsurface of the Pahute Mesa study area, while the Yucca Mountain site is underlain primarily by multiple ash-flow sheets of the Paintbrush Group. This is advantageous for the modeling efforts of the Pahute Mesa study area because extensive physical properties data and hydrologic measurements of the Paintbrush Group have been obtained for the rocks along the length of Yucca Mountain. These rocks were extensively studied at Yucca Mountain because the target horizon for the location of the potential underground repository is in the densely welded, devitrified interior of the Topopah Spring Formation of the Paintbrush Group.

B.4.3 Alteration

The alteration of volcanic rocks can also influence flow and transport parameters. For example, it was seen in [Section B.3.0](#) of this appendix that alteration of volcanic rocks can directly effect fracture geometry. Therefore, any lithologic comparison between the two areas must also include an examination of possible alteration products. The transfer of data from one specific area to another is supported by demonstrating that the two areas have comparable types and degrees of alteration. Broxton et al. (1987) state that alteration of volcanic rocks at Yucca Mountain is mostly observed in nonwelded ash-flow tuff, bedded tuff, and in thin envelopes of nonwelded tuff at the top and bottom of cooling units that have densely welded, devitrified interiors. The tuffs were vitric after emplacement and were highly susceptible to alteration because of the instability of volcanic glass in the presence of groundwater. This has important implications for the modeling of UGTA CAUs because the Pahute Mesa study area has undergone similar types of alteration as the Yucca Mountain area. However, the altered volcanic rocks at Yucca Mountain have been extensively studied. For example, the alteration history of a thick sequence of vitric and zeolitized ash-fall tuffs of the Calico Hills Formation has been carefully studied as part of the YMP site characterization study. These volcanic rocks were studied extensively because they form a major vertical transport barrier between the target horizon of the Topopah Springs Formation and the water table at Yucca Mountain. These studies would provide a valuable source of comparable data for the modeling efforts of the Central and Western Pahute Mesa CAUs because related rocks of the Paintbrush Group and the Calico Hills Formation, for example, are present in the Central and Western Pahute Mesa CAUs.

B.4.4 Influence of Stress

Stress can influence fracture orientation, aperture distribution, and fracture connectivity. Extensional regions tend to form extensional fractures that are open to flow. The orientation of these open fractures is generally parallel to the intermediate stress direction. Permeability tends to be enhanced in the direction of the fracture orientation unless fractures are filled (NRC, 1996).

In addition, the interaction and linkage of joints is influenced by the state of stress. Nearby fractures tend to interact and connect if the differential regional stress is small. When differential stress is large, the tendency to connect is weak (NRC, 1996).

Regional stress is characterized by the directions and magnitudes of the principal stresses. Directions of horizontal stress have been determined by tectonic and structural analyses and by analyses of borehole elongation. Magnitudes of the least horizontal principal stress, S_h , can be directly measured using the hydraulic fracturing method and the greatest horizontal principal stress, S_H , can be estimated indirectly from this method (Stock and Healy, 1988).

Stress Directions

A model proposed by Carr (1974) based on tectonic and structural analyses suggests the NTS region is undergoing extension with the direction of the least

principal stress being North 50° West. Measurements made by Stock and Healy (1988) in four boreholes at Yucca Mountain found the direction of least principal stress to range from North 60° West to North 65° West. Stress directions were determined in seven boreholes on Pahute Mesa by Springer et al. (1984) using borehole elongation information. The distribution of orientation of borehole elongations was slightly bimodal with the major mode corresponding to a direction of least principal stress of North 56° West. The orientation of borehole elongation was evaluated in 12 additional boreholes on Pahute Mesa by Gillson (1993). The mean orientation of the direction of least principal stress from these analyses was also North 56° West. These results show good agreement between Yucca Mountain and Pahute Mesa in measured directions of least horizontal principal stress.

Stress Magnitudes

Seven measurements of the magnitude of the least horizontal principal stress (S_h) and seven corresponding estimates of the magnitude of the greatest horizontal principal stress (S_H) were obtained from three boreholes on Yucca Mountain by Stock and Healy (1988). No measurements of stress magnitude were found for Pahute Mesa; however, Carr (1974) reports two measurements of the maximum excess horizontal stress at two depths in tunnels under Rainier Mesa. These measurements along with the maximum excess horizontal stress ($S_H - S_h$) from the data of Stock and Healy (1988) are plotted in [Figure B.4-1](#).

Measurements on Yucca Mountain were made at depths ranging from 1,026 to 1,573 m. The increase in maximum excess horizontal stress with depth for the Yucca Mountain measurements can be seen in [Figure B.4-1](#). An exponential relationship was fit to the Yucca Mountain data and is shown in the figure.

Given the increase of maximum excess horizontal stress with depth evidenced by the Yucca Mountain measurements, the stress magnitudes for Rainier Mesa measured at a relatively shallow depth are consistent with stress magnitudes measured at Yucca Mountain. These similarities in the regional stress regime suggest that the influence of regional stress on fracture network characteristics is similar for Pahute Mesa and Yucca Mountain.

B.4.5 Groundwater Chemistry

Groundwater chemistry is an important component of flow and transport models because it influences everything from mineral dissolution/precipitation reactions to fracture geometry. Examination of the groundwater chemistry for the Pahute Mesa and the Yucca Mountain areas reveals that both locations have similar geochemical signatures for wells that penetrate Tertiary volcanic rocks. This also has important implications for the transfer of data from the Yucca Mountain area to the Pahute Mesa study area because it supports the argument that both areas contain similar types of rocks. It is well documented that groundwater acquires a chemical signature, or fingerprint, by reaction with aquifer solids along the flow path. Similar chemical signatures indicate that groundwater is flowing through similar types of aquifer material. [Figure B.4-2](#) is a trilinear diagram showing the relative concentrations of major ions in composite groundwater samples from selected wells in the Pahute Mesa and Yucca Mountain regions. The figure

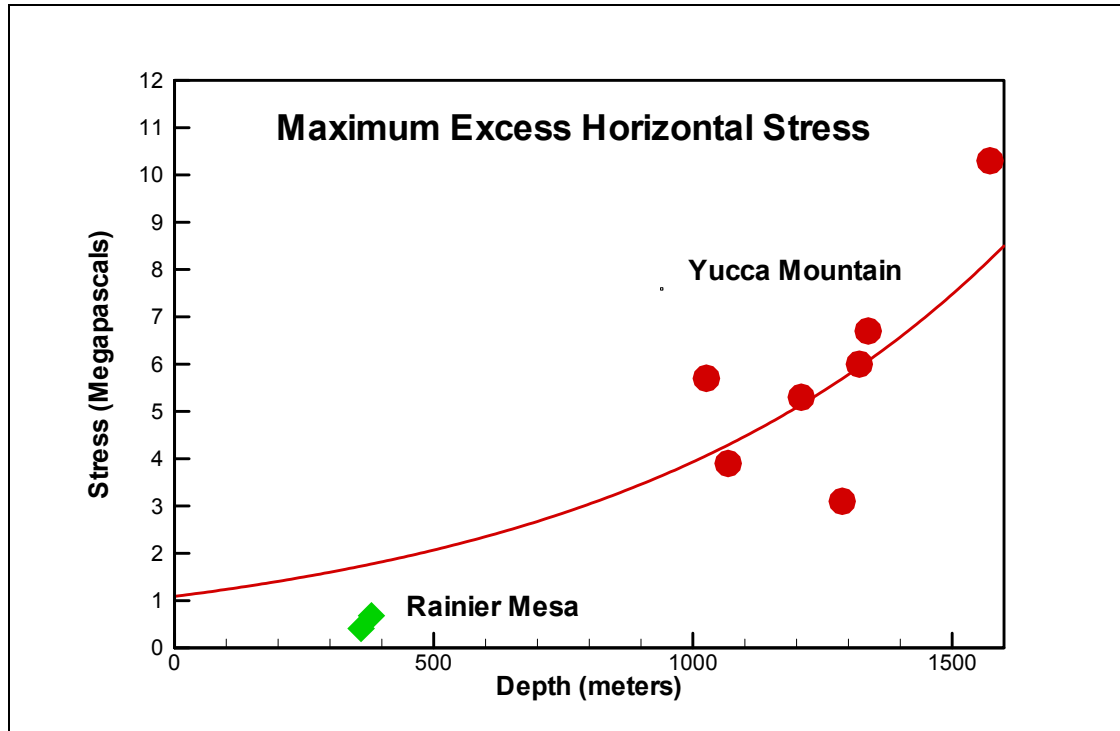


Figure B.4-1
Maximum Excess Horizontal Stress from Yucca Mountain Boreholes
(Stock and Healy, 1988) and Rainier Mesa (Carr, 1974)

contains three different plots of major-ion chemistry. The concentrations on the trilinear diagram are expressed in percent milliequivalents per liter. Trilinear diagrams are useful for illustrating various groundwater chemistry types and relationships that may exist between the types. It can be seen from the trilinear diagram that sodium is the dominant cation for both regions with minor amounts of calcium and magnesium. Further examination of the figure reveals that bicarbonate is the dominant anion for both regions with minor amounts of sulfate and chloride. However, it can be seen from the figure, in general, the Pahute Mesa study area has greater amounts of chloride and sulfate than the Yucca Mountain area. It has been suggested that the higher proportions of chloride and sulfate in the eastern side of Pahute Mesa are a result of the interaction of groundwater with hydrothermally altered zones (Blankennagel and Weir, 1973). The Pahute Mesa study area, however, has greater amounts of chloride and sulfate than the Yucca Mountain area. Groundwater with chemical compositions such as these can be classified as sodium-potassium-bicarbonate type water. This water type is typically found in volcanic terrain and alluvium derived from volcanic material. The similarity in groundwater composition between the two areas for wells that penetrate the Tertiary rocks illustrates that the groundwater in both regions is in contact with similar types of volcanic rocks.

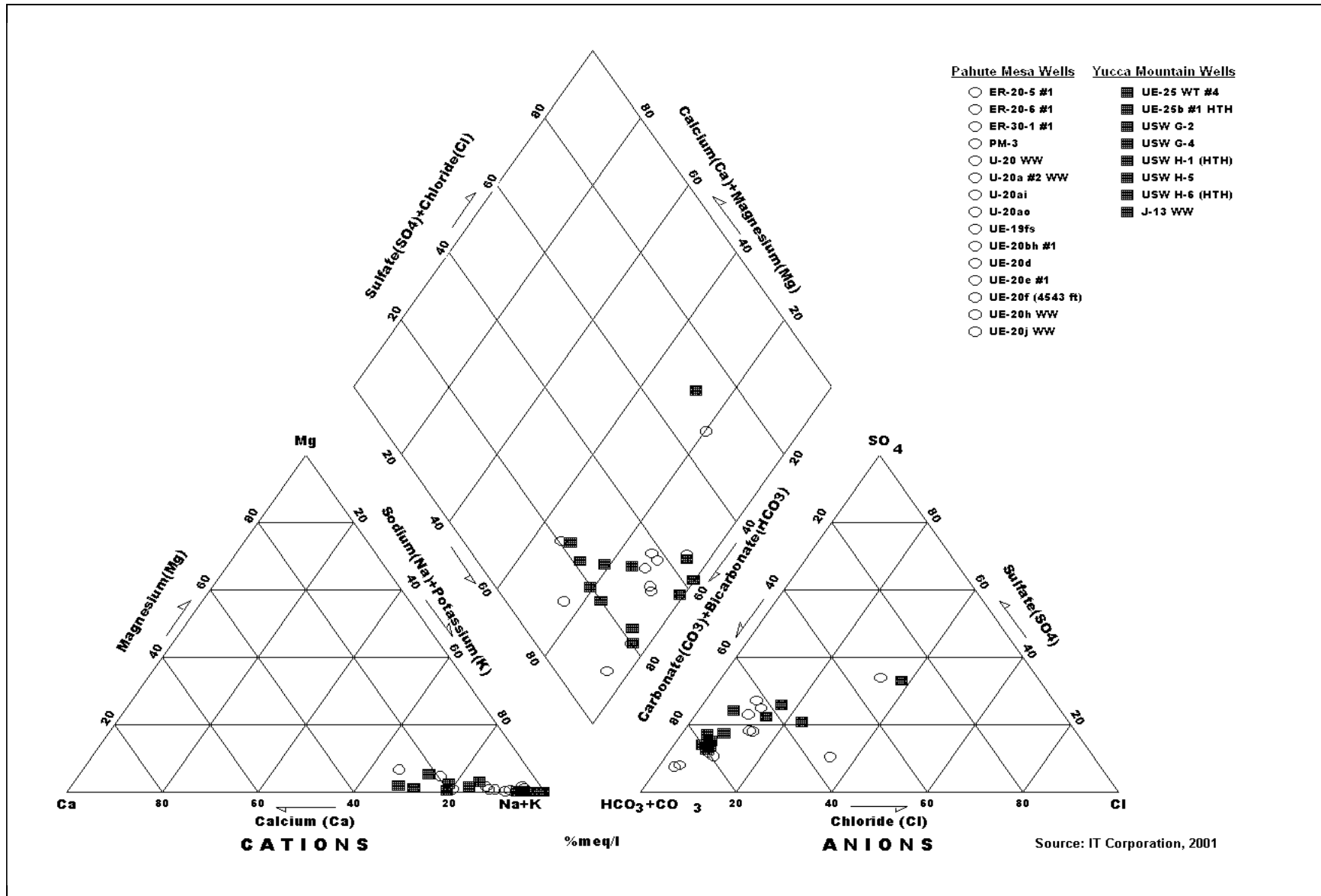


Figure B.4-2
Trilinear Diagram Showing Relative Major Ion Percentages for Groundwater from Pahute Mesa and Yucca Mountain (IT, 2001)

B.4.6 Summary

The use of data from the Yucca Mountain area to develop parameter distributions for flow and transport modeling of UGTA CAUs can be supported by examining specific similarities between the two areas.

- Both areas are located in the SWNVF.
- The volcanic rocks in both areas are the results of similar deposition processes.
- Both areas contain similar lithologic units and even lithologic units from the same source area.
- In addition, both areas have experienced similar types of alteration including devitrification and zeolitization of volcanic material.
- The two areas have also undergone similar types of regional tectonic stresses, resulting in a similarity in the two areas of regional fracture orientations.
- Finally, the two areas have similar groundwater chemistry.

B.5.0 Uncertainties in Data Transfer

While much hydrologic and transport information can be transferred from comparable sources of data, there are several cautions that must accompany the transfer and interpretation of this type of data.

First, and most importantly, hydrologic properties of volcanic tuff are strongly controlled by the fracture properties of the rocks. These properties are controlled in part by the vertical and lateral distribution of cooling joints that can be systematically related to the welding properties of the ash-flow sheets. However, an additional and locally dominant component of fracture permeability is associated with tectonic fractures. These fractures are controlled by the local tectonic setting and the presence and nature of faulting, particularly basin and range faults associated with extensional faulting and basin formation. As a result, hydrologic properties of jointed volcanic rocks can vary dramatically in proximity to major fault systems. Studies of fracture frequency in the exploratory studies facility at Yucca Mountain showed that fracture frequency in the immediate vicinity of faults was influenced in a zone that ranged from less than 1 m to about 7 m (CRWMS M&O, 2000). In addition, the hydrologic properties of the faults themselves can vary significantly depending on the nature of the faulting, the presence or absence of alteration products in the fault zones, and the orientation of the faults with respect to the groundwater flow directions.

A second cause of local spatial variability of fracture properties of ash-flow tuff is the effect of paleotopography or the topography of the surface beneath the

ash-flow tuff (emplacement surface). Ash-flows move as turbulent, high-particle concentration flows and are channeled by underlying topography. Consequently, the resulting thickness of local ash-flow units can change markedly by thickening in depressions and thinning over topographic highs. The general effect of ash-flow channeling is significant increases in the thickness of welded zones and the production of more intense and more closely spaced fractures that can transmit water. For example, the Topopah Springs Formation at Yucca Mountain is thickened relative to adjacent depressions from ponding in the Miocene Crater Flat tectonic basin.

Finally, the alteration history of individual sections of tuff can vary with local settings dependent on the history and access of both groundwater and hydrothermal fluids to the rocks. For example, high-porosity sections of vitric fallout and reworked tuff can decrease in porosity from alteration. Characterization studies at the YMP have also shown that sections of zeolitized tuff can vary by a factor of two or three in abundance of secondary alteration minerals. As a result, fracture permeability in both non-welded and welded tuff can change dramatically dependent on whether the fracture is filled or not filled with secondary alteration products.

B.6.0 References

- Blankennagel, R.K., and J.E. Weir. 1973. *Geohydrology of the Eastern Part of the Pahute Mesa, Nevada Test Site, Nye County, Nevada*, Professional Paper 712B. Denver, CO: U.S. Geological Survey.
- Broxton, D.E., D.L. Bish, and R.G. Warren. 1987. "Distribution and Chemistry of Diagenetic Minerals at Yucca Mountain, Nye Co., Nevada." In *The Clay Minerals Society*, v. 35, p. 89. Aurora, CO: The Clay Minerals Society.
- Broxton, D.E., R.G. Warren, F.M. Byers, Jr., and R.B. Scott. 1989. "Chemical and Mineralogic Trends within the Timber Mountain-Oasis Valley Caldera Complex, Nevada: Evidence for Multiple Cycles of Chemical Evolution in a Long-Lived Silicic Magma System." In *Journal Geophysical Research*, v. 94, 5961-5985. Washington, DC: American Geophysical Union.
- Byers, F.M., Jr., W.J. Carr, P.P. Orkild, W.D. Quinlivan, and K.A. Sargent. 1976. *Volcanic Suites and Related Cauldrons of Timber Mountain-Oasis Valley Caldera Complex, Southern Nevada*, Professional Paper 919. Denver, CO: U.S. Geological Survey.
- Byers, F.M., Jr., W.J. Carr, and P.P. Orkild. 1989. "Volcanic Centers of Southwestern Nevada: Evolution of Understanding 1960-1988." In *Journal Geophysical Research*, v. 94, pp. 5908-5924. Washington, DC: American Geophysical Union.
- CRWMS M&O, see Civilian Radioactive Waste Management System and Operating Contractor.

- Carr, W.J. 1974. *Summary of Tectonic and Structural Evidence for Stress Orientation at the Nevada Test Site*, U.S. Geological Survey Open File Report 74-176. Denver, CO. U.S. Geological Survey.
- Cas, R.A.F., and J.V. Wright. 1988. *Volcanic Successions: Modern and Ancient*. New York, NY: Chapman & Hall.
- Christiansen, R.L., P.W. Lipman, W.J. Carr, F.M. Byers, Jr., P.P. Orkild, and K.A. Sargent. 1977. "The Timber Mountain-Oasis Caldera Complex of Southern Nevada." In *Geological Society America*, v. 88, pp. 943-949. Boulder, CO: Geological Society of America, Inc.
- Civilian Radioactive Waste Management System and Operating Contractor. 2000. *Fault Displacement Effects on Transport in the Unsaturated Zone*, ANL-NBS-HS-000020, REV 00. Las Vegas, NV.
- Drellack, S.L., Jr., and L.B. Prothro. 1997. *Descriptive Narrative for the Hydrogeologic Model of Western and Central Pahute Mesa Corrective Action Units*. Prepared for the U.S. Department of Energy, Nevada Operations Office. Las Vegas, NV: Bechtel Nevada.
- Freeze, R.A., J. Massman, L. Smith, T. Sperling, and B. James. 1990. "Hydrologically Decision Analysis: 1. A Framework." In *Ground Water*, v. 28., pp. 738-766. Columbus, OH: Groundwater Publishing Co.
- Gillson III, R.G. 1993. *Analysis of Borehole Elongation in Yucca Flat and Pahute Mesa, Using the Digital Downhole Surveyor*; Thesis (M.S.). Fayetteville, AR: University of Arkansas.
- IT Corporation. 2001. *A User's Guide to the Comprehensive Chemistry Database for Groundwater at the Nevada Test Site*, ITLV/13052--070. Prepared for U.S. Department of Energy, Nevada Operations Office. Las Vegas, NV.
- Laczniaik, R.J., J.C. Cole, D.A. Sawyer, and D.A. Trudeau. 1996. *Summary of Hydrogeologic Controls on Groundwater Flow at the Nevada Test Site, Nye County, Nevada*, Water-Resources Investigations Report 96-4109. Denver, CO: U.S. Geological Survey.
- NRC, see U.S. National Research Council.
- Prothro, L.B., and S.L. Drellack, Jr. 1997. *Nature and Extent of Lava-Flow Aquifers Beneath Pahute Mesa, Nevada Test Site*, DOE/NV/11718-156. Las Vegas, NV.
- Sawyer, D.A., R.J. Fleck, M.A. Lanphere, R.G. Warren, and D.E. Broxton. 1994. "Episodic Caldera Volcanism in the Miocene Southwestern Nevada Volcanic Field: Revised Stratigraphic Framework, $^{40}\text{Ar}/^{39}\text{Ar}$ Geochronology, and Implications for Magmatism and Extension." In *Geological Society of America Bulletin*, v.106, pp. 1304-1318. Boulder, CO: Geological Society of America, Inc.

- Smith, R.L. 1960a. "Ash Flows." In *Geological Society America*, Special Paper 67. Boulder, CO: Geological Society of America, Inc.
- Smith, R.L. 1960b. *Zones and Zonal Variations in Welded Ash Flows*, U.S. Geological Survey Professional Paper No. 345-F, pp. 138-143. Denver, CO: U.S. Geological Survey.
- Springer, J.E., R.K. Thorpe, and H.L. McKague. 1984. *Borehole Elongation and Its Relation to Tectonic Stress at the Nevada Test Site*, UCRL-53528. Livermore, CA: Lawrence Livermore National Laboratory.
- Stock, J.M, and J.H. Healy. 1988. "Stress Field at Yucca Mountain, Nevada." In *Geologic and Hydrologic Investigations of a Potential Nuclear Waste Disposal Site at Yucca Mountain, Southern Nevada*, U.S. Geological Survey Bulletin No. 1790, pp. 87-93. Carr, M.D. and J.C. Yount, eds. Denver, CO: U.S. Geological Survey.
- U.S. Department of Energy, Nevada Operations Office. 1997. *Regional Groundwater Flow and Tritium Transport Modeling and Risk Assessment of the Underground Test Area, Nevada Test Site, Nevada*, DOE/NV--477. Las Vegas, NV.
- U.S. Department of Energy, Nevada Operations Office. 1999. *Corrective Action Investigation Plan for Corrective Action Units 101 and 102: Central and Western Pahute Mesa, Nevada Test Site, Nevada*, DOE/NV--516. Las Vegas, NV.
- U.S. National Research Council. 1996. *Rock Fractures and Fluid Flow: Contemporary Understanding and Applications*. Washington DC.: National Academy Press.
- Winograd, I. J., and W. Thordarson. 1975. *Hydrogeologic and Hydrochemical Framework, South Central Great Basin, Nevada-California, with Special Reference to the Nevada Test Site*, Professional Paper No. 712-G. Denver, CO: U.S. Geological Survey.
- YMP, see Yucca Mountain Project.
- Yucca Mountain Project. 1998. *Yucca Mountain Project 1998 Geographic Information System CD-ROM Project*. Las Vegas, NV.



Appendix C

Analyses of Past Aquifer Tests Conducted on the NTS

C.1.0 Introduction

This appendix presents reanalyses of past aquifer and slug tests that had been conducted on NTS wells. These older tests provide much of the NTS-specific formation hydraulic property information.

C.2.0 Aquifer Test Data Reanalysis

The reanalyses of the aquifer tests focused on tests run in carbonate and volcanic rocks which are generally fractured and may be expected to respond to pumping with a dual-porosity response. A summary of the approach and results are presented in this appendix. Detailed information on each test and reanalysis is presented in an attachment to this appendix named "Attachment-to-Appendix-C." The attachment is located on the CD included with this document.

C.2.1 Reanalysis Objectives

The objective was to determine if the drawdown responses were consistent with dual-porosity behavior and would be better analyzed using a dual-porosity model. In addition, since K is the parameter of interest, the tested interval thickness was used to calculate K , and the uncertainty in the appropriate thickness was reviewed.

The tests that were reanalyzed were selected first by reviewing the USGS database of hydraulic properties (Belcher and Elliott, 2001) to identify constant-rate pumping tests that had been conducted in fractured formations. The records for these tests were then located and evaluated to determine that sufficient information was available to conduct reanalysis and that the drawdown response was amenable to interpretation.

Most of the subject tests had previously been analyzed using the Theis single-porosity model (Theis, 1935) for a confined aquifer, often using the Cooper-Jacob straight-line method (Cooper and Jacob, 1946). When graphed against log time, the drawdown responses of these tests typically exhibit multiple-segment drawdown behavior. The changes in slope were speculatively attributed to changing aquifer properties or boundary conditions, and the various straight-line segments of the responses yielded different values for transmissivity (T). However, a three-segment response is characteristic of dual-porosity, and the interpretation of a dual-porosity response is more restrictive. Only the Cooper-Jacob analysis of a fully developed third segment would yield a correct T for a test in dual-porosity media. T values derived from the first or second segment of a dual-porosity response are not representative for the tested

formation. The past tests were typically short, one day or less, although some were longer. Some of the longer tests exhibit well developed three-segment responses and others only show the beginning of a third segment in the late time. The rest of the tests, generally the shorter ones, only exhibit a two-segment response. The premise for these reanalyses was that the tested formation should respond as dual-porosity due to the fractured nature of the formations. All of the tests were evaluated using a dual-porosity model to determine if the responses were consistent with dual-porosity and to derive transmissivities where appropriate. In all cases, the dual-porosity model was found to be as good or better than the single-porosity model for simulating the drawdown response using reasonable parameter values. Average K is the parameter value that is ultimately desired, which is calculated by dividing the transmissivity by the aquifer thickness. Determination of the aquifer thickness to associate with each test is not definitive, and assignment of an aquifer thickness introduces uncertainty in the resultant K value. This will be discussed further.

Reanalyses discussed in this appendix were conducted by both the UGTA ER Contractor and the USGS Water Resources Branch in Las Vegas. There are some differences in approach and method between these two sets of reanalyses which are discussed in detail in the following sections.

C.2.2 Approaches to Reanalysis

The reanalyses discussed in this appendix were conducted by both the ER Contractor and the USGS. There are some differences in approach and method between these two sets of reanalyses which is discussed in detail in the following sections. The differences in results for each well are discussed individually.

C.2.2.1 ER Contractor Reanalysis Approach

Reanalysis of the drawdown responses generally found that the multi-segment behavior was consistent with wellbore storage and secondary storage (dual-porosity or delayed-gravity drainage), and that the different segments of the responses could be simulated with one consistent set of hydraulic parameter values. These analyses do not invoke multiple changes in aquifer properties. Analyses of tests for which the third segment of the drawdown response was not fully developed introduces some uncertainty into the results. Fitting the dual-porosity model to test datasets that exhibited only two segments of the response was even more speculative, but arguably provides a more accurate result than the Cooper-Jacob analyses of the second segment.

The Papadopoulos-Cooper model (Papadopoulos and Cooper, 1967), a single-porosity model that incorporates a finite well diameter and simulates wellbore storage, was used as a baseline for analyzing tests with only two segments of response. Modeling wellbore storage also provided some guidance for specifying borehole sizes when records were incomplete. Comparison to the Moench dual-porosity model (Moench, 1984), which also simulates wellbore storage, provides a view of the amount of dual-porosity information in the first segment of response helping to determine the solution fit. For a few tests, the top of the tested interval was also unconfined, and an unconfined model incorporating

delayed gravity drainage (Moench, 1997) was used to analyze these tests. In these cases, the dual-porosity model and the unconfined delayed gravity drainage models usually produced similar K values, but the dual-porosity model yielded the better result. In one case a leaky aquifer, constant-head case was applied (Moench, 1985). These analyses were conducted using the commercial software program AQTESOLV Ver. 3.50 (HydroSOLVE, Inc., 1996-2002).

The primary parameter of interest is K, specifically fracture K in the case of dual porosity. Determination of K requires specification of the aquifer thickness representing the tested section of the formation. Many of the wells accessed long intervals of formation, extremely long intervals in a few wells. However, it is questionable that the pumping stress uniformly affected the entire accessed length due to such factors as vertical gradient, internal well flow losses, and variable development. For some wells, flow logs during pumping were available showing variable distribution of production along the well completions. The construction information for other wells left some uncertainty about the extent of the formation accessed by the well. All of the available data for each test were evaluated to determine if there was any basis for specifying different aquifer thicknesses. The basis for assigning thicknesses is discussed for each well. Partial penetration effects were not considered in the analyses due to the inability to specify the upper and lower boundaries of distinct aquifers.

Most of these past aquifer tests were single-well tests, and the drawdown response was only observed in the production well. Storage parameter values cannot necessarily be accurately determined from such data because of the sensitivity of the models to uncertainties in the effective well radius. Since storage parameter values significantly interact with the conductivity values in the models, the values for the storage parameters were initially constrained to ranges believed to be realistic this was done to ensure that the dual-porosity analyses for these single-well tests were realistic. The solutions were evaluated for the sensitivity of the K value to the storage parameter values where optimal values were outside of the constraint ranges. The calculated ranges for specific storage are listed in [Table C.2-1](#).

The ranges for the storage parameters were calculated based on the theory of confined storage using general values from literature bounding the possible values of the parameters. Specific storage was calculated using the following formula (Freeze and Cherry, 1979, p.59):

$$S_s = \rho g (\alpha + n\beta)$$

where:

ρ = Density
 g = Gravity
 α = Bulk compressibility
 n = Matrix porosity
 β = Matrix compressibility

Upper and lower bounds for specific storage, both fracture system (Ss) and matrix (Ss') were calculated using upper and lower bound values for compressibility and porosity. The values used for rock compressibility were general ranges for jointed and sound rock (Freeze and Cherry, 1979, p.55). NTS-specific information was not generally available. The values used for porosity were taken from the NTS Regional Flow and Transport Model documentation for the LCA (for carbonate completion wells) and for tuffs and lava flow aquifers (for volcanic completion wells) (DOE/NV, 1997). These parameter values are also listed in [Table C.2-1](#).

**Table C.2-1
Storage Parameter Constraints**

Parameter	Carbonate Rocks		Volcanic Rocks	
	Upper Bound	Lower Bound	Upper Bound	Lower Bound
Fracture Storativity (Ss) [1/ft]	3.0E-05	3.0E-07	3.0E-05	3.0E-7
Matrix Storativity (Ss') [1/ft]	3.1E-06	3.4E-08	3.4E-6	3.1E-8
Bulk Compressibility [m ² /N]	1.00E-8	1.00E-10	1.00E-8	1.00E-10
Matrix Compressibility [m ² /N]	1.00E-9	1.00E-11	1.00E-9	1.00E-11
Fracture Porosity	0.1	0.001	0.10	0.000001
Matrix Porosity	0.099	0.003	0.30	0.001

The best-fit solutions generally had parameter values within the predetermined range, with a larger matrix specific storage parameter value the most common discrepancy. For some tests, the best-fit was achieved with matrix specific storage values larger than the specified range by an order of magnitude. However, a good fit could be achieved for these with the storage parameter values the specified ranges. The larger apparent matrix specific storage values may reflect greater compressibility of the matrix rock than reflected in laboratory values derived from small samples due to micro-fracturing of the matrix, as has been suggested in the literature (Moench, 1984). Alternately, this could also result from an effective well radius larger than the nominal hole diameter. While this approach does not necessarily produce very accurate storage parameters, solution fits were generally sufficiently unique to give confidence that the parameter values were representative.

There was generally no specific information on the degree of fracturing in the formations for each well; therefore, a standard conceptual model was assumed. The Moench dual-porosity model was applied using the slab configuration with a standard spacing of 3.3 ft (1 meter). This fracture spacing is probably near the upper end of the fracture density. The UGTA Phase I Data Documentation Package, Volume V (IT, 1996) gives the average fracture spacing in carbonate rocks at Well ER-6-2 as 0.72 ft, and average spacing for volcanic rocks from 1 to 19.7 ft. An average spacing of 6.3 ft was derived from the results of analyses of the fracture logs for the WPM-OV ER wells (volcanic rocks). Data on laboratory measurement of hydraulic conductivity for core indicate that matrix hydraulic

conductivity may reasonably range from $10E-2$ to $10E-6$ ft/d. The matrix hydraulic conductivity interacts with the fracture spacing such that higher conductivity compensates for a greater fracture spacing. The dual-porosity solution was not found to be sensitive to the fracture spacing within the range allowed for the matrix hydraulic conductivity. Consequently, the uncertainty in the fracture spacing does not affect the resultant hydraulic conductivity. This latitude even accommodates uncertainty due to alternate conceptualizations of the slab model with greater average spacing for flowing fractures (~10 m), or an even greater average spacing yet for flowing intervals (~100 m). The Moench dual porosity model, spherical configuration was evaluated in some cases when well information noted heavy fracturing, and was sometimes found to improve the solution fit. However, results using that model are not included here because of a lack of information to support the spacing value.

Using the AQTESOLV software, the match between the solution type curve and the drawdown response were optimized for all parameters, maintaining the parameter values within reasonable constraints. For tests that clearly had a three-segment drawdown response, only the dual-porosity model and the delayed-gravity drainage model (where appropriate), which could simulate the response were used. For tests that exhibited only two segments of response, both the single-porosity and dual-porosity models were applied. Typically the single-porosity model solutions had unrealistic low storage coefficients. The discrepancies between the single-porosity storage coefficients and realistic values were much greater than can be attributed to other uncertainties in the analysis. However, the dual-porosity model generally produced good solutions with realistic values for all of the parameters. The dual-porosity results have an unquantified uncertainty in the cases where the drawdown response had only two segments, but these solutions appear more realistic than the single-parameter solutions because the solutions are consistent with realistic storage parameter values.

The solutions were only fit to the drawdown data even when recovery data were available. Typically, the wells on the NTS recover faster than the drawdown analysis parameter values predict. This situation is believed to result from temperature increases in the water column during pumping decreasing the average density, resulting in an increase in water level. This theory is supported by observation of temperature increases at the wellhead during pumping, and review of the recovery curves. For some wells with longer recovery records, the water levels have been observed to initially over-recover and then drop back to the static water level. For shorter records, the recovery curves can be seen to approach the original static water level steeply, and projecting the curves indicates over recovery. Recovery data are displayed on the figures to illustrate the discrepancies.

C.2.2.2 USGS Reanalysis Approach

The USGS approached the reanalyses somewhat differently. Their analyses were conducted with AQTESOLV Ver. 3.01 software (HydroSOLVE, Inc., 1996-2000). They used the Cooper-Jacob straight-line method to reanalyze the late-time data, and also fit the Moench dual-porosity model to the same data using

eight specified pairs of parameter values for the matrix K and specific storage. The paired values for matrix K and specific storage were selected from predetermined ranges of values for these parameters. Their effort focused on determining transmissivity and did not specifically evaluate hydraulic conductivity. They did not optimize all parameter values but ran the automated fitting routine in AQTESOLV for a specified number of iterations, 700. The early-time data during the wellbore storage period were not used in fitting the solution, and, in several cases, some late-time data were also excluded from the analysis because pumping rates were not constant. For the dual-porosity analyses, the fracture spacing was conceptualized differently, and solutions were developed for slab models with 500-ft spacing and spherical models with 10-ft spacing. In some cases, the resultant fit between the type curve and the drawdown response was poor. Further information on these reanalyses can be found in the summary report available on the UGTA Common Data Repository (CDR), DTN 1274 Component 5824 and in the full reports for each well located on the UGTA CDR, DTN 1274, Component 5853.

C.2.2.3 Aquifer Thickness

The aquifer parameter of primary interest is K. The single-porosity models produce values for transmissivity which are independent of aquifer thickness. The transmissivity must be divided by the aquifer thickness to yield K. The dual-porosity model produces a value for K which is associated with an input value for the aquifer thickness. Transmissivity is calculated from the K and aquifer thickness. In both cases, an aquifer thickness has to be specified to calculate a hydraulic conductivity value.

Specification of the appropriate aquifer thickness presents considerable uncertainty in many cases. For some wells, details of the well construction are not known and there is some uncertainty in the extent of the formation accessed by the well. Flow logging during pumping in a variety of wells has shown great variation in the productivity along the long completions as well as intervals of no production. Use of only the combined length of the productive intervals yields the actual K of the productive intervals, but use of the entire length of the accessed formation characterizes the average K of the formation. Analysis of the downhole hydraulics of production in wells has found that the stress applied to the formation varies with depth depending upon the K distribution and the vertical gradient. This effect can limit production to short intervals of the accessed formation regardless of the K of the deeper formation. For most wells, there is little or no data on the production distribution during pumping or any of the other information needed to quantify vertical gradient or flow losses. In some cases, the published records indicate intervals described as productive or permeable, but do not provide quantitative information. It cannot be assumed that all of the formation accessed by the well completion is being tested or is equally represented in the drawdown response. For these reasons, the appropriate aquifer thickness to associate with the drawdown response may be some fraction of the total length of accessed formation. However, partial penetration effects, which are not considered due to lack of information defining the functional extent of the aquifer unit and vertical anisotropy, could result in a greater appropriate aquifer thickness.

The aquifer thicknesses used for these analyses were the length of access to the formation. Alternative thicknesses were specified based on well-specific factors and information. Specific considerations are detailed in the individual discussions for each test that can be found in an attachment to this appendix named "Attachment-to-Appendix-C" located on the CD included with this document.

C.2.3 Results

[Table C.2-2](#) presents T and K values selected by the ER Contractor as the most representative values for each test cross-referenced to lithology and formation of the tested interval. Ranges are presented where there are alternate analyses of equal validity, indicating uncertainty in the analysis due to different models. Greater detail on the ER Contractor reanalyses and the combined ER Contractor and USGS results can be found in the attachment to this appendix which is located in the "Attachment-to-Appendix-C." This attachment contains discussions of the reanalyses for each test and conclusions about which analyses are most representative. For most of the tests, several different models were evaluated, depending upon the physical situation and the form of the well response. The results for the different models are presented and compared, and the best estimate for the T and K values identified. As noted in [Section C.2.2.2](#), reports for the USGS reanalyses are located on the UGTA CDR.

**Table C.2-2
Summary of Aquifer Test Data Reanalysis Results**

Well Name	Test Date	Lithology	Stratigraphy	Aquifer Thickness (ft)	T (ft ² /d)	K (ft/d)	K (m/d)
Tests in Carbonate Rocks							
Army 1	9/11/1962	dolomite, limestone	Windfall Fm., Bonanza King Fm.	969	1,279-1,748	1.3-1.8	0.40-0.55
TW-1	8/10/1962	dolomite	Nevada Fm., Devils Gate Fm.	495	374	0.76	0.23
TW-2	3/16/1962	dolomite, limestone	Pogonip Grp.	246	88	0.36	0.11
TW-3	5/9/1962	limestone, dolomite	Pogonip Grp.	750	259	0.35	0.11
TW-4	9/11/1962	limestone, dolomite	Pogonip Grp.	740	761-889	1.0-1.2	0.30-0.37
TW-10	2/24/1963	dolomite	Bonanza King Fm.	281	1,801	6.4	2.0
UE-16d	6/13/1977	carbonate	Tippipah Fm.	730	1,938-2,447	2.7-3.4	0.82-1.0
UE-1q	7/17/1992	carbonate	Nopah Fm.	141	1,506	11	3.4
UE-10j	4/27/1993	carbonate	Bonanza King Fm.	344	8,094-8,318	24	7.3
UE-7ns	3/1984	carbonate	Pogonip Grp.	230	2.6-2.9	0.011-0.013	0.0034-0.0040
ER-6-1	10/6/1992	carbonate	Sevy, Laketown, Ely Springs Dolomite	334	3,124-3,623	9.3-11	2.8-3.4
ER-12-1	1/5/1993	dolomite	Upper Simonson Fm., Lower Guilmette Fm.	97	101-144	1.0-1.5	0.30-0.46
MX-CE-VF-2	2/6/1986	carbonate	Bird Spring Fm.	361	2,578	7.1	2.2
MX-CSV-2	6/7/1987	carbonate	Bird Spring Fm.	87	1,153	13	4.0
Tests in Volcanic Rocks							
TW-8	1/4/1963	tuff	Tuff of Yucca Flat	3,459	39	0.011	0.0034
TW-8	1/10/1963	rhyolite, tuff	Rhyolite of Split Ridge	782	11,000-14,477	19-21	5.8-6.4
UE-19fs	8/17/1965	rhyolite, welded tuff	Crater Flat Grp.	2,214	891	0.40	0.12
UE-19gs	5/26/1965	rhyolite, ash flow tuff	Belted Range Grp.	1,858	1,076	0.58	0.18
UE-19i	9/2/1965	rhyolite, welded tuff	Belted Range Grp.	5,104	126-162	0.025-0.032	0.0076-0.0098
U-20-a2	2/10/1965	rhyolite	Calico Hills Fm.	2,417	2,393-2,400	1.0	0.30
UE-20f	8/9/1964	rhyolite	Unknown	9,230	28	0.0030	0.00091
UE-25 J-11	12/18/1958	basalt	Basalt of Jackass Flat	289	526	1.8	0.55
UE-25 J-13	2/18/1964	ash flow tuff	Topapah Spring Member, Paintbrush Grp.	2,298	3,424	1.5	0.46
UE-25 b#1	8/29/1981	ash flow tuff	Calico Hills, Crater Flat Tuffs	1,312	3,422-3,653	2.6-2.8	0.80-0.85
UE-25 p#1	2/1983	ash flow tuff	Calico Hills, Crater Flat, Lithic Ridge, Older Tuffs	3,015	478-745	0.16-0.25	0.049-0.076

C.3.0 Slug Test Data Reanalysis

This section discusses the reanalysis of a large number of packer tests conducted in the 1960s in the volcanic rocks of Pahute Mesa. The discussion includes descriptions of the objectives, approach and results of the reanalysis.

C.3.1 Reanalysis Objectives

A large number of packer tests were conducted in the 1960s in the volcanic rocks of Pahute Mesa. Multiple tests were run over a series of short intervals, typically around 200 ft, along deep open boreholes to evaluate the variation of hydraulic conductivity in the rocks. The tests were originally interpreted using a proprietary method (Blankennagel, 1967) that yielded information on relative hydraulic conductivity between different test intervals. Many of the recorded responses exhibit forms that do not conform to the basic model of a slug injection, indicating that a variety of other things occurred during the test. The objective for this exercise was to analyze the tests using slug test models to calculate the actual values of hydraulic conductivity.

C.3.2 Approach

The USGS database contained in a file named 'short_term_aquifer_tests.xls' contains extensive data on a series of pumping tests and packer-injection tests that were conducted in the past on Pahute Mesa in volcanic rocks in uncased boreholes. Original field notes on each test were not available. General information on testing procedures used at the NTS in the time frame of these tests is covered in the publication *Hydraulic Testing Techniques of Deep Drill Holes at Pahute Mesa, Nevada Test Site* (Blankennagel, 1967) was reviewed. The individual tests are identified in the database by well name, test sequence and number, and test interval. The data rows for the tests for individual wells were copied from the original database intact and unmodified into a well-specific spreadsheet, preserving the integrity of the raw data. Individual worksheets were created for each test, importing the raw data for the test by reference, and showing subsequent manipulations and calculations explicitly.

The test data include elapsed time versus head (i.e., depth-to-water), parameters for the physical system, and test system parameters. The required physical parameters are the vertical location of the upper and lower confining layers, and the test interval equilibrium head. The test system parameters are the test interval defined by the packers, the borehole radius of the injection interval, the injection tubing radius, and the initial head. This information is not complete for every test, and assumptions about missing parameter values were made, where necessary, based on general information on test procedures and information on associated tests.

An initial evaluation of the data revealed that some of the pumping test data suffered from apparent measurement problems, revealed as inconsistencies in the response or significant noise. Often the pumping test data supplied in the database

lacked information that would have helped to deal with a variety of problems in the well responses. Some data gaps concerned well construction, some were related to variation in pumping rates during the tests, and others resulted from lack of hydrologic information for the very deep well completions. For some of the tests, attempts to fit aquifer hydraulic models constrained to realistic parameter values for storage indicated that a more sophisticated understanding of the test response was required than could not readily be developed. As a result, the results of the analysis of the pumping test data are not reliable and are not discussed any further in this report.

The final analysis was conducted for slug injection tests only. A total of 261 tests were found to be suitable for analysis. Two particular pieces of information that were not available or specifically given in the database for many of these tests are the static water level (or test interval-specific head) and the initial injection head.

The responses were graphed with a consistent format so that varieties of response forms could be identified. Several characteristic forms were found, and the features of the responses were interpreted based on the available data for each test and similar characteristics of tests with similar forms. Based on the interpretation, the section of the response believed to be most representative of the formation response was identified, and the analysis was conducted on that portion of the response.

C.3.2.1 Interval-Specific Equilibrium Head

The interval-specific equilibrium head was rarely available as an initial static water level for the test interval. In some cases, the test data show the head declining to a stable value or the test data can be trended to indicate the asymptotic value which was assumed to indicate the interval-specific equilibrium head. Otherwise, the overall static water level for the entire well or the interval-specific head from a test for a nearby test interval was used, corrected for vertical gradient if the available information indicated a clear trend. Equilibrium head values for individual test intervals were estimated while preserving consistency with the head distribution in the well. In most cases, the packer-injection tests were conducted using very large injection displacements, and small uncertainties in the interval-specific head would not result in substantial uncertainties in the calculated hydraulic conductivities. The datasets used for analysis were truncated at the first instance of a minimum value, assumed to be the equilibrium water level, when the measurements extended to equilibrium. However, many datasets did not extend to equilibrium when equilibrium was not achieved in several hours, and general data or data from other intervals were used in these cases to estimate the interval-specific equilibrium head. Displacement values less than one foot were generally disregarded in fitting the slug test solutions since the accuracy of measurements at this level is suspect.

C.3.2.2 Initial Injection Head

The initial displacement values (0) was also commonly not provided. General information on the testing procedure suggests that the injection tubing was commonly filled up to the top of the tubing, located a specified distance above the

rig floor. This was used as the initial value in the fitting process. However, the value for initial head that produced the best model fit to the data was often less than the height that the tubing was filled to. There are several reasons for this. The process of filling the tubing with water entrained and entrapped air in the water column which functionally reduced the initial injection head. The general information on testing procedures indicates that bubbles were allowed to escape before starting the test, but this may not have removed all of the trapped air. It is not known how much residual trapped air may have affected the initial injection head because there were no data available on the downhole pressure. Other factors affecting the early time response include measurement problems and packer leakage. Very high injection heads were used, usually between 1,000 to 2,000 ft. For some of the more permeable intervals, the rate of head decline was initially rapid and it was probably difficult to collect time versus depth-to-water measurements with great precision. For the tests with rapid head declines, the data are probably less definitive.

Data from many of the head versus time responses suggest that the packer seals for the injection intervals may have leaked at these high heads, often appearing to seal after the head declines to substantially lower values. Leakage from the test interval might also occur due to the high head opening fractures behind the packers.

The appropriate value for the initial head was estimated for each test and for different models based on judgement about the nature of the head decline response, and was optimized individually for the different model solutions. This will be discussed later in the section on fitting model solutions. The possible range of the actual physical value for the initial injection head was bounded by two constraints: the maximum value is the top of the injection tubing, and the minimum value is the first depth-to-water measurement. It is recognized that this latter value may also be affected by the reduced water column density, but there is no basis for correcting for this.

C.3.3 Analysis

The packer-injection tests were analyzed as slug tests with positive displacement. Three models for slug test analysis were used: the Hvorslev (1951) model which is based on a steady-flow assumption; the Butler (1998) model which is a modification of the Horslev (1951) model that includes inertial effects and friction losses; and the Cooper et al., (1967) model which is based on unsteady flow. These models are based on a number of assumptions that are honored to various degrees by the test method and the physical conditions of the test. The analyses were conducted using the aquifer test analysis software package AQTESOLV (HydroSOLVE, 2002).

The assumption that is substantially violated for these models is that the injection intervals fully penetrate an isotropic, confined aquifer. The formations tested do not conform clearly to the simple physical model of a permeable interval bounded by confining layers. The volcanic formations tested are made up of various forms of tuff (e.g., ash flow, air fall, vitrified, welded, fractured, zeolitized, etc.) with embedded lavas, and detailed information on the lithologic variations along the

boreholes was not available for these analyses. In general, the test intervals were selected to include relatively consistent geology, but are not known to be distinctly bounded by confining layers. General experience with these volcanic formations as well as results of the individual test analyses indicate that the horizontal hydraulic conductivity varies substantially (multiple orders of magnitude) vertically depending on the character of the rock in the particular test interval. The test intervals were located substantial distances below the water table, and would be expected to respond as confined due to the distance isolation from the water table as well as intervening low permeability intervals. Consequently, there are insufficient data to implement more sophisticated analyses. Research by Hyder et al. (1994) quantified the error resulting from partial penetration for the Cooper et al., (1967) and the Hvorslev (1951) models. Using typical system dimensions for these tests to compute the dimensionless parameter values used in the graphs ($\psi \sim 0.002$, $\alpha \sim 0.064$) the ratio of K_{est}/K_r is between 1 and 2 for the various models (Cooper et al., 1967 and Hvorslev, 1951) and cases examined. This is also evaluated in Butler 1998 with similar conclusions.

The Hvorslev (1951) model is the most basic and least restrictive model, determining hydraulic conductivity based upon an assumption of steady flow and consequently does not incorporate storage. The model predicts a straight-line decline in head in log time. The AQTESOLV implementation optimizes the value for initial displacement using linear regression to fit a straight line to the data in log time. The Butler (1998) model is based on the Hvorslev (1951) model and incorporates inertial effects and flow friction losses in the injection tubing, determining hydraulic conductivity and optimizing the inertial damping factor. This is particularly relevant to these tests due to the high injection heads and long tubing lengths. The Cooper et al., (1967) model is based on unsteady flow and compressible storage, and yields hydraulic conductivity and the storage coefficient values. The versions of these models implemented in AQTESOLV assume full penetration and horizontal flow. Application of these models was guided by reference to Butler 1998 for analyzing slug tests in confined formations.

The analyses were conducted using these three slug test models applied in sequence to employ their distinct features to focus the solution process and evaluate the uncertainty in the analysis related to the particular features of each model. The AQTESOLV program includes an automated fitting routine to optimize the parameter values derived from the least-squares fit of the solution to the data, and gives a standard error (SE) for the fit. The solution was restricted to the portion of the total dataset judged to be representative of formation properties by unweighting the data that appear to be affected by other factors. The Hvorslev (1951) and Butler (1998) solutions for each test use the same data and weights, allowing comparison of the fits using the SE values. The early-time data that were interpreted to be affected by storage were also used for the Cooper et al., (1967) analyses; consequently the SE is not directly comparable. The results of all of the analyses are presented in electronic form in an Excel table named "Slug_Test." This table presents all results and identifies the analysis that provided the best solution fit as determined by the least value for the SE. In a few cases, the Cooper et al., (1967) model provided the best fit, but did not have the lowest SE due to the additional data points used in that analysis.

C.3.3.1 Types of Head Decline Responses

The head decline curves show complex behavior that was interpreted so that the appropriate part of the response curves could be identified for analysis. In some cases, the rate of head decline decreased in log time (i.e. early-time head decline was more rapid). The change in the rate of decline was sometimes short and minor, sometimes gradual with significant duration, and sometimes abrupt after significant duration. These differences have been interpreted to indicate different conditions. The short, minor changes are probably the result of storage in the test interval and possibly additional de-aeration of the water column. The Cooper et al., (1967) model usually simulated these responses well. Large changes indicate that the packer-seals leaked under the high differential pressure condition, resulting in initial losses to the whole wellbore. Alternately, the high injection heads could have opened fractures in the formation and possibly even induced fracturing. In either case, reduction in the injection head would reduce the rate of leakage and allow the leakage path to reseal. The resealing of the test interval apparently may be either gradual or abrupt. For these responses, the later-time data after apparent resealing were analyzed.

In other cases, the rate of head decline increased later in the response time. This assumed several different forms. One form exhibited an initial, gradual decline that abruptly steepened. This was interpreted as packer-seal failure of a low permeability interval after an initial period. In these cases, the initial decline curve was analyzed. In other cases, the head decline response appeared to be consistent until late-time and low head, at which time the rate abruptly increased. Here, the late-time data were ignored.

The general rule followed was that the later-time, lower-head data were believed to be most representative of the formation response. If the head decline response had features that did not conform to the basic form of response exhibited by the analysis models, those features discussed above were eliminated from the analysis by unweighting those data.

Cases in which there was a very rapid early-time response were probably affected or limited by the flow resistance of the straddle-packer tool, in particular, the injection ports. This situation could occur when the formation hydraulic conductivity is greater than the conductivity of the straddle-packer tool. There are no specific data available on the tool to estimate such losses. However, these losses are a function of the square of the velocity and would diminish with the rate of decline, which generally diminishes with displacement.

C.3.3.2 Application of the Different Models

The models were applied in the order: Hvorslev (1951), Butler (1998), and Cooper et al., (1967). The Hvorslev (1951) model presents the data in log time for evaluation of the overall response curve. The portion of the response curve to be analyzed was identified and the data weighted appropriately. An optimized initial displacement was determined for the selected segment of the dataset. Even when none of the problems with early-time data discussed previously were present, the early-time response typically had a concave-upwards lead-in that is identified as a

storage effect not accounted for by the Hvorslev (1951) or Butler (1998) models. This effect was discounted by unweighting the data points, removing them from the analysis. The $s(0)$ parameter is a fitting parameter for the Hvorslev (1951) model and the automated fitting routine was used to optimize the $s(0)$ value for this model. The Butler (1998) model was applied after the Hvorslev (1951) model to evaluate whether incorporation of the effect of flow friction in the tubing improved the fit and substantially affected the result. This model also includes inertial effects and optimizes the damping factor. The Butler (1998) model presents the Hvorslev (1951) model on axes identical to the Cooper et al., (1967) model for comparison purposes. The Cooper et al., (1967) model was then applied to refine the analysis with a model considering unsteady flow and compressible storage to see if the more complete model fit the data better. This model fits a storage parameter value, and the storage parameter values were restricted to a range based on supporting information for the tested formations to ensure that the solution was realistic.

For these tests, the actual total formation thickness was not known, and due to the nature of the tested formations, an appropriate value would be difficult to estimate. The top of the aquifer was considered to be the static water level, and the formation thickness input to the models was the distance from the static water level or interval-specific head to the bottom of the well, either drilled depth or top of fill if specified. Likewise, the test interval was located in the formation relative to the static water level or interval-specific head.

As noted previously, data weighting adjustments were often made to the individual slug test datasets prior to fitting with each of the three models (Hvorslev, 1951; Butler, 1998; and Cooper et al., 1967). The same weighting adjustments used for the Hvorslev 1951 model were also used for the Butler 1998 model, but not necessarily for Cooper et al., (1967). These adjustments, which involved setting the weight value to zero, were made based on either comments in the original data file to exclude certain data or observable effects in the data. The observed effects were characterized by applicable elapsed time(s) in the model summary result tables as one or more of four categories: (1) Storage effects (S), (2) Packer leakage (P), (3) Tool losses (T), and (4) Data (D).

As neither the Hvorslev (1951) nor Butler (1998) models account for storage, the storage effects designation (S) was only applied to these two models and not for Cooper et al., (1967). Evidence of storage effects was generally characterized by a concave-upward dataset in Hvorslev axes (log-linear) that could be divided into two linear portions, with the later-time data fitted with the model and the early-time data weighted to zero. An example of storage effects used for justifying weighting adjustments is injection test 15-8 from Well UE-18r. All data less than or equal to 18 minutes (min) elapsed time was weighted to zero for both the Hvorslev (1951) and Butler (1998) fits, while no weighting changes were necessary for the Cooper et al., (1967) fit. The Hvorslev (1951) model fit is shown in [Figure C.3-1](#).

Packer leakage (P) effects were generally observed in the later-time data of a given test, exhibiting a dramatic decrease in displacement with time subsequent to an apparent stabilizing period in the dataset. An example of packer leakage effects is

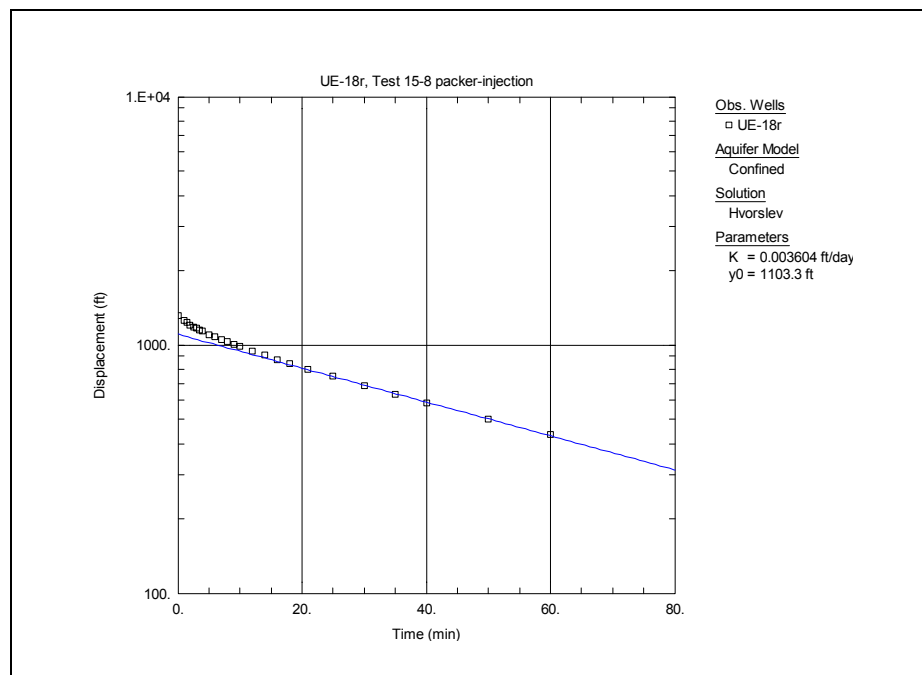


Figure C.3-1
Well UE-18r - Injection Test 15-8
Early-Time Storage Effect

injection test 6-4 of Well UE-19e, in which a displacement of approximately 600 ft was observed between 35 and 40 min elapsed time (120 ft/min), after ranging roughly 25 to 30 ft/min for the previous 20 min of the test. For this test, a comment in the original data worksheet indicated that the packers might have failed during the test. Figure C.3-2 shows the Cooper et al., (1967) model fit to the dataset after weighting data collected from 40 min to the end of the test to zero.

Packer-seal leakage with tool loss (T) effects, generally within the first few minutes of an injection test, were characterized by a sharp linear change in displacement different from storage effects. Figure C.3-3 illustrates the leakage/tool loss effect model fit using the Hvorslev (1951) model after unweighting later-time data, for injection test 1-1 at well UE-20p. The model fit shown in the Figure C.3-4 shows unweighting of the early-time data through 20 min, which eliminates both tool loss and storage effects in this case. The results from this model fit are included in the main summary table.

Weighting adjustments based on data (D) were primarily due to values being greater than 1,000 ft (beyond the first 1 to 2 min) or less than 1 ft displacement, or not fitting the majority of the dataset visually. The latter case was obviously much more subjective, but an attempt was made to be consistent in the use of this justification for eliminating data from the fitting process. Figure C.3-5 for Well UE-20h, injection test 3-1b, illustrates the application of the Butler (1998) model to a dataset in which displacement values from 7 min to the end of the test were all less than 1 ft.

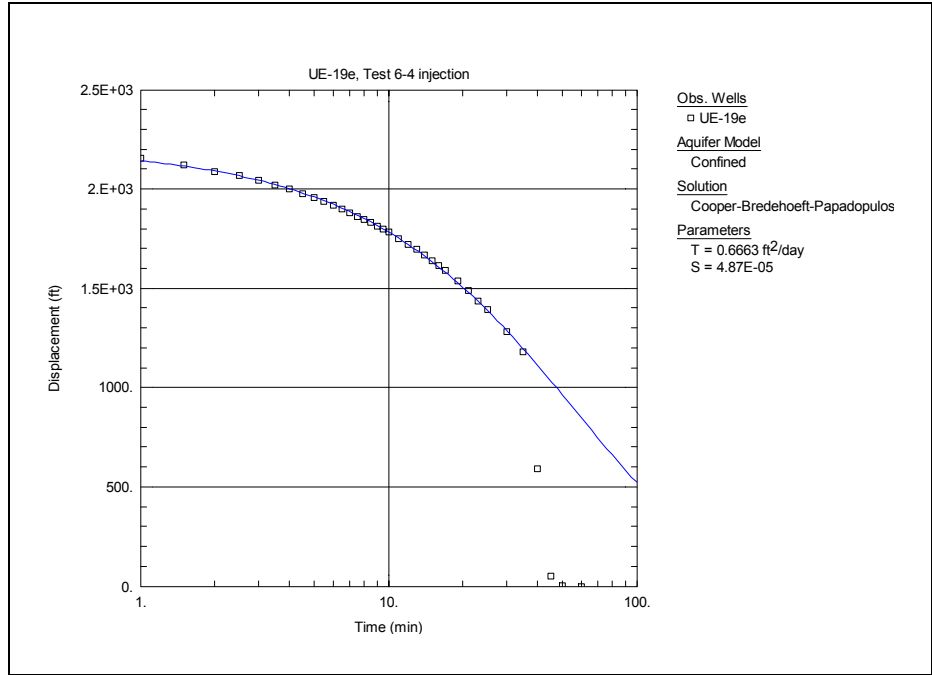


Figure C.3-2
Well UE-19e - Injection Test 6-4
Late-Time Packer-Seal Failure

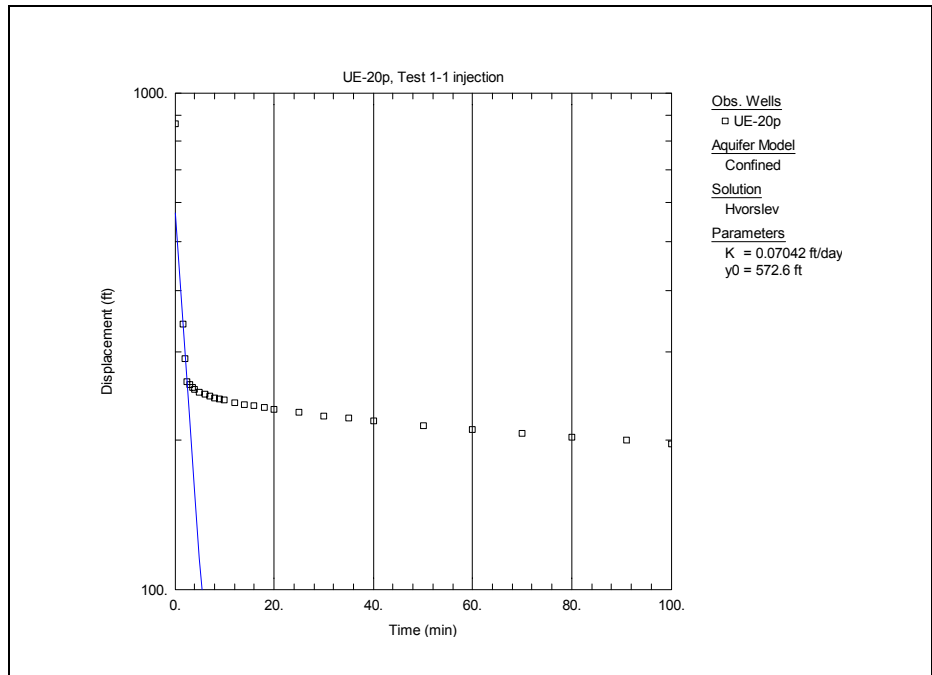


Figure C.3-3
Well UE-20p - Injection Test 1-1
Early-Time Packer-Seal Leakage

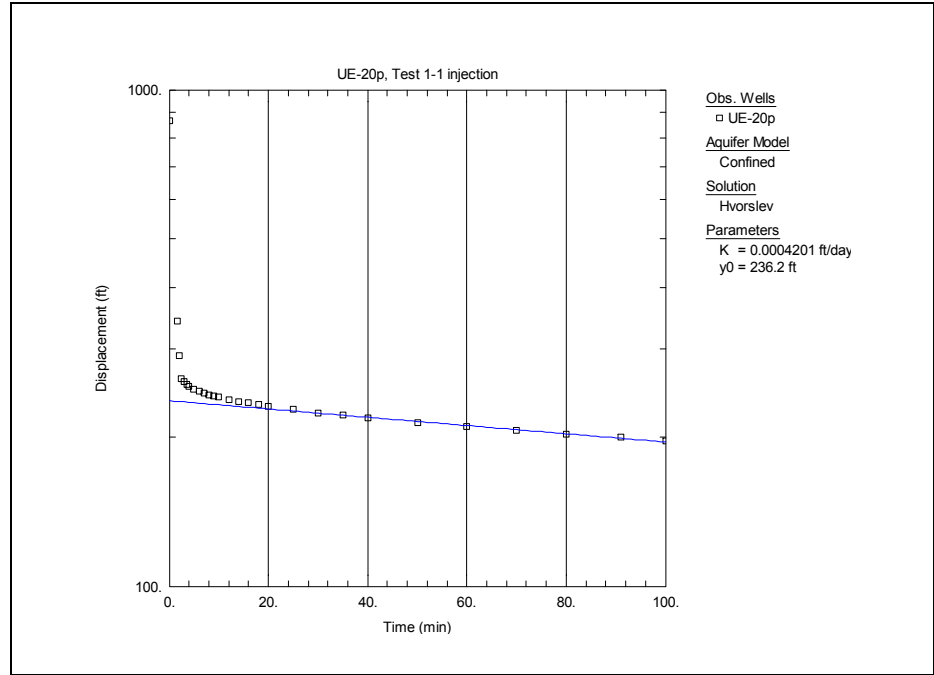


Figure C.3-4
Well UE-20p - Injection Test 1-1
Later-Time Formation Response

C.3.3.3 Results

Figure C.3-6 shows the distribution of analysis results for all of the tests plotted as percent versus log K (feet per day [ft/d]). Hydraulic conductivity generally has a log normal distribution, but this graph appears to indicate a bimodal distribution of log K. The second peak of this distribution starts around a log K of -1.5 ft/d. This is thought to be in the range of the hydraulic conductivity of the straddle-packer tool. One interpretation of this result is that the tests with log K values greater than -1.5 ft/d, which generally resemble the test shown in Figure C.3-5, actually represent packer-seal leakage for the duration of the test. The resultant head decline response would have been limited by the tool. Consequently, the log K values above -1.5 ft/d would not be representative of formation hydraulic conductivity.

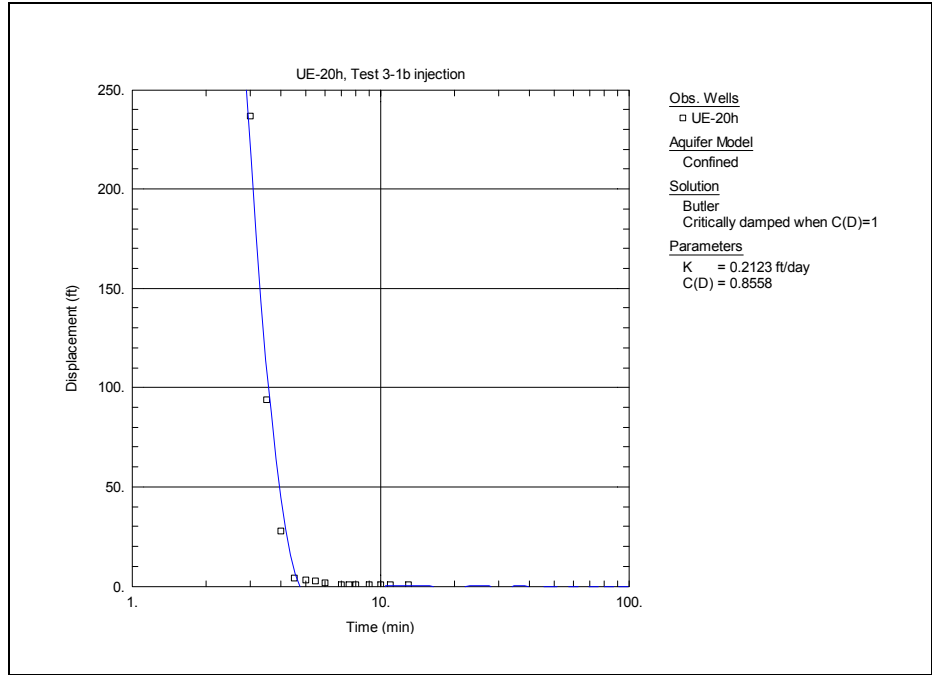


Figure C.3-5
Well UE-20h - Injection Test 3-1b
Questionable Test

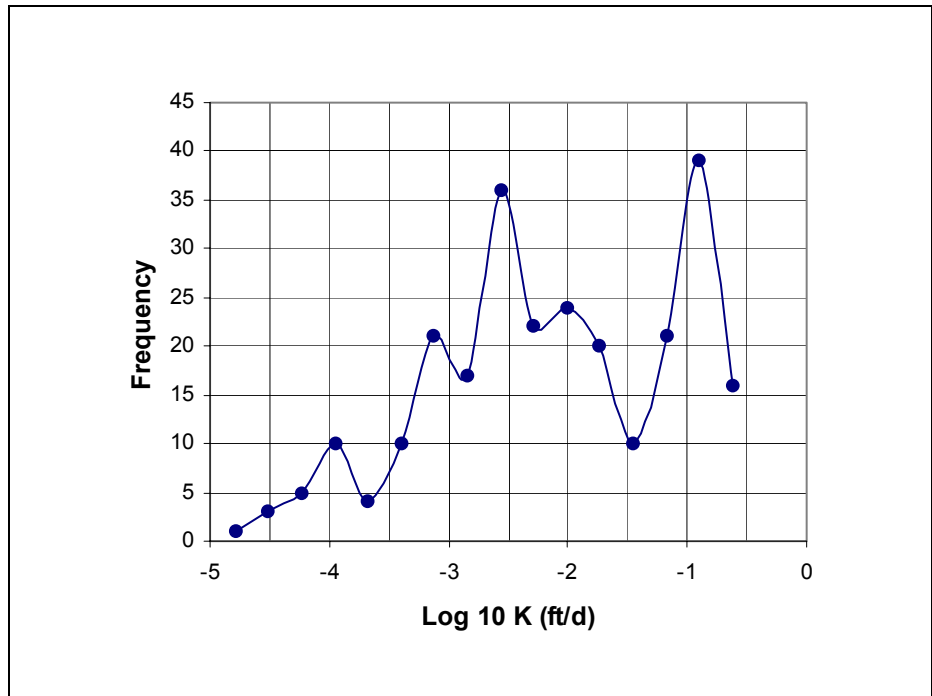


Figure C.3-6
Distribution of Results as Log K (ft/d)

C.4.0 References

- Belcher, W.R., and P.E. Elliott. 2001. *Hydraulic-Property Estimates for Use With a Transient Ground-Water Flow Model of the Death Valley Regional Ground-Water Flow System, Nevada and California*, WRIR 01-4210. Carson City, NV: U.S. Department of the Interior, U.S. Geological Survey.
- Blankennagel, R.K., 1967. Hydraulic Testing Techniques of Deep Drill Holes at Pahute Mesa, Nevada Test Site. United States Department of the Interior Geological Survey. Washington.
- Butler, 1998. The design, performance and analysis of slug tests. Lewis Publishers; Boca Raton, FL.
- Cooper, H.H., Jr., and C.E. Jacob. 1946. "A Generalized Graphical Method for Evaluating Formation Constants and Summarizing Well-field History." In *Transaction American Geophysical Union*, Vol. 27:526-534. Washington, DC: American Geophysical Union.
- Cooper, H.H., J.D. Bredehoeft, and J.S. Papadopoulos. 1967. "Response of a Finite-Diameter Well to an Instantaneous Change of Water." In *Water Resources Research*, Volume 3, No. 1 First Quarter of 1967. Water Resources Division, USGS. Washington, DC: American Geophysical Union.
- Freeze, R.A. and J.A. Cherry. 1979. *Groundwater*. Englewood Cliffs, NJ: Prentice-Hall, Inc.
- Hvorslev, M.J. 1951. Time Lag and Soil Permeability in Ground-Water Observations, Bull. No. 36, Waterways Exper. Sta. Corps of Engrs, U.S. Army, Vicksburg, Mississippi, pp. 1-50.
- Hyder Z., J.J. Butler Jr., and W. Liu. C.D. McElwee. 1994. "Slug Tests In Partially Penetrating Wells." *Water Resources Research*, Vol. 30, No. 11, pp 2945-2957. Washington, DC: American Geophysical Union.
- HydroSOLVE, Inc. 1996-2000. *AQTESOLV for Windows, User's Guide*. Reston, VA.
- IT Corporation. 1996. *Transport Parameter and Source Term Data Documentation Package (Phase I Data Analysis Documentation, Volume V)*. Prepared for the U.S. Department of Energy, Nevada Operations Office. Las Vegas, NV.
- Moench, A.F. 1984. "Double-Porosity Models for a Fissured Groundwater Reservoir With Fracture Skin." In *Water Resources Research*, Vol. 20, No. 7 pp. 8-31 to 8-46. Washington, DC: American Geophysical Union.

- Moench, A.F. 1985. "Transient Flow to a Large-diameter Well in an Aquifer With Storative Semiconfining Layers." In *Water Resources Research*, Vol. 21, No. 8. Washington, DC: American Geophysical Union.
- Moench, A.F. 1997. "Flow to a Well of Finite Diameter in a Homogeneous, Anisotropic Water Table Aquifer." In *Water Resources Research*, Vol. 33, No. 6. Washington, DC: American Geophysical Union.
- Papadopoulos, I.S., and H.H. Cooper. 1967. "Drawdown in a Well of Large Diameter." In *Water Resources Research*, Vol. 3. Washington, DC: American Geophysical Union.
- Theis, C.V. 1935. *The Relation Between the Lowering of the Piezometric Surface and the Rate and Duration of Discharge of a Well Using Groundwater Storage*, In *American Geophysical Union Transactions*, Vol. 16. Washington, DC: American Geophysical Union.
- U.S. Department of Energy, Nevada Operations Office. 1997. *Regional Groundwater Flow and Tritium Transport Modeling and Risk Assessment of the Underground Test Area, Nevada Test Site, Nevada*, DOE/NV--477. Las Vegas, NV.



Appendix D

Description of Well Discharge Data

D.1.0 Introduction

This appendix describes data relating to groundwater discharge by wells located within the PM-OV area and vicinity. The description includes the following items:

- A summary of the well discharge data
- A description of the full dataset
- Directions on how to access the data in electronic form

D.2.0 Summary Data

The well information for all wells considered is presented in [Table D.2-1](#). The total yearly water withdrawals for all wells considered are presented in [Table D.2-2](#). [Table D.2-2](#) indicates whether a given well is located within the boundaries of the PM-OV area or out of it but near its boundaries.

Table D.2-1
Pumping Well Information
(Page 1 of 2)

Reporting Name	UTM Easting (m)	UTM Northing (m)	Open Interval		HSU
			Depth to Top (m bgs)	Depth to bottom (m bgs)	
Wells Located within the Pahute Mesa-Oasis Valley Area					
Beatty Well No 1	522765.49	4086193.6	28.956	48.768	AA
Gexa Well 4	534072.61	4086108.2	243.84	487.7	PCM
U-20 WW (Cased)	550627.96	4122707.7	692.2	996.1	CHZCM
U-20a 2 WW	551348.24	4121756.8	629	1371.6	CHZCM
UE-19b 1 WW	562105.26	4129780.4	667.5	1371.6	BRA
UE-19c WW	560344.84	4124713.5	737.9	1377.696	BRA
UE-19c WW	560344.84	4124713.5	737.9	2401.8	BRA
UE-19c WW	560344.84	4124713.5	2401.8	2587.45	PBRCM
UE-19e WW	559115.78	4127848.1	754.38	894	BFCU
UE-19e WW	559115.78	4127848.1	894	1830.47	BRA

Table D.2-1
Pumping Well Information
 (Page 2 of 2)

Reporting Name	UTM Easting (m)	UTM Northing (m)	Open Interval		HSU
			Depth to Top (m bgs)	Depth to bottom (m bgs)	
UE-19gS WW	556297.17	4129062.8	807.72	2002.5	BRA
UE-19gS WW	556297.17	4129062.8	2002.5	2286	PBRCM
UE-20h WW	550195.52	4124985.6	763.82	1653.8	CHZCM
UE-20h WW	550195.52	4124985.6	1653.8	2196.4	BFCU
UE-20h WW	550195.52	4124985.6	2196.4	2196.69	CFCM
WW-8	563115.44	4113269.7	381	542.5	BRA
Wells Located Outside the Pahute Mesa-Oasis Valley Area					
Beatty Indian Spring Well	517538.38	4089416.7	147	210.3	DVA
Beatty Middle Well	516848.99	4087874.6	30.48	213.36	DVA
Beatty Summit Well	517990.17	4086274.6	115	213.3	DVA
Beatty Well No 2	521707.47	4083879.8	27.432	59.436	AA
Beatty Well No 3	521533.42	4084218.3	21.336	39.624	AA
UE-16d WW	574307.16	4102759.7	229	252.98	UCA

Table D.2-2
Historical Groundwater Discharge Volumes and Rates
 (Page 1 of 5)

Reporting Name	Year	Discharge Volume (m ³)	Discharge Rate (m ³ /d)
Wells Located within the Pahute Mesa-Oasis Valley Area			
Beatty Well No 1	1994	55,157	151.12
Beatty Well No 1	1995	63,709	174.55
Beatty Well No 1	1996	54,396	148.62
Beatty Well No 1	1997	52,793	144.64
Beatty Well No 1	1998	53,410	146.33
Beatty Well No 1	1999	35,771	98.00
Beatty Well No 1	2000	34,523	94.58
GEXA W 4	1997	237,409	650.44
GEXA W 4	1998	109,812	300.86

Table D.2-2
Historical Groundwater Discharge Volumes and Rates
 (Page 2 of 5)

Reporting Name	Year	Discharge Volume (m ³)	Discharge Rate (m ³ /d)
GEWA W 4	1999	254,992	698.61
GEWA W 4	2000	96,412	264.14
PW-2 ^a	1997	118,427	324.46
PW-2	1998	147,315	403.60
PW-2	1999	61,501	168.50
PW-2	2000	1,767	4.84
U-20 WW (cased)	1985	157,600	431.78
U-20 WW (cased)	1986	288,300	789.86
U-20 WW (cased)	1987	260,000	712.33
U-20 WW (cased)	1988	399,100	1090.44
U-20 WW (cased)	1989	426,100	1167.40
U-20 WW (cased)	1990	351,600	963.29
U-20 WW (cased)	1991	116,500	319.18
U-20 WW (cased)	1992	313,300	856.01
U-20 WW (cased)	1993	105,800	289.86
U-20 WW (cased)	1994	76,400	209.32
U-20 WW (cased)	1995	116,700	319.73
U-20 WW (cased)	1996	144,200	393.99
U-20 WW (cased)	1997	-	0.00
U-20 WW (cased)	1998	73,500	201.37
U-20 WW (cased)	1999	57,400	157.26
U-20 WW (cased)	2000	-	0.00
U-20a 2 WW	1964	64,300	175.68
U-20a 2 WW	1965	34,400	94.25
U-20a 2 WW	1966	23,800	65.21
U-20a 2 WW	1967	86,300	236.44
UE-19c WW	1983	158,400	433.97
UE-19c WW	1984	242,600	662.84
UE-19c WW	1985	390,700	1070.41
UE-19c WW	1986	322,000	882.19
UE-19c WW	1987	193,400	529.86
UE-19c WW	1988	243,300	664.75
UE-19c WW	1989	524,700	1437.53
UE-19c WW	1990	418,500	1146.58
UE-19c WW	1991	477,200	1307.40
UE-19c WW	1992	184,100	503.01
UE-19c WW	1993	26,900	73.70

Table D.2-2
Historical Groundwater Discharge Volumes and Rates
 (Page 3 of 5)

Reporting Name	Year	Discharge Volume (m ³)	Discharge Rate (m ³ /d)
UE-19c WW	1994	2,500	6.85
UE-19c WW	1995	-	0.00
UE-19c WW	1996	-	0.00
UE-19c WW	1997	-	0.00
UE-19c WW	1998	-	0.00
UE-19c WW	1999	-	0.00
UE-19c WW	2000	-	0.00
UE-19e WW	1965	42,400	116.16
UE-19e WW	1966	23,800	65.21
UE-19e WW	1967	38,600	105.75
UE-19gS WW	1967	79,500	217.81
WW-8	1963	20,100	55.07
WW-8	1964	423,500	1157.10
WW-8	1965	122,300	335.07
WW-8	1966	137,000	375.34
WW-8	1967	217,600	596.16
WW-8	1983	222,900	610.68
WW-8	1984	231,400	632.24
WW-8	1985	228,000	624.66
WW-8	1986	143,400	392.88
WW-8	1987	258,700	708.77
WW-8	1988	247,100	675.14
WW-8	1989	203,900	558.63
WW-8	1991	217,900	596.99
WW-8	1992	214,200	585.25
WW-8	1993	118,600	324.93
WW-8	1994	114,000	312.33
WW-8	1995	78,500	215.07
WW-8	1996	66,400	181.42
WW-8	1997	47,000	128.77
WW-8	1998	43,000	117.81
WW-8	1999	52,300	143.29
WW-8	2000	59,536	163.11
Wells Located Outside the Pahute Mesa-Oasis Valley Area			
Beatty Middle Well	1995	30,455	83.44
Beatty Middle Well	1996	9,251	25.28
Beatty Middle Well	1997	21,463	58.80

Table D.2-2
Historical Groundwater Discharge Volumes and Rates
 (Page 4 of 5)

Reporting Name	Year	Discharge Volume (m ³)	Discharge Rate (m ³ /d)
Beatty Middle Well	1998	15,419	42.24
Beatty Middle Well	1999	379	1.04
Beatty Middle Well	2000	-	0.00
Beatty Middle Well	2001	-	0.00
Beatty Summit Well	1991	146,377	401.03
Beatty Summit Well	1992	97,131	266.11
Beatty Summit Well	1993	100,406	275.08
Beatty Summit Well	1994	89,525	245.27
Beatty Summit Well	1995	80,176	219.66
Beatty Summit Well	1996	79,559	217.38
Beatty Summit Well	1997	69,938	191.61
Beatty Summit Well	1998	72,035	197.36
Beatty Summit Well	1999	73,762	202.09
Beatty Summit Well	2000	48,643	133.27
Beatty Summit Well	2001	37,778	103.50
Beatty Upper Indian Well	1991	200,144	548.34
Beatty Upper Indian Well	1992	175,194	479.98
Beatty Upper Indian Well	1993	171,688	470.38
Beatty Upper Indian Well	1994	162,242	444.50
Beatty Upper Indian Well	1995	159,057	435.77
Beatty Upper Indian Well	1996	154,185	421.27
Beatty Upper Indian Well	1997	140,617	385.25
Beatty Upper Indian Well	1998	121,004	331.52
Beatty Upper Indian Well	1999	109,286	299.41
Beatty Upper Indian Well	2000	71,658	196.32
Beatty Well No 2	1994	87,928	240.90
Beatty Well No 2	1995	69,420	190.19
Beatty Well No 2	1996	76,599	209.29
Beatty Well No 2	1997	68,458	187.56
Beatty Well No 2	1998	-	0.00
Beatty Well No 2	1999	-	0.00
Beatty Well No 2	2000	11,848	32.46
Beatty Well No 3	1994	88,718	243.06
Beatty Well No 3	1995	82,224	225.27
Beatty Well No 3	1996	131,982	360.61
Beatty Well No 3	1997	106,079	290.63
Beatty Well No 3	1998	22,203	60.83

Table D.2-2
Historical Groundwater Discharge Volumes and Rates
 (Page 5 of 5)

Reporting Name	Year	Discharge Volume (m ³)	Discharge Rate (m ³ /d)
Beatty Well No 3	1999	2,011	5.51
Beatty Well No 3	2000	-	0.00
UE-16d WW	1983	17,200	47.12
UE-16d WW	1984	30,700	83.88
UE-16d WW	1985	96,000	263.01
UE-16d WW	1986	145,600	398.90
UE-16d WW	1987	128,800	352.88
UE-16d WW	1988	144,100	393.72
UE-16d WW	1989	98,500	269.86
UE-16d WW	1990	124,700	341.64
UE-16d WW	1991	103,300	283.01
UE-16d WW	1992	124,400	339.89
UE-16d WW	1993	181,300	496.71
UE-16d WW	1994	195,500	535.62
UE-16d WW	1995	134,400	368.22
UE-16d WW	1996	145,400	397.27
UE-16d WW	1997	156,900	429.86
UE-16d WW	1998	77,700	212.88
UE-16d WW	1999	139,600	382.47
UE-16d WW	2000	93,609	256.46

^a Well PW-2 is located within 500 m of GEXA Well 4. It was used as a substitute pumping well for GEXA Well 4 during 1997 and 1998.

D.3.0 Full Dataset

This description of the full well discharge dataset includes the following items:

- A summary of the contents of the dataset
- The structure of the table containing the dataset

Directions on how to access the dataset are presented in [Section D.4.0](#).

D.3.1 Dataset Content Summary

The dataset contains information about the well, yearly discharge volume, and ancillary information related to the measurement. The well discharge dataset contains 144 records for 15 wells located within the PM-OV area and vicinity. Each record in the well discharge dataset contains information relating single well discharge measurement.

D.3.2 Table Structure

The well discharge table contains the following fields:

WPM_DA_reporting_name: WPM_DA reporting name for the site

hyd_area: Nevada Hydrographic Area

- 147 - Gold Flat
- 159 - Yucca Flat, essentially northeastern section of NTS
- 227B - Upper Fortymile, essentially Area 18 and parts of 20, 19, and 30 (2271)
- 228 - Oasis Valley
- 229 - Crater Flat

nts_area: Nevada Test Site Area number

g_bsn: Groundwater sub-basin

- AFFCR - Alkali Flat-Furnace Creek Ranch
- AM - Ash Meadows
- OV - Oasis Valley

yield_unt: Primary water yielding unit

- B - Basin fill
- C - Carbonate rock
- V - Volcanic rock

duration: Period of time (specific date as year, month and year, or year, month and day), over which the total volume of water withdrawn from the well is reported or the discharge is reported

dur_type: Year, month, or day - Left blank if discharge rate rather than volume is reported

- Y - Yearly

dis_vol (gal): Discharge volume in gallons over 'duration' of interest -- [Provided only when reported]

dis_vol (mg): Discharge volume in millions of gallons over 'duration' of interest -- obtained by dividing 'dis_vol (gal)' by 1E6

dis_vol (af): Discharge volume reported in acre-feet over 'duration' of interest -- obtained by multiplying 'dis_vol (mg)' by a factor of 3.069

dis_vol (ml): Discharge volume reported in million liters over 'duration' of interest -- obtained by multiplying 'dis_vol (mg)' by a factor of 3.785

dis_vol (m3): Discharge volume in cubic meters over 'duration' of interest -- Conversion formula is: 'dis_vol (m3) = ['dis_vol (ml)' * (1e6/ml)] / [1,000 m³/L]

rpt_days: Number of days of record (was used to convert discharge volume to daily discharge rate)

dys_est: Number of days of record for which volume was estimated

dis_rate (m³/d): Discharge rate in cubic meters per day. Obtained by converting the water use from millions of liters -- The conversion formula is: [dis_rate (m³/d)] = [dis_vol(m³)]/[rpt_dys], or = dis_rate(gpm)*60*24*3.78541e-3, or = dis_vol (af) * 1,233.48.

data_source: Name of, or code for the entity that collected the data

- A - Estimated from pump run times recorded on daily ammeter charts supplied by BN or Reynolds Electrical & Engineering Co., Inc. (REECO)
- E - Taken from BN or REECO water production reports and includes estimated values
- M - Taken from BN or REECO water production reports
- R - Taken from Claassen, H.C., (1973) *Water Quality And Physical Characteristics Of Nevada Test Site Water-supply Well*
- BWS - Beatty Water and Sanitation District
- NDWR - Nevada Division of Water Resources
- PUBUT - Public Utility

ref_id: Unique identifier of a given document or file from which the data were extracted. If the same reference is used more than once, a sequential number is added at the end of the ref_id [Example: PC-5-01]

DDE_F: Data documentation evaluation flag

- 4 - Level 4: Data are collected by a participating NNSA/NSO ERP or other organization prior to the issuance and implementation of project-approved standard policies, procedures, or practices governing data acquisition and qualification

reported_by: Organization, person, or agency reporting the NTS well discharge data

load_file: Name of the file from which the data were loaded into the database

dis_meth: Method of volume or discharge measurement

- E - Estimated
- F - Measured with flow meter installed at well head

dis_type: Type of discharge: pumped or flowing

- P - Pumped discharge
- F - Flowing discharge

water_use: Water use or proposed water use

- P - Public supply
- U - Unused
- N - Industrial

dis_rate (gpm): Discharge rate in gallons per minute - Provided as reported by others

D.4.0 Access to Data

To access the datasets from the paper copy of this document, use the CD provided at the end of the document and open the desired file. To access the dataset from the electronic version of this document, click on the desired filename listed below.

The well information table and the full well discharge dataset are presented in an electronic format. The tables include wells located within and outside of the PM-OV area boundary and may be found in the following EXCEL and ASCII files:

EXCEL:

- Pumping-Well-Information.xls
- tblDischarge_Well.xls

ASCII:

- Pumping-Well-Information.txt
- tblDischarge_Well.txt

D.5.0 *References*

Claassen, H.C. 1973. *Water Quality and Physical Characteristics of Nevada Test Site Water-Supply Wells*. U.S. Geological Survey, USGS-474-158.
U.S. Geological Survey.



Appendix E

Description of Hydraulic Head Dataset

E.1.0 Introduction

This appendix contains summary information on the hydraulic heads, the complete water elevations dataset, and the hydrograph analysis documentation.

E.1.1 Hydraulic Head Summary Data

The hydraulic head summary data discussed in the main text of this document is shown in [Table E.1-1](#) and [Table E.1-2](#). The mean water level elevations shown in [Table E.1-2](#) are the suggested target heads for flow model calibration.

E.1.2 Water Elevations Dataset and Hydrograph Analysis

This description of the water elevations dataset and hydrograph analysis includes the following items:

- A summary of the contents of the dataset and analysis
- The structure of the table containing the dataset
- Directions on how to access the full dataset and analysis

E.2.0 Dataset and Analysis Summary

Each record in the water elevations dataset contains information for a single water-level measurement. The water elevations dataset contains 3,822 records for roughly 292 different locations or borehole intervals on or near the NTS. The dataset contains information about the well, water level depth, and ancillary information related to the measurement.

The hydrograph analysis contains a hydrograph as well as a description of the data for a well or intervals within a well. Hydrographs were not prepared for wells or intervals with a limited amount of data.

E.3.0 Table Structure

The water elevations table contains the following fields:

- ID - Database identifier

Table E.1-1
Site Information for Selected Wells, Boreholes, and Springs Located in the
Pahute Mesa-Oasis Valley Area and Vicinity
(Page 1 of 7)

Site Name	UTM Easting (m) ^a	UTM Northing (m)	Total Depth (mbgs) ^b	Ref. Point Elevation (m amsl) ^c	Ref. Point Elevation Accuracy (m)	EOI Top Elevation (m amsl) ^d	EOI Bottom Elevation (m amsl)	Primary HSU(s) ^e
Beatty Wash Terrace Well	524858.14	4088542.31	22.86	1,054.61	6.096	1,037.84	1,031.75	AA
Beatty Well No 1	521378.38	4085329.17	—	1,025.65	6.096	996.70	976.88	AA
Boiling Pot Road Well	524817.51	4093904.62	3.75	1,103.38	6.096	1,103.38	1,099.63	AA
Coffer Dune Well	526403.82	4100288.03	5.18	1,183.54	3.048	1,183.54	1,178.36	AA
Coffer Lower ET Well	525961.02	4099700.94	3.38	1,176.83	3.048	1,176.83	1,173.45	AA
Coffer Middle ET Well	525664.24	4099915.24	3.41	1,175.31	3.048	1,175.31	1,171.90	AA
Coffer Windmill Well	539420.80	4095192.45	146.30	1,341.12	3.048	1,231.39	1,194.82	AA
ER-18-2	555724.60	4106388.73	762.00	1,657.20	0.3048	1,245.4	899.30	TMCM
ER-19-1-1 (deep)	567541.60	4114743.34	1,095.80	1,871.41	0.03048	893.32	786.62	UCCU
ER-19-1-2 (middle)	567541.60	4114743.34	1,095.80	1,871.41	0.03048	1,094.52	1,037.22	PBRCM
ER-19-1-3 (shallow)	567541.60	4114743.34	1,095.80	1,871.41	0.03048	1,475.22	1,438.32	PBRCM
ER-20-1	545113.11	4119467.75	627.89	1,883.94	0.03048	1,293.26	1,254.26	TCA
ER-20-2-1	553210.64	4118447.10	768.10	2,042.16	6.096	1,346.56	1,272.96	CHZCM
ER-20-5-1 (3-in string)	546385.91	4119208.35	860.50	1,902.50	0.03048	1,217	1,093.30	TSA/CHZCM
ER-20-6-1 (3-in string)	551362.94	4123691.83	975.40	1,973.52	0.03048	1,230.7	1,075.30	CHZCM
ER-20-6-2 (3-in string)	551328.01	4123661.84	975.40	1,973.61	0.03048	1,237.81	1,076.01	CHZCM
ER-20-6-3 (3-in string)	551295.69	4123578.84	975.40	1,970.84	0.03048	1,228.34	1,115.24	CHZCM
ER-30-1	560804.66	4100462.97	434.60	1,416.53	0.03048	1,280.06	1,176.20	FCCM
ER-EC-1	541729.80	4117659.54	1,524.00	1,836.72	0.3048	1,148.8	361.80	BA/UPCU/TCA/LPCU/TSA/CHCU/CFCM
ER-EC-2A (498.3-681.5 m)	538420.77	4110841.15	1,516.10	1,494.13	0.3048	996.5	813.30	FCCM
ER-EC-2A (498.35-1515.8 m)	538420.77	4110841.15	1,516.60	1,494.13	0.3048	996.5	-21.30	FCCM/TMCM
ER-EC-4 (290.2-1062.8 m)	532759.63	4112355.80	1,063.10	1,450.74	0.3048	1,160.6	393.80	TMA/FCCM/TCVA
ER-EC-4 (290.2-699.5 m)	532759.63	4112355.80	1,063.10	1,450.74	0.3048	1,160.6	751.30	TMA/FCCM/TCVA
ER-EC-4 (Lower Interval)	532759.63	4112355.80	—	1,450.74	0.3048	526.7	393.80	TMA
ER-EC-5	538701.80	4104136.85	762.00	1,547.47	0.3048	1,191.2	791.60	TMCM
ER-EC-6 (481.9-1164.3 m)	544673.45	4115728.54	1,524.00	1,708.10	0.3048	1,226.42	543.97	BA/UPCU/TCA/LPCU/TSA/CHCU
ER-EC-6 (481.9-1524 m)	544673.45	4115728.54	1,524.00	1,708.10	0.3048	1,226.42	184.30	BA/UPCU/TCA/LPCU/TSA/CHCU/CFCM
ER-EC-7	546483.54	4093127.26	422.50	1,464.56	0.3048	1,190.2	1,063.70	FCCM
ER-EC-8	532763.77	4106141.76	609.60	1,320.70	0.3048	1,101.4	687.40	FCCM/TMCM

Table E.1-1
Site Information for Selected Wells, Boreholes, and Springs Located in the
Pahute Mesa-Oasis Valley Area and Vicinity
 (Page 2 of 7)

Site Name	UTM Easting (m) ^a	UTM Northing (m)	Total Depth (mbgs) ^b	Ref. Point Elevation (m amsl) ^c	Ref. Point Elevation Accuracy (m)	EOI Top Elevation (m amsl) ^d	EOI Bottom Elevation (m amsl)	Primary HSU(s) ^e
ER-OV-01	528416.67	4104084.05	54.86	1,241.40	0.3048	1,198.88	1,187.26	FCCM
ER-OV-02	526310.01	4098715.82	60.96	1,182.72	0.3048	1,134.74	1,122.54	AA
ER-OV-03a	526298.82	4094586.88	76.50	1,171.76	0.3048	1,112.25	1,096.10	DVCM
ER-OV-03a2	526298.82	4094586.88	250.24	1,171.58	0.3048	1,001.42	972.52	DVCM
ER-OV-03a3	526298.82	4094586.88	250.24	1,171.58	0.3048	1,145.32	1,123.37	DVCM
ER-OV-03b	531007.58	4097776.60	121.92	1,290.12	0.3048	1,184.52	1,168.81	AA
ER-OV-03c	535494.16	4094374.14	165.20	1,277.57	0.3048	1,127.24	1,113.24	TMA
ER-OV-03c2	535494.16	4094374.14	97.84	1,277.69	0.3048	1,196.33	1,180.83	TMA
ER-OV-04a	525671.45	4089315.70	46.02	1,064.17	0.3048	1,037.78	1,018.88	AA
ER-OV-05	520280.13	4099808.54	60.96	1,200.25	0.3048	1,159.37	1,139.82	AA
ER-OV-06a	528416.67	4104084.05	163.37	1,241.46	0.3048	1,092.36	1,077.66	FCCM
ER-OV-06a2	528416.67	4104084.05	21.64	1,241.32	0.3048	1,228.60	1,222.20	FCCM
Gexa Well 4	534242.30	4085955.88	487.68	1,198.14	0.03048	954.30	710.44	PCM
Hagestad 1	569542.26	4116259.67	591.62	2,281.52	0.03048	1,841.84	1,697.95	PBRCM
Matheny Well	525009.22	4087433.45	53.34	1,069.85	6.096	1,069.85	1,016.51	AA
MOV ET Well	524614.14	4095906.35	4.02	1,124.10	3.048	1,121.51	1,120.14	AA
Pioneer Road Seep Well	524051.77	4093748.21	2.21	1,112.52	6.096	1,112.52	1,110.31	AA
PM-1 (2356.408 m)	552668.11	4125925.14	2,395.12	1,998.82	0.03048	-300.18	-396.18	BRA
PM-2	538256.72	4133028.18	2,676.75	1,704.38	0.03048	938.49	-973.51	PBRCM
PM-3 (Upper Borehole)	539011.77	4121281.28	502.01	1,774.79	0.03048	1,330.42	1,272.79	UPCU
PM-3 (Lower Borehole)	539011.77	4121281.28	920.19	1,774.79	0.03048	1,325.82	854.60	UPCU/TCA/LPCU/CHCU/BFCU/BRA/PBRCM
PM-3-1 (Piez 1)	539011.77	4121281.28	920.20	1,774.79	0.03048	1,204.19	1,106.69	LPCU/TCA/UPCU
PM-3-2 (Piez 2)	539011.77	4121281.28	920.20	1,774.79	0.03048	1,331.18	1,260.59	UPCU
Springdale ET Deep Well	523992.86	4096952.87	2.83	1,131.42	3.048	1,131.42	1,128.58	AA
Springdale ET Shallow Well	523992.86	4096952.87	1.71	1,131.42	3.048	1,131.42	1,129.71	AA
Springdale Lower Well	523894.12	4096952.59	3.51	1,130.81	6.096	1,130.81	1,127.30	AA
Springdale Upper Well	523521.64	4097506.21	—	1,150.62	3.048	1,150.62	1,122.88	AA
Springdale Windmill Well	521469.33	4098301.69	—	1,179.58	3.048	1,167.38	1,143.00	AA

Table E.1-1
Site Information for Selected Wells, Boreholes, and Springs Located in the
Pahute Mesa-Oasis Valley Area and Vicinity
(Page 3 of 7)

Site Name	UTM Easting (m) ^a	UTM Northing (m)	Total Depth (mbgs) ^b	Ref. Point Elevation (m amsl) ^c	Ref. Point Elevation Accuracy (m)	EOI Top Elevation (m amsl) ^d	EOI Bottom Elevation (m amsl)	Primary HSU(s) ^e
TW-1 (1125 m)	569000.27	4112499.01	1,281.99	1,876.29	0.03048	1,294.12	1,135.62	PBRCM
TW-1 (1127-1137 m)	569000.27	4112499.01	1,137.21	1,876.29	0.03048	748.53	739.08	LCA3
TW-1 (170 m)	569000.27	4112499.01	170.69	1,876.29	0.03048	1,751.17	1,705.60	PBRCM
TW-1 (492 m)	569000.27	4112499.01	492.25	1,876.29	0.03048	1,749.67	1,384.04	PBRCM
TW-1 (560 m)	569000.27	4112499.01	560.83	1,876.29	0.03048	1,384.04	1,315.46	PBRCM
TW-1 (826 m)	569000.27	4112499.01	1,281.99	1,876.29	0.03048	1,294.12	1,135.62	PBRCM
TW-1 (839 m)	569000.27	4112499.01	1,281.99	1,876.29	0.03048	1294.12	1,135.62	PBRCM
TW-1 (839-1279 m)	569000.27	4112499.01	1,281.99	1,876.29	0.03048	748.53	594.30	LCA3
U-12s (451.1 m)	569567.09	4120287.29	486.46	2,070.87	0.03048	1,784.75	1,619.77	MGCU
U-19ab	559842.41	4122993.41	685.80	2,111.65	0.03048	1,442.35	1,438.35	BFCU
U-19ab 2	559864.00	4123005.98	731.52	2,112.26	0.03048	1,497.89	1,380.76	CFCU/BFCU
U-19ad	557182.93	4125122.57	685.80	2,039.72	0.03048	1,372.21	1,353.92	PLFA
U-19ae	555867.14	4121059.06	832.10	2,065.02	0.03048	1,369.77	1,233.02	CHCU/CFCU
U-19ai	560675.01	4130919.10	632.46	2,054.96	0.03048	1,428.99	1,422.50	BFCU
U-19aj	559768.33	4128539.07	670.56	2,100.38	1.524	1,432.38	1,429.78	BFCU
U-19aq	555471.48	4120144.12	662.94	2,072.18	0.03048	1,428.95	1,409.28	PLFA
U-19ar	557127.29	4125777.83	670.56	2,043.99	—	1,398.93	1,373.39	PLFA
U-19aS (857 m)	555856.82	4125370.82	857.40	2,060.75	0.03048	1,392.69	1,203.35	CHVTA/CFCU
U-19au	555278.49	4122855.75	670.56	1,991.56	0.03048	1,358.57	1,321.00	CHVCM
U-19au 1	555285.52	4122848.77	660.50	1,991.50	0.3048	1,358.78	1,331.00	CHVCM
U-19ay	557311.38	4125422.57	657.15	2,045.82	0.03048	1,396.93	1,388.72	PLFA
U-19az	555779.16	4120082.43	649.22	2,058.25	0.03048	1,424.58	1,409.05	PLFA
U-19ba	560899.24	4127735.55	663.55	2,144.94	0.03048	1,488.78	1,481.44	KA
U-19bg 1	556767.57	4125059.53	685.80	2,040.27	0.03048	1,394.51	1,354.47	PLFA/CHVTA
U-19bh	555683.61	4120389.25	654.71	2,062.86	0.03048	1,425.93	1,407.86	PLFA
U-19bj	560900.36	4127416.21	656.23	2,144.27	0.3048	1,493.23	1,488.07	KA
U-19bk	554585.64	4126722.95	669.95	2,033.00	0.03048	1,427.93	1,363.05	unk
U-19d 2	560056.34	4133534.77	2,343.61	2,091.11	0.03048	1,310.81	-252.49	BRA/PBRCM
U-19e	559100.94	4127774.92	1,539.24	2,109.12	0.03048	580.22	569.92	BRA

Table E.1-1
Site Information for Selected Wells, Boreholes, and Springs Located in the
Pahute Mesa-Oasis Valley Area and Vicinity
 (Page 4 of 7)

Site Name	UTM Easting (m) ^a	UTM Northing (m)	Total Depth (mbgs) ^b	Ref. Point Elevation (m amsl) ^c	Ref. Point Elevation Accuracy (m)	EOI Top Elevation (m amsl) ^d	EOI Bottom Elevation (m amsl)	Primary HSU(s) ^e
U-19g	556340.47	4129243.99	1,003.40	2,052.52	0.03048	1,074.12	1,061.92	BRA
U-19x	556020.56	4120757.93	679.70	2,066.85	0.03048	1,392.02	1,387.15	PLFA
U-20 WW (Open)	550614.04	4122711.65	996.09	1,971.45	0.03048	1,351.54	975.36	CHZCM
U-20a	550480.65	4121740.04	774.19	1,987.21	0.003048	1,221.86	1,213.01	CHZCM
U-20a 2 WW	551333.24	4121743.04	1,371.60	1,972.67	0.3048	1,343.25	601.68	CHZCM
U-20ah	551224.79	4123206.53	701.04	1,964.44	0.03048	1,354.02	1,263.44	CHZCM
U-20ai	549637.35	4124115.40	656.54	1,982.11	0.03048	1,356.20	1,325.61	CHZCM
U-20ak	545315.27	4122286.80	640.08	1,900.43	0.03048	1,278.45	1,260.43	BA
U-20am	552255.84	4124536.00	670.56	2,009.55	0.03048	1,356.97	1,338.55	CHVCM
U-20an	549804.18	4127791.81	617.52	1,969.62	0.03048	1,363.10	1,352.12	CHZCM
U-20ao	546767.80	4121180.00	655.32	1,913.84	0.03048	1,317.29	1,258.54	BA
U-20ar 1	546841.11	4129690.73	696.47	1,926.03	0.3048	1,364.42	1,229.56	UNK/CHZCM
U-20as	547764.68	4119233.62	640.08	1,897.99	0.03048	1,284.43	1,257.89	UPCU
U-20at 1	543540.04	4122270.49	670.56	1,902.17	0.03048	1,284.41	1,232.57	UPCU
U-20av	551172.75	4120677.79	640.08	1,970.23	0.3048	1,338.00	1,330.13	LPCU
U-20aw	552097.89	4126211.40	640.08	2,007.11	0.03048	1,371.43	1,367.11	CHZCM
U-20ax	549116.89	4120396.31	670.56	1,992.20	0.03048	1,329.93	1,321.60	CHZCM
U-20ay	549562.42	4123673.30	640.08	1,987.45	0.03048	1,360.98	1,347.35	CHZCM
U-20az	552392.36	4120468.47	685.80	2,003.42	0.03048	1,345.05	1,317.42	CHZCM
U-20bb (579.12 m)	544857.89	4122285.19	579.12	1,897.78	1.524	1,367.70	1,318.66	PVTA
U-20bb (676.66 m)	544857.89	4122285.19	676.66	1,897.78	1.524	1,272.94	1,221.12	PVTA/BA/UPCU
U-20bb 1	544858.27	4122265.38	714.76	1,897.99	3.048	1,280.00	1,183.23	PVTA/BA/UPCU
U-20bc	545158.17	4123977.74	609.60	1,873.36	0.03048	1,303.07	1,263.76	UPCU
U-20bd (689.15 m)	551420.29	4123847.44	689.15	1,976.96	0.03048	1,355.79	1,287.81	UPCU/LPCU/CHZCM
U-20bd 1	551402.86	4123865.05	732.13	1,976.78	0.03048	1,355.50	1,244.65	LPCU/CHZCM
U-20bd 2	551437.63	4123857.55	746.76	1,977.24	0.3048	1,355.86	1,249.92	UPCU/LPCU/CHZCM
U-20be	550733.50	4119853.20	676.66	1,978.64	0.03048	1,303.78	1,301.94	CHZCM
U-20bf	549522.46	4122042.60	685.80	1,988.00	0.03048	1,338.18	1,302.20	CHZCM
U-20bg	552511.89	4121139.28	670.56	2,001.68	0.03048	1,352.49	1,331.12	CHZCM

Table E.1-1
Site Information for Selected Wells, Boreholes, and Springs Located in the
Pahute Mesa-Oasis Valley Area and Vicinity
 (Page 5 of 7)

Site Name	UTM Easting (m) ^a	UTM Northing (m)	Total Depth (mbgs) ^b	Ref. Point Elevation (m amsl) ^c	Ref. Point Elevation Accuracy (m)	EOI Top Elevation (m amsl) ^d	EOI Bottom Elevation (m amsl)	Primary HSU(s) ^e
U-20c	546698.66	4120477.68	1,463.04	1,914.45	0.03048	465.13	451.41	CHZCM
U-20e	547789.21	4129655.07	1,174.39	1,925.12	0.03048	1,360.32	750.72	CHZCM
U-20g	552440.19	4128343.51	1,280.16	1,972.06	0.03048	697.69	691.90	BFCU
U-20i	548242.94	4127580.93	1,434.08	1,941.58	0.03048	1,941.58	510.50	TCVA/TMA/CHZCM/CFCM
U-20m	541289.57	4128104.30	1,264.01	1,799.23	0.03048	549.55	535.23	PBRCM
U-20n PS 1DD-H (922 m)	551149.81	4121479.12	922.02	1,971.48	0.03048	1,159.18	1,058.60	CHZCM
U-20y	546651.34	4119290.95	793.09	1,907.13	0.03048	1,276.94	1,114.13	LPCU/TSA
UE-12n 15a	569702.98	4117954.50	589.48	2,246.13	0.03048	1,841.00	1,656.65	YF-LCU
UE-18r	549321.87	4109762.04	1,525.22	1,688.04	0.03048	1,191.54	162.84	TMCM
UE-18t	559591.45	4109095.12	792.48	1,585.26	0.3048	1,306.27	792.76	FCCM/TMCM
UE-19b 1 WW	562090.74	4129796.62	1,371.60	2,073.25	0.3048	1,405.75	701.65	BRA
UE-19c WW	560338.88	4124701.60	2,587.45	2,143.69	0.03048	1,405.79	766.15	BRA
UE-19e WW	559111.73	4127849.31	1,830.32	2,108.79	0.03048	1,354.41	278.32	BRA/BFCU
UE-19fs	556107.49	4119780.70	2,118.36	2,052.89	0.03048	1,271.08	-65.47	CHCU/IA/CFCU/BFCU/BRA
UE-19gS	556306.09	4129056.77	2,286.00	2,048.07	0.03048	2,047.95	-208.05	BRA/PBRCM
UE-19gS WW	556306.09	4129056.77	1,374.04	2,047.95	0.3048	1,240.23	673.91	BRA/PBRCM
UE-19h	555488.44	4132881.78	698.91	2,066.57	0.03048	1,423.14	1,370.67	BRA
UE-19i	557922.26	4122592.04	2,438.40	2,084.50	0.03048	1,201.80	-353.90	CFCU/BFCU/BRA
UE-19z	559665.02	4128109.05	853.44	2,099.46	—	1,429.66	1,246.02	BFCU
UE-20ab	552284.53	4125130.30	777.24	2,005.89	1.524	1,357.88	1,228.65	CHVCM
UE-20av	551258.81	4120728.07	788.52	1,968.40	0.3048	1,319.66	1,171.66	LPCU/CHZCM
UE-20bh 1	552402.18	4122007.34	856.50	2,022.84	0.03048	1,348.55	1,166.46	CHZCM
UE-20c	546865.74	4120450.24	1,627.02	1,915.06	0.03048	1,267.05	285.06	TCA/LPCU/TSA/CHZCM
UE-20d	546102.70	4122275.25	1,371.60	1,905.91	0.3048	1,160.37	536.75	UPCU/TCA/TSA/LPCU/CHZCM
UE-20e 1	548110.45	4129980.73	1,949.20	1,919.33	0.03048	1,365.47	-29.67	CHZCM/CFCM/BRA
UE-20f (1384.7 m)	545400.83	4124900.36	1,384.71	1,864.25	0.03048	1,268.62	479.54	UPCU/TCA/LPCU/CHZCM/IA
UE-20f (4171 m)	545400.83	4124900.36	4,171.49	1,864.25	0.03048	506.07	-2,307.24	IA/CFCM/BFCU/BRA/PBRCM
UE-20h WW	550191.74	4124986.54	2,197.61	1,998.45	0.03048	1,234.63	-198.24	CHZCM/BFCU/CFCM
UE-20j WW	541285.30	4128082.01	1,734.31	1,799.17	0.03048	1,268.82	64.87	PVTA/CFCM/BRA/PBRCM

Table E.1-1
Site Information for Selected Wells, Boreholes, and Springs Located in the
Pahute Mesa-Oasis Valley Area and Vicinity
 (Page 6 of 7)

Site Name	UTM Easting (m) ^a	UTM Northing (m)	Total Depth (mbgs) ^b	Ref. Point Elevation (m amsl) ^c	Ref. Point Elevation Accuracy (m)	EOI Top Elevation (m amsl) ^d	EOI Bottom Elevation (m amsl)	Primary HSU(s) ^e
UE-20n 1 (1005.84 m)	551273.21	4121483.82	1,005.84	1,969.22	0.03048	1,273.67	963.42	CHZCM
UE-20n 1 (863.8 m)	551273.21	4121483.82	1,005.84	1,969.22	0.03048	1,273.67	1,106.22	CHZCM
UE-20p	542331.42	4132503.21	1,365.50	1,692.55	0.03048	1,692.55	327.05	TCVA/TMA/BRA/PBRCM
UE-29a 1 HTH	555757.96	4088341.18	65.53	1,215.39	0.03048	1,189.97	1,149.86	UNK
UE-29a 2 HTH	555749.41	4088346.03	421.54	1,215.39	0.03048	1,128.83	793.85	YMCFCM
USW UZ-N91	555687.14	4088202.59	28.65	1,203.05	0.3048	1,203.05	1,174.40	UNK
Ute Spr Drainage Well	525399.15	4089561.15	3.26	1,066.80	6.096	1,066.80	1,063.54	AA
WW-8	563113.05	4113274.55	1,673.35	1,735.84	0.03048	1,354.84	1,193.34	BRA
Spring	521843.23	4098424.43	—	1,171.96	3.05	—	—	AA ^f
Crystal Springs Area	522029.68	4093217.28	—	1,188.72	6.10	—	—	AA ^f
Revert Springs Channel	522145.51	4085299.85	—	1,018.03	6.10	—	—	AA ^f
Revert Springs Area	522742.47	4085546.45	—	1,027.18	7.62	—	—	AA ^f
Revert Springs Area	522766.64	4085762.20	—	1,027.18	—	—	—	AA ^f
Spring (Report R10)	524072.36	4096458.34	—	1,127.76	6.10	—	—	AA ^f
Spring	524169.39	4088416.09	—	1,057.66	6.10	—	—	AA ^f
Springdale Culvert	524340.84	4096306.46	—	1,126.24	3.05	—	—	AA ^f
Torrance Spring	524573.05	4094210.34	—	1,121.66	3.05	—	—	AA ^f
Ute Springs Area	524705.61	4091129.29	—	1,083.56	1.52	—	—	AA ^f
Spring	524728.01	4091930.52	—	1,097.28	—	—	—	AA ^f
OVU Culvert Spring	524754.97	4098341.50	—	1,149.10	3.05	—	—	AA ^f
Hot Springs Area	524777.61	4091869.03	—	1,097.28	6.10	—	—	AA ^f
Hot Springs Pump House	524798.64	4091870.52	—	1,094.23	6.10	—	—	AA ^f
Hot Springs Bath House 1	524823.47	4091839.86	—	1,094.23	6.10	—	—	AA ^f
Hot Springs Bath House 2	524823.56	4091809.02	—	1,094.23	6.10	—	—	AA ^f
Hot Springs blw Culvert 1	524873.05	4091778.33	—	1,094.23	6.10	—	—	AA ^f
Hot Springs Culvert 2	524897.98	4091716.84	—	1,092.71	6.10	—	—	AA ^f
Hot Springs abv Culvert 2	524922.63	4091747.64	—	1,092.71	6.10	—	—	AA ^f
Ute Springs Area	524954.28	4090667.80	—	1,085.09	7.62	—	—	AA ^f
Spring	524976.02	4091684.74	—	1,097.28	—	—	—	AA ^f

Table E.1-1
Site Information for Selected Wells, Boreholes, and Springs Located in the
Pahute Mesa-Oasis Valley Area and Vicinity
 (Page 7 of 7)

Site Name	UTM Easting (m) ^a	UTM Northing (m)	Total Depth (mbgs) ^b	Ref. Point Elevation (m amsl) ^c	Ref. Point Elevation Accuracy (m)	EOI Top Elevation (m amsl) ^d	EOI Bottom Elevation (m amsl)	Primary HSU(s) ^e
Ute Springs Culvert	525227.73	4088913.69	—	1,051.56	6.10	—	—	AA ^f
Ute Springs	525351.54	4090114.32	—	1,085.09	7.62	—	—	AA ^f
Oleo Road Spring	525925.42	4095325.20	—	1,167.38	3.05	—	—	AA ^f
Goss Springs - North	526100.47	4094647.72	—	1,164.34	6.10	—	—	AA ^f
Goss Springs	526128.44	4094800.46	—	1,188.72	6.10	—	—	AA ^f
Spring	526697.22	4094709.79	—	1,158.24	—	—	—	AA ^f
Spring	532646.80	4102958.21	—	1,211.58	3.05	—	—	AA ^f

^aUniversal Transverse Mercator Zone 11, North American Datum 1927 in meters

^bTotal drilled depth in meters below ground surface

^cReference point elevation in meters above mean sea level

^dEffective open interval top elevation in meters above mean sea level

^ePrimary hydrostratigraphic unit(s)

^fThe water moves upwards through faults from Tertiary volcanics through the alluvium.

Table E.1-2
Summary of Hydraulic Heads at Selected Sites within the
Pahute Mesa-Oasis Valley Area and Vicinity
(Page 1 of 8)

Site Name	Mean Hydraulic Head (m amsl) ^a	Minimum Hydraulic Head (m amsl) ^b	Maximum Hydraulic Head (m amsl) ^b	Standard Deviation ^c	Variance on the Mean ^d	Total Uncertainty ^e	Data Points Used	First Measurement ^b	Last Measurement ^b	Comments ^f
Beatty Wash Terrace Well	1,048.77	1,044.85	1,049.44	0.35	0.10	9.39	48	10/13/1984	09/27/2001	—
Beatty Well No 1	996.70	—	—	—	—	—	1	10/26/1962	—	—
Boiling Pot Road Well	1,102.77	1,102.39	1,103.25	0.28	0.09	9.38	42	05/08/1997	06/26/2001	—
Coffer Dune Well	1,181.47	1,181.26	1,181.69	0.12	0.04	2.36	37	04/13/1998	06/26/2001	—
Coffer Lower ET Well	1,175.36	1,174.96	1,176.02	0.31	0.11	2.43	31	08/03/1998	06/26/2001	—
Coffer Middle ET Well	1,174.46	1,173.92	1,175.03	0.36	0.14	2.46	26	01/07/1999	06/26/2001	—
Coffer Windmill Well	1,231.39	—	—	—	—	—	1	07/30/1970	—	—
ER-18-2	1,287.90	1,283.98	1,287.90	—	—	—	1	05/24/1999	06/06/2001	—
ER-19-1-1 (deep)	1,326.01	1,324.55	1,338.67	0.95	0.35	0.35	29	02/03/1994	09/25/2001	—
ER-19-1-2 (middle)	1,498.92	1,468.87	1,533.33	15.75	5.25	5.25	36	02/15/1994	09/25/2001	—
ER-19-1-3 (shallow)	1,564.44	1,564.06	1,566.70	0.2	0.10	0.10	17	02/03/1994	04/11/2001	—
ER-20-1	1,277.68	1,277.55	1,278.94	0.1	0.04	0.04	28	09/18/1992	09/24/2001	—
ER-20-2-1	1,341.04	1,340.42	1,350.20	0.34	0.13	9.42	29	08/03/1993	09/25/2001	—
ER-20-5-1 (3-in string)	1,275.54	1,275.13	1,276.43	0.38	0.18	0.18	17	11/17/1995	05/14/1996	—
ER-20-6-1 (3-in string)	1,356.61	1,354.78	1,359.25	0.07	0.04	0.04	10	03/21/1996	03/20/2001	—
ER-20-6-2 (3-in string)	1,356.62	1,354.29	1,356.64	0.03	0.03	0.03	4	04/01/1996	03/20/2001	—
ER-20-6-3 (3-in string)	1,356.50	1,355.25	1,356.58	0.08	0.05	0.05	11	04/16/1996	09/24/2001	—
ER-30-1	1,280.06	1,280.01	1,280.13	0.05	0.03	0.03	9	06/21/1994	06/24/1994	—
ER-EC-1	1,271.08	1,270.98	1,271.81	0.02	0.01	0.04	8	05/10/1999	09/24/2001	—
ER-EC-2A (498.3-681.5 m)	1,264.22	1,263.06	1,264.24	0.03	0.04	0.07	2	02/18/2000	03/26/2001	—
ER-EC-2A (498.35-1515.8 m)	1,266.26	1,260.14	1,266.36	0.10	0.12	0.14	3	02/18/2000	08/07/2000	—
ER-EC-4 (290.2-1062.8 m)	1,222.46	1,222.40	1,222.48	0.02	0.02	0.04	4	07/18/1999	08/24/2000	—
ER-EC-4 (290.2-699.5 m)	1,222.50	1,222.49	1,222.53	0.02	0.02	0.04	5	10/05/2000	10/03/2001	—

Table E.1-2
Summary of Hydraulic Heads at Selected Sites within the
Pahute Mesa-Oasis Valley Area and Vicinity
 (Page 2 of 8)

Site Name	Mean Hydraulic Head (m amsl) ^a	Minimum Hydraulic Head (m amsl) ^b	Maximum Hydraulic Head (m amsl) ^b	Standard Deviation ^c	Variance on the Mean ^d	Total Uncertainty ^e	Data Points Used	First Measurement ^b	Last Measurement ^b	Comments ^f
ER-EC-4 (Lower Interval)	1,220.17	—	—	—	—	—	1	02/16/2000	—	—
ER-EC-5	1,237.55	1,237.34	1,237.62	0.05	0.04	0.06	7	07/19/1999	03/26/2001	—
ER-EC-6 (481.9-1164.3 m)	1,273.53	1,273.50	1,273.55	0.02	0.02	0.04	6	06/06/2000	09/24/2001	—
ER-EC-6 (481.9-1524 m)	1,273.60	1,273.58	1,274.25	0.01	0.01	0.03	4	04/20/1999	03/13/2000	—
ER-EC-7	1,236.67	1,236.46	1,236.76	0.1	0.08	0.10	7	08/30/1999	03/26/2001	—
ER-EC-8	1,222.36	1,222.24	1,222.43	0.05	0.04	0.06	8	08/04/1999	10/03/2001	—
ER-OV-01	1,235.86	1,235.61	1,236.48	0.02	0.01	0.03	17	10/02/1997	09/13/2001	—
ER-OV-02	1,174.04	1,173.67	1,174.10	0.05	0.02	0.05	17	10/02/1997	09/13/2001	—
ER-OV-03a	1,154.35	1,154.13	1,154.54	0.13	0.07	0.09	16	10/02/1997	09/13/2001	—
ER-OV-03a2	1,122.86	1,122.48	1,123.01	0.09	0.04	0.07	17	10/02/1997	09/13/2001	—
ER-OV-03a3	1,154.24	1,154.08	1,154.44	0.13	0.06	0.09	17	10/02/1997	09/13/2001	—
ER-OV-03b	1,184.52	1,184.29	1,184.61	0.07	0.03	0.06	17	10/02/1997	09/13/2001	—
ER-OV-03c	1,212.28	1,211.97	1,212.33	0.04	0.02	0.04	17	10/02/1997	09/13/2001	—
ER-OV-03c2	1,212.31	1,211.98	1,212.41	0.04	0.02	0.04	23	10/02/1997	09/13/2001	—
ER-OV-04a	1,056.85	1,056.36	1,057.02	0.12	0.06	0.08	17	10/02/1997	09/13/2001	—
ER-OV-05	1,190.50	1,190.19	1,190.52	0.02	0.01	0.03	17	10/02/1997	09/13/2001	—
ER-OV-06a	1,236.82	1,236.76	1,236.99	0.03	0.01	0.03	27	10/02/1997	09/13/2001	—
ER-OV-06a2	1,235.64	1,235.41	1,235.67	0.03	0.01	0.04	17	10/02/1997	09/13/2001	—
Gexa Well 4	1,010.05	954.99	1,010.10	—	—	—	1	09/01/1989	03/14/1996	—
Hagestad 1	1,841.84	1,802.13	1,843.77	1.48	0.53	0.53	31	01/24/1958	12/05/1963	—
Matheny Well	1,039.12	1,037.54	1,039.12	—	—	—	1	04/12/1988	03/21/1997	—
MOV ET Well	1,123.26	1,122.76	1,124.04	0.37	0.11	2.43	46	05/08/1997	06/26/2001	—
Pioneer Road Seep Well	1,112.22	1,111.73	1,112.61	0.25	0.08	9.37	43	05/22/1997	06/26/2001	—

Table E.1-2
Summary of Hydraulic Heads at Selected Sites within the
Pahute Mesa-Oasis Valley Area and Vicinity
(Page 3 of 8)

Site Name	Mean Hydraulic Head (m amsl) ^a	Minimum Hydraulic Head (m amsl) ^b	Maximum Hydraulic Head (m amsl) ^b	Standard Deviation ^c	Variance on the Mean ^d	Total Uncertainty ^e	Data Points Used	First Measurement ^b	Last Measurement ^b	Comments ^f
PM-1 (2356.408 m)	1,359.49	1,355.14	1,360.53	0.5	0.13	0.13	61	01/01/1969	06/06/2001	—
PM-2	1,442.76	1,439.27	1,447.37	0.13	0.04	0.04	54	01/01/1969	09/24/2001	—
PM-3 (Upper Borehole)	1,330.42	1,331.00	1,331.61	—	—	—	1	09/09/1988	09/13/1988	—
PM-3 (Lower Borehole)	1,330.35	1,329.57	1,331.00	0.41	0.18	0.18	21	09/21/88	09/30/91	—
PM-3-1 (Piez 1)	1,330.58	1,329.72	1,330.58	—	—	—	1	04/10/1992	06/05/2001	—
PM-3-2 (Piez 2)	1,331.18	1,330.42	1,331.18	—	—	—	1	04/10/1992	06/05/2001	—
Springdale ET Deep Well	1,131.67	1,131.18	1,132.12	0.28	0.07	2.39	60	06/20/1996	06/26/2001	—
Springdale ET Shallow Well	1,131.13	1,130.56	1,131.50	0.36	0.10	2.42	57	08/14/1996	06/26/2001	—
Springdale Lower Well	1,129.70	1,128.33	1,130.82	0.81	0.21	9.50	58	06/20/1996	06/26/2001	—
Springdale Upper Well	1,143.29	1,143.13	1,143.45	0.09	0.02	2.35	60	06/06/1996	09/27/2001	—
Springdale Windmill Well	1,175.24	1,174.39	1,175.43	0.09	0.03	2.35	44	04/01/1941	09/25/2000	—
TW-1 (1125 m)	1,430.40	1,428.93	1,430.49	0.02	0.02	0.02	5	04/07/1980	07/26/2001	—
TW-1 (1127-1137 m)	1,271.57	—	—	—	—	—	1	06/09/1961	—	—
TW-1 (170 m)	1,751.17	—	—	—	—	—	1	09/30/1960	—	—
TW-1 (492 m)	1,749.67	1,749.61	1,749.67	—	—	—	1	11/10/1960	11/18/1960	—
TW-1 (560 m)	1,564.20	1,564.20	1,564.36	—	—	—	1	02/17/1961	02/21/1961	—
TW-1 (826 m)	1,437.07	1,437.07	1,437.16	—	—	—	1	08/14/1962	08/16/1962	—
TW-1 (839 m)	1,437.31	1,437.01	1,437.71	0.26	0.17	0.17	9	09/25/1963	10/17/1963	—
TW-1 (839-1279 m)	1,277.25	1,276.41	1,277.33	0.06	0.05	0.05	6	09/25/1963	12/05/1963	—
U-12s (451.1 m)	1,784.75	1,778.87	1,791.00	1.92	0.51	0.51	57	08/06/1966	07/25/2001	—
U-19ab	1,494.97	1,494.74	1,495.35	0.29	0.29	0.29	4	07/17/1980	06/30/1985	—
U-19ab 2	1,497.89	1,497.48	1,498.11	0.36	0.42	0.42	3	12/03/1984	12/12/1984	—
U-19ad	1,372.21	—	—	—	—	—	1	06/16/1979	—	—

Table E.1-2
Summary of Hydraulic Heads at Selected Sites within the
Pahute Mesa-Oasis Valley Area and Vicinity
(Page 4 of 8)

Site Name	Mean Hydraulic Head (m amsl) ^a	Minimum Hydraulic Head (m amsl) ^b	Maximum Hydraulic Head (m amsl) ^b	Standard Deviation ^c	Variance on the Mean ^d	Total Uncertainty ^e	Data Points Used	First Measurement ^b	Last Measurement ^b	Comments ^f
U-19ae	1,369.77	1,369.47	1,370.08	0.43	0.61	0.61	2	01/24/1982	02/23/1982	—
U-19ai	1,428.99	1,428.29	1,429.82	0.46	0.29	0.29	10	06/30/1980	10/11/1980	—
U-19aj	1,432.38	—	—	—	—	0.58	1	02/23/1981	—	—
U-19aq	1,428.95	1,428.45	1,429.36	0.47	0.54	0.54	3	01/10/1987	06/17/1987	—
U-19ar	1,398.93	1,398.12	1,399.64	0.77	0.89	—	3	11/05/1985	03/28/1986	—
U-19aS (857 m)	1,392.69	—	—	—	—	—	1	07/27/1964	—	—
U-19au	1,358.57	1,358.28	1,360.02	0.14	0.09	0.09	9	06/05/1987	06/30/1988	—
U-19au 1	1,358.78	1,358.62	1,359.10	0.28	0.32	0.35	3	02/22/1988	03/02/1988	—
U-19ay	1,396.93	1,396.87	1,399.15	0.05	0.06	0.06	3	12/22/1987	01/09/1989	—
U-19az	1,424.58	1,417.08	1,425.06	0.18	0.07	0.07	26	12/16/1988	07/02/1990	—
U-19ba	1,488.78	1,484.44	1,488.89	0.05	0.03	0.03	10	09/15/1989	12/11/1990	—
U-19bg 1	1,394.52	1,394.34	1,394.70	0.14	0.13	0.13	5	08/20/1991	11/18/1991	—
U-19bh	1,425.93	1,410.52	1,426.06	0.08	0.06	0.06	7	06/24/1991	06/12/2001	—
U-19bj	1,493.23	1,493.23	1,495.90	—	—	—	1	09/24/1992	06/12/2001	—
U-19bk	1,427.93	1,427.67	1,428.14	0.14	0.06	0.06	24	09/24/1992	06/11/2001	—
U-19d 2	1,427.59	1,417.59	1,428.45	—	—	—	1	06/23/1964	01/13/1965	—
U-19e	1,432.87	1,425.46	1,432.87	—	—	—	1	09/06/1966	01/01/1969	—
U-19g	1,424.23	1,422.81	1,425.25	0.98	0.80	0.80	6	09/27/1965	01/04/1976	—
U-19x	1,392.02	—	—	0	0	—	2	08/21/1976	06/30/1978	—
U-20 WW (Open)	1,351.54	1,351.48	1,351.61	0.09	0.13	0.13	2	07/01/1982	07/16/1985	—
U-20a	1,328.66	1,328.66	1,328.93	—	—	—	1	02/13/1964	01/01/1969	—
U-20a 2 WW	1,343.25	1,342.95	1,345.39	—	—	—	1	03/30/1964	10/23/1975	—
U-20ah	1,354.02	1,352.40	1,355.75	1.02	0.59	0.59	12	12/15/1980	04/01/1981	—

Table E.1-2
Summary of Hydraulic Heads at Selected Sites within the
Pahute Mesa-Oasis Valley Area and Vicinity
(Page 5 of 8)

Site Name	Mean Hydraulic Head (m amsl) ^a	Minimum Hydraulic Head (m amsl) ^b	Maximum Hydraulic Head (m amsl) ^b	Standard Deviation ^c	Variance on the Mean ^d	Total Uncertainty ^e	Data Points Used	First Measurement ^b	Last Measurement ^b	Comments ^f
U-20ai	1,356.20	1,355.14	1,357.27	0.67	0.51	0.51	7	09/26/1981	10/30/1985	—
U-20ak	1,278.46	1,277.72	1,279.25	0.54	0.41	0.41	7	07/11/1982	11/30/1985	—
U-20am	1,356.97	1,356.67	1,357.27	0.43	0.61	0.61	2	10/13/1983	02/01/1984	—
U-20an	1,363.10	1,362.88	1,363.37	0.25	0.29	0.29	3	10/10/1984	03/12/1985	—
U-20ao	1,317.29	—	—	—	—	—	1	05/17/1985	—	—
U-20ar 1	1,364.42	1,363.50	1,366.17	0.49	0.35	0.37	8	02/09/1987	05/08/1987	—
U-20as	1,284.43	1,284.41	1,284.70	0.03	0.03	0.03	4	04/22/1986	06/06/1986	—
U-20at 1	1,284.41	1,284.03	1,284.64	0.29	0.29	0.29	4	12/09/1986	02/13/1987	—
U-20av	1,338.00	1,336.20	1,338.38	0.53	0.75	0.77	2	08/04/1986	12/08/1986	—
U-20aw	1,371.43	1,371.30	1,371.60	0.1	0.06	0.06	10	12/10/1986	11/04/1988	—
U-20ax	1,329.93	1,328.87	1,367.12	0.24	0.08	0.08	37	08/31/1987	05/26/1993	—
U-20ay	1,360.98	1,357.82	1,363.89	0.06	0.04	0.04	9	06/22/1987	01/11/1988	—
U-20az	1,345.05	1,334.48	1,345.05	—	—	—	1	12/12/1988	08/31/1989	+1 to 5 m
U-20bb (579.12 m)	1,367.70	1,341.03	1,367.70	—	—	—	1	07/15/1988	12/18/1989	+10 to 20 m
U-20bb (676.66 m)	1,272.94	1,272.94	1,298.11	—	—	—	1	02/13/1990	04/19/1990	-1 to 5 m
U-20bb 1	1,280.00	1,279.71	1,280.23	0.16	0.08	2.40	17	05/15/1990	07/09/1990	—
U-20bc	1,303.07	1,299.70	1,303.87	0.13	0.05	0.05	23	07/07/1988	08/02/1989	—
U-20bd (689.15 m)	1,355.79	1,355.72	1,355.87	0.05	0.04	0.04	7	04/28/1989	05/16/1989	—
U-20bd 1	1,355.50	1,355.35	1,355.68	0.14	0.13	0.13	5	01/09/1990	03/14/1990	—
U-20bd 2	1,355.86	1,355.58	1,356.21	0.24	0.21	0.24	5	01/09/1990	03/14/1990	—
U-20be	1,303.78	1,303.48	1,319.39	0.2	0.10	0.10	15	06/14/1989	06/05/1991	—
U-20bf	1,338.18	1,332.77	1,353.98	0.43	0.15	0.15	31	08/28/1989	01/30/1991	—
U-20bg	1,352.49	1,350.07	1,352.98	—	—	—	1	01/08/1991	09/25/2001	+5 m

Table E.1-2
Summary of Hydraulic Heads at Selected Sites within the
Pahute Mesa-Oasis Valley Area and Vicinity
(Page 6 of 8)

Site Name	Mean Hydraulic Head (m amsl) ^a	Minimum Hydraulic Head (m amsl) ^b	Maximum Hydraulic Head (m amsl) ^b	Standard Deviation ^c	Variance on the Mean ^d	Total Uncertainty ^e	Data Points Used	First Measurement ^b	Last Measurement ^b	Comments ^f
U-20c	1,275.28	1,273.15	1,275.28	—	—	—	1	02/25/1965	11/13/2000	—
U-20e	1,360.32	—	—	—	—	—	1	02/07/1969	—	—
U-20g	1,357.27	—	—	—	—	—	1	10/30/1964	—	—
U-20i	1,361.24	—	—	—	—	—	1	08/30/1967	—	—
U-20m	1,412.14	—	—	—	—	—	1	10/04/1968	—	—
U-20n PS 1DD-H (922 m)	1,350.32	1,345.84	1,350.32	—	—	—	1	05/17/1985	07/09/1998	—
U-20y	1,276.94	1,275.28	1,278.03	0.76	0.51	0.51	9	12/18/1974	02/18/1975	—
UE-12n 15a	1,841.00	1,840.44	1,841.97	0.64	0.57	0.57	5	05/31/1988	06/20/1988	—
UE-18r	1,271.89	1,269.74	1,272.34	0.61	0.21	0.21	35	01/29/1968	06/06/2001	—
UE-18t	1,306.27	1,305.73	1,307.35	0.22	0.07	0.09	43	10/06/1978	06/06/2001	—
UE-19b 1 WW	1,427.93	1,427.90	1,427.96	0.04	0.06	0.08	2	06/19/1964	01/13/1965	—
UE-19c WW	1,430.50	1,428.32	1,438.38	0.47	0.18	0.18	26	04/30/1964	06/12/2001	—
UE-19e WW	1,432.03	1,429.70	1,433.02	1.56	1.56	1.56	4	09/03/1964	06/26/1975	—
UE-19fs	1,350.02	1,349.11	1,351.24	—	—	—	1	08/17/1965	—	—
UE-19gS	1,424.76	1,423.11	1,425.25	—	—	—	1	05/06/1965	—	—
UE-19gS WW	1,425.24	1,413.05	1,428.60	0	0	0.02	3	03/24/1965	01/13/1976	—
UE-19h	1,423.14	1,422.84	1,472.70	0.11	0.04	0.04	35	08/09/1965	06/11/2001	—
UE-19i	1,396.26	1,396.26	1,408.45	—	—	—	1	09/01/1965	01/01/1969	—
UE-19z	1,429.66	1,429.21	1,429.82	0.26	0.21	—	6	07/12/1977	09/24/1977	—
UE-20ab	1,357.88	1,355.75	1,357.88	—	—	—	1	06/02/1978	10/30/1978	—
UE-20av	1,319.66	1,319.32	1,319.66	—	—	—	1	12/15/1986	01/15/1987	—
UE-20bh 1	1,348.55	1,347.63	1,349.47	0.54	0.20	0.20	30	10/29/1991	09/25/2001	—
UE-20c	1,267.05	—	—	—	—	—	1	02/28/1964	11/13/2000	—

Table E.1-2
Summary of Hydraulic Heads at Selected Sites within the
Pahute Mesa-Oasis Valley Area and Vicinity
(Page 7 of 8)

Site Name	Mean Hydraulic Head (m amsl) ^a	Minimum Hydraulic Head (m amsl) ^b	Maximum Hydraulic Head (m amsl) ^b	Standard Deviation ^c	Variance on the Mean ^d	Total Uncertainty ^e	Data Points Used	First Measurement ^b	Last Measurement ^b	Comments ^f
UE-20d	1,273.90	1,272.54	1292.35	0.67	0.95	0.97	2	08/19/1964	01/14/1965	—
UE-20e 1	1,365.47	1,359.49	1365.50	—	—	—	1	06/04/1964	04/05/1975	—
UE-20f (1384.7 m)	1,268.62	1,268.58	1,268.67	0.06	0.08	0.09	2	04/07/1964	11/13/2000	—
UE-20f (4171 m)	1,322.86	1,269.19	1,337.55	1.22	1.41	1.41	3	01/13/1965	11/24/1974	—
UE-20h WW	1,356.48	1,353.50	1,356.97	0.69	0.98	0.98	2	08/20/1964	01/01/1969	—
UE-20j WW	1,411.96	—	—	—	—	—	1	10/23/1964	—	—
UE-20n 1 (1005.84 m)	1,318.78	—	—	—	—	—	1	06/01/1987	—	—
UE-20n 1 (863.8 m)	1,349.75	1,346.16	1,349.75	0	0	—	2	06/12/1987	10/16/2000	—
UE-20p	1,423.11	1,412.29	1,423.11	—	—	—	1	10/01/1968	09/27/1970	—
UE-29a 1 HTH	1,189.97	1,188.12	1,194.45	1.42	0.19	0.19	219	06/21/1982	09/26/1997	—
UE-29a 2 HTH	1,187.62	1,186.24	1,191.31	1.1	0.15	0.15	219	06/21/1982	09/26/1997	—
USW UZ-N91	1,186.72	1,185.59	1,191.34	1.1	0.15	0.17	217	01/21/1986	09/26/1997	—
Ute Spr Drainage Well	1,066.02	1,065.00	1,066.82	0.63	0.19	9.48	43	05/22/1997	06/26/2001	—
WW-8	1,410.46	1,404.21	1,410.46	—	—	—	1	01/03/1963	09/13/2000	—
Spring	1,171.96	—	—	—	—	2.32	1	—	—	—
Crystal Springs Area	1,188.72	—	—	—	—	9.29	1	—	—	—
Revert Springs Channel	1,018.03	—	—	—	—	9.29	1	—	—	—
Revert Springs Area	1,027.18	—	—	—	—	14.52	1	—	—	—
Revert Springs Area	1,027.18	—	—	—	—	æ	1	—	—	—
Spring (Report R10)	1,127.76	—	—	—	—	9.29	1	—	—	—
Spring	1,057.66	—	—	—	—	9.29	1	—	—	—
Springdale Culvert	1,126.24	—	—	—	—	2.32	1	—	—	—
Torrance Spring	1,121.66	—	—	—	—	2.32	1	—	—	—

Table E.1-2
Summary of Hydraulic Heads at Selected Sites within the
Pahute Mesa-Oasis Valley Area and Vicinity
(Page 8 of 8)

Site Name	Mean Hydraulic Head (m amsl) ^a	Minimum Hydraulic Head (m amsl) ^b	Maximum Hydraulic Head (m amsl) ^b	Standard Deviation ^c	Variance on the Mean ^d	Total Uncertainty ^e	Data Points Used	First Measurement ^b	Last Measurement ^b	Comments ^f
Ute Springs Area	1,083.56	—	—	—	—	0.58	1	—	—	—
Spring	1,097.28	—	—	—	—	—	1	—	—	—
OVU Culvert Spring	1,149.10	—	—	—	—	2.32	1	—	—	—
Hot Springs Area	1,097.28	—	—	—	—	9.29	1	—	—	—
Hot Springs Pump House	1,094.23	—	—	—	—	9.29	1	—	—	—
Hot Springs Bath House 1	1,094.23	—	—	—	—	9.29	1	—	—	—
Hot Springs Bath House 2	1,094.23	—	—	—	—	9.29	1	—	—	—
Hot Springs blw Culvert 1	1,094.23	—	—	—	—	9.29	1	—	—	—
Hot Springs Culvert 2	1,092.71	—	—	—	—	9.29	1	—	—	—
Hot Springs abv Culvert 2	1,092.71	—	—	—	—	9.29	1	—	—	—
Ute Springs Area	1,085.09	—	—	—	—	14.52	1	—	—	—
Spring	1,097.28	—	—	—	—	—	1	—	—	—
Ute Springs Culvert	1,051.56	—	—	—	—	9.29	1	—	—	—
Ute Springs	1,085.09	—	—	—	—	14.52	1	—	—	—
Oleo Road Spring	1,167.38	—	—	—	—	2.32	1	—	—	—
Goss Springs - North	1,164.34	—	—	—	—	9.29	1	—	—	—
Goss Springs	1,188.72	—	—	—	—	9.29	1	—	—	—
Spring	1,158.24	—	—	—	—	—	1	—	—	—
Spring	1,211.58	—	—	—	—	2.32	1	—	—	—

^aMeters above mean sea level

^bApplies to all data available

^cApplies only to data used

^d $(2 \times \text{Standard Deviation})/\text{Square Root (Number of Data Points Used)}$

^eTotal uncertainty is the variance on the mean plus variance associated with the land surface elevation

^fShows sites that should be used with caution with a positive or negative error associated with the hydraulic head

— Not Applicable or Not Available

- official_name - Official USGS station name
- WPM_DA_reporting_name - Database name for the site.
- ref_pt_el (masl) - Elevation, relative to sea level, of the reference point for depth-to-water measurements.
- ref_el_ac (m) - Accuracy of the reference point elevation in meters.
- ref_el_meth - Method used to determine the reference point elevation.
- ref_pt - Location of reference point elevation for depth-to-water measurements (e.g., ground surface)
- depth_to_wat (mbrp) - Depth to groundwater in meters below the reference point.
- depth_acc (m) - Accuracy of the depth-to-water measurement in meters.
- DDE_F - Data Documentation Evaluation Flag - Data qualifier for Environmental Restoration Project data; indicates the level and quality of documentation available for a given depth-to-water measurement.
- meth_of_meas - Method by which the depth to groundwater was measured.
- meas_date - Date the depth of groundwater was measured.
- meas_time - Time of day the depth of groundwater was measured.
- site_status - Status of site (e.g., known conditions at site that may affect measured depth to water)
- data_source - Source of the water level data where known.
- lev_party_id - NWIS Code C246. Source agency, State/County code, or acronym.
- agency_cd - NWIS Code C004. Source agency of water-level measurement personnel.
- elev (masl) - Groundwater elevation in meters above mean sea level
- ref_id - ITLV library number or YMP (www.ymp.gov) Site and Engineering Properties database data tracking number.
- mon_int_depth_top (mbgs) - Depth to the top of the monitored interval (may not be reliable, use with caution).

- mon_int_depth_bot (mbgs) - Depth to the bottom of the monitored interval (may not be reliable, use with caution).
- remarks - Additional information pertaining to the water elevation information.
- Analysis_Code - Code applied to the record based on hydrograph analysis.

E.4.0 Access to Data

E.4.1 Water Elevations Table

The full water elevations dataset, a combined electronic version of [Table E.1-1](#) and [Table E.1-2](#) (tblTarget_heads.xls), the water elevations used for vertical gradient analysis (tbl3danalysis.xls) and the additional water-level elevations, for the region outside the model boundary, used to construct the potentiometric map may be found in the following EXCEL and ASCII files:

EXCEL:

- tblWater_Elevations.xls
- tblTarget_heads.xls
- tbl3danalysis.xls
- tblAdditonal_Map_Elevations.xls

ASCII:

- tblWater_Elevations.txt
- tblTarget_heads.txt
- tbl3danalysis.txt
- tblAdditional_Map_Elevations.txt

E.4.2 Hydrograph Analysis

The hydrographs and well summaries are provided in HTML format in the following file:

- hydrographs.htm

To access the data from the paper copy of the document, use the CD provided at the end of the document and open the desired file. To access the dataset from the electronic version of the document, click on the desired file.



Appendix F

Flux Calculations Using Regional Flow Model

F.1.0 Introduction

The Pahute Mesa-Oasis Valley flow system contains the Western and Central Pahute Mesa CAUs, the sites of 85 underground nuclear tests. The flow system is comprised of hydrostratigraphic units through which the radionuclides from these tests could potentially reach the Oasis Valley discharge area. The flow system includes areas within and around the NTS, as shown in [Figure F.1-1](#). As a precursor to the CAU-scale modeling of the PM-OV flow system, groundwater fluxes need to be estimated to define the boundary conditions for the lateral sides of the CAU flow model.

On a practical scale, the technology does not exist to directly measure groundwater fluxes at the spatial frequency needed to define boundary conditions for the Pahute Mesa CAU-scale flow model. An acceptable alternative, to derive boundary fluxes for complex models, such as the CAU flow model, is based upon interpolation of fluxes generated from a calibrated larger-scale flow model. Such an approach is common practice, and is described in Ward et al. (1987). For the case of the Pahute Mesa, the UGTA NTS regional flow model is the logical choice of sources for boundary fluxes that can be used in the more refined CAU-scale modeling effort.

In developing the data needed for the CAU-scale model, the uncertainty associated with parameters such as boundary fluxes must also be considered. To some degree, uncertainty associated with the boundary fluxes can be considered by assuming the spatial distribution of boundary fluxes as derived from the NTS regional model is correct, then adjusting the flux levels by a factor which covers the possible range of fluxes through the area. Additionally though, uncertainty in the fluxes must also be considered to be a function of the choice of plausible geologic and recharge models from alternative models that still honor the site data. Since the NTS regional model was based upon a specific conceptual (and associated geologic) model and recharge model, to consider these sources of uncertainty, alternative conceptual models and recharge models must also be considered in the CAU flow modeling task.

The boundary fluxes generated from the NTS regional model simulations will be used to set bounds on the total flux through each of the CAU-scale model boundaries. The precise location of flux in the NTS regional model will not be required to be replicated in the CAU model, only the total amount. In this way, differences in the amount of detail in the two models will not lead to assignment of inappropriate fluxes at the CAU scale.

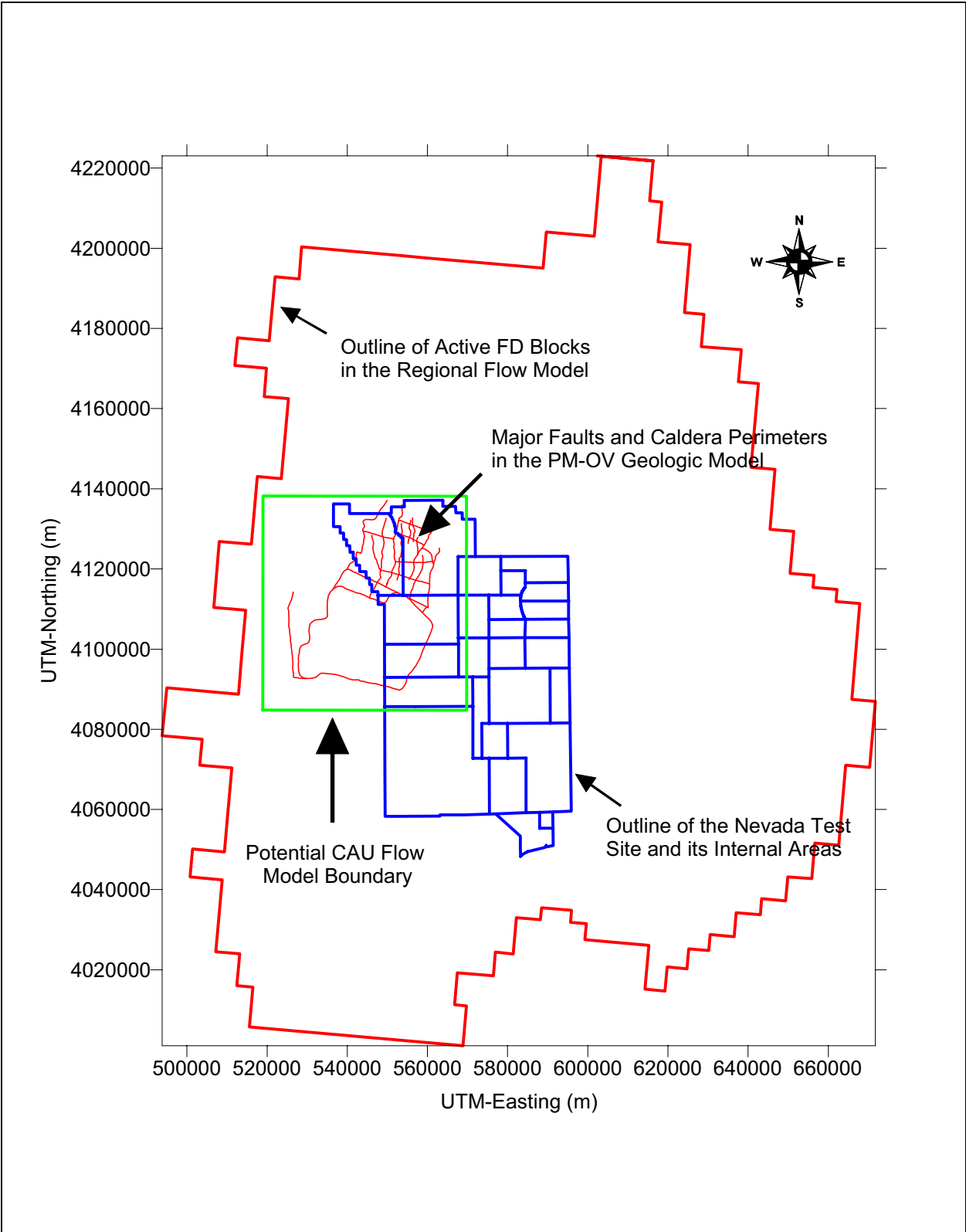


Figure F.1-1
Outline of the Regional Groundwater Flow Model Grid with NTS Perimeter and Area Boundaries
Along with Traces of the Major PM-OV Faults and Caldera Perimeters

In the event that calibration of the CAU groundwater flow model is not possible with the constraints imposed by the boundary fluxes, a detailed explanation will be provided in the CAU model documenting the deviation from bounding ranges.

F.2.0 Models Evaluated in the Calibration Process

F.2.1 Geologic Model Alternatives

In the hydrostratigraphic model report for the PM-OV area (BN, 2002), several alternative hydrostratigraphic models of the Pahute Mesa CAUs are described. Each of these alternative models honors the data available, with differences between the models representing differences in interpretations of various features defined by the data. A group of experts was queried to provide a subset of these alternatives, that would be likely to span the range of system responses to system stresses. For the subset of models selected by the group of experts, the question needing to be answered was which of the conceptual models, if any, could provide alternate radionuclide transport pathways that could strongly influence the results of an associated transport simulation.

Since a full calibration of each alternative model would be a time and resource consuming effort, a screening process was developed. The objective of this process was to evaluate to what degree the models would differ in response to system stresses and which, if any, of the alternative geologic models would be important to consider for further analysis (see [Appendix A](#)). To determine the importance of considering the uncertainty in the conceptualization of the geologic model, flow and transport simulations were performed to evaluate to what degree the choice of the alternate geologic models affect the results of "particle-tracking" analyses (see [Appendix A](#)). Statistically, the results of the "particle-tracking" analyses were similar for all the PM-OV geologic models compared with the BN PM-OV model (see [Appendix A](#)). Particle-tracking results for the USGS PM-OV geologic model, a structurally uncoupled alternative model for the Silent Canyon Caldera, differed radically. From this analysis it was decided to consider both the base-case BN PM-OV geologic model and the USGS PM-OV geologic model.

To generate fluxes for the PM-OV CAU-scale model, the NTS regional flow model was first updated by regenerating its hydraulic conductivity fields from two hybrid geologic models. The hybrid models were derived by taking the two refined PM-OV hydrostratigraphic models (BN base case and USGS) and patching them into the coarse gridded BN regional geologic model (see [Appendix A](#)). In addition, separate models were constructed for different conceptualizations of the northern portion of the LCA. Speculation as to the continuity of the LCA in the northern section of the flow model led to the development of the two alternatives. Both were considered because of potential effects on fluxes applied to the northern boundary of the CAU flow model. This created four conceptual hydrostratigraphic flow models, which were then used in conjunction with several different recharge distributions, to create a set of models that were each calibrated. The calibrated results were in turn used to generate fluxes along the PM-OV CAU-scale model boundaries.

F.2.2 Recharge Distribution Models

In the PM-OV area, the groundwater flow system is replenished by interbasin subsurface flow and areal recharge. Quantification of precipitation recharge to the subsurface flow system is quite difficult. In an attempt to estimate the uncertainty associated with the quantification of surficial recharge to the PM-OV CAU-scale model, three different methods were used (see [Section 6.0](#)). The three methods are an empirical mass-balance method and two derivatives of this method, a deterministic mechanistic method and a chloride mass-balance method (see [Section 6.0](#)). Including subsets of the first and third method, five different recharge models were generated from the three different recharge generation methods.

The first method, a Maxey-Eakin approach (see [Section 6.0](#), Maxey and Eakin, 1949 and Eakin et al., 1951) is an empirically derived approach relating recharge to precipitation zones from a base precipitation map. The original UGTA regional recharge model was based upon a Maxey-Eakin approach applied to a recreation of edited Hardman (1965) and James (1993) precipitation contour maps. During the NTS regional flow model calibration process (DOE/NV, 1997), it was found that there was insufficient recharge in the southeast portion of the NTS area (see [Section 6.0](#)). To correct for this problem, a precipitation distribution developed by USGS (Hevesi et al., 1992) was inserted into this southeastern area (see [Section 6.0](#)). Then, utilizing the same approach, recharge values that were more amenable to the calibration process were assigned to the corresponding model cells. This updated recharge model included a revision of the parameter controlling the minimum amount of precipitation needed to generate recharge. It was the final version that was used in the calibrated NTS regional flow model (IT, 1996).

Due to the differences in total infiltration between the original and upgraded Maxey-Eakin recharge models, both recharge models were considered when generating sets of boundary fluxes for the CAU-scale model. [Figures F.2-1](#) and [F.2-2](#) depict the recharge distributions over the NTS regional flow model area for the original and calibrated NTS regional flow models. It is the original recharge model ([Figure F.2-1](#)) that is referred to as the UGTA base-case in [Section 6.0](#). Note that the recharge figures in this appendix represent recharge that was applied to the model for the present analysis; therefore, they differ slightly from the original distributions as noted above.

The USGS deterministic mechanistic approach is based upon modeling the processes that affect the net rate of infiltration past the root zone (see [Section 6.0](#) and Hevesi et al., 2003). Parameters controlling the net rate of infiltration include precipitation, evaporation, soil type, percent and type of vegetative cover, and numerous other parameters. The USGS approach included two versions, one which includes overland flow of excess precipitation and redistribution of this water to downstream areas of more permeable soils and one version without redistribution. In the first version, the recharge redistribution along channels was discontinuous. As a result only the version without redistribution was used in the boundary-flux generation simulations. Contours of the recharge-rate distribution

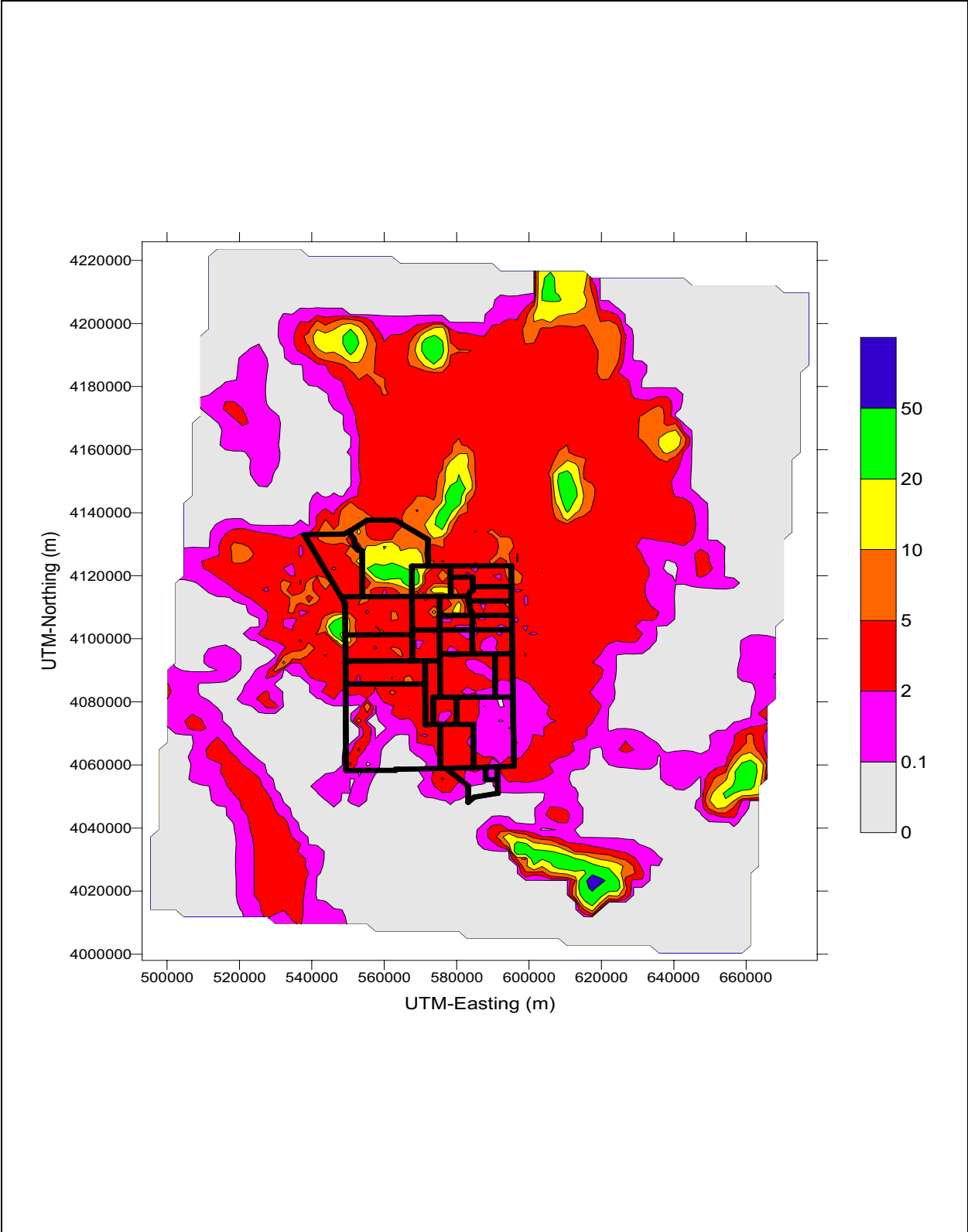


Figure F.2-1
Recharge Distribution in mm/y for UGTA Recharge Model Used
in Final Calibrated Regional Flow Model

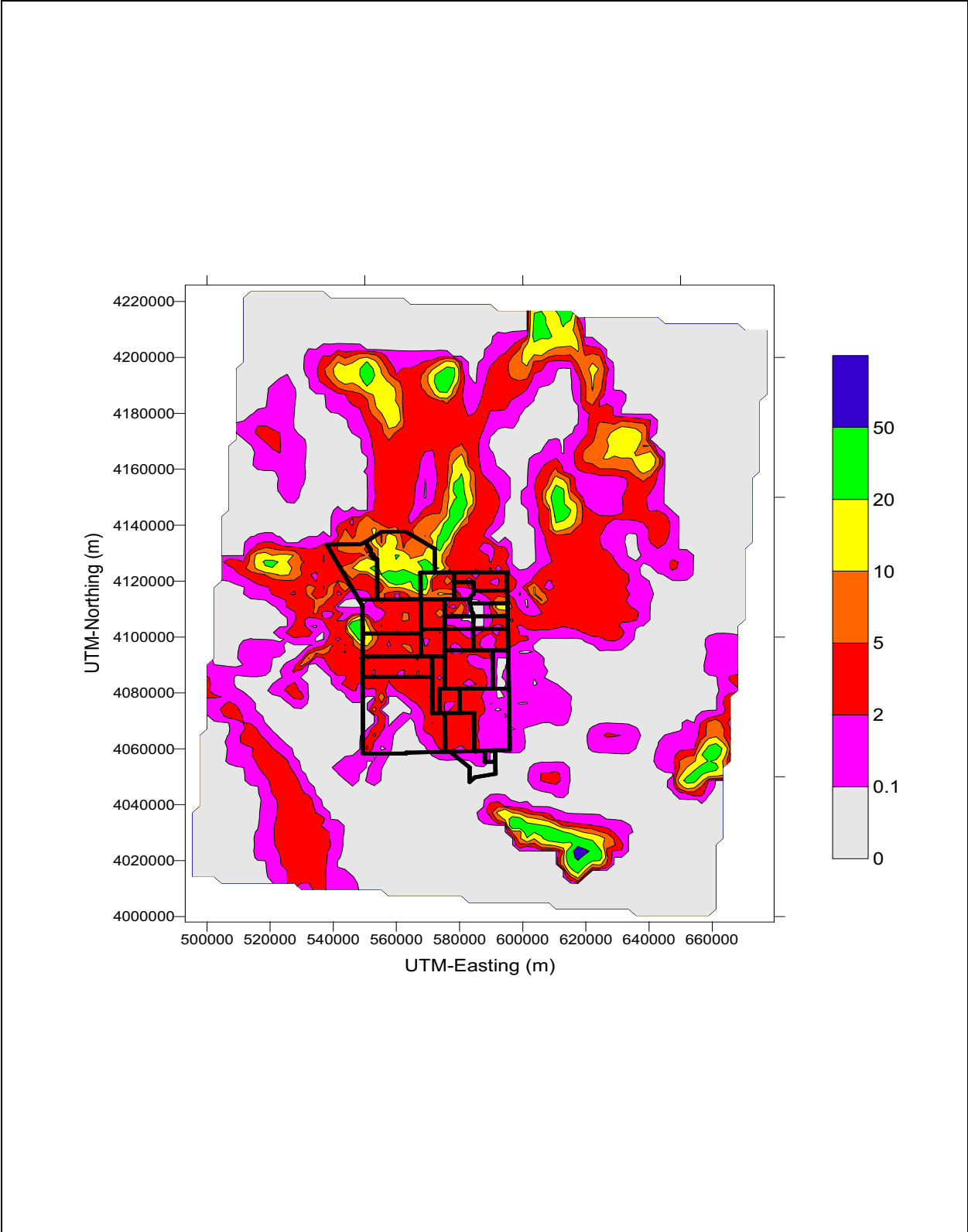


Figure F.2-2
Original Recharge Distribution in mm/y for UGTA Recharge Model Used in Regional Flow Model

over the NTS regional flow model area for the USGS recharge model are presented in [Figure F.2-3](#).

The third method is a chloride mass-balance approach developed by DRI, which estimates recharge by analyzing and comparing the chloride ratios of precipitation and groundwater (see [Section 6.0](#) and Russell and Minor, 2002). As noted in [Section 6.0](#), higher chloride concentrations in groundwater discharged from springs result from evapotranspiration of precipitation that contains low amounts of conservative atmospheric chloride ion, presenting a relative gauge of recharge. DRI used this information along with soil chloride profiles in different recharge locations to estimate recharge rates and associated confidence intervals. DRI presented two versions of the model, both assuming zero recharge in the alluvium and a second also assuming zero recharge in all other surface materials if they are found below 1,237 m (see [Section 6.0](#) and Russell and Minor, 2002). Both versions were used to generate flux boundary conditions. Contours of the recharge-rate distribution over the NTS regional flow model area for the DRI recharge models are presented in [Figures F.2-4](#) and [F.2-5](#).

A comparison between approximate total daily recharge rates for all five recharge models is presented in [Table F.2-1](#). As can be seen by comparing [Figures F.2-1](#) through [F.2-5](#), the general trend of high recharge in the mountains and low in the valleys is consistent with all the approaches. The recharge distribution used in the calibrated NTS regional flow model ([Figure F.2-1](#)) is similar to the distribution in the original UGTA recharge model ([Figure F.2-2](#)), but differs in the southeast NTS area where the addition of the Hevesi data (Hevesi et al., 1992) increases the recharge. Changes in the minimal precipitation level needed for recharge also increase the recharge in the southeast of the original model. Other areas of higher elevation in the northern and western areas of the distribution used in the calibrated NTS regional flow model have lower recharge rates than found in the original model. The USGS recharge model has a much lower total volume than the UGTA models ([Table F.2-1](#)), and the recharge distribution pattern is much more widely spread (see [Figures F.2-3](#), [F.2-1](#) and [F.2-2](#)). The DRI recharge models show a similar recharge distribution to the UGTA models, but recharge in the highlands is much greater (see [Figures F.2-1](#), [F.2-2](#), [F.2-4](#) and [F.2-5](#)).

As noted in [Section 6.0](#), the original UGTA recharge model (the UGTA Revised Maxey Eakin approach) is considered the base model for the recharge analysis. It was chosen because it provides a good starting point for modeling that falls in the middle of the ranges of recharge estimates. In general, the volumes for the base model are bracketed by the other models volumes and fall within the 5 and 95 percent confidence intervals for the DRI methods where available ([Table 6-5](#)). A detailed comparison of the recharge volumes as determined by the various methods, for the study area hydrostratigraphic basins and subbasins (see [Figure 6-1](#)) is presented in [Table 6-5](#).

F.2.3 Models Calibrated

Based upon the combinations of geologic and recharge models described above, eight separate models were calibrated to produce a range of flux boundary

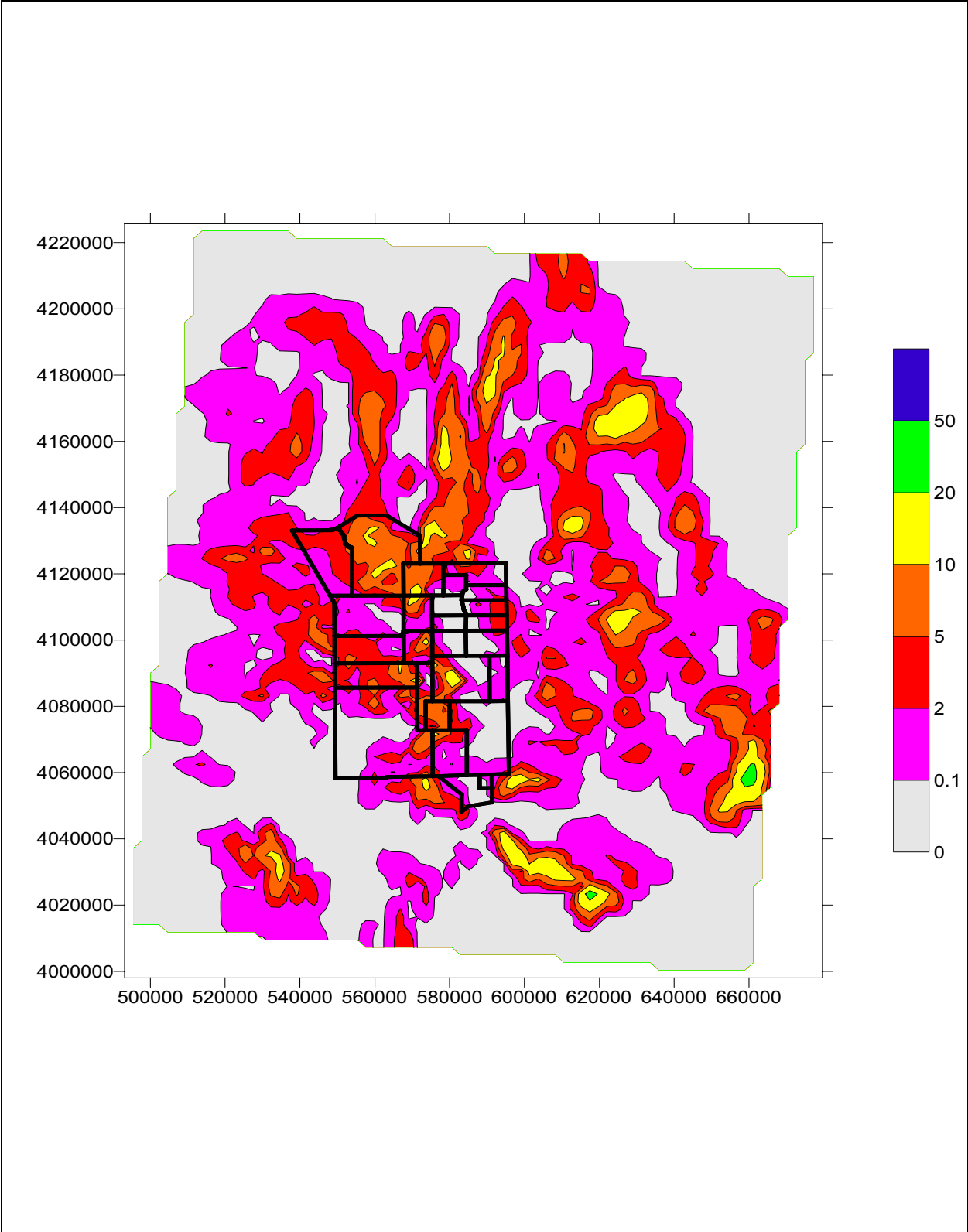


Figure F.2-3
Recharge Distribution in mm/y for USGS Recharge Model Without Redistribution of Recharge

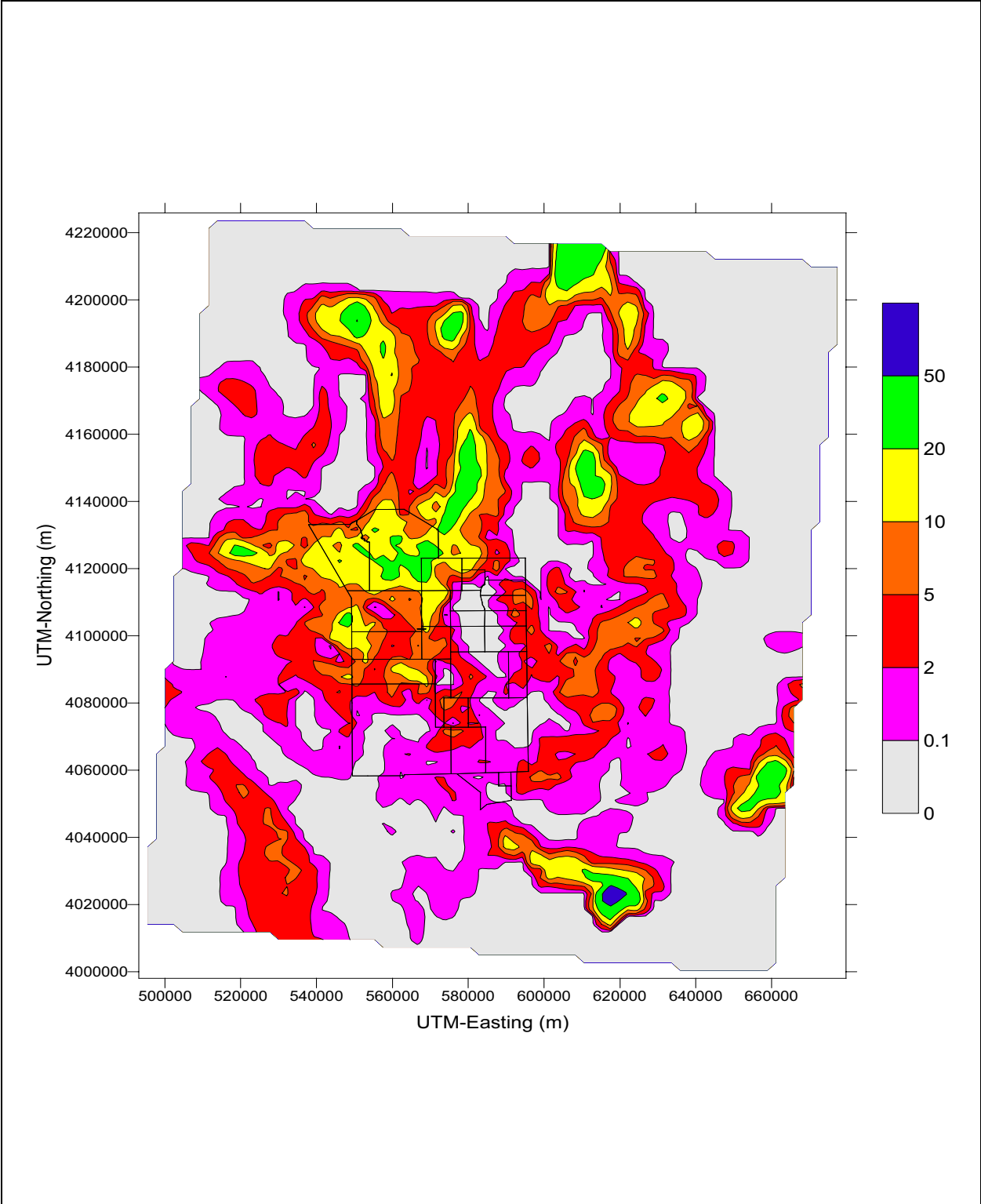


Figure F.2-4
Recharge Distribution in mm/y for DRI Recharge Model with
Recharge Allowed Below an Elevation of 1,237 m

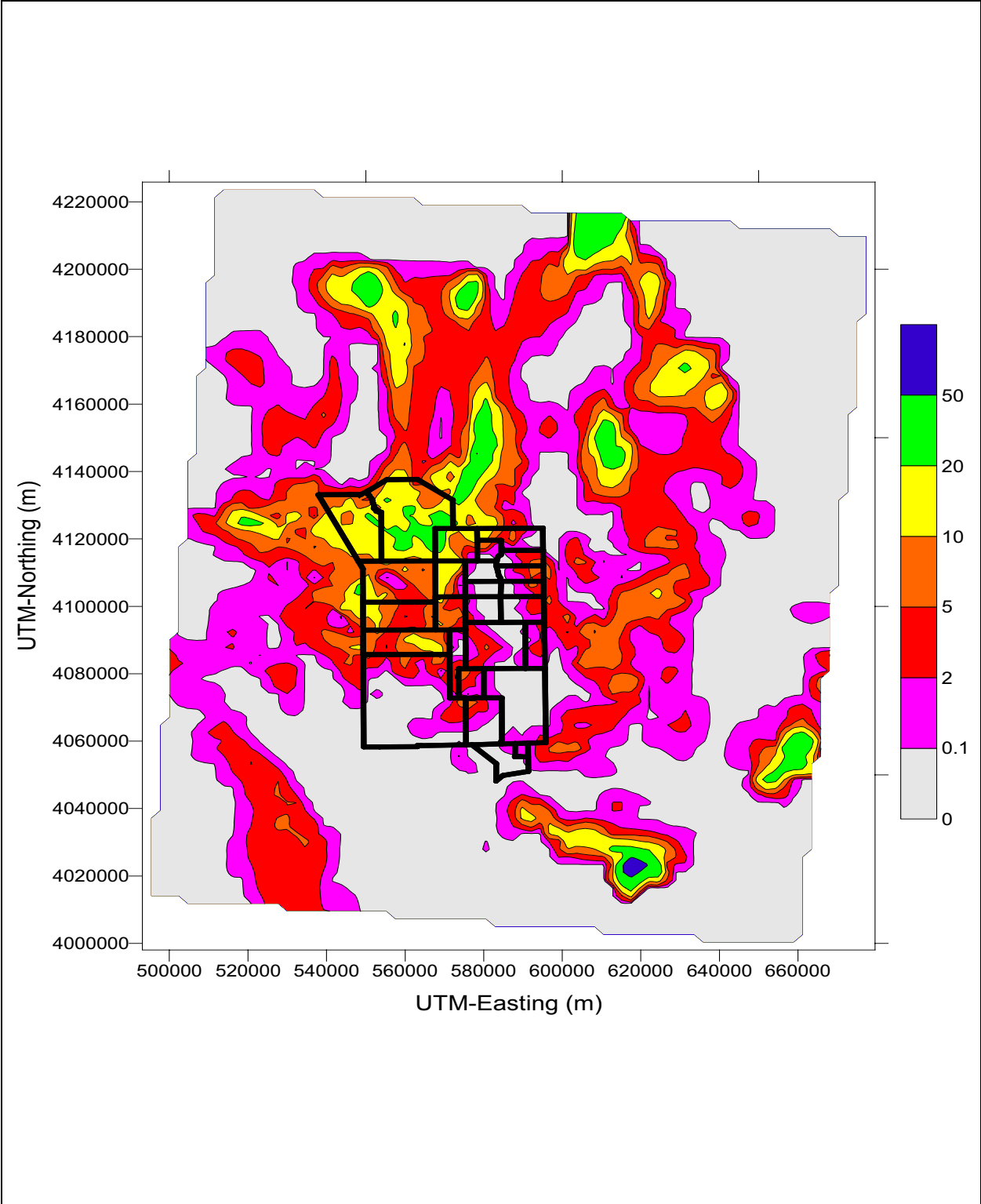


Figure F.2-5
Recharge Distribution in mm/y for DRI Recharge Model
Without Recharge Allowed Below an Elevation of 1,237 m

Table F.2-1
Recharge Models Flux Rates in m³/d

Recharge Model	Recharge Rate in m ³ /d
UGTA Regional Model (original)	213,000
UGTA Regional Model (calibrated)	234,000
USGS (no redistribution)	144,000
DRI (recharge below 1,237 m elevation)	268,000
DRI (no recharge below 1,237 m elevation)	262,000

conditions for the CAU flow model. The models that were calibrated are listed in [Table F.2-2](#) along with the model name as they will be referred to in the following text.

Table F.2-2
Simulation Names and Associated Hydrostratigraphic and Recharge Models

Model Name	Pahute Mesa-Oasis Valley Hydrostratigraphic Model	Northern Region LCA Submodel	Recharge Model
G1aR1a	Bechtel Nevada	Discontinuous LCA	UGTA Calibrated Regional
G1bR1a	Bechtel Nevada	Continuous LCA	UGTA Calibrated Regional
G1aR1b	Bechtel Nevada	Discontinuous LCA	UGTA Original Regional
G1aR2	Bechtel Nevada	Discontinuous LCA	USGS - No Redistribution
G2aR1a	USGS	Discontinuous LCA	UGTA Calibrated Regional
G2bR1a	USGS	Continuous LCA	UGTA Calibrated Regional
G1aR3a	Bechtel Nevada	Discontinuous LCA	DRI
G1aR3b	Bechtel Nevada	Discontinuous LCA	DRI - no recharge below 1,237 m

F.3.0 Calibration Process

An automated calibration approach was considered for generating a set of flux boundary conditions for the CAU flow model from the set of regional-scale flow models, with alternative recharge models and PM-OV geologic submodels. Visual PEST (Doherty, 2000) was selected as the driver for this multi-model parameter estimation exercise. Since the total number of parameters in the model that could be estimated was 354, several simplifying assumptions were made. Two sets of parameters, the ratios of vertical to horizontal hydraulic conductivities and the hydraulic conductivity depth decay coefficients were assumed to be the same as derived in the original regional model calibration. Only the horizontal hydraulic conductivities were recalibrated for each model. This brought the number of estimated parameters down to 118. In addition, it was decided that due to the complexity of the system (the number and geometry of the HSU's), the number of unknown parameters, and the nonlinearity associated with the

MODFLOW water-table model, that the automated approach would be adhered to only if it was effective. As it turned out, the automated approach produced severe problems associated with nonconvergence of the variable water-table model. In addition, grouping of parameters into smaller subsets of unknowns due to practical limitations on the number of unknowns that can be estimated at once, was also problematic. Basing the groupings on parameter sensitivity was difficult since the sensitivity of the system to specific parameters chosen was greatly influenced by the parameter values at adjacent HSUs. Due to these concerns, the calibration process was initiated using PEST, but when difficulties arose, the final calibrations were performed by hand allowing for individual adjustments.

F.3.1 Calibration Criteria

The model calibration process is comprised of adjusting various modeling parameters until an acceptable agreement between model-related values and those values measured in the groundwater system. For these simulations, the horizontal hydraulic conductivity was the variable that was estimated. Calibrated values for the NTS regional model (IT, 1996) were used for the vertical to horizontal conductivity ratios and the decay terms describing the decrease of conductivity with depth. Note that the recharge rates were based upon different models describing conceptual uncertainties, so they were not adjusted except for places where the recharge model was totally incompatible with the geologic model (e.g., high recharge rate applied to a near-surface igneous intrusion). This incompatibility generated unrealistic water levels and typically nonconvergence of the model associated with MODFLOW's nonlinear water-table option. For the calibration criteria, agreement of modeled-measured values of hydraulic head, boundary fluxes and general flow direction was examined. The calibration criteria for the measured versus simulated heads as given in IT (1996) are presented in [Table F.3-1](#). The agreement criteria for the boundary fluxes are presented in [Table F.3-2](#). The range of values in [Table F.3-2](#) is based on minimum and maximum values in Laczniaik et al. (2001). This large range is considered appropriate for the regional-scale simulations. The CAU-scale model will use slightly smaller ranges based on 5 and 95 percent values from Laczniaik et al. (2001). Additionally, combined values of fluxes from Ash Meadows and Alkali Flat (Peter's Playa) were considered more important than just the individual values.

It should also be noted that calibration in the PM-OV area of the model was given preference over calibration in areas that were not as critical to determining the flow field in the PM-OV area. For example, if the recharge model generates excess recharge, the water must exit somewhere. Therefore, an over-estimate of discharge in the Ash Meadows/Death Valley area was considered acceptable in some cases.

Table F.3-1
Calibration Criteria for Weighted Hydraulic-Head Residuals by Zone
(IT, 1996)

Zone	Area	Mean Weighted Residual (m)	Root Mean Square of Weighted Residuals (m)	Range in Measured Heads (m)
	All	20	100	1,687.4
1	Northern Area	100	150	202.7
2	Oasis Valley	15	75	533.7
3	Pahute Mesa	25	35	230.7
4	Barrier	300	350	565.3
5	W. Yucca Flat	45	110	632.2
6	E. Yucca Flat	35	80	101.3
7	Shoshone	20	50	285.8
8	Death Valley	80	100	728.4
9	Lower Carbonate Aquifer	5	40	205
10	SW. of Pahrangat Valley	40	40	15.3
11	Spring Mountain	150	150	278.9
12	Sheep Range	100	100	39.9
13	Timber Mountain	100	100	220.7
14	Armagosa Farm	10	50	58.3
15	Frenchman Flat	10	50	20.6

Table F.3-2
Calculation of Criteria for Model-Area Discharge
(brackets denote inflow)

Discharge Area	Total Discharge Range (m ³ /d)	Target Discharge Rate (m ³ /d)
Death Valley	17,500 - 60,200	60,100
Oasis Valley	14,089 - 30,152	21,275
Amargosa River	2,400 - 5,100	2,500
Ash Meadows	33,484 - 95,527	60,022
Franklin Lake/Alkali Flats	800 - 42,600	35,500
Alkali Flat (Peter's Playa)	5,000 - 7,300	6,100
Penoyer Valley	13,000 - 27,000	20,300
Indian Springs	1,600 - 2,400	2,400
Pahrump Valley	(5,000) - (7,600)	(5,000)
Eagle mountain	850 - 3,400	3,400

F.4.0 Calibration Results

The calibration efforts produced a set of eight results that were used to generate boundary conditions for use in the CAU flow model. Root mean square of weighted residual values for individual residual zones and combined zones are presented in [Table F.4-1](#). Discharge (recharge) zone flux results for each alternative model are presented in [Table F.4-2](#).

Water table-contours for the eight alternative regional-scale flow models are presented in [Figures F.4-1](#) through [F.4-8](#).

The regional-scale model results for inflow at the CAU flow model lateral boundaries are presented in [Table F.4-3](#). Outflow rates for the CAU flow model lateral boundaries are presented in [Table F.4-4](#).

A satisfactory calibration was achieved for all cases. The PM-OV model boundary fluxes for all the models had common general tendencies including net inflow on the northern and eastern boundaries, and net outflow on the southern boundary. The western boundary showed fairly balanced inflows and outflows. Note that the flow generated for the western boundary of the PM-OV model is highly controlled by the proximity of the NTS regional flow model western boundary.

Table F.4-1
Root Mean Square of Weighted Residuals Values for Individual Residual Zones
and Combined Zones in Meters

#	Residual Zone	G1aR1a	G1bRa1	G1aR1b	G1aR2	G2aR1a	G2bRa1	G1aR3a	G1aR3b
	All	58.5	58.7	56.2	61.4	68.8	67.6	58.2	56.3
1	Northern	63.9	68.0	54.9	58.7	71.1	75.7	51.1	54.8
2	Oasis Valley	49.2	48.7	48.6	60.9	36.0	36.2	52.4	51.5
3	Pahute Mesa	28.7	30.2	31.0	45.7	44.0	43.4	39.5	39.3
4	Barrier	161.0	167.8	153.8	167.0	145.1	150.8	153.3	153.7
5	Western Yucca Flat	139.6	131.2	138.4	167.0	172.8	160.6	158.4	155.2
6	Eastern Yucca Flat	54.0	55.5	43.0	28.9	56.2	48.5	42.0	27.8
7	Shoshone	92.1	88.2	89.0	116.3	119.1	130.5	98.5	100.5
8	Death Valley	55.4	56.8	54.6	62.1	36.0	36.1	43.9	38.0
9	LCA	39.6	41.5	40.5	49.3	70.3	72.8	36.9	36.3
10	SW of Pahranaagat Valley	22.6	23.1	22.7	57.7	22.4	23.0	49.4	45.5
11	Spring Mountain	103.0	102.8	104.6	49.8	99.3	99.5	90.6	95.4
12	Sheep Range	29.4	29.3	30.5	35.8	26.2	26.5	38.9	43.6
13	Timber Mountain	30.5	28.3	34.0	42.2	39.9	39.1	41.0	40.1
14	Amargosa Farm Area	19.6	19.8	17.9	10.5	10.0	10.1	14.5	14.5
15	Frenchman Flat	16.1	15.1	14.7	26.6	7.7	7.6	5.2	4.9

Table F.4-2
Simulation Discharge Rates in m³/d at Discharge Calibration Zones

#	Discharge Zone	G1aR1a	G1bRa1	G1aR1b	G1aR2	G2aR1a	G2bRa1	G1aR3a	G1aR3b
1	Death Valley	-69,418	-69,434	-69,425	-47,268	-65,236	-65,405	-87,978	-88,662
2	Oasis Valley	-22,224	-23,732	-29,188	-15,054	-18,273	-20,679	-51,376	-47,492
3	Amargosa River	-8,150	-8,213	-7,701	-406	-889	-891	-521	-532
4	Ash Meadows	-82,027	-82,616	-78,108	-77,561	-65,993	-65,793	-100,503	-100,188
5	Franklin Lake/Alkali Flat	-16,186	-16,317	-16,197	-27,726	-26,905	-26,915	-32,503	-32,962
6	Alkali Flat (Peter's Playa)	-31,049	-31,863	-24,737	-863	-47,658	-47,043	-15,488	-14,362
7	Penoyer Valley	-9,764	-6,654	-7,267	-7,185	-16,990	-15,225	-21,610	-24,757
8	Indian Springs	0	0	0	0	0	0	0	0
9	Pahrump Valley	3,301	3,293	3,371	1,329	3,336	3,343	2,887	2,998
10	Eagle Mountain	-7,363	-7,378	-7,135	-1,662	-4,266	-4,267	-2,705	-2,726

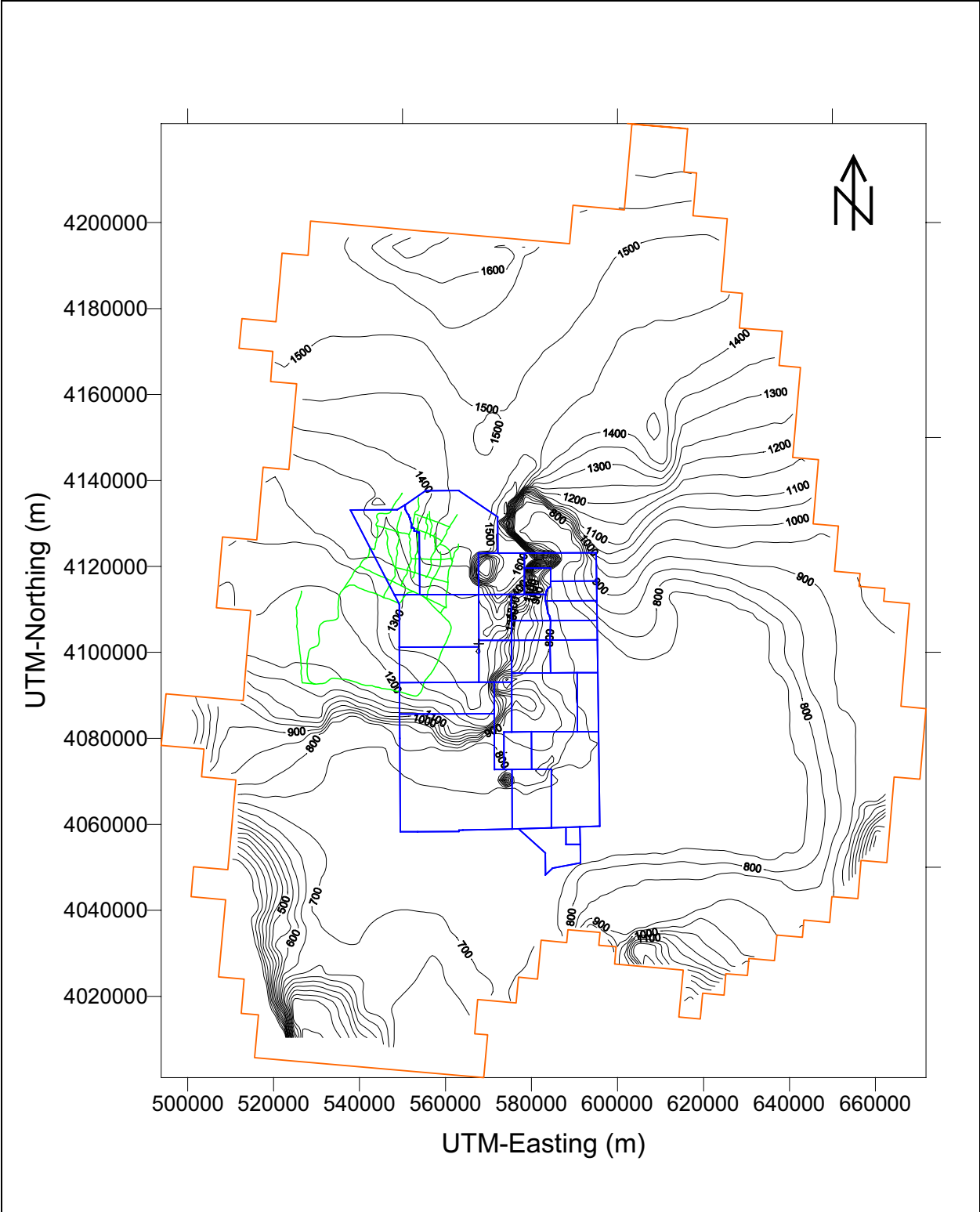


Figure F.4-1
Water-Table Contours in m amsl for Regional Groundwater Flow Model with BN PM-OV Geologic Model, Discontinuous LCA and Final Regional Model Recharge (Model G1aR1a)

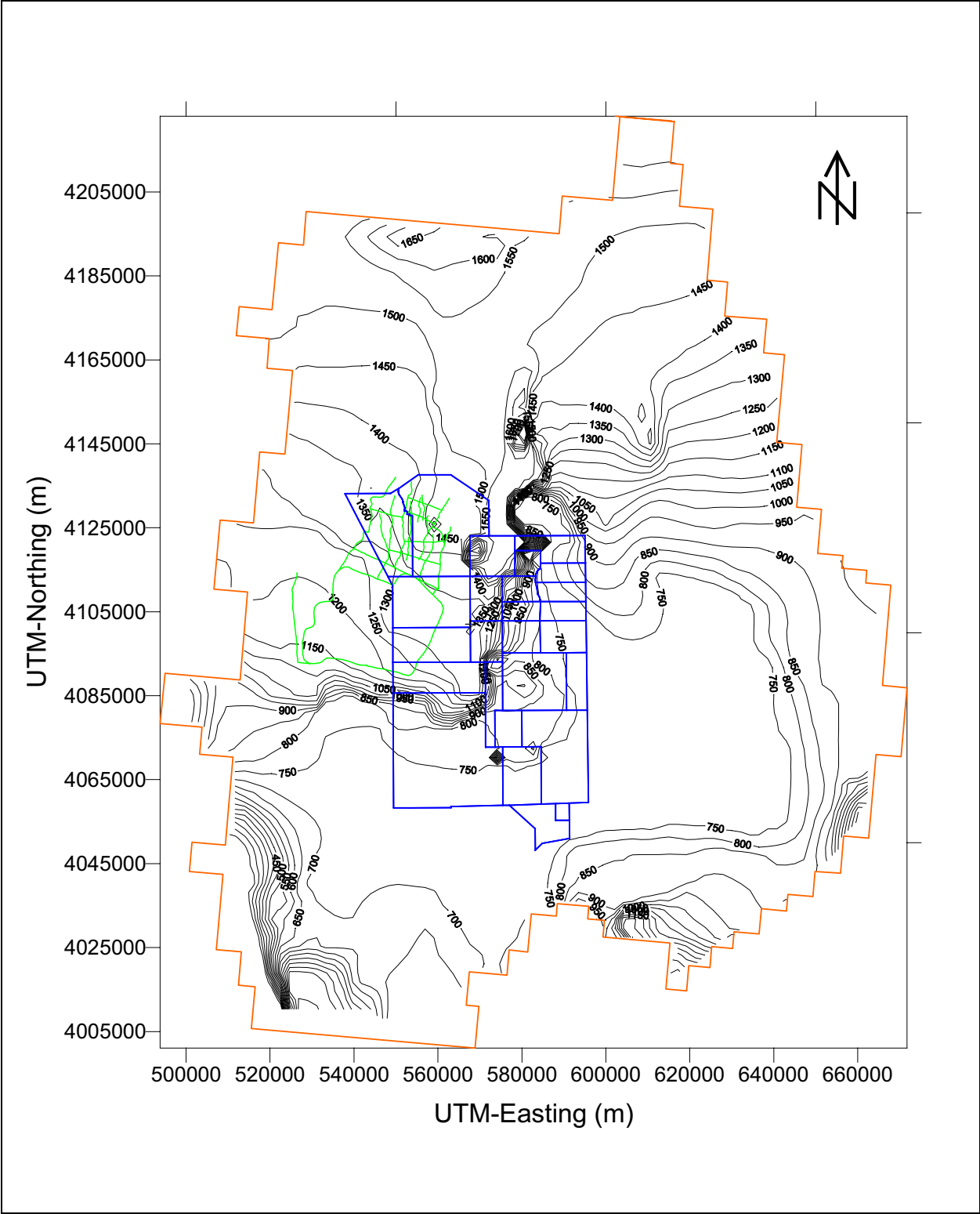


Figure F.4-2
Water-Table Contours in m amsl for Regional Groundwater Flow Model with BN PM-OV
Geologic Model, Continuous LCA and Final Regional Model Recharge (Model G1bR1a)

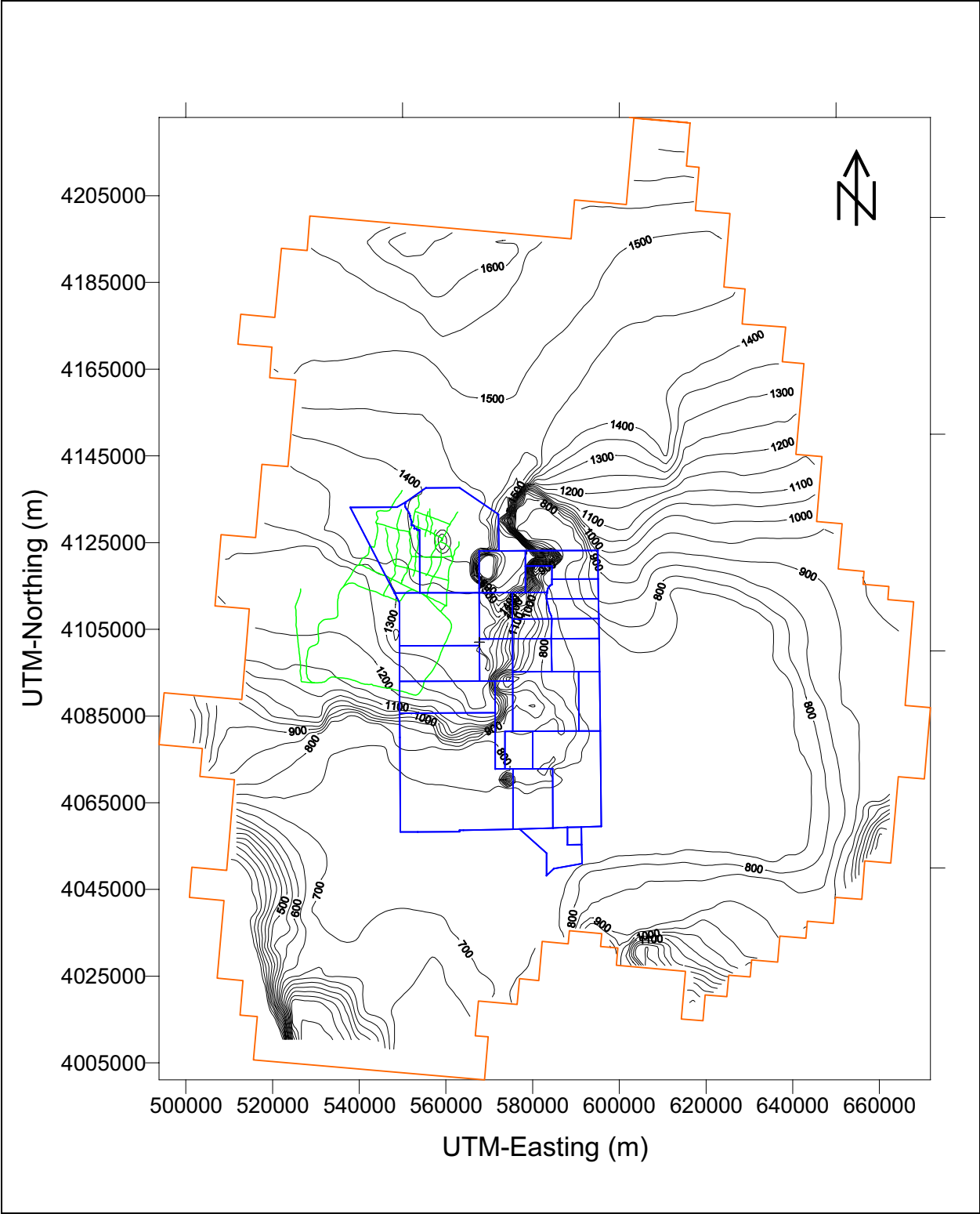


Figure F.4-3
Water-Table Contours in m amsl for Regional Groundwater Flow Model with BN PM-OV
Geologic Model, Discontinuous LCA and Original Regional Model Recharge (Model G1aR1b)

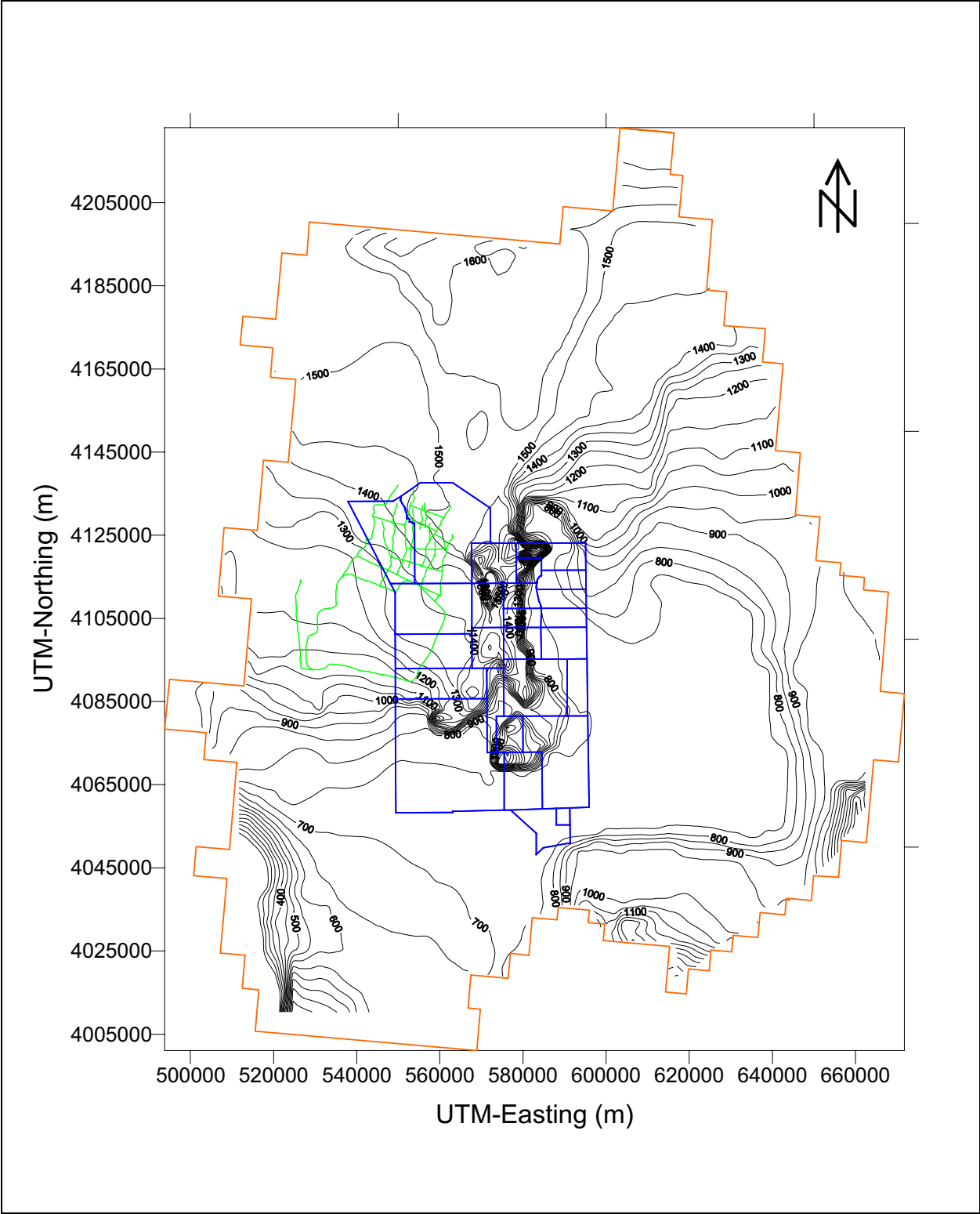


Figure F.4-4
Water-Table Contours in m amsl for Regional Groundwater Flow Model with BN PM-OV
Geologic Model, Discontinuous LCA and USGS Recharge Model with no Redistribution
(Model G1aR2)

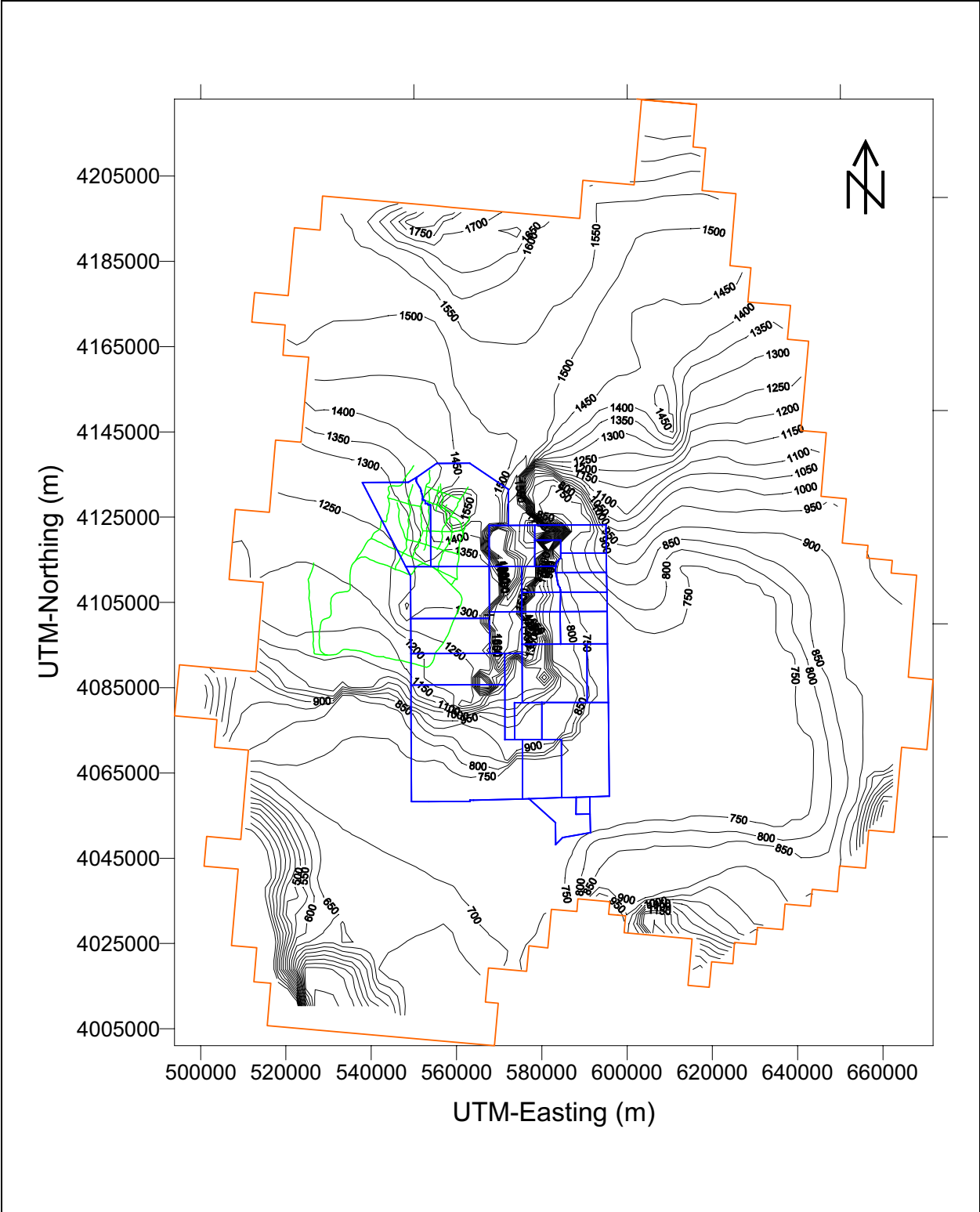


Figure F.4-5
Water-Table Contours in m amsl for Regional Groundwater Flow Model with USGS PM-OV Geologic Model, Discontinuous LCA and Final Regional Model Recharge (Model G2R1a)

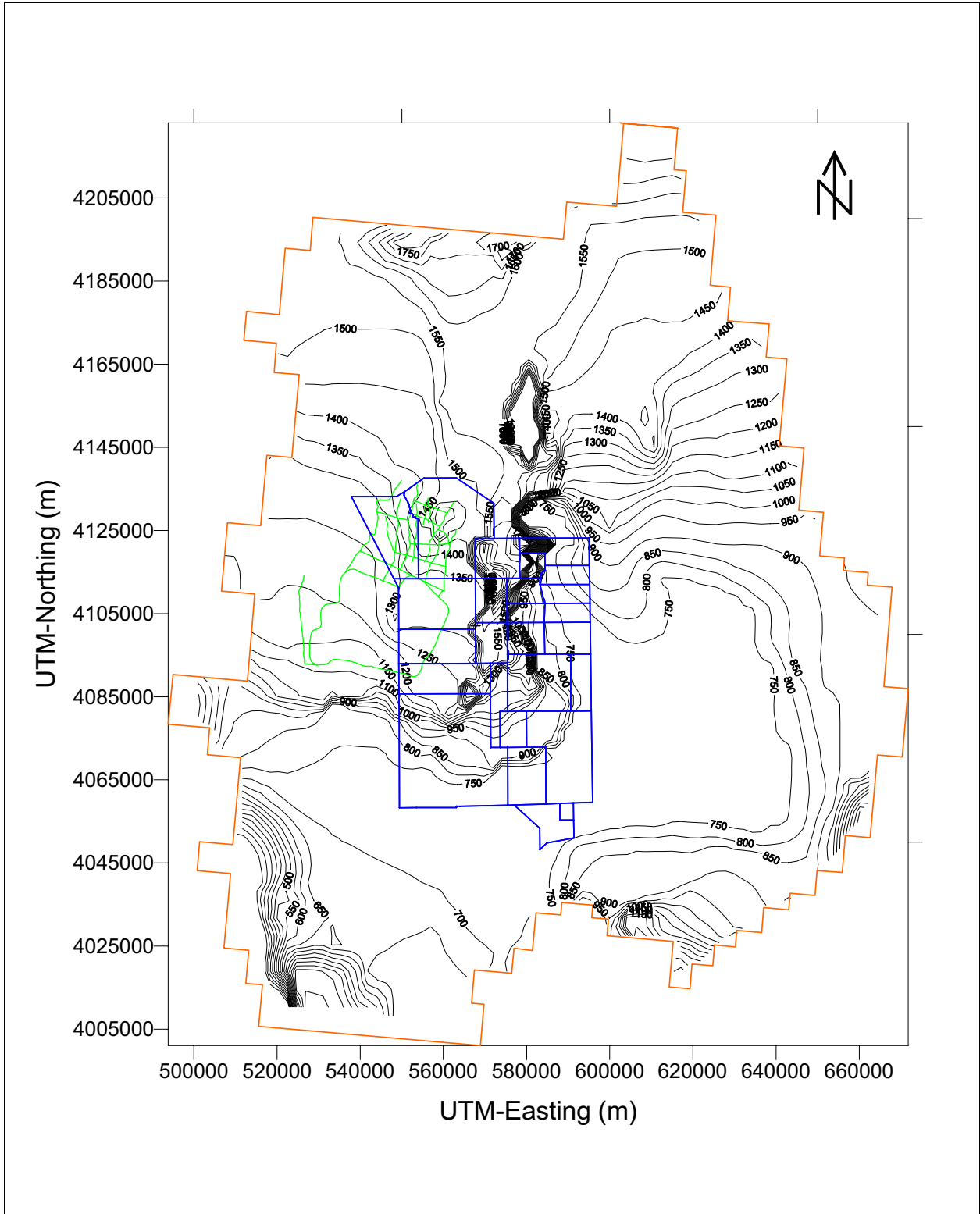


Figure F.4-6
Water-Table Contours in m amsl for Regional Groundwater Flow Model with USGS PM-OV
Geologic Model, Continuous LCA and Final Regional Model Recharge (Model G2bR1a)

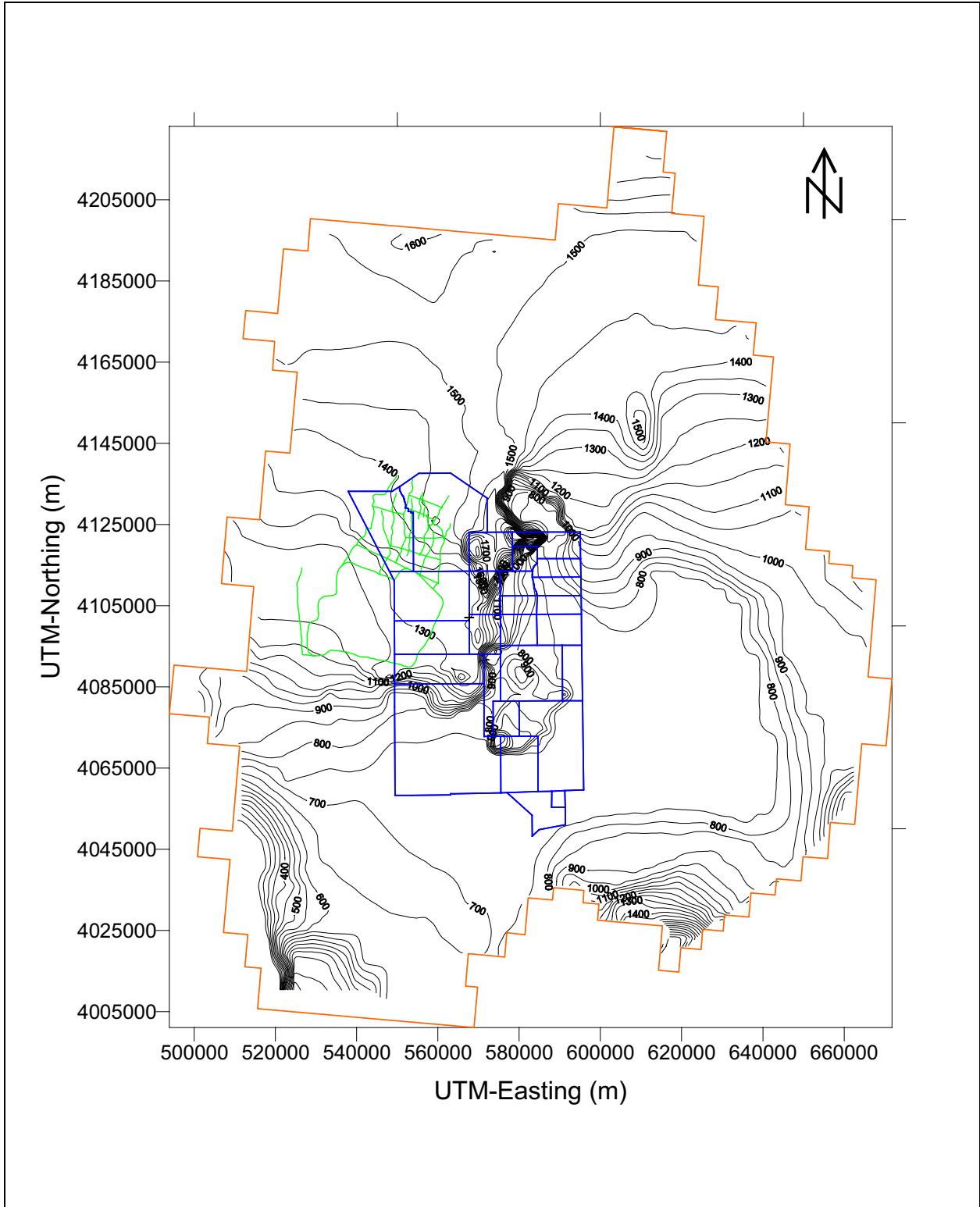


Figure F.4-7
Water-Table Contours in m amsl for Regional Groundwater Flow Model with BN PM-OV
Geologic Model, Discontinuous LCA and DRI Recharge Model (Model G1aR3a)

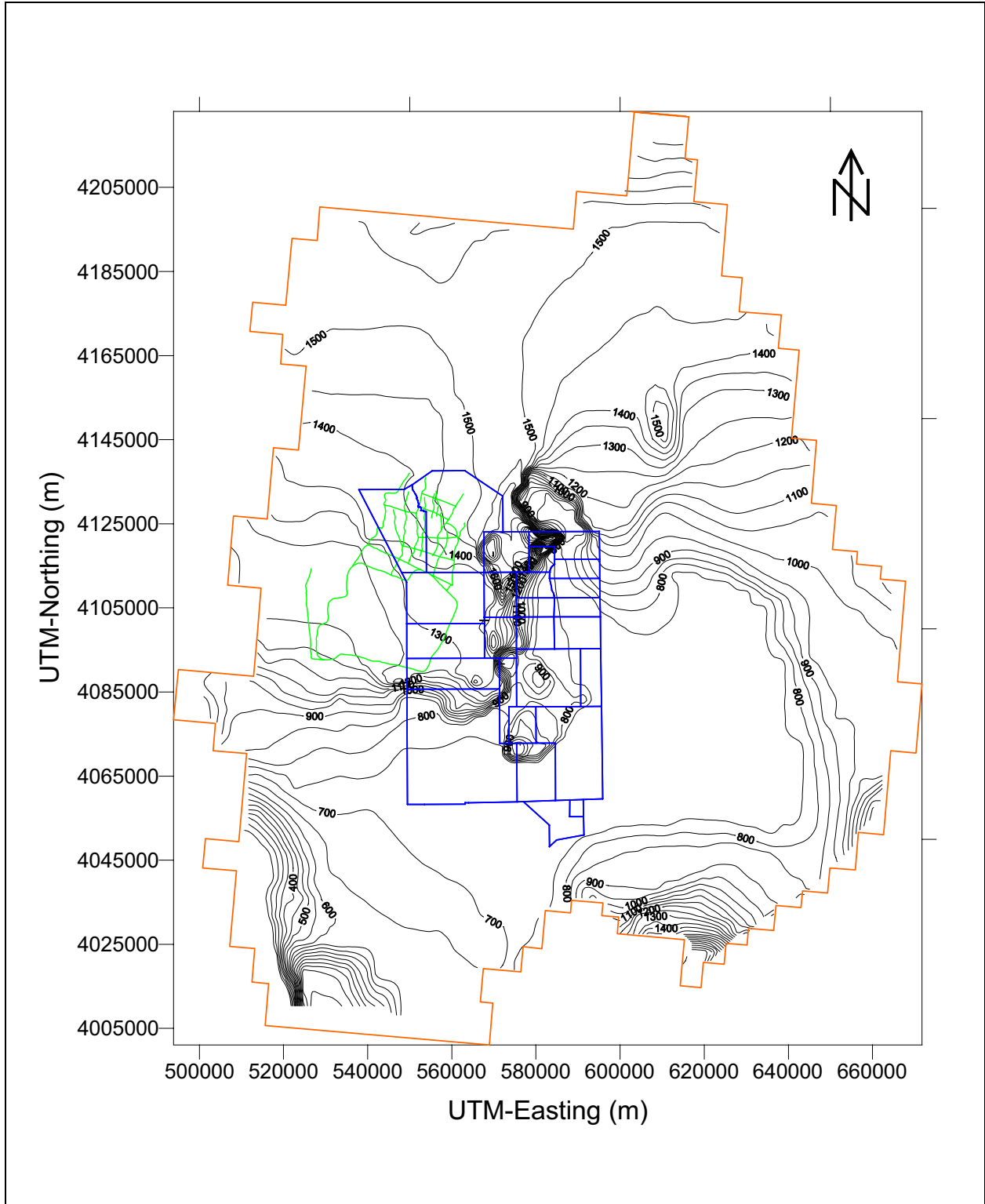


Figure F.4-8
Water-Table Contours in m amsl for Regional Groundwater Flow Model with BN PM-OV
Geologic Model, Discontinuous LCA and DRI Recharge Model Without Recharge Below 1,237 m
(Model G1aR3b)

**Table F.4-3
Regional Model Groundwater Inflows at CAU-Scale
Model Boundaries in m³/d**

Model Number	Northern Boundary Influx	Southern Boundary Influx	Eastern Boundary Influx	Western Boundary Influx
G1aR1a	22,763	452	10,453	13,478
G1bR1a	22,494	458	12,407	14,652
G1aR1b	23,880	413	11,828	17,257
G1aR2	13,828	248	5,572	1,723
G2aR1a	26,895	3,280	13,950	8,325
G2bR1a	27,693	3,477	16,943	9,285
G1aR3a	27,948	502	13,678	8,803
G1aR3b	24,216	804	10,531	5,815

**Table F.4-4
Regional Model Groundwater Outflows at CAU-Scale
Model Boundaries in m³/d**

Model Number	Northern Boundary Outflow	Southern Boundary Outflow	Eastern Boundary Outflow	Western Boundary Outflow
G1aR1a	5,127	40,747	4,598	13,858
G1bR1a	4,985	41,651	4,507	14,676
G1aR1b	5,034	41,996	3,979	17,305
G1aR2	139	26,339	305	2,440
G2aR1a	6,703	53,109	4,120	9,537
G2bRa1	6,669	54,405	5,007	10,225
G1aR3a	2,417	50,979	1,959	7,251
G1aR3b	1,419	50,224	1,568	5,839


F.5.0 References

- Bechtel Nevada. 2002. *Hydrostratigraphic Model of the Pahute Mesa-Oasis Valley Area, Nye County, Nevada*, DOE/NV/11718-646. Prepared for U.S. Department of Energy, National Nuclear Security Administration Nevada Operations Office. Las Vegas, NV.
- DOE/NV, see U.S. Department of Energy, Nevada Operations Office.
- Doherty, J. 2000. *Visual Pest User's Manual (Includes Pest2000 & WinPEST)*, Waterloo, Canada: Waterloo Hydrogeologic/Watermark Numerical Company.
- Eakin, T.E., G.B. Maxey, T.W. Robinson, J.C. Fredericks and O.J. Loeltz. 1951. *Contributions to the Hydrology of Eastern Nevada*, Water Resources Bulletin No. 12. State of Nevada, Office of the State Engineer/U.S. Geological Survey. Carson City, NV.
- Hardman, G. 1965. *Nevada Precipitation and Acreages of Land by Rainfall Zones*. Reno, NV: U.S. Department of Agriculture, University of Nevada Experimental Station.
- Hevesi, J.A., A.L. Flint, and J.D. Istok. 1992. "Precipitation Estimation in Mountainous Terrain Using Multivariate Geostatistics, Part II: Isohyetal Maps." In *Journal of Applied Meteorology*, 31(7): 677-688. Boston, MA: American Meteorological Society.
- Hevesi, J.A., A.L. Flint, and L.E. Flint. 2003. *Simulation of Net Infiltration Using A Distributed Parameter Watershed Model For The Death Valley Regional Flow System, Nevada And California*, USGS, Draft.
- IT Corporation. 1996. *Groundwater Flow Model Documentation Package, (Phase I Data Analysis Documentation, Volume VI)*. Las Vegas, NV.
- James, J.W. 1993. *Climate of the Death Valley Region, Nevada/California*. Prepared for the National Park Service. Reno, NV: State of Nevada, Office of the State Climatologist.
- Laczniak, R.J., J.L. Smith, P.E. Elliot, G.A. DeMeo, M.A. Chatigny, and G.A. Roemer. 2001. *Ground-Water Discharge Determined from Estimates of Evapotranspiration, Death Valley Regional Flow System, Nevada, and California*. U.S. Geological Survey Water-Resources Investigation Report 01-4195, 51 p. Carson City, NV: U.S. Geological Survey.
- Maxey, G.B. and T.E. Eakin. 1949. *Groundwater in White River Valley, White Pine, Nye and Lincoln Counties, Nevada*, Water Resources Bulletin No. 8. Carson City, NV: State of Nevada, Office of the State Engineer.

Russell, C.E. and T. Minor. 2002. *Reconnaissance Estimates of Recharge Based on an Elevation-dependent Chloride Mass-balance Approach*, DOE/NV/11508-37, Prepared for U.S. Department of Energy, National Nuclear Security Administration Nevada Operations Office. Las Vegas, NV: Desert Research Institute.

U.S. Department of Energy, Nevada Operations Office. 1997. *Regional Groundwater Flow and Tritium Transport Modeling and Risk Assessment of the Underground Test Area, Nevada Test Site, Nevada*, DOE/NV--477. Las Vegas, NV.

Ward, D.S., D.R. Buss, J.W. Mercer, and S.S. Hughes. 1987. "Evaluation of a Groundwater Corrective Action at the Chem-Dyne Hazardous Waste Site Using a Telescopic Mesh Refinement Modeling Approach." In *Water Resources Research*, 24(4): 603-617. Washington, DC: American Geophysical Union.



Appendix G
Supplemental Information

G.1.0 Introduction

This appendix contains a description of the supplemental information provided on the Compact disk-read only memory (CD-ROM). This information is provided to help the reader enhance their understanding of material provided in the document. The supplemental information consists of a Hydrostratigraphic Unit Gallery.

The PM-OV Valley EarthVision[®] hydrostratigraphic model (BN, 2002) was completed in September 2001. The model was constructed using an existing model for Western Pahute Mesa and increasing the area of the model to include Eastern Pahute Mesa, Oasis Valley south to Beatty, to the north of the NTS boundary, and west of Beatty. This tripled the size of the original model. The model incorporated the new PM-OV series of wells along with data supplied by the Yucca Mountain Project to provide consistency with the northern end of that model. The USGS provided input for the depth to Paleozoic surface and intrusive bodies based on their gravity and magnetics studies. The model has 73 fault blocks and 48 layers. In addition, six alternative models were constructed to evaluate different conceptual models that honor the data but have different interpretations of structure and HSUs where data are not available. The EarthVision[®] models have been exported to create meshes for the next step in the workflow, numerical modeling of groundwater flow and transport.

G.2.0 Data Summary

The "HSU Model Gallery" file contains images of the HSUs with a brief description for each HSU. Additional information can be found within the "HSU Descriptions" table.

G.3.0 Access to Data

The HSU Model Gallery is provided in HTML format in the following file:

- Pahute Mesa-Oasis Valley HSU Gallery.html

The HSU Descriptive table is provided in EXCEL format in the following file:

- HSU-descriptions.xls

To access the gallery and associated table from the paper copy of this document, use the CD provided in this document and open the desired file within the Supplemental Information subdirectory. To access the gallery and associated table from the electronic version of this document, click on the desired filename listed above.

G.4.0 *References*

Bechtel Nevada. 2002. *Hydrostratigraphic Model of the Pahute Mesa-Oasis Valley Area, Nye County, Nevada*, Report DOE/NV/11718--646. Las Vegas, NV.



Plates

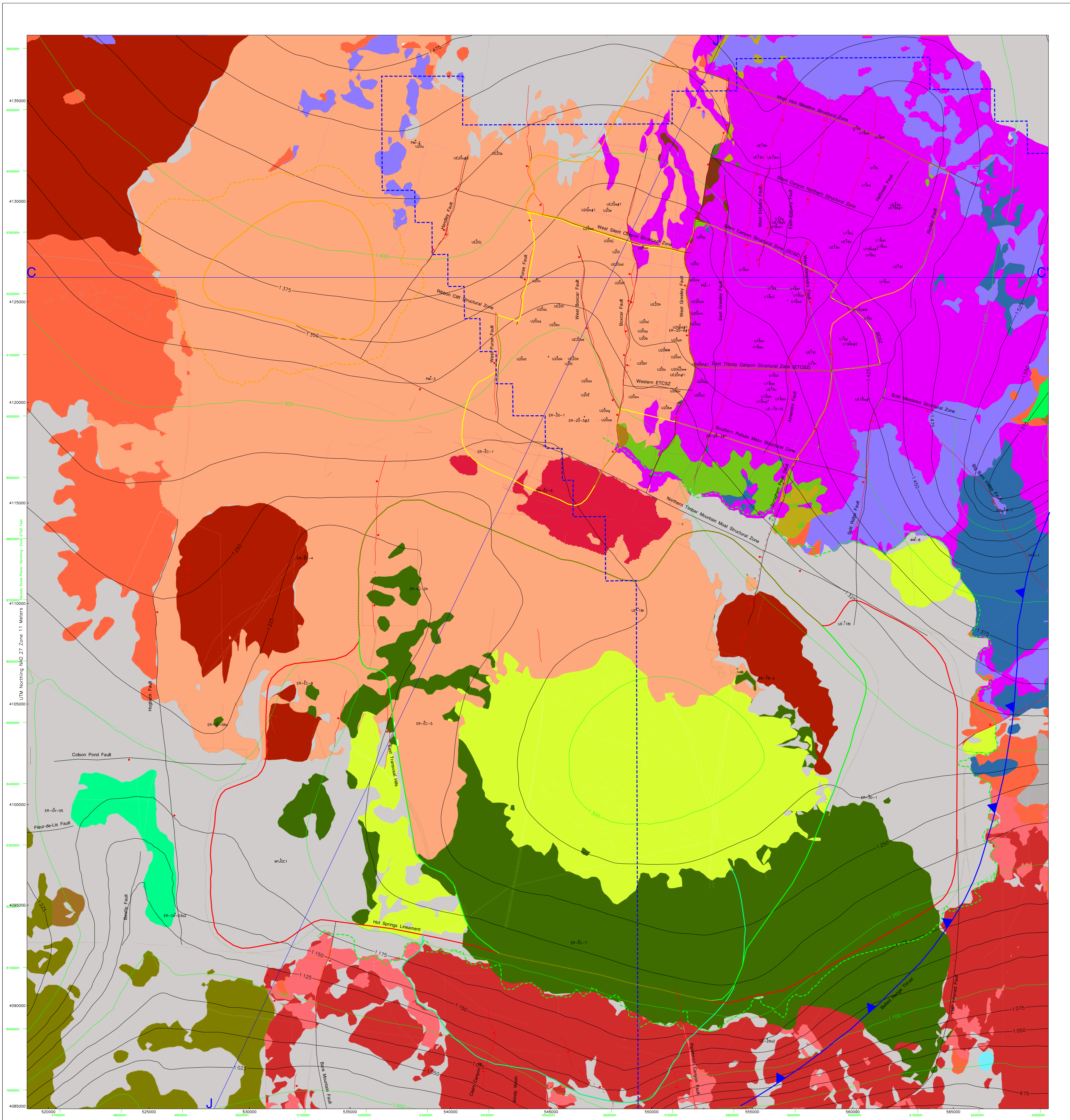
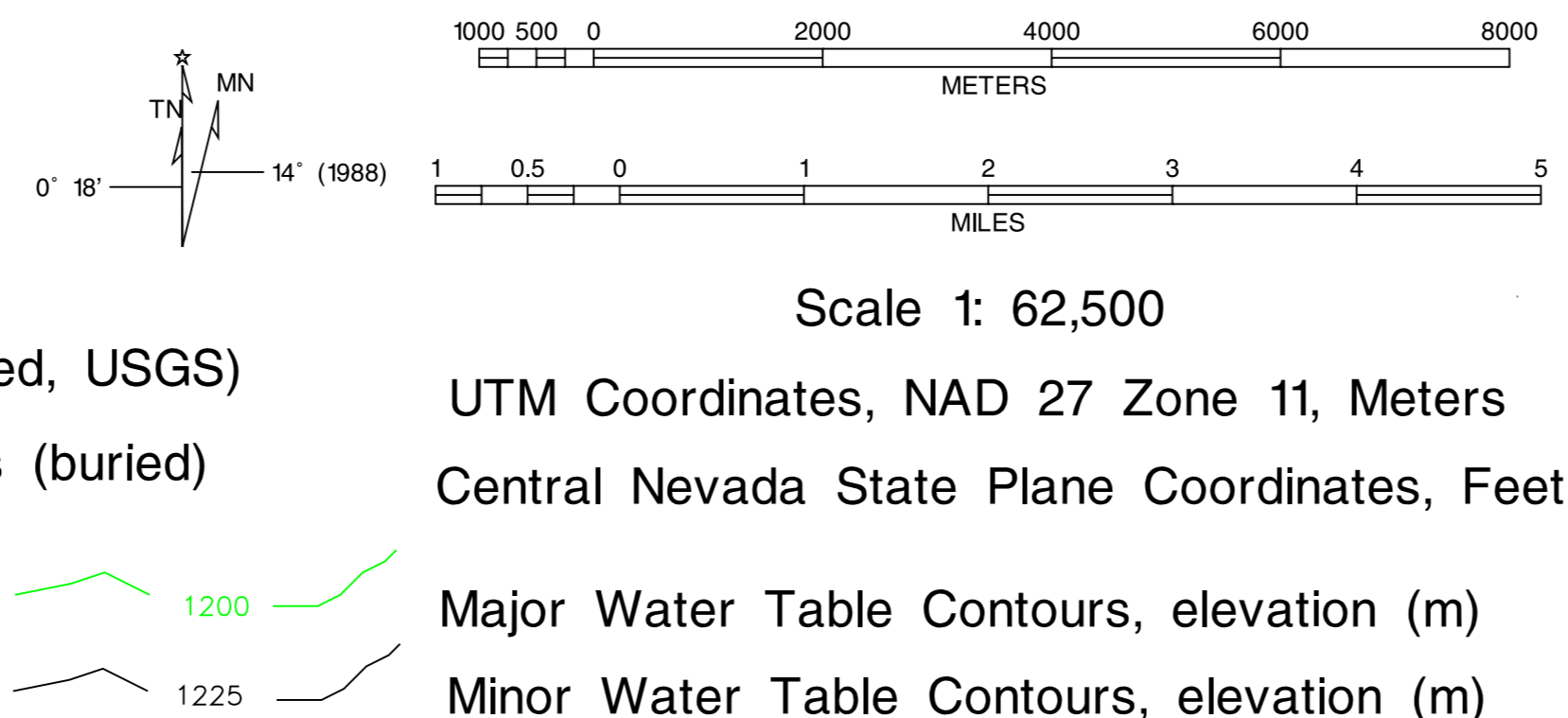


Plate 1 Hydrostratigraphic Units for the Pahute Mesa - Oasis Valley Area

EXPLANATION

- Black Mountain Caldera Topographic Margin
- Black Mountain Caldera Structural Margin (buried)
- Ammonia Tanks Caldera Structural Margin (buried)
- Timber Mountain Caldera Complex Topographic Margin (mapped, USGS)
- Common Ammonia Tanks and Rainier Mesa Structural Margins (buried)
- PM-OV Hydrogeologic Framework Model Cross Section Lines
- Borehole



- NTS boundary
- Surface faults, Wahl et al., 1997, ball and bar on downthrown side
- Buried faults and structural zones
- ▲ Thrust fault, sawteeth on upper plate (buried)
- Rainier Mesa Caldera Structural Margin (buried)
- Grouse Canyon Caldera Margin (buried)
- Area 20 Caldera Margin (buried)
- Claim Canyon Caldera Margin (buried)

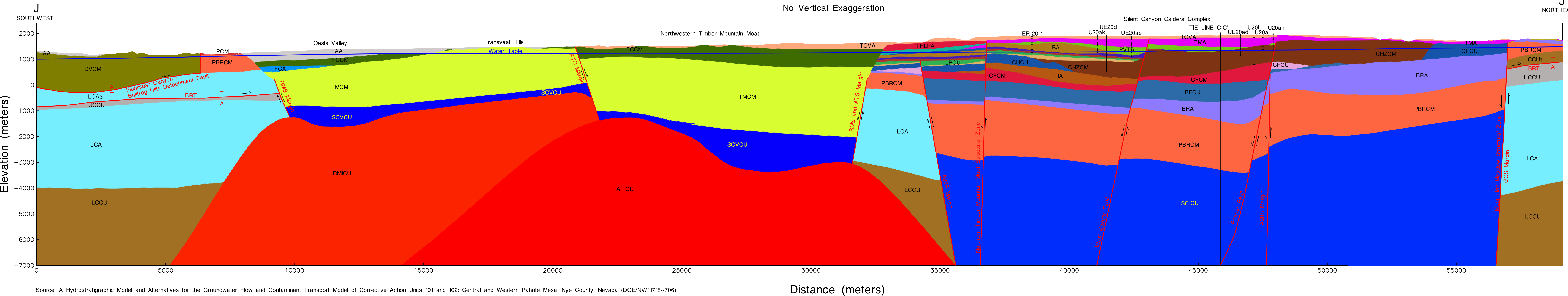
Hydrostratigraphic Units

AN	TCA	PRBCW
DNA	PULFA	TUCW
DNM	LCPU	SCOCU
YCM	TSA	LEA3
TCVA	YMEFCM	LCOU
FCCM	CHVTA	UCOU
FCA	CHVCM	LCA
THLFA	CHZCM	SCOU
THCM	CHZCU	LCCU
TMA	IA	MCCU
WVA	CFM	BCOU
PCM	CFU	CHCU
PVTA	KA	SCOU
FCU	BA	BRUCU
BA	BA	ATCU
UPCU		

August 8, 2002

Plate 2 - Southwest to Northeast Hydrostratigraphic Cross Section J-J' through the Pahute Mesa - Oasis Valley Area

Scale - 1:62,500
No Vertical Exaggeration



Hydrostratigraphic Units	
AA	CHZCM
DVA	CHCU
DVCM	IA
YVCM	CFCM
TCVA	CFCU
FCCM	KA
FCA	BFCU
THLFA	BRA
THCM	PBRCM
TMA	TMCM
WWA	SCVCU
PCM	LCA3
PVTA	LCCU1
FCCU	LCCU
BA	LCA
UPCU	LCCU
TCA	MGCU
PLFA	CHICU
LPCU	BMICU
TSA	CHICU
YMCFCM	CCICU
CHVTA	RMICU
CHVCM	ATICU

EXPLANATION

ER-20-1

 Drill hole in line of cross section. Tick marks represent tops of hydrostratigraphic units determined from drill hole data. Dashed line indicates drill hole projected into line of cross section (up to 1000 meters).

Fault with half arrows indicate sense of displacement. "T" indicates sense of movement is toward the reader. "A" indicates sense of movement is away from the reader.

TIE LINE J-J'

 Tie line indicates the location where another cross section intersects this cross section.

ATS - Ammonia Tanks caldera structural margin
 A20S - Area 20 caldera structural margin
 BMS - Black Mountain caldera structural margin
 BRT - Belted Range thrust fault
 CCS - Claim Canyon structural margin
 GCS - Grouse Canyon structural margin
 RMS - Rainier Mesa structural margin

Note: See Appendix A for definitions of hydrostratigraphic units.

Source: A Hydrostratigraphic Model and Alternatives for the Groundwater Flow and Contaminant Transport Model of Corrective Action Units 101 and 102: Central and Western Pahute Mesa, Nye County, Nevada (DOE/NV/11718--706)

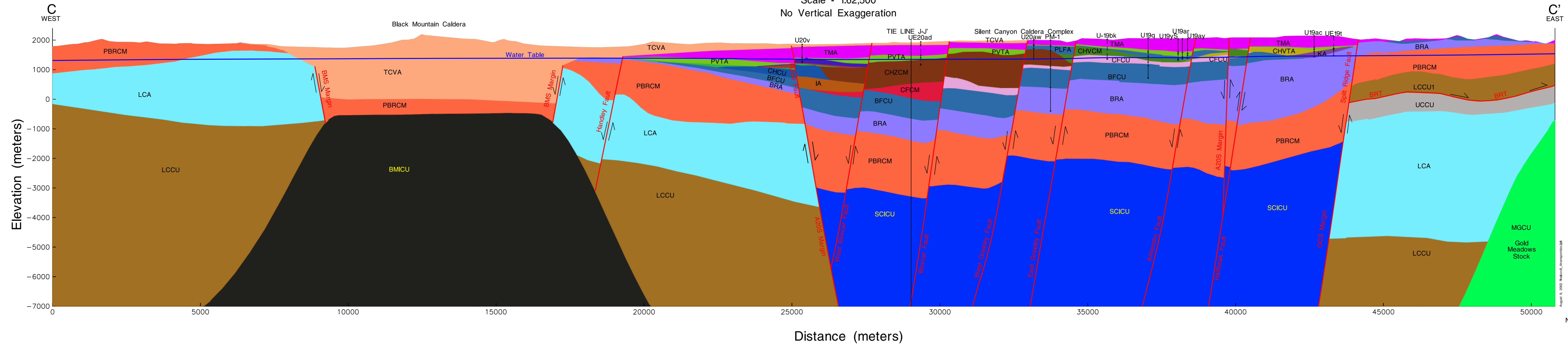
Distance (meters)

August 9, 2002 (file:///C:/Users/robert/...

Plate 3 - West to East Hydrostratigraphic Cross Section C-C' through the Pahute Mesa - Oasis Valley Area

Scale - 1:62,500

No Vertical Exaggeration



Hydrostratigraphic Units	
AA	CHZCM
DVA	CHCU
DVCM	IA
YVCM	CFCM
TCVA	CFCU
FCCM	KA
FCA	BFCU
THLFA	BRA
THCM	PBRCM
TMA	TMCM
WWA	SCVCU
PCM	LCA3
PVTA	LCCU1
FCCU	UCCU
BA	LCA
UPCU	LCCU
TCA	SCICU
PLFA	MCCU
LPCU	BMICU
TSA	CHICU
YMCFM	CCICU
CHVTA	RMICU
CHVCM	ATICU

EXPLANATION

ER-20-1
 Drill hole in line of cross section. Tick marks represent tops of hydrostratigraphic units determined from drill hole data. Dashed line indicates drill hole projected into line of cross section (up to 1000 meters).

Fault with half arrows indicate sense of displacement. "T" indicates sense of movement is toward the reader. "A" indicates sense of movement is away from the reader.

TIE LINE J-J'
 Tie line indicates the location where another cross section intersects this cross section.

ATS - Ammonia Tanks caldera structural margin
 A20S - Area 20 caldera structural margin
 BMS - Black Mountain caldera structural margin
 BRT - Belted Range thrust fault
 CCS - Claim Canyon structural margin
 GCS - Grouse Canyon structural margin
 RMS - Rainier Mesa structural margin

Note: See Appendix A for description of hydrostratigraphic units.

Source: A Hydrostratigraphic Model and Alternatives for the Groundwater Flow and Contaminant Transport Model of Corrective Action Units 101 and 102: Central and Western Pahute Mesa, Nye County, Nevada (DOE/NV/11718--706)

Distribution

<p>Terre A. Maize State of Nevada Bureau of Federal Facilities Division of Environmental Protection 1771 E. Flamingo Road, Suite 121A Las Vegas, NV 89119</p>	1
<p>State of Nevada Division of Environmental Protection Bureau of Federal Facilities 333 West Nye Lane, Suite 138 Carson City, NV 89706-0851</p>	1
<p>Robert Bangerter Environmental Restoration Division U.S. Department of Energy National Nuclear Security Administration Nevada Site Office P.O. Box 98518, M/S 505 Las Vegas, NV 89193-8518</p>	1
<p>Bill Wilborn Environmental Restoration Division U.S. Department of Energy National Nuclear Security Administration Nevada Site Office P.O. Box 98518, M/S 505 Las Vegas, NV 89193-8518</p>	1
<p>Shirley Doty Environmental Restoration Division U.S. Department of Energy National Nuclear Security Administration Nevada Site Office P.O. Box 98518, M/S 505 Las Vegas, NV 89193-8518</p>	1 Electronic
<p>Ken Ortego Bechtel Nevada P.O. Box 98521 MS/NLV 82 Las Vegas, NV 89193</p>	1
<p>Chuck Russell Desert Research Institute 755 E. Flamingo Las Vegas, NV 89119</p>	1

Hydrologic Data for CAUs 101 and 102

John McCord Stoller-Navarro Joint Venture 7710 W. Cheyenne Ave., Bldg. 3 Las Vegas, NV 89129	1
Jim Aldrich Los Alamos National Laboratory Box 1663, MS-J514 CST-7 Los Alamos, NM 87545	1
Gayle Pawloski Lawrence Livermore National Laboratory P.O. Box 808, L-221 Livermore, CA 94551	1
Tim Rose Lawrence Livermore National Laboratory P.O. Box 808, L-221 Livermore, CA 94551	1
Bonnie Thompson U.S. Geological Survey 160 Stephanie Street Henderson, NV 89074	1
U.S. Department of Energy National Nuclear Security Administration Nevada Site Office Technical Library P.O. Box 98518, M/S 505 Las Vegas, NV 89193-8518	1
U.S. Department of Energy Office of Scientific and Technical Information P.O. Box 62 Oak Ridge, TN 37831-0062	1
Southern Nevada Public Reading Facility c/o Nuclear Testing Archive P.O. Box 98521, M/S 400 Las Vegas, NV 89193	2
Manager, Northern Nevada FFACO Public Reading Facility c/o Nevada State Library & Archives Carson City, NV 89701-4285	1
Sig Drellack Bechtel Nevada P.O. Box 98521 MS/NLV 82 Las Vegas, NV 89193	1 (CD)

Hydrologic Data for CAUs 101 and 102

Paul Reimus Los Alamos National Laboratory Bikini Atoll Rd., SM 30 Los Alamos, NM 87545	1 (CD)
Robert Graves U.S. Geological Survey 160 Stephanie Street Henderson, NV 89074	1 (CD)
Joseph Fenelon U.S. Geological Survey 160 N. Stephanie Street Henderson, NV 89074	1 (CD)
Reed Maxwell Lawrence Livermore National Laboratory 7000 East Ave. Livermore, CA 94550-9234	1 (CD)
Rick Waddell GeoTrans, Inc. 363 Centennial Parkway, Suite 210 Louisville, CO 80027	1 (CD)
Greg Pohl Desert Research Institute 2215 Raggio Parkway Reno, NV 89512	1 (CD)
FFACO Support Office Stoller-Navarro Joint Venture 7710 W. Cheyenne Ave., Bldg. 3 Las Vegas, NV 89129	1
John Pickens Stoller-Navarro Joint Venture 7710 W. Cheyenne Ave., Bldg. 3 Las Vegas, NV 89129	1
Warda Drici Stoller-Navarro Joint Venture 7710 W. Cheyenne Ave., Bldg. 3 Las Vegas, NV 89129	1
Bill Fryer Stoller Corp. 990 South Public Road, Suite A Lafayette, CO 80026	1 (CD)

Hydrologic Data for CAUs 101 and 102

James Watrus Stoller-Navarro Joint Venture 7710 W. Cheyenne Ave., Bldg. 3 Las Vegas, NV 89129	1 (CD)
Derek Sloop Stoller-Navarro Joint Venture 7710 W. Cheyenne Ave., Bldg. 3 Las Vegas, NV 89129	1 (CD)
Tad Beard Stoller-Navarro Joint Venture 7710 W. Cheyenne Ave., Bldg. 3 Las Vegas, NV 89129	1 (CD)
Ken Rehfeldt Yucca Mountain Project 1180 Town Center Drive Mail Stop 423 Las Vegas, NV 89144	1 (CD)
Stoller-Navarro Joint Venture Central Files 7710 W. Cheyenne Ave., Bldg. 3 Las Vegas, NV 89129	1 1 (CD)